

NANOGOLD AND NANOSILVER HYBRID POLYMER MATERIALS

By

Maria Parry

A thesis

submitted to the Victoria University of Wellington

in fulfilment of the requirements for the degree of

Doctor of Philosophy

Victoria University of Wellington

2013

Abstract

Significant opportunities exist in both the scientific and industrial sectors for the development of new generation hybrid materials. These multifunctional hybrid materials favourably combine the often disparate characteristics of both precursor components in one material. As such, this field can be very innovative due to the many possible combinations of components providing the opportunity to create a wide variety of new generation materials with a range of known and as yet unknown properties. In this manner the research carried out in this PhD research programme combines particular polymer substrates with gold, silver or silver halide nanoparticles, generating multifunctional hybrid materials which exhibit novel and useful optical, antimicrobial and antifouling properties. As such, these hybrid materials are well suited for applications in the healthcare and biomedical devices, food and packaging, surface coatings and the personal hygiene industries.

The novel approach developed and used for the production of these nanogold, nanosilver and nanosilver halide hybrid polymer materials did not use conventional external reducing or stabilising agents. Instead, for the nanogold and nanosilver hybrid polymer materials, the Au^{3+} or Ag^+ ions were first absorbed into the polymer substrates (polyurethane, nylon 6,6, polyurethane K5000 latex paint base and amine coated polyethylene terephthalate) and then upon heating the nitrogen-containing functional groups in the polymer matrices reduced the metal ions to their respective metal nanoparticles Au^0 and Ag^0 . Simultaneously a chemical interaction between the metal nanoparticles and the polymer matrix was facilitated. Hence the reduction reaction was effected by the coupled to the oxidation reaction of the nitrogen-containing functional groups. The polymer matrix also afforded control over the nanoparticle size. Silica based BULK ISOLUTE® SORBENTS were used to help elucidate this particular chemistry taking place in the formation of the hybrid polymer materials.

The synthesis of the nanosilver halide hybrid polymer materials involved the initial absorption of halide ions into the polymer matrix followed by treatment with silver ions to effect precipitation of nanosize silver halide particles within the polymer matrix, wherein the particle size was similarly controlled by the polymer matrix and precipitation conditions. All formed nanoparticles were therefore stabilised by the polymer matrix.

The colour of the resultant hybrid polymer materials is due to the surface plasmon resonance effect of gold and silver nanoparticles. The colour is dependent on the particle size and shape of the nanoparticles and on the refractive index of the surrounding medium. Nanogold hybrid polymers are pink/purple in colour whereas nanosilver hybrid polymers reflect yellow/brown colour. Nanosilver halide hybrid polymers absorb light in the UV range of light and are therefore white in colour. However, due to their photosensitive properties, once exposed to light, silver halides undergo a self-photosensitisation process resulting in formation of silver nanodomains (smaller nanoparticles) on the surface of the silver halide nanoparticles. This gives rise to their absorption in the visible range of light making the hybrid polymer materials appear purple/brown in colour. Nanosilver iodide hybrid polymer materials do not show this effect to any extent and remain as their typical yellow colour. The reflected colours of the hybrid polymer materials and therefore the particle sizes and shapes of metal nanoparticles were investigated by the UV-Vis spectroscopy. The electron microscopy (SEM and TEM) studies showed the morphology of the hybrid polymer materials and that the nanoparticles were not only deposited on the surface but distributed within the polymer matrix. The metal nanoparticles varied in sizes and shapes, particle agglomerates were observed. The confirmation of gold, silver or silver halide species was undertaken using energy dispersive spectroscopy (EDS), scanning transmission spectroscopy (STEM) and X-ray diffraction (XRD). Furthermore, X-ray photoelectron spectroscopy (XPS) was carried out in order to study the nature of the interaction between the formed metal nanoparticles and the polymer matrix. It was demonstrated that the gold and silver nanoparticles are bound to the polymer matrices via Au-N and Ag-N bonds respectively, through the nitrogen-containing functional groups of the polymer matrices. The presence of the oxidised

nitrogen species (NO_x) confirmed that the electrons required for the reduction of Au^{3+} and Ag^+ to the respective nanoparticles were provided by the coupled oxidation reaction of the nitrogen-containing groups in the polymer matrices. The XPS studies showed there is an interaction between the silver on the surface of the AgX nanoparticles and the nitrogen and oxygen groups present in the polymer matrix. The observation that only very small amounts of Au^{3+} and Ag^+ ions could be leached from the nanogold and nanosilver hybrid materials confirmed the integrity of this chemical bonding between the gold or silver nanoparticles and the polymer matrix. The nanogold, nanosilver and nanosilver halide polymer materials showed effective antimicrobial properties. They were successfully tested against gram negative bacteria *Escherichia coli*. Additionally, the new generation nanogold and nanosilver hybrid polymer materials have been shown to exhibit antifouling properties.

Acknowledgements

I would like to express my heartfelt gratitude to my supervisor Professor Jim Johnston, who is not only a mentor but also a friend. I could not have asked for better inspiration, support and patience I have received from you. A big thank you to the research group of LB 107/108, it has been a pleasure working with you all. Especially thank you Mathew for your help, advice and proof reading. My friends Matthias, Thomas and Eldon, you guys have been a great influence, always. My dearest friend Kerstin, thank you for providing support and friendship that I needed, I will always be grateful for it.

To the VUW and University of Auckland staff, in particular David Flynn and Dr. Colin Doyle, I am very thankful for the help and support in all aspects of electron microscopy and X-ray photoelectron microscopy respectively. I would like to acknowledge and thank Dr. David Ackerley and his research group for letting me use your laboratory and helping me with the developing and running of the antimicrobial tests. Thanks to the Polymer Group Ltd in Auckland for running the antifouling tests.

I would not have contemplated this road without my entire family. Thank you mama for always believing in me. Dave, I am very grateful for your eager eye and quick proof reading. To the best dog in the world, thank you Lily for being there by my side and not letting me go crazy while writing up this thesis. To my husband and my best friend Elliot, thank you for your unconditional love, support, encouragement, long evening hours of proof reading and also the enormous interest and understanding you have developed for this science project.

Funding for the research and the provision of a scholarship from the University of Auckland "Hybrid Plastics" Programme, FRST RFI UOAX0812, through a sub contract to Professor Jim Johnston, Victoria University of Wellington and also a Submission Scholarship from Victoria University of Wellington are gratefully acknowledged.

Table of Contents

| | |
|---|--------|
| Abstract..... | i |
| Acknowledgements | iv |
| Table of Contents..... | v |
| List of Figures..... | xiii |
| List of Tables | xxx |
| List of Abbreviations | xxxiii |
| Generic terms and definitions | xxxv |
| List of conference presentations and published conference papers..... | xxxvi |
| 1 Hybrid materials | 1 |
| 1.1 Background | 1 |
| 1.2 Polymer nanocomposites..... | 2 |
| 1.3 Substrates | 5 |
| 1.3.1 Thermoplastic elastomers | 5 |
| 1.3.1.1 Background..... | 5 |
| 1.3.1.2 Polyurethane | 8 |
| 1.3.1.2.1 Background | 8 |
| 1.3.1.2.2 Synthesis of polyurethane | 11 |
| 1.3.1.2.3 Polyols | 12 |
| 1.3.1.2.4 Isocyanates | 15 |
| 1.3.1.2.5 Chain extenders | 16 |
| 1.3.1.3 Polyamide – nylon..... | 17 |
| 1.3.1.3.1 Background | 17 |
| 1.3.1.3.2 Synthesis of nylon | 18 |
| 1.3.1.4 Polyethylene terephthalate..... | 19 |
| 1.4 Gold, silver and silver halide nanoparticles | 21 |
| 1.4.1 Background | 21 |

| | | |
|-----------|--|----|
| 1.4.2 | Surface Plasmon Resonance..... | 23 |
| 1.4.3 | Optical properties of gold and silver nanoparticles | 27 |
| 1.4.4 | Synthesis of gold and silver nanoparticles..... | 29 |
| 1.4.5 | Silver halide..... | 32 |
| 1.4.5.1 | Background..... | 32 |
| 1.4.5.2 | Photochemistry of silver halide | 34 |
| 1.4.5.3 | Synthesis of silver halide nanoparticles..... | 36 |
| 1.4.5.4 | Optical properties of silver halides..... | 37 |
| 1.4.6 | Antimicrobial properties of gold and silver | 39 |
| 1.5 | Antifouling paints | 44 |
| 1.5.1 | Background | 44 |
| 1.6 | Scope of Thesis..... | 49 |
| 2 | Experimental methodology | 51 |
| 2.1 | Materials..... | 51 |
| 2.2 | Preparation | 52 |
| 2.2.1 | <i>In situ</i> preparation of gold / silver nanoparticles in the presence of polyurethane or nylon 6,6 and their subsequent binding to the polymer matrix | 52 |
| 2.2.1.1 | Larger scale <i>in situ</i> preparation of gold / silver nanoparticles in the presence of polyurethane or nylon 6,6 and their subsequent binding to the polymer matrix | 53 |
| 2.2.1.2 | <i>In situ</i> preparation of gold / silver nanoparticles in the presence of alternative substrates..... | 54 |
| 2.2.1.2.1 | <i>In situ</i> preparation of gold / silver nanoparticles in the presence of amine coated PET sail cloth and their subsequent binding to the sail cloth..... | 55 |
| 2.2.1.2.2 | <i>In situ</i> preparation of gold / silver nanoparticles in the presence of BULK ISOLUTE® SORBENTS and octadecyl- functionalized silica gel | 56 |

| | | |
|---------|---|----|
| 2.2.2 | <i>In situ</i> preparation of gold / silver nanoparticles in the presence of polyurethane K5000 latex paint base polymer and their subsequent binding to the polymer matrix | 56 |
| 2.2.3 | Preparation of nanosilver halide hybrid polymers | 57 |
| 2.2.3.1 | Preparation of nanosilver halide hybrid polymers in the presence of polyurethane and nylon 6,6 | 58 |
| 2.2.3.2 | Preparation of nanosilver halide hybrid paint materials in the presence of polyurethane K5000 latex paint base polymer | 58 |
| 2.2.4 | Gold and silver uptake | 59 |
| 2.2.5 | Leaching test for nanogold and nanosilver hybrid PU and PU K5000 materials | 59 |
| 2.3 | Characterisation | 60 |
| 2.3.1 | Scanning Electron Microscopy | 60 |
| 2.3.2 | Transmission Electron Microscopy | 61 |
| 2.3.3 | Atomic Absorption Spectroscopy | 61 |
| 2.3.4 | X-ray Diffraction | 62 |
| 2.3.5 | Infrared Spectroscopy | 63 |
| 2.3.6 | X-ray Photoelectron Spectroscopy | 63 |
| 2.3.7 | UV-Visible Spectroscopy | 64 |
| 2.3.8 | Antimicrobial and antifouling testing | 65 |
| 2.3.8.1 | Antimicrobial testing | 65 |
| 2.3.8.2 | Antifouling testing | 66 |
| 3 | Nanogold and nanosilver hybrid polymer materials: nanoparticles formed in the presence of polyurethane and nylon 6,6 using their reducing nature | 67 |
| 3.1 | Uptake studies | 70 |
| 3.1.1 | Extent of gold uptake by polyurethane and nylon 6,6 | 70 |
| 3.1.2 | Extent of silver uptake by polyurethane and nylon 6,6 | 74 |

| | | |
|-------|--|-----|
| 3.2 | Formation of gold and silver nanoparticles within the polymer matrix | 79 |
| 3.3 | Scale up of nanogold and nanosilver hybrid PU materials | 81 |
| 3.4 | UV visible spectroscopy - colour of nanogold and nanosilver hybrid polyurethane and nylon 6,6 materials | 82 |
| 3.4.1 | UV visible spectroscopy - nanogold hybrid polyurethane and nylon 6,6 materials..... | 85 |
| 3.4.2 | UV visible spectroscopy - colour of nanosilver hybrid polyurethane and nylon 6,6 materials | 90 |
| 3.5 | Scanning electron microscopy and energy dispersive X-ray analysis of nanogold and nanosilver hybrid polymer materials | 94 |
| 3.5.1 | Scanning electron microscopy and energy dispersive X-ray analysis of nanogold and nanosilver hybrid polyurethane materials..... | 95 |
| 3.5.2 | Scanning electron microscopy and energy dispersive X-ray analysis of nanogold and nanosilver hybrid nylon 6,6 materials | 108 |
| 3.6 | Transmission electron microscopy and energy dispersive X-ray analysis of nanogold and nanosilver hybrid polymer | 120 |
| 3.6.1 | Transmission electron microscopy and energy dispersive X-ray analysis of nanogold hybrid polyurethane and nylon 6,6 materials..... | 121 |
| 3.6.2 | Transmission electron microscopy and energy dispersive X-ray analysis of nanosilver hybrid polyurethane materials..... | 125 |
| 3.7 | X-ray diffraction analysis of nanogold and nanosilver hybrid polyurethane and nylon 6,6 materials..... | 126 |
| 3.7.1 | X-ray diffraction analysis of nanogold and nanosilver hybrid polyurethane materials..... | 127 |
| 3.7.2 | X-ray diffraction analysis of nanogold and nanosilver hybrid nylon 6,6 materials..... | 130 |
| 3.8 | X-ray photoelectron spectroscopy analysis of nanogold and nanosilver hybrid polyurethane and nylon 6,6 materials..... | 132 |

| | | |
|-------|--|-----|
| 3.8.1 | X-ray photoelectron spectroscopy analysis of nanogold hybrid polyurethane materials..... | 133 |
| 3.8.2 | X-ray photoelectron spectroscopy analysis of nanogold hybrid nylon 6,6 materials..... | 139 |
| 3.8.3 | Proposed mechanism of formation of gold nanoparticles in hybrid PU and nylon 6,6 materials | 151 |
| 3.8.4 | X-ray photoelectron spectroscopy analysis of nanosilver hybrid polyurethane materials..... | 152 |
| 3.8.5 | X-ray photoelectron spectroscopy analysis of nanosilver hybrid nylon 6,6 materials..... | 156 |
| 3.8.6 | Proposed mechanism of formation of silver nanoparticles in hybrid PU and nylon 6,6 materials | 161 |
| 3.9 | Infrared and Raman spectroscopy analysis of nanogold and nanosilver hybrid PU and nylon 6,6 materials | 162 |
| 3.10 | Leaching test on nanogold and nanosilver hybrid polyurethane materials | 164 |
| 3.11 | Antimicrobial properties of nanogold and nanosilver hybrid PU materials | 165 |
| 3.12 | Conclusions | 169 |
| 4 | Nanogold and nanosilver hybrid polymer materials: nanoparticles formed in the presence of alternative substrates such as amine coated polyethylene terephthalate sail cloth and silica based Bulk isolate® sorbent | 172 |
| 4.1 | Nanogold and nanosilver hybrid PET sail cloth and ISOLUTE sorbents materials | 173 |
| 4.2 | Extent of gold and silver uptake by PET sail cloth and silica based BULK ISOLUTE® NH ₂ sorbent materials..... | 175 |
| 4.3 | UV Visible spectroscopy – colour of nanogold and nanosilver hybrid PET sail cloth and silica based BULK ISOLUTE® NH ₂ sorbent materials | 178 |

| | | |
|-------|---|-----|
| 4.4 | SEM and EDS analyses of hybrid PET sail cloth and silica based BULK ISOLUTE® NH ₂ sorbent materials..... | 182 |
| 4.5 | X-ray diffraction on nanogold and nanosilver hybrid PET sail cloth and silica based BULK ISOLUTE® NH ₂ sorbent materials | 188 |
| 4.6 | X-ray photoelectron spectroscopy on nanogold and nanosilver hybrid PET sail cloth materials | 190 |
| 4.7 | Conclusions | 196 |
| 5 | Nanogold and nanosilver hybrid materials: nanoparticles formed directly in polyurethane K5000 latex paint base material | 198 |
| 5.1 | Formation of gold and silver nanoparticles within the polyurethane K5000 latex paint base polymer | 200 |
| 5.2 | UV Visible spectroscopy - colour of nanogold and nanosilver hybrid polyurethane K5000 latex paint base materials | 203 |
| 5.3 | Scanning electron microscopy and energy dispersive X-ray analysis of nanogold and nanosilver hybrid polyurethane K5000 latex paint base materials | 211 |
| 5.4 | Transmission electron microscopy and energy dispersive X-ray analysis of nanogold and nanosilver hybrid polyurethane K5000 latex paint base materials | 219 |
| 5.5 | X-ray diffraction analysis of nanogold and nanosilver hybrid polyurethane K5000 latex paint base materials | 224 |
| 5.6 | X-ray photoelectron spectroscopy analysis of nanogold and nanosilver hybrid polyurethane K5000 latex paint base materials..... | 230 |
| 5.6.1 | X-ray photoelectron spectroscopy analysis of nanogold hybrid polyurethane K5000 latex paint base materials - proposed mechanism for gold nanoparticles formation and their binding to the PU K5000 matrix..... | 231 |
| 5.6.2 | X-ray photoelectron spectroscopy analysis of nanosilver hybrid polyurethane K5000 latex paint base materials – proposed mechanism for silver nanoparticles formation and their binding to the PU K5000 matrix | 237 |

| | | |
|-------|--|-----|
| 5.7 | Infrared spectroscopy analysis of nanogold and nanosilver hybrid polyurethane K5000 latex paint base materials | 242 |
| 5.8 | Leaching tests on nanogold and nanosilver hybrid polyurethane K5000 latex paint base materials | 244 |
| 5.9 | Antimicrobial and antifouling properties of nanogold and nanosilver hybrid polyurethane K5000 latex paint base materials | 245 |
| 5.10 | Conclusions | 251 |
| 6 | Nanosilver halide hybrid materials: silver halide formed in the presence of polyurethane, nylon 6,6 and polyurethane K5000 latex paint base materials..... | 254 |
| 6.1 | UV Visible spectroscopy - colour of nanosilver halide hybrid polymer materials | 256 |
| 6.2 | Scanning electron microscopy and energy dispersive X-ray analysis of nanosilver halide polymer materials..... | 264 |
| 6.2.1 | Scanning electron microscopy and energy dispersive X-ray analysis of nanosilver halide hybrid polyurethane materials | 264 |
| 6.2.2 | Scanning electron microscopy and energy dispersive X-ray analysis of nanosilver halide hybrid nylon 6,6 materials..... | 272 |
| 6.2.3 | Scanning electron microscopy and energy dispersive X-ray analysis of nanosilver halide hybrid polyurethane K5000 latex paint base materials | 275 |
| 6.3 | Transmission electron microscopy and energy dispersive X-ray analysis of nanosilver halide hybrid polymer materials..... | 278 |
| 6.4 | X-ray diffraction analysis of nanosilver halide hybrid polymer materials | 286 |
| 6.5 | X-ray photoelectron spectroscopy analysis of nanosilver halide hybrid polymer materials | 298 |
| 6.6 | Infrared spectroscopy analysis of nanosilver halide hybrid polymer materials | 311 |
| 6.7 | Antimicrobial properties of nanogold and nanosilver hybrid polymer materials | 312 |

| | | |
|-----|---|-----|
| 6.8 | Conclusions | 317 |
| 7 | Summary of Thesis | 320 |
| 7.1 | Nanogold and nanosilver hybrid polyurethane and nylon 6,6, materials | 320 |
| 7.2 | Nanogold and nanosilver hybrid polyethylene terephthalate and silica based BULK ISOLUTE® SORBENTS (NH ₂) | 322 |
| 7.3 | Nanogold and nanosilver hybrid polyurethane K5000 latex paint base materials | 322 |
| 7.4 | Nanosilver halide hybrid polyurethane, nylon 6,6 and PU K5000 latex paint base materials | 324 |
| 8 | References..... | 327 |

List of Figures

| | |
|---|----|
| Figure 1.1: Schematic representation of segmented block copolymer..... | 6 |
| Figure 1.2: Consumer products containing TPEs as a) polyurethane shoe sole, ³⁵ b) copolyester cutlery, ³⁶ c) power cords made of halogen-free flame-retardant (HFFR) TPEs. ³⁷ | 7 |
| Figure 1.3: Simplified schematic representation of a PU. ⁵⁶ | 9 |
| Figure 1.4: "one shot" process reaction for PU synthesis. | 16 |
| Figure 1.5: Synthesis of nylon 6,6..... | 19 |
| Figure 1.6: The Lycurgus Cup in a) reflected and b) transmitted light, Department of Prehistory and Europe, The British Museum. ⁸⁹ c) The deep red colours in some stained glass windows created during the Middle Ages were the result of the optical properties of the gold nanoparticles..... | 22 |
| Figure 1.7: Schematic representation for the excitation of the dipole surface plasmon oscillation for a metal nanosphere. ⁹⁴ | 23 |
| Figure 1.8: a) Schematic presentation of the interaction of electromagnetic radiation with a metal nanosphere: a dipole is induced, which oscillates in phase with the electric field of the incoming light. b) Transversal and longitudinal oscillation of electrons in a metal nanorod. ⁹⁶ | 25 |
| Figure 1.9: Summary of silver and gold nanoparticle morphologies with their respective typical locations of SPR bands in the visible range. ⁹⁸ | 26 |
| Figure 1.10: UV-Vis spectrum of gold nanoparticles with different shapes and sizes. ¹⁰⁶ | 27 |
| Figure 1.11: Brust's two-phase method for gold nanoparticle synthesis. ¹²⁹ | 31 |
| Figure 2.1: Setup for scale up reaction: a) circulating pump, b) water bath, c) reaction vessel, d) sintered glass plate, e) reaction solution containing metal ions and f) substrate polymer beads. | 54 |

| | |
|---|----|
| Figure 3.1: Hybrid PU beads prepared from a) gold solution and b) silver solution with increasing gold / silver concentrations (5 – 100 mg kg ⁻¹ Au ³⁺ or Ag ⁺ from left to right)..... | 69 |
| Figure 3.2: Gold uptake by PU beads at 50 °C, utilising a solution with an initial gold concentration of 10, 20 and 50 mg kg ⁻¹ Au ³⁺ | 71 |
| Figure 3.3: Gold uptake by nylon 6,6 beads at 50 °C, utilising a solution with an initial gold concentration of 5, 10 and 50 mg kg ⁻¹ Au ³⁺ | 72 |
| Figure 3.4: Gold uptake by PU beads measured at 50, 70 and 90 °C. | 73 |
| Figure 3.5: Gold uptake by nylon 6,6 beads measured at 50, 70 and 90 °C. | 73 |
| Figure 3.6: Comparison of gold uptake by PU versus nylon 6,6 beads. The experiment was undertaken at 50 °C. | 74 |
| Figure 3.7: Silver uptake by PU beads at 90 °C, utilising a solution with an initial silver concentration of 10, 20 and 50 mg kg ⁻¹ Ag ⁺ | 75 |
| Figure 3.8: Silver uptake by nylon 6,6 beads at 90 °C, utilising a solution with an initial silver concentration of 10, 20 and 50 mg kg ⁻¹ Ag ⁺ | 75 |
| Figure 3.9: Silver uptake by PU beads measured at 50, 70 and 90 °C utilising a solution with an initial silver concentration of 50 mg kg ⁻¹ Ag ⁺ | 76 |
| Figure 3.10: Silver uptake by nylon 6,6 beads measured at 50 and 90 °C utilising a solution with an initial silver concentration of 50 mg kg ⁻¹ Ag ⁺ | 76 |
| Figure 3.11: Comparison of silver absorption by PU beads versus nylon 6,6 beads. The experiment was undertaken at 90 °C. | 77 |
| Figure 3.12: PU beads during absorption process a) after 30 minutes in contact with gold solution with an initial concentrations of 10, 20, 50, 500 mg kg ⁻¹ Au ³⁺ (from left to right); b) after 120 min in silver solution with an initial concentrations of 10, 20, 50, 500 mg kg ⁻¹ Ag ⁺ | 80 |
| Figure 3.13: a) From left to right moulded <i>dog bone</i> strips from the untreated PU beads, beads which were produced from 1, 5, 10, 50, 100 mg kg ⁻¹ Au ³⁺ solution; b) from left to right | |

| | |
|--|----|
| moulded <i>dog bone</i> strips from the untreated PU beads, beads which were produced from 1, 10 and 50 mg kg ⁻¹ Ag ⁺ solution. | 82 |
| Figure 3.14: Photograph of the nanogold and nanosilver hybrid PU and nylon 6,6 beads: a) (from left to right) untreated PU beads, PU-b-5Au, PU-b-10Au, PU-b-20Au and PU-b-50Au samples; b) (from left to right) untreated PU beads, PU-b-5Ag, PU-b-10Ag, PU-b-20 and PU-b-50Ag samples; c) (from left to right) untreated nylon 6,6 beads, Ny-b-5Au, Ny-b-10Au, and Ny-b-50Au samples; d) (from left to right) untreated nylon 6,6 beads, Ny-b-5Ag, Ny-b-10Ag, and Ny-b-50Ag samples. | 83 |
| Figure 3.15: Photograph of the sliced nanogold and nanosilver hybrid PU and nylon 6,6 beads: a) (from left to right) PU-b-20Au, PU-b-50Au and PU-b-500Au samples; b) (from left to right) Ny-b-50Au and Ny-b-500Au samples..... | 85 |
| Figure 3.16: Kubelka Munk transformed UV-Vis reflectance spectra of the nanogold hybrid PU polymer materials with different quantities of gold..... | 88 |
| Figure 3.17: Kubelka Munk transformed UV-Vis reflectance spectra of the nanogold hybrid nylon 6,6 beads polymer materials with different quantities of gold. | 89 |
| Figure 3.18: Kubelka Munk transformed UV-Vis reflectance spectra for the nanosilver hybrid polyurethane <i>dog bone</i> samples with different amounts of silver. | 92 |
| Figure 3.19: Kubelka Munk transformed UV-Vis reflectance spectra for the nanosilver hybrid nylon 6,6 beads with different amounts of silver..... | 93 |
| Figure 3.20: Kubelka Munk transformed UV-Vis reflectance spectra of nanosilver hybrid nylon 6,6 sheets with different amounts of silver. | 94 |
| Figure 3.21: SEM micrographs in backscatter mode of the untreated PU bead surface at a) 230 and b) 7500 times magnification..... | 96 |
| Figure 3.22: SEM micrographs in backscatter mode of the surface of the PU-b-50Au sample at a) 230 and b) 8000 times | |

| | |
|---|-----|
| magnification with c) the respective EDS elemental analysis Au map. | 97 |
| Figure 3.23: SEM micrographs in backscatter mode of the surface of the PU-b-500Au sample at a) 230 and b) 8000 times magnification with c) the respective EDS elemental analysis Au map. | 98 |
| Figure 3.24: Photographs of the a) PU-b-50Au, b) PU-b-500Au, c) PU-b-50Ag and d) PU-b-500Ag samples..... | 98 |
| Figure 3.25: SEM micrographs in backscatter mode of the surface of the PU-b-50Ag sample at a) 9500 and b) 27000 times magnification with c) the respective EDS elemental analysis spectrum. | 100 |
| Figure 3.26: SEM micrographs in backscatter mode of the surface of the PU-b-500Ag sample at a) 8000 and b) 37000 times magnification with c) the respective EDS elemental analysis Ag map. | 101 |
| Figure 3.27: SEM micrographs in backscatter mode of a cross section of the PU-b-50Au sample at a) 55 times magnification, b) 22000 times magnification on the edge of the bead and c) 25000 times magnification in the centre of the bead. | 103 |
| Figure 3.28: Photographs of sliced cross sections of the PU-b-50Au (left) and PU-b-500Au (right) samples..... | 103 |
| Figure 3.29: SEM micrographs in backscatter mode of a cross section area of the PU-b-500Au sample at a) 25 times magnification, b) 500 times magnification on the edge of the bead and c) 7000 times magnification around the centre of the PU bead..... | 104 |
| Figure 3.30: SEM micrograph of the nanogold hybrid PU <i>dog bone</i> strip (left) the corresponding Au EDS map (right). | 105 |
| Figure 3.31: SEM micrographs in backscatter mode of a cross section area of the PU-b-50Ag sample at a) 1400 times magnification on the edge of the bead and b) at 40 000 times magnification in the centre of the bead together with c) the respective EDS spectrum. | 106 |

| | |
|--|-----|
| Figure 3.32: SEM micrographs in backscatter mode of a cross section of the PU-b-500Ag sample at a) 2200 and b) 25000 times magnification near the edge of the bead. | 107 |
| Figure 3.33: SEM micrographs of the untreated nylon 6,6 bead surface (secondary electron and backscatter mode). | 109 |
| Figure 3.34: SEM micrographs in backscatter mode at increasing magnifications of the surface Ny-b-50Au sample..... | 109 |
| Figure 3.35: SEM micrographs in backscatter mode at increasing magnifications of a-b) the surface of the Ny-b-500Au sample with c-d) respective elemental analyses spectrum and Au map. | 110 |
| Figure 3.36: Photographs of Ny-b-50Au (left) and Ny-b-500Au (right) samples with their respective cross sections below..... | 111 |
| Figure 3.37: SEM micrographs in backscatter mode at increasing magnifications of a-b) the surface of the Ny-b-50Ag sample with c) the respective elemental analysis spectrum. | 112 |
| Figure 3.38: SEM micrographs in backscatter mode at increasing magnifications of a-b) the surface of the Ny-b-500Ag sample with c) the respective elemental analysis spectrum. | 113 |
| Figure 3.39: SEM micrograph in backscatter mode of the surface cross section of an untreated nylon 6,6 bead..... | 115 |
| Figure 3.40: SEM micrograph in backscatter mode of a) a surface cross section of the Ny-b-50Au sample with b) respective EDS elemental analysis map. | 117 |
| Figure 3.41: SEM micrographs in backscatter mode at increasing magnifications of a-b) a surface cross section of the Ny-b-500Au sample with c) the respective EDS elemental analysis spectrum. | 118 |
| Figure 3.42: SEM micrographs in backscatter mode of the cross section area of a) the nanogold hybrid nylon 6,6 bead prepared by soaking the bead in 500 mg kg ⁻¹ gold solution at room temperature for 24 hours subsequently increasing the | |

| | |
|--|-----|
| temperature to 50 °C for further 24 hours; b) the respective EDS elemental analysis spectrum. | 119 |
| Figure 3.43: SEM micrographs in backscatter mode of the cross section area of the Ny-b-500Ag sample at different magnifications. . | 120 |
| Figure 3.44: TEM micrographs of some geometrical shape examples of gold nanoparticles found in the PU-b-50Au sample (left) with the respective EDS elemental analyses (right): a-b) spherical, c) triangular, d) truncated triangular, e) hexagonal, f) cubical and g) fivefold twinned particle and h) particle agglomeration..... | 124 |
| Figure 3.45: TEM micrograph of gold nanoparticles found in a) the Ny-b-500Au sample with b) the respective EDS elemental analysis spectrum (right). | 125 |
| Figure 3.46: TEM micrographs of silver nanoparticles found in a) the PU-b-50Ag sample with b) the respective EDS elemental analysis spectrum. | 126 |
| Figure 3.47: XRD patterns for the nanogold and nanosilver hybrid PU materials: PU <i>dog bone</i> strip by itself, PU-db-50Ag and PU-db-50Au samples..... | 128 |
| Figure 3.48: XRD patterns for the nanogold hybrid PU materials: PU sheet by itself, PU-s-100Au and PU-s-500Au samples..... | 129 |
| Figure 3.49: XRD patterns for nanosilver hybrid PU materials: PU sheet by itself, PU-s-100Ag and PU-s-500Ag samples. | 130 |
| Figure 3.50: XRD patterns for nanogold and nanosilver hybrid nylon 6,6 beads and nylon 6,6 beads by themselves..... | 131 |
| Figure 3.51: Survey XPS scans of a) a cross section of the untreated PU bead and b) the cross section of the PU-b-500Au sample. | 133 |
| Figure 3.52: Deconvoluted high resolution XPS spectra for the untreated PU: a) C 1s peaks, c) N 1s peaks and e) O 1s peaks; for the PU-b-500Au sample: b) C 1s peaks, d) N 1s peaks and f) O 1s peaks. Experimental data points are shown by circles. | 135 |
| Figure 3.53: Deconvoluted high resolution Au 4f XPS spectrum for the cross section of the bead PU-b-500Au sample. | 138 |

| | |
|--|-----|
| Figure 3.54: Survey XPS scan of a) the untreated nylon 6,6 sheet and b) the Ny-s-500Au sample. | 140 |
| Figure 3.55: Deconvoluted high resolution XPS spectra for the untreated nylon 6,6 sheet: a) C 1s peaks, c) N 1s peaks and e) O 1s peaks; for the Ny-s-500Au sample: b) C 1s peaks, d) N 1s peaks and f) O 1s peaks..... | 142 |
| Figure 3.56: Deconvoluted high resolution Au 4f XPS spectrum for the Ny-s-500Au sample. | 145 |
| Figure 3.57: Photographs of the Ny-b-500Au beads (left) and the beads prepared via the same method but with a changed pH value of 1.4 (right)..... | 147 |
| Figure 3.58: Deconvoluted high resolution Au 4f XPS spectrum for hybrid nylon 6,6 sheet prepared from a 500 mg kg ⁻¹ gold solution at 50 °C for 24 hours. | 149 |
| Figure 3.59: XRD patterns of the nanogold hybrid nylon 6,6 sheets produced employing 500 mg kg ⁻¹ gold solutions with different pH values..... | 150 |
| Figure 3.60: Survey XPS scans of the surfaces of the untreated PU bead (a) and PU-b-500Au sample. | 153 |
| Figure 3.61: Deconvoluted high resolution XPS spectra for the untreated polyurethane bead: a) N 1s peaks and c) O 1s peaks; for the PU-b-500Ag sample: b) N 1s peaks, d) O 1s peaks and e) Ag 3d peaks..... | 154 |
| Figure 3.62: Survey XPS scan for (a) the untreated nylon 6,6 sheet and b) the Ny-s-1000Ag sample. | 157 |
| Figure 3.63: Deconvoluted high resolution XPS spectra for the untreated nylon 6,6 sheet: a) C 1s peaks and c) N 1s peaks; for the Ny-s-1000Ag sample: b) C 1s peaks, d) N 1s peaks and e) Ag 3d peaks..... | 159 |
| Figure 3.64: XRD patterns of the untreated nylon 6,6 sheet and the Ny-s-1000Ag sample..... | 161 |
| Figure 3.65: FT-IR spectra for the untreated PU sheet, nanogold and nanosilver hybrid PU sheets. | 163 |
| Figure 3.66: Percentage cell survival relative to the untreated PU as control sample after 7 days of bacteria being in contact | |

| | |
|--|-----|
| with the PU and gold and silver hybrid PU materials. (Note the vertical axis is in log scale.)..... | 166 |
| Figure 4.1: Survey XPS scan of the untreated PET sail cloth fabric..... | 174 |
| Figure 4.2: Gold uptake by the PET sail cloth at 80 °C, utilising a solution with an initial gold concentration of 50 mg kg ⁻¹ Au ³⁺ | 176 |
| Figure 4.3: Silver uptake by the PET sail cloth at 80 °C, utilising a solution with an initial silver concentration of 50 mg kg ⁻¹ Ag ⁺ | 176 |
| Figure 4.4: Photograph of the untreated PET sail cloth, PET-50Au and PET-50Ag samples (from left to right). | 178 |
| Figure 4.5: Photograph of the NH2-500Au, NH2-500Ag and untreated NH2 sorbent material samples (from left to right). | 179 |
| Figure 4.6: Kubelka Munk transformed UV-Vis reflectance spectra of the untreated PET sail cloth, nanogold and nanosilver hybrid PET sail cloth materials. | 180 |
| Figure 4.7: Kubelka Munk transformed UV-Vis reflectance spectra of the untreated NH2 sorbent particles, nanogold and nanosilver hybrid NH2 sorbent materials..... | 181 |
| Figure 4.8: SEM micrographs of the surface of the PET-50Au sample a) at 25 times (SEI), b) 2500 times (COMPO), c) 23000 times magnification (COMPO) with d) the respective EDS elemental analysis spectrum. | 183 |
| Figure 4.9: SEM micrographs of the PET-50Ag surface a) at 11000 times (COMPO) with b) the respective EDS elemental analysis map..... | 184 |
| Figure 4.10: SEM micrograph (COMPO) of a cross section of the PET-50Au sample at a) 7000 times magnification (COMPO) with b) the respective EDS elemental analysis spectrum..... | 185 |
| Figure 4.11: SEM micrographs in backscatter mode of the NH2-500Au surface a) at 170 times, b) 1300 times and c) 23000 times magnification with d) the respective EDS elemental analysis spectrum. | 186 |

| | |
|--|-----|
| Figure 4.12: SEM micrographs in backscatter mode of the NH2-500Ag surface a) at 12000 times and b) 45000 times with c) the respective EDS elemental analysis spectrum. | 187 |
| Figure 4.13: XRD patterns of the untreated PET sail cloth and the nanogold and nanosilver hybrid PET materials. | 189 |
| Figure 4.14: XRD patterns of the untreated PET sail cloth and the nanogold and nanosilver hybrid PET materials at higher concentration of Au and Ag. | 190 |
| Figure 4.15: Survey XPS scans of the surface of a) the untreated PET sail cloth b) the PET-50Au and c) the PET-50Ag samples. | 191 |
| Figure 4.16: Deconvoluted high resolution XPS N 1s spectra for a) the untreated PET sail clot and b) the PET-50Au sample. Deconvoluted high resolution Au 4f XPS spectrum for the hybrid PET sail cloth prepared from a 50 mg kg ⁻¹ gold solution at 80 °C for 24 hours is shown in c). Experimental data points are shown by circles. | 193 |
| Figure 4.17: Deconvoluted high resolution XPS N 1s spectra for a) the untreated PET sail clot and b) the PET-50Ag sample. Deconvoluted high resolution Ag 3d XPS spectrum for the hybrid PET sail cloth prepared from a 50 mg kg ⁻¹ silver solution at 80 °C for 24 hours is shown in c). Experimental data points are shown by circles. | 195 |
| Figure 5.1: Picture nanogold (left) and nanosilver (right) hybrid polyurethane K5000 paint materials containing 0.1 wt % of Au ³⁺ / Ag ⁺ | 200 |
| Figure 5.2: Photographs of the a) untreated PU K5000 paint base, b) K5000-1000Au-1:2 (left) and K5000-200Au-1:2 (right) after 24 hours of reaction time and c) K5000-1000Au-1:2 (left) and K5000-200Au-1:2 (right) after seven days of reaction time. | 202 |
| Figure 5.3: Photographs of the a) untreated PU K5000 paint base and b) the K5000-1000Ag-1:2 sample on day 1, day 2, day 3 and day 7 of reaction time (from left to right). | 202 |
| Figure 5.4: Photographs of dried nanogold and nanosilver hybrid PU K5000 paint films: a) K5000-200Au-1:4, b) | |

| | | | |
|---------------------------|----|-------------------|--------|
| K5000-600Au-1:4, | c) | K5000-1000Au-1:4, | d) |
| K5000-200Au-1:2, | e) | K5000-600Au-1:2, | f) |
| K5000-1000Au-1:2, | g) | K5000-200Ag-1:4, | h) |
| K5000-600Ag-1:4, | i) | K5000-1000Ag-1:4, | j) |
| K5000-200Ag-1:2, | k) | K5000-600Ag-1:2 | and l) |
| K5000-1000Ag-1:2.204 | | | |

Figure 5.5: UV-Vis absorption spectra of the nanogold hybrid polyurethane K5000 latex paint base materials prepared from 1.25 ml solution with different amounts of Au^{3+} to 5 g of polyurethane K5000 paint base.206

Figure 5.6: UV-Vis absorption spectra of the nanogold hybrid polyurethane K5000 latex paint base materials prepared from 2.5 ml solution with different amounts of Au^{3+} to 5 g of PU K5000 paint base.208

Figure 5.7: UV-Vis absorption spectra of nanosilver hybrid polyurethane K5000 latex paint base materials prepared from 1.25 ml solution with different amounts of Ag^+ to 5 g of PU K5000 paint base.209

Figure 5.8: UV-Vis absorption spectra of nanosilver hybrid polyurethane K5000 latex paint base materials prepared from 2.5 ml solution with different amounts of Ag^+ to 5 g of PU K5000 paint base.211

Figure 5.9: a-b) Cross sectional SEM micrographs in backscatter mode of the dry film nanogold hybrid polyurethane K5000 latex paint base sample (K5000-1000Au-1:2) at increasing magnification with c-d) the corresponding elemental analysis spectrum and gold EDS map.212

Figure 5.10: Cryo-SEM micrograph in backscatter mode of a) an untreated polyurethane K5000 latex paint base with b) the corresponding EDS micrograph and c) EDS spectrum.214

Figure 5.11: Cryo-SEM micrograph in backscatter mode of a) the K5000-1000Au-1:2 sample with b-c) the corresponding EDS micrographs and d) the EDS C and Au overlay map.216

| | |
|---|-----|
| Figure 5.12: Cryo-SEM micrograph in backscatter mode a) of a K5000-1000Au-1:2 sample and b) respective EDS spectrum at higher magnification..... | 217 |
| Figure 5.13: Cryo-SEM micrograph of a) a nanosilver hybrid PU K5000 paint sample with b-c) the corresponding EDS micrographs and d) the EDS Ag and C overlay map..... | 219 |
| Figure 5.14: TEM micrographs of a,c,d) gold nanoparticles found in the K5000-1000Au-1:2 sample with b) the EDS spectrum of the particle shown in a)..... | 221 |
| Figure 5.15: TEM and corresponding Au STEM micrographs of the K5000-1000Au-1:2 sample. | 221 |
| Figure 5.16: TEM micrographs of the K5000-1000Ag-1:2 sample: a, c) various shaped silver nanoparticles with b, d) their respective EDS spectra, e-f) nanosilver particle aggregates. | 223 |
| Figure 5.17: XRD patterns of the nanogold hybrid PU K5000 latex paint base materials prepared from 1.25 ml solution with different quantities of gold..... | 226 |
| Figure 5.18: XRD patterns of the nanogold hybrid PU K5000 latex paint base materials prepared from 2.5 ml solution with different quantities of gold..... | 226 |
| Figure 5.19: XRD patterns of the nanosilver hybrid polyurethane K5000 latex paint base materials prepared from 1.25 ml solution with different quantities of silver..... | 228 |
| Figure 5.20: XRD patterns of the nanosilver hybrid polyurethane K5000 latex paint base materials prepared from 2.5 ml solution with different quantities of silver..... | 229 |
| Figure 5.21: Survey XPS scans of a) the reference PU K5000 paint sample and b) the K5000-1000Au-1:2 sample which was heated to 50 °C during its preparation..... | 231 |
| Figure 5.22: Deconvoluted high resolution XPS spectra for the reference PU K5000 paint sample: a) C 1s peaks, c) N 1s peak and e) O 1s peaks; for the K5000-1000Au-1:2 sample: b) C 1s peaks, d) N 1s peaks and f) O 1s peaks. Experimental data points are shown by circles..... | 233 |

| | |
|---|-----|
| Figure 5.23: Deconvoluted high resolution Au 4f XPS spectrum for the nanogold hybrid PU K5000 paint sample (K5000-1000Au-1:2). | 235 |
| Figure 5.24: Survey XPS scans of the surfaces for a) the reference PU K5000 paint and b) the K5000-1000Ag-1:2 sample. | 238 |
| Figure 5.25: Deconvoluted high resolution XPS spectra for the reference PU K5000 paint sample: a) C 1s peaks, c) N 1s peak and e) O 1s peaks; for the K5000-1000Ag-1:2 sample: b) C 1s peaks, d) N 1s peaks and f) O 1s peaks. Experimental data points are shown by circles. | 240 |
| Figure 5.26: Deconvoluted high resolution Ag 3d XPS spectrum for the nanosilver hybrid PU K5000 paint sample (K5000-1000Ag-1:2). | 241 |
| Figure 5.27: FT-IR spectra of the dry untreated PU K5000 paint and the nanogold and nanosilver hybrid PU K5000 paint materials. | 243 |
| Figure 5.28: Percentage cell survival relative to untreated PU K5000 paint as control after two days of bacteria being in contact with the control, gold and silver hybrid PU K5000 materials. (Note the vertical axis is a log scale.) | 246 |
| Figure 5.29: Percentage cell survival relative to untreated PU K5000 paint as control after four days of bacteria being in contact with the control, gold and silver hybrid PU K5000 materials. (Note the vertical axis is a log scale.) | 247 |
| Figure 5.30: Photographs of panel surfaces painted with a) the untreated PU K5000 paint, b) the K5000-1000Au-1:2, c) the K5000-1000Au-1:4, d) the K5000-1000Ag-1:2 and e) the K5000-1000Ag-1:4 samples after being submerged in seawater for six months. | 250 |
| Figure 6.1: Photographs of a) the untreated polyurethane sheet and nanosilver hybrid polyurethane sheets; b) the PU-200AgCl sample before (top) and after exposure to light for four days (bottom); c) the PU-200AgBr sample before (top) and after exposure to light for four days (bottom). | 257 |

| | |
|--|-----|
| Figure 6.2: Photographs of a) the untreated nylon 6,6 sheet and nanosilver hybrid nylon 6,6 sheets; b) the Ny-200AgCl sample before (top) and after exposure to light for four days (bottom); c) the Ny-200AgBr sample before (top) and after exposure to light for four days (bottom); d) the Ny-200AgI sample before (top) and after exposure to light for four days (bottom)..... | 258 |
| Figure 6.3: Photographs of dried films of a) the untreated PU K5000 sample; b) the K5000-1000AgCl sample before (left) and after exposure to light for four days (right); c) the K5000-1000AgBr sample before (left) and after exposure to light for four days (right); d) the K5000-1000AgI sample before (left) and after exposure to light for four days (right). The photographs were taken on a black background in order to improve the image contrast. | 259 |
| Figure 6.4: UV-Vis spectra of nanosilver chloride hybrid nylon 6,6 materials before and after light exposure..... | 261 |
| Figure 6.5: UV-Vis spectra of nanosilver bromide hybrid nylon 6,6 materials before and after light exposure..... | 262 |
| Figure 6.6: UV-Vis spectra of nanosilver iodide hybrid nylon 6,6 materials before and after light exposure..... | 263 |
| Figure 6.7: SEM micrograph in backscatter mode of the surface cross section of the PU-200AgCl sample at a magnification of 200 times with b-c) the corresponding EDS micrographs, d) the EDS Ag and Cl overlay map and e) the corresponding elemental analysis spectrum. The sample surface is located to the right side of the red arrow..... | 266 |
| Figure 6.8: SEM micrographs a-b) of the surface cross section of the PU-200AgCl sample (secondary electron and backscatter mode) at a magnification of 23000 times with c-d) the corresponding EDS micrographs and e) the corresponding elemental analysis spectrum. | 267 |
| Figure 6.9: SEM micrograph in backscatter mode of the surface cross section of the PU-200AgCl sample at a magnification of | |

| | |
|---|-----|
| 50000 times with b) the respective EDS elemental analysis spectrum. | 269 |
| Figure 6.10: SEM micrograph in backscatter mode of the surface cross section of the PU-200AgCl sample at a magnification of 55000 times with b) the respective EDS elemental analysis spectrum. | 269 |
| Figure 6.11: SEM micrographs a-b) of the surface cross section of the PU-200AgBr sample (secondary electron and backscatter mode). Above the red arrow is the interior, below the red arrow is the surface of the PU sheet and the red represents the edge of the sheet), c) at an increasing magnification of 30000 times with d) the respective EDS elemental analysis spectrum. | 270 |
| Figure 6.12: SEM micrograph in backscatter mode of the surface cross section of the PU-200AgI sample at a magnification of 3300 times with b-c) the corresponding EDS micrographs, d) the EDS Ag and Cl overlay map and e) the corresponding elemental analysis spectrum. | 271 |
| Figure 6.13: SEM micrograph in backscatter mode of the surface cross section of the PU-200AgI sample at a magnification of 12000 times with b) the respective EDS elemental analysis spectrum. | 272 |
| Figure 6.14: SEM micrograph in backscatter mode of the surface cross section of the Ny-200AgCl sample with b) the respective EDS elemental analysis spectrum. | 273 |
| Figure 6.15: SEM micrograph in backscatter mode of the surface cross section of the Ny-200AgCl sample with b-c) the corresponding EDS micrographs, d) the EDS Ag and Cl overlay map and e) the corresponding elemental analysis spectrum. | 274 |
| Figure 6.16: Cryo-SEM micrograph in backscatter mode of the K5000-1000AgCl sample. | 276 |
| Figure 6.17: Cryo-SEM micrograph in backscatter mode of the K5000-1000AgCl sample with b-c) the corresponding EDS | |

| | |
|---|-----|
| micrographs, d) the EDS Ag and Cl overlay map and e) the corresponding elemental analysis spectrum. | 277 |
| Figure 6.18: TEM micrographs of the Ag/AgCl nanoparticles found in the K5000-1000AgCl sample after the exposure to light (left) with their corresponding EDS spectra (right). | 279 |
| Figure 6.19: TEM micrograph of the silver chloride particle in the K5000-1000AgI sample, the corresponding Ag and Cl STEM micrographs and the Ag and Cl overlay. | 280 |
| Figure 6.20: TEM micrographs of the Ag/AgCl nanoparticles found in the K5000-1000AgCl sample after the exposure to light (left) with their corresponding EDS spectra (right). | 281 |
| Figure 6.21: a-c) TEM micrographs of an Ag/AgBr particle found in the K5000-1000AgBr sample taken over a period of three minutes with d) the respective EDS analysis spectrum of the particle shown in a). | 283 |
| Figure 6.22: TEM micrographs of the Ag/AgI nanoparticles found in the K5000-1000AgCl sample after the exposure to light (left) with their corresponding EDS spectra (right). | 284 |
| Figure 6.23: a) TEM micrograph of the silver iodide particles in the K5000-1000AgI sample, the corresponding b) Ag and c) I STEM micrographs. The Ag and I overlay is shown in d). | 285 |
| Figure 6.24: XRD patterns of the nanosilver halide hybrid PU materials before exposure to light. | 288 |
| Figure 6.25 XRD patterns of the nanosilver halide hybrid nylon 6,6 materials before exposure to light. | 289 |
| Figure 6.26: XRD patterns of the nanosilver halide hybrid polyurethane K5000 latex paint base materials before exposure to light. .. | 291 |
| Figure 6.27: XRD patterns of the nanosilver chloride hybrid PU materials before and after exposure to light. | 293 |
| Figure 6.28: XRD patterns of the nanosilver bromide hybrid PU materials before and after exposure to light. | 294 |
| Figure 6.29: Photographs of a) the PU-200AgCl sample before the exposure to light, 4 and 61 days of exposure to natural light (from left to right) and b) the PU-200AgBr sample | |

| | |
|---|-----|
| before the exposure to light, 4 and 61 days of exposure to natural light (from left to right). | 295 |
| Figure 6.30: XRD patterns of the nanosilver chloride hybrid polyurethane K5000 latex paint base materials before and after exposure to light. | 297 |
| Figure 6.31: XRD patterns of the nanosilver bromide hybrid polyurethane K5000 latex paint base materials before and after exposure to light. | 297 |
| Figure 6.32: Survey XPS scans of a) the PU sheet used as reference sample, b) the PU-200AgCl sample, c) the PU-200AgBr sample and d) the PU-200AgI sample..... | 299 |
| Figure 6.33: Deconvoluted high resolution XPS spectra for the PU sheet used as used as reference sample: a) C 1s peaks, c) N 1s peak and e) O 1s peaks; for the PU-200AgCl sample: b) C 1s peaks, d) N 1s peaks and f) O 1s peaks. Experimental data points are shown by circles..... | 301 |
| Figure 6.34: Deconvoluted high resolution XPS spectra for the PU-200AgCl sample: a) Ag 3d peaks and b) Cl 2p peaks. Experimental data points are shown by circles..... | 302 |
| Figure 6.35: Deconvoluted high resolution XPS spectra for the PU sheet used as used as reference sample: a) C 1s peaks, c) N 1s peak and e) O 1s peaks; for the PU-200AgBr sample: b) C 1s peaks, d) N 1s peaks and f) O 1s peaks. Experimental data points are shown by circles..... | 305 |
| Figure 6.36: Deconvoluted high resolution XPS spectra for the PU-200AgBr sample: a) Ag 3d peaks and b) Br 3d peaks. Experimental data points are shown by circles..... | 306 |
| Figure 6.37: Deconvoluted high resolution XPS spectra for the PU sheet used as used as reference sample: a) C 1s peaks, c) N 1s peak and e) O 1s peaks; for the PU-200AgI sample: b) C 1s peaks, d) N 1s peaks and f) O 1s peaks. Experimental data points are shown by circles..... | 309 |
| Figure 6.38: Deconvoluted high resolution XPS spectra for the PU-200AgI sample: a) Ag 3d peaks and b) I 3d peaks. Experimental data points are shown by circles..... | 310 |

| | |
|---|-----|
| Figure 6.39: FT-IR spectra of the dry untreated PU K5000 paint base and the nanosilver halide hybrid polyurethane K5000 latex paint base materials..... | 312 |
| Figure 6.40: Percentage cell survival relative to untreated PU K5000 paint as control after five days of bacteria being in contact with the control and the nanosilver halide hybrid PU K5000 samples. The bars depicted in red represent the samples tested in dark conditions, whereas the bars depicted in blue relate to the samples tested in natural light. (Note the vertical axis is in log scale.) | 314 |

List of Tables

| | | |
|------------|---|-----|
| Table 1.1: | Some commercial available polyols for PU synthesis. ⁷¹ | 13 |
| Table 1.2: | Some commercial available isocyanates for PU synthesis. ^{56,70,71} | 14 |
| Table 1.3: | Differences between physical polyester based and polyether based PUs. ⁷² | 15 |
| Table 1.4: | Commercial available polyamides with their respective monomers. ⁸³ | 19 |
| Table 1.5: | Solubility constants of silver compounds. ¹⁹⁵ | 43 |
| Table 1.6: | Antifouling strategies. ²³⁴ | 46 |
| Table 1.7: | Key advantages and disadvantages of past and present antifouling systems. ²³⁴ | 47 |
| Table 3.1: | The names and their respective reaction parameters for the hybrid polymer materials. The reaction time for all samples was 24 hours; the solution volume was 10 mL. | 68 |
| Table 3.2: | Nomenclature of moulded hybrid PU <i>dog bone</i> strips names and their respective precursor hybrid PU beads. | 69 |
| Table 3.3: | Summary of standard reduction potentials for gold and silver couples in aqueous solutions. ²⁴⁹ | 78 |
| Table 3.4: | XPS assignments for the untreated PU bead and the PU-b-500Au sample. | 134 |
| Table 3.5: | XPS assignments for the untreated nylon 6,6 sheet and the Ny-s-500Au sample. | 141 |
| Table 3.6: | XPS assignments for gold present in the Ny-s-500Au sample and hybrid nylon 6,6 sheet prepared from a 500 mg kg ⁻¹ gold solution at 50 °C for 24 hours. | 149 |
| Table 3.7: | XPS assignments for the untreated PU bead and the PU-b-500Ag sample. | 155 |
| Table 3.8: | XPS assignments for the untreated nylon 6,6 sheet and the Ny-s-1000Ag sample. | 157 |
| Table 3.9: | Gold or silver leached from nanogold and nanosilver hybrid PU materials, leaching tests were carried out at room temperature for seven days. | 165 |

| | | |
|------------|---|-----|
| Table 4.1: | The sample names and their respective reaction parameters for the nanogold and nanosilver hybrid materials. The mass for each substrate was 0.2 g. The reaction time for all samples was 24 hours. The solution volume was 10 mL..... | 173 |
| Table 5.1: | The names and their respective reaction parameters for the nanogold and nanosilver hybrid polyurethane K5000 latex paint base materials. All samples were prepared at room temperature, reaction time was seven days. | 199 |
| Table 5.2: | Parameters for X-ray diffraction patterns of the nanogold hybrid K5000 samples shown in Figure 5.17 -Figure 5.18. ... | 225 |
| Table 5.3: | Parameters for X-ray diffraction patterns of the nanosilver hybrid PU K5000 samples shown in Figure 5.19 -Figure 5.20..... | 228 |
| Table 5.4: | XPS assignments for dry films of the reference PU K5000 paint sample and the K5000-1000Au-1:2 sample..... | 232 |
| Table 5.5: | XPS assignments for dry films of the reference PU K5000 paint sample and K5000-1000Ag-1:2 sample. | 238 |
| Table 5.6: | Gold or silver leached from nanogold and nanosilver hybrid PU K5000 materials, leaching tests were carried out at room temperature for seven days. | 245 |
| Table 6.1: | The sample names and their respective reaction parameters for the silver hybrid PU, nylon 6,6 and polyurethane K5000 latex paint base materials. All samples were prepared at room temperature. | 255 |
| Table 6.2: | Band gap values for silver halides. ³²⁰ | 257 |
| Table 6.3: | Parameters for X-ray diffraction patterns of the nanosilver halide hybrid PU and polyurethane K5000 latex paint base samples..... | 287 |
| Table 6.4: | XPS assignments for the PU sheet as the reference sample and the nanosilver chloride hybrid PU material. | 300 |
| Table 6.5: | XPS assignments for the PU sheet as the reference sample and the nanosilver bromide hybrid PU material..... | 303 |
| Table 6.6: | XPS assignments for the PU sheet as the reference sample and the nanosilver iodide hybrid PU material..... | 308 |

| | |
|--|-----|
| Table 6.7: Remaining percentage of <i>E. coli</i> CFU after being in contact with the nanosilver halide hybrid PU K5000 materials for five days..... | 315 |
|--|-----|

List of Abbreviations

AA: Atomic absorption
CNTs: Carbon nanotubes
CFU: Total colony-forming unit
DMF: Dimethylformamide
EDS: Energy dispersive spectroscopy
E. coli: Escherichia coli
FWHM: Full width at half maximum
HRTEM: High resolution transmission electron microscopy
HFFR: Halogen-free flame-retardant
IR: Infrared spectroscopy
K5000: Kamthane 5000
LB: Luria Bertani Broth
MeOH: Methanol
PC: Polycarbonate
PBS: Phosphate-buffered saline
PCLm: Polycaprolactam
PEI: Polyethyleneimine
PET: Polyethylene terephthalate
PMMA: Polymethylmethacrylate
PU: Polyurethane
PVA: Polyvinyl acetate
PVP: Polyvinylpyrrolidone
SEM: Scanning electron microscopy
SPR: Surface plasmon resonance
SPRB: Surface plasmon resonance band
Staph aureus: Staphylococcus aureus
STEM: Scanning transmission electron microscopy
TBT: Tributyltin
TEM: Transmission electron microscopy
THF: Tetrahydrofuran
TPEs: Thermoplastic elastomers
TSC: Trisodium citrate
UV-Vis: Ultra violet visible spectroscopy

XPS: X-ray photoelectron spectroscopy

XRD: X-ray diffraction

Generic terms and definitions

Elastomer is a thermoplastic or thermoset polymer that can stretch and then return to its original shape without permanent deformation.

Glass-liquid transition (or glass transition) temperature is the temperature range where the reversible transition in amorphous materials (or in amorphous regions within semicrystalline materials) from a hard and relatively brittle state into a molten or rubber-like state occurs.

Thermosetting plastics or thermosets are independent macromolecules before curing process. Upon curing they reach their final state. They then exhibit a 3D structure acquired by irreversible chemical crosslinking formed during or after the processing (e.g. injection moulding, spray-up moulding).

Thermosoftening plastic or thermoplastics are polymers which are mouldable above a specific temperature. They return to a solid state when cooled, exhibiting a 3D structure acquired by reversible crosslinking during or after the processing.

To *pellet* - gather the precipitate ("pellet") on the bottom of the tube via the centrifugation process.

List of conference presentations and published conference papers

Pobedinsky M, Johnston J, "Nanogold and nanosilver hybrid plastics", 6th Annual Polymer Electronic Research Centre PERC Symposium, (Auckland, NZ, December 2009).

Pobedinsky M, Johnston J, "Nanogold and nanosilver plastics", TechConnect NSTI Nano Science and Technology Institute Conference (Anaheim, CA, United States, June 21-24, 2010).

Pobedinsky M, Johnston J, "Nanogold and nanosilver hybrid plastics", AMN-5 Advanced Materials and Nanotechnology Conference (Wellington, NZ, February 2011).

Pobedinsky M, Johnston J, "New generation hybrid plastics functionalised by nanogold and nanosilver", TechConnect NSTI Nano Science and Technology Institute Conference (Boston, MA, United States, June 13-16, 2011).

Pobedinsky M, Johnston J, "New generation hybrid plastics functionalised by nanogold and nanosilver", 7th Annual Polymer Electronic Research Centre PERC / 2nd Hybrid Polymers Symposium, (Auckland, NZ, December 2011).

Parry M, Johnston J H, "New silver chloride - silver hybrid polymers with nylon and polyurethane showing enhanced antimicrobial and photocatalytic properties", CIMTEC 2012 the 4th International Conference on Smart Materials, Structures and Systems (Montecatini Terme, Italy, June 2012).

Parry M, Johnston J H, "New silver - silver halide hybrid polymers with enhanced antimicrobial properties" Annual Polymer Electronic Research Centre PERC Symposium, (Auckland, NZ, December 2012).

1 Hybrid materials

1.1 Background

The world of science and technology grows every day. This creates new requirements for novel materials and provides new ways of making them. The demand for doing things smaller, lighter, faster and stronger has become a challenge for scientists and engineers. Well studied materials such as metals, polymers, glasses or ceramics do not always accomplish desires for new technologies. Material science has shown that a mixture of two different moieties on the molecular scale can produce a new composite that exhibits either characteristics in between the two components or remarkably different and unique properties.

These novel functionalised materials are defined as hybrid materials and they comprise a broad area of different materials, such as crystalline highly ordered coordination polymers, amorphous sol-gel compounds, materials with and without interactions between the inorganic and organic units.¹ Natural materials often play as an important model for scientists to develop new hybrid materials in as much as almost all materials of nature (e.g. wood, bone, skin, leaf) are hybrid materials, for example bone is a combination of collagen with hydroxyapatite.² Hybrid materials mainly consist of organic and inorganic building blocks. Their properties can be tuned and altered by modifications of their composition on the molecular scale, the relative content of the constitutive organic and inorganic components.

One of the well-known examples of hybrid materials is inorganic fibre-reinforced polymers. Due to their lightweight, corrosion resistance and high strength they have been utilised extensively in the medical, sports equipment, automotive and small ship industries, aerospace applications and the construction industry.^{3,4} Carbon nanotubes-inorganic hybrids, produced from carbon nanotubes (CNTs) and inorganic glasses or ceramics, have been utilised in photocatalysis, electrocatalysis, environmental catalysis, gas sensors, supercapacitors, and field emission devices.

1.2 Polymer nanocomposites

A polymer nanocomposite is a hybrid material and defined as a two-phase system, where at least one dimension of the reinforcing filler is on the nanometre scale. Clay minerals have been discussed as candidates for a filler material to improve the characteristics of conventional polymers, such as increased modulus, strength, fracture toughness, impact resistance, gas and liquid barrier, flame retardance.^{5,6} Clay polymer nanocomposites are applicable in a range of areas – from adhesives to coatings, from microelectronic applications to composite systems, in automotive components, food packaging, hoses for automotive, domestic electrical appliances.⁷

Using metal nanoparticles as additives in polymer matrices is an enormously important progress for modern technology and a wide range of potential applications. Polymers exhibit electrical and thermal insulator or conductor properties, they can be of a hydrophobic or hydrophilic nature, mechanically hard, plastic or rubbery.⁸ Depending on nano-scale structure metal particles show unique physical and chemical properties (optical, electronic, magnetic, catalytic and antimicrobial). Metal polymer nanocomposites not only combine the advantageous properties of metal nanoparticles and polymers but also exhibit new multifunctional and high performance polymer characteristics.

The incorporation of metal nanoparticles into polymer matrices can be achieved either by *in situ* or *ex situ* method. In the latter nanoparticles are first produced by the reduction of metal ions following by the distribution of the preformed metal nanoparticles into a polymer solution or monomer solution to polymerise. The *in situ* technique involves the production of nanoparticles inside the polymer matrix. The monomer is polymerised in solution containing metal salts, then metal nanoparticles are generated by reducing metal ions through a reduction process.⁹⁻¹¹ In a third method, the combined solutions containing the metal precursor and the polymer are deposited onto a substrate, and the reduction to the metal colloids is performed within the thin solid film after removal of the solvent.¹² Different approaches have been applied to reduce metal ions to metal

nanoparticles such as UV or γ -ray irradiation, microwave- and sonochemical-assisted reduction, or by using chemical reductants.

Silver nanoparticles can be coated onto polyurethane by producing nanoparticles *ex situ* following by soaking the polymer with the nanoparticles. Nitrogen groups (e.g. urethane) are expected to bind with the surface of the nanoparticles.¹³ In a similar manner, nanocomposites showing antibiofilm effects were prepared by using gold and silver nanoparticles as fillers in polyurethane (PU), polycaprolactam (PCLm), polycarbonate (PC) and polymethylmethacrylate (PMMA) polymers.¹⁴ Silver nanoparticles as well as silver halide nanoparticles have been synthesised and deposited on nylon or polyethylene using ultrasound irradiation resulting in a physical adsorption of the nanoparticles onto the polymers.¹⁵⁻¹⁷ Antibacterial silver halide nanoparticles have been synthesised inside the pores of a mesoporous silica SBA-15, which then can be incorporated into a variety of fabrics and polymers as a filler.¹⁸ Antimicrobial metal nanoparticle-filled polymer nanofibres containing 0.5 - 1.25 wt % silver have been produced by using the electrospinning solvent (formic acid) as a reducing agent and the electrospinning polymer, nylon 6, as a stabilizing agent.¹⁹ Metal nanoparticles can be added to the polymer solution and the resulting suspension can be cast into polymer-metal composite films.^{11,14,20} Natural biopolymer wool has been utilised as the redox active biotemplate. The S-containing cystine amino acids in the wool reduced *in situ* Au^{3+} or Ag^+ to nanoparticulate Au^0 or Ag^0 respectively on and within the fibres. The reaction was coupled by the oxidation reaction of cystine in the fibre resulting in chemical bonds between the metal nanoparticles and the sulfur groups of the biopolymer.^{21,22} It has been reported that gold nanocrystals were successfully prepared in a single step synthesis by the addition of polyethyleneimine (PEI) to gold tetrachloroaurate solution.²³ The produced nanoparticles were then absorbed by wool fibres and chemically bound via the amino nitrogen at the gold surface to the keratin fibre.²⁴

The present research has focused on the synthesis of new generation hybrid polymer materials, the characterisation and analysis of their novel optical, antimicrobial and antifouling properties. The new functionalised hybrid materials consist of an organic matrix (polyurethane, nylon 6,6 and polyurethane K5000

latex paint base polymers) and inorganic building block (gold, silver and silver halide nanoparticles).

The following sections provide a background to the various components which were used for development of these hybrid polymer materials.

1.3 Substrates

The properties of the polymer substrates used in the preparation of nanogold, nanosilver and nanosilver halide hybrid polymer materials are discussed below.

1.3.1 Thermoplastic elastomers

1.3.1.1 Background

Thermoplastic elastomers (TPEs) are a unique class of high molecular weight polymers, which consist of materials with both thermoplastic and elastomeric properties. TPEs become plastic when heated and return to being elastic when cooled. The crosslinks in TPEs are of a weak dipole or hydrogen bond nature and are therefore reversible crosslinks. This is why TPEs can be processed by conventional extrusion and moulding techniques, the same as those which are used for thermoplastics such as injection moulding, extrusion, blow moulding and vacuum forming. The final products have similar mechanical properties to those produced from conventional vulcanized elastomers. The microphase-separated morphology of the TPE is responsible for the specific properties of the material. A typical bimicrophasic TPE material consists of two structural units (Figure 1.1): a segmented block copolymer which contains an amorphous or semicrystalline polymer block with a low glass transition temperature and a crystalline block that physically crosslinks the polymer chains into a reversible network. The amorphous or semicrystalline polymer block defined as the soft segment which is incompatible with the hard segment at service temperatures to avoid the interpenetration of the segments. The hard segment consists of an immiscible crystalline copolymer,^{25,26} and a hydrogen-bonding^{27,28} urethane²⁸⁻³¹ or urea segment.^{28,32,33} The soft segment is responsible for the material's flexibility and suppleness; whilst the hard segment acts as a reinforcing filler in addition to a physical crosslink, giving the material its stiffness. At a low temperature the hard segment accounts for mechanical stability in TPEs.

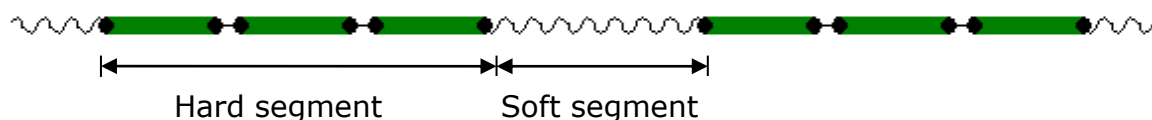


Figure 1.1: Schematic representation of segmented block copolymer.

The reversible crosslinks can be disturbed by thermal or mechanical means and irreparable changes in the morphology of TPEs may occur, resulting in a plastic deformation of the material.

The properties of TPEs are highly dependent on which phases are present and how those are spatially arranged. The crystallinity and crystal defects of the hard segment, the composition of the amorphous phase, the relative proportion of the hard and soft segments and the nature of their continuity and the processing history of the TPE are important parameters. The desired properties, for example porosity and density of TPEs can be obtained by altering of the polymerisation conditions or by changing the ratios of soft and hard segments or by varying the soft segment.

TPEs have a wide range of useful products and applications in a variety of markets such as automotives, building and construction, wires and cables, biomedical fields,³⁴ sports equipment, packaging and hygiene products, etc. Figure 1.2 shows some examples of different TPE products.

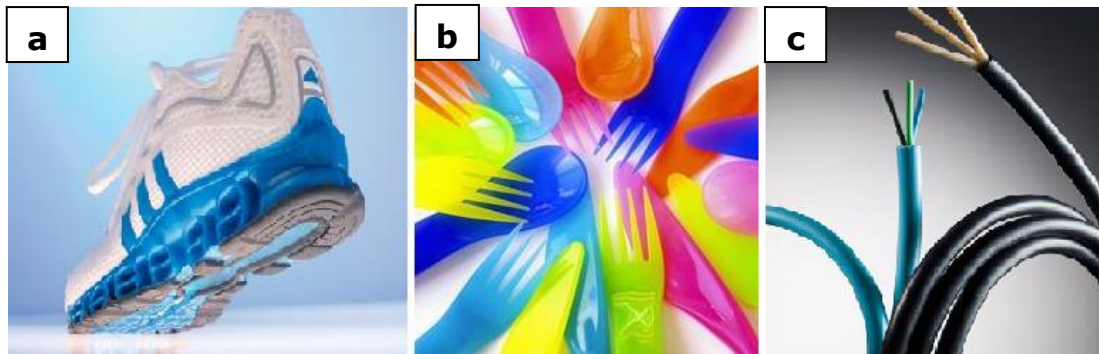


Figure 1.2: Consumer products containing TPEs as a) polyurethane shoe sole,³⁵ b) copolyester cutlery,³⁶ c) power cords made of halogen-free flame-retardant (HFFR) TPEs.³⁷

TPEs may be rationally classified into the following classes due to their chemistry and morphology:³⁸

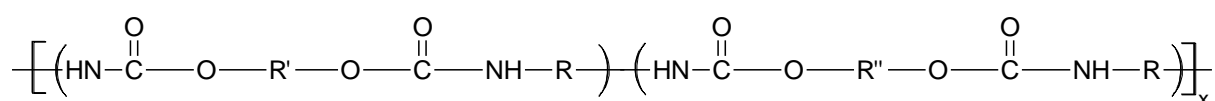
1. Block copolymers
 - a. Styrenic block copolymers
 - b. Thermoplastic copolyesters
 - c. Thermoplastic polyurethanes
 - d. Thermoplastic polyamides
2. Blends and elastomeric alloys
 - a. Elastomeric rubber –plastic blends
 - b. Thermoplastic vulcanizates
 - c. Melt processable rubber
3. Crystalline –amorphous block copolymers
4. Ionomers
 - a. Sulfonated-EPDM rubber
 - b. Zn or Na salt of ethylene acrylic acids
5. Miscellaneous

This thesis will be mainly focused on the block copolymers of the TPEs, with particular reference to polyurethanes and polyamides.

1.3.1.2 Polyurethane

1.3.1.2.1 Background

Thermoplastic polyurethanes (PU) have been available for longer than any other TPEs. They are the well-known and widely used materials of the segmented copolymer class. A typical polyurethane structure is shown below:



A significant break-through occurred in 1937 when Otto Bayer and his co-workers discovered the basic isocyanate polyaddition reaction in Main Scientific Laboratories of I.G. Farbenindustrie, Leverkusen, Germany.³⁹ The discovery was the first step towards the production of polyurethane fibres, trademarked as Perlon U, which were expected to compete with the nylons developed by DuPont some years earlier.^{40,41} In the following years the elastomeric properties of some polyurethanes were recognized independently by chemists at DuPont^{42,43} and ICI.⁴⁴ Otto Bayer et al. first analysed the behaviour of polyurethane in a theoretical study which contained a truly linear polyurethane preparation through a sequence of steps.³¹ It was the first time that the polyaddition was systematically used, which opened the door to the development of many other TPEs (a typical process reaction for a PU synthesis is shown in Figure 1.4). Soon after, it was discovered that the replacement of the short-chain diol by a long-chain diol improved the performance of the polyurethanes. This yielded highly elastic fibres. Further developments of PU proceeded through the 1950's and 1960's. Polyurethanes were first commercially established in the 1950s by B. F. Goodrich in the United States and by Bayer A.G. in Germany. In 1958 Schollenberger and his group from the B.F. Goodrich Company published a paper on a polyurethane which was soluble, offered good elasticity, high abrasion resistance and high tensile strength, and could be processed as a thermoplastic.⁴⁵ In 1960 one of the most interesting thermoplastic polyurethane

fibres, spandex (Lycra), was invented by chemist Joseph Shivers at DuPont's Benger Laboratory in Waynesboro, Virginia. The aim of the fibre was to replace natural rubber⁴⁶ and nowadays it is in use for ladies' garments, and is also expanding into all areas of clothing, including sports and swimwear, at a very rapid rate.⁴⁷

Today, the thermoplastic PUs are an important group of polyurethane products due to their favourable properties such as high hardness for a given modulus, excellent mechanical and elastic characteristics, high abrasion and chemical resistance, low stress relaxation and resistance to long term cyclic flex failure, good resistance to biodegradation, good biocompatibility, structural versatility, good wear and tear resistance, good oil and grease resistance, flame retardant characteristics, transparency, good processability, and protective barrier characteristics.⁴⁸⁻⁵⁵

The properties of thermoplastic polyurethanes are highly influenced by their two-phase microstructure notably the nature and functionality of the component monomers and their ratios. By varying the different parameters the structure of the polymer can be tuned and the desired final properties of the material can be achieved. Simplified linear block copolymer PU (Figure 1.3) consists of a long chain diol, a diisocyanate and a chain extender such as short chain diol.

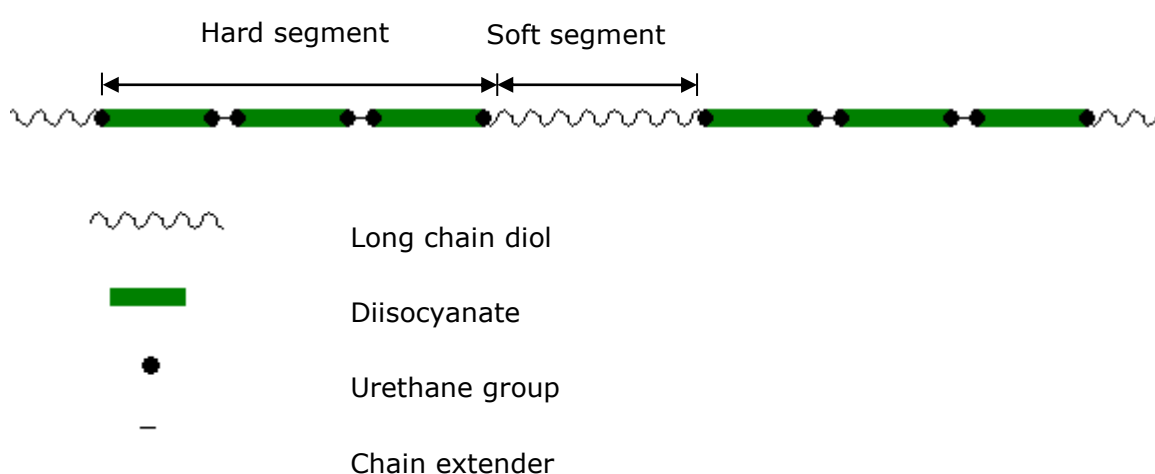


Figure 1.3: Simplified schematic representation of a PU.⁵⁶

The hard segment of polyurethane which has a crystalline nature is formed by extending a diisocyanate (Table 1.2) with a low molecular weight chain extender such as 1,4-butanediol (or alternatively a diamine). The soft segment consists of flexible long chain diols (Table 1.1) with a polyether or polyester backbone (Table 1.3) which connects it to two hard segments. As mentioned in Section 1.3.1.1, thermoplastic polyurethane is a phase-separated multiblock, in which the hard and soft segments are incompatible at the service temperature due to the difference in the chemical structure of both segments. The important parameters which control the degree of microphase separation include the copolymer composition, block length, crystallinity of the hard segment, their production conditions, as well as the difference in the melting points and the polarity of both segments.

The rigid hard segments act as physical crosslinks providing filler-like reinforcement to the soft segments. The soft segments form an elastomeric matrix which accounts for the elastic properties of thermoplastic PU. The melting points and polarity of soft segment are much less than those of the hard segment.

Due to the reversible cross links in the polymer matrix of PU, at temperatures higher than the melting point of the hard segment, the polymer becomes a homogenous viscous melt. Hence, polyurethane can be processed using conventional extrusion and moulding techniques.⁵³ Cooling the melt results in a separation of the phases and reorganising of crosslinks in the matrix. The original properties are retained in the final product.

Thermoplastic PUs are one of the most versatile materials which are suitable for demanding applications in almost all sectors of industry today. PU's application can be found in engineering materials, coatings, adhesives as well as films.⁵⁷ PU has been meeting the needs of a worldwide marketplace in sportswear and footwear because of their protective barrier properties like waterproofness whilst providing comfort through moisture vapour transmission.⁵⁸ Due to excellent abrasion resistance, low density, high elasticity and flexibility, PU is ideal for producing thinner and lighter shoe soles.⁵⁹ It has been used considerably in the automotive industry for instrument panel skins and several car interior parts,

like belts, hoses and tubing, gear knobs, inner door handles, seals, bushings etc.^{51,60,61} PUs have made inroads into biomedical and biotechnological fields due to their good biocompatibility, processing ability and excellent physical-mechanical properties.^{62,63}

1.3.1.2.2 Synthesis of polyurethane

The synthesis of a polyurethane can be accomplished by two polymerisation processes, the “one-shot method”⁶⁴ or the “prepolymer” method.³⁸ In the exothermic “one-shot” process the three reaction components, polyols (Table 1.1), isocyanates (Table 1.2) and chain extenders are simultaneously mixed and all reactions occur at once forming polyurethane. Alternatively polyurethane can be formed via the prepolymer method which involves the initial formation of an isocyanate functionalized prepolymer. Subsequently the low molecular weight, linear isocyanate prepolymer reacts with the added chain extender resulting in the formation of the final high molecular weight linear PU. Here for example, the hardness of PU can be regulated by increasing the diisocyanate and chain extender concentrations. When using diamine as the chain extender, the PU also contains urea groups, which raise the melting temperature of the hard segment. There have been a number of patents and other literature published on the synthesis of thermoplastic polyurethanes.^{38,65-69} However, because of the broad range of hard and soft segment variations possible, the final PU product can be tuned from extremely soft flexible, elastomeric materials to more brittle, high-modulus plastics.

There are many possible variations of polyols, isocyanates and chain extenders or curatives, which can be used to manufacture thermoplastic PU. However only a limited number are of practical interest to the work presented in this thesis and these are discussed in the following sections.

1.3.1.2.3 Polyols

The long flexible soft segments consisting of high molecular weight polyols are mainly responsible for the low temperature properties, the resistance to solvents and the weather-resistant properties of PUs. Polyols are primarily variations of hydroxyl terminated polyesters and hydroxyl terminated polyethers. The polyesters of commercial interest are adipates, polycaprolactones, and aliphatic polycarbonates.⁷⁰ The polyethers used in large scale synthesis are poly(oxypropylene) glycols and poly (oxytetramethylene) glycols.⁷⁰ Some commercially available polyols used for PU synthesis are represented in Table 2.1. Mixtures of polyethers and polyesters are sometimes used and yield a very useful combination of properties at an attractive cost.⁵⁶

Generally more polyesters are used than polyethers. Table 1.1 represents the main differences between polyester based and polyether based PUs. The polyether based PUs are only of practical importance in cases where excellent hydrolysis, microbial resistance and extreme low temperature flexibility are required.

Table 1.1: Some commercial available polyols for PU synthesis.⁷¹

| Polyol | Structure |
|---|---|
| Poly (tetramethylene adipate) glycol | $\text{HO}-(\text{CH}_2)_4[\text{O}-\overset{\text{O}}{\parallel}{\text{C}}-\text{CH}_2-\overset{\text{O}}{\parallel}{\text{C}}-\text{O}-(\text{CH}_2)_4]_n\text{HO}$ |
| Poly (ϵ -caprolactone) glycol | $\text{H}-\left[\text{O}-(\text{CH}_2)_5-\overset{\text{O}}{\parallel}{\text{C}}\right]_x\text{ORO}-\left[\overset{\text{O}}{\parallel}{\text{C}}-(\text{CH}_2)_5\text{O}\right]_y\text{H}$ |
| Poly (hexamethylenecarbonate) glycol | $\text{HO}-\left[(\text{CH}_2)_6\text{O}-\overset{\text{O}}{\parallel}{\text{C}}-\text{O}\right]_n(\text{CH}_2)_6\text{OH}$ |
| Poly (oxytetramethylene) glycol | $\text{HO}-\left[(\text{CH}_2)_4\text{O}\right]_n\text{H}$ |
| Poly (1,2-oxypropylene) glycol | $\text{HO}-\left[\overset{\text{CH}_3}{\underset{ }{\text{CH}}}-\text{CH}_2-\text{O}\right]_n\text{CH}_2-\overset{\text{CH}_3}{\underset{ }{\text{CH}}}-\text{OH}$ |

Table 1.2: Some commercial available isocyanates for PU synthesis.^{56,70,71}

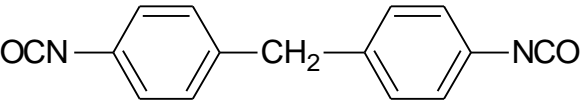
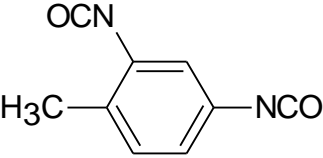
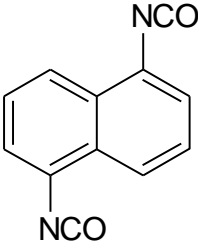
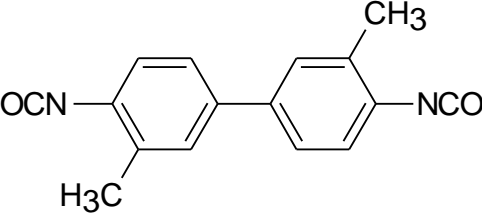
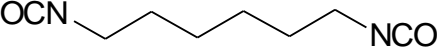
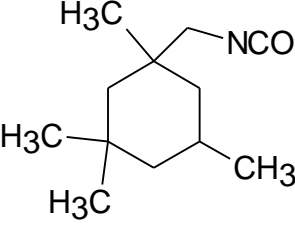
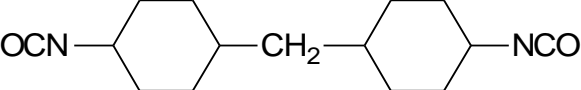
| Isocyanate | Structure |
|---|--|
| 4,4'-methylene-bis(phenyl isocyanate) |  |
| 2,4-toluene diisocyanate |  |
| 1,5-naphthalene diisocyanate |  |
| 3,3'-dimethyl-4,4'-biphenyl-diisocyanate |  |
| 1,6-hexamethylene diisocyanate |  |
| 5-isocyanato-1-(isocyanatomethyl)-1,3,3-trimethyl-cyclohexane |  |
| 4,4'-diisocyanato-dicyclohexylmethane |  |

Table 1.3: Differences between physical polyester based and polyether based PUs.⁷²

| Property | Polyester based PU | Polyether based PU |
|------------------------------------|--------------------|--------------------|
| Abrasion | excellent | acceptable |
| Mechanical properties | excellent | good |
| Low temperature flexibility | acceptable | excellent |
| Heat ageing | good | poor |
| Hydrolysis resistance | very poor | excellent |
| Chemical resistance | excellent | poor |
| Resistance to microbes, fungi etc. | very poor | good |
| Adhesion strength | good | poor |
| Injectability (cycle time) | excellent | acceptable |

1.3.1.2.4 Isocyanates

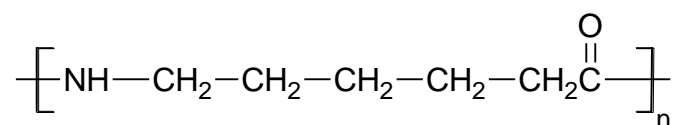
Isocyanate groups react with chain extenders and compose the hard segment of the PU. These hard regions in the PU matrix have relatively inflexible chain sequences but regular structures and a high capability for hydrogen bonding thus forming physical crosslinks with the soft segments.⁷³ The hard segments comprise domains within the continuous softer PU matrix and act as reinforcing filler. Among the commercially available isocyanates only a few are appropriate for the synthesis of PUs. The isocyanates are divided into two types, aromatic isocyanates and aliphatic isocyanates. Isocyanates are commercially prepared by phosgenation of primary amines. Some commercially available and suitable isocyanates are presented in Table 1.2. Aromatic isocyanates are more reactive and economical to use than aliphatic isocyanates. Aliphatic isocyanates are used if special properties of the final product are essential, for example more UV- or light-stable PUs.

1.3.1.3 Polyamide – nylon

1.3.1.3.1 Background

Thermoplastic polyamides are generally known as “nylons”. Nylons are characterised by their repeating amide linkage - the amide group (-CO-NH-) alternating with a (CH₂)_n, group. Much like PU, nylon is one of the most versatile polymers today. The discovery of nylon has been considered as one of the greatest achievements of chemistry in the 20th century. Polymeric amides can be found naturally in the polypeptides which represent every life form and in the composition of silk and wool.⁷⁵ In the early 1930s the DuPont Company started their research on making man-made fibres in order to find a substitute for silk. In 1935 Wallace Hume Carothers and his researchers succeeded in creating a fibre referred to simply as “6,6” because both of the reactants hexamethylene diamine and adipic acid had six carbon atoms.⁷⁶ Polyamide was developed. Although polymer 6,6 was patented in 1937, it took a further 2 years for its first appearance in the real world when it premiered at the New York World Fair and gained the name 'nylon', the 'ny' part of the name standing for the initials of New York. In 1941 researchers from I.G.Farben Industrie's in Germany managed to synthesise nylon 6, which was sold as Perlon. Since the discovery of Nylon 6,6 and Nylon 6 a wide variety of nylon types have been synthesised and commercialised.

Nylons are semicrystalline materials with their crystalline character reflected in their performance and processing properties. The most common nylons are nylon 6, nylon 11, nylon 12, nylon 6,6, nylon 6,10 and nylon 6,12.⁷⁷ A typical linear structure of Nylon 6 is shown below:



Polyamides can be processed by most thermoplastic processing techniques, e. g. injection and blow molding, extrusion, co-injection and gas-assist injection. Polyamides are hygroscopic which has to be considered during their processing. The moisture content should be below 0.2 % or hydrolytic degradation and significant loss of properties may occur.⁷⁸

Polyamides have high performance characteristics such as excellent chemical, physical and mechanical properties.^{79,80} Many characteristics of nylons are attributable to the formation of hydrogen bonds between the NH and CO groups of neighbouring macromolecules.⁸¹ Nylons are suitable for demanding applications in almost all sectors of industry today. Nylons can be found in clothing, tyre cords, sails and rigging, fishing lines, insulators, electrical connectors, automotive industry, packaging industry, engineering and construction industry, racket strings, rope, musical strings, surgical sutures, etc.

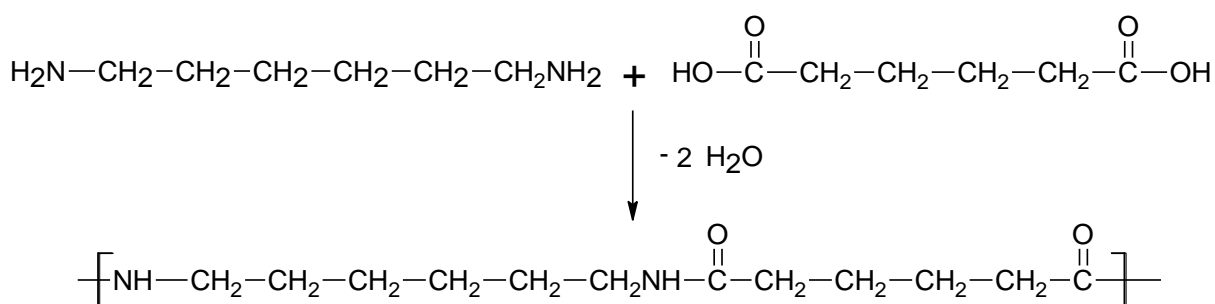
1.3.1.3.2 Synthesis of nylon

A wide selection of nylons with synthesis routes to their production exist. The reactions utilised for the synthesis of polyamides are: polycondensation of ω - aminocarboxylic acids, polycondensation of diamines with dicarboxylic acids (or their derivatives such as acid chlorides) and ring-opening polymerisation of lactams.⁸¹

By varying the monomer composition many different varieties of polyamides can be developed. The monomers required for the synthesis of some commercially available nylons are outlined in Table 1.4. The nylon of specific relevance to this thesis was nylon 6,6. The simplified synthesis scheme involves the condensation polymerization of adipic acid and 1,6 hexanediamine (Figure 1.5).⁸²

Table 1.4: Commercial available polyamides with their respective monomers.⁸³

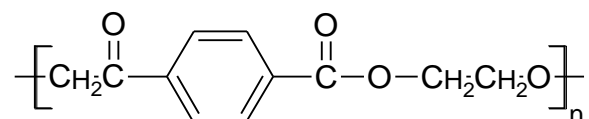
| Polyamide | Monomer(s) |
|----------------|--|
| Polyamide 6 | ϵ -caprolactam |
| Polyamide 11 | 11-amino undecanoic acid |
| Polyamide 12 | laurolactam |
| Polyamide 6,6 | hexamethylene diamine and adipic acid |
| Polyamide 6,10 | hexamethylene diamine and sebacic acid |
| Polyamide 6,12 | hexamethylene diamine and 1,12-dodecanedionic acid |

**Figure 1.5: Synthesis of nylon 6,6.**

1.3.1.4 Polyethylene terephthalate

Polyethylene terephthalate (PET) is a thermoplastic polymer from the polyethylene family and is one of the most versatile thermoplastics. Although polyethylene has been known since the 19th century, PET was first developed by Whinfield and Dixon in 1941 and commercialised by ICI and DuPont.⁸⁴ Early

grades were designed for use as fibres and in 1970s PET was first introduced to manufacture drink bottles due to its good barrier properties against oxygen and carbon dioxide. PET is made via a direct polycondensation reaction between terephthalic acid and ethylene glycol.⁸⁵ A typical structure is shown below:



PET exists as both an amorphous and semicrystalline thermoplastic material. It has good resistance to mineral oils, solvents and acids but not to bases. The semicrystalline PET has good strength, ductility, stiffness and hardness. The amorphous PET has better ductility but less stiffness and hardness. PET can be processed by extrusion and moulding techniques and is used as synthetic fibres, in food packaging, as materials for microwave ovens and in thermal insulation etc.

1.4 Gold, silver and silver halide nanoparticles

1.4.1 Background

The prefix 'nano' is derived from the old greek word nannos and means dwarf. One nanometer is 10^{-9} metres. To provide a reference scale a typical human white blood cell size is about 10000 nm, a cell of the bacterium *E. coli* is 1000 nm and a polymer coil is 40 nm.^{86,87}

A nanoparticle is defined as a particle with at least one dimension between 1 and 100 nm. In this size-range quantum effects start to predominate and a decrease in the particle size of metal nanoparticles to the nanometer length scale increases the surface to volume ratio significantly. Hence, the surface chemistry and physical properties become much more important. These two factors may provide novel and unique physical, chemical and biological properties to the metal nanoparticles with respect to their bulk forms.

The origin of nanoparticles dates back to ancient Egyptian and Roman times⁸⁸ where the brilliant colours of silver and gold metal colloids were used to colour glass. In the 4th century AD Romans utilised colloidal gold combined with smaller amounts of silver and copper nanoparticles as colourants for the Lycurgus Cup (Figure 1.6) which represents one of the outstanding achievements of the ancient glass industry.⁸⁹

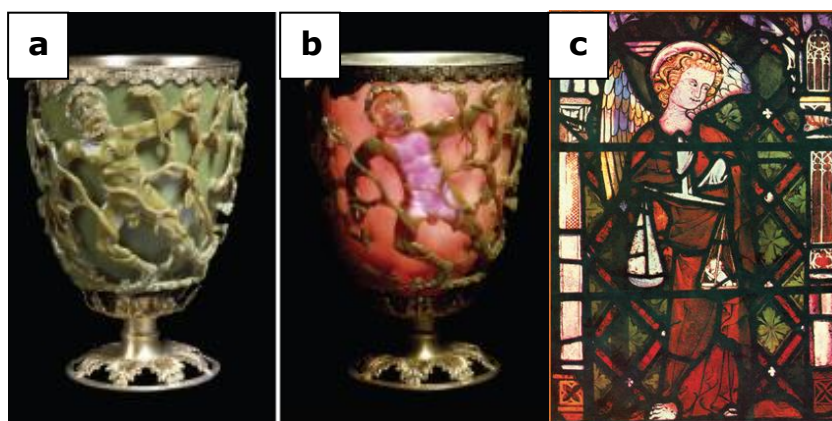


Figure 1.6: The Lycurgus Cup in a) reflected and b) transmitted light, Department of Prehistory and Europe, The British Museum.⁸⁹ c) The deep red colours in some stained glass windows created during the Middle Ages were the result of the optical properties of the gold nanoparticles.

In the Middle Ages gold and silver nanoparticles were used throughout Europe in stained glass windows of cathedrals and by the Chinese in colouring vases and other ornaments. Medieval artisans mixed metal salts for example gold chloride and silver nitrate into the molten glass and obtained a variety of different colours. Silver nanoparticles stained the glass yellow, while gold and copper nanoparticles were utilized to make ruby glass. However, the science behind it was not understood until the 19th century. In 1857 Michael Faraday observed that colloidal gold exists in the reduced state as extremely fine particles and these finely divided metals are responsible for their optical properties. When he reduced an aqueous solution of HAuCl_4 using white phosphorus,⁹⁰ his samples resulted in a stable, ruby-red colour, and some of them are still conserved today in the Faraday Museum in London. From his studies of the optical properties of thin films prepared from dried colloidal solutions, he elucidated the mechanism of formation of colloidal metals.⁹¹

In 1908 by the solving Maxwell's equations for spherical particles, with appropriate interface conditions, Gustav Mie first provided a theoretical quantitative explanation that the colour reflected by exceedingly small metal particles is due to strong visible absorptions known as Surface Plasmon Resonances (SPRs).⁹² These arise from the interaction of light with metal

nanoparticles which can generate hybrid surface waves (light waves coupled to free electrons in a metal), referred to as surface plasmons.⁸⁸

1.4.2 Surface Plasmon Resonance

The electron plasma in metal nanoparticles is spread in diverse spatial dimensions depending on the metal nanoparticle shape and it is smaller than the wavelength of light.⁹³ When excited with incident electromagnetic radiation, the free electrons are displaced by the electric vector and a net charge difference at the surface of the nanoparticle originates. The main restoring force between the electron cloud and nuclei is the Columbic attraction.⁹⁴ A dipolar oscillation of all the electrons with the same phase is created (Figure 1.7).⁹³ The observed colour is due to the strong absorption of the metal nanoparticles when the incident photon frequency is resonant with the collective oscillation of the conduction band electrons. The resonance wavelength is defined as surface plasmon resonance band (SPRB). Because of the d-d transitions, the SPRB of silver and gold nanoparticle is localised at the visible wavelength of electromagnetic radiation.⁹⁵

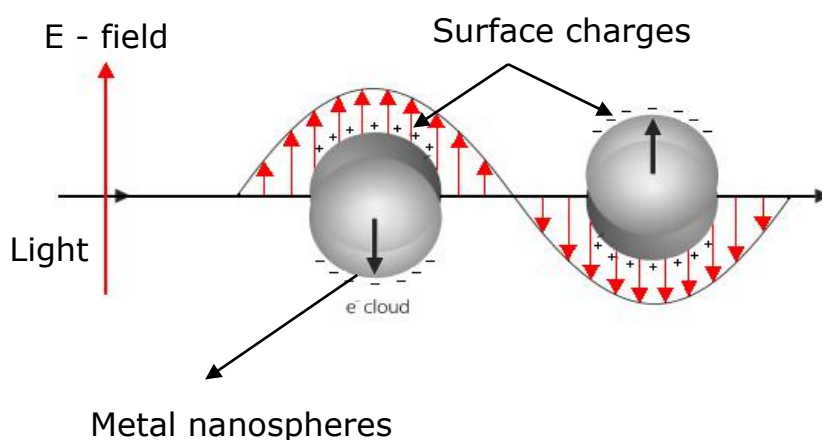


Figure 1.7: Schematic representation for the excitation of the dipole surface plasmon oscillation for a metal nanosphere.⁹⁴

The frequency (i.e., absorption maxima or colour) and intensity of the SPRB depend upon a variety of factors, such as the size and shape of the metal nanoparticles as well as on their dielectric environment.⁹⁶

The optical properties of dispersions of spherical metal particles with a radius R can be calculated by Mie theory, through expressions for the extinction cross section C_{ext} (scattering + absorption). For very small particles with a frequency dependent, the complex dielectric function, $\varepsilon = \varepsilon' + i\varepsilon''$, surrounded by a medium of dielectric constant ε_m , this can be expressed by the equation shown below:

$$C_{ext} = \frac{24\pi^2 \varepsilon_m^{3/2} R^3}{\lambda} \frac{\varepsilon''}{(\varepsilon' + 2\varepsilon_m)^2 + \varepsilon''^2}$$

The resonance condition is fulfilled when $\varepsilon' = -2\varepsilon_m$ for spheres. With increasing particle size, higher order modes become more dominant. As the size increases, the plasmon absorption band shifts to longer wavelengths and the observed colour changes towards blue. The light cannot polarise larger nanoparticles homogeneously and retardation effects lead to the excitation of higher order modes.⁹³ The optical absorption spectra depend directly on the size of the nanoparticles. This phenomenon is known as the extrinsic size effect.⁹³ Aggregation of colloidal metal particles can also lower their plasmon frequencies and shifts the plasmon absorbance to longer wavelengths.

The shape of the nanoparticle is another factor which has a large influence on the presence and position of SPRB. A material with a large flat surface does not feature any resonance band due to surface plasmons which exhibit a strictly longitudinal propagation. They are not able to couple with light and the electric field will be uniform.

The interaction of electromagnetic radiation with a metal nanosphere causes a dipole which oscillates in phase with the electric field of the incoming light. For that reason spherical nanoparticles exhibit one distinct SPRB. For nonspherical particles, such as rods and ellipsoids, the resonance wavelength is influenced by the orientation of the electric field with respect to the metal nanoparticle. Hence, they display two distinct SPRBs due to longitudinal and transversal oscillations of electrons (Figure 1.8).⁹⁵ Concerning the dimensionality of anisotropic shapes, the frequencies related with the diverse resonance modes can be different, therefore optical properties can be largely affected.

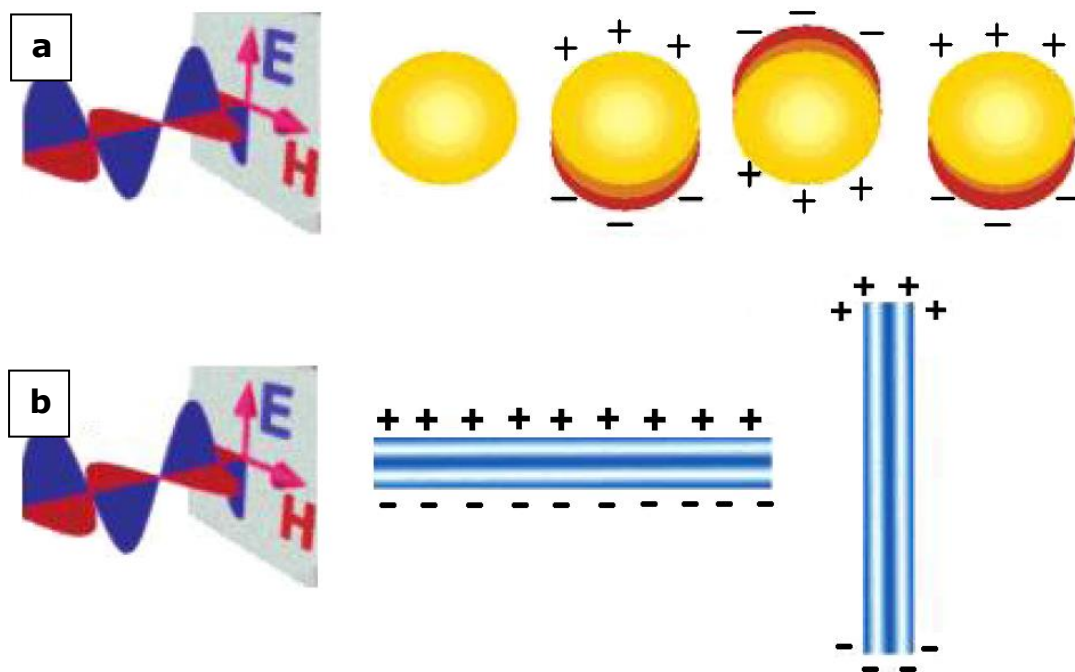


Figure 1.8: a) Schematic presentation of the interaction of electromagnetic radiation with a metal nanosphere: a dipole is induced, which oscillates in phase with the electric field of the incoming light. b) Transversal and longitudinal oscillation of electrons in a metal nanorod.⁹⁶

The surface plasmon band of metal nanoparticles is greatly influenced by the local dielectric environment. Here the plasmon band position depends on the refractive index of the surrounding medium. The dependence of the wavelength of the SPRB on the medium dielectric constant can be determined

spectroscopically from reflectance and absorbance measurements. For spherical nanoparticles where $\lambda \gg$ particle diameter, the resonant frequency is described by the equation:⁹⁷

$$\lambda = \sqrt{\lambda_p(\epsilon^\infty + 2\epsilon_m)}$$

where λ is the resonance wavelength, λ_p is the wavelength of the bulk plasmon, ϵ^∞ is the high frequency dielectric constant of the metal and ϵ_m is the dielectric constant of the medium. The temperature affects the dielectric constant, for that reason this factor has an influence on the position of the SPRB as well.

Figure 1.9 represents a summary of silver and gold nanoparticles with different morphologies, compositions, and structures, with their respective typical locations of SPR absorption bands in the visible range.

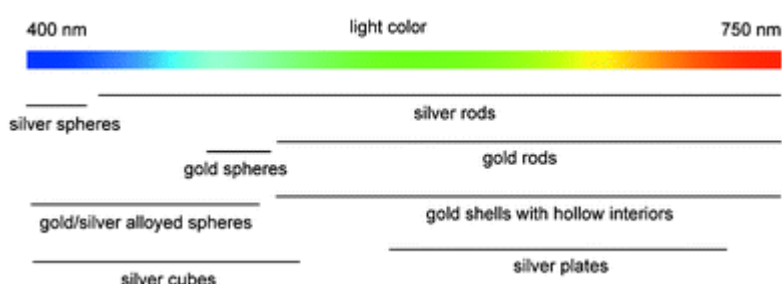


Figure 1.9: Summary of silver and gold nanoparticle morphologies with their respective typical locations of SPR bands in the visible range.⁹⁸

The exploration of unique physical, chemical and biological properties of noble metal nanoparticles has gained momentum as the metal nanoparticles exhibit enormous potential to be utilised in a variety of applications such as catalysis, optics, electronics, environmental biomedical and biotechnology, medical

diagnostics, high performance engineering materials, conducting adhesives, surface enhanced Raman scattering, etc.^{99–105}

1.4.3 Optical properties of gold and silver nanoparticles

As described above, the position of the SPR absorption band depends on the size and shape (Figure 1.10) of the metal nanoparticles as well as the nature of the surrounding medium.

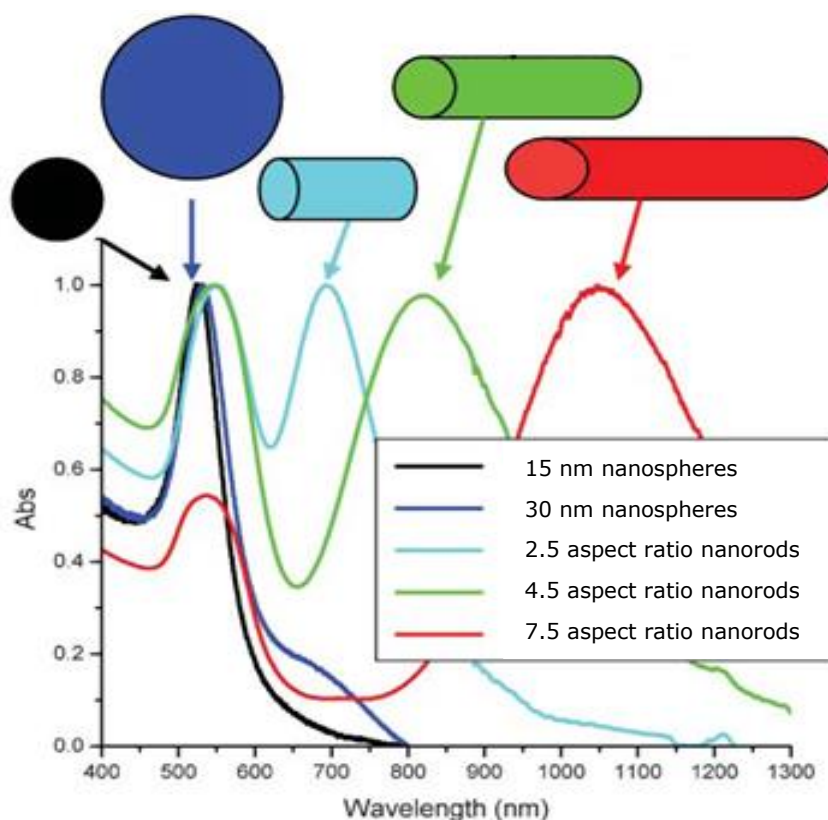


Figure 1.10: UV-Vis spectrum of gold nanoparticles with different shapes and sizes.¹⁰⁶

As the size of the nanoparticle increases, the surface plasmon resonance band shifts to the red.¹⁰⁷ For example, there is a single, strong SPR absorption band in the visible region around 520 nm for a spherical gold nanoparticle of 20 nm diameter which red shifts to 560 nm as the nanoparticle diameter increases to 100 nm.¹⁰⁸

However, for nanoparticles of anisotropic shapes, several plasmon resonance modes could appear resulting from diverse orientations of the multiple particle axes relative to the electric field of light.¹⁰⁷ Two typical absorption bands exist in the UV-visible absorption for gold nanoparticles of anisotropic shapes: one corresponds to the absorption of transverse plasmon band, and at the longer wavelength a band that is ascribed to the absorption of the longitudinal plasmon band (Figure 1.10).¹⁰⁹ For instance gold nanoparticles consisting of a mixture of triangular/hexagonal shaped and smaller, close to spherical particles show one SPRB at 540 nm and another at 680 nm.¹¹⁰ Secondly, nanorods exhibit two plasmon resonances, one at about 520 nm for gold (transverse oscillation of the electrons) and the other due to the longitudinal plasmon resonance at longer wavelengths. The transverse surface plasmon resonance is at the same wavelength as the plasmon resonance of spheres and is not dependent on the aspect ratio. However, the absorption band of the longitudinal surface plasmon resonance increases with larger aspect ratios (Figure 1.10).¹⁰⁶

The more irregular nanoparticles possess the more red-shifted and wider absorption peaks.¹¹¹ Plasmon resonance UV-Vis spectra with three or more SPRB have also been studied for silver nanocrystals with different shapes, such as silver nanodisks and silver nanoprisms.^{93,112,113}

Another influential parameter is the nature of the surrounding medium to the nanoparticles. The refractive index of the solvent has been shown to provoke a shift of the SPRB. For example, the UV-Vis spectroscopy measurements have shown that a solution of gold nanoparticles of 5.2 nm average diameter results in an 8 nm shift in SPRB when the solvent refractive index is varied from $n_d^{20} = 1.33$ to $n_d^{20} = 1.55$.¹¹⁰ The SPRB of a silver nanoparticle of 80 nm in diameter in water is located at 445 nm. The same nanoparticle in air reveals a plasmon resonance peak with a wavelength of 380 nm, giving a blue shift of

65 nm; hence, the observed colour turns from yellow to yellow green due to the shoulder of this 380 nm peak being in the violet end of the spectrum.

1.4.4 Synthesis of gold and silver nanoparticles

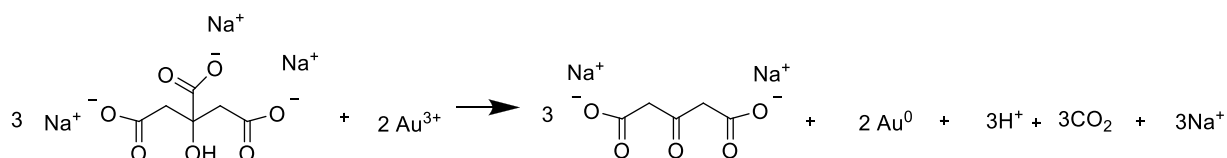
Nowadays numerous chemical and physical procedures exist for the preparation of noble metal nanoparticles. Nanoparticles can be synthesised with great precision by controlling the size and shape of the nanoparticle. Nanoparticles are produced generally by the reduction of their corresponding precursor salt in the presence of a stabilising agent. Physical methods usually need a high temperature (over 1000 °C), vacuum and expensive equipment.¹¹⁴ Chemical methods are more convenient and do not require complex equipment. Chemical methods involve reduction using a reducing agent, electrochemical reduction,¹¹⁵ photochemical reduction.^{116,117} In general, the chemical reduction reactions involve reducing agents that react with metal salts in an aqueous, organic or two-phase system.

Nanoparticles have a very high surface area to volume ratio resulting in a higher reactivity thus they generally undergo an agglomeration based on van der Waals forces. To avoid the aggregation or precipitation, various stabilisers are used which bind to the surface of the metallic nanoparticles, imparting high stability and the desired charge and solubility properties. The main classes of stabilisers described in the literature are carboxylic acids, trisodium citrate (TSC), tannic acid, polymers and block copolymers; P, N, and S donors (e.g., thiols, phosphanes, amines, thioethers); solvents such as THF, THF/MeOH, and propylene carbonate, long-chain alcohols; surfactants and dendrimers.¹¹⁸ Apart from stabilising the nanoparticle dispersion, the stabilising agents can also play an important role in controlling the particle morphology.¹¹⁹

Tetrachloroauric acid is the most commonly used precursor for the synthesis of gold nanoparticles and silver nitrate is suitable for production of silver nanoparticles. Reducing agents such as tri-sodium citrate, sodium or potassium

borohydride,^{120,121} hydrazine,¹²² ascorbic acid,¹²³ dimethylformamide,¹²⁴ salicylic acid¹²⁵ are often used.

The first scientifically reported preparation of gold nanoparticles was done by Michael Faraday. By using an aqueous solution of gold chloride and phosphorus as the reducing agent which was dissolved in a solution of carbon disulphide, he prepared stable gold nanoparticles. In 1951, almost one century later, Turkevich described one of the most popular methods for synthesis of gold nanoparticles.¹²⁶ The method is based on reduction of gold tetrachloride to gold nanospheres using boiling trisodium citrate solution which acts as the reducing agent and simultaneously as the stabilising agent. The reaction is shown below:



By varying the concentration ratio of gold salt and tri-sodium citrate, the nanoparticle diameter can be tuned over a range of 10 to 100 nm. The same method can be applied to the reduction of silver salts, but control of the particle size is very limited.⁹⁶

An alternative method for the synthesis of metal nanoparticles (in particular gold) is the two-phase method which was published by Brust and co-workers in 1994.^{127,128} They reported on reduction of controlled size gold nanoparticles which were thermally stable and air stable. In general, the method includes mixing aqueous gold tetrachloride solution with an organic solvent such as toluene. Following the addition of a phase transfer agent such as tetraoctylammonium bromide, a phase separation occurs and the dissolved gold salt is transferred to the organic phase. Subsequent addition of stabilising agents such as organic thiols (dodecanethiol) and reducing agents such as sodium borohydride leads to the formation of thiolate protected gold nanoparticles

(Figure 1.11). By variation of the metal salt, stabilising agent and reducing agent concentration, the nanoparticle size can be tuned.

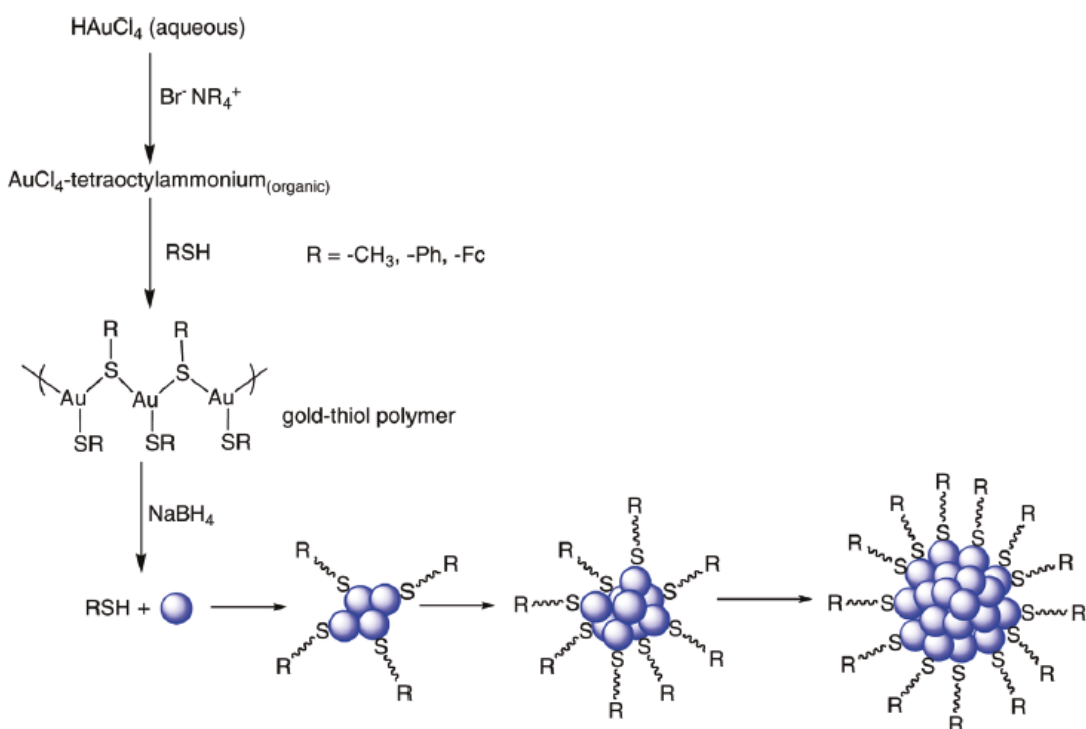


Figure 1.11: Brust's two-phase method for gold nanoparticle synthesis.¹²⁹

Microemulsions, copolymer micelles, reversed micelles, surfactants, and membranes have also been utilized in the two-phase system for synthesis of gold nanoparticles.¹¹⁰ The surfactants provide the formation of the microemulsion or the micelle maintaining a favourable microenvironment, also the extraction of metal ions from the aqueous phase to the organic phase is ensured.

Recently, more advanced attempts have been made towards implementing 'green chemistry' by using both uni- and multicellular organisms in order to create metal nanoparticles.¹³⁰⁻¹³² The advantages of the metal nanoparticles produced by plants, algae, fungi, bacteria and viruses include the energy-efficient synthesis and toxic organic solvents, external reducing agents and

stabilising agents are avoided. The synthesis is expected to yield novel and complex structural entities compared with those obtained by the conventional methods.^{133,134}

As mentioned in Section 1.2, wool has been utilised as a redox active biotemplate. Gold and silver nanoparticles have been reduced *in situ*. The controlled reduction of Au^{3+} or Ag^+ to Au^0 or Ag^0 respectively with the coupled oxidation reaction of S and N in the cystine amino acids in the keratin protein of the wool fibre, leads to chemical bonding between the metal nanoparticles and the sulfur groups of the wool.^{21,22} The matrix of the wool stabilises the metal nanoparticles.

Other methods for the syntheses of noble metal nanoparticles include sonochemical reduction,^{135,136} laser ablation,¹³⁷ electrochemical or ultrasound-assisted reduction,^{138,139} UV-, laser-, or microwave-assisted syntheses,^{140–142} γ -radiolysis¹⁴³ and thermal decomposition.¹⁴⁴

1.4.5 Silver halide

1.4.5.1 Background

When silver undergoes a reaction with a halogen a silver halide compound is formed which comprises a mix of ionic and covalent bonding. The difference, relative to their alkaline halide counterparts, is due to the presence of the *4d* electrons in silver which are nearly degenerate with the halide valence *p* electrons, resulting in a strong hybridisation between them.¹⁴⁵ Silver halides are given a pseudo-chemical notation AgX , where X represents one of fluoride, chloride, bromide or iodide. However, for the purpose of this thesis X will refer only to chloride, bromide and iodide.

Because of their unique characteristics photosensitive silver halides are used in photographic materials, X-ray films and photocatalysis.^{146,147} For instance AgCl ,

AgBr and AgI, known as widely applied photosensitive materials, were firstly reported as photocatalysts for water splitting in 1999.^{148,149}

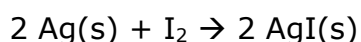
AgX crystals, with the exception of one crystal modification of AgI, have cubic structures. At atmospheric pressure and low temperature AgCl and AgBr have the rock salt NaCl structure, which is typical of ionic compounds.¹⁵⁰ Silver iodide, on the other hand, is found in the face centred cubic (fcc) zincblende (γ -AgI form), which is metastable, often coexisting with the hexagonal wurtzite (β -AgI form) phase where silver cations are tetrahedrally coordinated to iodide ions. This type is linked with covalent compounds.¹⁵¹ At elevated temperature (420 K), β -AgI will undergo a first-order phase transition and transform into the α -AgI phase.¹⁵²

Silver halides are semiconductors and their nanosized crystals show notable quantum size effects; AgI was one of the first materials in which excitonic quantum confinement effects were detected.¹⁵³ Another remarkable property of silver halides is their high ionic conductivity. The transport properties of these materials at room temperature are dominated by intrinsic ionic defects.¹⁵⁴ Such defects are formed when silver ions are removed from their regular site and transferred to an interstitial site leaving silver ion vacancies within the silver halide crystal lattice. The ionic conductivity in such crystallites may be up to two orders of magnitude higher than in a bulk crystal.¹⁵⁵ Ionic conductivity can be enhanced either by the dispersion of a second phase in the ionic conductivity matrix or by the heterogeneous mixture with other solid ionic conductors.¹⁵⁶ Interesting variations in the ionic conductivity performances can be expected when nanosized crystals are used as the dispersed phase, due to critical size-dependent changes in the nanoparticle's free energy.

Silver halides exhibit antimicrobial properties (Section 1.4.6). However, the most well-known characteristic of silver halides is their behaviour when exposed to light, which makes them suitable as source materials in photographic processes.

1.4.5.2 Photochemistry of silver halide

Since the 16th century scientists observed the darkening of silver salts upon exposure to light – a fundamental process for photography. In the 19th century Louis Daguerre plated silver onto sheets of copper and exposed them to iodine vapour. The iodine oxidised the silver as shown in equation below:

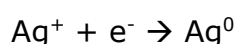


Daguerre kept the produced plates in the dark. He used a lens to focus an image of a person onto a plate and everywhere where light fell on the coating, a black deposit of finely divided silver formed, this image was called a “daguerreotype”. Film photography is not much different to the process as that used by Daguerre. Black and white photographic film is composed of microscopic crystals of silver bromide and small amounts of silver iodide in gelatine coated on cellulose acetate plastic sheet. When the emulsion is exposed to light, the following mechanism for the photochemical reaction, first proposed by Gurney and Mott takes place:¹⁵⁷ the absorption of a photon by the silver halide excites an electron from the valence band to the conduction band of the crystal, leaving an electron hole in the valence band. The photo-electron migrates to a trap (either a defect or an impurity centre) in the lattice where it reduces a silver ion to atomic silver. Following this, photo-electrons and mobile interstitial silver ions migrate alternately to the same trap to enhance the cluster of silver atoms. The positive hole can also diffuse to the surface of the crystal, where it oxidises a halide ion to halogen atom. The reactive halogen atom is prevented from re-oxidising reaction with the silver atom by the presence of sulphide compounds in the surrounding gelatine. This process is called *photosensitisation*.

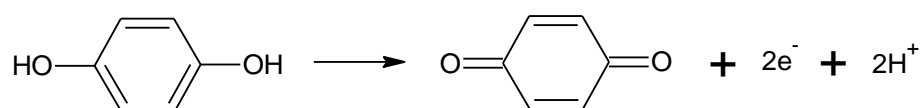
The equation shown below represents silver halides (X=Cl, Br, I, F) when exposed to light:



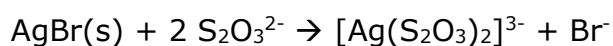
The electron reduces silver ion to atomic silver:



In the *developing* process only the sensitised crystals are reduced to metallic silver by means of reducing agents such as hydroquinone which is oxidised to quinone as shown below:



In this process the amount of metallic silver is increased by a factor of about 10^{10} , thus intensifying the image by the same factor. The undeveloped silver halide crystals are dissolved by a solution of sodium thiosulfate in the *fixing* process:



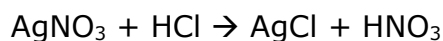
Without this step the non-sensitised crystals would continue being reduced to silver by light and the film would eventually turn black. Following the *fixing* a *negative* is created. When light is shone through the negative onto photographic paper which is covered with photographic emulsion, a positive print is obtained by essentially the same process.

1.4.5.3 Synthesis of silver halide nanoparticles

Among the variety of methods developed for the preparation of silver halide nanoparticles, microemulsions, or reverse micelles are popular as these are easy to handle, thermodynamically stable, systems which provide production of highly homogeneous materials with controlled particle sizes.^{158–161} Microemulsions are colloidal dispersions of two immiscible solvents which are stabilised by a layer of surfactant molecules at the liquid–liquid interface. Microemulsions may be classified as water-in-oil (w/o) or oil-in-water (o/w) depending on the dispersed and continuous phases.¹⁶² In a microemulsion the diameter of the micelles is typically of 3–20 nm, and co-surfactants, such as alcohols, are often added to support a more rigid interface, with a higher curvature towards the inside of the micelle.¹⁶³ Silver halide nanoparticles are prepared by mixing two identical microemulsions, containing Ag^+ and X^- reactants separately.^{164–166} Upon mixing of both microemulsions, reverse micelles containing the two reactants migrate due to mixing and Brownian motion, collide, and their surfactant surface layers open up allowing the reaction to take place. The resultant precipitate is stabilised in the water phase by the surrounding surfactant layer upon decoalescence of the reverse micelles. Alternatively, a silver containing aqueous solution can be introduced in an organic microemulsion which contains a halide releasing material, or vice versa. An example for the preparation of silver halide nanoparticles via a microemulsion method involves the solubilising of two aqueous solutions into dioctyl sodium sulfosuccinate (surfactant) and alkane (n-heptane) mixtures under stirring. The aqueous phase in the first microemulsion is composed of silver nitrate whereas the aqueous phase in the second microemulsion contains either NaCl or NaBr. Mixing of both microemulsions results in exchange of reactants between water droplets and allows precipitation of AgCl or AgBr nanoparticles.¹⁶²

Due to its simplicity and effectivity, aqueous synthesis of nanoparticles is an attractive method to produce silver halide nanoparticles. The method involves metal ions present in the aqueous solution of metal salt being reduced by a reducing agent. The synthesis is carried out in the presence of stabilisers in

order to avoid undesired agglomeration of the nanoparticles. For precipitation of silver halide nanoparticles, as opposed to using reducing agent, HCl or NaCl can be added to an aqueous solution containing AgNO₃ in the presence of a stabiliser such as PVP or PVA.^{167,168} The chemical reaction is shown below:



The large difference in the lattice energies between AgCl and AgNO₃ is the driving force for this reaction.

The silver halide nanoparticles thus formed can be used as precursors for the synthesis of Ag/AgX nanoparticles using the photoactive properties of silver halide materials. When exposed to light, silver clusters or domains are formed at the surface of the silver halide nanoparticles and can be described by a mechanisms first reported by first proposed by Gurney and Mott (Section 1.4.5.2).

1.4.5.4 Optical properties of silver halides

Silver halides have an intrinsic absorption in the blue region of the UV-Vis spectrum. AgCl has a direct and an indirect band gap of 5.2 eV (~ 240 nm) and 3.3 eV (~ 380 nm) respectively; with regard to AgBr the direct band gap is 4.3 eV (~ 290 nm) and the indirect band gap is 2.7 eV (~ 460 nm);¹⁶⁹ the direct band gap of γ-AgI is found to be 2.9 eV (~ 430 nm).¹⁷⁰ Thus silver chloride and silver bromide as bulk- or nanoscale crystals are white in colour, whereas α-AgI gives dark brown nanoparticles, and β- and γ-AgI nanoparticles are yellow.^{171,172}

As a result of their photosensitive properties, silver halides are not stable under light radiation. Once exposed to UV-Visible light, silver halide particles undergo a self-photosensitisation resulting in partial reduction of Ag⁺ to Ag⁰ nanoparticles

at the surface of the silver halide particles, thus forming Ag/AgX nanoparticles. Once sufficient Ag^0 particles are formed, the resultant Ag/AgX particles become photo-stable under further irradiation, preventing a total reduction of Ag^+ to Ag^0 .^{173–175} The stability can be explained as follows. The surface of AgX particles is most likely terminated by X^- ions, therefore it is negatively charged.¹⁷⁴ The formed silver nanoparticles on the surface of an AgX particle polarise their electron distribution so that the regions of their negative charges are far from the Ag/AgX interface and their positive charges are close to the Ag/AgX interface. Under irradiation, due to the dipolar properties of the surface plasmon resonance effect of a silver nanoparticle, an absorbed photon would be efficiently separated into an electron and a hole such that an electron is transferred to the surface of the nanoparticle as far away as possible from the Ag/AgX interface, and a hole to the surface of the AgX particle bearing the nanoparticle.¹⁷⁶ The migration of photo-excited electrons away from the AgX core avoids further photo-reduction of AgX to Ag^0 , resulting in stability of these Ag/AgX particles.¹⁷⁷ The combination between the polarisation field provided by the AgX core and the enhanced absorption of visible light by SPR of the Ag nanoparticles assists electron hole separation and interfacial charge transfer which allow these Ag/AgX materials to be utilised as plasmonic photocatalysis under visible light for the degradation of organic molecules.^{168,177–179} However, due to time constraints in the present research programme the photocatalytic properties of Ag/AgX hybrid materials could not be investigated, thus the photocatalytic Ag/AgX materials will not be discussed in detail.

Once exposed to light, the Ag/AgX particles change their colour, for instance silver chloride or silver bromide nanoparticles change from being white to purple upon such exposure to light.^{22,180} AgCl has a wide band gap of 3.3 eV, therefore, absorption of light with a wavelength larger than 380 nm is not possible by AgCl alone. There are literature reports on wide absorption band of silver/silver chloride or silver/silver bromide nanoparticles in the wavelength range of 420 - 800 nm attributable to the SPR effect of metallic Ag nanoparticles which are formed on the surface of the AgCl or AgBr nanoparticles respectively.^{174,181–183} As mentioned in Section 1.4.5.4, silver nanoparticles exhibit unique optical properties which arise from the collective oscillation of the conduction electrons upon interaction with electromagnetic radiation. The frequency, shape and

amplitude of the maximum absorbance of the surface plasmon absorption band depend on their morphology and size distribution as well as the effective dielectric constant of the surrounding medium. For example, decreasing the refractive index, n , of the surrounding environment will shift the SPR band of silver nanoparticles to shorter wavelengths. Ware et al. reported purple silver halides with absorption maxima at ca. 550 nm after exposure to light.¹⁸⁴ The absorption band arose due to 10 nm silver nanoparticles which were formed within the silver halide lattice. Generally, silver particles of this size dispersed in water ($n=1$) exhibit their characteristic SPR absorption at around 400 nm.^{21,185} However, since the silver particles were surrounded by a silver chloride matrix with a refractive index of $n=2$ the absorption band is shifted towards a higher wavelength.¹⁸⁴ Shape and size distribution of silver nanoparticles also create a variety of SPR absorption band shifts.

1.4.6 Antimicrobial properties of gold and silver

The concept of the use of gold as an antibacterial therapy has a long history and can be traced back to the Chinese in 2500 BC. In the 8th century AD, gold was considered to be the cure-all for every known disease¹⁸⁶ In the 13th century Roger Bacon recommended auric chloride for the treatment of leprosy.¹⁸⁷ In 1890, gold cyanide was used for *in vitro* inhibition of tuberculosis. Around 1925 the first clinical tests were carried out on bacteriostatic effect of gold towards bacilli.¹⁸⁸ Since chronic polyarthritis was believed to be infectious disease, some patients suffering from rheumatoid arthritis also received the same gold compounds, gold therapy was shown to be clinically efficient.¹⁸⁸ Extensive research since has revealed that a variety of gold complexes were active against a broad spectrum of microorganisms. The antimicrobial activity of gold(III) complexes is believed to be due to the instability of Au(III) in biological environments. Au(III) complexes often have strong oxidising properties as they are able to be reduced to Au(I). The major mode of action involves the highly specific coordination of Au(I) to thiol groups in proteins, and particularly with L-cysteine, inhibiting processes essential to cellular survival.¹⁸⁹

Several studies have shown that gold nanoparticles alone do not kill bacteria.^{190,191} However, when used in conjunction with a photosensitiser, they enhance the photosensitiser's ability to kill bacteria. Gold nanoparticles prepared by using hyperbranched poly(amidoamine) with terminal dimethylamine groups (HPAMAM-N(CH₃)₂) as the reducing and stabilising agent¹⁹² could inhibit the growth and multiplication of gram positive or gram negative bacteria and fungi efficiently. Although the antimicrobial mechanism of gold nanoparticles is not fully understood, it is likely to be due to existing Au(I) and Au(III) species on the surface of the particles making the particles bacteriostatic.

The antimicrobial properties of silver in various forms have been used throughout history. The ancient Greeks, Romans, Egyptians, and many others used metallic silver vessels for preservation of water and wine.^{193,194} Alexander the Great used to drink only from silver vessels. In the 19th century silver nitrate became the most useful tool in the treatment of burns or wounds.¹⁹⁵ Today silver based antimicrobial systems can be found in the medical field (e.g. orthopedic implants, prostheses, vascular grafts, wound dressings, cream gels, surgical instruments), food packaging, home appliances (e.g. refrigerators, washing machines), cosmetics and hygiene products (creams, lotions, soaps, deodorants, toothbrushes), textiles (clothing, underwear, socks), in air or water purifications systems, antifouling and antimicrobial paints and many more.^{141,196–198}

Silver is considered to exhibit low toxicity to human cells.¹⁹⁹ The biocidal characteristics of bulk silver arise through the constant oxidation and release of very small amounts of silver ions to an aqueous or moist environment, making silver cups, vessels, pots famous for their antimicrobial activity. Contrary to the biocidal effects of ionic silver, the antimicrobial activity of colloidal silver particles depend on their size, and a decrease of the particle size reflects in the increase of the antimicrobial effect.²⁰⁰ Morones investigated the effect of silver nanoparticles with a broad size distribution, ranging between 1–100 nm on gram negative bacteria.²⁰¹ The results indicated that the only silver nanoparticles to present a direct interaction with the bacteria preferentially had a diameter of ca. 1–10 nm. Not only the size but also the shape²⁰² of the nano silver can have significant effects on their antimicrobial activity against a broad range of microorganisms.^{203,204} Pal reported that truncated triangular silver nanoplates

displayed the strongest biocidal action, compared with spherical and rod-shaped silver nanoparticles.²⁰² Silver nanoparticles exhibit biocidal effects in over 650 disease-causing organisms (bacteria, viruses, fungi, parasites etc.)^{114,205} in the body even at low concentrations.²⁰⁶

Although the antimicrobial activity of silver ions, silver nanoparticles, and silver nanoparticle polymer composites is believed to be due to morphological and structural changes found in the bacterial cells, to date the exact antimicrobial mechanism of silver is still not fully understood.

In respect of silver ions, it has been reported that silver ions inactivate vital proteins by reacting with thiol groups of the proteins.²⁰⁷ Other researchers report on interaction of silver ions with peptidoglycan in the cell wall and the plasma membrane, resulting in cell lysis. The silver ions are also capable of disrupting protein synthesis and inhibiting DNA replication of the microorganisms.^{208–210} It has been reported that silver nanoparticles react in a similar way to silver ions. For comparison, there are reports in the literature that show there is an electrostatic attraction between the negatively charged bacterial cell walls and the positively charged surface of the nanoparticles.²¹¹ Deposition of these nanoparticles on the bacterial surface can affect cell wall permeability, thus altering the normal transport of electrolytes and other metabolites.²¹² Silver nanoparticles can directly enter the cell²⁰¹ causing the changes of redox cycle in the cytosol, interference with the cellular S-containing compounds, intracellular radical accumulation, and dissipation of the proton motive force for ATP synthesis.^{212–214} Silver nanoparticles are not inert and are sensitive to oxidation in aqueous solutions exposed to air.^{215,216} Thus, the efficacious properties of silver arise through the partial oxidation and release of silver ions to an aqueous or moist environment²¹⁷. The dissolution of silver nanoparticles to silver ions in the bacterial cells results in enhanced antimicrobial activity.²¹⁸ Although the explanation remains unclear, it is accepted that these effects rely either on the increase in released silver ions or the increase in the reactivity of the particles resulting from the high active surface area.

The possibility of incorporation of metal nanoparticles within a polymer matrix has attracted considerable global attention. Polymers are found to be very

effective support for the spatial stabilisation of metal nanoparticles; additionally the matrix provides a physical immobilisation of the nanoparticles at the polymer surface. The incorporation of metal nanoparticles into the polymer or paint matrix can enable a controlled slow migration of the antimicrobial metal ions or/and nanoparticles into environment due to the porosity of the matrix, thus making the new composites a powerful option for a variety of antimicrobial applications. There are diverse techniques to introduce metal nanoparticles into a polymer matrix. Several antimicrobial polymer nanocomposites have been prepared by mixing pre-formed particles with polymers. However, generally the production of a metal nanoparticle polymer composite involves chemical *in situ* reduction of metal ions (e.g. Ag^+ from AgNO_3) resulting in formation of the metallic nanoparticles within the polymer matrix.²¹⁹

A nylon 6,6 nanocomposite containing silver nanoparticles (1 wt % silver in the polymer) has been successfully produced by means of ultrasound-assisted reduction method of silver nitrate.²²⁰ The composite was successfully tested against *Staphylococcus aureus* and *Pseudomonas aeruginosa*. In other work, porous films with silver were produced from PVA electrospun fibres doped with AgNO_3 (10 wt %).²²¹ In these films the proliferation and biological activity of yeast cells was effectively inhibited. Polycarbonate and silver nanoparticles were mixed and moulded to prepare a composite in dichloromethane.²²² The composite showed antifungal properties. Ag nanoparticles could be successfully loaded on the DBD (dielectric barrier discharge) plasma-treated woven PET surface by submerging into AgNO_3 aqueous solution.²²³ The Ag nanoparticle-loaded woven PET exhibited a strong antimicrobial activity against both *Staph aureus* and *E. coli*. Hyperbranched polyurethane composites containing silver nanoparticles (1, 2.5 and 5 wt % silver in the polymer) were prepared by an *in situ* polymerisation process.²²⁴ Dimethylformamide (DMF) was acting as a diluent as well as a reducing agent for silver ions. The composites showed antimicrobial activity against *Staphylococcus aureus* and *Escherichia coli*. Also antifouling activity was successfully tested against the yeast *Candida albicans*.

Silver nanoparticle polymer composites show a low release rate of silver ions. Replacing of the silver nanoparticles with a moderately soluble silver salt can significantly improve the dissolution rate of silver ions and therefore increase the

antimicrobial efficacy in the short term. Solubility constants of some silver salts are listed in Table 1.5. Apart from silver nitrate these are all very small. Silver halides such as AgCl or AgBr which have low solubility exhibit the potential to provide a constant low concentration of silver ions in aqueous or moist environments over extended periods of time.

Table 1.5: Solubility constants of silver compounds.¹⁹⁵

| Silver compound | Solubility constant |
|---------------------------------|--------------------------|
| AgNO ₃ | 51.60 |
| Ag ₂ SO ₄ | 1.58 x 10 ⁻⁵ |
| Ag ₃ PO ₄ | 2.51 x 10 ⁻¹⁸ |
| AgCl | 1.58 x 10 ⁻¹⁰ |
| AgBr | 7.70 x 10 ⁻¹³ |
| AgI | 1.50 x 10 ⁻¹⁶ |
| Ag ₂ S | 7.94 x 10 ⁻⁵¹ |

Furthermore, visible light irradiated silver halide species produce oxidative radicals (OH[•], O₂^{•-}, H₂O₂) which inactivate bacteria by decomposing its cell wall and cell membrane leading to the leakage of intracellular molecules and causing the cell death.²²⁵

Antimicrobial composites consisting of a cationic polymer, poly(4-vinyl-N-hexylpyridinium bromide) and silver bromide nanoparticles have been produced.¹¹⁴ The bromide anions associated with the polymer side chains of the amphiphilic pyridinium polymer were precipitated by the addition of a silver salt. Surfaces coated with these composites resisted biofilm formation. Silver chloride nanoparticles were synthesized inside the pores of a mesoporous silica (SBA-15).¹⁸ The AgCl SBA-15 composites were blended with polypropylene into pellets by injection moulding which showed effective antimicrobial results against *E. coli*.

1.5 Antifouling paints

Because of their unique properties and increasing popularity, antifouling nano composite coatings have been the subject of numerous books, journal articles, reports, etc. This section is intended to provide an overview of recent developments in these coatings.

1.5.1 Background

External surfaces of submerged structures in seawater, such as hulls of vessels, pontoons, piers, aquaculture nets, buoys, pipelines and drilling platforms can show settlement and growth of undesirable microorganisms, algae, slime and animals, so called marine biofouling. Biofouling can be roughly separated into two categories, microfouling (bacteria and diatomic biofilms) and macrofouling (e.g., macroalgae, barnacles, mussels, tubeworms, and bryozoans).²²⁶ Such accumulations of biofouling can result in lower speeds, greater fuel and power consumption due to the increase of frictional drag of vessels moving through water.²²⁷ Thus, biofouling is a major problem for the shipping industry. To prevent biofouling surfaces can be treated with antifouling paints to inhibit the settlement of marine organisms. These paints consist of solvents, pigments, extenders, fillers and binder.²²⁸ With the discovery of the antifouling effectiveness of organotin compounds in the 20th century, all hull fouling problems seemed to have been solved. However, Tributyltin (TBT) has shown extensive detrimental effects on non-target marine organisms and was internationally banned by International Maritime Organisation in 2008.²²⁹ After the prohibition of triorganotin formulations, copper has once again become the predominant antifouling biocide, as already the early Phoenicians (1500–300 BC) used copper sheets to prevent biofouling on their wooden boats.²³⁰ Cuprous oxide (Cu_2O) is a common pigment of antifouling paints. However, Cu(I) thiocyanate and Zn(II) oxide can also be used as pigments. Zinc oxide is generally utilised in combination with Cu(I) as a booster, increasing the toxicity

of the formulation by 200-fold, and/or to impart flexibility and facilitate the erosion process of the coating.²³¹ Some diatoms and algae are resistant to inorganic Cu and Zn, so the effectiveness of the antifouling paints can be further enhanced by the addition of one or more secondary or booster co-biocides.²²⁷ These include zinc and copper pyrithione, Irgarol 1051®, chlorothalonil, TCMS pyridine, Sea-nine 211®, ziram, zineb, dichlofluanid and diuron.²³² These are often herbicides (e.g., Irgarol 1051® and diuron) which negatively affect the growth rate of photosynthetic organisms.²³³ Legislation now exists in some countries to regulate the use of some booster biocides in antifouling paints.²³⁴

Incorporating the biocides into the paint matrix allows them to leach out gradually from the surface layer and inhibit the settlement of marine organisms.²³⁵ However, not only desired organisms will be affected by the antifouling paints but there is also a very real potential for harmful effects on non-target organisms. In comparison with the application, maintenance or removal of the paints, a greater risk to the aquatic environment is present due to greater amounts of biocides released slowly through the leaching process from the antifouling paint into a marine or freshwater environment.²³⁶ Leaching is of particular concern in marinas where large numbers of vessels are moored for long periods of time. As such, antifouling paints containing toxins are elevating levels of contamination in the environment raising concerns about their effects on marine communities.²³⁷

Consequently the development of more environmentally friendly antifouling paints has gained the interest of researchers. Some non-toxic foul release coatings which are silicone based have been developed.^{238,239} Instead of preventing the settlement of marine organisms these paints reduce the attachment strength of the settling organisms. When the vessel is moving any accumulated biofouling will be sheared off the paint surface due to increasing drag and turbulence. The drawback of these foul release coatings is that the self-clean efficacy is only achieved on high speed vessels. Other non-toxic technologies include integrating natural antifouling compounds from marine organisms (algae and sponges) into the paint matrix, though these are not yet in commercially available. Existing major antifouling strategies with their advantages and disadvantages are summarised in Table 1.6 and Table 1.7.

Table 1.6: Antifouling strategies.²³⁴

| Antifouling system | Mode of action |
|--|--|
| Tin-free self-polishing copolymer coatings | Cu/Zn/Silyl copolymer resin with Cu particles and booster biocides dispersed through the paint matrix – hydrolysis with seawater results in slow and consistent release of biocide |
| Tin-free conventional coatings | Cu particles and booster biocides dispersed through soluble or insoluble paint binder – dissolution in seawater results in slow and decreasing release of biocide |
| Booster biocides | Most often herbicides/pesticides incorporated into Tin-free conventional and self-polishing copolymer antifouling paints to increase efficacy against copper tolerant algae |
| Foul-release coatings | Low energy, minimally adhesive surfaces, mostly silicone elastomers and often incorporating silicone oils |
| Biomimetics | Incorporation of natural AF compounds produced by marine organisms or surfaces based on natural microtopography |

Table 1.7: Key advantages and disadvantages of past and present antifouling systems.²³⁴

| Antifouling system | Key advantages | Key disadvantages |
|--------------------------------|---|---|
| Tin-free SPC coatings | Effective against a range of invertebrate foulers, long lifetime (~5 years) | Cu and booster biocide impacts on non-target species, Cu persistent in marine environment (depends on pH, salinity and dissolved organic matter – also determines toxicity) |
| Tin-free conventional coatings | Effective against a range of invertebrate foulers | Short lifetime (~12–18 months), Cu and booster biocide impacts on non-target species, Cu persistent in marine environment (depends on pH, salinity and dissolved organic matter – also determines toxicity) |
| Booster biocides | Effective against a range of bacterial, algal and fungal foulers | Impacts on non-target species, e.g., algae, seagrasses, corals, invertebrates, some persistent in marine environment |
| Foul-release coatings | Effective at reducing strength of fouling attachment, do not leach, no or low toxicity, potential long life (~10 years) | Only self-clean on high speed /high activity vessels, or otherwise require regular cleaning, susceptible to abrasion damage |
| Biomimetics | Natural alternatives “environmentally friendly” | Not commercially available yet, difficult to source adequate supply of compound |

Traditional biocides have revealed limited efficacy against biofouling in aquatic and terrestrial environments. Another problem of liquid biocide use is the environmental pollution from antifouling biocides. Currently the Environmental Protection Authority is reassessing all biocides used as active ingredients in antifouling paints imported to, manufactured and used in New Zealand about the harmful effects they have on both aquatic and human health.²⁴⁰ All of these paints contain copper compounds. As such, more research is needed to find alternative strategies with more effective outcomes and minimised environmental impact.

1.6 Scope of Thesis

The present research focused on the synthesis of new generation hybrid polymer materials, the characterisation and analysis of their novel optical, antimicrobial and antifouling properties. These new functionalised hybrid polymer materials consist of an organic substrate matrix (polyurethane, nylon 6,6 and polyurethane K5000 latex paint polymers) and gold, silver and silver halide nanoparticles respectively.

The proposed technology for the formation of the nanogold and nanosilver particles in the polymer matrices comprises the uptake of gold or silver ions by the polymers and an *in situ* reduction of metal ions to metal nanoparticles within and on the polymer matrix. The oxidation potential and chemical affinity of nitrogen in the PU or nylon 6,6 polymer for gold and silver²⁴¹ was utilised to reduce Au^{3+} and Ag^+ to Au^0 and Ag^0 respectively and bind them chemically to the polymer matrix. The metal nanoparticles are stabilised by the polymer matrix which also serves as a control on their particle size. In a similar manner, gold and silver nanoparticles were formed by means of nitrogen containing compounds which are first incorporated into a polyethylene terephthalate (PET) polymer. Silica based BULK ISOLUTE® SORBENT (NH_2) material was used as an additional substrate for the purpose of building up a simple model to confirm the chemical affinity of gold and silver for nitrogen, and the ability of the nitrogen-containing functional groups to reduce Au^{3+} and Ag^+ ions to Au^0 and Ag^0 nanoparticles respectively.

Photoactive nanosilver halide hybrid polymer materials were prepared by doping the polymer matrix with Cl^- , Br^- or I^- ions and accomplishing the precipitation reaction of silver halide nanoparticles with silver ions in solution. The silver halide nanoparticles are similarly stabilised by the substrate matrix and form chemical interaction with the polymer matrix.

The nanogold, nanosilver and nanosilver halide hybrid materials were characterised by a number of different methods. The uptake of gold and silver

ions by the polymer substrates and the amount of gold and silver later leached from the hybrid materials were analysed by atomic absorption spectroscopy. The optical properties were measured by ultra violet visible spectroscopy. The morphology of the hybrid materials was studied with scanning electron microscopy, energy dispersive spectroscopy and transmission electron microscopy. X-ray diffraction measurements were carried out to confirm the formation of crystalline gold, silver or silver halide within the hybrid materials. X-ray photoelectron spectroscopy and infra-red spectroscopy were used to determine the nature of the interaction between the metal nanoparticles and the polymer substrates. The antimicrobial properties of the hybrid materials were investigated against gram negative *Escherichia coli* bacteria. The Polymer Group Ltd in Auckland assisted in the testing of the antifouling properties of nanogold and nanosilver hybrid K5000 paint materials.

These new generation nanogold, nanosilver and nanosilver halide hybrid polymer materials have significant potential in various commercial applications.

2 Experimental methodology

2.1 Materials

Polyurethane beads, nylon 6,6 and polyethylene terephthalate beads were supplied by the Centre for Advanced Composite Materials and the Plastics Centre of Excellence at the University of Auckland, New Zealand. Liquid PU Kamthane 5000 (K5000) latex paint base polymer was provided by The Polymer Group Ltd in Auckland. Sail cloth material was provided by Doyle Sails Ltd, Auckland. Polycarbonate and nylon 6,6 sheets were purchased from Mulford Plastics. BULK ISOLUTE® SORBENTS were supplied by International Sorbent Technology Ltd. Octadecyl-functionalized silica gel was purchased from Aldrich Chemical Company, Inc.

All chemicals employed are of analytical grade unless otherwise stated. Distilled water was used. Silver nitrate was purchased from Scientific and Chemical Supplies and hydrogen tetrachloroaurate(III)hydrate ($\text{HAuCl}_4 \cdot 3\text{H}_2\text{O}$ (99%)) was sourced from Sigma Aldrich. Sodium chloride, sodium bromide and sodium iodide were supplied by Unilab. All other chemicals used were purchased from Sigma Aldrich.

All laboratory equipment used for experiments was metal-free to eliminate any undesirable reduction of Au^{3+} to Au^0 or Ag^+ to Ag^0 , by for example contact with stainless steel equipment, and resulting in the deposition of Au^0 or Ag^0 onto the stainless steel equipment. All laboratory glassware was washed with aqua regia before use to prevent any contamination.

2.2 Preparation

2.2.1 *In situ* preparation of gold / silver nanoparticles in the presence of polyurethane or nylon 6,6 and their subsequent binding to the polymer matrix

The preparation of nanosilver / nanogold hybrid plastic beads for the small scale approach involved immersing plastic polyurethane or nylon 6,6 beads (1 g) in an aqueous tetrachloroaurate or silver nitrate solution (10 mL, 10-1000 mg kg⁻¹ Au³⁺ / Ag⁺) for 24 hours under heat (in a water bath). The temperature was altered from room temperature to 50 °C (ideal for gold samples) and to 90 °C (ideal for silver samples). During heating, metal ions were absorbed by the polymer matrix and simultaneously reduced to Au⁰ or Ag⁰ by the nitrogen groups in the polymer, and subsequently stabilised and bound to the polymer matrix. With the appearance of purple/pink or yellow/brown colours on the plastic beads, the formation of gold and silver nanoparticles on/in the plastics was observed. At the same time the initial yellow gold solution became colourless. Following the absorption/reduction reaction, the resulting coloured beads were removed from solution, washed thoroughly with distilled water and air dried.

For nylon or polyurethane in the form of sheets the following procedure was undertaken. Polyurethane sheets with dimensions of 20 x 20 x 3 mm (ca. 1.5 g) or 20 x 20 x 1 mm nylon sheets (ca. 0.5 g) were heated in an aqueous gold tetrachloride or silver nitrate solution (10 mL, 500 mg kg⁻¹ Au³⁺ / Ag⁺), for 24 hours (gold solution at 50 °C, silver at 90 °C).

2.2.1.1 Larger scale *in situ* preparation of gold / silver nanoparticles in the presence of polyurethane or nylon 6,6 and their subsequent binding to the polymer matrix

A new reaction vessel was designed for larger scale processing. Figure 2.1 shows a typical setup which includes an elongated reaction glass vessel, with a glass lid and a sintered glass plate on the bottom. The sintered glass plate acts as a filter for the plastic beads and the lid prevents the water evaporation. A circulating pump was connected via silicon tubing to the vessel to pump the reagents through. The whole reaction vessel was immersed in a water bath set at 50 °C (gold samples) or 90 °C (silver samples). 100 g of plastic beads were immersed in an aqueous gold tetrachloride or silver nitrate solution (1000 mL, 10 - 1000 mg kg⁻¹ Au³⁺ / Ag⁺). The reaction solution was pumped through the beads for 24 hours to provide the maximum absorption of metal ions by the plastics. As mentioned in Section 2.2.1 the beads were rinsed with distilled water and dried at room temperature.

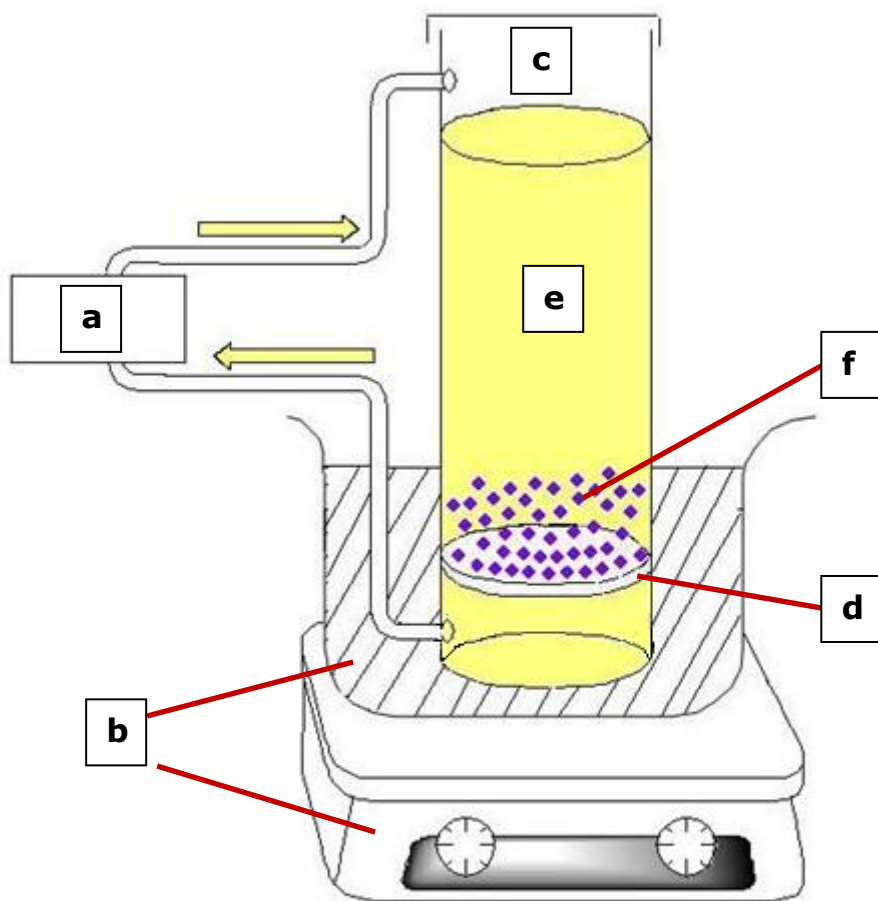


Figure 2.1: Setup for scale up reaction: a) circulating pump, b) water bath, c) reaction vessel, d) sintered glass plate, e) reaction solution containing metal ions and f) substrate polymer beads.

2.2.1.2 *In situ* preparation of gold / silver nanoparticles in the presence of alternative substrates

Polymer substrates which do not normally contain functional groups capable of reducing Au^{3+} or Ag^+ to their respective metallic nanoparticles were modified to include thiol or amine groups on the surface of these substrates. Such modified substrates included amine coated polyethylene terephthalate sail cloth.

Additionally Bulk isolate® sorbent (containing amine functional groups) and octadecyl-functionalised silica gel were used as alternative substrates. It was hoped that the nitrogen-containing functional groups on the surface of the substrates would reduce Au^{3+} and Ag^+ to Au^0 and Ag^0 respectively, whilst simultaneously stabilising the resultant metal nanoparticles.

2.2.1.2.1 *In situ* preparation of gold / silver nanoparticles in the presence of amine coated PET sail cloth and their subsequent binding to the sail cloth

A fine PET fabric treated with an amine based light stabiliser was provided by Doyle Sails Ltd. Treatment details are unknown as they are proprietary.

PET sail cloth (0.2 g) was immersed in an aqueous gold tetrachloride or silver nitrate solution (10 mL, 10-100 mg kg^{-1} Au^{3+} / Ag^+) and heated in a water bath (80 °C for gold and silver samples) for up to 24 hours. A pink or yellow colour was observed, which corresponds to the SPRB of gold and silver nanoparticles respectively (Section 1.4.2). The coloured sail cloth was then removed from the solution, rinsed with distilled water and air dried.

As a control, 1 g of untreated PET beads were immersed in an aqueous gold tetrachloride or silver nitrate solution (10 mL, 10-1000 mg kg^{-1} Au^{3+} / Ag^+) and heated for 24 hours at 80 °C. After 24 hours the samples were rinsed with distilled water and dried at RT.

2.2.1.2.2 *In situ* preparation of gold / silver nanoparticles in the presence of BULK ISOLUTE® SORBENTS and octadecyl-functionalized silica gel

0.2 g of Bulk isolate® sorbent were dispersed in an aqueous gold tetrachloride or silver nitrate solution (10 mL, 500 mg kg⁻¹ Au³⁺ / Ag⁺) and heated for 24 hours in a water bath at 70 °C. After 24 hours, the samples were filtered, rinsed with water and air dried at room temperature.

2.2.2 *In situ* preparation of gold / silver nanoparticles in the presence of polyurethane K5000 latex paint base polymer and their subsequent binding to the polymer matrix

The supplied K5000 is a polyurethane latex paint base polymer on a polyether/polyester/acrylic composite backbone. The preparation of nanosilver or nanogold hybrid polyurethane K5000 paint materials proceeded using the following methodology. Aqueous gold tetrachloride or silver nitrate solution (2.5 mL, 20-2000 mg kg⁻¹ Au³⁺ / Ag⁺; or 1.5 mL, 33-3333 mg kg⁻¹ Au³⁺ / Ag⁺) was slowly added to 5 g Kamthane 5000 liquid polyurethane via a pipette under constant stirring. High concentrations of acidic metal ion solutions may cause flocculation of the paint. To prevent the flocculation of the paint, the solution was diluted with water (whilst keeping the polymer to metal ion ratio constant). Increasing the pH of the gold solution with NaOH from its initial value of approximately 1.5 to a value of approximately 5 avoids the flocculation. Once Au³⁺ / Ag⁺ was added, the reactions tubes were heated in a water bath (50 °C for gold and 70 °C for silver samples) for up to 24 hours. The ideal temperature for the preparation of the nanogold and nanosilver hybrid PU K5000 materials proved to be room temperature. However, this needed at least seven days of reaction time to reduce Au³⁺ or Ag⁺ to Au⁰ or Ag⁰ respectively. The reduction of metal ions to Au⁰ and Ag⁰ was indicated by the development of stable colours,

purple for nanogold and brown for nanosilver hybrid PU K5000 materials respectively.

For characterisation, the samples were spread out on a clean optical microscope slide and placed on a window sill or in the dark to dry. The preparation process was scaled up by a direct scaling of the procedure above.

2.2.3 Preparation of nanosilver halide hybrid polymers

Nanosilver halide hybrid polyurethane and nylon 6,6 materials were produced via the following two approaches. In the first approach PU or nylon 6,6 polymer substrates were soaked in silver nitrate solution for 2 hours at room temperature. The substrates were then removed from the solution, thoroughly rinsed with distilled water and air dried at room temperature. With the assumption that Ag^+ had been absorbed by the polymers, the samples were then soaked in NaX ($\text{X}=\text{Cl}, \text{Br}, \text{I}$) solution for 2 hours at room temperature. However, this method was not successful and a second approach was utilised. In this second approach, the polymer substrates were first soaked in a halide solution (Cl^- , Br^- , I^-) at RT for different amounts of time, rinsed and air dried. These were then immersed in a silver nitrate solution in the absence of light. Samples that were isolated from light did not develop any colour once the silver nitrate solution was added to the samples. Once they were exposed to UV-Vis light (direct light), they changed in colour depending upon the dopant. This is discussed in further detail in Chapter 5.

2.2.3.1 Preparation of nanosilver halide hybrid polymers in the presence of polyurethane and nylon 6,6

PU sheets (1.5 g, 20 x 20 x 3 mm) and nylon 6,6 sheets (0.5 g, 20 x 20 x 1 mm) were immersed in 10 mL of 0.1 M NaX (X= Cl, I, Br) solution. The reaction vials were agitated on a shaking table at room temperature in order to allow the polymer sheets to absorb the Cl⁻, I⁻ or Br⁻ ions. After 12 hours the plastics were removed, rinsed with distilled water and allowed to air dry. Subsequently, the doped plastics were added to a silver nitrate solution (10 mL, 200 mg kg⁻¹ Ag⁺) and agitated for 12 hours at room temperature. The reaction vials were wrapped in aluminium foil. When removed from the solution, the silver chloride and silver bromide hybrid plastic materials were white in colour, silver iodide hybrid materials were yellow in colour.

2.2.3.2 Preparation of nanosilver halide hybrid paint materials in the presence of polyurethane K5000 latex paint base polymer

The synthesis of nanosilver halide hybrid PU K5000 latex paint base polymer materials was achieved via the following methodology. 1 mL of 0.5 M NaX solution was added to 5 g of liquid polyurethane Kamthane 5000 latex paint base. The mixture was set on a shaking table at room temperature for two hours. Thereafter, the reaction was completed by the drop wise addition of a silver nitrate (1.5 mL, 3333 mg kg⁻¹ Ag⁺) solution under vigorous stirring. The reaction tubes were covered in aluminium foil and as expected the silver chloride (or bromide, iodide) containing PU K5000 paint materials remained white in colour. Upon exposure to sun light a purple to brown colour development occurred within hours (for silver chloride and silver bromide samples). Silver iodide samples remained white in colour. For characterisation, the samples were spread out on clean optical microscope slides and placed on a window sill or in the dark as required for drying to form thin films.

2.2.4 Gold and silver uptake

During the preparation of nanogold and nanosilver hybrid materials the uptake of metal ions by the substrates was quantitatively analysed by means of atomic absorption spectroscopy (AAS) (Section 2.3.3). This involved immersing the plastic beads (1 g) or sail cloth (0.2 g) in a gold tetrachloride or silver nitrate solution (10 mL, 10-100 mg kg⁻¹ Au³⁺ / Ag⁺) at room temperature to 90 °C. After different periods of time, (15 minutes, 30 minutes and up to 24 hours), the plastics were removed and the residual solution was quantitatively analysed by AAS for any remaining gold or silver ions.

2.2.5 Leaching test for nanogold and nanosilver hybrid PU and PU K5000 materials

The amount of silver or gold leached from the nanogold and nanosilver hybrid PU beads or PU K5000 paint materials was determined. Nanogold and nanosilver hybrid PU beads and polyurethane K5000 paint base samples were produced via the methods outlined in Sections 2.2.1 and 2.2.2 respectively. For the leaching test, 1 g of produced nanogold or nanosilver hybrid PU samples was rinsed with distilled water, air dried and immersed in 10 mL of distilled water. As for the produced nanogold and nanosilver hybrid PU K5000 materials, the samples were dried on microscope glass slides, the dry paint films were peeled off the microscope slide, resulting in ca. 3 g of dry paint. The paint samples then were rinsed with distilled water and immersed in 30 mL distilled water. All samples were agitated for seven days at room temperature. The samples were removed and the residual solutions were quantitatively analysed by atomic absorption spectroscopy (Section 2.3.3) for any leached gold or silver.

2.3 Characterisation

2.3.1 Scanning Electron Microscopy

Scanning electron microscopy (SEM) is an important characterisation method for studying the surface morphology of the produced hybrid polymer materials comparing it to that of the untreated plastic substrates. Backscatter conditions were used as these give a better contrast between the metals and the polymers due to the high atomic weight of metals and the lower atomic weight of the C, N, and O elements in the polymers. In order to get an overall picture of the surface morphology of the materials, imaging was carried out at various positions throughout the samples. A JEOL 6500 F field emission gun scanning electron microscope operating in a high-vacuum mode at 15 kV was used with a working distance of 9 and 11 mm.

The dispersion of nanoparticles in the polymer matrix and the size of the particles were analysed by SEM. Samples were prepared for SEM analyses by cutting the plastic beads, sheets and dry paint films in half and mounting the cross section area upwards on an aluminium stub using double sided carbon adhesive tape. Six coats of carbon were applied by a JEOL JEC-560 carbon coater to allow discharge of electrons from the surface of the sample. Bulk isolute® sorbent and hybrid sail cloth materials were spread out on double sided carbon adhesive tape which was stuck on top of an aluminium stub. Liquid hybrid polyurethane K5000 paint materials were studied under cryogenic conditions. By means of the Cryo SEM attachment the sample can be frozen rapidly in liquid nitrogen, thus preserving the pristine matrix structure of the resin. The frozen hybrid PU K5000 materials were fractured under vacuum. A thin layer of carbon was sputtered onto the fractured surface of the material to provide conductance of electrons. The imaging of the surface of the inner structure was carried out.

Energy-dispersive X-ray spectroscopy (EDS) was utilized in 2D scans to give the distribution of elements such as Au, Ag, Cl, C, N, O on the surface of the polymer samples for their corresponding SEM image. The technique enables the

study of the correlation between the metals and other elements in the plastic matrix.

2.3.2 Transmission Electron Microscopy

High resolution transmission electron microscopy (HRTEM) and scanning transmission electron microscopy (STEM) are complementary techniques to SEM and EDS but due to their higher spatial resolution, a more accurate picture of the morphological fine structure of the nanoparticles within the polymer matrices can be obtained. TEM analyses of the hybrid materials were carried out on a JEOL 2011 high-resolution instrument with a $L_{\alpha}B_6$ filament operated at a 200 kV accelerating voltage. Solid polymer samples were dissolved in high purity dimethylformamide or methanol. A drop of the resulting solution was placed onto carbon-coated copper grid (200 mesh), air dried and further carbon coated by a JEOL JEC-560. Elemental analyses and elemental maps of the samples were performed on the JEOL 2011 TEM microscope in STEM mode.

2.3.3 Atomic Absorption Spectroscopy

The analyses for Au and Ag in the solutions used in the uptake studies were performed by means of flame Atomic Absorption Spectroscopy (AAS). Following the hybrid materials preparation and also leaching tests (Section 2.2) the resulting solutions were analysed for the residual amounts of gold or silver on a GBC 906AA. The operating conditions for the Atomic Absorption Spectrometer followed those recommended by the manufacturer. An air-acetylene flame, light with a wavelength of 242.8 nm for gold and 324.0 nm for silver was used. All solutions were diluted so that gold or silver concentrations were within the optimum working range (1 to 14 mg kg⁻¹ for gold and 1 to 12 mg kg⁻¹ for silver). Calibration curves were obtained with standard solutions of the following

concentrations: Au³⁺: 3.5, 7.5, 10, 12, 14 mg kg⁻¹ and Ag⁺: 3, 5, 7, 9, 11 mg kg⁻¹.

2.3.4 X-ray Diffraction

X-ray Diffraction (XRD) is an experimental non-destructive technique which is used to provide structural information of crystal lattices and to identify a crystalline substance. XRD was used to obtain information on the crystallographic form and the mean crystallite size of the gold, silver and silver halide nanoparticles within the hybrid polymer materials.

XRD measurements were carried out using PANalytical X'Pert Pro to analyse the hybrid materials which contained higher gold, silver and silver chloride concentrations. The instrument utilised the Bragg-Brentano geometry in which the sample is fixed horizontally and both the X-ray tube and detector rotate. Typically, scans were run using the Cu K_α radiation. In order to determine the exact peak position and peak width for the crystallite size determination of the nanoparticles, the peaks obtained in XRD data were deconvoluted with PANalytical HighScore software. The reference patterns were taken from the ICDD Powder Diffraction File Version 4+²⁴² and were of either Star or Indexed quality. A silicon standard was used to ascertain and correct the instrumental broadening. The standard was run under identical instrumental conditions to those used to obtain patterns for the samples, and thus the broadening of the standard is exactly the same as the instrumental broadening in the pattern of the samples.

To estimate the mean particle size of gold, silver and silver halide nanoparticles in the hybrid materials, in the simplest case where particles are stress-free, a single diffraction peak from the XRD pattern was used for the Scherrer equation:²⁴³

$$d = \frac{B\lambda}{(\beta \cos \theta)}$$

where, d is the mean crystallite size of the nanoparticles, B is the Scherrer constant (0.89 for integral breadth of spherical crystals w/ cubic symmetry), λ is the wavelength of X-ray radiation source, β is the angular full width at half maximum (FWHM) of the X-ray diffraction peak and θ is the diffraction angle (the angle between incident beam and the lattice planes).²⁴⁴

2.3.5 Infrared Spectroscopy

Infrared Spectroscopy (IR) is an absorption spectroscopic technique and deals in the infrared region of the electromagnetic spectrum. IR was used to study the interactions between the metallic nanoparticles and the polymers. Spectra of untreated substrates were compared to the spectra of hybrid materials containing metallic nanoparticles to determine any changes in the vibrational modes. Spectra were recorded on a Perkin Elmer Spectrum One FT-IR Spectrometer.

2.3.6 X-ray Photoelectron Spectroscopy

X-ray photoelectron spectroscopy (XPS) is a spectroscopic technique that is based on the process of photoemission. XPS provides analytical and chemical information about the top 5-10 nm of a material. XPS was used to elucidate the nature of the chemical bonding between the substrates and nanoparticles in the produced hybrid materials. The XPS spectra were collected under a high vacuum with an aluminium K_{α} X-ray source operating at 15 kV. XPS analyses were

performed using Kratos XSAM800 photoelectron spectrometer at the University of Auckland, Surface Science Department with the assistance of Dr Colin Doyle. Charging caused by the samples was minimised by the charge neutraliser – a thorium coated filament with tuneable current, filament voltage and bias settings of 1.95-2.1 A, 2.9-3.3 V and 1.1-1.3 V respectively. Spectra for Ag, Au, Cl, C, N, S, O were obtained and Gaussian-Lorentzian (70:30) peaks were fitted to the recorded spectra using the CasaXPS Version 2.3.13 program. All collected spectra were calibrated to the C 1s line at 285.0 eV.

2.3.7 UV-Visible Spectroscopy

Ultra violet visible (UV-Vis) spectroscopy was utilised to characterise the optical properties of the produced hybrid materials. As gold and silver nanoparticles exhibit distinctive absorptions in the visible region, UV-Vis spectroscopy was used to determine the presence of nanoparticles in the produced hybrid polymer samples. Also by comparing the UV-Vis spectra between various hybrid materials it was possible to compare the size of the present nanoparticles by determining the absorption peak positions and their shifts and peak broadenings. Absorption and reflectance (incorporating Kubelka-Munk transformations) UV-Vis spectra were collected on a Varian Cary 100 scan spectrometer UV-Vis spectrophotometer, in the spectral region of 200-800 nm. The Kubelka-Munk theory provides a correlation between reflectance and absorbance and the reflectance values are transformed into Kubelka-Munk units (K/S), using the equation below:

$$\frac{k}{s} = \frac{(1 - R)^2}{2R}$$

where R is the absolute reflectance of the sampled layer, k is the molar absorption coefficient and s the scattering coefficient of the sample at a given wavelength²⁴⁵. This transformation was performed by software which was incorporated in the spectrometer's analysis program.

2.3.8 Antimicrobial and antifouling testing

The antimicrobial effectiveness of the produced hybrid plastic materials was tested against *Escherichia coli* (*E. coli*) bacteria. The microorganism is a gram negative commensal commonly found in both human and animal intestines. *E. coli* was chosen as it is easy to grow and reproduce. Most *E. coli* strains are harmless.²⁴⁶ Furthermore, the nanogold and nanosilver hybrid polyurethane paint materials were tested for their potential as marine antifouling agents.

2.3.8.1 Antimicrobial testing

Due to time constraints, only the antimicrobial activity of produced hybrid polyurethane *dog bone* test strips and hybrid polyurethane K5000 paint materials were tested against *E. coli*. The tests were performed in triplicate for each sample and were achieved via the following method: a 5 mL stationary phase (16 hour) overnight culture of *E. coli* strain W3110 was grown in Luria Bertani Broth (LB). 3 mL of culture were pelleted in sterile Eppendorf tubes and resuspended and mixed in 3 mL of standard phosphate-buffered saline (PBS). This process was repeated twice to wash the cells and remove all traces of LB. 50 μ L aliquots of the washed and homogenously resuspended *E. coli* and 20 mg of hybrid polymer sample (each sample was cut finely cut into small pieces) was transferred into sterile Eppendorf tubes. It was important that the polymer sample pieces were completely covered by the liquid bacteria suspension. The Eppendorf tubes were incubated for up to 7 days (nanosilver halide hybrid

samples were also incubated in the dark). For the quantification of viable bacteria, the plastic samples were resuspended in 1 mL PBS and then vortexed for 30 seconds. 10 μ L from each tube was transferred to 990 μ L fresh PBS (10^{-2} dilution) followed by shaking and vortexing the suspension. The process was repeated to give a 10^{-4} dilution for each sample. 100 μ L of each dilution was then plated onto individual LB agar plates. Plates were incubated at 37 °C for 16 hours, and the resulting colonies were counted. The total colony-forming unit (CFU) was calculated by multiplying the mean number of colonies for each sample by the dilution factor. CFU is a measure of viable bacterial numbers. All samples were tested against reference samples, notably untreated polyurethane *dog bone* or dry untreated PU K5000 paint base. The antimicrobial activity was determined on the basis of the relative difference in CFU between new hybrid samples and their reference sample.

2.3.8.2 Antifouling testing

Antifouling effects of nanogold, nanosilver and nanosilver chloride hybrid PU K5000 materials were investigated. The experiment on prevention of marine biofouling on hybrid PU K5000 materials was performed by Polymer Group Ltd in Auckland. Pieces of wooden surfaces were painted with hybrid polyurethane K5000 materials and set in seawater (Whangaparaoa Peninsula). A control surface was painted with an untreated PU K5000 paint and also kept under the same conditions. After approximately six months the painted panels were taken out of sea water and the extent of marine growth on the surfaces were compared to that of control sample.

3 Nanogold and nanosilver hybrid polymer materials: nanoparticles formed in the presence of polyurethane and nylon 6,6 using their reducing nature

Hybrid polyurethane and nylon 6,6 materials containing gold and silver nanoparticles were synthesised using the approach described in Section 2.2.1. The methodology involved immersing the substrates (polyurethane or nylon 6,6 beads or sheets respectively) in aqueous hydrogen tetrachloroaurate or silver nitrate solutions followed by heating the reaction vials to 50 °C for gold or 90 °C for silver samples to complete the reduction of metal ions to metal nanoparticles. Unless otherwise mentioned, the mass of the substrates was 1 g for PU and nylon 6,6 beads and 1.5 g for PU and 0.5 g for nylon 6,6 sheets; the solution volume was 10 mL. All experiments were stopped after 24 hours in order to keep the process more economical. PU and nylon 6,6 simultaneously act as the substrate and reducing agents due to their amine functionality. For larger scale preparation a reaction vessel of ten times the size was designed and constructed, to produce suitably larger amounts of the nanogold and nanosilver hybrid polymer materials (Section 2.2.1.1) which were then moulded into plastic sheets, and *dog bone* test strips.

The sample names for the hybrid polymer materials produced and their respective reaction parameters are summarised in Table 3.1. The sample names for the hybrid PU beads produced which were moulded into *dog bone* test strips are summarised in Table 3.2.

Table 3.1: The names and their respective reaction parameters for the hybrid polymer materials. The reaction time for all samples was 24 hours; the solution volume was 10 mL.

| Name of hybrid material | Substrate | Metal ion conc. [mg kg⁻¹] | Metal ion species | Reaction temp. [°C] | % of metal in polymer |
|--------------------------------|------------------|---|--------------------------|----------------------------|------------------------------|
| PU-b-10Au | PU bead | 10 | Au ³⁺ | 50 | 0.01 |
| : | : | : | : | : | : |
| PU-b-1000Au | PU bead | 1000 | Au ³⁺ | 50 | 1 |
| PU-s-10Au | PU sheet | 10 | Au ³⁺ | 50 | 0.008 |
| : | : | : | : | : | : |
| PU-s-1000Au | PU sheet | 1000 | Au ³⁺ | 50 | 0.77 |
| PU-b-10Ag | PU bead | 10 | Ag ⁺ | 90 | 0.01 |
| : | : | : | : | : | : |
| PU-b-1000Ag | PU bead | 1000 | Ag ⁺ | 90 | 1 |
| PU-s-10Ag | PU sheet | 10 | Ag ⁺ | 90 | 0.008 |
| : | : | : | : | : | : |
| PU-s-1000Ag | PU sheet | 1000 | Ag ⁺ | 90 | 0.77 |
| Ny-b-10Au | Nylon 6,6 bead | 10 | Au ³⁺ | 50 | 0.01 |
| : | : | : | : | : | : |
| Ny-b-1000Au | Nylon 6,6 bead | 1000 | Au ³⁺ | 50 | 1 |
| Ny-s-10Au | Nylon 6,6 sheet | 10 | Au ³⁺ | 50 | 0.02 |
| : | : | : | : | : | : |
| Ny-s-1000Au | Nylon 6,6 sheet | 1000 | Au ³⁺ | 50 | 2 |
| Ny-b-10Ag | Nylon 6,6 bead | 10 | Ag ⁺ | 90 | 0.01 |
| : | : | : | : | : | : |
| Ny-b-1000Ag | Nylon 6,6 bead | 1000 | Ag ⁺ | 90 | 1 |
| Ny-s-10Ag | Nylon 6,6 sheet | 10 | Ag ⁺ | 90 | 0.02 |
| : | : | : | : | : | : |
| Ny-s-1000Ag | Nylon 6,6 sheet | 1000 | Ag ⁺ | 90 | 2 |

Table 3.2: Nomenclature of moulded hybrid PU *dog bone* strips names and their respective precursor hybrid PU beads.

| Name of PU <i>dog bone</i> strip | Hybrid PU beads used for moulding PU <i>dog bone</i> strips |
|----------------------------------|---|
| PU-db | Untreated PU beads |
| PU-db-1Au | PU-b-10Au |
| PU-db-5Au | PU-b-5Au |
| PU-db-10Au | PU-b-10Au |
| PU-db-50Au | PU-b-50Au |
| PU-db-100Au | PU-b-100Au |
| PU-db-1Ag | PU-b-1Ag |
| PU-db-10Ag | PU-b-10Ag |
| PU-db-50Ag | PU-b-50Ag |

The formation of nanogold or nanosilver on and within the nylon 6,6 and polyurethane polymers is evident by the appearance of a pink-purple or yellow-brown colour resulting from the surface plasmon resonance scattering of light by gold and silver nanoparticles respectively (Section 1.4.2). The shade and intensity of the colour can be altered by systematically altering the concentration of Au^{3+} or Ag^+ ions, the reaction time and the temperature. An example of this can be seen in Figure 3.1 below.

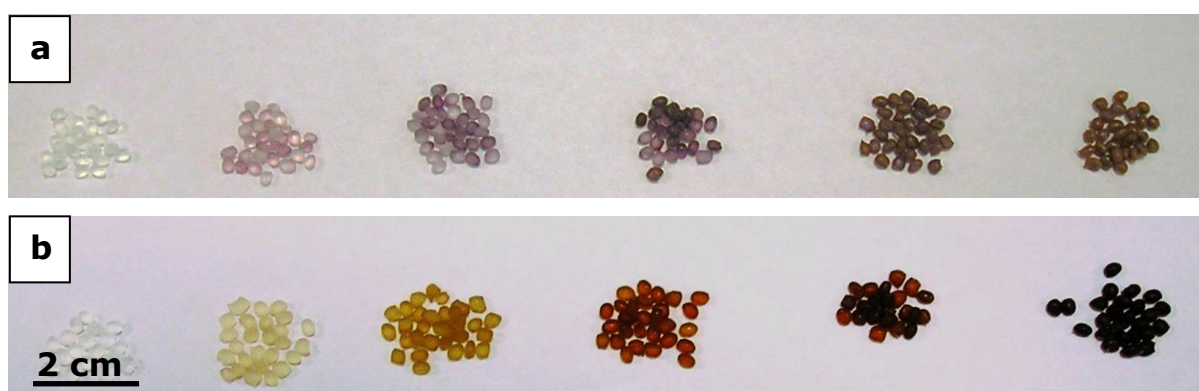


Figure 3.1: Hybrid PU beads prepared from a) gold solution and b) silver solution with increasing gold / silver concentrations (5 – 100 mg kg⁻¹ Au^{3+} or Ag^+ from left to right).

3.1 Uptake studies

The uptake of dissolved gold (Au^{3+}) and silver (Ag^+) by substrates such as PU and nylon 6,6 was quantitatively analysed by atomic absorption spectroscopy (Section 2.3.3). This was facilitated by soaking the polymer substrates in different concentrations of gold or silver solutions for different periods of time at different temperatures, then analysing the resulting solution for any residual gold or silver. The difference between the starting concentration and the residual concentration in the soaking solution was determined to be the amount of gold or silver ions absorbed by the polymer substrates. The effect of concentration and temperature of the ion solution on uptake were studied.

3.1.1 Extent of gold uptake by polyurethane and nylon 6,6

Figure 3.2 and Figure 3.3 present the effect of concentration on the uptake of gold ions by PU and nylon 6,6. All experiments were run at a constant temperature of 50 °C with starting solution concentrations of 10, 20 and 50 mg kg^{-1} Au^{3+} and 5, 10 and 50 mg kg^{-1} Au^{3+} for PU and nylon 6,6 samples respectively. The solutions were analysed for residual gold within 24 hours of absorption.

It was observed that the uptake rate of metal ions by both PU and nylon 6,6 increased with increasing concentrations of metal ions in the starting solutions. For example, when 10 mg kg^{-1} of Au^{3+} solution was employed, the total uptake after 24 hours at 50 °C was 8.2 mg kg^{-1} which conforms to ca. 81.3 % of gold ions taken up by polyurethane, whereas the absorption from the 20 and 50 mg kg^{-1} Au^{3+} conform to 95.5 % and 97.4 % respectively. Similar results were observed for nylon 6,6.

Taking these results into consideration, the uptake process can be described with Fick's law:²⁴⁷

$$J_i = -AD \frac{dC_i}{dz}$$

where J_i is the rate of diffusion transport per unit area, A is the area across which diffusion is taking place, D is the diffusion coefficient, C_i is the concentration and z is the distance over which the diffusion is taking place. Thus, the rate of uptake increases directly with the concentration of metal ions, in other words the increase in concentration gradient (dC_i/dz) acts as increase to the driving force of diffusion.

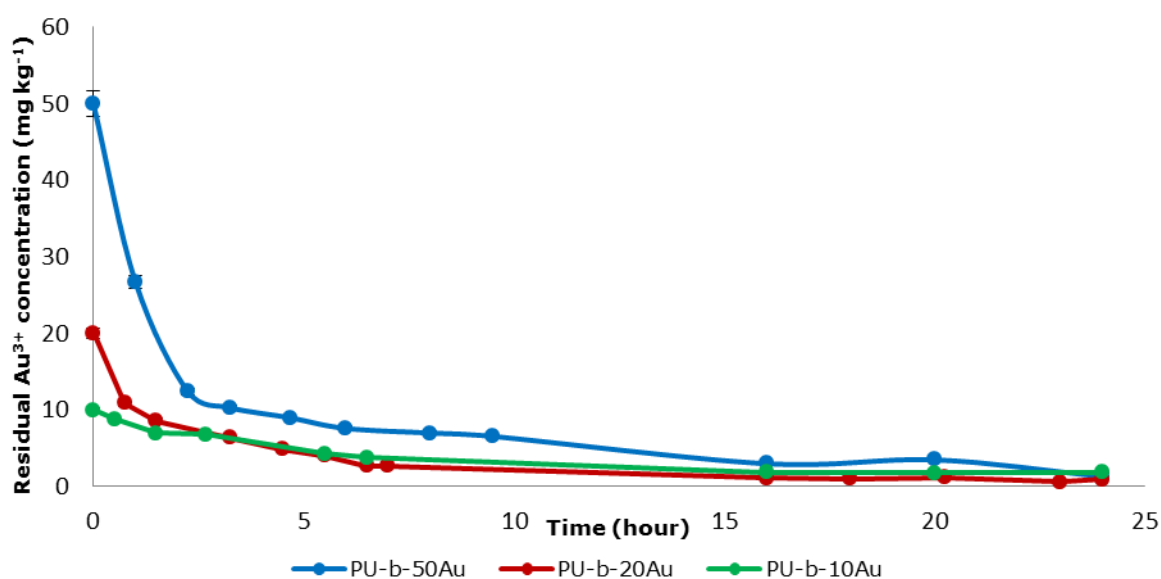


Figure 3.2: Gold uptake by PU beads at 50 °C, utilising a solution with an initial gold concentration of 10, 20 and 50 mg kg⁻¹ Au³⁺.

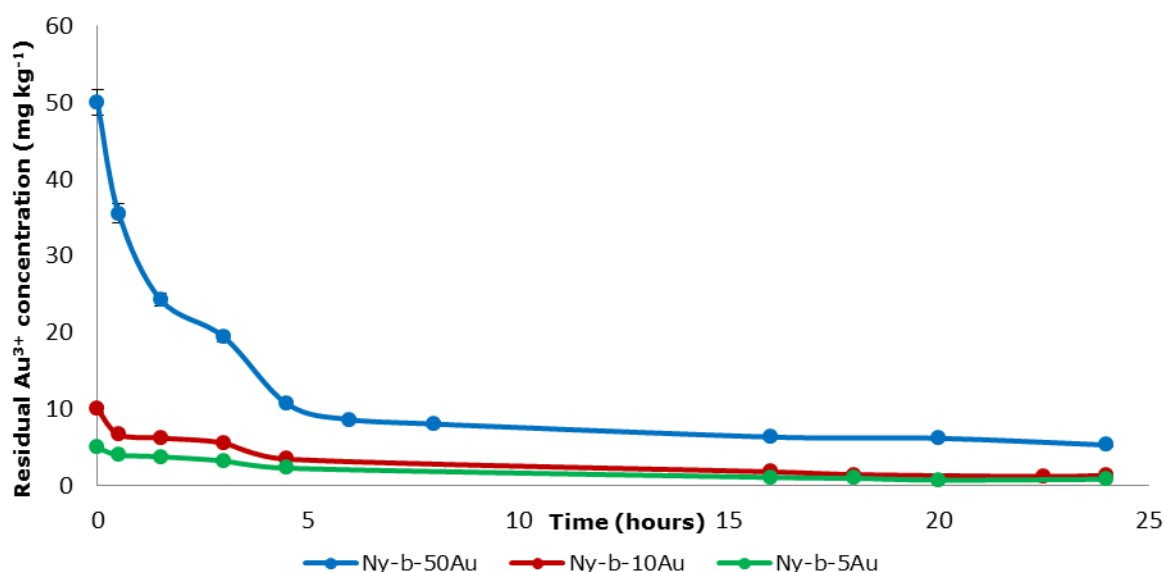


Figure 3.3: Gold uptake by nylon 6,6 beads at 50 °C, utilising a solution with an initial gold concentration of 5, 10 and 50 mg kg⁻¹ Au³⁺.

When changing the reaction temperature from 50 to 90 °C and keeping the starting concentration constant, it was shown that the temperature at which the uptake process occurs greatly affects the value of the diffusion coefficient. This is illustrated with a 50 mg kg⁻¹ gold solution (Figure 3.4 and Figure 3.5) showing that for both PU and nylon 6,6 substrates an increase in temperature results in an increased gold absorption rate.

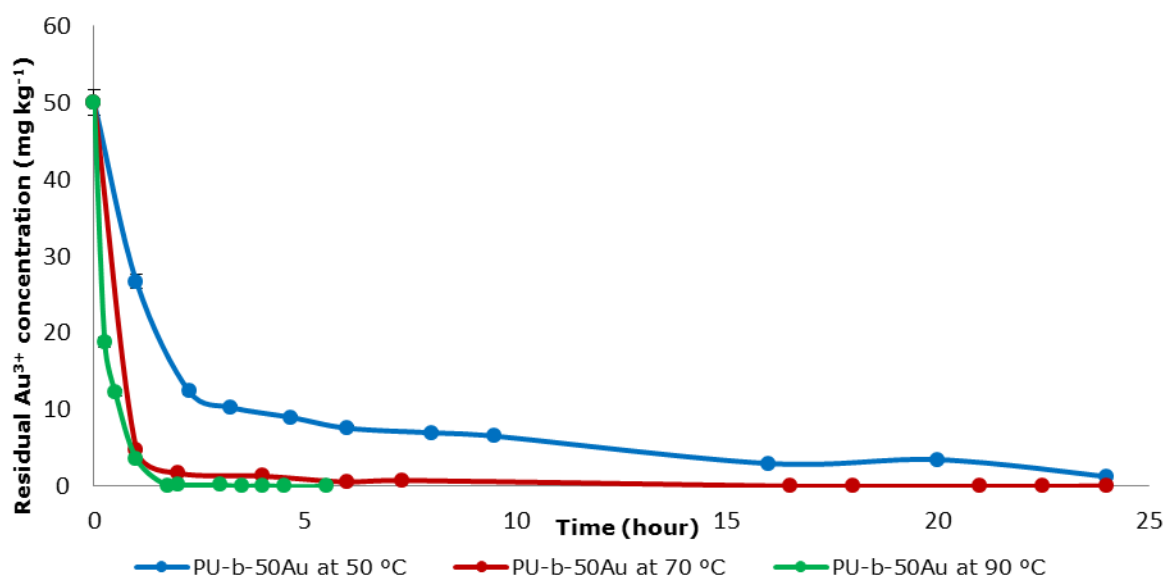


Figure 3.4: Gold uptake by PU beads measured at 50, 70 and 90 °C.

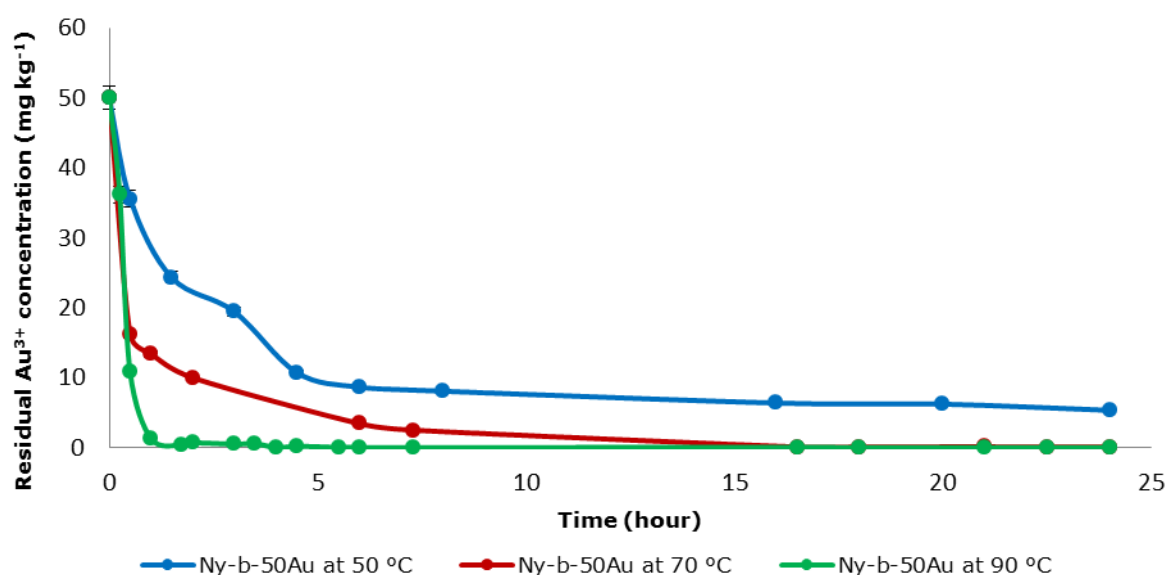


Figure 3.5: Gold uptake by nylon 6,6 beads measured at 50, 70 and 90 °C.

Due to the porosity of the PU and nylon 6,6 structures both substrates have the capacity to absorb significant amounts of gold ions within 24 hours when tested at a temperature of 50 °C. Figure 3.6 shows that the amount of gold absorbed by PU is slightly higher than being absorbed by nylon 6,6. The maximum absorption level of gold ions by both substrates is reached after about 16 hours

and amounts to ca. 97 % for polyurethane and 89 % for nylon 6,6. The difference in the total amount of gold absorbed between polyurethane and nylon 6,6 may be due to the fact that polyurethane has higher porosity than nylon 6,6. In order to keep the experiments more economical and provide gentle reaction conditions for the substrates the reaction temperature for production of all nanogold hybrid polyurethane and nylon 6,6 materials was set to 50 °C.

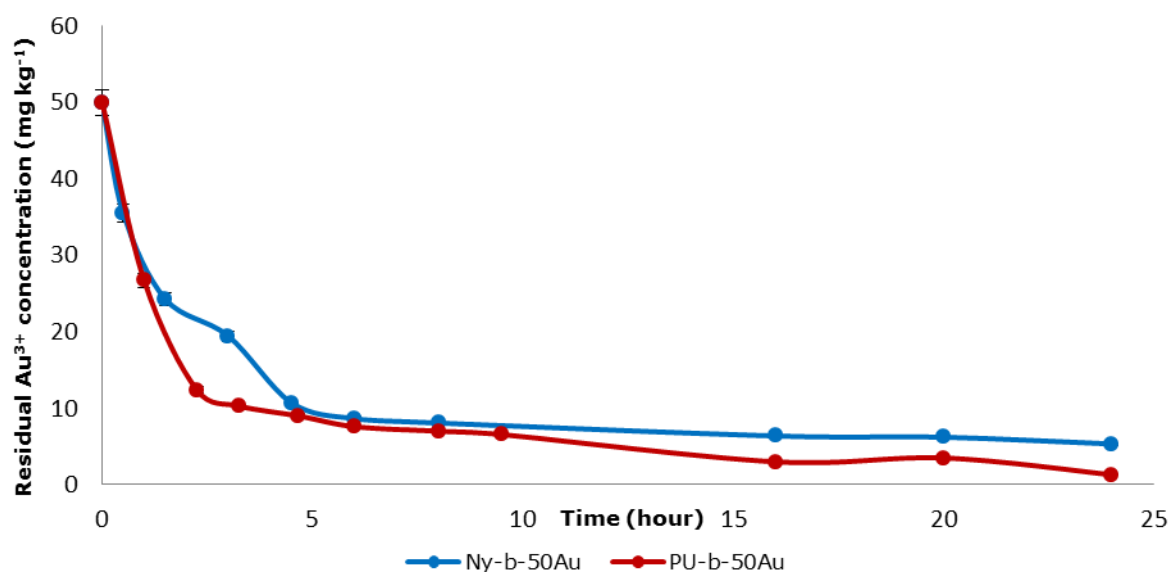


Figure 3.6: Comparison of gold uptake by PU versus nylon 6,6 beads. The experiment was undertaken at 50 °C.

3.1.2 Extent of silver uptake by polyurethane and nylon 6,6

Similar to gold, uptake studies were undertaken to determine the effect of temperature on the absorption of silver ions by polyurethane or nylon 6,6 substrates. Figure 3.7 and Figure 3.8 show that the shape of the uptake curves of silver are generally similar to that observed for gold. The absorption temperature was set to 50, 70 and 90 °C for polyurethane (Figure 3.9) and 50 and 90 °C for nylon 6,6 (Figure 3.10). For both substrates absorption was not complete - even after 24 hours. At 50 or 70 °C the uptake was more limited with only 20 % of the silver ions absorbed by PU or nylon 6,6. To achieve the

maximum silver ion absorption the reaction temperature of 90 °C was used for preparation of the nanosilver hybrid polyurethane and nylon 6,6 materials.

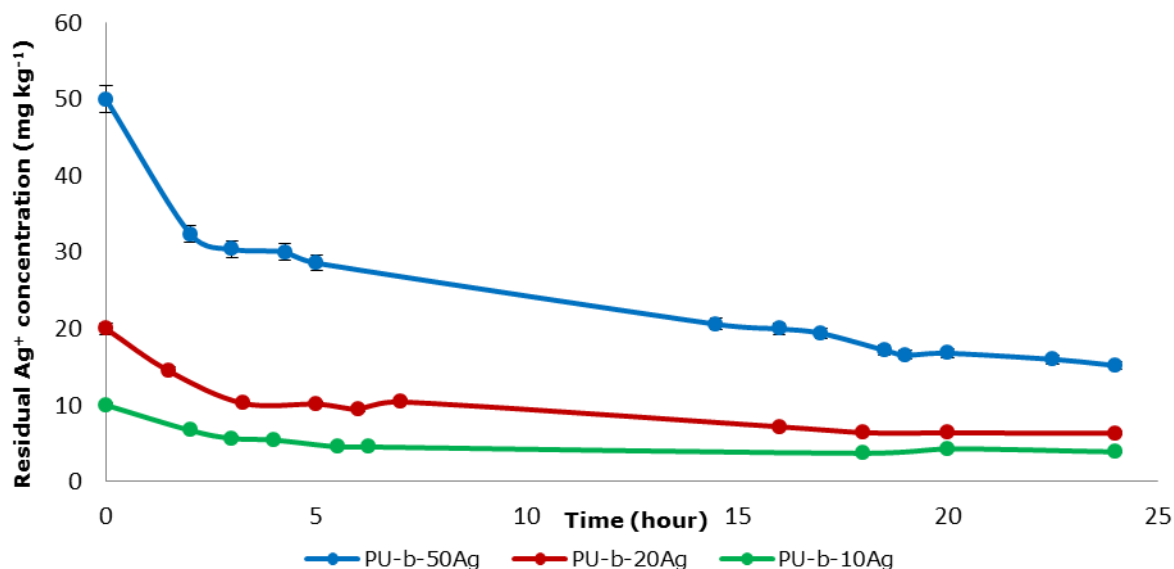


Figure 3.7: Silver uptake by PU beads at 90 °C, utilising a solution with an initial silver concentration of 10, 20 and 50 mg kg⁻¹ Ag⁺.

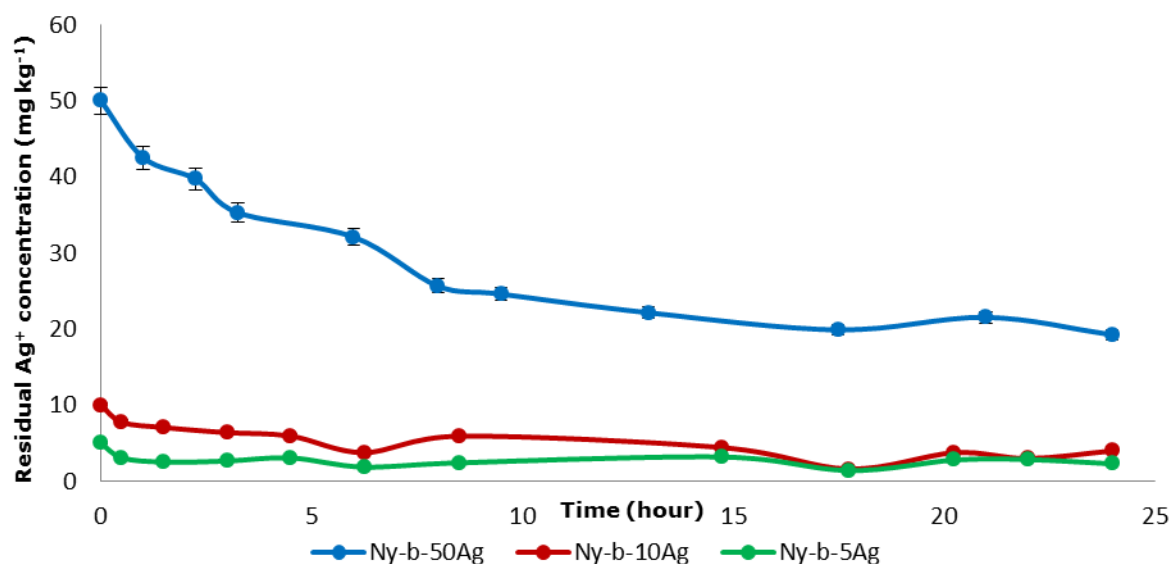


Figure 3.8: Silver uptake by nylon 6,6 beads at 90 °C, utilising a solution with an initial silver concentration of 10, 20 and 50 mg kg⁻¹ Ag⁺.

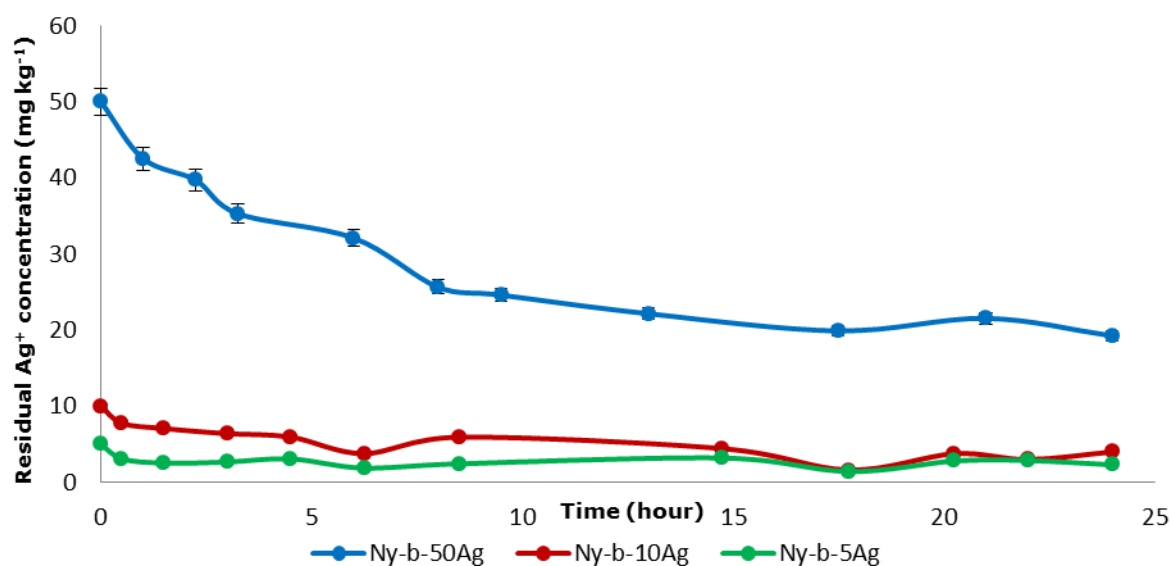


Figure 3.9: Silver uptake by PU beads measured at 50, 70 and 90 °C utilising a solution with an initial silver concentration of 50 mg kg⁻¹ Ag⁺.

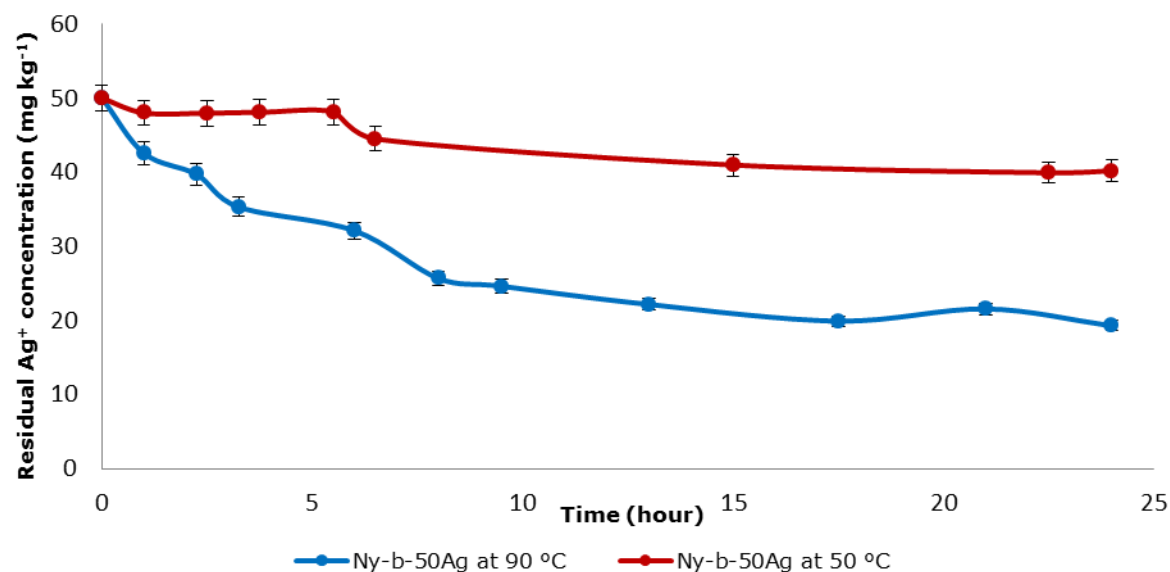


Figure 3.10: Silver uptake by nylon 6,6 beads measured at 50 and 90 °C utilising a solution with an initial silver concentration of 50 mg kg⁻¹ Ag⁺.

In terms of the differences between the two substrates on the uptake of silver ions, it was shown that PU absorbed slightly more silver ions than nylon 6,6. Figure 3.11 shows silver uptake with a starting concentration of 50 mg kg⁻¹.

After a period of 24 hours at 90 °C polyurethane absorbed ca. 70 % of silver ions with nylon 6,6 only absorbing 62 %. This confirms the observations made during the absorption of gold by PU and nylon 6,6 – whereby a more porous polymer matrix (as seen in PU) allows for a greater absorption.

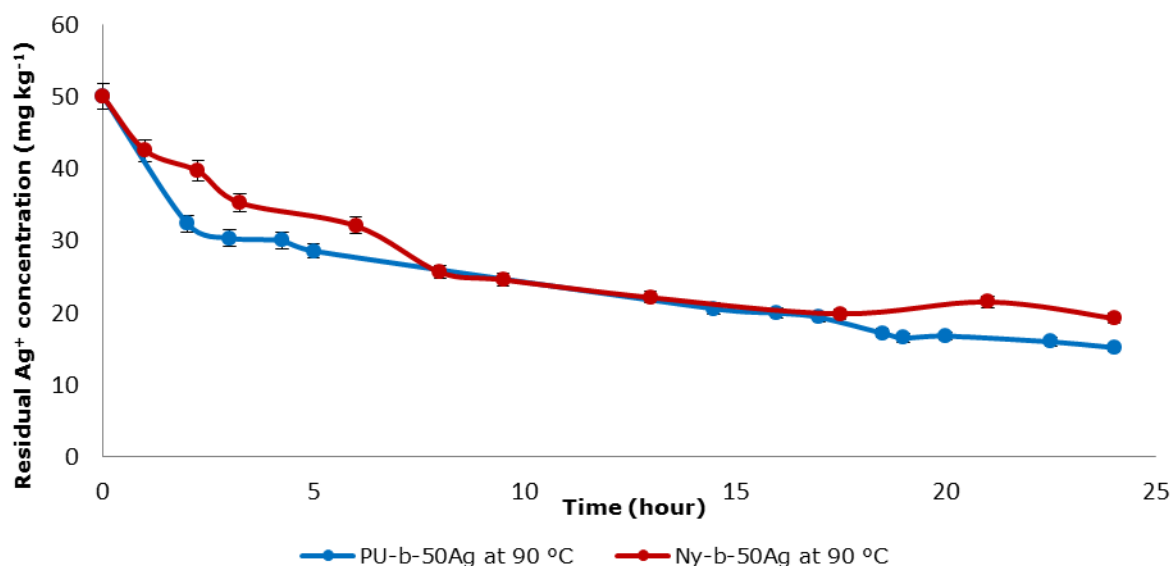


Figure 3.11: Comparison of silver absorption by PU beads versus nylon 6,6 beads. The experiment was undertaken at 90 °C.

When comparing the uptake of gold and silver ions by both PU and nylon 6,6 it can be seen that the uptake of silver is not as efficient nor complete even after a 24 hour absorption period at 90 °C (Figure 3.11). One possible reason for this observation could be that under the slightly acidic reaction conditions (pH 4-5) employed substrates may be protonated and thus exhibit a net positive charge. Because gold ions are being absorbed as the $[\text{AuCl}_4]^-$ complex²¹ it is possible that there would be an electrostatic attraction between the gold complex and the positively charged substrates. Silver ions are positively charged and therefore they would be electrostatically repelled by the substrates providing a slower uptake rate.

A second reason for the differences in gold and silver absorption might be due to the greater chemical affinity of gold for nitrogen functional groups compared to

silver. The comparison of the respective metal-nitrogen bond enthalpies in the metal-ammonia complexes has shown that the enthalpy of formation for the Au-NH₃ bond is $-30.17 \text{ kJ mol}^{-1}$ and for Ag-NH₃ the enthalpy is $-20.45 \text{ kJ mol}^{-1}$.²⁴⁸ A further reason for the difference in uptake rate could likely be due to the different reduction potentials of gold and silver ions to their corresponding metallic nanoparticles. As mentioned above, while the absorption process is taking place, a reduction of gold or silver ions to metallic gold or silver also occurs. The driving force for the reduction reaction is provided by the difference between the two potentials; the reduction of the metal ion to the metal and the corresponding oxidation of the amine functional groups of the polymer substrates. These potential differences are known as the electrochemical overpotential. Table 3.3 shows that the standard redox potential for the reduction of Au³⁺ or [AuCl₄]⁻ to Au⁰ is higher than that of Ag⁺ to Ag⁰. As such, the reduction of gold ions/complexes to gold nanoparticles is the thermodynamically preferred reaction, the gold ions reduce more readily providing the driving force for more [AuCl₄]⁻ ions to be absorbed and subsequently reduced.

Table 3.3: Summary of standard reduction potentials for gold and silver couples in aqueous solutions.²⁴⁹

| Reaction | Standard potential, E ⁰ (V) |
|---|--|
| Au ³⁺ + 3e → Au | 1.42 to 1.52 |
| AuCl ₄ ⁻ + 3e → Au + 4Cl ⁻ | 0.994 to 1.002 |
| Ag ⁺ + e → Ag | 0.799 |

Overall, the results show that the majority of the gold (at 50 °C) and more than 60 % of the silver content (90 °C) in the 10 mL starting solutions is taken up by the 1 g quantities of PU or nylon 6,6 beads.

3.2 Formation of gold and silver nanoparticles within the polymer matrix

During the uptake of gold or silver ions by the substrates at different temperatures the appearance of pink-purple or yellow-brown colours within the substrates were observed which are evidence for the formation of gold and silver nanoparticles respectively. Here the PU or nylon 6,6 acted both as the substrates and simultaneously as the reducing agents presumably due to their carbamate and amide functionalities respectively. The purple colour was observed in the hybrid PU and nylon 6,6 materials after approximately 15 minutes for PU and 3 hours for nylon 6,6 into the gold ion uptake process from a 500 mg kg^{-1} gold starting solution concentration. When using a 500 mg kg^{-1} silver starting solution the typical yellow colour of silver nanoparticles appears in the PU samples approximately 90 minutes into the silver ion uptake process. However, it takes approximately 5 hours to observe the yellow colour in nylon 6,6 materials. Figure 3.12 shows the colour development of hybrid PU beads in gold and silver solutions with different initial concentrations after 30 minutes (for gold) and 90 minutes (for silver) into metal ion absorption and the nanoparticle formation process. This observation together with the respective uptake curves confirms that both the absorption of the gold ions and their reduction to metallic gold nanoparticles is taking place simultaneously.

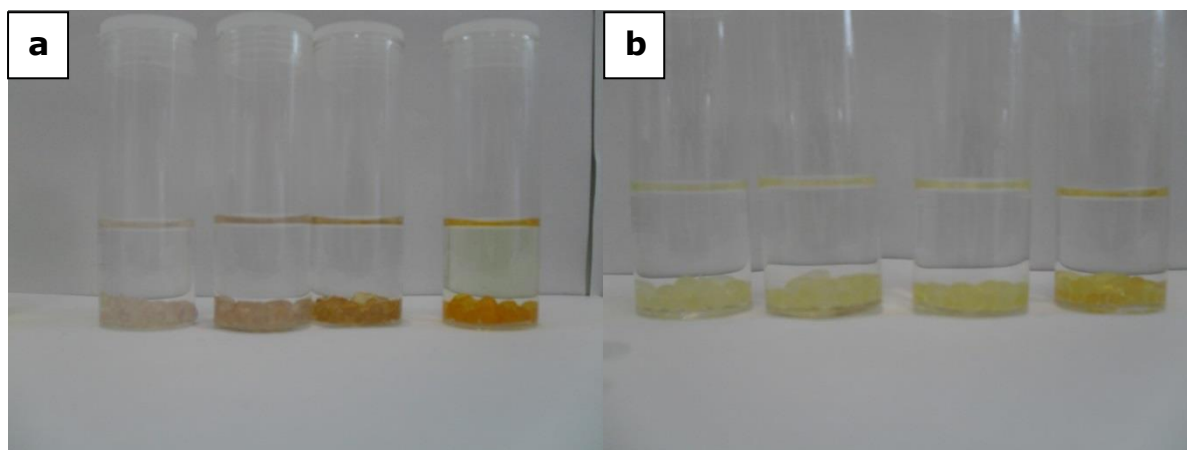


Figure 3.12: PU beads during absorption process a) after 30 minutes in contact with gold solution with an initial concentrations of 10, 20, 50, 500 mg kg⁻¹ Au³⁺ (from left to right); b) after 120 min in silver solution with an initial concentrations of 10, 20, 50, 500 mg kg⁻¹ Ag⁺.

The beads were not uniformly coloured; this is due to the contact area between the solution and the polymer beads which was not provided evenly to every bead in the reaction vial (Figure 3.14a-d). This behaviour was not observed in production of the nanogold and nanosilver hybrid polymer beads during the scaling up process (Section 3.3).

The perceived colours of the hybrid polymer materials derive from response of light receptors in the human eye to the particular wavelengths of light absorbed, transmitted or reflected by the produced hybrid polymer materials. These wavelengths are the result of the resonance interaction of the incident light with the conduction band electrons of gold or silver nanoparticles formed within the polymers. When conduction electrons confined in a very small volume interact with light they undergo a collective oscillation with respect to the positive ion nuclei, creating a negative charge distribution at the surface. This effect is surface plasmon resonance phenomenon (Section 1.4.2). The excitation of surface plasmon resonances on the metal nanoparticles is what creates a very selective absorption and strong scattering of light of particular colours.

Various factors such as reaction temperature, time, initial metal ion concentration and ratio of metal ion to polymer beads (or sheets) influence the

colour of the produced hybrid polymer materials. The colour change of the hybrid polymer materials and the relationship between the size and shape of nanogold and nanosilver particles were characterised through the use of UV-Vis spectroscopy, SEM, TEM and XRD.

3.3 Scale up of nanogold and nanosilver hybrid PU materials

The nanogold and nanosilver hybrid polymer materials were produced in ten times greater quantities in a reactor designed and operated as discussed in Section 2.2.1.1. After 24 hours of reaction the beads were uniform in colour as the flow of reaction solution through the beads ensured a better contact between the solution and the PU polymer beads in comparison to the reaction which took place on a small scale in a glass vial. The nanogold and nanosilver hybrid PU beads produced in this way were moulded into *dog bone* strips via a conventional thermoplastic moulding process by the Centre for Advanced Composite Materials and the Plastics Centre of Excellence at the University of Auckland. The resulting *dog bone* strips produced from the nanogold and nanosilver hybrid PU beads are illustrated in Figure 3.13. These are very uniform in colour and show that nanogold and nanosilver entities are distributed evenly through the moulded plastic (uniform coloured cross section of the *dog bone* strips), confirming that these nano-entities do not affect the thermoplastic forming properties of the polymer substrates.

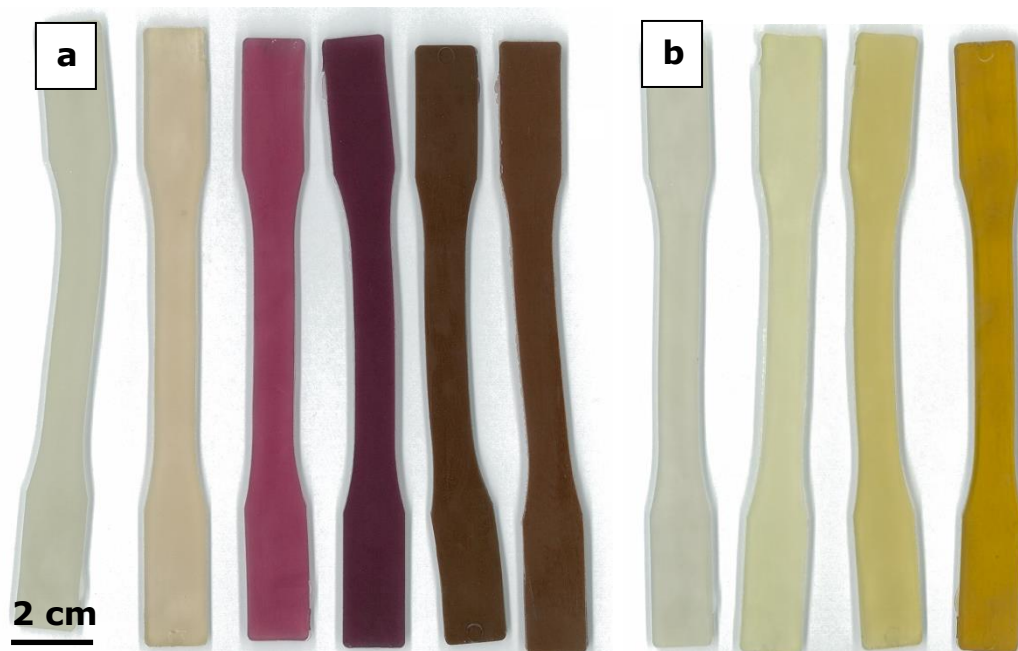


Figure 3.13: a) From left to right moulded *dog bone* strips from the untreated PU beads, beads which were produced from 1, 5, 10, 50, 100 mg kg⁻¹ Au³⁺ solution; b) from left to right moulded *dog bone* strips from the untreated PU beads, beads which were produced from 1, 10 and 50 mg kg⁻¹ Ag⁺ solution.

3.4 UV visible spectroscopy - colour of nanogold and nanosilver hybrid polyurethane and nylon 6,6 materials

As mentioned above, the pink-purple or yellow brown colour development that was observed in the PU and nylon 6,6 substrates during the uptake of gold or silver ions indicated the subsequent reduction of these ions to metallic nanoparticles. Figure 3.14 shows a picture of the nanogold and nanosilver hybrid PU and nylon 6,6 polymer beads after a period of 24 hours of reaction with Au³⁺ and Ag⁺ containing solution of different concentrations. During the reaction, gold or silver ions were absorbed by the polymer substrates and simultaneously reduced to gold or silver nanoparticles respectively. With increasing initial gold concentrations the colour of the resultant materials changes from a pink to purple and then brown. Similarly, with increasing initial silver concentrations, the colour of the resultant materials changes from yellow to dark brown.

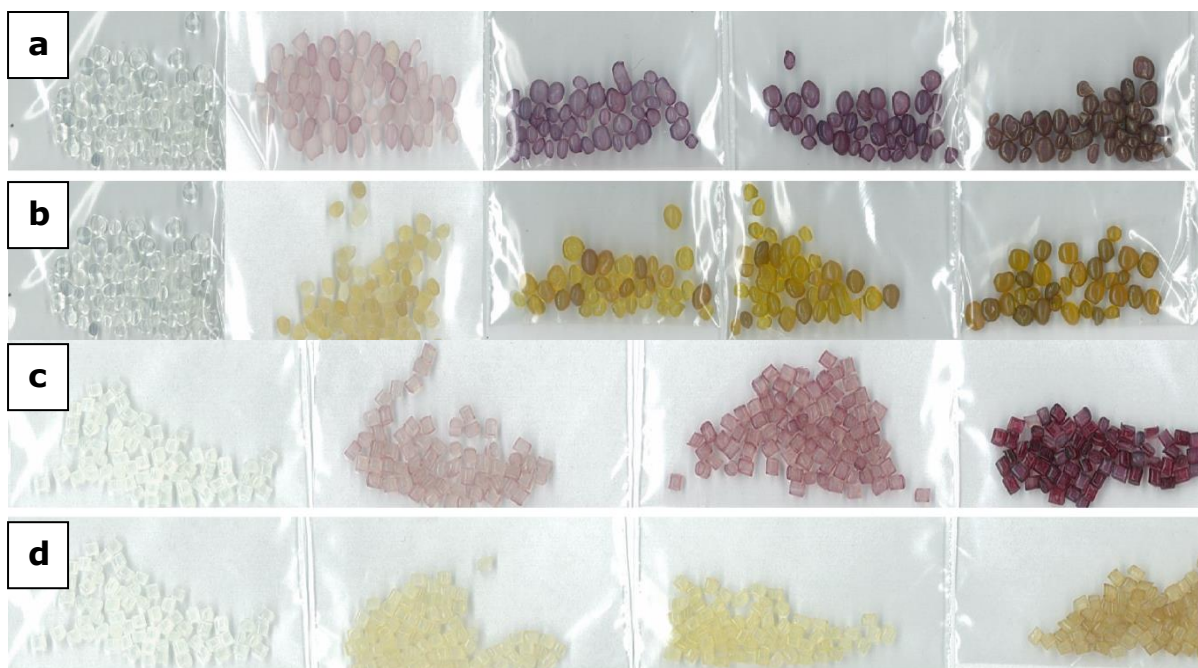


Figure 3.14: Photograph of the nanogold and nanosilver hybrid PU and nylon 6,6 beads: a) (from left to right) untreated PU beads, PU-b-5Au, PU-b-10Au, PU-b-20Au and PU-b-50Au samples; b) (from left to right) untreated PU beads, PU-b-5Ag, PU-b-10Ag, PU-b-20 and PU-b-50Ag samples; c) (from left to right) untreated nylon 6,6 beads, Ny-b-5Au, Ny-b-10Au, and Ny-b-50Au samples; d) (from left to right) untreated nylon 6,6 beads, Ny-b-5Ag, Ny-b-10Ag, and Ny-b-50Ag samples.

In order to ascertain the extent of the formation and distribution of the nanoparticles through the interior of the hybrid polymer materials, the nanogold and nanosilver hybrid PU and nylon 6,6 beads were cut into slices (Figure 3.15). At low gold concentrations the surface of the PU was coloured purple due to the surface plasmon resonance effect, and the centre was almost colourless (PU-b-20Au sample). However, when the gold concentration of the solution was increased to $50 \text{ mg kg}^{-1} \text{ Au}^{3+}$ to prepare the PU-50-Au sample, the cross section of this bead showed that the purple colour, which was the same on the surface of the bead, became lighter when moving towards the centre of the bead and eventually became colourless around the core of the bead. Increasing the concentration of the gold solution further to $500 \text{ mg kg}^{-1} \text{ Au}^{3+}$ (as in PU-b-500Au sample) resulted in a change in the colour of the surface of the bead from purple to brown. Moving towards the centre of such a bead saw a gradual colour change back to purple due to discrete and separated gold nanoparticles. Similar

observations were made for the nanosilver hybrid PU beads. For the PU-b-20Ag sample, the yellow colour, which is the typical colour for silver nanoparticles due to surface plasmon resonance, was observed on the surface of the bead. With increasing concentration, the PU-b-50Ag sample was evenly yellow throughout the entire hybrid PU bead. As the concentration was further increased to $500 \text{ mg kg}^{-1} \text{ Ag}^+$ to prepare the PU-b-500Ag sample, the beads were brown on the surface turning yellow when moving towards the centre of the beads.

The cross sectional variation in colour seen in the PU beads produced from solutions with increasing gold or silver concentrations, notably from purple or yellow on the outer edge and colourless in the centre to purple or yellow all of the way through and finally brown on the outer edge and purple or yellow in the centre is likely due to the formation of different sized gold or silver nanoparticles exhibiting different extents of agglomeration. With a low initial gold or silver concentration the majority of metal ions would form as discrete nanoparticles on the outer edges of the beads. Increasing the gold or silver concentration slightly would increase the rate of absorption and diffusion, meaning there would be a greater spread of metal ions right throughout the bead, resulting in the formation of nanoparticles both on the surface and also within the interior of the beads. Increasing the gold or silver concentration further may saturate the beads. On the outer edges of the beads the gold or silver concentration would be so high that more nanoparticles may form than are able to be stabilised by the substrate, resulting in particle growth via agglomeration and hence the appearance of a brown colour. Due to diffusion, the concentration of metal ions in the centre of the beads produced with a high gold or silver concentration would be less than that on the outer edges, and hence the amount of nanoparticles formed would be less. As these produce a purple or yellow colour respectively it is likely that they are sufficiently stabilised by the polymer matrix and exist as discrete nanoparticles sufficiently separated, and therefore do not undergo agglomeration.

The observation made for the nanogold and nanosilver hybrid nylon 6,6 beads was slightly different. The sliced Ny-b-50Au sample (Figure 3.15b) was purple on the surface and as the concentration was increased the colour penetrated the bead admittedly not as intensive as for the analogue PU sample (Figure 3.15a)

which is likely due to the different porosity degrees of the polymers. This agrees well with the uptake study results (Section 3.1), the amount of the gold ions absorbed by the PU beads was higher than the amount of the gold ions absorbed by the nylon 6,6 beads.

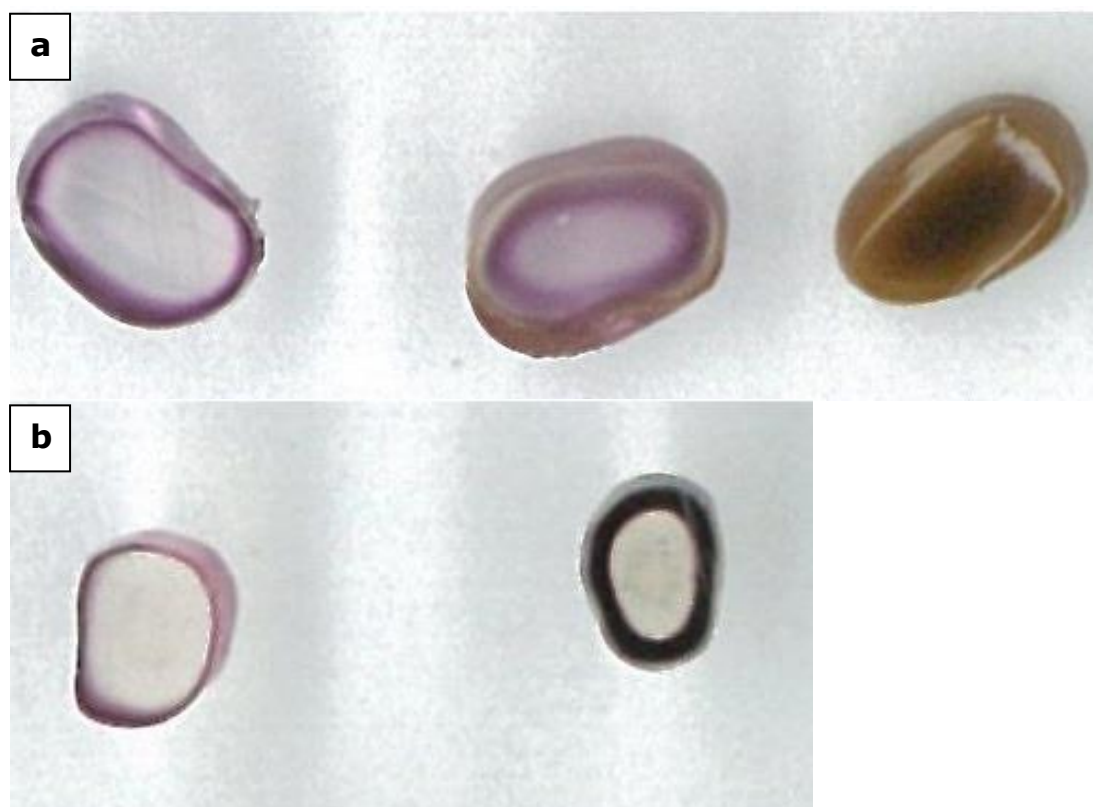


Figure 3.15: Photograph of the sliced nanogold and nanosilver hybrid PU and nylon 6,6 beads: a) (from left to right) PU-b-20Au, PU-b-50Au and PU-b-500Au samples; b) (from left to right) Ny-b-50Au and Ny-b-500Au samples.

3.4.1 UV visible spectroscopy - nanogold hybrid polyurethane and nylon 6,6 materials

For gold, the absorption edge due to the interband transitions is in the visible range at around 470 nm²⁵⁰, yielding the distinct golden yellow colour. A thin film of gold absorbs in the blue region at 480 nm.²⁵¹ Gold nanoparticles exhibit an

intense visible absorption, generally centred between approximately 500–700 nm.¹⁰⁶ For example spherical gold nanoparticles exhibit an intense ruby red colour and an extinction band around 520 nm with nanoparticles of an approximate size between 10 and 20 nm dispersed in water.^{108,110} As mentioned in Section 1.4.2, the surface plasmon resonance band depends strongly not only on the size and the shape of the nanoparticle but also on the dielectric constant of the surrounding medium, presence of the adsorbed species and the distance between neighbouring nanoparticles.²⁵²

Figure 3.16 shows the Kubelka Munk transformed UV-Vis reflectance spectra for the nanogold hybrid polyurethane materials prepared from different concentrations of gold in the uptake solutions ranging from 5 to 50 mg kg⁻¹ Au³⁺. Their respective photographed colours are presented in Figure 3.14a. For all samples two peaks, around 505 and 700 nm, should be ignored as the peaks are artefacts of the UV Vis spectrometer used. The PU beads prepared from a 5 mg kg⁻¹ gold solution exhibit two absorption peaks, one at around 512 nm and another one at 547 nm. The peak around 512 nm which is clearly blue-shifted from the typical surface plasmon resonance band at 520 nm for small spherical gold nanoparticles matches with the peaks reported on gold nanoparticles which absorb between 500 and 510 nm and are around 2 nm and smaller in size.^{253–255} The peak position and shape depend on the dielectric constant of the surrounding medium of the nanoparticles. The optical properties of spherical metal particles can be calculated by Mie theory. As previously introduced (Section 1.4.2), in the equation shown below:

$$C_{ext} = \frac{24\pi^2 \varepsilon_m^{3/2} R^3}{\lambda} \frac{\varepsilon''}{(\varepsilon' + 2\varepsilon_m)^2 + \varepsilon''^2}$$

the resonance condition is fulfilled when $\varepsilon' = -2\varepsilon_m$ for spheres. For noble metal nanoparticles ε' is negative and decreases with increasing wavelength so that as ε_m increases, the resonance condition is fulfilled at higher wavelengths. Additionally the peak shifts to higher wavelengths with increases in the refractive index of the surrounding medium.²⁵⁶ The refractive index of the surrounding medium is close ca. 1.5 for polyurethane, therefore as expected the peak is red-shifted from 520 nm absorption band for small gold nanoparticles which are dispersed in aqueous solution with refractive index of 1.33 for water. Thus, the peak at 547 nm represents very small nanoparticles appearing to reflect a pink colour to the eye. Due to the small concentration of the nanoparticles in this sample the particle size could not be determined by TEM analyses. When analysing the spectrum curve for PU beads produced from a 10 mg kg⁻¹ gold solution the absorption peaks have shifted and broadened. The first peak is slightly shifted from 512 to 514 nm, indicating particle growth due to an increased number of absorbed gold ions by the substrate. The second peak is broadened significantly and has its absorption maxima at 555 nm. If it is assumed the particles are spherical then the broadening and red-shift is caused by the increased particle diameter and also possible agglomeration of the particles which results in the coupling of surface plasmon resonance bands of closely adjacent nanoparticles. Larger spherical gold nanoparticles scatter more light²⁵⁷ due to larger optical cross sections and increasing ratio of scattering to total extinction with increasing size. The colour changed from pink to slightly purple shade.

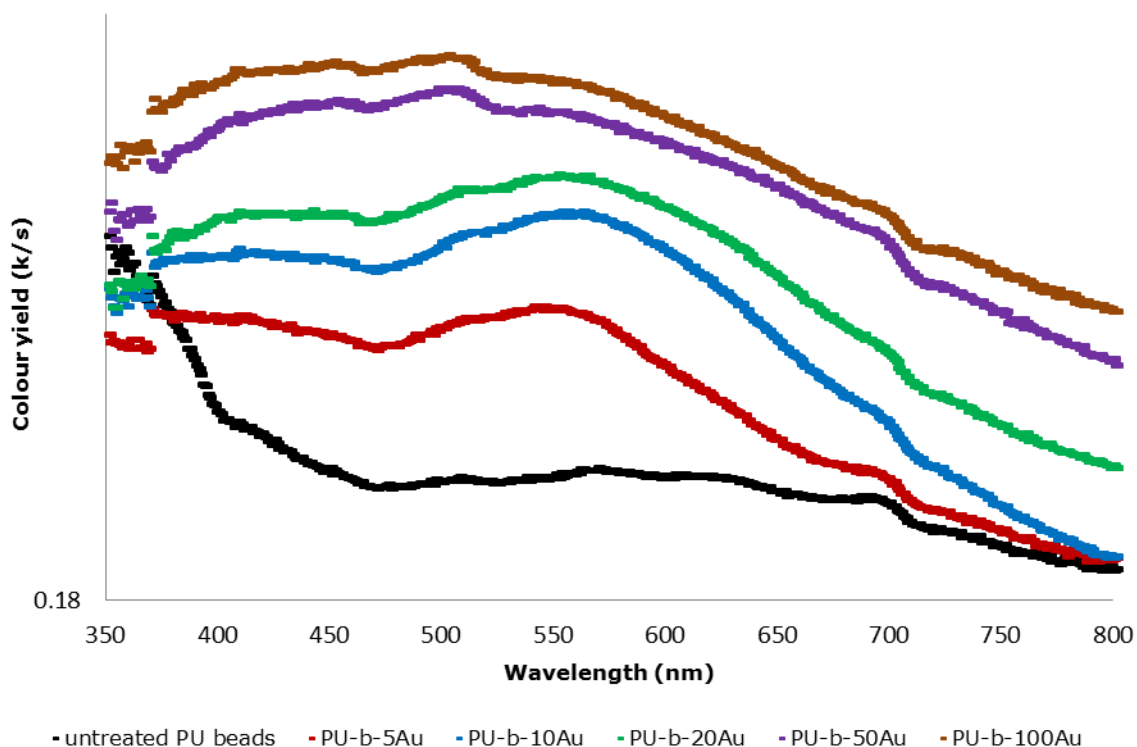


Figure 3.16: Kubelka Munk transformed UV-Vis reflectance spectra of the nanogold hybrid PU polymer materials with different quantities of gold.

As the concentration of the soaking solution was increased from 10 to 100 mg kg⁻¹ Au³⁺ to produce the PU-b-100Au sample, the colour changed from purple to dark purple and then brown (Figure 3.14a), covering the entire range in the UV-Vis absorption spectrum. The broadening and the intensity suggest an inhomogeneity in particle size and shape and a possible presence of aggregates of the nanoparticles as was confirmed by the SEM and TEM analyses (Sections 3.5.1 and 3.6.1).

Figure 3.17 presents the Kubelka Munk transformed UV-Vis reflectance spectra for the nanogold hybrid nylon 6,6 beads materials prepared with different levels of Au³⁺ in the uptake solutions from 5 to 50 mg kg⁻¹ Au³⁺. The beads show the typical pink-purple colours for gold nanoparticles which were presented in Figure 3.14c.

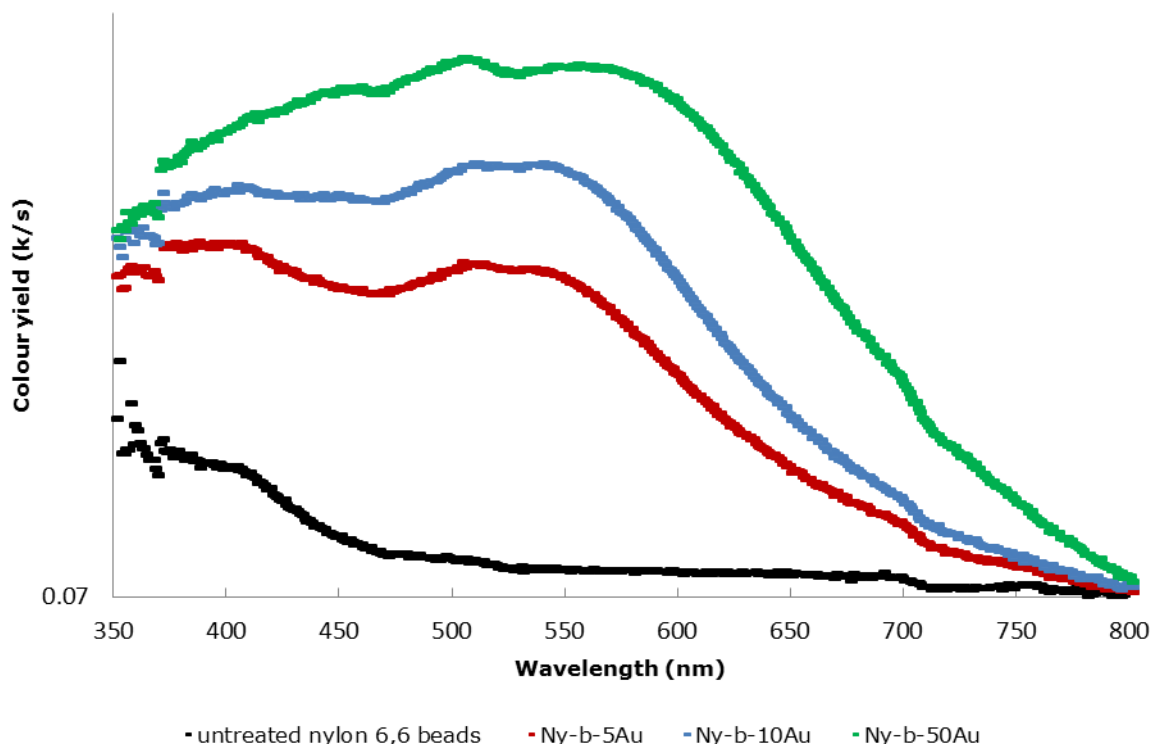


Figure 3.17: Kubelka Munk transformed UV-Vis reflectance spectra of the nanogold hybrid nylon 6,6 beads polymer materials with different quantities of gold.

For all samples the peaks at around 505 and 700 nm should be ignored as mentioned above. Nylon 6,6 beads prepared from a solution with an initial gold concentration of 5 mg kg^{-1} exhibit a peak at 510 nm and an additional peak at 535 nm which could mean the sample contains gold nanoparticles with the size of smaller than 2 nm and also nanoparticles with the size between 2 and 20 nm assuming the nanoparticles are spherical (Figure 3.17). As mentioned above, the peak position is strongly dependent on the refractive index of surrounding medium. In this case the refractive index of nylon 6,6, similar to PU, has the value of ca. 1.5 and is higher than water, resulting in a redshift to a higher wavelength. After the increasing of the Au^{3+} content from a 5 mg kg^{-1} to 10 mg kg^{-1} in the soaking solution the peak at 510 nm remains and a second peak appears at around 538 nm, which is slightly broadened due to an increase of the particle diameter and also the presence of different particle sizes of the gold nanoparticles. The colour change from light pink to pink is shown in Figure

3.14c. The third curve of Figure 3.17 characterises the sample of nylon 6,6 beads produced from a soaking solution of $50 \text{ mg kg}^{-1} \text{ Au}^{3+}$. The shift of the peak maximum from 538 nm to 556 nm and also the significant peak broadening indicates a range of particle sizes, the increase in available Au^{3+} ions leads to the formation of new small nanoparticles in addition to growth of existing particles. Furthermore, a possible aggregation of gold nanospheres results in a pronounced colour transition from pink to purple (Figure 3.14c). This is due to plasmonic coupling between particles.²⁵⁸ TEM analysis of the Ny-b-50Au sample confirmed that the gold nanoparticles exist in a variety of sizes and shapes, additionally some agglomerates of the gold nanoparticles in this material were observed (Section 3.6.1).

3.4.2 UV visible spectroscopy - colour of nanosilver hybrid polyurethane and nylon 6,6 materials

In comparison with gold, the interband transition for silver occurs in the ultraviolet region at 320 nm due to the wider energy gap between the 4d to 5sp orbitals, giving silver its shiny grey colour.^{259,260} Surface plasmon absorption bands of silver nanoparticle sols in water vary enormously in position ranging from 375 to 405 nm⁹⁷, Berry reported that spherical silver nanoparticles 5.6 nm in size dispersed in water exhibit an absorption band at 376 nm.²⁶¹ However, due to several factors such as particle size and shape as well as the dielectric constant of the surrounding medium, the presence of adsorbed species and the distance between neighbouring nanoparticles, the surface plasmon resonance band of silver nanoparticles can be shifted to longer wavelengths, in the blue region of the visible spectrum from about 400 – 490 nm²² appearing yellow to the eye. Another important factor is that silver nanoparticles are sensitive to oxidation and the presence of a silver oxide outer surface also causes a red shift of the SPRB.²¹⁵

The Kubelka Munk transformed UV-Vis reflectance spectra for the nanosilver hybrid polyurethane *dog bone* strips moulded from nanosilver hybrid PU beads

prepared with different levels of silver in the uptake solutions from a 1 to 50 mg kg⁻¹ Ag⁺, are presented in Figure 3.18. Their respective colours can be seen in Figure 3.14b. The sample which was produced from a 1 mg kg⁻¹ Ag⁺ solution showed that at around 437 nm a small peak started to form. The peak can be ascribed to the surface plasmon resonance absorption band of silver nanoparticles. This peak was more pronounced for the sample with 10 times more silver content but at an unchanged absorption position of 437 nm meaning the particle size remained the same but the particle concentration increased. Klein and Metz observed silver spheres of a size larger than 20 nm in dry gelatine which gave an absorption peak near 450 nm.²⁶¹ The refractive index of gelatine (n=1.5)⁹⁷ is very similar to those of PU and nylon 6,6 thus it is reasonable to assume that the formed silver nanoparticles in the polyurethane matrix are smaller than 20 nm. As the concentration increased to 50 mg kg⁻¹ Ag⁺ the peak of the hybrid PU *dog bone* sample broadened and the absorption maxima shifted to around 466 nm indicating an increasing size of the nanoparticles as well as a variation in particle size and the formation of some agglomerates of the silver nanoparticles as confirmed by TEM (Section 3.6.2). Again, here for all samples the peaks at around 505 and 700 nm should be ignored as these are artificial signals caused by the spectrometer.

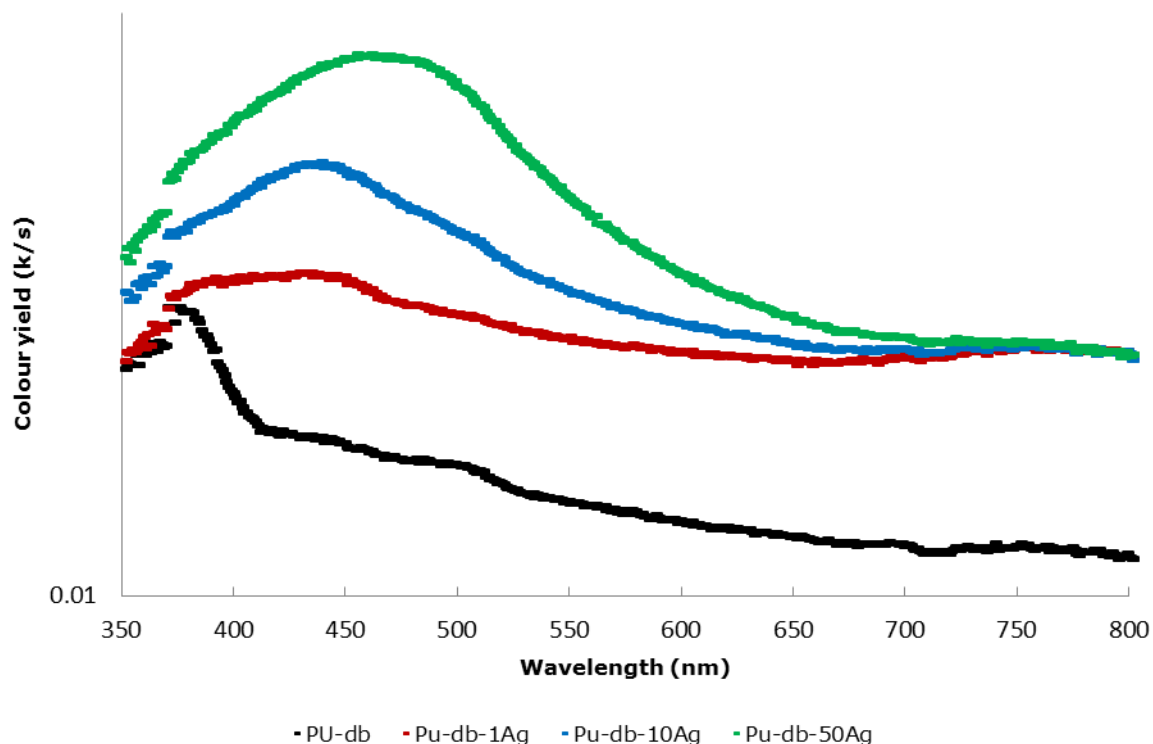


Figure 3.18: Kubelka Munk transformed UV-Vis reflectance spectra for the nanosilver hybrid polyurethane *dog bone* samples with different amounts of silver.

For the UV-Vis reflectance spectrum measurement of the nanosilver hybrid nylon 6,6 beads the peaks appearing for all samples at 410 nm can be ascribed to the nylon 6,6 itself. Figure 3.19 shows the spectra for the nanosilver hybrid nylon 6,6 beads prepared with different levels of silver in the uptake solutions from 5 to 50 mg kg⁻¹ Ag⁺. The 450 nm peak is not discernible in the hybrid nylon 6,6 beads prepared from a 5 mg kg⁻¹ silver solution but is discernible for the hybrid polymer materials prepared from a 10 mg kg⁻¹ Ag⁺ solution. This peak becomes progressively more prominent for the hybrid polymer material prepared from a 50 mg kg⁻¹ silver solution. The 450 nm peak may contain, as reported earlier similar to the nanosilver hybrid PU beads, silver nanoparticles which are around 20 nm in size. Because the peak position remains at 450 nm this could mean the particle size is not changing but more particles are formed with increasing Ag⁺ concentration which reflects in no colour change but in increase in intensity of the yellow colour shown in Figure 3.14d.

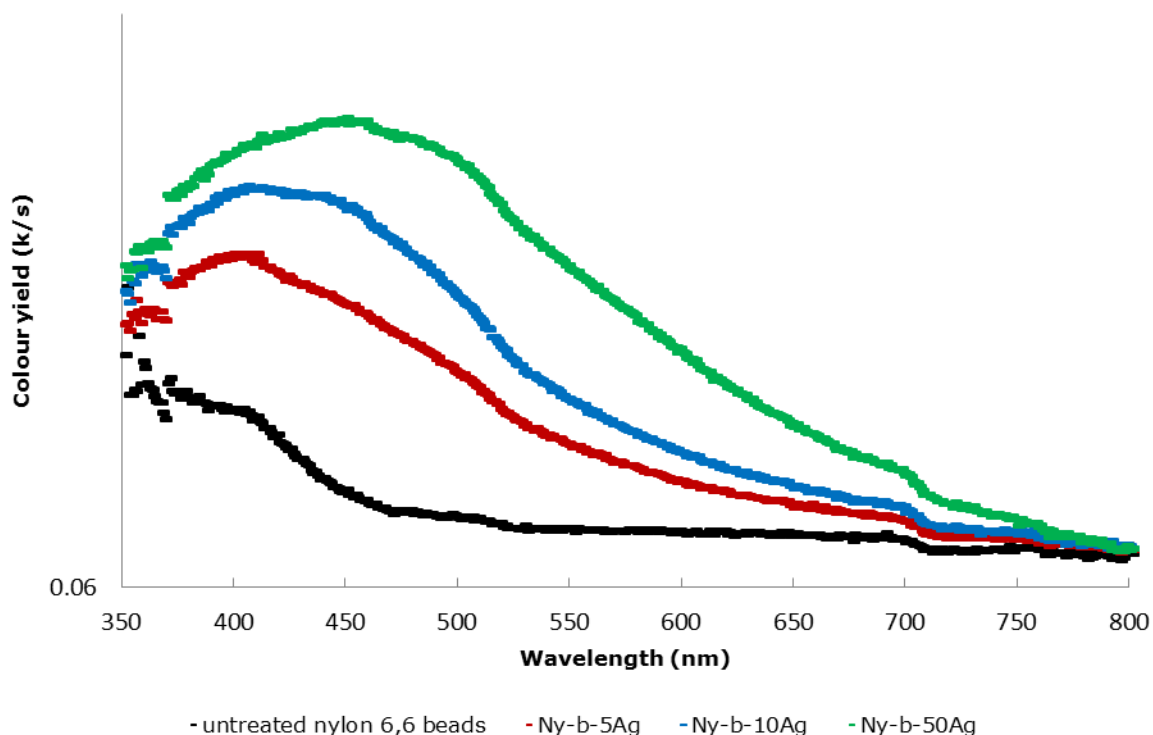


Figure 3.19: Kubelka Munk transformed UV-Vis reflectance spectra for the nanosilver hybrid nylon 6,6 beads with different amounts of silver.

Figure 3.20 presents the UV-Visible reflectance spectra for the nanosilver hybrid nylon 6,6 polymer materials in the form of sheets. The samples were prepared from solutions with starting concentrations of 10, 20, 50 and 100 mg kg⁻¹ of Ag⁺. The sample which was prepared from a 10 mg kg⁻¹ Ag⁺ solution exhibits a peak at 430 nm. With increasing the Ag⁺ concentration to 20 mg kg⁻¹ there is essentially no shift or broadening of the peak, meaning the particle size does not change with higher levels of Ag⁺ in the uptake solution. Rather, again more nanoparticles of the same size are formed which provides an increase in colour intensity. There is a noticeable peak broadening of the sample which was prepared from a 100 mg kg⁻¹ Ag⁺ soaking solution. The broadening is most likely due to particle agglomeration.

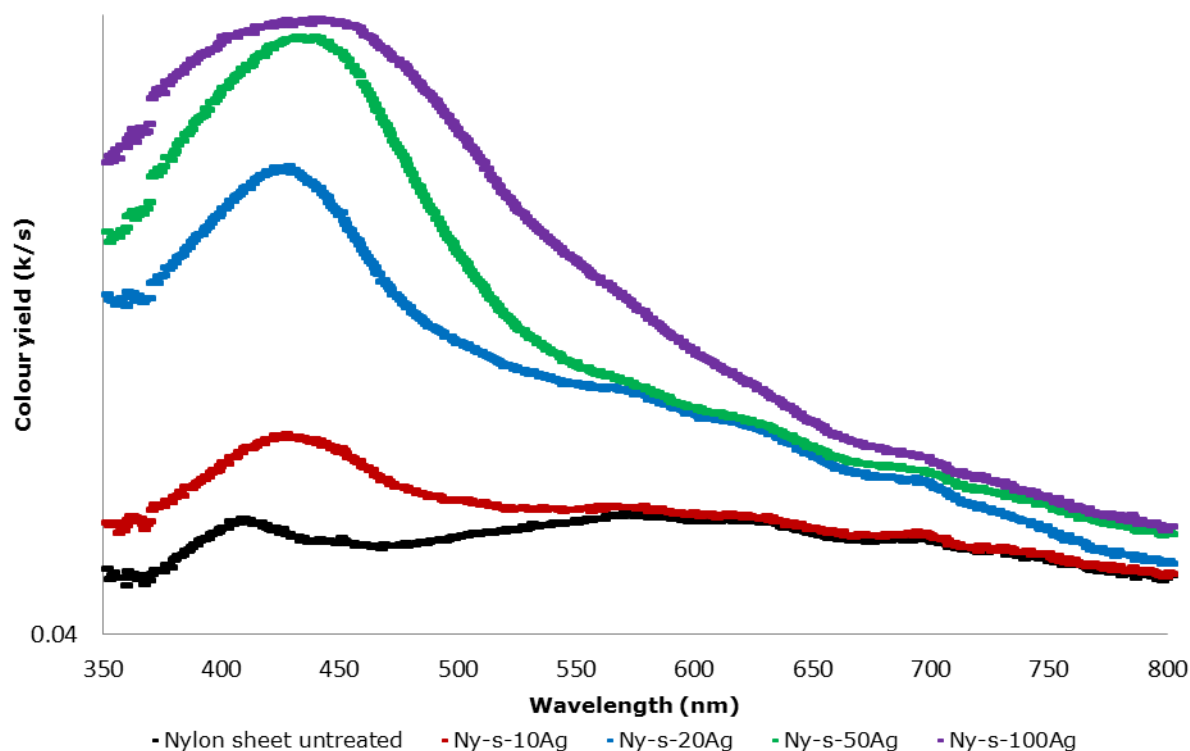


Figure 3.20: Kubelka Munk transformed UV-Vis reflectance spectra of nanosilver hybrid nylon 6,6 sheets with different amounts of silver.

3.5 Scanning electron microscopy and energy dispersive X-ray analysis of nanogold and nanosilver hybrid polymer materials

SEM analyses were run on the hybrid polymer samples with at least 0.05 % metal loading on the beads. The typical colour for gold or silver nanoparticles could already be seen in samples which contained 0.005% of metal, due to the very high extinction coefficient in the visible region from the surface plasmon resonance effect of nanogold or nanosilver. However, in the SEM nanoparticles could only be observed on samples with a higher amount of particles. To observe the interior of the hybrid polymer materials, cross sections of the PU samples were made by freezing the PU beads or sheets in liquid nitrogen following by breaking the beads or sheets into two fractions. Due to the small size of nylon 6,6 beads and the thickness of the nylon 6,6 sheets, cross sections were made by cutting the samples with a clean razor blade into two halves.

3.5.1 Scanning electron microscopy and energy dispersive X-ray analysis of nanogold and nanosilver hybrid polyurethane materials

Figure 3.21 shows SEM micrographs of surfaces of the untreated PU beads. Organic matrices such as PU and nylon 6,6 seem to suffer beam damage under high energy electron beam resulting in dark areas, an example can be seen in Figure 3.21b. The surface of the untreated PU beads appears to be smooth. SEM micrographs of the nanogold hybrid PU beads, the PU-b-50Au sample and the PU-b-500Au sample confirmed the presence of gold nanoparticles on the polymer surface at low resolution (Figure 3.22a and Figure 3.23a). The gold nanoparticles are observable in the backscatter mode as white dots. The contrast between the metal and the polymer is due to the high atomic weight of gold and the low atomic weight of the polymer atoms. A further magnification of the PU-b-50Au sample to 8000 times (Figure 3.22.b) shows a surface with high coverage of gold nanoparticles which are predominantly spherical; however, occasional larger triangular, hexagonal and rod shapes were observed. This result matched well the TEM results of the sample (Section 3.6.1). EDS elemental mapping analysis confirmed that the nanoparticles present on the PU surface are gold (Figure 3.22c). The distribution of the gold nanoparticles is reasonably uniform across the PU surface, and the intense surface plasmon band of these gold nanoparticles is responsible for the dark purple colouration of the hybrid polymer (Figure 3.24a). When the gold solution was increased from 50 to 500 mg kg⁻¹ Au³⁺ to produce the PU-b-500Au sample, nanoparticles found on the surface of the sample were larger and showed a wider spread in particle size. A few very large particles of about 1 - 2 µm were present (Figure 3.23b) which EDS analysis verifies as being gold (Figure 3.23c). Increasing the gold concentration possibly saturated the surface of the beads such that the gold concentration on the bead surfaces was so high that more nanoparticles were formed than were able to be stabilised by the substrate matrix. This resulted in particle growth via agglomeration. These particles produce the brown and metallic shiny colour of the nanogold hybrid PU beads (Figure 3.24b). As previously mentioned, the SPRB of gold or silver nanoparticles depends on the particle size and shape. Since at higher gold concentrations the formed particles on the surface of the bead have a wide range of sizes and likely exist as

agglomerates, the particles do not exhibit a distinct absorption band but cover the entire range in visible absorption spectrum thus appearing brown to our eye. A further increase of gold ion concentration results in the formation of even bigger gold particles on the surface of PU materials. These particles then assume the optical properties of the bulk metal and appear a shiny metallic colour to the eye. Additionally, EDS analysis did not detect any peaks for chlorine, implying all gold ions were reduced to metallic gold. The Cl^- ions were washed out of the beads following the reduction step in the preparation.

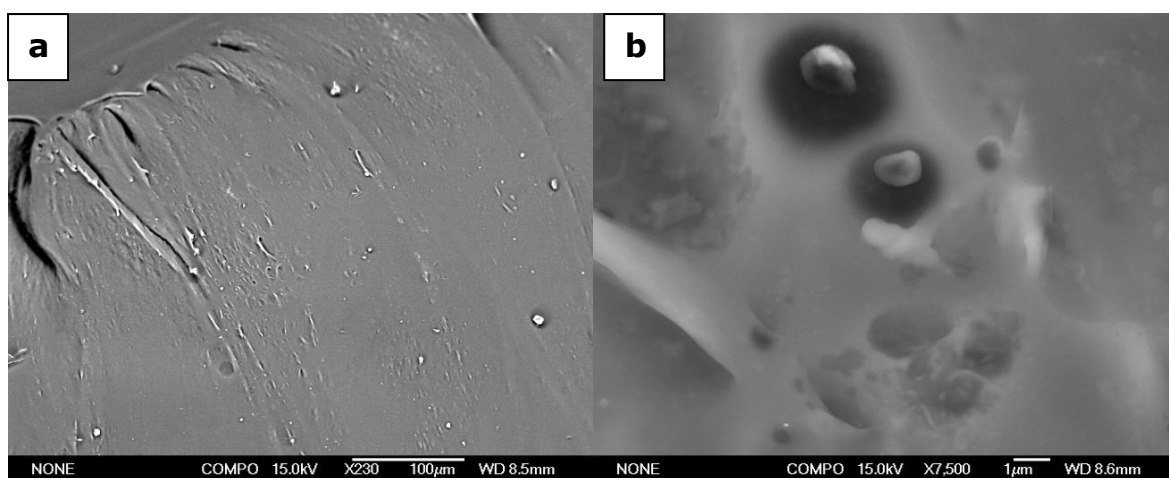


Figure 3.21: SEM micrographs in backscatter mode of the untreated PU bead surface at a) 230 and b) 7500 times magnification.

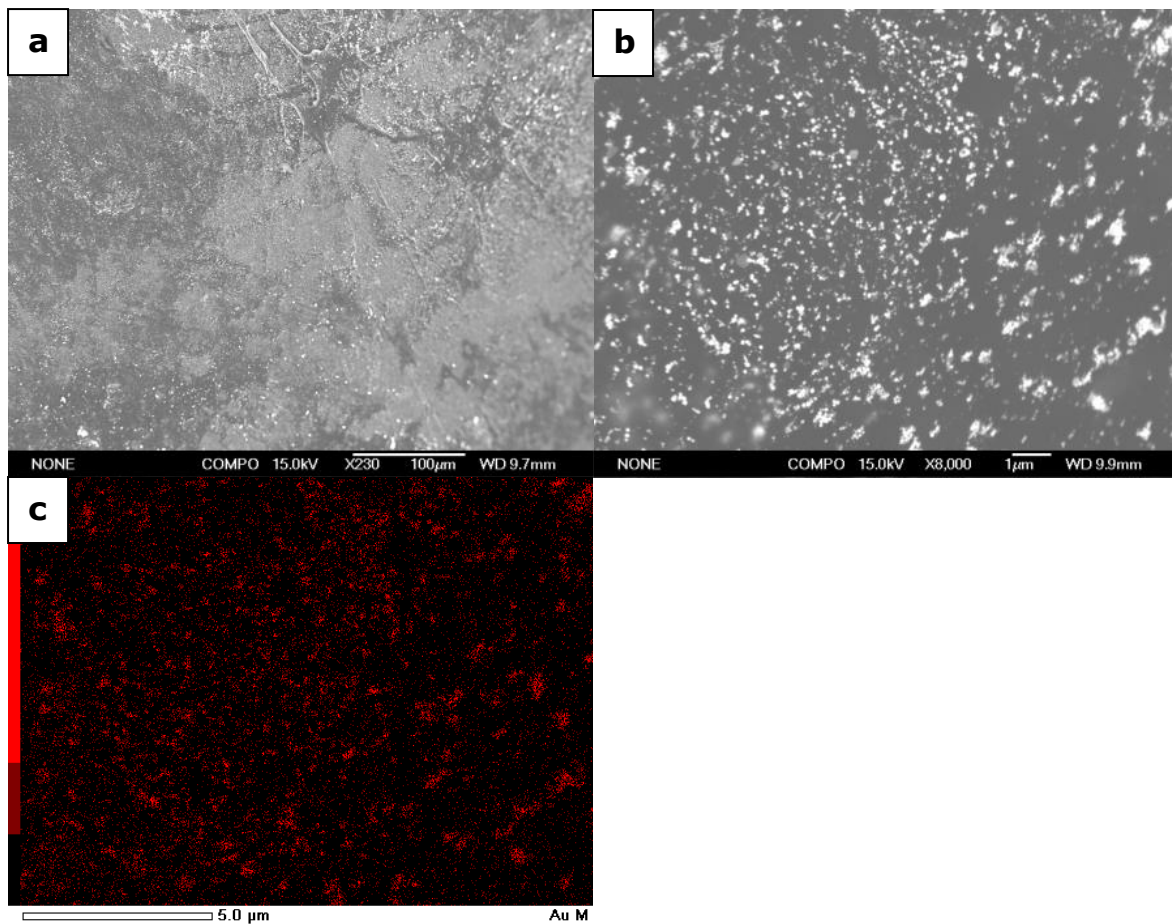


Figure 3.22: SEM micrographs in backscatter mode of the surface of the PU-b-50Au sample at a) 230 and b) 8000 times magnification with c) the respective EDS elemental analysis Au map.

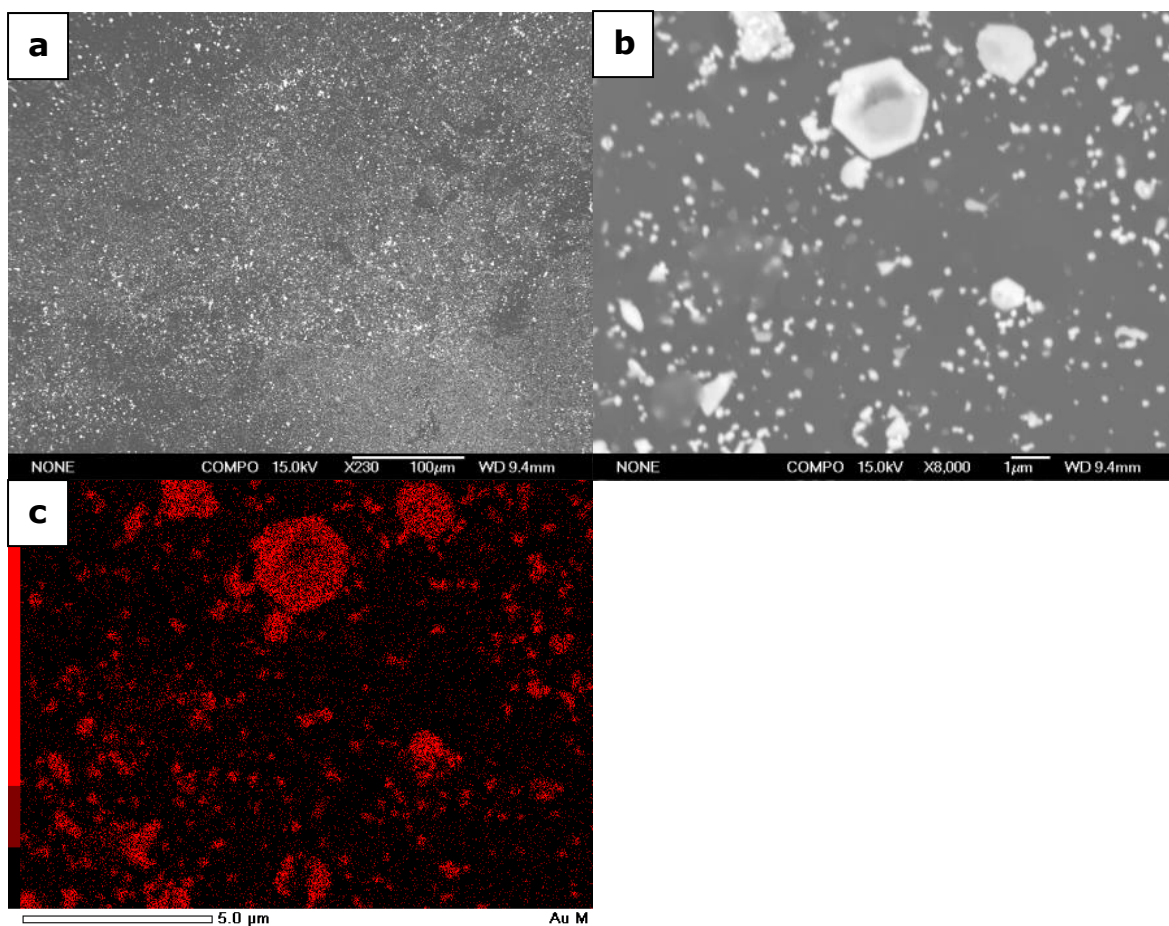


Figure 3.23: SEM micrographs in backscatter mode of the surface of the PU-b-500Au sample at a) 230 and b) 8000 times magnification with c) the respective EDS elemental analysis Au map.

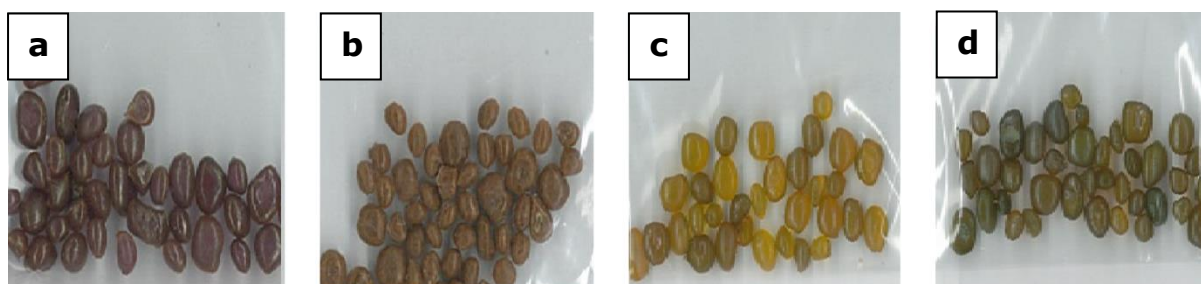


Figure 3.24: Photographs of the a) PU-b-50Au, b) PU-b-500Au, c) PU-b-50Ag and d) PU-b-500Ag samples.

At a low magnification, SEM images of nanosilver hybrid PU beads, the PU-b-50Ag and the PU-b-500Ag samples appeared similar to the untreated PU

beads. However, at a high magnification of 9500 times, the surface of the PU-b-50Ag sample exhibits high coverage of spherical bright dots smaller than 100 nm in diameter (Figure 3.25a). However, it is difficult to determine the precise size by SEM. EDS confirmed that the particles are silver (Figure 3.25c). Magnification of one of the brighter areas of high silver content shows that the silver nanoparticles are smaller than the gold nanoparticles of the PU-b-50Au sample. This was expected as studies have shown that the uptake of silver ions by polymers is generally much poorer than the uptake of gold (Sections 3.1.1 and 3.1.2) therefore less ions are present so less particle growth and agglomeration is expected. As the silver ion concentration was increased to produce the PU-b-500Ag sample, the colour of the hybrid PU beads turned from yellow to brown with metallic shimmering effect (Figure 3.24b-c). The examination of the surface by SEM revealed the formation of silver agglomerates. Figure 3.26a shows the surface of the PU-b-500Ag sample at a magnification of 8000 times. Although the nanoparticles are well distributed on the surface of the substrate, there are some different areas of varying brightness which show different densities of silver nanoparticles across the hybrid PU surface. A further magnification to 37000 times shows some areas with well distributed spherical silver nanoparticles smaller than 100 nm in diameter coexisting with some agglomerates appearing as bright round areas consisting of little spherical dots (Figure 3.26b). These agglomerates were also confirmed to be silver by the EDS mapping analysis (Figure 3.26c). Similar to the nanogold hybrid PU materials, increasing of the silver ion concentration led to particle growth on the surface of the PU polymer which is responsible for the metallic appearance of the surface of the nanosilver hybrid PU beads.

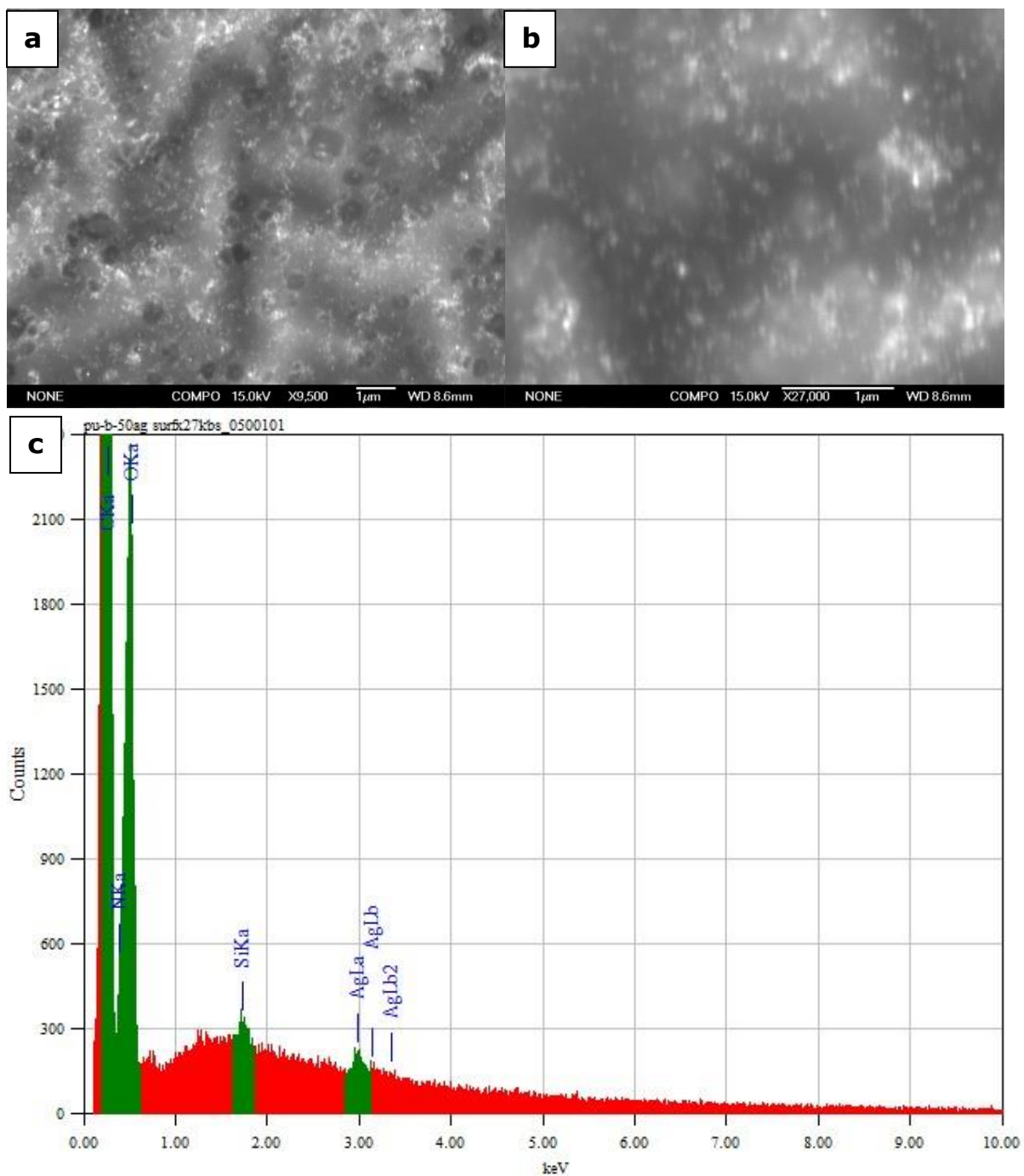


Figure 3.25: SEM micrographs in backscatter mode of the surface of the PU-b-50Ag sample at a) 9500 and b) 27000 times magnification with c) the respective EDS elemental analysis spectrum.

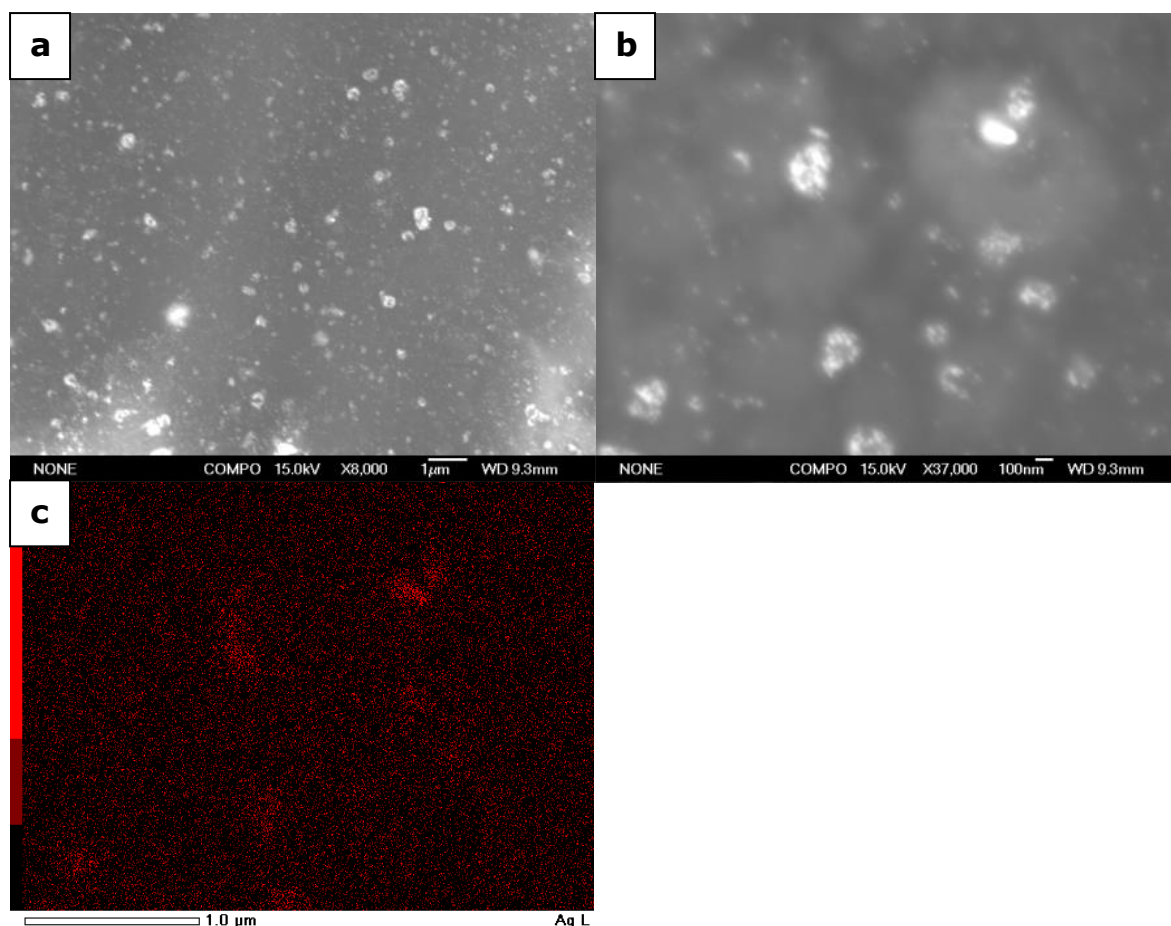


Figure 3.26: SEM micrographs in backscatter mode of the surface of the PU-b-500Ag sample at a) 8000 and b) 37000 times magnification with c) the respective EDS elemental analysis Ag map.

A cross sectional analysis was undertaken to determine the nanoparticle distribution in the polymer interior relative to the surface coverage. Figure 3.27a-c shows SEM images recorded in the backscatter mode of a cross section of the PU-b-50Au sample. At lower resolution only occasional bright particles located on the cross sectioned surface are noted, however these particles are in fact contamination particles sitting loosely on the surface. With a higher magnification an image was taken near the edge, the gold particles, appearing bright, are found on the surface and just below the surface of the PU-b-50Au sample. Some occasional spherical gold nanoparticles smaller than 100 nm in diameter were found in the centre of the bead (Figure 3.27c). However, due to instability of organic matrix under the SEM beam it was difficult to obtain higher resolution images at higher magnifications and thus to ascertain the exact size

and shape of the gold particles. The distribution of gold nanoparticles in the interior of the bead was very irregular. The colour of the cross section and hence the interior is shown in Figure 3.28a, as going from the surface towards the centre of the bead the colour loses its intensity, turning from purple to very light purple and almost transparent in the centre. The increasing of the gold solution concentration to produce the PU-b-500Au sample resulted in a complete colouration of the PU bead interior, the colour of the bead core turned dark purple while the surface appeared brown with a metallic shiny effect as previously mentioned (Figure 3.28b). The reason for the colour development in the centre of the bead is due to the higher amount of absorbed gold ions which could penetrate further into the polymer matrix where they were reduced to metallic gold nanoparticles. The colour is dependent on the particle size and shape (Section 1.4.2). Because the concentration of absorbed gold ions decreases with increasing distance to the surface, it is likely that formed gold nanoparticles in the centre of the bead are fully stabilised and isolated by the polymer matrix and therefore do not undergo agglomeration. This contrasts with the surface where the particles exhaust the stabilisation capability of the polymer resulting in aggregates and therefore exhibiting a brown colour. At a very low magnification the cross section of the PU-b-500Au sample shows a rich coverage of gold particles only on the surface (Figure 3.29a). A further magnification to 22000 times, which is presented in Figure 3.29b, shows a surface cross section of the sample near the edge. The surface of the bead is depicted on the right hand side of the image and is covered by larger gold particles, most likely agglomerates. The particles in the centre of the bead, which appeared spherical, were easily detectable (Figure 3.29c) and well distributed.

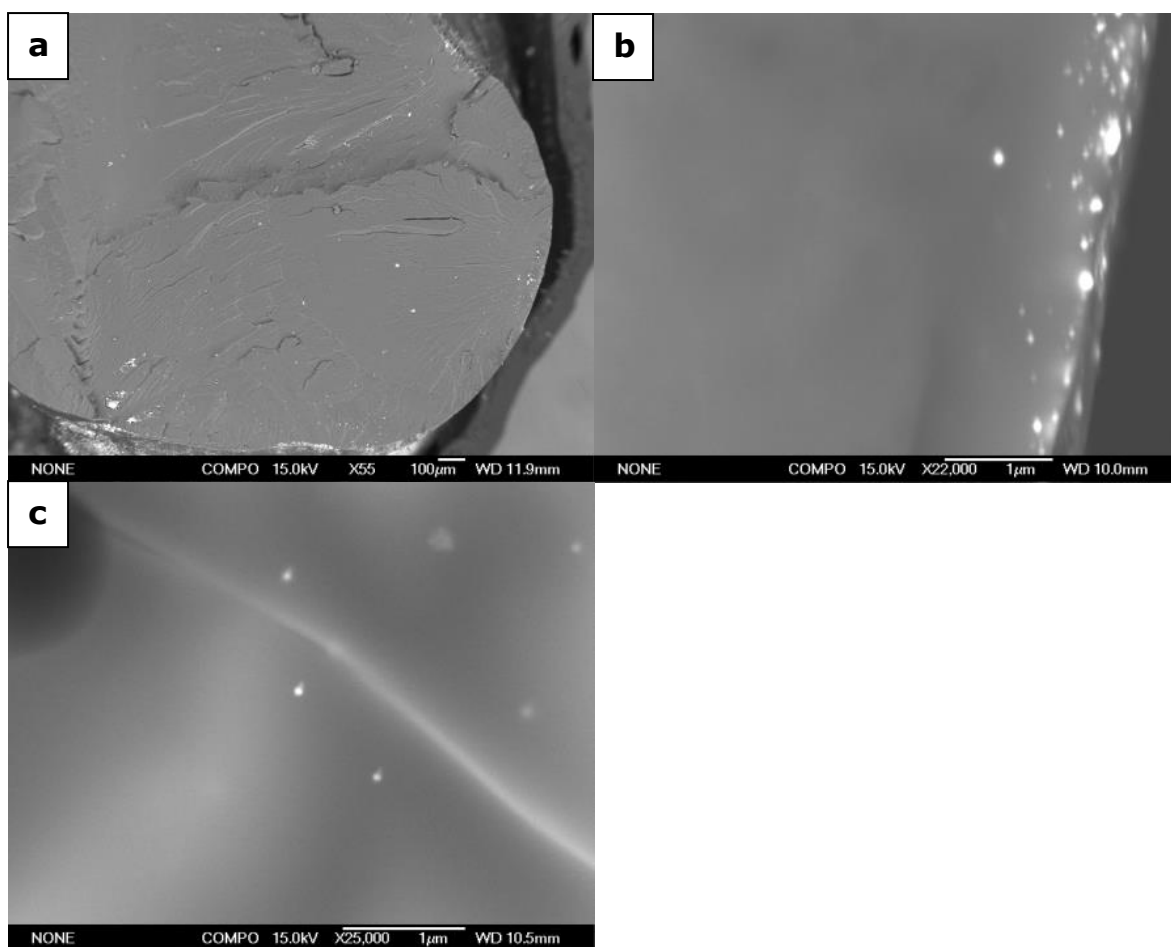


Figure 3.27: SEM micrographs in backscatter mode of a cross section of the PU-b-50Au sample at a) 55 times magnification, b) 22000 times magnification on the edge of the bead and c) 25000 times magnification in the centre of the bead.



Figure 3.28: Photographs of sliced cross sections of the PU-b-50Au (left) and PU-b-500Au (right) samples.

Figure 3.30 shows SEM micrographs and corresponding gold EDS maps of a nanogold hybrid polyurethane *dog bone* strip which was moulded from the PU beads produced from a 50 mg kg^{-1} gold solution (PU-b-50Au). The sample is brown in colour. SEM confirmed that during the moulding process the gold nanoparticles were distributed evenly throughout the plastic. At a magnification of 6500 times, the particles were found to be varying in sizes and shapes but mostly spherical particles could be seen. However, occasional triangles, hexagonal and rod shaped particles were also observed.

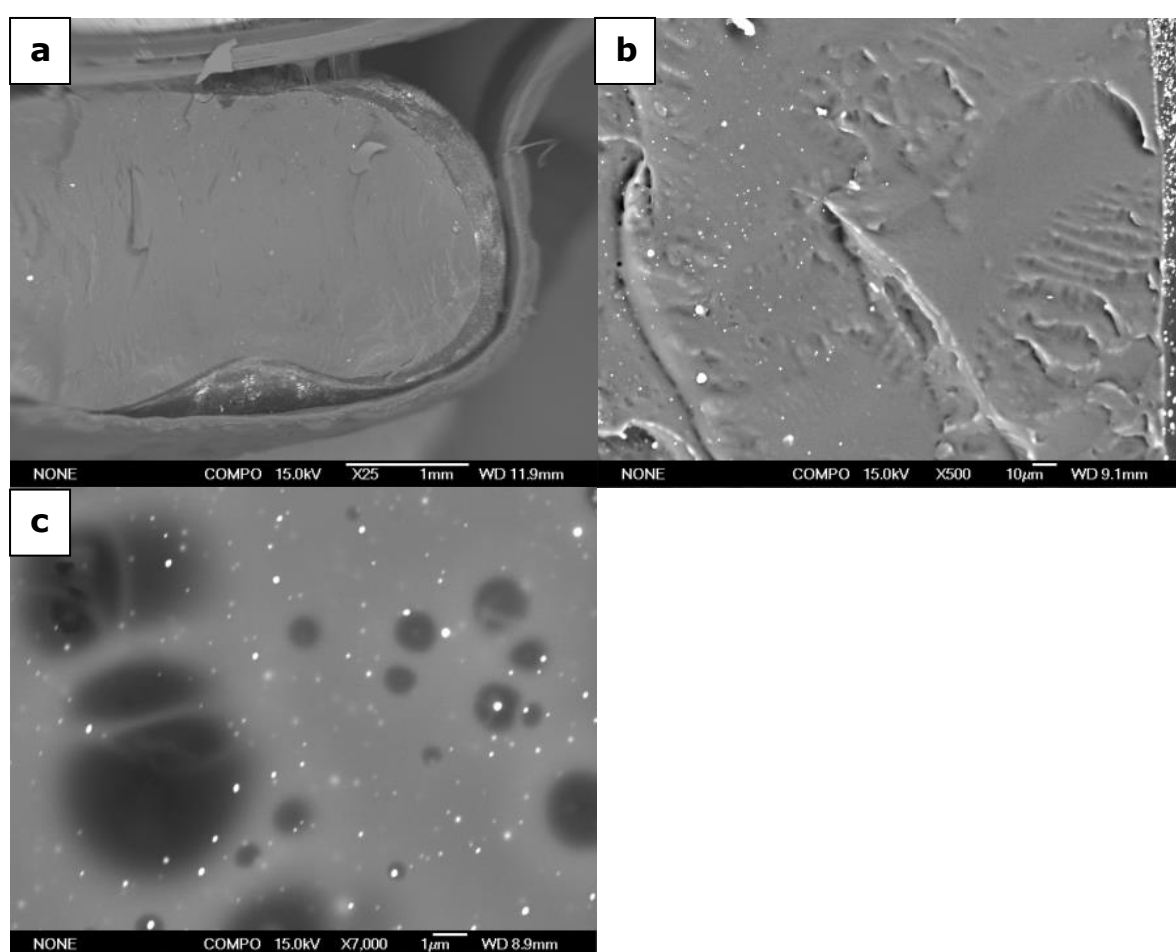


Figure 3.29: SEM micrographs in backscatter mode of a cross section area of the PU-b-500Au sample at a) 25 times magnification, b) 500 times magnification on the edge of the bead and c) 7000 times magnification around the centre of the PU bead.

This confirms that during the moulding process of the PU-b-50Au the larger particles which were located on the surface were mixed with smaller gold particles of the bead interior. This result is consistent with the UV-Vis spectrum (Figure 3.16) of the PU-b-50Au sample showing no typical distinct surface plasmon resonance band for gold nanoparticles at about 530 nm but rather covering the whole visible absorbance range. EDS confirmed the bright white particles evident within the nanogold hybrid PU *dog bone* sample were gold. In TEM analysis of the PU-b-50Au sample particles up to 450 nm in size and particle agglomerates were observed.

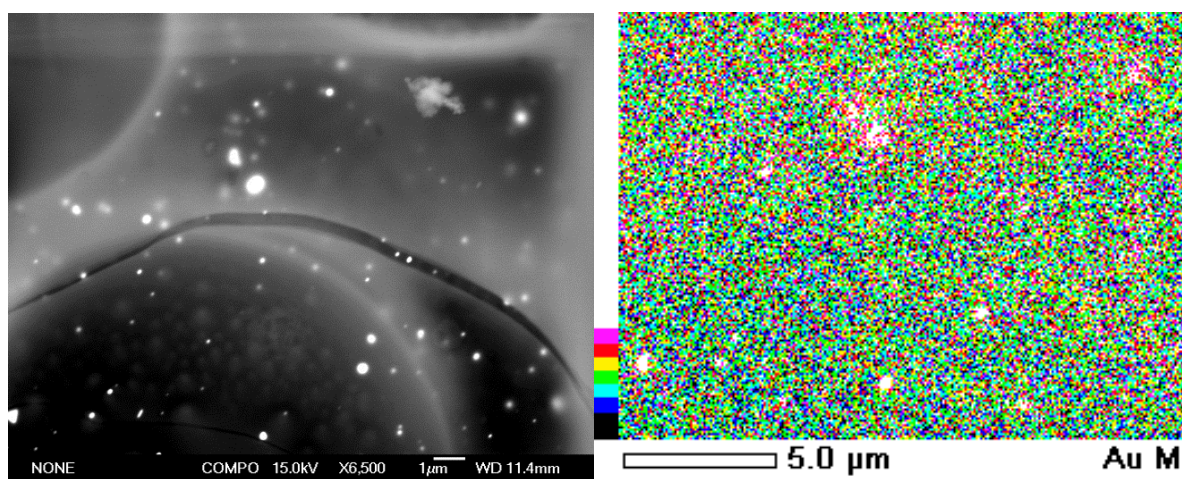


Figure 3.30: SEM micrograph of the nanogold hybrid PU *dog bone* strip (left) the corresponding Au EDS map (right).

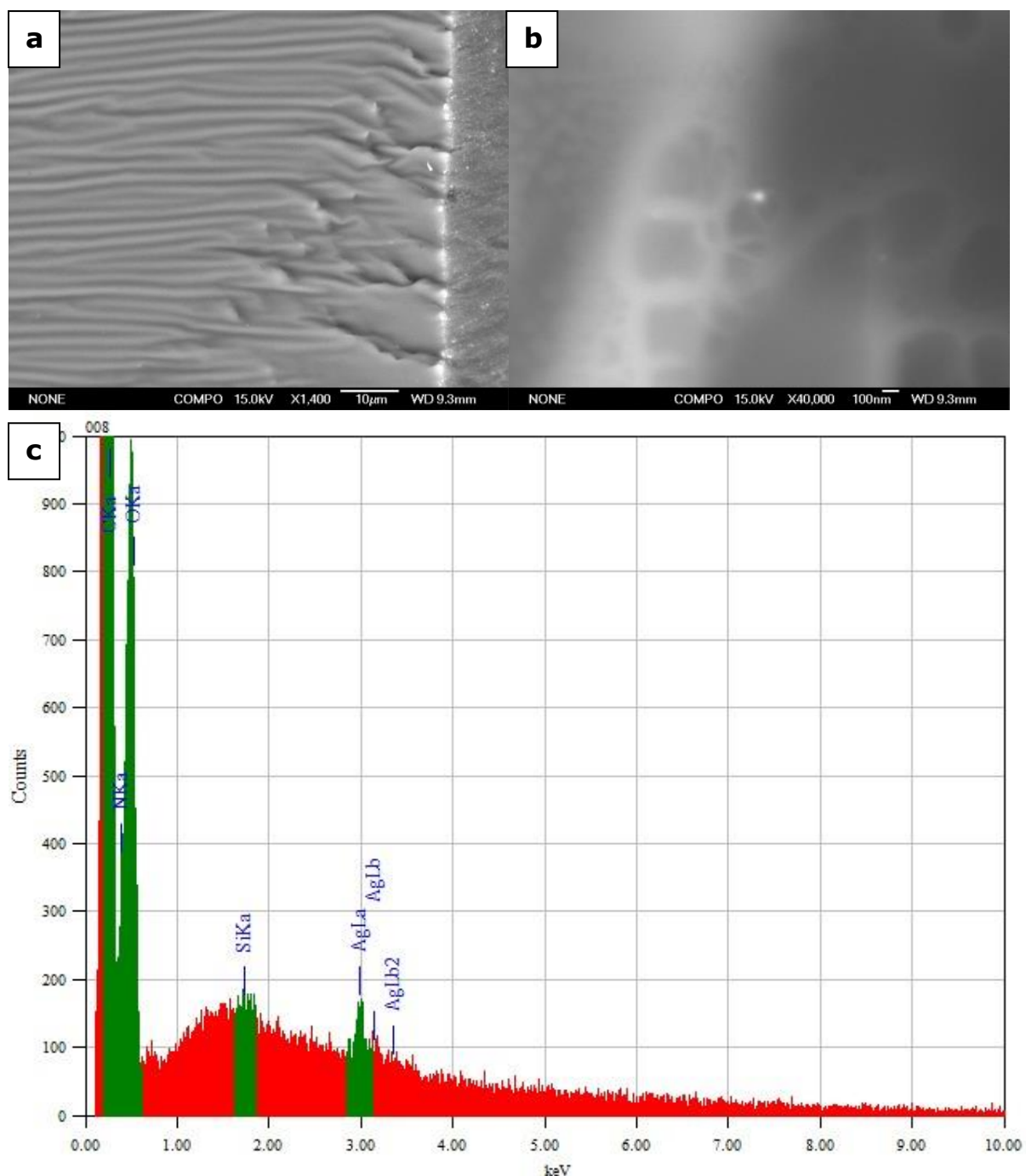


Figure 3.31: SEM micrographs in backscatter mode of a cross section area of the PU-b-50Ag sample at a) 1400 times magnification on the edge of the bead and b) at 40 000 times magnification in the centre of the bead together with c) the respective EDS spectrum.

SEM analyses of cross sections of the nanosilver hybrid PU materials proved to be somewhat difficult. Similar to the surface analysis, the particles in the interior seem to be smaller and scarcer than those observed in the corresponding

nanogold hybrid PU materials. Uptake studies have shown that uptake of silver ions by the polymer substrates was not as efficient or abundant as that of gold ions. Thus, imaging at a higher magnification was required. Figure 3.31a presents the image of the cross section area of the PU-b-50Ag sample. At a magnification of 1400 times, silver particles appear to be on the surface and just under the surface respectively (Figure 3.31b). The EDS elemental analysis verified the particles as being silver. When analysing the area near the centre of the bead single sparsely distributed spherical particles were observed. The size of the particles was smaller than 100 nm in diameter; however, it was difficult to determine the exact size by SEM. These particles give rise to the interior of the bead being evenly yellow coloured with a dark yellow tending to a brown surface colour instead of gradually changing colour when moving towards the centre, as observed in the nanogold hybrid PU beads. TEM analysis of this sample showed that in general the particles were spherical and of a size between 5 and 50 nm in diameter. Figure 3.32a-b shows a SEM image of the cross section of the PU-b-500Ag sample. The silver nanoparticles observed in the bead interior were spherical and smaller than 100 nm in diameter. The coverage over the entire bead seems to be rich and uniform, indicating that the Ag^+ penetrated the entire bead where they were reduced to Ag^0 and simultaneously stabilised by PU matrix.

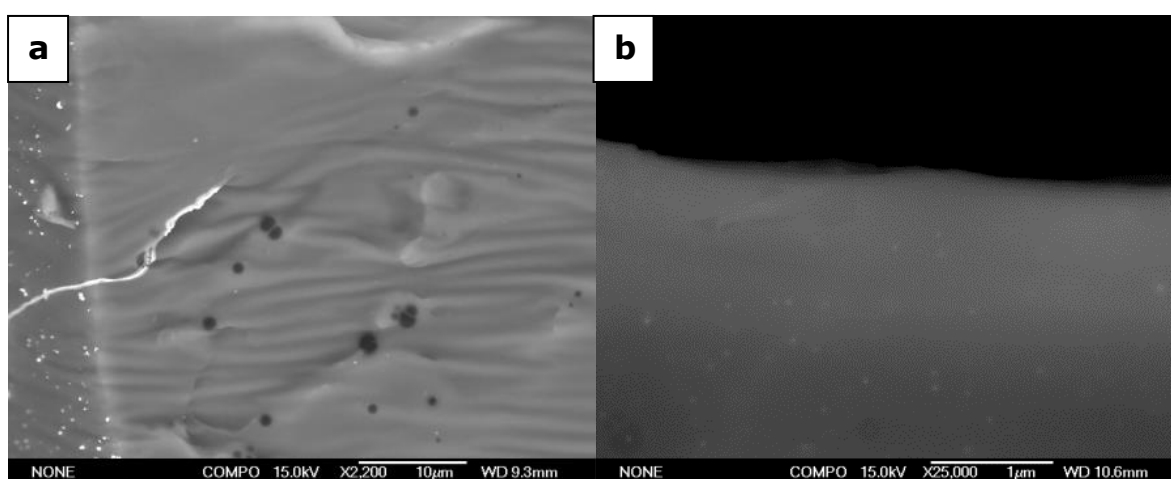


Figure 3.32: SEM micrographs in backscatter mode of a cross section of the PU-b-500Ag sample at a) 2200 and b) 25000 times magnification near the edge of the bead.

3.5.2 Scanning electron microscopy and energy dispersive X-ray analysis of nanogold and nanosilver hybrid nylon 6,6 materials

The examination of the surface of the untreated and the nanogold and nanosilver hybrid nylon 6,6 beads was similarly carried out via SEM analyses. Figure 3.33 presents secondary electron and backscatter mode of the surface of the untreated nylon 6,6 bead at a low magnification. The surface appears to be relatively smooth. SEM studies, recorded in backscatter mode, show that at low magnifications the Ny-b-50Au sample appears similar to the untreated nylon 6,6 bead (Figure 3.34a). However, on increasing the magnification to 40000 times (Figure 3.34b) bright white spots become observable, which were confirmed by EDS elemental analysis to be gold. The particles appeared to be smaller than 100 nm, however some agglomerates were observed. In general the particles seem to be smaller than the analogue polyurethane sample, which could be due to the available gold ions in the nylon 6,6 matrix that can be reduced by the polymer to gold nanoparticles. As the uptake studies have shown, PU is able to absorb higher amounts of gold ions than nylon 6,6 substrate which is presumably due to the higher porosity of the PU compared to the nylon 6,6 substrates. Examination of the Ny-b-500Au sample has revealed a high coverage of gold particles on the surface of the bead which were easily detectable at a low magnification of 60 times (Figure 3.35a). At a higher magnification of 9500 times, gold particles with distinct geometrical shapes, such as triangular, hexagonal and rods were observed (Figure 3.35b). Although occasionally spherical particles smaller than 100 nm are seen, most gold particles were formed on the microscale. The gold particles were confirmed by EDS (Figure 3.35c-d). Similar to the nanogold hybrid PU materials, due to the oversaturation of the bead surface with gold ions, more particles were formed than were able to be stabilised by the polymer matrix of the nylon 6,6 substrate. This resulted in the continued aggregation of the nanoparticles producing large, microscale gold particles. This lowers the surface energy of the nanoparticles, and stabilises the nanoparticles by aggregation. As expected, the Ny-b-500Au sample in comparison to the Ny-b-50Au sample was dark purple, almost brown in colour and exhibited a typical gold lustre, similar to the comparable nanogold hybrid PU samples. Figure 3.36 presents the photographs of both samples. In the EDS

elemental analysis for the Ny-b-50Au and the Ny-b-500Au samples respectively, chlorine was also detected, which is due to unreduced $[\text{AuCl}_4]^-$ and also free Cl^- ions. However, this is discussed further in Section 3.8.1.

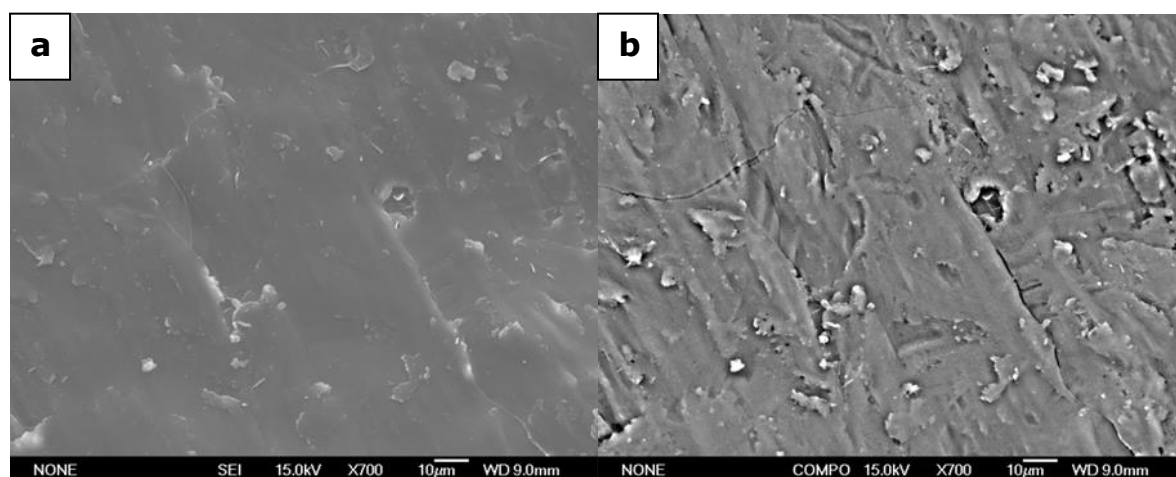


Figure 3.33: SEM micrographs of the untreated nylon 6,6 bead surface (secondary electron and backscatter mode).

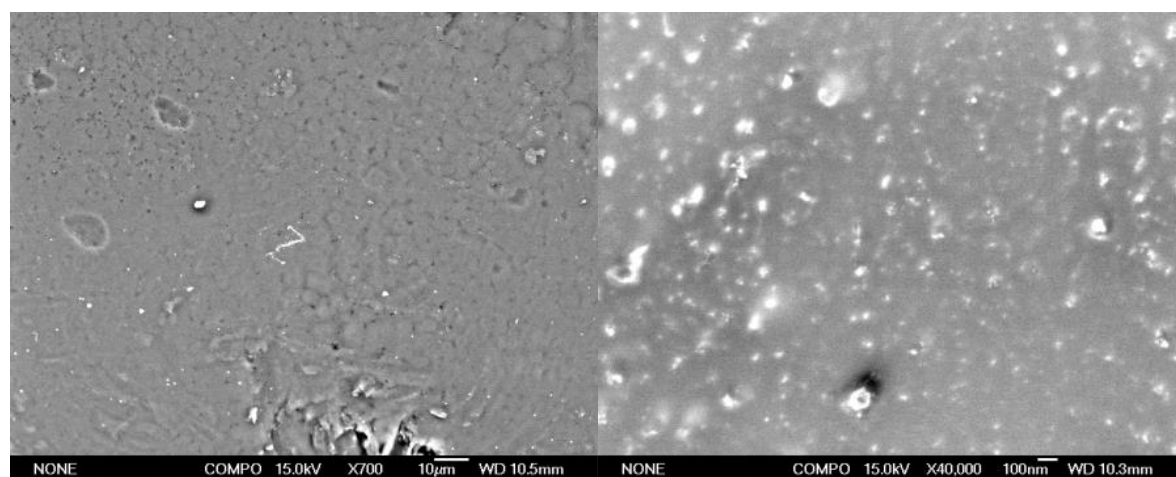


Figure 3.34: SEM micrographs in backscatter mode at increasing magnifications of the surface Ny-b-50Au sample.

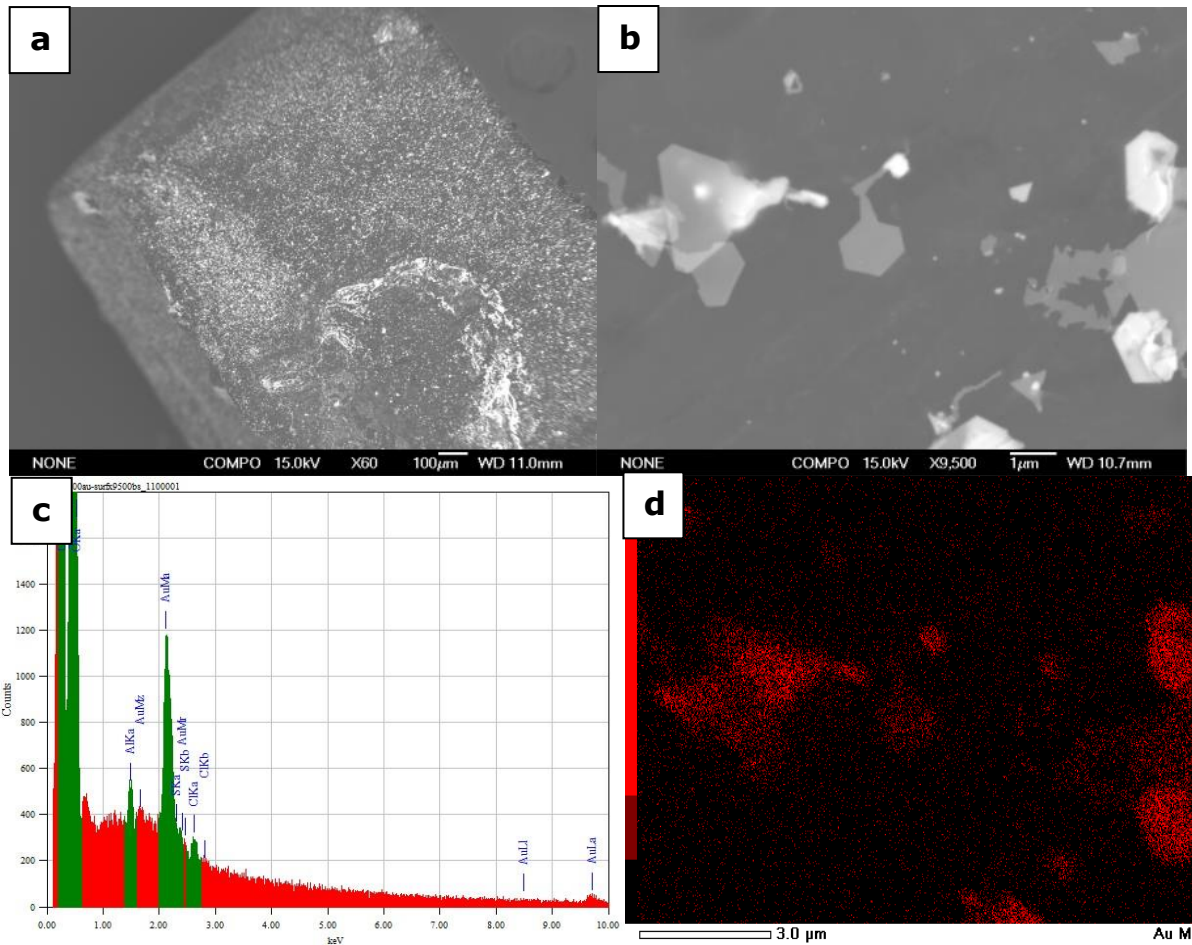


Figure 3.35: SEM micrographs in backscatter mode at increasing magnifications of a-b) the surface of the Ny-b-500Au sample with c-d) respective elemental analyses spectrum and Au map.



Figure 3.36: Photographs of Ny-b-50Au (left) and Ny-b-500Au (right) samples with their respective cross sections below.

Figure 3.37 shows SEM photographs of the surface of the Ny-b-50Ag sample at different magnifications with the respective EDS elemental analysis spectrum. At a low magnification the surface of the Ny-b-50Ag sample seems to be similar to the untreated nylon 6,6 bead. However, with further magnification to 9500 times the surface shows a high coverage of bright dots which EDS confirms as being silver (Figure 3.37c). The particles are in nanoscale however it is difficult to accurately ascertain the size of the silver nanoparticles on the surface of the nylon 6,6 bead due to the resolution limit of the SEM and slight charging of the materials. Thus, particle agglomeration cannot be excluded.

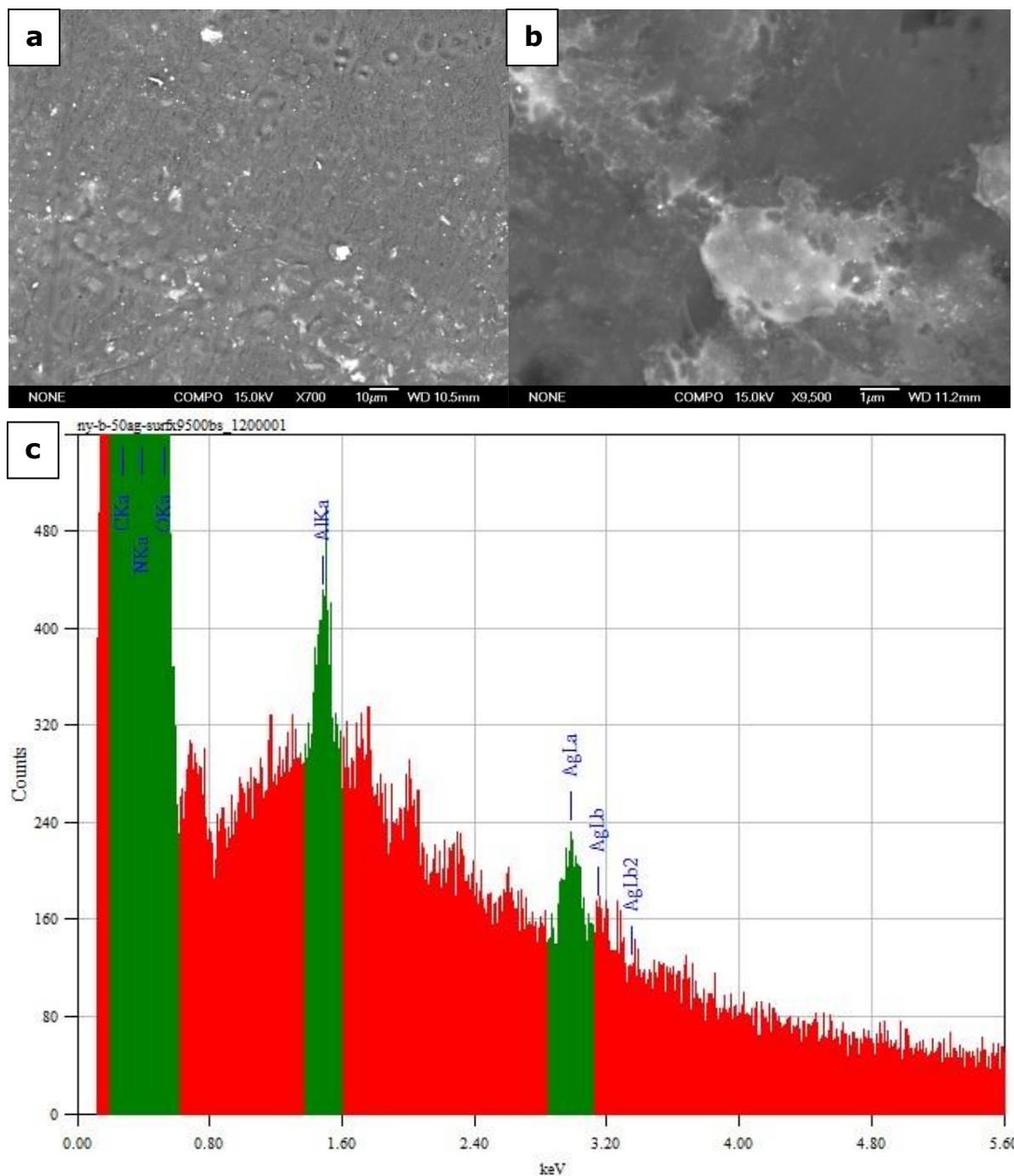


Figure 3.37: SEM micrographs in backscatter mode at increasing magnifications of a-b) the surface of the Ny-b-50Ag sample with c) the respective elemental analysis spectrum.

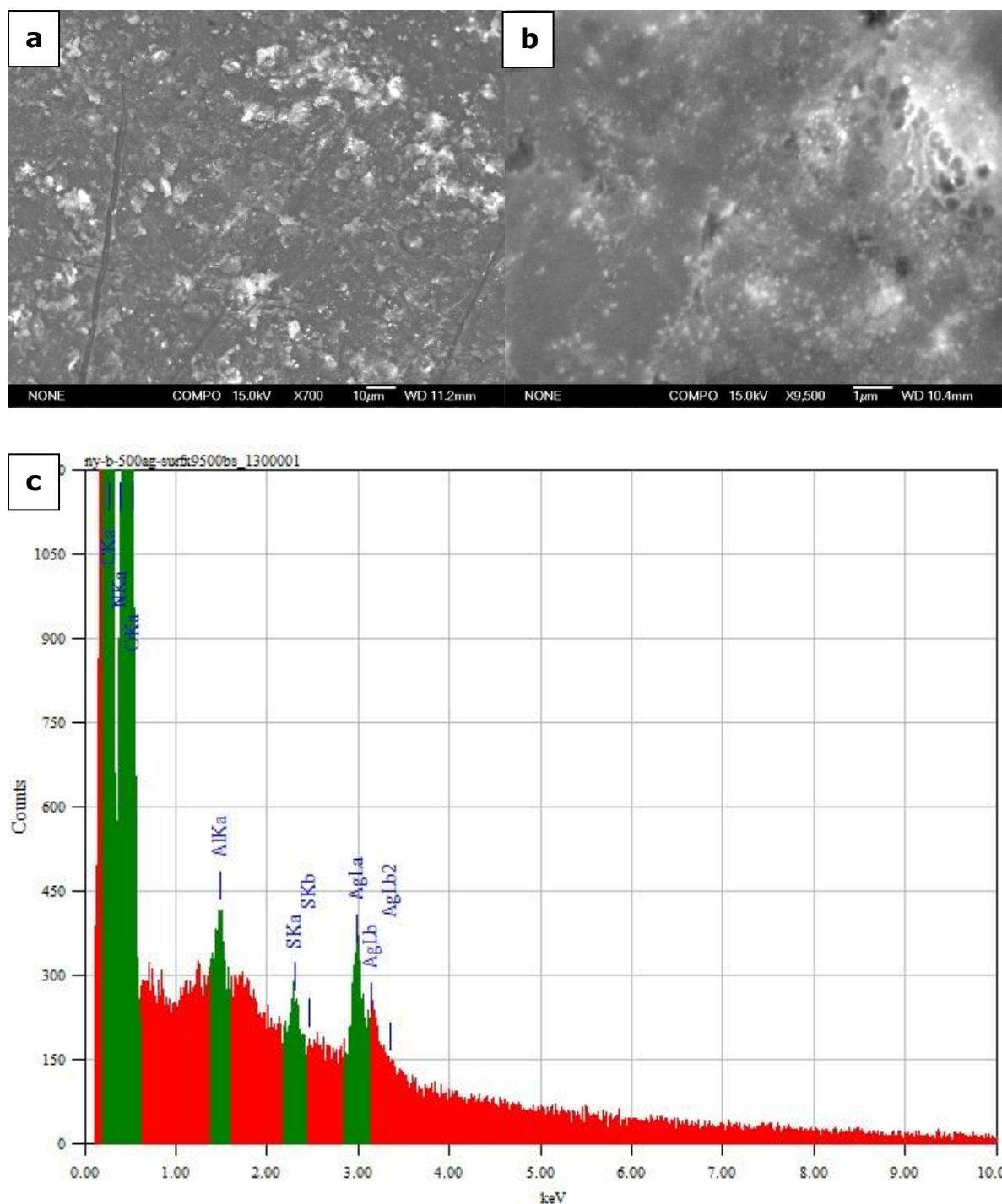


Figure 3.38: SEM micrographs in backscatter mode at increasing magnifications of a-b) the surface of the Ny-b-500Ag sample with c) the respective elemental analysis spectrum.

As the silver ion concentration was increased to synthesise Ny-b-500Ag sample, the surface colour of the hybrid PU beads turned light brown. Figure 3.38 shows SEM images of the surface of the Ny-b-500Ag sample with the corresponding

EDS elemental analysis spectrum shown in Figure 3.38c. In contrast to the Ny-b-50Ag sample the surface of the Ny-b-500Ag sample at the magnification of 700 times shows small bright spots depicting silver. Increasing the silver ion concentration, from 50 to 500 mg kg⁻¹ Ag⁺ led to particle propagation and a possible particle growth via agglomeration on the surface of nylon 6,6. A further magnification to 9500 times shows that the surface has essentially a full coverage of silver particles (Figure 3.38b). Again, the particle size could not be measured accurately due to the resolution of the SEM and charging behaviour of the materials. Generally, the silver nanoparticles appear to be spherical and smaller than the analogue nanogold sample. Similar behaviour was seen in nanogold and nanosilver hybrid PU materials and is again believed to be due to the difference in the uptake of gold and silver ions by the polymer substrates. As reported in Sections 3.1.1 and 3.1.2 the uptake studies have shown that the uptake of silver ions by the polymer substrates is usually much poorer than the uptake of gold. Thus, smaller amounts of silver ions are present for reduction to nanosilver particles, which are stabilised by the nylon 6,6 matrix.

In a similar approach to characterise the interior of synthesised hybrid nylon 6,6 materials, cross sections were prepared by cutting the nylon 6,6 beads into slices. The slices were then studied by SEM and EDS. Figure 3.39 shows a cross section of the untreated nylon 6,6 bead. The surface appears very smooth due to the clean cut with a blade.

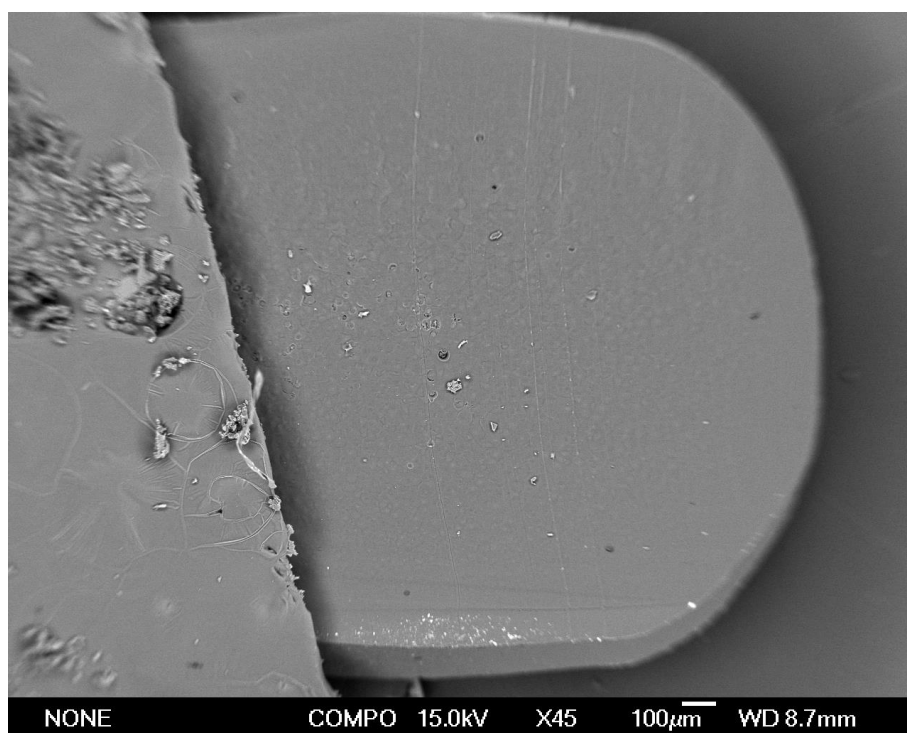


Figure 3.39: SEM micrograph in backscatter mode of the surface cross section of an untreated nylon 6,6 bead.

Figure 3.40a presents the SEM micrographs recorded in the backscatter mode of the cross section surface of the Ny-b-50Au sample. At a magnification of 90 times, a bright ring about 60 μm from the edge into the bead interior was observed. The bright ring in the backscatter image corresponds with the area of high gold concentration in the gold EDS analysis image (Figure 3.40b). This suggests that within the 24 hours reaction time the gold ions (in form of $[\text{AuCl}_4]^-$) penetrated the first ca. 60 μm of the nylon 6,6 bead where they were reduced to metallic gold and subsequently stabilised by the surrounding nylon 6,6 matrix. When the concentration of the gold ion solution was increased to 500 $\text{mg kg}^{-1}\text{Au}^{3+}$, the gold ions penetrated the beads further into the matrix. A similar behaviour to the cross section of the Ny-b-50Au sample was observed for the Ny-b-500Au sample. The gold particles were concentrated mostly in a 160 μm thick ring which was ca. 80 μm in from the edge of the bead (Figure 3.41a). A further magnification to 15000 times revealed that the particles within this ring are spherical and generally smaller than 100 nm in diameter. However, some randomly distributed agglomerates were observed which are several 100

nm in size, indicating that the nylon 6,6 matrix, composed of randomly orientated polymer chains, is not able to provide a uniform stabilisation of gold particles. The penetration of the gold was also confirmed by the photographs of a cross section area of the Ny-b-50Au and Ny-b-500Au sample respectively which are shown in Figure 3.36. The sample with the lower concentration of gold (Ny-b-50Au) appears purple only on the surface or just below the surface, whereas the sample with higher concentration of gold (Ny-b-500Au) has a rather transparent edge and dark purple ring in from the edge of the nylon 6,6 bead. As previously mentioned, these colours are due to surface plasmon resonance effect of gold nanoparticles. To investigate how the soaking time and reaction temperature influenced the penetration of the gold into the polymer matrix the reaction conditions were changed slightly and a new nanogold hybrid nylon 6,6 sample was prepared. Instead of heating the beads in 500 mg kg⁻¹ gold solution for 24 hours, the beads were immersed in 500 mg kg⁻¹ gold solution and left at room temperature for 24 hours. Subsequently the sample was heated to 50 °C for another 24 hours. It was hoped that in first 24 hours the gold ions had time to penetrate the polymer matrix further without being reduced to Au⁰. Then, a temperature increase to 50 °C for further 24 hours was employed to promote the reduction of absorbed ions in order to form metallic gold nanoparticles. Within the first 24 hours at the room temperature, the colour of the gold solution progressively lost its yellow intensity due to the (AuCl₄⁻) ions in solution while the beads became yellow showing that these (AuCl₄⁻) ions had diffused into the polymer matrix. The typical purple colour for gold nanoparticles first started to appear when the temperature was increased to 50 °C. Figure 3.42a-b presents SEM micrographs of the cross section of such sample with the respective EDS map. The gold particles were mostly concentrated in the centre and on the surface of the nylon 6,6 bead.

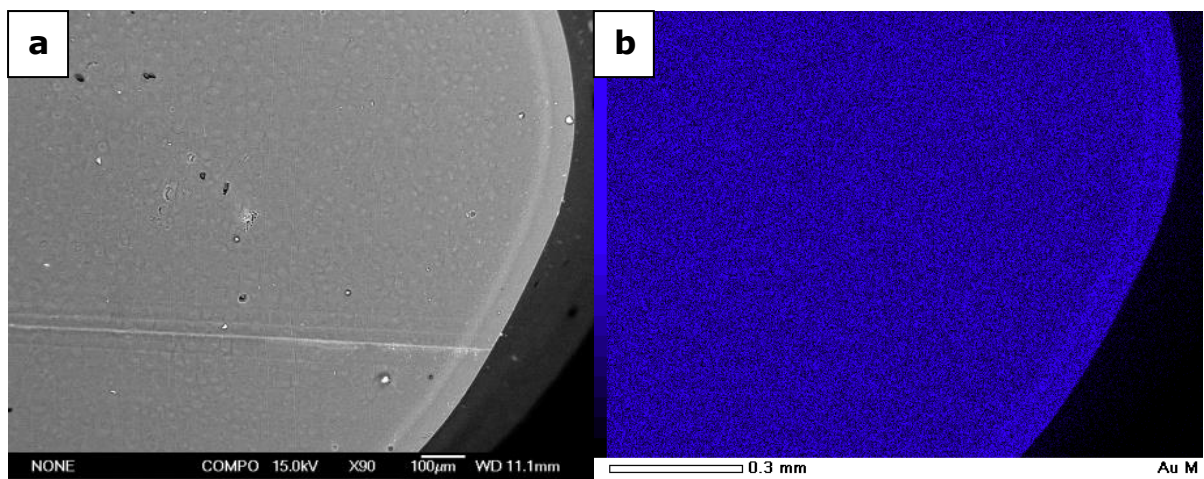


Figure 3.40: SEM micrograph in backscatter mode of a) a surface cross section of the Ny-b-50Au sample with b) respective EDS elemental analysis map.

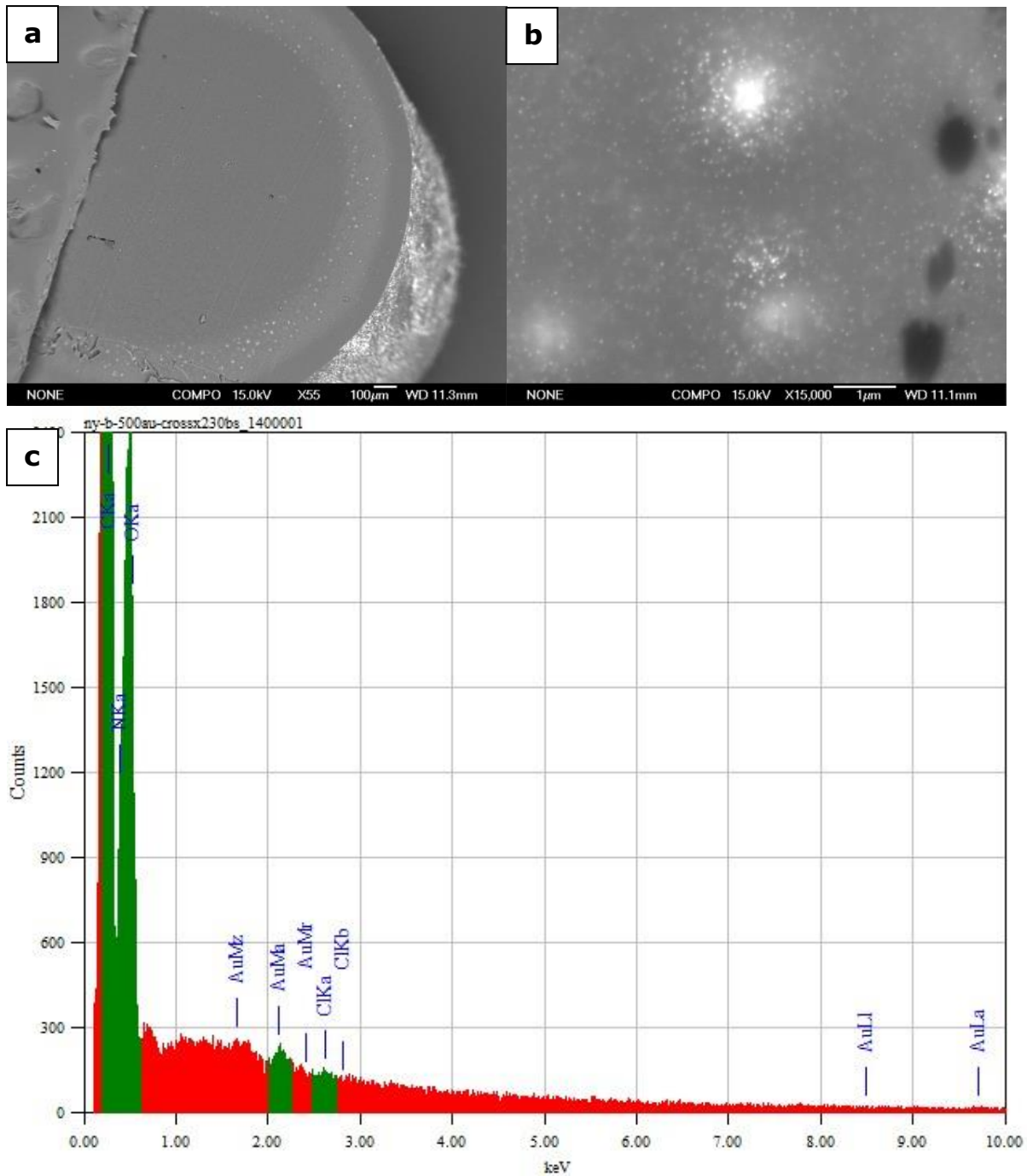


Figure 3.41: SEM micrographs in backscatter mode at increasing magnifications of a-b) a surface cross section of the Ny-b-500Au sample with c) the respective EDS elemental analysis spectrum.

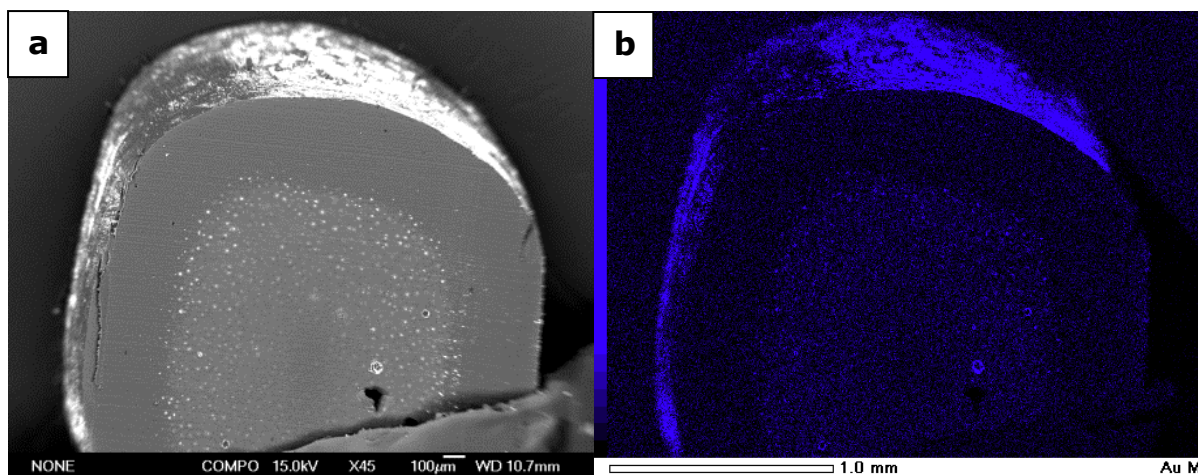


Figure 3.42: SEM micrographs in backscatter mode of the cross section area of a) the nanogold hybrid nylon 6,6 bead prepared by soaking the bead in 500 mg kg⁻¹ gold solution at room temperature for 24 hours subsequently increasing the temperature to 50 °C for further 24 hours; b) the respective EDS elemental analysis spectrum.

Examination of the nanosilver hybrid nylon 6,6 beads proved to be rather difficult. For the cross section area of the Ny-b-50Ag sample no silver could be detected in the centre of the bead. Rather the silver nanoparticles seemed to be located on the surface or just below the surface. However, it could not be ruled out that the nanoparticles found below the surface were particles carried by the razor blade while cutting the cross section. The cross sectioned bead was colourless throughout the bead but exhibited yellow colour on the surface. This colour is consistent with surface plasmon resonance band of silver nanoparticles (Section 1.4.2). When the concentration of silver ions was increased to prepare the Ny-b-500Ag sample, the colour of the surface became brown. However the interior of the bead again remained colourless. Figure 3.43 presents the SEM micrographs of a cross section area of the Ny-b-500Ag sample at different magnifications. Again, due to the resolution of the SEM and charging of the material silver particles it was difficult to image at higher magnifications. However, very small nanoparticles were found just under the surface. Since the silver solution is slightly acidic (pH 5) the nylon 6,6 polymer functional groups are protonated during the production of nanosilver hybrid nylon 6,6 materials and thus have a positive net charge. This positive net charge hinders the positive charged silver ions from penetrating the polymer matrix further where

they then can be reduced and stabilised. Thus, the absorption and reduction of silver ions to metallic silver takes place on the top layer of the nylon 6,6 surface. By contrast, the gold ions are absorbed in form of $[\text{AuCl}_4]^-$. There is electrostatical interaction of protonated nylon 6,6 functional groups and the $[\text{AuCl}_4]^-$ ions, thus the gold nanoparticles are formed within the polymer matrix, as already reported.

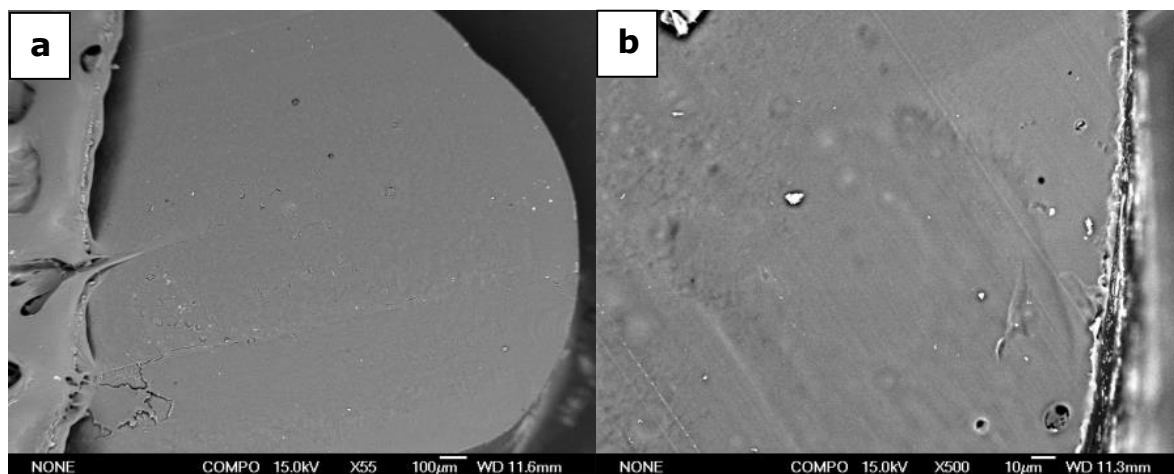


Figure 3.43: SEM micrographs in backscatter mode of the cross section area of the Ny-b-500Ag sample at different magnifications.

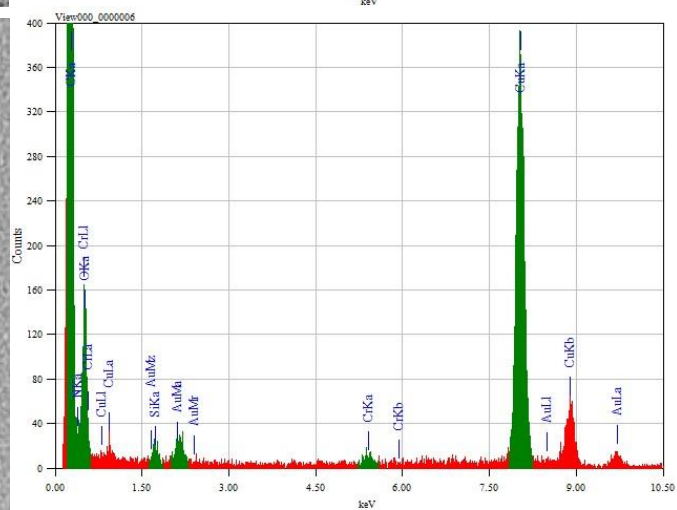
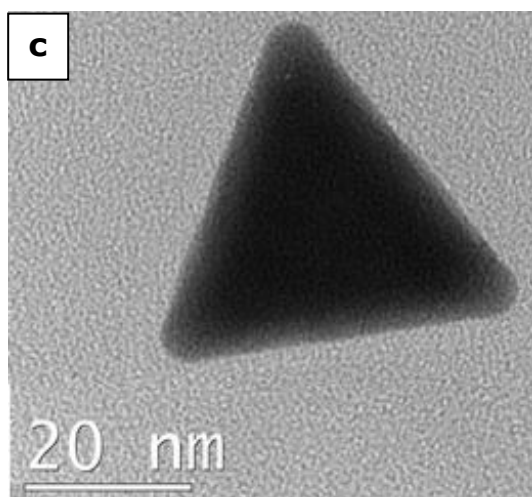
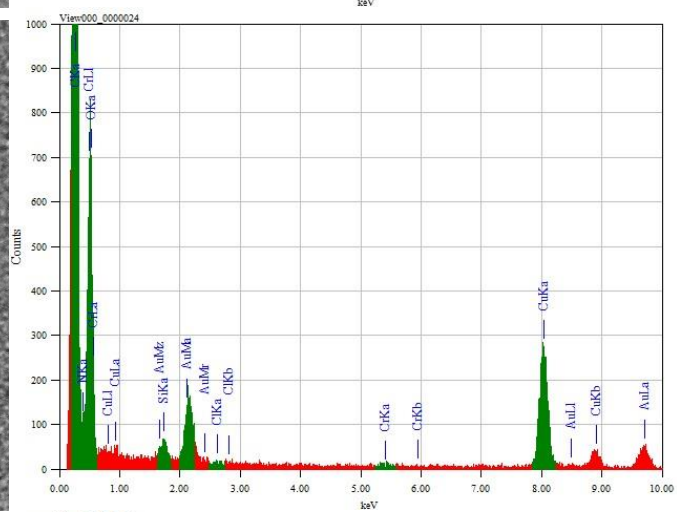
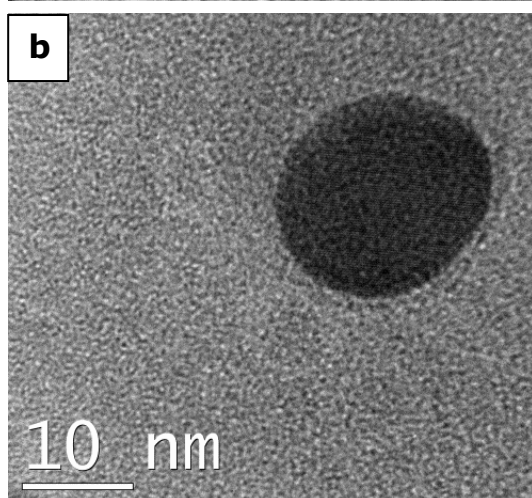
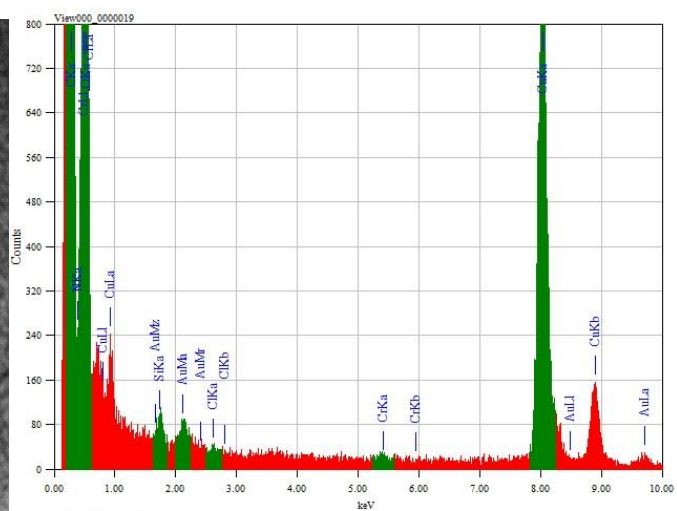
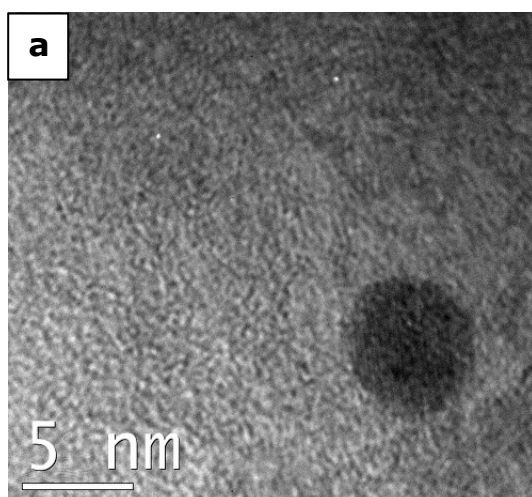
3.6 Transmission electron microscopy and energy dispersive X-ray analysis of nanogold and nanosilver hybrid polymer

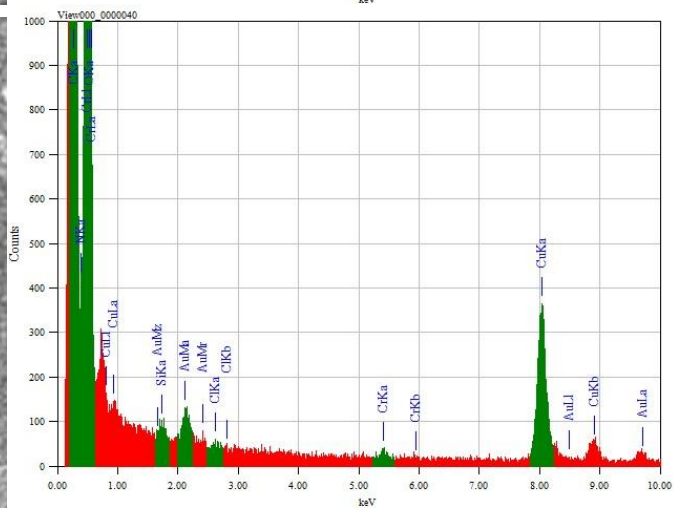
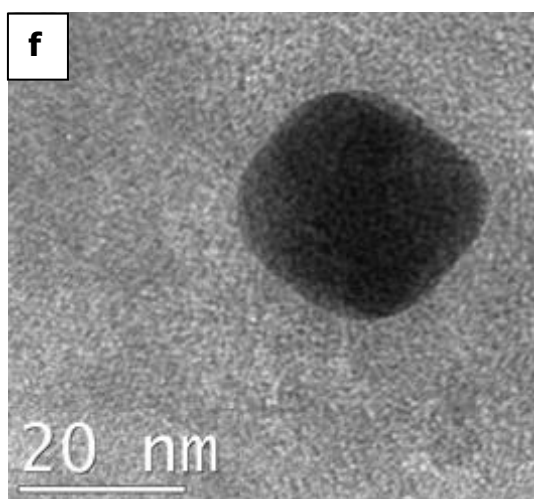
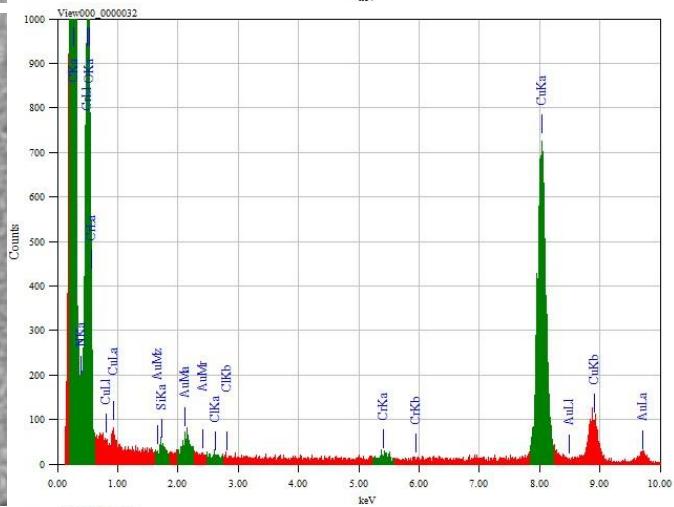
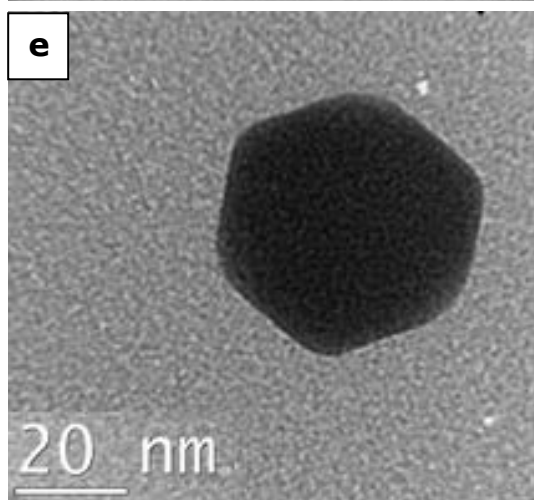
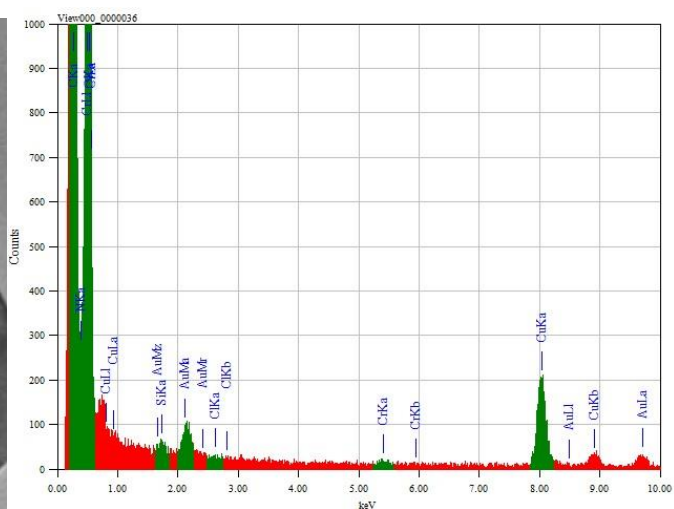
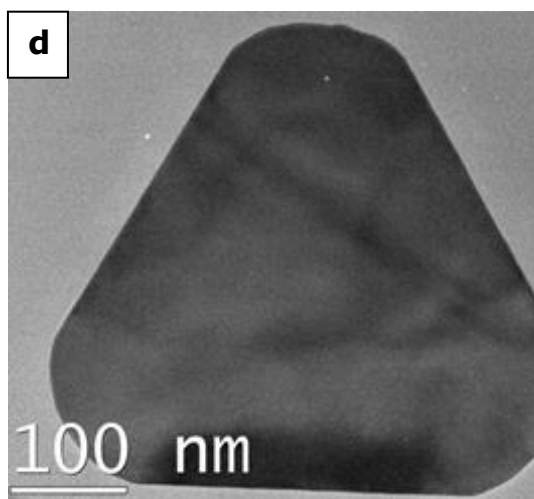
The sample preparation conditions used for TEM analyses on the hybrid polymer materials were extremely harsh, and it is possible that the distribution of the metal nanoparticles may have been affected and therefore may not be a true representation of those present in the hybrid polymer materials. Also there were difficulties imaging samples, prepared from solutions with metal ion concentrations below 50 mg kg^{-1} , as the nanoparticle concentration in the polymer sample was too low for them to be observed by the TEM. With the available cutting technique it was not possible to cut the nanogold and nanosilver hybrid polymer materials into thin cross sections because of the soft

nature of the polymers, which then could be analysed by TEM. Thus, the information on the relationship between the different particle sizes and shapes to their respective location in the polymer beads or sheets could not be obtained. Therefore in order to characterise the nanoparticles the nanoparticle hybrid PU beads were dissolved in DMF and the nanogold hybrid nylon 6,6 beads were dissolved in 6 molar HCl. A drop of resulting solution was placed on a copper grid where the solvent then was evaporated and the residual solid carbon coated. All imaged particles were also characterised by EDS elemental analyses. EDS showed the existence of carbon, nitrogen and oxygen which are present in PU, as well as copper X-ray peaks from the copper grid on which the sample was placed. Peaks for magnesium, silicon, sulfur and chromium are either due to impurity in the beads or from other contaminations in the laboratory. Hence they can be ignored.

3.6.1 Transmission electron microscopy and energy dispersive X-ray analysis of nanogold hybrid polyurethane and nylon 6,6 materials

As a face centred cubic metal, gold nanoparticles can take a variety of geometrical shapes, defined by the crystallographic orientation of the surface facets.²⁶² Figure 3.44 presents TEM micrographs of a nanogold hybrid PU material which was treated with a 50 mg kg⁻¹ gold solution (PU-b-50Au sample). The particles show a variety of particle shapes and sizes. Spherical, hexagonal, cubic and triangular-shaped (including truncated triangles) nanoparticles of different sizes covering a wide interval of sizes from approximately 5 to 450 nm were observed. As reported in Section 3.4.1, the UV-Vis spectrum confirmed the presence of particles with different sizes and shapes and also particle agglomeration, making the sample appear brown in colour. The presence of gold within the nanogold hybrid polymer material was confirmed by a peak at 2.12 keV corresponding to Au M_α in EDS spectrum (Figure 3.44 in the right side).





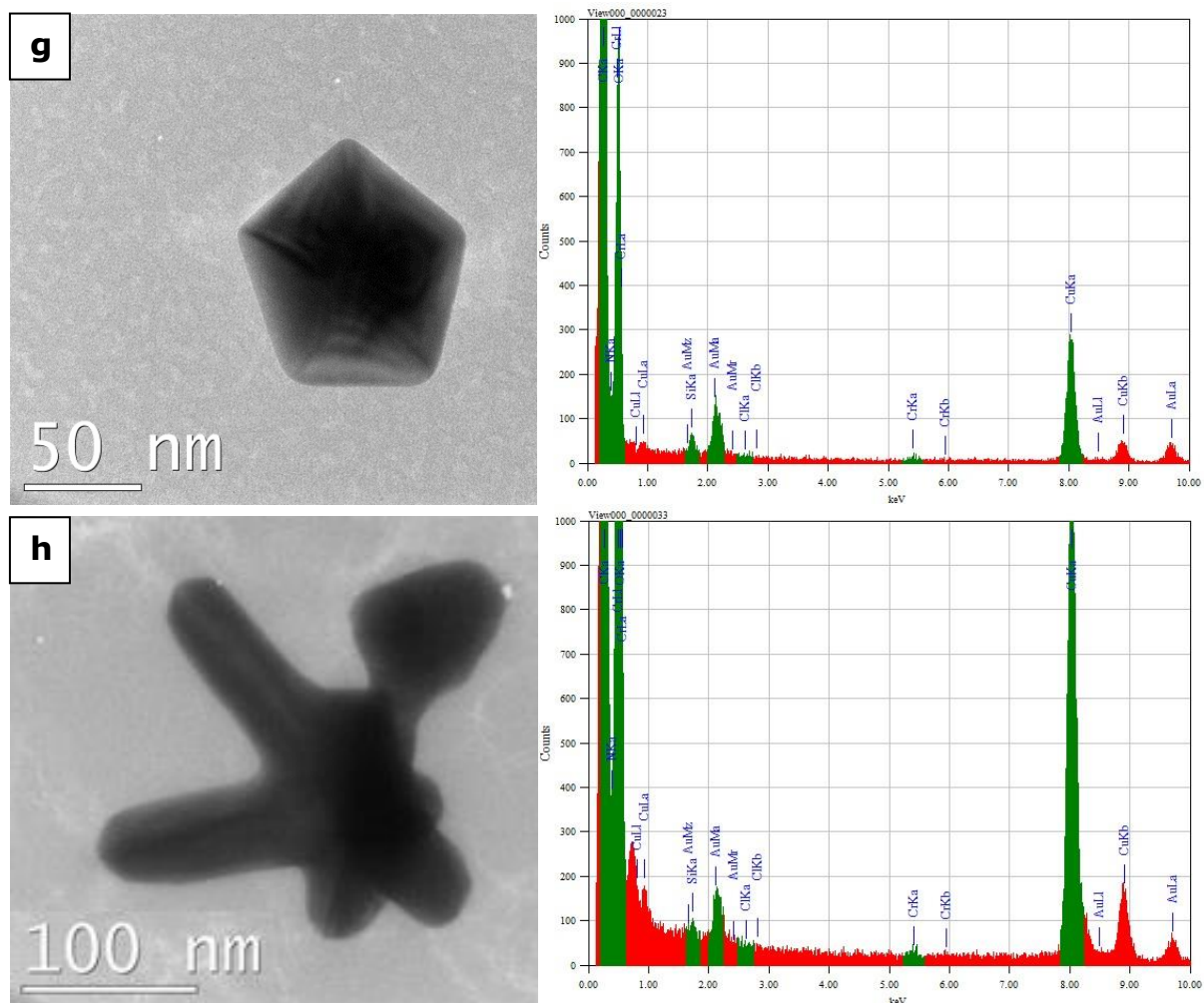


Figure 3.44: TEM micrographs of some geometrical shape examples of gold nanoparticles found in the PU-b-50Au sample (left) with the respective EDS elemental analyses (right): a-b) spherical, c) triangular, d) truncated triangular, e) hexagonal, f) cubical and g) fivefold twinned particle and h) particle agglomeration.

Since the hybrid nylon 6,6 beads were dissolved in concentrated HCl, only nanogold hybrid nylon 6,6 samples were investigated by TEM as there was a possibility to form silver chloride particles as a byproduct during the dissolution process of the nanosilver hybrid nylon 6,6 materials. Figure 3.45 shows a TEM micrograph of the Ny-b-500Au sample. EDS elemental analysis confirmed the presence of gold by a peak located at 2.12 keV corresponding to the Au M_α line. The gold nanoparticles were mostly spherical or spherical like in shape however some hexagonal, truncated triangular and rod shaped particles were occasionally

found. The spherical particles were less than 60 nm in diameter. However, as a result of the high concentration of dissolved organic matrix of nylon 6,6 it was difficult to image at a higher magnification in order to determine the size of the smallest gold nanoparticles.

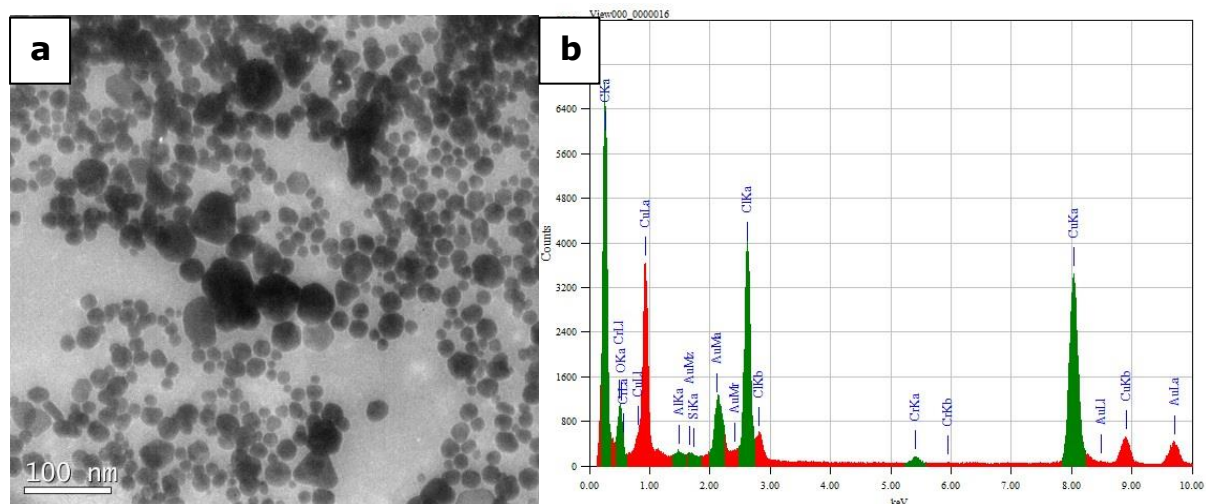


Figure 3.45: TEM micrograph of gold nanoparticles found in a) the Ny-b-500Au sample with b) the respective EDS elemental analysis spectrum (right).

3.6.2 Transmission electron microscopy and energy dispersive X-ray analysis of nanosilver hybrid polyurethane materials

Figure 3.46 presents TEM micrographs of the nanosilver hybrid PU beads which were produced from a $50 \text{ mg kg}^{-1} \text{ Ag}^+$ solution (PU-b-50Ag sample). In the case of silver, particles found in the sample were mostly spherical, from approximately 2 to 50 nm in diameter. Some particle agglomerations were also observed which was consistent with the UV-Vis spectrum showing a broadening of the SPR band for the silver nanoparticles (Section 3.4.2). SEM analysis also confirmed that the silver particles on the surface of the bead were agglomerated due to the lack of stabilisation from the polymer matrix. The presence of silver within the nanosilver hybrid polymer material was confirmed by a peak at 2.98 keV corresponding to the Ag L_α line in the EDS elemental analysis spectrum (Figure 3.46).

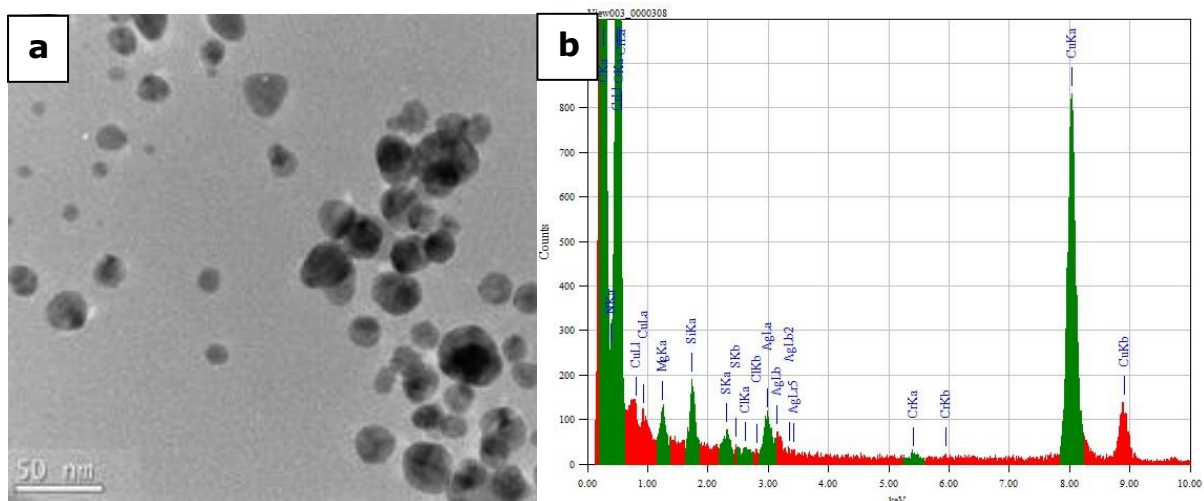


Figure 3.46: TEM micrographs of silver nanoparticles found in a) the PU-b-50Ag sample with b) the respective EDS elemental analysis spectrum.

3.7 X-ray diffraction analysis of nanogold and nanosilver hybrid polyurethane and nylon 6,6 materials

Confirmation of the formation of gold and silver nanoparticles in the PU and nylon 6,6 polymer matrices was carried out using X-ray diffraction analyses. XRD patterns matched nicely with the standard PDF 04-001-2616 for gold and the PDF 04-001-2617 for silver pattern.²⁴² The XRD patterns were analysed to determine peak intensity, position and width. To determine the mean particle diameter, full width at half maximum (FWHM) values were used in the Scherrer equation.

3.7.1 X-ray diffraction analysis of nanogold and nanosilver hybrid polyurethane materials

Due to having a flat surface and an even distribution of metal nanoparticles throughout the PU matrix, hybrid *dog bone* samples were well suited for XRD measurements. The XRD patterns of hybrid PU *dog bone* strips, PU-b-50Au sample, PU-b-50Ag sample and blank PU *dog bone* strip, PU-db, are shown in Figure 3.47. Results from X-ray diffraction analyses indeed demonstrate the presence of gold nanoparticles in the hybrid PU *dog bone* strip. The Bragg diffraction peaks centred at $2\theta = 38.22^\circ$ (1 1 1), 44.37° (2 0 0), 64.56° (2 2 0), 77.54° (3 1 1) and 81.70° (2 2 2) are indexed to the face centred cubic structure of gold and are a good match with the database.²⁴² The synthesized gold nanoparticles were primarily dominated by (1 1 1) facets.

From TEM analysis, the Au nanoparticles in the PU-b-50Au sample appear to range in size from ca. 5 - 450 nm (Section 3.6.1). Due to the residual PU on the TEM grid it was difficult to locate and view these particles on the TEM, and as such the average size of the particles or the relative percentage of different size particles could not be determined. Larger particles were much easier to view and image than smaller ones. Using the Scherrer equation (Section 2.3.4) the average estimated crystallite particle size of this PU-db-50Au sample was 44 nm.

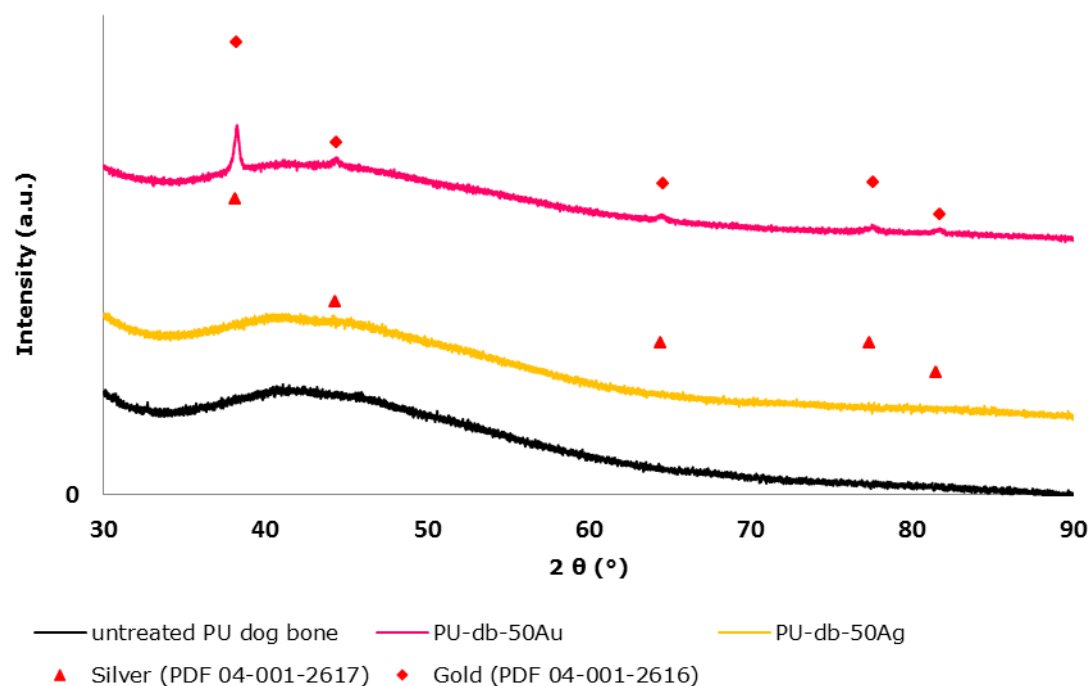


Figure 3.47: XRD patterns for the nanogold and nanosilver hybrid PU materials: PU *dog bone* strip by itself, PU-db-50Ag and PU-db-50Au samples.

The XRD pattern for the PU-db-50Ag sample showed only a background curve with no observable peaks for silver. Although silver was present as shown by the typical nanosilver SPRB in UV-Vis spectrum (Figure 3.18) and also in TEM analyses (Figure 3.46), it was not possible to detect any silver nanoparticles by XRD or SEM. This was due to the very small amount present within the PU polymer and also the small size of silver nanoparticles which were further distributed when the beads were moulded into the *dog bone* test strips. As mentioned in Section 3.1, the uptake studies showed that the uptake of gold ions from the solution by PU substrates were higher than that for silver ions (for gold almost 100 % of gold ions and 70 % of silver ions were absorbed after 24 hours soaking time) which would have affected the number of nanoparticles formed.

The nanogold and nanosilver hybrid PU sheets were also analysed by XRD. The presence of gold and silver nanoparticles was confirmed by the characteristic peaks observed in the XRD patterns shown in Figure 3.48 and Figure 3.49. All the diffraction peaks correspond to the characteristic face centred cubic gold

(PDF 04-001-2616) and silver (PDF 04-001-2617) lines respectively.²⁴² The diffraction patterns were observed at 2θ angle 38.17° (1 1 1), 44.36° (2 0 0), 64.68° (2 2 0) and 77.61° (3 1 1) for gold (PU-s-500Au sample) and 38.26° (1 1 1), 44.10° (2 0 0), 64.61° (2 2 0) and 77.49° (3 1 1) for silver (PU-s-500Ag sample). The mean crystallite size of gold nanoparticles was estimated as 29 nm for the PU-s-100Au sample, 34 nm for the PU-s-500Au sample, 21 nm for the PU-s-100Ag sample and 25 nm for the PU-s-500Ag sample. The results obtained by Scherrer equation show an increase in the crystallite size with increasing concentration of gold solution used to produce nanogold hybrid PU sheets.

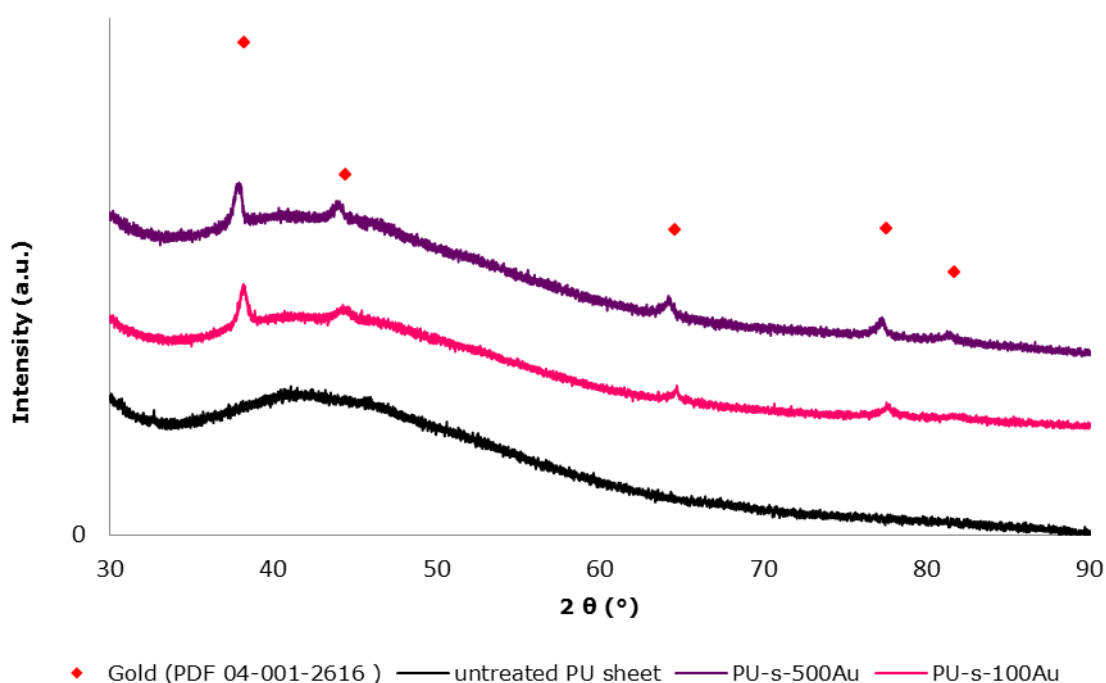


Figure 3.48: XRD patterns for the nanogold hybrid PU materials: PU sheet by itself, PU-s-100Au and PU-s-500Au samples.

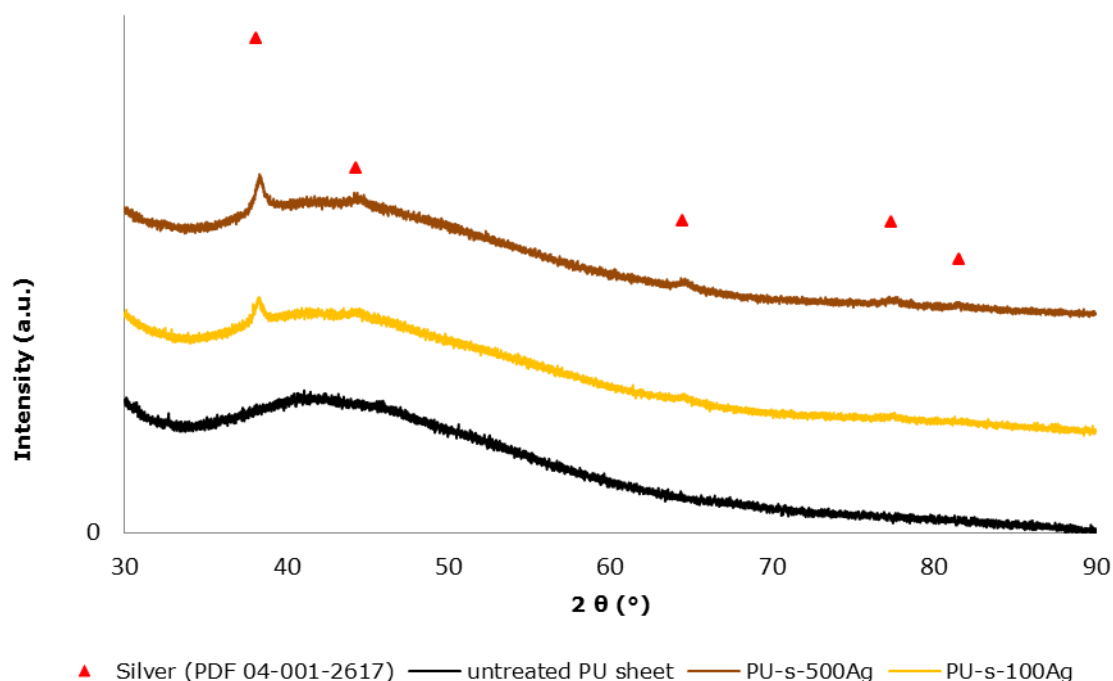


Figure 3.49: XRD patterns for nanosilver hybrid PU materials: PU sheet by itself, PU-s-100Ag and PU-s-500Ag samples.

3.7.2 X-ray diffraction analysis of nanogold and nanosilver hybrid nylon 6,6 materials

The XRD pattern of the untreated nylon 6,6 beads is shown in Figure 3.50. The black curve in the spectrum exhibits two broad peaks at 2θ angles of 37.6° and 40.8° and a third peak at around $2\theta = 81.4^\circ$ depicting the semi-crystalline structure of nylon 6,6 beads.

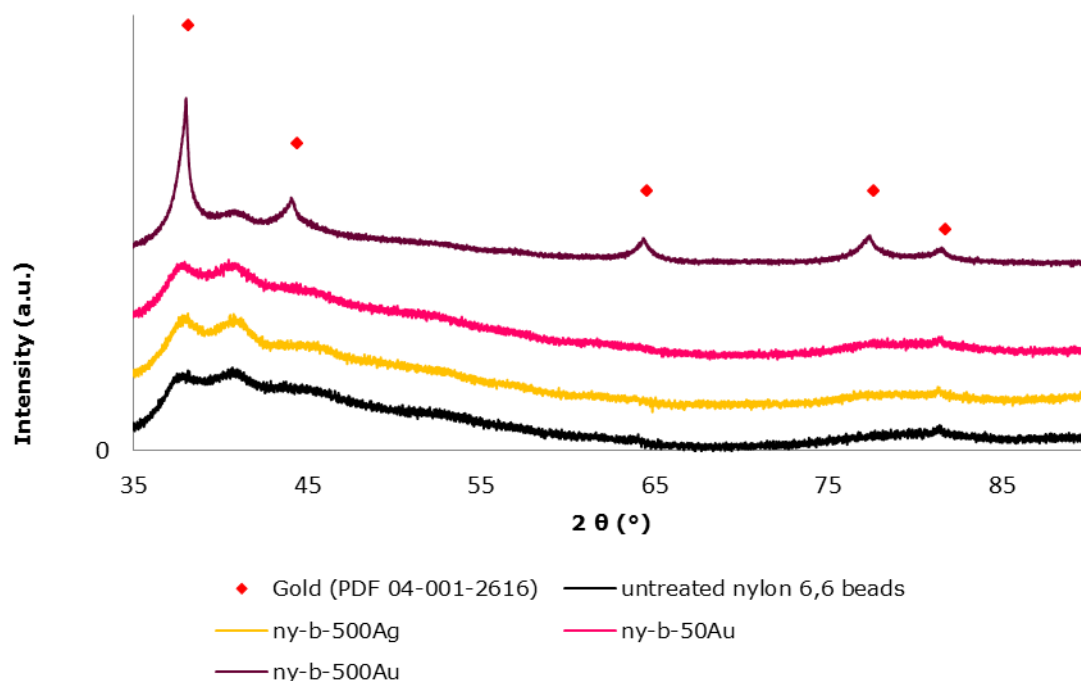


Figure 3.50: XRD patterns for nanogold and nanosilver hybrid nylon 6,6 beads and nylon 6,6 beads by themselves.

No diffraction peaks for gold were detected for the nanogold hybrid nylon 6,6 beads which were prepared using 50 mg kg^{-1} gold solution. However, when the reaction solution concentration was increased to 500 mg kg^{-1} of gold solution to produce nanogold hybrid nylon 6,6 beads (Ny-b-500Au sample) the XRD pattern showed the characteristic Bragg diffraction peaks of gold in the face centred cubic phase confirming the presence of gold nanoparticles on the surface of hybrid nylon 6,6 beads. These diffraction peaks located at 2θ angle 37.9° , 44.08° , 64.35° , 77.29° and 81.42° respectively, have been indexed as (1 1 1), (2 0 0), (2 2 0), (3 1 1) and (2 2 2) planes for gold respectively. The calculation for the mean crystallite size for gold (2 0 0), (2 2 0), (3 1 1) peaks yielded an average value of 22 nm, whereas no calculation was done for (1 1 1) and (3 1 1) peaks as they are located at a very similar position to the peaks of the untreated nylon 6,6 beads. A slight angular offset between the XRD peaks of the Ny-b-500Au sample and the reference peaks was observed as the result from the hybrid beads not sitting at the correct height in the XRD stage. Secondly, slight variations in the position of the peaks indicate the existence of some strain in the crystal structure, often characteristics of nanocrystals.²⁶³

The XRD analysis of the Ny-b-500Ag sample showed no Bragg diffraction peaks that can be indexed on the basis of the fcc structure of silver. However, with a closer look, the broader peak from nylon 6,6, which was located at around 2θ angle 37.6° , exhibits a shift to around 37.8° . Additionally, its intensity is slightly increased in proportion to the nylon's second broad peak at $2\theta = 40.8^\circ$. This suggests the possible presence of the silver (1 1 1) peak in the Ny-b-500Ag sample.

3.8 X-ray photoelectron spectroscopy analysis of nanogold and nanosilver hybrid polyurethane and nylon 6,6 materials

As described in Sections 1.3.1.2 and 1.3.1.3 polyurethane and nylon 6,6 possess nitrogen-containing groups. In order to understand how the carbamate groups of PU and amide groups of nylon 6,6 are involved in the reduction of gold or silver ions to their respective metallic nanoparticles and their subsequent binding to the polymer matrix, XPS study of the hybrid polyurethane and nylon 6,6 materials was carried out. An initial survey scan from a binding energy of 600 to 0 eV for all polymer samples showed the presence of carbon, nitrogen and oxygen groups on the polymer surface, together with gold for nanogold hybrid polymers and silver for nanosilver hybrid polymers. High resolution scans were subsequently carried out across the peaks for each of the elements in the nanogold and nanosilver hybrid polymer materials respectively, and also for carbon, nitrogen and oxygen in the untreated PU or nylon 6,6, as the control samples. The control samples were prepared under the same conditions employed to prepare the hybrid polymer materials. Hence the control samples were heated for 24 hours in 50 or 90 °C in distilled water, the pH of water was adjusted to 4.5 - 5, subsequently all control samples were rinsed with distilled water. Peaks for calcium and silicon should be ignored due to contamination of the samples.

3.8.1 X-ray photoelectron spectroscopy analysis of nanogold hybrid polyurethane materials

Peaks from characteristic elements (C, O, N) of the untreated polyurethane and the nanogold hybrid polyurethane beads (C, O, N and Au) were observed in the survey XPS scan of the PU-b-500Au sample (Figure 3.51).

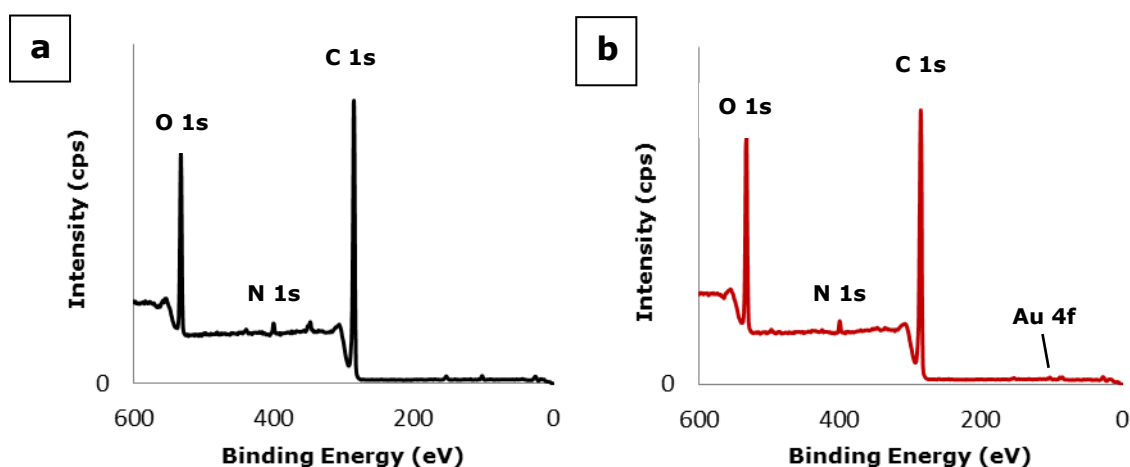


Figure 3.51: Survey XPS scans of a) a cross section of the untreated PU bead and b) the cross section of the PU-b-500Au sample.

Figure 3.52 (a, c, e) shows C, N and O 1s high resolution XPS spectra acquired from the cross section area of the untreated polyurethane bead. This high resolution C 1s spectrum was deconvoluted into four components at positions 285 eV, 285.6 eV, 286.6 eV and 289.4 eV which can be attributed to a carbon bound to adjacent carbon (C-C), a carbon singly bound to nitrogen environment (C-N), a carbon singly bound to oxygen (C-O) and a carbonyl carbon derived from the urethane linkages of PU matrix (RNH-COOR').²⁶⁴ Examination of the deconvoluted high resolution, narrow scan N 1s revealed that PU possess a major peak at about 400.3 eV which is due to the transition from the N 1s core level into the antibonding π^* orbital of the carbamate bond. The XPS O 1s spectrum was deconvoluted into one peak with the maximum at around

532.7 eV and was assigned to the average oxygen environment of PU. A complete list of peak assignments is presented in Table 3.4.

Table 3.4: XPS assignments for the untreated PU bead and the PU-b-500Au sample.

| | | Untreated PU beads | Nanogold hybrid PU beads |
|--------------|---------------------------------|-------------------------------------|--------------------------|
| | | Binding Energy [eV] and (FWHM) [eV] | |
| C 1s | C-C, C-H | 285.00 (0.97) | 285.00 (1.15) |
| | C-N | 285.58 (0.73) | 285.60 (0.83) |
| | C-O | 286.57 (1.16) | 286.75 (1.29) |
| | O-C=O | 289.35 (1.27) | 289.60 (1.16) |
| | C-N-Au | - | 284.09 (1.33) |
| N 1s | N-H | 400.31 (1.06) | 400.45 (1.31) |
| | N-Au | - | 398.58 (1.12) |
| O 1s | Average O environment | 532.71 (1.77) | 533.03 (1.69) |
| | Unidentified O species | - | 531.10 (1.17) |
| | | | |
| Au 4f | Au ⁰ _{7/2} | - | 82.87 (0.81) |
| | Au ⁺ _{7/2} | - | 83.59 (1.02) |
| | Au ³⁺ _{7/2} | - | 84.55 (1.48) |
| | Au ⁰ _{5/2} | - | 86.54 (0.81) |
| | Au ⁺ _{5/2} | - | 87.26 (1.02) |
| | Au ³⁺ _{5/2} | - | 88.14 (1.48) |

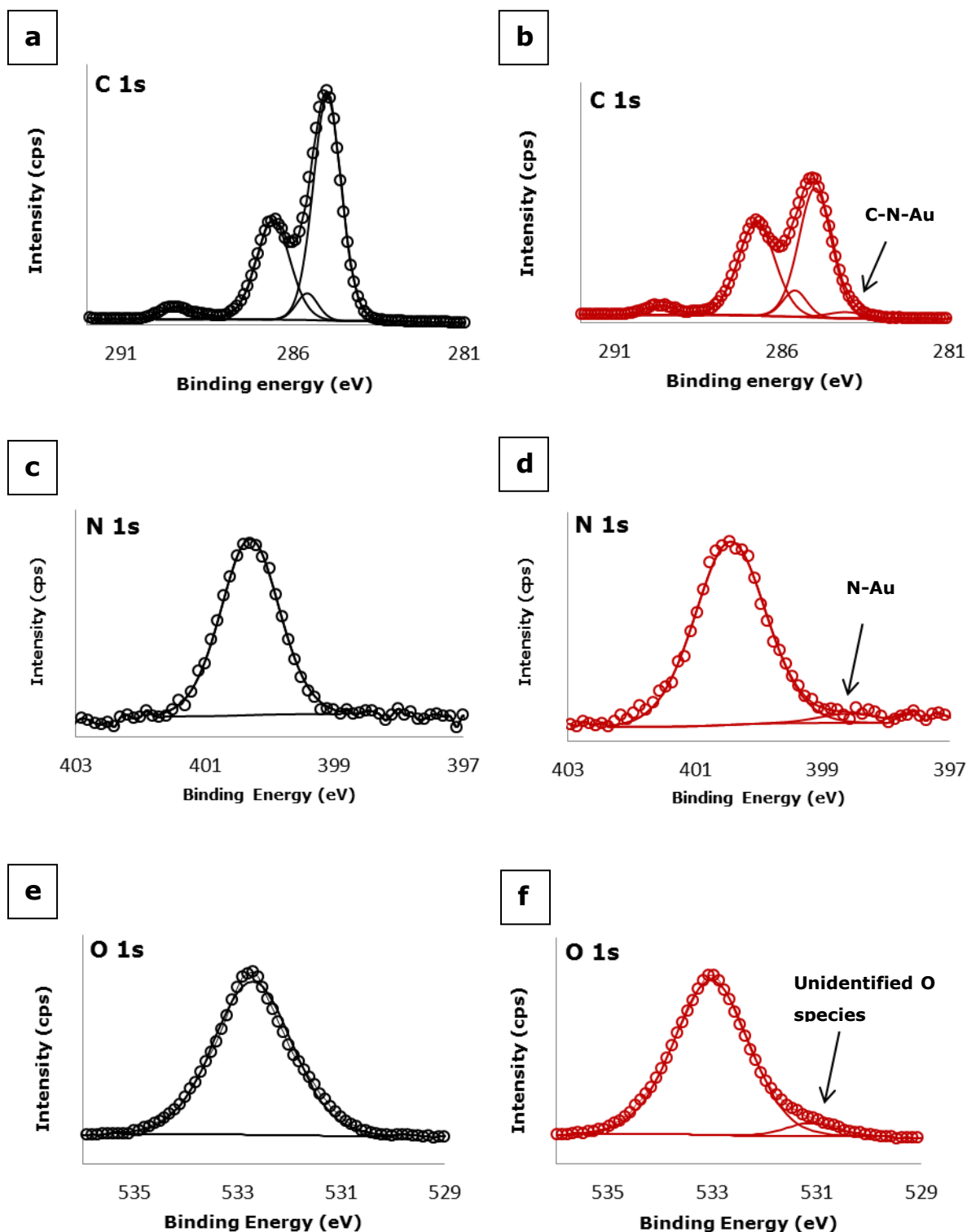


Figure 3.52: Deconvoluted high resolution XPS spectra for the untreated PU: a) C 1s peaks, c) N 1s peaks and e) O 1s peaks; for the PU-b-500Au sample: b) C 1s peaks, d) N 1s peaks and f) O 1s peaks. Experimental data points are shown by circles.

Owing to the affinity of gold for nitrogen in the carbamate group, PU offers an opportunity to reduce gold ions to nanoparticles and subsequently bind them to the polymer matrix. This gold nitrogen interaction was confirmed in XPS analysis of the nanogold hybrid PU sample. The interaction was first observed in the high resolution C 1s scan of the cross section of the nanogold hybrid PU bead sample. The cross section of the bead provided a cleaner surface, therefore stronger XPS peaks, and the opportunity to examine the interior matrix of hybrid PU. Figure 3.52b shows that the treatment of the PU beads with 500 mg kg⁻¹ gold solution for 24 hours at 50 °C (PU-b-500Au sample) led to changes in the positions of C-O, C-N and carbamate C 1s peaks suggesting O- and N-containing moieties of the polyurethane matrix were involved in the reduction of gold ions to gold nanoparticles. Additionally a new peak which was consistent with the formation of a C-N-Au bond²⁴ was observed at 284.1 eV.

Likewise, the high resolution N1s spectrum of the PU-b-500Au sample provided further confirmation of the potential binding (Figure 3.52d). Deconvolution of the N 1s spectrum using a two-peak fitting routine revealed binding energies of 400.5 eV and 398.6 eV. The latter peak is representative of a N-Au interaction^{21,24,265} consistent with the chemical affinity of gold for nitrogen. This is provided by the interaction of the electrons on the nitrogen with gold to form an Au-N bond, which lowers the electron density on the nitrogen atom. Similar binding energies were reported for gold to nitrogen interaction.^{24,266} As the amount of gold in this sample which corresponds to less than 0.5 wt % gold loading and more gold was formed on the surface rather than interior of the bead (Section 3.5.1), the changes of the nitrogen were expected to be minimal, as most of the nitrogen is associated with the remaining polymer and only 4.3 % area of nitrogen species form bonds to gold. The N 1s spectral component occurring at higher binding energy values showed a shift of ~ 0.14 eV compared to the untreated PU sample, as well as an increase in full (FWHM) value. It is considered that the reduction of the Au³⁺ ions to Au⁰ is facilitated by the oxidation of the carbamate groups in the polyurethane matrix, resulting in a shift to higher binding energies which indicates the formation of oxidised nitrogen species. The corresponding increase in FWHM is due to a consequent increase in the variability of the binding environment of the nitrogen.

The high resolution O 1s spectrum of the hybrid PU material shows a shift of around 0.3 eV to higher binding energies and additionally a new peak which was not seen in the untreated PU sample (Figure 3.52f). The shift to higher binding energies is consistent with the oxidation of the nitrogen in the PU, which is necessary for the gold ions to be reduced. The peak at lower binding energy is centred at ca. 531.1 eV. According to Wagner et al., for all known oxides or hydroxides the binding energy of the oxygen 1s electron varies between 525 and 531 eV.²⁶⁷ Reports showed that an Au-O bond is expected to have a peak centred at approximately 529.7 eV for Au₂O₃.²⁶⁸ It is most unlikely that there is a formation of oxidised gold species in the nanogold hybrid PU materials. Au₂O₃ is normally formed only under exceptional conditions such as the exposure of Au to highly reactive ozone²⁶⁹, atomic oxygen²⁷⁰ or oxygen plasma.²⁷¹ Gold nanoparticles can catalyse the oxidation of CO however it is necessary for them to be highly dispersed and deposited on reducible semiconductor metal oxides, hydroxides of alkaline earth metals or amorphous ZrO₂.²⁷² Since none of the support materials are present in the PU matrix, the formation of an Au-O bond can be ruled out. Although Au(III) hydroxide is more likely to be formed, because it is more thermodynamically stable than Au₂O₃²⁷³, the formation of such gold(III)hydroxide can be eliminated as basic conditions are required for its formation, whereas acidic conditions prevail here.²⁷⁴

In this case the peak at lower binding energies is likely to be due to an interaction between partially reduced gold ions, Au⁺, which are present on the surface of the gold nanoparticles and the lone pairs of oxygen in the carbamate group of PU polymer matrix. In a similar way, Burridge reported on the interaction of TSC with positively charged gold nanoparticles resulting in O 1s peak at around 530 eV.²¹ There are many more oxygens compared to nitrogen species present in the PU polymer matrix, which interact with unreduced surface of gold nanoparticles. As such, the variation of oxygen environment appears to be greater than that for nitrogen. However, to confirm this proposed assignment it would be interesting to measure the XPS spectra of *ex situ* produced gold nanoparticles which are introduced into the PU matrix. This would be the subject of further research work.

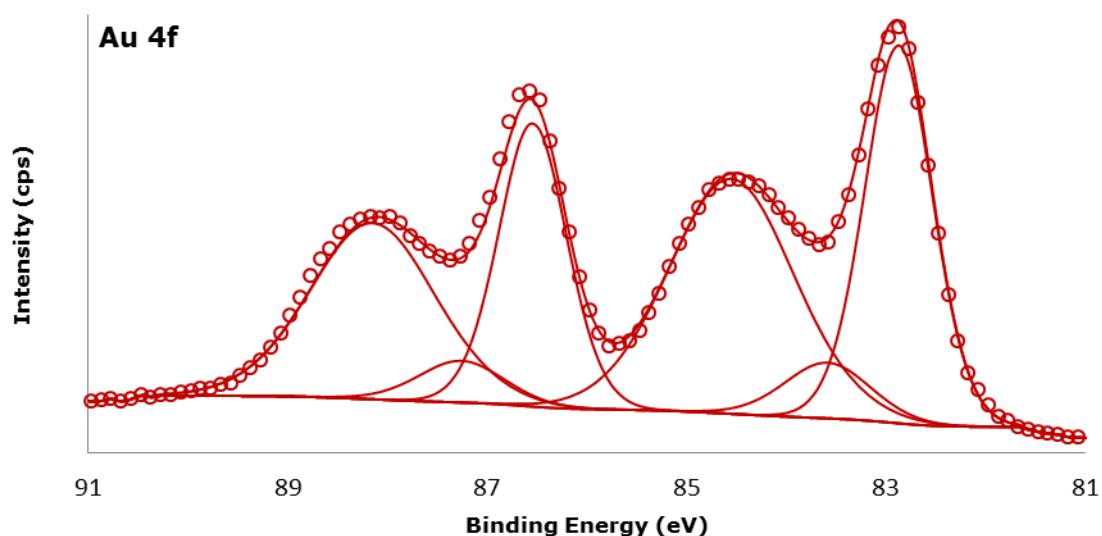


Figure 3.53: Deconvoluted high resolution Au 4f XPS spectrum for the cross section of the bead PU-b-500Au sample.

Figure 3.53 shows the high resolution Au 4f XPS spectrum for the cross section area of the PU-b-500Au sample. The spectrum comprises a doublet of the $7/2$ and $5/2$ photoemission peaks due to spin orbit splitting.²⁷⁵ The doublet peaks with an intensity ratio of 4:3 are positioned around 82.9 eV ($4f_{7/2}$) and 86.6 eV ($4f_{5/2}$) and are attributable to Au^0 , which further confirms that gold ions were reduced to metallic gold when PU substrate was soaked with gold ion solution at 50 °C for 24 hours. While the spacing between the two peaks matches that of the bulk metal, both peaks are shifted to lower binding energies by approximately 1 eV. Similar effects have been observed for gold nanoparticles capped with nitrogen-containing groups.²⁴ The negative shift is believed to be due to the N of the carbamate groups bound to the gold providing greater negative charge at the gold surface, leading to greater screening of the gold and therefore a lower binding energy. A second broader doublet composed of asymmetrical Au $4f_{5/2}$ and Au $4f_{7/2}$ peaks was located at around 83.6 eV and 87.3 eV respectively, consistent with the characteristic separation of these Au 4f peaks (3.67 eV) and indicating a higher oxidation state of gold. These peaks were attributed to Au^+ that bind to the polymer matrix via Au-N bonds to the nitrogen-containing carbamate group of the PU. However, they may also

represent partially reduced Au^+ on the surface of the nanoparticles, which do not bond to the PU matrix. Additional broad peaks indicative of Au^{3+} were present at approximately 84.6 eV and 88.1 eV suggesting a small percentage of unreduced Au^{3+} . It is likely that the gold nanoparticles bound to the polymer matrix of the PU have Au^0 cores which are surrounded by Au^+ ions, with some of them binding to the polymer via Au-N bonds, through the nitrogen-containing carbamate groups of PU, as discussed above. The unreduced Au^{3+} species may accumulate on the formed nanoparticles or in the polymer matrix. Some interaction between gold and oxygen may exist to stabilize the Au nanoparticles although no obvious evidence for any oxidised gold species is available.

3.8.2 X-ray photoelectron spectroscopy analysis of nanogold hybrid nylon 6,6 materials

It was not possible to prepare a cross section of the nylon 6,6 sheet samples. Thus, XPS analyses were carried out of the top 10 nm of the surface of nylon 6,6 samples. Figure 3.54 presents wide XPS spectra of an untreated nylon 6,6 sheet and a nanogold hybrid nylon 6,6 sample (Ny-s-500Au) with their characteristic elements (C, N, O and Au), which additionally confirm the presence of gold in the Ny-s-500Au sample. In contrast to the nanogold hybrid PU sample, an X-ray peak for chlorine was detected in all the nanogold hybrid nylon 6,6 samples.

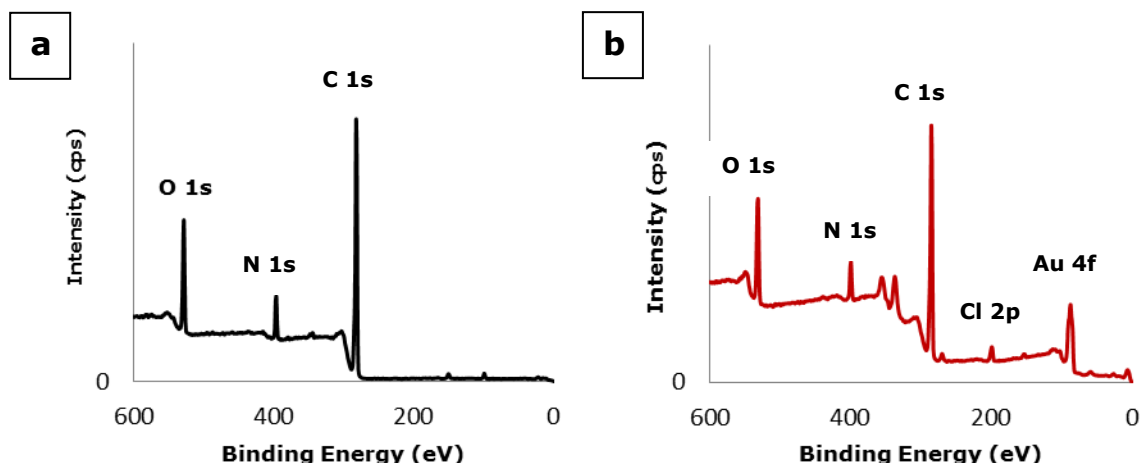


Figure 3.54: Survey XPS scan of a) the untreated nylon 6,6 sheet and b) the Ny-s-500Au sample.

Figure 3.55a-b shows the C 1s, O 1s and N 1s spectra, respectively, for the untreated nylon 6,6 sheet which was employed as a control. The high resolution C 1s spectrum of the untreated nylon 6,6 sheet was deconvoluted into three main peaks, 285.0 eV, 285.5 eV and 288.1 eV, respectively. The lowest binding energy peak at 285 eV is due to the C–C or C–H carbons in the nylon 6,6 polymer chain while the higher binding energy peaks at approximately 285.5 eV and 287.8 eV are attributable to the carbon nitrogen bond (C–N) and the amide group of nylon 6,6 (NH–C=O) respectively. The resolved N 1s spectrum of the untreated nylon 6,6 is shown in Figure 3.55c. Theoretically only one species of amide nitrogen should be present in the nylon 6,6 material. However, in the case of these nylon 6,6 samples the N 1s spectrum was deconvoluted into two nitrogen peaks. Due to complexity and disorder of the polymer chains within the nylon 6,6 matrix it is possible that the amide functional groups exist in a number of environments depicted by fitting the experimental envelope to two end number peaks representing the range of these different chemical environments. Hence one type of amide group is interacting more with some adjacent electron withdrawing groups (e.g. oxygen containing groups) than the other, resulting in slightly higher binding energy. Hence both peaks at 399.7 eV and 400.1 eV respectively were assigned to amide group (N–C=O) of nylon 6,6.²⁷⁶ In a similar way to nitrogen, the analysis of the O 1s spectrum proved to be difficult as there are likely three chemical environments of oxygen atoms contributing to the O 1s

peak. Hence, in all samples, the O 1s spectra were fitted into three peaks (with equal FWHM), corresponding to oxygen in the carbonyl group of polyamide linkage centred at ca. 531.4 eV and two another types of carrier oxygen atom belonging presumably to some additives of nylon 6,6 at approximately 532.4 eV and 533.5 eV. Table 3.5 presents a complete list of peak assignments.

Table 3.5: XPS assignments for the untreated nylon 6,6 sheet and the Ny-s-500Au sample.

| | | Untreated nylon 6,6 sheet | Nanogold hybrid nylon 6,6 sheet |
|--------------|---------------------------------|-------------------------------------|---------------------------------|
| | | Binding Energy [eV] and (FWHM) [eV] | |
| C 1s | C-C, C-H | 285.00 (0.87) | 285.00 (1.04) |
| | C-N | 285.54 (1.52) | 285.72 (1.61) |
| | N-C=O | 288.08 (1.13) | 287.91 (1.87) |
| | C-N-Au | - | 283.79 (0.81) |
| N 1s | N-H | 399.67 (0.95) | 399.64 (1.22) |
| | | 400.06 (1.16) | 400.27 (1.31) |
| | N-Au | - | 398.44 (1.18) |
| | NH ₃ ⁺ | - | 401.21 (1.50) |
| O 1s | N-C=O | 531.38 (1.12) | 531.31 (1.42) |
| | Unidentified O species | 532.29 (1.12) | 532.22 (1.42) |
| | | 533.24 (1.12) | 533.40 (1.42) |
| Au 4f | Au ⁰ _{7/2} | - | 84.76 (1.19) |
| | Au ⁺ _{7/2} | - | 85.41 (1.23) |
| | Au ³⁺ _{7/2} | - | 87.06 (1.58) |
| | Au ⁰ _{5/2} | - | 88.41 (1.19) |
| | Au ⁺ _{5/2} | - | 89.08 (1.23) |
| | Au ³⁺ _{5/2} | - | 90.73 (1.58) |

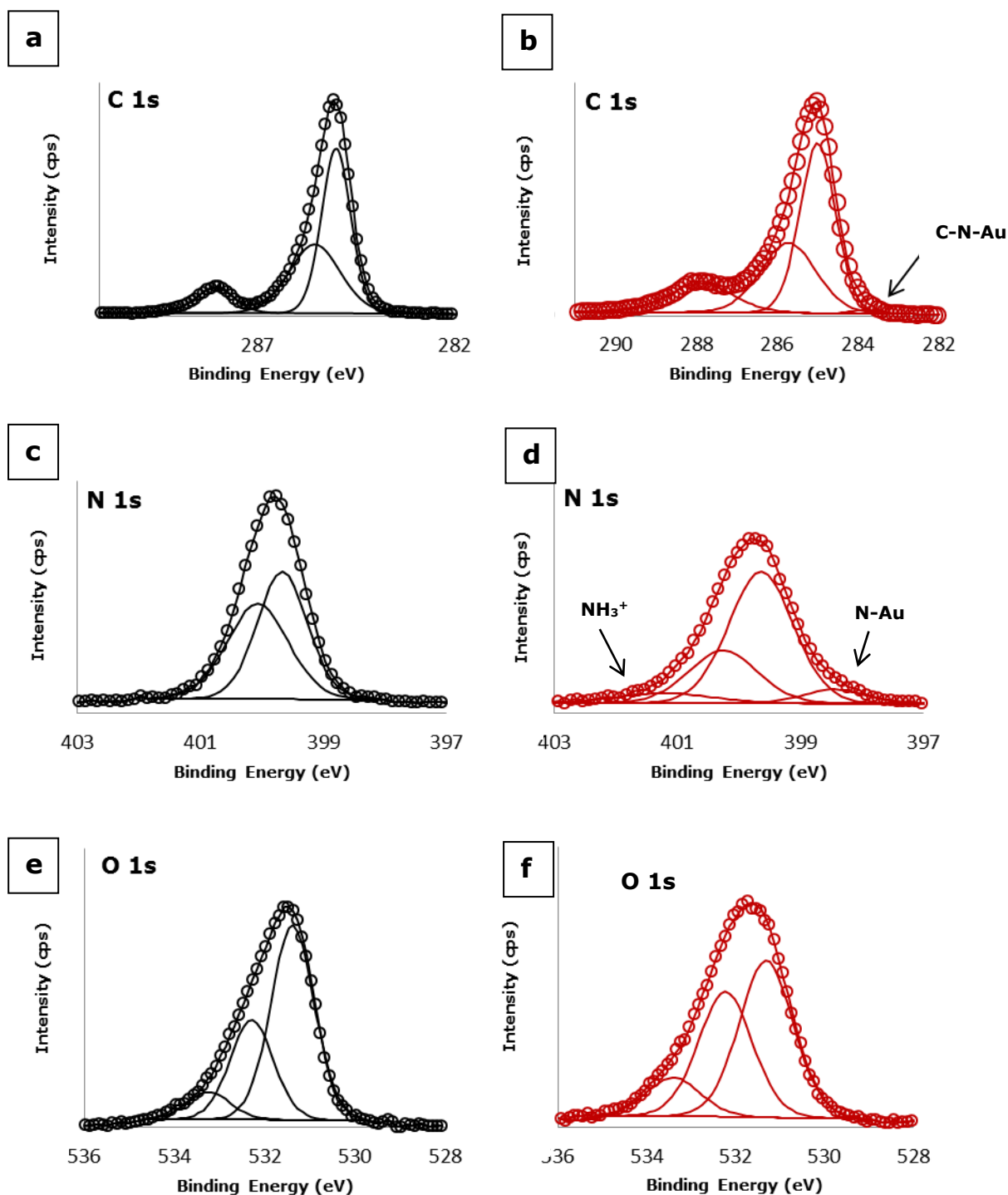
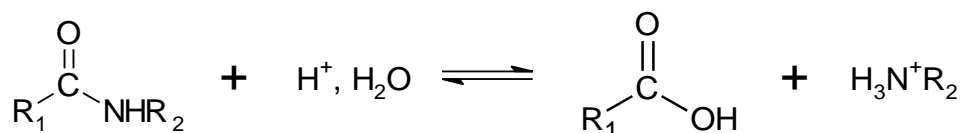


Figure 3.55: Deconvoluted high resolution XPS spectra for the untreated nylon 6,6 sheet: a) C 1s peaks, c) N 1s peaks and e) O 1s peaks; for the Ny-s-500Au sample: b) C 1s peaks, d) N 1s peaks and f) O 1s peaks.

As previously mentioned, gold has an affinity for nitrogen and this interaction was seen in high resolution spectrum of carbon for the nanogold hybrid

nylon 6,6 sample. A summary of the XPS data is shown in Table 3.5. Figure 3.55b shows that the experimental envelope of the C 1s spectrum of the nanogold hybrid nylon 6,6 sheet has two maxima. However, the spectrum was deconvoluted into four components. The weak peak centred at 283.8 eV suggests a formation of a C-N-Au bond, in a similar peak position as that observed for the nanogold hybrid polyurethane sample (Section 3.8.1) and being consistent with similar values for binding energy of Au-N bond reported in the literature²⁴. Nylon 6,6 has a considerable number of nitrogen-containing groups, thus it was expected that the amount of Au-N bonds formed would give only small signal in the C 1s spectrum due to 1 wt % of gold loading in the nylon 6,6 sheet (0.5 g). For the C-N peak of the nanogold hybrid nylon 6,6 sample, a shift from 285.5 to 285.7 eV as well as broadening of the peak was noted when comparing to the C-N peak of the untreated nylon 6,6 sample. The shift of this peak to higher binding energy suggests a higher oxidation state of nitrogen, the greater width at half maximum of the peak is due to an increase in the variability of the binding environment. Both factors suggest that the nitrogen group is likely to be involved in the reduction of the gold ions to metallic gold and also in the binding of formed gold nanoparticles to the nylon 6,6 polymer matrix.

The significant broadening of N-C=O peak which is located at approximately 287.92 eV could mask an additional HO-C=O peak at slightly higher binding energies which can result from the hydrolysis of the amide linkage of nylon 6,6 in acidic gold solution (pH 4.5). This hydrolysis reaction for the amide occurs according to the equation below:²⁷⁷



Examination of the high resolution N 1s XPS spectrum for the nanogold hybrid nylon 6,6 sheet (Ny-s-500Au sample) supports the conclusion that nitrogen has

an affinity to gold resulting in nitrogen gold interaction. Figure 3.55d shows the XPS spectrum in the region of the N 1s envelope for the Ny-s-500Au sample which was deconvoluted into four peaks. The two peaks centred at approximately 399.6 eV and 400.3 eV respectively were assigned to the nitrogen of the amide group in the nylon 6,6 matrix. Both peaks, in comparison to the peaks of the untreated nylon 6,6 sheet, exhibit greater FWHM values, implying greater variations in the nature of the bonding around the nitrogen species, as well as changes in the surrounding environment. The peak locating at 400.3 eV is shifted by 0.2 eV towards higher binding energies implying a formation of some oxidised nitrogen entities. While this peak also decreased in intensity, two new peaks for nitrogen appeared upon absorption and subsequent reduction of Au^{3+} as $([\text{AuCl}_4]^-)$ to Au^0 by the nylon 6,6 polymer matrix. The peak at lower binding energy was ascribed to a N-Au bond as its binding energy of ca. 398.4 eV matched the binding energy of N-Au bond found in nanogold hybrid PU materials (Section 3.8.1). The peak observed at around 401.2 eV indicates the presence of protonated nitrogen.^{278,279} Addition of gold solution to nylon 6,6 materials leads to hydrolysis of the amide groups in the polymer matrix as shown in equation above, resulting in positively charged nitrogen groups. The positive charge on the nitrogen atom invokes a core-level chemical shift to higher energies. As such, there exists the possibility of an ionic interaction between the free $[\text{AuCl}_4]^-$ ions and protonated nitrogen groups of nylon 6,6. The protonated nitrogen peak could not be detected in nanogold hybrid polyurethane materials. However, Chapman studied amides and polyurethanes under the acid conditions (pH 1.34) and reported that the polyurethanes are somewhat more stable than the amides.²⁸⁰

O 1s spectrum acquired after nylon 6,6 was reacted with gold solution is shown in Figure 3.55f. The high resolution O 1s spectrum was deconvoluted into three peaks centred at ca. 531.4 eV, 532.3 eV and 533.6 eV respectively. It is evident from these spectra that the chemical environment of O in general does not change to a great extent. The increasing of width-at half-maximum of the peaks is due to an increase in the variability of the binding environment. It is also expected that protonation of the oxygen occurs. However, because the nylon 6,6 matrix is very complex it is difficult to confirm with any certainty an interaction

between oxygen and gold or whether oxygen was involved in the reduction of gold ions to metallic gold.

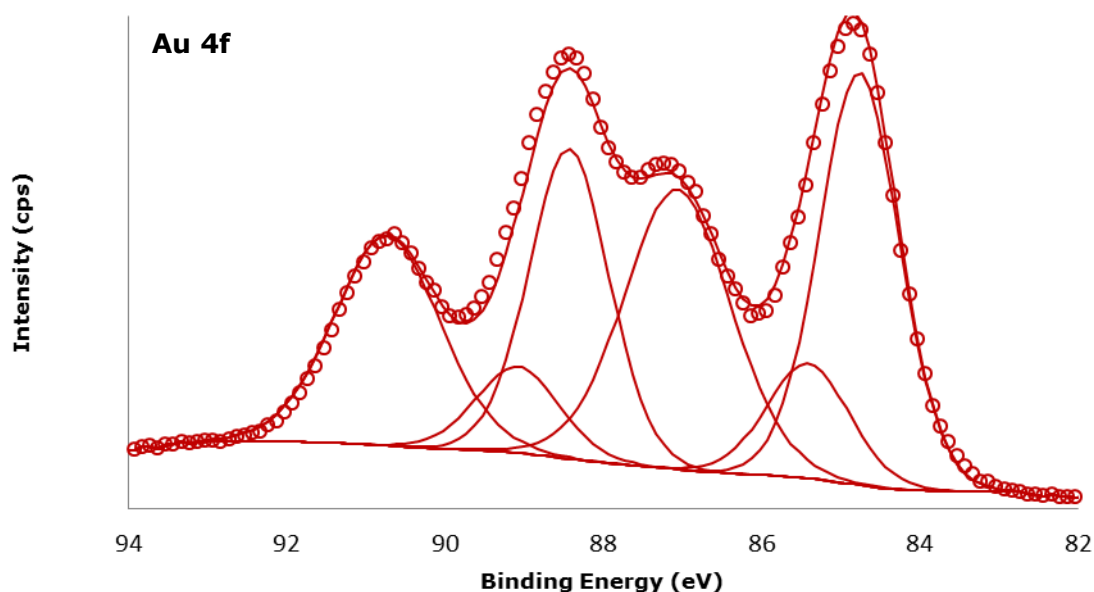


Figure 3.56: Deconvoluted high resolution Au 4f XPS spectrum for the Ny-s-500Au sample.

Figure 3.56 shows a high resolution Au 4f spectrum for the Ny-s-500Au sample. The deconvolution of the lineshape resulted in three doublets, indicating three different species of gold being present in the nanogold hybrid nylon 6,6 sheet. All three doublets have the required intensity ratio of 4:3 and the spin orbital separation of 3.67 eV. The presence of Au^0 in the nanogold hybrid nylon 6,6 sample is marked by the appearance of the doublet located at approximately 84.8 ($4f_{7/2}$) and 88.4 eV ($4f_{5/2}$) confirming that Au^{3+} ions were reduced to metallic gold. These values are located at higher binding energies in comparison to the values of Au^0 present in the analogue nanogold hybrid PU materials. The binding energy depends on the particle size, where such binding energy is larger in nanoparticle clusters than in the bulk metal and increases with decreasing size.²⁸¹ Hence, it is assumed the nanoparticles present in the nanogold hybrid nylon 6,6 materials are smaller than the ones formed in the PU matrix. This was confirmed by TEM. The doublet occurring at slightly higher binding energies from

the Au⁰ doublet is indicative of Au⁺ and has component peaks at 85.4 eV (4f_{7/2}) and 89.0 eV (4f_{5/2}) respectively. It is similarly considered that the gold nanoparticles formed in the nylon 6,6 matrix comprise Au⁰ cores, surrounded by Au⁺. Thus, these latter peaks may be due to partially reduced gold within the nylon 6,6 matrix. However, they are most likely due to the surface Au⁺ ions of the nanoparticle bound to the nylon 6,6 surface via the Au-N bond through the main containing amide groups of the polymer, and those Au⁺ ions on the surface of the nanoparticle, not bound to the polymer matrix. It is evident from the high resolution N 1s spectrum that there is a presence of a further nitrogen species at higher binding energies (Figure 3.55d) which was not seen in nanogold hybrid PU materials, thus the nitrogen species are assigned to positively charged nitrogen groups. Kitagawa et al. reported on tetrabutylammonium gold tetrachloride compound, [(C₄H₉)₄N][AuCl₄], whose Au 4f_{7/2} peak was located at around 86.9 eV²⁸², McNeillie also investigated some gold compounds and found that the Au 4f_{7/2} peak of the tetra-alkylammonium tetrachloroaurate(III) was centred at approximately 87 eV.²⁸³ Thus, protonated nitrogen groups can also be involved in gold – nitrogen interaction. As such, the third doublet of the Ny-s-500Au sample which is centred at around 87.0 (4f_{7/2}) and 90.7 eV (4f_{5/2}) respectively, is indicative of an ionic interaction between the unreduced negatively charged [AuCl₄]⁻ complex and the protonated nitrogen groups of nylon 6,6. The existence of [AuCl₄]⁻ species was also confirmed by the chlorine peak in the XPS wide scan of all the nanogold hybrid nylon 6,6 samples (Figure 3.54b). The broadness of the doublet could be due to the variation in the binding energies of the [AuCl₄]⁻ ions to different binding sites in the polymer matrix, such as protonated oxygen groups. Table 3.5 shows a summary of the XPS data obtained for the Ny-s-500Au sample.

In order to understand the extent to which the amide groups of nylon 6,6 are involved in reduction of Au³⁺ to Au⁰ the pH of the reaction medium was decreased from 4.5 to 1.4 to increase the number of protonated nitrogen groups and consequently reduce the number of original nitrogen-containing amide groups, which potentially act as reducing agents. A new sample was prepared as follows. A nylon 6,6 sheet (or beads) was immersed in 10 mL of 500 mg kg⁻¹ gold solution with pH 1.4 and heated at 50 °C for 24 hours. Contrary to the dark purple Ny-s-500Au sample, the resulting nylon 6,6 product was yellow in colour.

An identical yellow colour was noted when nylon 6,6 beads were used as the substrate in a similar reaction. Figure 3.57 shows the photograph of such resulting hybrid nylon 6,6 beads from the 500 mg kg⁻¹ gold solution with pH value of 1.4 versus the Ny-b-500Au sample. The dark purple colour of the Ny-b-500Au sample is typical of the surface plasmon resonance colour observed for gold particles in the nanoscale (Section 1.4.2). The yellow colour of the nylon beads 6,6 suggests that there are either no gold nanoparticles formed or the particles are very small in size; the colour is rather due to the absorbed [AuCl₄]⁻ ions.



Figure 3.57: Photographs of the Ny-b-500Au beads (left) and the beads prepared via the same method but with a changed pH value of 1.4 (right).

The deconvoluted, high resolution Au 4f XPS spectra of the yellow coloured nylon 6,6 sheet (prepared from a 500 mg kg⁻¹ gold solution, pH 1.4, and heating at 50 °C for 24 hours) is shown in Figure 3.58. The examination of the spectrum showed that the dominant doublet is located at higher binding energies, around 87.4 eV and 91.0 eV respectively. Thus, the gold in this material exists mainly as unreduced [AuCl₄]⁻ (62 %) which presumably forms an ionic interaction with the protonated nitrogen groups. It is evident from this spectrum that there also exist small amounts of Au⁺ and Au⁰ species. The doublet peaks located approximately 85.1 eV and 88.7 eV respectively suggests that some Au³⁺ have been reduced to

Au^+ . The percentage of Au^+ species is 28 % which can interact with the nitrogen of the nylon 6,6 matrix via an Au-N bond through the amide functional groups of nylon 6,6. Although there was no appearance of a typical pink-purple colour of gold nanoparticles in the sample, a doublet for Au^0 was evident at ca. 84.7 eV and 88.4 eV respectively. Presumably the concentration of formed gold nanoparticles was too low to exhibit a purple colour. Since nylon 6,6 possesses a considerable number of amide groups the decrease of pH value to 1.4 did not hydrolyse the amide functional groups completely so the reduction of Au^{3+} to Au^+ and Au^+ to Au^0 facilitated by the amide groups took place to a small extent. The relative percentage of formed Au^0 (75 %) in the Ny-s-500Au sample, which was prepared in the reaction medium with pH value of 4.5, was significantly higher than the relative percentage of Au^0 (10 %) found in the sample prepared at lower pH of 1.4. The binding energies of gold species present in both samples and their relative percentages are summarised in Table 3.6. Through the hydrolysis at pH 1.4, more polymer chains of nylon 6,6 break via the amide groups into positively charged amine and carboxylic acid terminated polymer chains. This process decreases the amount of amide functional groups in the nylon 6,6 matrix influencing the oxidation ability of the amide groups thus decreasing reduction of $[\text{AuCl}_4]^-$ ions to Au^0 . The increase in protonated nitrogen groups, in turn, causes an attraction of $[\text{AuCl}_4]^-$ ions forming an ionic bond.

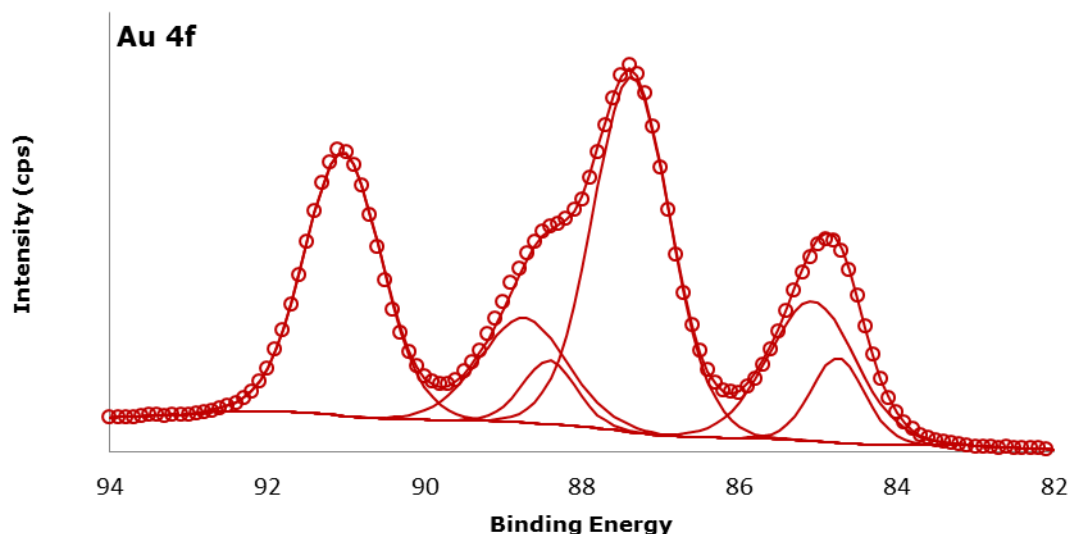


Figure 3.58: Deconvoluted high resolution Au 4f XPS spectrum for hybrid nylon 6,6 sheet prepared from a 500 mg kg⁻¹ gold solution at 50 °C for 24 hours.

Table 3.6: XPS assignments for gold present in the Ny-s-500Au sample and hybrid nylon 6,6 sheet prepared from a 500 mg kg⁻¹ gold solution at 50 °C for 24 hours.

| | | Ny-s-500Au | Ny-s-500Au prepared in pH 1.4 |
|--------------|---------------------------------|---|----------------------------------|
| | | Binding Energy [eV] and (relative percentage) | |
| Au 4f | Au ⁰ _{7/2} | 84.76 (42.62 %) | 84.74 (5.92 %) |
| | Au ⁺ _{7/2} | 85.41 (12.28 %) | 85.07 (15.74 %) |
| | Au ³⁺ _{7/2} | 87.06 (2.24 %) | 87.37 (35.66 %) |
| | Au ⁰ _{5/2} | 88.41 (31.97 %) | 88.41 (4.44 %) |
| | Au ⁺ _{5/2} | 89.08 (9.21 %) | 88.74 (11.80 %) |
| | Au ³⁺ _{5/2} | 90.73 (1.68 %) | 91.04 (26.45 %) |

Although the typical pink – purple colour for gold nanoparticles was not visible in the sample prepared at pH 1.4, the presence of metallic gold was also confirmed via XRD measurements. Figure 3.59 shows XRD patterns of an untreated nylon 6,6 sheet, a Ny-s-500Au sample and a nylon 6,6 sheet treated with a 500 mg kg⁻¹ gold solution (pH 1.4) at 50 °C for 24 hours, respectively. For the

Ny-s-500Au sample the XRD pattern showed the characteristic Bragg diffraction peaks of gold in the face centred cubic phase confirming the presence of gold nanoparticles on the surface of the hybrid nylon 6,6 sheet. The diffraction pattern of the nanogold hybrid nylon 6,6 sheet which was produced at pH 1.4 confirms the presence of gold in the sample as shown by the (1 1 1) diffraction peak at a 2θ angle of 37.9° . Gold nanoparticles larger than 2 nm in size exhibit size- and shape-dependent surface plasmon resonance absorption bands (Section 1.4.2) thus the Ny-s-500Au sample appears dark purple to our eye (Figure 3.57a). However, for gold nanoparticles smaller than 2 nm in diameter, the surface plasmon resonance absorption band disappears because the electron density in the conduction band becomes very small.¹⁰⁷ Thus, formed gold nanoparticles in the sample produced from the gold solution with pH 1.4 are very small and the colour appears yellow (Figure 3.57b) resulting from absorbed and mainly unreduced $[\text{AuCl}_4]^-$.

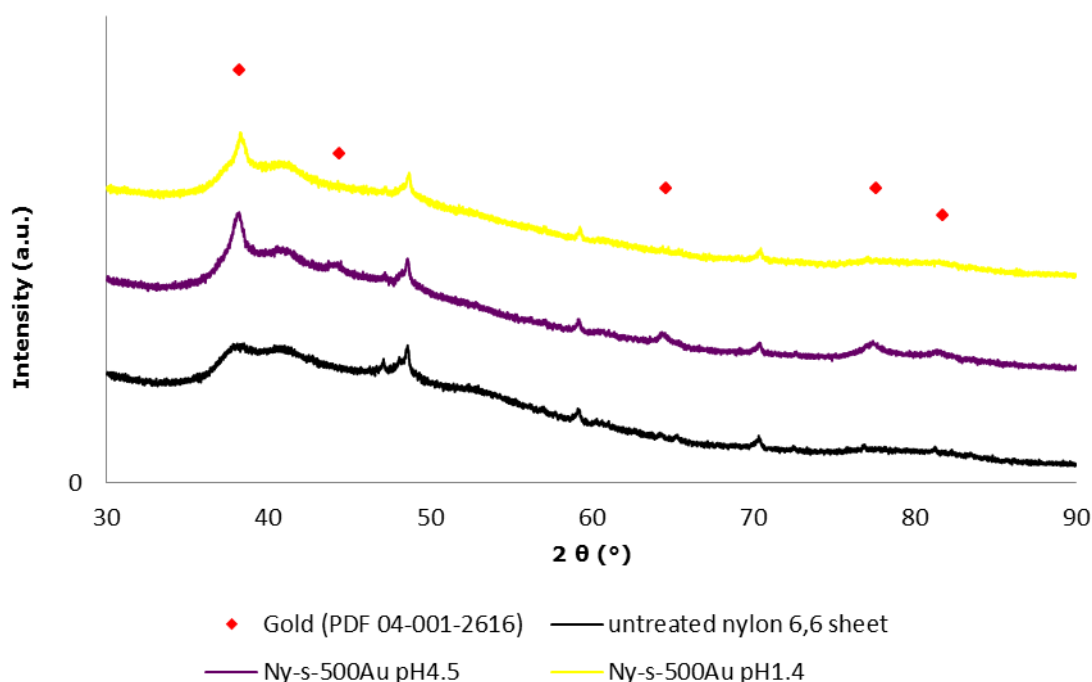


Figure 3.59: XRD patterns of the nanogold hybrid nylon 6,6 sheets produced employing 500 mg kg^{-1} gold solutions with different pH values.

3.8.3 Proposed mechanism of formation of gold nanoparticles in hybrid PU and nylon 6,6 materials

As presented and discussed above, the preparation of the nanogold hybrid PU and nylon 6,6 materials involved the reduction of gold ions to metallic nanoparticles on the surface and within the polymer matrix. The polymer matrix acts as a reducing agent and simultaneously as a stabilising agent for the gold nanoparticles which were bound chemically to the matrix. The reduction was facilitated by nitrogen-containing groups which are present in PU and nylon 6,6 polymers. The oxidation of the nitrogen functional groups form a redox couple and provide the electrons required for gold ions to be reduced to metallic gold.

In light of the results presented in Sections 3.8.1 and 3.8.2, the following mechanism is proposed for the formation of the nanogold hybrid polyurethane and nylon 6,6 materials produced through the redox properties of the nitrogen-containing functional groups of the polymers. When immersing the polymer substrates in the aqueous gold solution, the dissociated hydrogen ions and gold ions as $[\text{AuCl}_4]^-$ complex penetrate the polymer. Some of the amide linkages of nylon 6,6 matrix will be hydrolysed, however polyurethane seems to be more stable under acidic conditions, thus presumably protonation of carbamate nitrogens takes place. The resulting positively charged nitrogen groups electrostatically attract Cl^- ions and destabilise the $[\text{AuCl}_4]^-$ complex. This facilitates the reduction of Au^{3+} to Au^+ by carbamate functional groups of polyurethane or unhydrolysed amide functional groups of nylon 6,6. As only a low concentration of gold solution is employed (up to 1 wt % of gold loading in the polymer) for production of the nanogold hybrid polymer materials, a large concentration of unoxidised nitrogen-containing functional groups would still remain. The resulting Au^+ ions bind to the polymer matrix via Au-N bonds, through the carbamate group of polyurethane or amide group of nylon 6,6, involving the expansion of the valence shell of gold to its 6s orbitals. Additional Au^{3+} ions will be reduced to Au^+ simultaneously coupled with further oxidation reaction of carbamate or amide groups respectively. Owing to the aurophilicity effect²¹ it is likely that the Au^+ in the Au-N complexes would be attracted to each other resulting in the formation of nanoclusters on which the additional Au^{3+} may

accumulate and be reduced accordingly to Au^0 forming gold nanoparticles in the polymer matrix. It is not necessary for the nitrogen-containing groups to be in direct contact with the gold nanoclusters because the reaction is carried out in ionic solutions and electrons liberated from the carbamate or amide group oxidation can be transferred to the adjacent gold nanoclusters, providing the required electrons for the Au^{3+} to Au^0 reduction. Since these gold nanoparticles are bound to the polymer matrix Au-N bonds (Sections 3.8.1 and 3.8.2), the surface energy of the nanoparticles will be decreased, making the nanoparticles stable against the aggregation.

Increasing of the pH of the reaction solution ($[\text{AuCl}_4]^-$) causes enhanced hydrolysis of the nylon 6,6 polymer chains resulting in a large number of broken amide linkages. Because less amide entities are available for oxidation in order to provide electrons for reduction of gold ions to metallic gold, metallic gold is formed to a smaller extent. Unreduced gold ions in $[\text{AuCl}_4]^-$ form ionic bonds to positively charged nitrogen atoms resulting in the yellow colour of the product.

3.8.4 X-ray photoelectron spectroscopy analysis of nanosilver hybrid polyurethane materials

XPS analysis was carried out on the surface of the PU-b-500Ag sample because, as it was observed by SEM, silver nanoparticles were mostly formed and found on the polyurethane bead surface. Figure 3.60 provides the survey XPS scans of the untreated polyurethane and the nanosilver hybrid polyurethane beads with their respective characteristic elements (C, N, O and Ag).

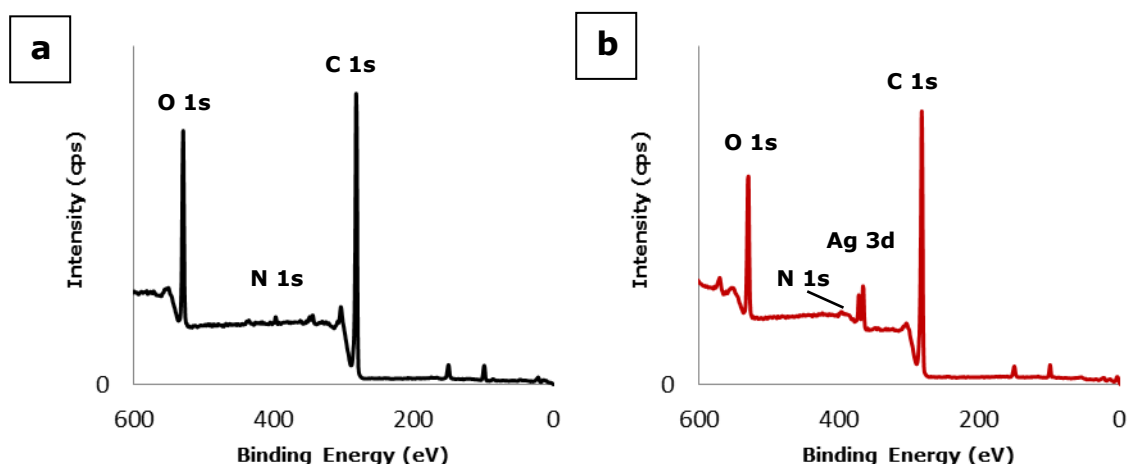


Figure 3.60: Survey XPS scans of the surfaces of the untreated PU bead (a) and PU-b-500Au sample.

From the examination of the deconvoluted high resolution C 1s spectra for the untreated polyurethane bead and the PU-b-500Ag sample (not illustrated) it was evident that the chemical environment of C did not change to a notable extent upon the reaction of polyurethane with silver. The high resolution N 1s and O 1s XPS spectra for the untreated PU and the nanosilver hybrid PU bead sample (PU-b-500Ag) are provided in Figure 3.61 and the list of the peak assignments is listed in Table 3.7. In the N 1s spectrum for the untreated PU bead a single peak was assigned to the carbamate group at 400.4 eV. In the spectrum for the PU-b-500Ag sample there was no significant shift to higher binding energies, however a significant broadening of the peak was observed. The increase of the FWHM by 0.3 eV suggests a greater range in the nature of the nitrogen species in addition to changes in the surrounding environment. As only 0.5 wt % of silver was employed to produce nanosilver hybrid PU material, very small changes are expected. Thus, it is also possible that the N 1s peak would mask further minor peaks at lower binding energies attributable to interaction of nitrogen with silver in the form of Ag-N bond, as well as a peak at higher binding energies representing oxidised nitrogen species, which provide electrons for the reduction of Ag^+ to Ag^0 .

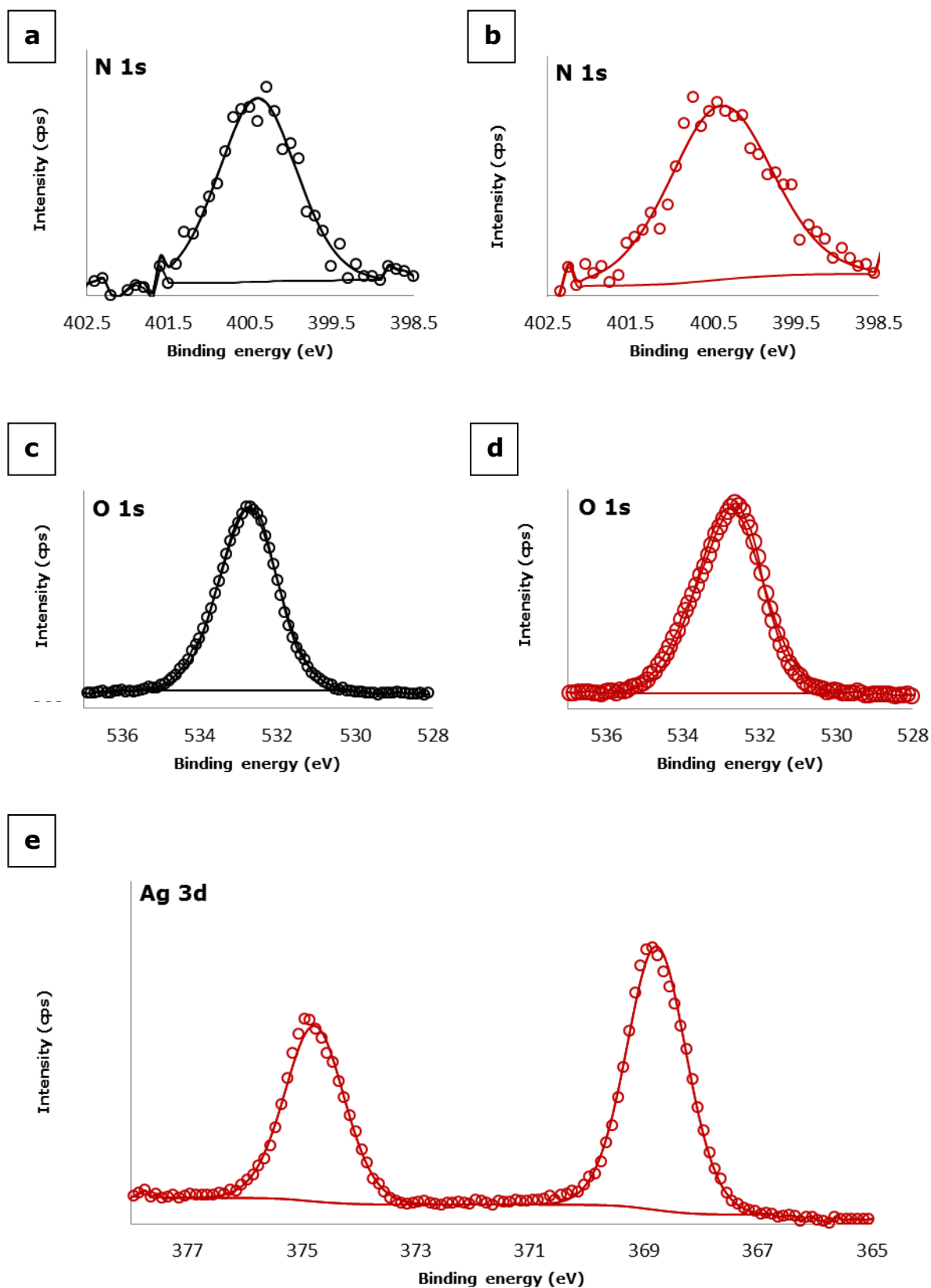


Figure 3.61: Deconvoluted high resolution XPS spectra for the untreated polyurethane bead: a) N 1s peaks and c) O 1s peaks; for the PU-b-500Ag sample: b) N 1s peaks, d) O 1s peaks and e) Ag 3d peaks.

The XPS O 1s spectrum was deconvoluted into one peak only with the maximum at around 532.8 eV and was considered to depict the average oxygen environment of PU. The analysis of high resolution O 1 s spectrum of the PU-b-500Ag sample showed similar broadening of the oxygen peak by 0.25 eV upon reaction with Ag⁺ ions. An interaction between silver and the lone pair electrons of oxygen species presented in PU is therefore likely.

Table 3.7: XPS assignments for the untreated PU bead and the PU-b-500Ag sample.

| | | Untreated PU beads | Nanosilver hybrid PU beads |
|--------------|--------------------------------|-------------------------------------|----------------------------|
| | | Binding Energy [eV] and (FWHM) [eV] | |
| C 1s | C-C, C-H | 285.00 (1.00) | 285.00 (1.17) |
| | C-N | 285.62 (0.92) | 285.61 (0.98) |
| | C-O | 286.73 (1.20) | 286.70 (1.47) |
| | O-C=O | 289.41 (0.97) | 289.44 (1.05) |
| | C-N-Ag | - | - |
| N 1s | N-H | 400.41 (1.12) | 400.42 (1.44) |
| | N-Ag | - | - |
| O 1s | Average O environment | 532.76 (1.78) | 532.78 (2.03) |
| Ag 3d | Ag ⁰ _{5/2} | - | 368.52 (1.14) |
| | Ag ⁰ _{3/2} | - | 374.52 (1.14) |

The high resolution Ag 3d spectrum of the PU-b-500Ag sample was deconvoluted into one doublet (Figure 3.61e). The peaks with an intensity ratio of 3:2 and the typical spin orbit splitting of 6 eV are positioned around 368.5 (3d_{5/2}) and 374.5 (3d_{3/2}) eV. These peaks are attributable to Ag⁰, which confirmed that silver ions were reduced to metallic silver when PU was exposed to AgNO₃ solution at 90 °C for 24 hours of reaction time. The position of the 3d_{5/2} peak is shifted slightly to higher binding energies compared with the binding energy of 3d_{5/2} peak of bulk silver which according to the literature is typically located between 368.0 to 368.3 eV.²² These shifts of the Ag 3d peaks of the nanosilver hybrid PU sample can be associated with decreasing particle size with respect to the Ag bulk value. The FWHM of the Ag⁰ peaks seem to be somewhat broader than expected. The

FWHM increases with decreasing of particle size; however it also may indicate more than one oxidation state of silver is present. It could also indicate that the association of silver with the nitrogen or oxygen groups of the polymer contributes to this peak. However, it is difficult to ascertain the nature of the bond existing between silver and the polymer matrix, since as mentioned above, the analyses of the N 1s and the O 1s spectra are not conclusive.

3.8.5 X-ray photoelectron spectroscopy analysis of nanosilver hybrid nylon 6,6 materials

For XPS analysis the Ny-s-1000Ag sample was chosen as a representative of the nanosilver hybrid nylon 6,6 materials in order to investigate how the amide groups of the nylon 6,6 matrix are involved in the reduction of silver ions to silver nanoparticles and their subsequent binding to the polymer matrix. By treating the nylon 6,6 sheet which with 1000 mg kg⁻¹ Ag⁺ solution at 90 °C for 24 hours, it was hoped to increase the likelihood of detecting any changes between the XPS spectra of the untreated nylon 6,6 sheet and its corresponding nanosilver hybrid polymer. The Ny-s-1000Ag sample possesses a very high concentration of silver nanoparticles on the hybrid polymer surfaces, thus the formation of an increased quantity of silver nanoparticles would necessitate the oxidation of an increased percentage of functional groups of the nylon 6,6 matrix. Figure 3.62 shows the survey XPS scans of the untreated nylon 6,6 sheet and the nanosilver hybrid nylon 6,6 sheet with their respective characteristic elements (C, N, O and Ag). A list of the peak assignments can be seen in Table 3.8.

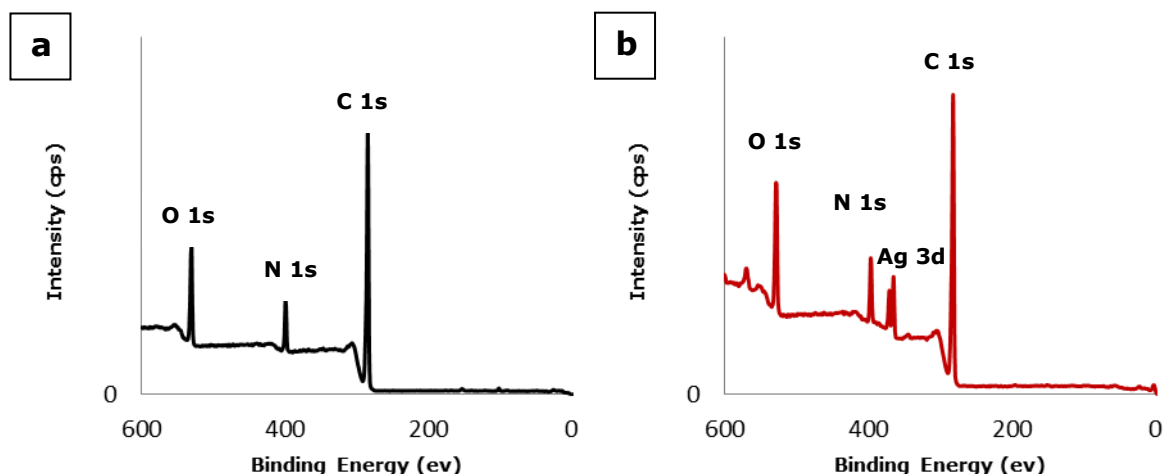


Figure 3.62: Survey XPS scan for (a) the untreated nylon 6,6 sheet and b) the Ny-s-1000Ag sample.

Table 3.8: XPS assignments for the untreated nylon 6,6 sheet and the Ny-s-1000Ag sample.

| | | Untreated nylon 6,6 sheet | Nanosilver hybrid nylon 6,6 sheet |
|--------------|--------------------------------|-------------------------------------|-----------------------------------|
| | | Binding Energy [eV] and (FWHM) [eV] | |
| C 1s | C-C, C-H | 285.00 (0.98) | 285.00 (0.99) |
| | C-N | 285.59 (1.59) | 285.79 (1.62) |
| | N-C=O | 288.04 (1.17) | 288.07 (1.24) |
| N 1s | N-H | 399.69 (1.14) | 399.79 (1.15) |
| | | 400.24 (1.52) | 400.53 (1.80) |
| O 1s | N-C=O | 531.16 (1.21) | 531.35 (1.22) |
| | Unidentified O species | 532.19 (1.21) | 532.41 (1.22) |
| | | 533.28 (1.21) | 533.44 (1.22) |
| Ag 3d | Ag ⁰ _{5/2} | - | 368.14 (0.86) |
| | Ag ⁺ _{5/2} | - | 368.77 (1.89) |
| | Ag ⁰ _{3/2} | - | 374.14 (0.86) |
| | Ag ⁺ _{3/2} | - | 374.77 (1.89) |

From a comparison of the deconvoluted high resolution C 1s spectra for the untreated nylon 6,6 sheet and the Ny-s-1000Ag sample it was apparent that the chemical environment of C changed upon the reaction of nylon 6,6 with silver.

The high resolution C 1s spectra for the untreated nylon 6,6 sheet and the nanosilver hybrid nylon 6,6 sheet were deconvoluted into three peaks respectively (Figure 3.63a-b). As described in Section 3.8.2, the peak of the untreated nylon 6,6 sheet at 285.0 eV was attributed to C-C or C-H carbons in the nylon 6,6 polymer chain, while the higher binding energy peaks at approximately 285.6 eV and 288.0 eV were assigned to the carbon nitrogen bond (C-N) and the carbon in the amide group of the nylon 6,6 (NH-C=O) respectively. The change in the Ny-s-1000Ag sample was notable in C-N peak which showed a positive core level shift by 0.2 eV. This shift can be associated with the higher oxidation state of the nitrogens consistent with the reduction of the Ag⁺ ions to Ag⁰ being facilitated by the oxidation of the amide groups of the nylon 6,6 matrix. A similar shift of ca. 0.2 eV was observed in the Ny-s-500Au sample (Section 3.8.2). The slight increase in FWHM of the C-N peak as well as the NH-C=O peak of the nanosilver hybrid sample is due to an increase in the variability of the environments surrounding these entities.

As previously mentioned (Section 3.8.2), owing to the complexity and the disorder of the nylon 6,6 polymer chains, it is likely that the amide functional groups exist in two different chemical environments. Thus, using a two-peak fitting routine deconvolution of the N 1s spectrum resulted in two peaks with the respective binding energies of 399.7 eV and 400.2 eV for the untreated nylon 6,6 sheet (Figure 3.63c). These peaks essentially represent the end number of a range of slightly different environments. After the reaction with silver, the two peaks which were assigned to amide nitrogen groups shifted to 399.8 eV and 400.5 eV respectively (Figure 3.63d). The shift to higher binding energies of both peaks implies oxidation of the nitrogen groups confirming the results seen in C 1s spectra analyses. Due to the broadness of peak at ca. 400.5 eV, it is also possible that this would mask any minor peaks which can be associated with protonated nitrogen groups formed during the reaction with silver solution with the pH value of 5.

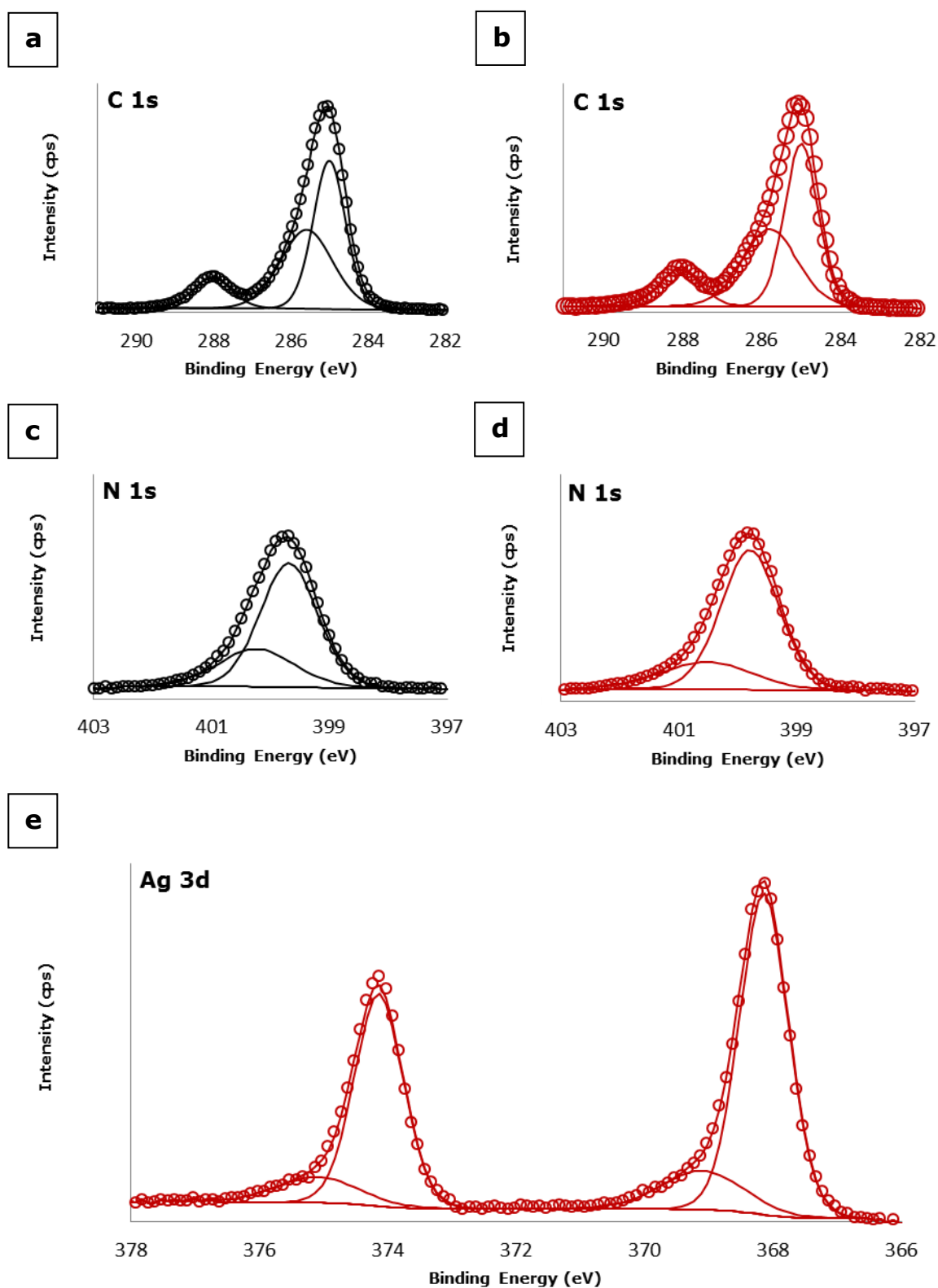


Figure 3.63: Deconvoluted high resolution XPS spectra for the untreated nylon 6,6 sheet: a) C 1s peaks and c) N 1s peaks; for the Ny-s-1000Ag sample: b) C 1s peaks, d) N 1s peaks and e) Ag 3d peaks.

Figure 3.63e shows the high resolution Ag 3d spectrum obtained of the Ny-s-1000Ag sample. Unlike the PU-b-500Ag sample (Section 3.8.4), the spectrum of the Ny-s-1000Ag sample was deconvoluted into two doublets. Matching the intensity ratio of 3:2 and the spin orbit splitting (6 eV) of bulk silver, the peaks positioned around 368.1 ($3d_{5/2}$) eV and 374.1 ($3d_{3/2}$) eV were attributed to Ag^0 , which confirmed that silver ions were reduced to metallic silver upon exposure of nylon 6,6 to $AgNO_3$ solution at 90 °C for 24 hours of reaction time. Evidence for the presence of a second species of silver was observed by the second doublet at higher binding energies with a positive core level shift of ca. 0.7 eV from the Ag^0 doublet. Although unlike other metals, silver shows a shift to lower binding energy with increased oxidation state, there are reports of shifts towards higher binding energies when silver is bound to sulphur or oxygen. Gerenser studied XPS measurements of Ag at the silver-poly(p-phenylene sulphide) interface and observed a positive shift of 0.6 eV for the Ag $3d_{5/2}$ peak, which was interpreted as the interaction of Ag with the S atoms of the poly(p-phenylene sulfide) polymer due to the strong affinity of Ag for S.²⁸⁴ Wagner reported on binding energy of 368.8 eV for Ag $3d_{5/2}$ peak for silver trifluoroacetate.²⁸⁵ Thus, with silver having a an affinity for nitrogen,^{241,286} the peaks found on the surface of the Ny-s-1000Ag sample located at around 368.8 eV and 374.8 eV respectively were attributed to the association of silver with the nitrogen atoms of nylon 6,6 matrix. The interaction of silver with oxygen atoms is likely. However, it is difficult to ascertain the nature of the bonding existing between silver and the polymer matrix. As reported above the interpretation of the high resolution of N 1s and O 1s spectrum analyses are similarly not conclusive.

The formation of nanosilver entities on nylon 6,6 surface were also confirmed by means of XRD analyses of the Ny-s-1000Ag sample. Figure 3.64 shows XRD pattern of the sample representing the appearance of (1 1 1), (2 0 0), (2 2 0) and (3 1 1) Bragg diffraction peaks of the fcc structure of silver.

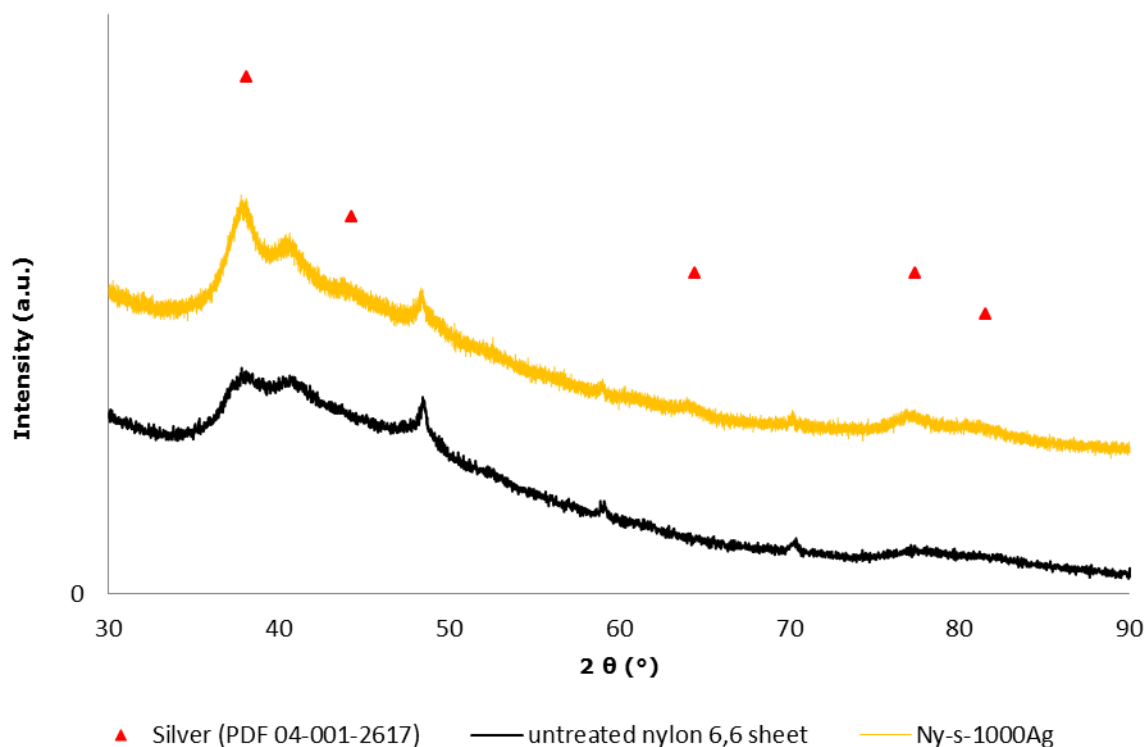


Figure 3.64: XRD patterns of the untreated nylon 6,6 sheet and the Ny-s-1000Ag sample.

3.8.6 Proposed mechanism of formation of silver nanoparticles in hybrid PU and nylon 6,6 materials

From the XPS results discussed in Sections 3.8.5 and 3.8.6, no unambiguous conclusion can be reached concerning the bonding nature of silver and the polymer matrix of polyurethane or nylon 6,6. However, the following mechanism for the formation of silver nanoparticles within the PU or nylon 6,6 polymer matrix can be suggested. Silver ions are firstly absorbed by the polymers. Due to their affinity for nitrogen, silver ions associate with nitrogen-containing groups such as carbamates or amides. The interaction between the silver ions and oxygen atoms of the polymer matrices is also possible. Acting as reducing agents nitrogen functionalities are oxidised and provide the electrons for Ag^+ ions to be reduced to Ag^0 , resulting in the formation of silver nanoparticles in the polymer matrix. The matrix restricts the size of the nanoparticles.

For a more conclusive statement of the proposed mechanism for the formation of silver nanoparticles in hybrid PU and nylon 6,6 materials further XPS studies are required, which could be carried out in the future. This work would include preparation of higher loading of silver in the polymers in order to achieve greater changes in the XPS spectra to confirm the proposed mechanism.

3.9 Infrared and Raman spectroscopy analysis of nanogold and nanosilver hybrid PU and nylon 6,6 materials

Infrared spectroscopy was used in an effort to further clarify the nature of bonding between the gold and silver nanoparticles and the polymer matrices of polyurethane and nylon 6,6 respectively. It was hoped that by comparing the spectra of the untreated polymers with the spectra of the nanogold and nanosilver hybrid polymers, such further clarification about the role of the carbamate and amide groups in the reduction of Au^{3+} to Au^0 or Ag^+ to Ag^0 respectively would emerge. The PU-b-500Au, PU-b-500Ag, Ny-b-500Au and Ny-b-500Ag samples were chosen as a representative of the nanogold and nanosilver hybrid PU and nylon 6,6 materials. These samples exhibit a very high concentration of metal nanoparticles at the hybrid polymer surfaces, increasing the probability of detecting any changes between the spectra of the untreated polymers and their respective hybrid polymers. The formation of an increased amount of nanoparticles would require the oxidation of an increased percentage of functional groups of the polymer matrix. Figure 3.65 shows a comparison between the untreated polyurethane, the PU-b-500Au and the PU-b-500Ag samples.

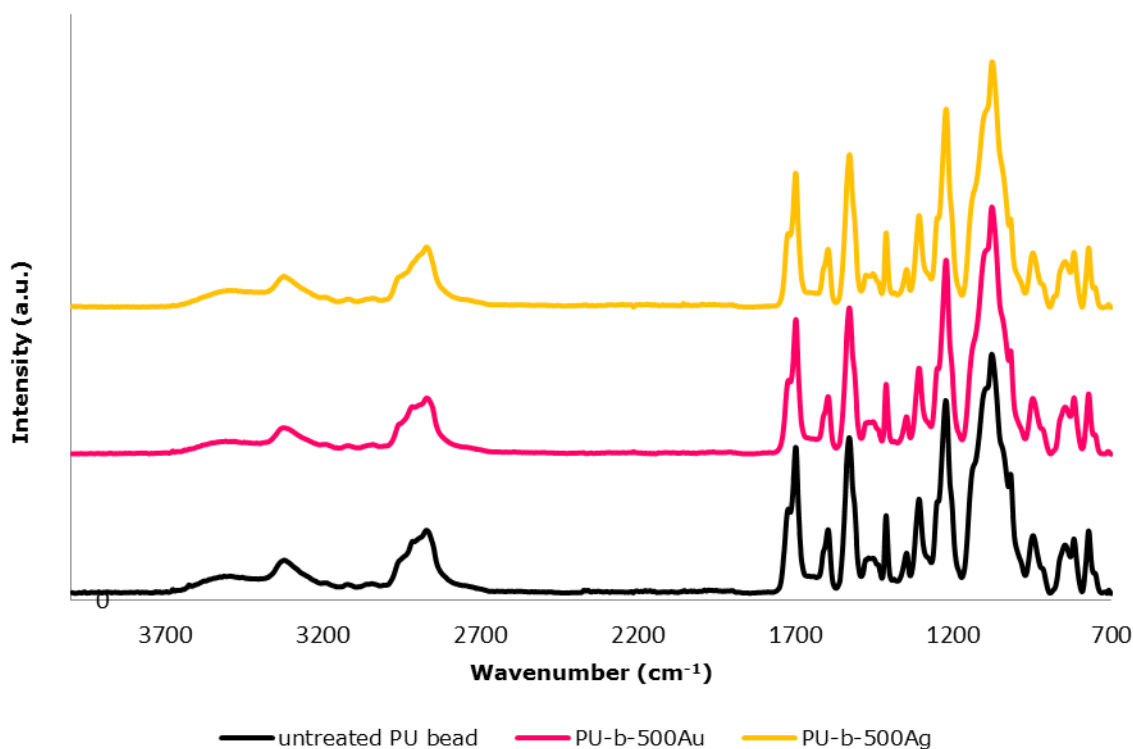


Figure 3.65: FT-IR spectra for the untreated PU sheet, nanogold and nanosilver hybrid PU sheets.

The characteristic features of polyurethane in the IR spectra are the 3420-3200 cm^{-1} bands assigned to N-H stretch, 3000-2800 cm^{-1} bands of the CH_2 and CH_3 stretch, 1701 cm^{-1} and 1726 cm^{-1} bands of the H-bonded urethane C=O and non-bonded urethane group respectively, the 1530 cm^{-1} band of the N-H bend and the 1080 cm^{-1} band of the C-O-C stretch.^{287,288} The nanogold and nanosilver hybrid PU samples exhibited identical peaks to those of the corresponding untreated PU sample (Figure 3.65). There were also no notable changes in the IR spectrum of the untreated nylon 6,6 compared with the hybrid nylon 6,6 samples upon reaction with gold or silver (not illustrated). Thus, due to the similarity of the two polymers to their resultant hybrid polymers, it was not possible to obtain any further information on the bonding between the metallic nanoparticles and PU or nylon 6,6 polymers using IR spectroscopy. This is likely due to the fact that IR spectroscopy is a bulk analysis technique on such samples, and hence is not particularly sensitive to the small quantity of

nanoparticles on the surface of the polymers relative to the quantity of polymer present.

Raman spectroscopy analysis showed that any potentially useful Raman signals were obscured by the fluorescent characteristics of the polymers, which also impaired the collection of spectra for the untreated polymers and their resultant nanogold and nanosilver hybrid polymers.

3.10 Leaching test on nanogold and nanosilver hybrid polyurethane materials

Nanoparticles are used in a host of consumer products. The antimicrobial properties of silver have encouraged many companies to incorporate silver nanoparticles in to plastic food containers, clothing, baby goods, cosmetic products etc. The lack of information however regarding the long term health or environmental impacts of these nanoparticles, the use of these consumer products is cause for concern. Hence, it is important to minimise the leaching of the nanoparticles from the consumer products. As such, quantitative AA analyses of the leaching solutions were undertaken in order to investigate the amount of gold and silver leached from the nanogold and nanosilver hybrid polymer materials. The PU-b-100Au and PU-b-100Ag samples were chosen as representatives for the hybrid polymer materials.

The preparation of the leaching solutions of these samples was achieved following the method described in Section 2.2.5. This was accomplished by immersing the produced nanogold or nanosilver hybrid PU samples in 10 ml of distilled water and agitating them for seven days at room temperature. The residual leaching solutions were analysed by AA spectroscopy for any gold or silver content respectively. AA spectroscopy studies showed that a small percentage of gold (0.27 wt % of total gold loading in the PU beads) and silver (0.19 wt % of total silver loading in the PU beads) was leached from the hybrid polyurethane materials (Table 3.9). These results endorse the XPS analyses

results of the materials suggesting that the gold and silver nanoparticles are chemically bound to the polymer matrix via Au-N and Ag-N bonds respectively (Sections 3.8.1 and 3.8.4). The detected amounts of gold or silver are likely related to the free gold or silver ions which are, as a result of an incomplete reduction reaction, confined in the PU matrix.

Table 3.9: Gold or silver leached from nanogold and nanosilver hybrid PU materials, leaching tests were carried out at room temperature for seven days.

| Sample | Metal species | Amount of metal in polymer [wt %] | Amount of leached metal [μg] | Amount of leached metal [% total metal loading] |
|------------|---------------|-----------------------------------|---|---|
| PU-b-100Au | gold | 0.1 | 2.7 | 0.27 |
| PU-b-100Ag | silver | 0.1 | 1.9 | 0.19 |

3.11 Antimicrobial properties of nanogold and nanosilver hybrid PU materials

Since the occurrence of antibiotic resistance by common microbes is increasing, it has become more challenging to treat microbial infections. Thus, there is growing interest in creating new and more effective antimicrobial materials and treatments. The antimicrobial properties of gold and silver in various forms have been used throughout history (Section 1.4.6). Silver is the element with the highest toxicity for microorganisms, followed by $\text{Hg} > \text{Cu} > \text{Cd} > \text{Cr} > \text{Pb} > \text{Co} > \text{Au} > \text{Zn} > \text{Fe} > \text{Mn} > \text{Mo} > \text{Sn}$.²⁸⁹ Due to their high surface area and high fraction of surface atoms, the use of gold and silver nanoparticles should exhibit more effective antimicrobial activity compared to their bulk metals. Consequently the nanogold and nanosilver hybrid PU *dog bone* strips were tested for their antimicrobial activity. Due to the time limitations, the test was performed only on the PU-db-50Au and PU-db-50Ag samples against the gram negative *Escherichia coli* bacteria (strain W3110). The tests were carried out using the method described in Section 2.3.8; in summary the untreated PU *dog bone* strip as the reference sample, the PU-db-50Au and the PU-db-50Ag

samples were cut into small pieces and dispersed in aqueous standard phosphate-buffered saline (PBS) suspension containing bacteria to provide contact between the hybrid polymer materials and the bacteria. The antimicrobial activity was determined on the basis of the relative difference in total colony-forming units (CFU) between the nanogold and nanosilver hybrid PU *dog bone* strips and the reference sample after seven days of contact with the bacteria. CFU is a measure of viable bacterial numbers.

Figure 3.66 presents the percentage of CFU remaining after the untreated PU *dog bone* strip, the PU-db-50Au and the PU-db-50Ag samples were exposed to *E. coli* bacteria for seven days. While the reference sample, the untreated PU, was as expected, not effective against the bacteria, ca. 51.74 % and 99.97 % of bacteria were killed for the PU-db-50Au and the PU-db-50Ag samples respectively after seven days of exposure.

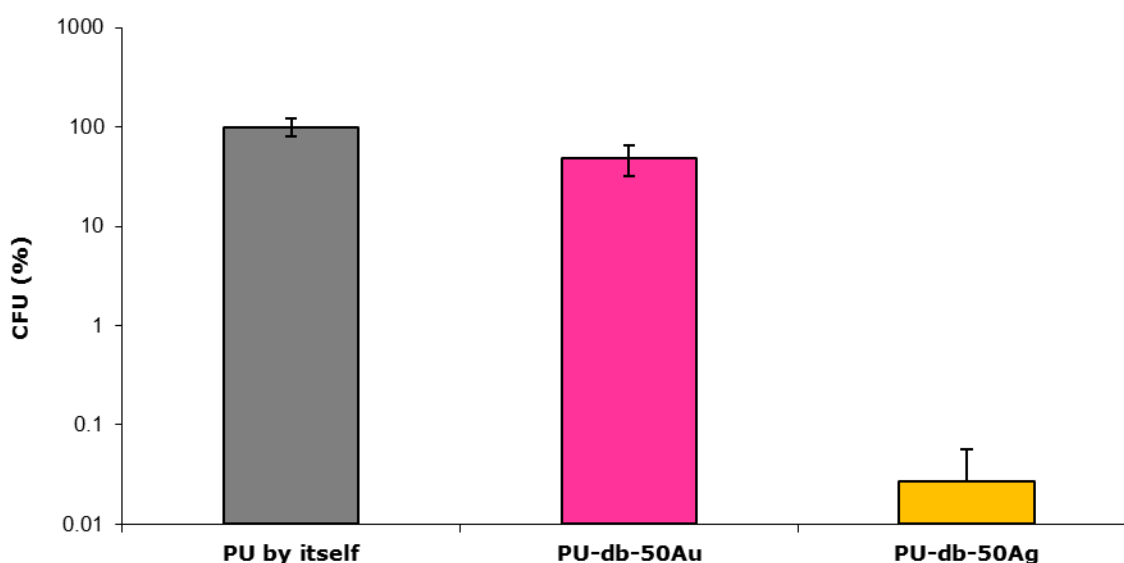
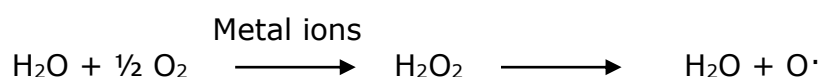


Figure 3.66: Percentage cell survival relative to the untreated PU as control sample after 7 days of bacteria being in contact with the PU and gold and silver hybrid PU materials. (Note the vertical axis is in log scale.)

Gold and silver nanoparticles have been explored for their broad-spectrum antimicrobial activity.^{192,290,291} When gold or silver nanoparticles are released into the pathogenic environment, the metallic nanoparticles attach to the surface of the bacterial cells and can also penetrate the cells. The nanoparticles exhibit strong binding affinity to the electron-donating groups in the bacterial cells, resulting in their antimicrobial activity.¹⁹² However, the mechanism of antimicrobial effects of gold or silver is still not fully understood (Section 2.3.8).

The gold and silver nanoparticles present in the hybrid PU and nylon 6,6 materials are chemically bound to the polymer matrix (Sections 3.8), thus the nanoparticles are not released into the pathogenic environment where they physically can interact with the bacteria. Burrige reported on bacteriostatic properties of gold nanoparticles wool composites, where gold nanoparticles chemically bound to wool resisted microbial attack.²¹ As shown by the XPS study (Section 3.8.1) the surface of formed nanoparticles is positively charged due to the presence of partially reduced Au^+ ions. Thus, there likely exists an electrostatic attraction between the positively charged gold ion and negatively charged bacterial cell wall resulting in association between the nanoparticles of the PU-db-50Au sample and the bacteria. This can facilitate electron transfer between the gold and the bacteria disrupting the cell function.

Another possibility is that the antibacterial activity of the nanogold hybrid PU materials may be related to the formation of free radicals from the surface of gold nanoparticles. It can be assumed that the Au^+ ions, which are on the surface of gold nanoparticles, catalyse the production of oxygen radicals which then oxidise the molecular structure of bacteria. Free radicals can then attack membrane lipids which leads to a breakdown of membrane function.²⁰⁷ During the antimicrobial tests the hybrid PU samples were immersed in aqueous PBS solution containing the bacteria. This would not exclude the formation of reactive oxygen species according to chemical reaction²⁹² below:



Because the reactive oxygen diffuses through the polymer matrix to the surrounding environment, there was no need for any direct contact between the nanogold of the hybrid PU material and the bacteria to induce the damage of the microorganism. However, the proposed model and the assumed formation of radicals needs to be studied further in order to verify it. This is work that could be carried out in the future.

As anticipated when comparing the nanogold and nanosilver hybrid PU *dog bone* strips (Figure 3.66) there is a major decrease in percentage of surviving *E. coli* cells for the PU-db-50Ag sample. Unlike gold, silver nanoparticles are not inert and are sensitive to oxidation.²¹⁵ Thus, the efficacious properties of silver are considered to arise through the partial oxidation and release of silver ions into an aqueous or moist environment.²¹⁷ The necessary conditions for this exist in the aqueous PBS suspension containing the *E. coli* bacteria. Once the suspension diffused into the PU-db-50Ag sample, the contact between the silver nanoparticles and water molecules leads to the slight dissolution of silver nanoparticles to silver ions and the subsequent migration of silver ions through the hybrid PU material leading to their release from the hybrid PU material to the aqueous environment. These released silver ions then can moderate the denaturation of proteins, leading to cell death. Additionally it is known that the binding of Ag^+ to bacterial DNA and RNA inhibits bacterial replication.^{209,293,294} Kaur reported that silver ions react with nucleophilic amino acid residues in proteins, and attach to sulfhydryl, amino, imidazole, phosphate and carboxyl groups of membrane or enzyme proteins.²⁹⁵ The reaction of silver ions with sulfhydryl (-S-H) groups on the cell wall to form R-S-S-R bonds, blocks respiration and causes cell death.²⁹⁶ Moreover, due to the electrostatic interaction with negatively charged bacterial cell walls the attachment of silver ions to the bacteria leads to cell death via the rupturing of the cell membrane.²⁹⁶ Reports have shown that low concentrations of silver ions induce a massive proton leakage through the bacterial membrane and cell death.^{297,298}

Additionally, the positively charged silver nanoparticles within the polymer matrix may form free radicals enhancing their antimicrobial properties. To verify this proposed effectiveness, it would be interesting to study the formation of free radicals in such a system. This work could be carried out in the future.

3.12 Conclusions

Nanogold and nanosilver hybrid polyurethane and nylon 6,6 polymer materials were successfully produced. For the redox reaction the carbamate and amide functional groups present in PU and nylon 6,6 matrices respectively were utilised in order to reduce Au^{3+} or Ag^+ to Au^0 or Ag^0 . Simultaneously formed metal nanoparticles were bound to the surface and within the polymer matrix of PU or nylon 6,6. Additionally, the polymer matrices provided stabilisation for gold and silver nanoparticles. The resultant hybrid materials showed to exhibit the typical colours for gold and silver nanoparticles.

For the redox reaction the ideal temperature was determined to be 50 °C for the production of nanogold and 90 °C for nanosilver hybrid polymer materials. Atomic absorption studies showed that after 24 hours of reaction time the majority of gold (in the form of AuCl_4^-) and more than 60 % of silver ions were absorbed by the polymer substrates. In general, the absorbed amount of metal ions was slightly higher by PU than by nylon 6,6 substrates. The reaction parameters, such as time, temperature and the concentration of the metal ion solution influenced the uptake rate of Au^{3+} / Ag^+ by the substrates and therefore the colour of the resultant hybrid materials.

The nanogold and nanosilver hybrid polymer materials were shown to exhibit absorption bands in the visible region of light consistent with the surface plasmon resonance bands of gold and silver nanoparticles respectively. When the concentration of the employed metal ion solution for the synthesis of the hybrid polymer materials was increased, the respective absorption bands showed not only broadening but also shifts towards higher wavelengths due to an increase in particle size and some agglomerations. The surface plasmon resonance absorption bands of gold and silver nanoparticles are influenced by particle size, shape and the dielectric constant of the surrounding medium.

Electron microscopy studies of the nanogold and nanosilver hybrid PU and nylon 6,6 materials demonstrated that the metal nanoparticles were formed not only on the surfaces but also within the polymer matrices. The gold or silver particle

distribution on the surface of the polyurethane or nylon 6,6 substrates was uniform. The higher the concentration of the employed metal ion solution for the production of the hybrid materials was the more particle agglomerates were formed on the surface of the polymer substrates due to the lack of stability by the substrates. This resulted in a brown colouration of the sample with a metallic shiny effect (for both nanogold and nanosilver hybrid polymer samples). The increased concentration of the metal ions also influenced the morphology of the interior of the substrates. The more the metal ions were absorbed the deeper they penetrated the substrates where they subsequently were reduced to metal nanoparticles. The interior of the polymer substrates provided better stabilisation of the nanoparticles resulting in smaller particle size compared to the particles found on the surface of the polymers. Generally, silver nanoparticles seem to be smaller than gold nanoparticles in both PU and nylon 6,6 substrates. The particles found in the PU polymer appear to be larger than the analogue hybrid nylon 6,6 materials which is believed to be due to the higher amount of metal ion uptake by PU compared to nylon 6,6 substrates. The gold nanoparticles in the hybrid polymer materials were mostly spherical or spherical like in shape, however some hexagonal, truncated triangular and rod shaped particles were observed. Silver nanoparticles were found to be predominantly spherical.

XPS studies suggest the gold and silver nanoparticles bind to the PU or nylon 6,6 matrix through the covalent Au-N and Ag-N bonds respectively in the nitrogen-containing carbamate or amine groups. Additionally, it was found that there is an ionic interaction between the unreduced negatively charged $[\text{AuCl}_4]^-$ complex and the protonated nitrogen groups of nylon 6,6.

The proposed mechanism of formation of the nanogold hybrid polyurethane and nylon 6,6 materials involves the reduction of Au^{3+} to nanoparticulate Au^0 by the coupled oxidation of the carbamate functional groups of polyurethane or amide functional groups of nylon 6,6. It is proposed that during the reaction some of the Au^{3+} ions will be reduced to Au^+ by nitrogen-containing groups, forming the Au-N bonds and acting as nucleation sites. Further Au^{3+} are attracted to these Au-N nucleation sites where they will be reduced to Au^0 , again facilitated by the oxidation of nearby nitrogen-containing groups of the polymers. No unambiguous conclusions concerning the bonding nature of silver and the

polymer matrix of polyurethane or nylon 6,6 could be made. However, the following can be suggested. Due to their affinity for nitrogen, silver ions interact with nitrogen-containing groups such as carbamates or amides. The interaction between the silver ions and oxygen atoms of the polymer matrices is not to be excluded. Acting as reducing agents nitrogen entities are oxidised and provide the electrons for Ag^+ ions to be reduced to Ag^0 , resulting in the formation of silver nanoparticles in the polymer matrix. The matrix restricts the size of the nanoparticles. The leaching tests confirmed that the gold and silver nanoparticles were chemically bound to the polymer matrix. It was demonstrated that only a very small amount of gold and silver leached out of the hybrid PU materials after seven days of leaching. These amounts are likely due to loosely bound gold or silver nanoparticles on the surface of the polymers.

It was found that the nanogold and nanosilver hybrid polyurethane materials have antimicrobial effects against gram negative *E. coli* bacteria.

The production of the nanogold and nanosilver hybrid PU materials has been scaled up to produce sufficient amounts of the materials which were moulded into *dog bone* test strips via a conventional thermoplastic moulding process by the Centre for Advanced Composite Materials and the Plastics Centre of Excellence at the University of Auckland. The resulting test strips show that nanogold and nanosilver entities are distributed evenly through the moulded plastic, confirming that these nanoparticles do not affect the thermoplastic forming properties of the polymer substrates.

4 Nanogold and nanosilver hybrid polymer materials: nanoparticles formed in the presence of alternative substrates such as amine coated polyethylene terephthalate sail cloth and silica based Bulk isolate® sorbent

Materials such as amine coated polyethylene terephthalate (PET) sail cloth and silica based Bulk isolate® sorbent (NH₂) were utilised as substrates. These substrates were used for the purpose of building up a simple model to confirm the ability of the nitrogen-containing functional groups to reduce Au³⁺ / Ag⁺ to Au⁰ / Ag⁰ respectively and subsequently bind the resultant metal nanoparticles to the substrate matrix (Section 3).

Hybrid PET sail cloth and silica based Bulk isolate® sorbent (NH₂) containing gold and silver nanoparticles were synthesised following the approach described in Section 2.2.1.2. The methodology involved immersing the substrates in aqueous hydrogen tetrachloroaurate or silver nitrate solutions followed by heating the reaction vials to complete the reduction of metal ions to metal nanoparticles. The employed temperatures are summarised in Table 4.1. Unless otherwise mentioned, the mass of the substrates was 0.2 g for PET sail cloth and 0.2 g for Bulk isolate® sorbent (NH₂) materials; the metal ion solution volume was 10 mL. All experiments were stopped after 24 hours. It was intended that the amine groups on the surface of the substrates would reduce Au³⁺ and Ag⁺ to Au⁰ and Ag⁰ respectively, whilst simultaneously stabilising the resultant metal nanoparticles and binding them to the substrate matrix.

The names for the hybrid polymer materials and their respective reaction parameters are listed in Table 4.1.

Table 4.1: The sample names and their respective reaction parameters for the nanogold and nanosilver hybrid materials. The mass for each substrate was 0.2 g. The reaction time for all samples was 24 hours. The solution volume was 10 mL.

| Name of hybrid polymer material | Substrate | Metal ion conc. [mg kg ⁻¹] | Metal ion species | Reaction temp. [°C] | wt % of metal in polymer |
|---------------------------------|--|--|-------------------|---------------------|--------------------------|
| PET-50Au | PET sail cloth | 50 | Au ³⁺ | 80 | 0.25 |
| PET-50Ag | PET sail cloth | 50 | Ag ⁺ | 80 | 0.25 |
| NH2-500Au | Bulk isolute® sorbent (NH2) ^a | 500 | Au ³⁺ | 70 | 2.5 |
| NH2-500Ag | Bulk isolute® sorbent (NH2) ^a | 500 | Ag ⁺ | 70 | 2.5 |

^a Bulk isolute® sorbent (NH2) substrates will be discussed below.

4.1 Nanogold and nanosilver hybrid PET sail cloth and ISOLUTE sorbents materials

In contrast to PU and nylon 6,6 materials, PET polymer does not contain any nitrogen-containing functional groups which are able to reduce Au³⁺ or Ag⁺ to Au⁰ or Ag⁰ respectively. To inhibit the aging of polymers, such as the PET sail cloth materials from the long term degradation effects of oxygen and UV light, stabilisers are used during the production of these materials. According to XPS analysis nitrogen-containing groups are present on the surface of the PET sail cloth. These are probably hindered amine light stabilisers. Figure 4.1 shows the survey XPS scans of the untreated sail cloth material with its respective characteristic major elements such as carbon and oxygen (X-ray peaks for Ca and Si should be ignored due to contaminations in the laboratory). Additionally, a peak for nitrogen was detected. The XPS analysis provided a quantitative estimation of nitrogen content on the surface of the sail cloth. The surface of the sail cloth substrate contained 0.6 % of nitrogen.

Hence, there exists an opportunity for these nitrogen-containing functional groups to reduce gold or silver ions to metallic gold or silver on the surface of the PET sail cloth and bind the metallic nanoparticles through the Au-N or Ag-N interaction.

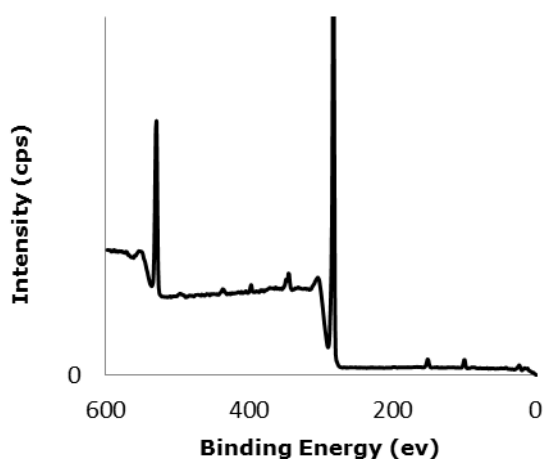
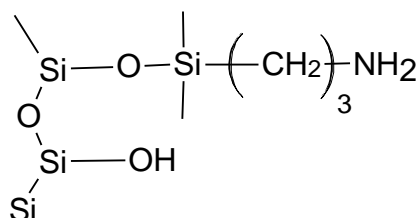


Figure 4.1: Survey XPS scan of the untreated PET sail cloth fabric.

Silica based Bulk isolate® polar sorbent (NH₂) is commonly utilised in solid phase chromatography to extract organic compounds such as drugs. They are irregular shaped aminopropyl functionalized silica particles with a size of ca. 50 µm. Typical NH₂ is shown below:



After immersing the fabrics or the sorbent materials in tetrachloroaurate or silver nitrate solutions for 24 hours at 80 °C or 70 °C respectively, the formation of metal nanoparticles on the substrates was apparent by the appearance of a pink

or yellow colour. As previously mentioned, these colours are typical for gold and silver nanoparticles respectively, resulting from the surface plasmon resonance scattering of light by these metallic nanoparticles (Section 1.4.2). The shade and intensity of the colour can be altered by systematically altering the concentration of the AuCl_4^- or Ag^+ solution and the reaction time. The resulting nanogold and nanosilver hybrid PET sail cloth and sorbent materials are shown in Figure 4.4 and Figure 4.5 respectively. For the control reaction 0.2 g of pure PET polymer beads or Silica based Bulk isolate® sorbents C18 sorbent material were immersed in equal concentrated tetrachloroaurate or silver nitrate solutions for 24 hours at 80 °C or 70 °C respectively. Silica based Bulk isolate® C18 sorbent are irregular shaped octadecyl-functionalized silica particles. After 24 hours of reaction time the PET beads or the C18 sorbent particles did not change their original colour. Hence, it is possible to rule out that the ester functional groups of the PET or silica groups of the C18 sorbent material are not involved in reduction of Au^{3+} or Ag^+ to Au^0 or Ag^0 respectively.

4.2 Extent of gold and silver uptake by PET sail cloth and silica based BULK ISOLUTE® NH₂ sorbent materials

The uptake of dissolved gold ($[\text{AuCl}_4]^-$) and silver (Ag^+) by the PET sail cloth material was quantitatively analysed by atomic absorption spectroscopy (Section 2.3.3). Similar to the PU and the nylon 6,6 substrates (Section 3.1.1) the PET sail cloth fabrics were soaked in 50 mg kg⁻¹ of gold or silver solutions for different periods of time at 80 °C. Subsequently the resulting solutions were analysed for any residual gold or silver. The difference between the starting concentration and the residual concentration was determined to be the amount of the gold or silver ions absorbed by the PET sail cloth substrates. Figure 4.2 and Figure 4.3 show the trend of gold and silver uptake by the PET sail cloth within 24 hours of absorption period.

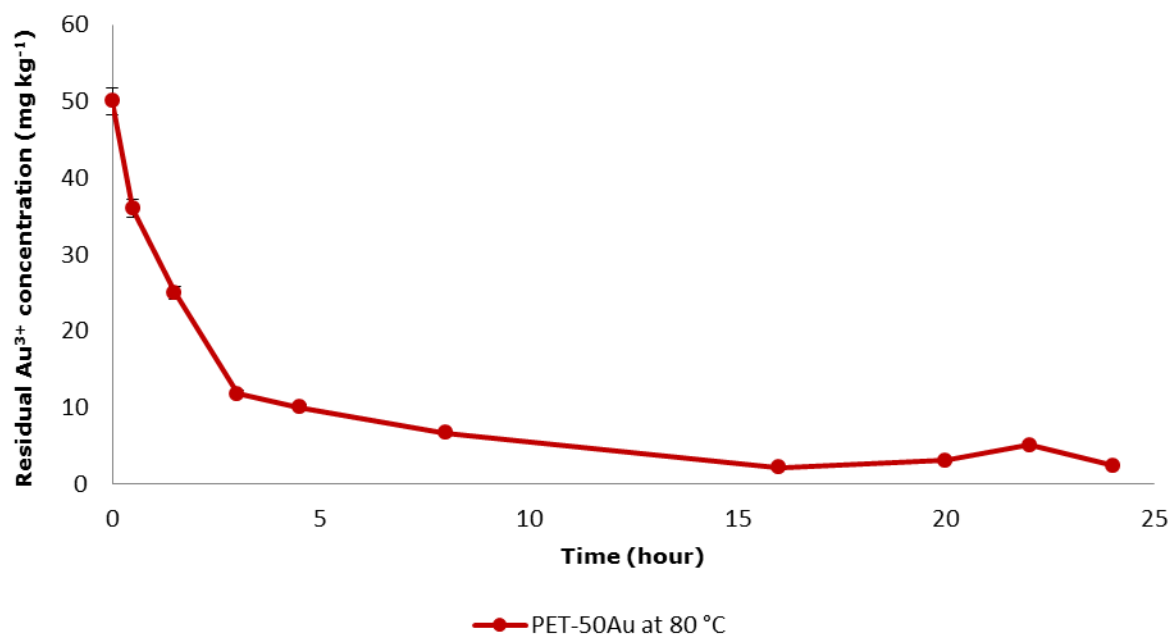


Figure 4.2: Gold uptake by the PET sail cloth at 80 °C, utilising a solution with an initial gold concentration of $50 \text{ mg kg}^{-1} \text{Au}^{3+}$.

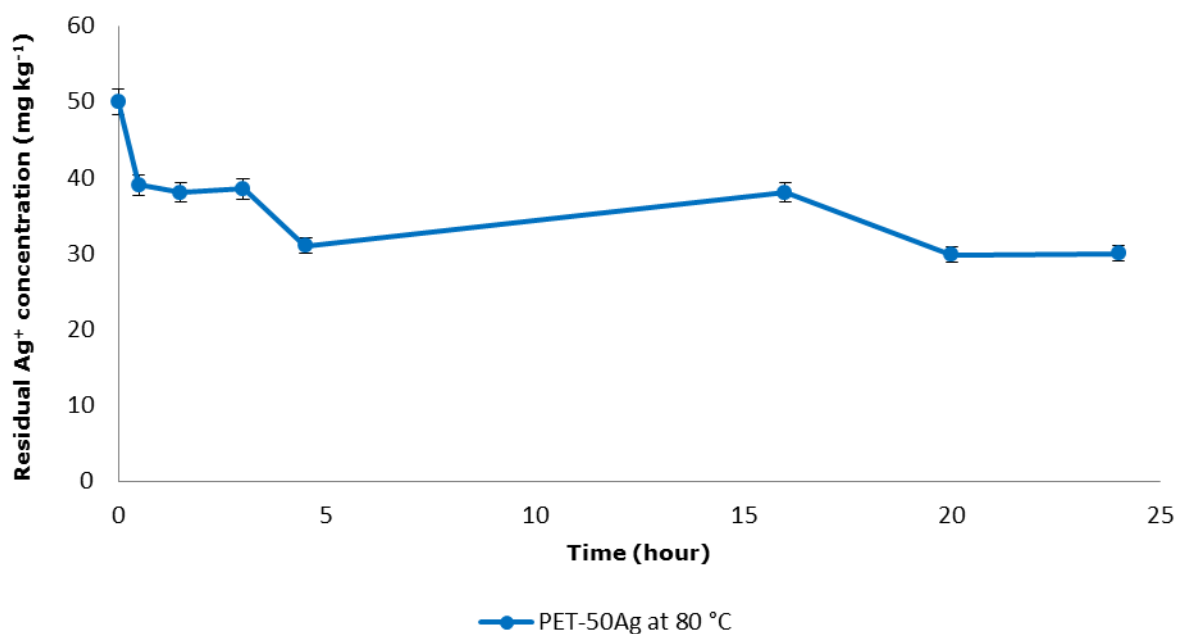


Figure 4.3: Silver uptake by the PET sail cloth at 80 °C, utilising a solution with an initial silver concentration of $50 \text{ mg kg}^{-1} \text{Ag}^{+}$.

When comparing the uptake of gold and silver ions by the PET sail cloth, the resulting curves show that nearly all of the gold and only ca. 40 % of silver content of the 10 mL starting solutions was absorbed by the 0.2 g of the PET sail cloth fabric after 24 hours absorption period at 80 °C. Similar behaviour was observed when PU or nylon 6,6 were used as substrates (Section 3.1). A possible explanation for this observation is that under slightly acidic reaction conditions (pH 4-5) the functional groups of the employed PET sail cloth substrates become protonated. Therefore these functional groups have a net positive charge. Gold ions are being absorbed as the $[\text{AuCl}_4]^-$ complex. Thus, it can be assumed that an electrostatic attraction exists between the gold complex and the positively charged PET sail cloth. Positive silver ions are electrostatically repelled by the PET substrates because of their positive charge leading to a decreased uptake rate.

Atomic absorption spectroscopy (Section 2.3.3) was also used to quantitatively analyse the uptake of dissolved gold and silver by the NH_2 sorbent material. However, due to the shortage of the material the uptake of gold or silver was only measured after 24 hours of reaction time. This was achieved by soaking the NH_2 particles (0.2 g) in 500 mg kg^{-1} of gold or silver solutions at 70 °C. After 24 hours the resulting solutions were analysed for any residual gold or silver. The difference between the starting concentration and the residual concentration was determined to be the amount of the gold or silver ions absorbed by the NH_2 sorbent substrates. After 24 hours of uptake period ca. 99 % of gold and approximately 80 % of silver ions were absorbed by these substrates. Again, as for the PET sail cloth substrate, under slightly acidic reaction conditions (pH 4-5) the amine groups of the employed NH_2 sorbent particles are protonated resulting in a net positive charge. The electrostatic attraction between the gold complex ($[\text{AuCl}_4]^-$) and the positively charged amine groups of NH_2 substrate lead to a complete uptake of the ions.

4.3 UV Visible spectroscopy – colour of nanogold and nanosilver hybrid PET sail cloth and silica based BULK ISOLUTE® NH₂ sorbent materials

The pink-purple or yellow-brown colour development of the nanogold and nanosilver hybrid PET sail cloth and silica based NH₂ sorbent samples was indicative of the reduction of the absorbed Au³⁺ or Ag⁺ to their respective metal nanoparticles. These colours are due to the interaction of light with nanosized gold or silver particles formed on the surface of the PET or NH₂ sorbent substrates. Similar pink and yellow colours were achieved for the nanogold and nanosilver hybrid PU and nylon 6,6 materials (Section 3). Figure 4.4 and Figure 4.5 show the photographs of the resultant hybrid PET or NH₂ materials next to their respective untreated substrates after a period of 24 hours of reaction, during which gold or silver ions were absorbed by the substrates, reduced to gold or silver nanoparticles respectively and simultaneously stabilised by the substrate matrix.



Figure 4.4: Photograph of the untreated PET sail cloth, PET-50Au and PET-50Ag samples (from left to right).



Figure 4.5: Photograph of the NH2-500Au, NH2-500Ag and untreated NH2 sorbent material samples (from left to right).

The formation of gold and silver nanoparticles in these substrates was studied by UV-Vis spectroscopy. When nanoparticles form, an intense visible surface plasmon resonance absorption band appears. The position of the SPR bands is dependent upon the size, shape of the nanoparticles and the dielectric constant of the surrounding medium.²⁵² Kubelka Munk transformed UV-Vis reflectance spectra for the nanogold and nanosilver hybrid PET materials as well as for the untreated PET sail cloth fabric are shown in Figure 4.6. The PET sail cloth sample prepared from a 50 mg kg⁻¹ gold solution (PET-50Au) exhibits an absorption peak at approximately 545 nm. The peak position is consistent with the surface plasmon resonance absorption of gold nanoparticles and similar positions were observed for SPR bands of the purple coloured nanogold hybrid PU and nylon 6,6 materials (Section 3.1.1). The peak at about 455 nm for the PET-50Ag sample is similarly consistent with the surface plasmon resonance absorption of silver nanoparticles appearing yellow to the eye. The broadness of both peaks

indicates a range of particle sizes and shapes as well as a possible presence of particle aggregates which was confirmed by the SEM analysis (Section 4.3).

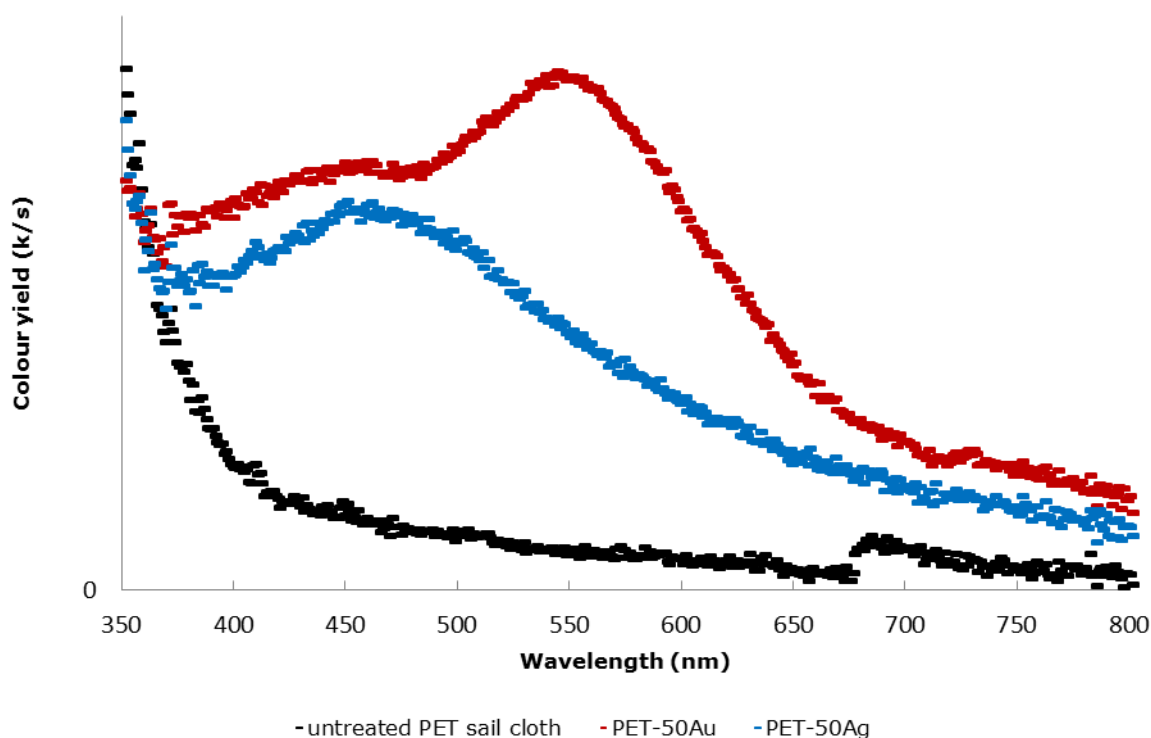


Figure 4.6: Kubelka Munk transformed UV-Vis reflectance spectra of the untreated PET sail cloth, nanogold and nanosilver hybrid PET sail cloth materials.

Figure 4.7 presents the Kubelka Munk transformed UV-Vis reflectance spectra for the nanogold and nanosilver hybrid NH₂ materials next to the untreated NH₂ sorbent material. The spectrum for the NH₂-500Au sample compared to the spectrum of the untreated NH₂ sorbent material shows that there is the development of a broad visible region absorption after the substrate reacted with the gold ion containing solution. This broad absorption band indicates the presence of gold nanoparticles in a wide range of particle size and shape as well as possible particle agglomeration resulting in a dark purple colouration of the sample shown in Figure 4.5. The Kubelka Munk transformed UV-Vis spectrum of the NH₂-500Ag sample (Figure 4.7) also displays a broad visible region absorption with its maximum between 400 nm and 500 nm, giving the sample

its brown appearance. This is consistent with the surface plasmon resonance band of silver nanoparticles.

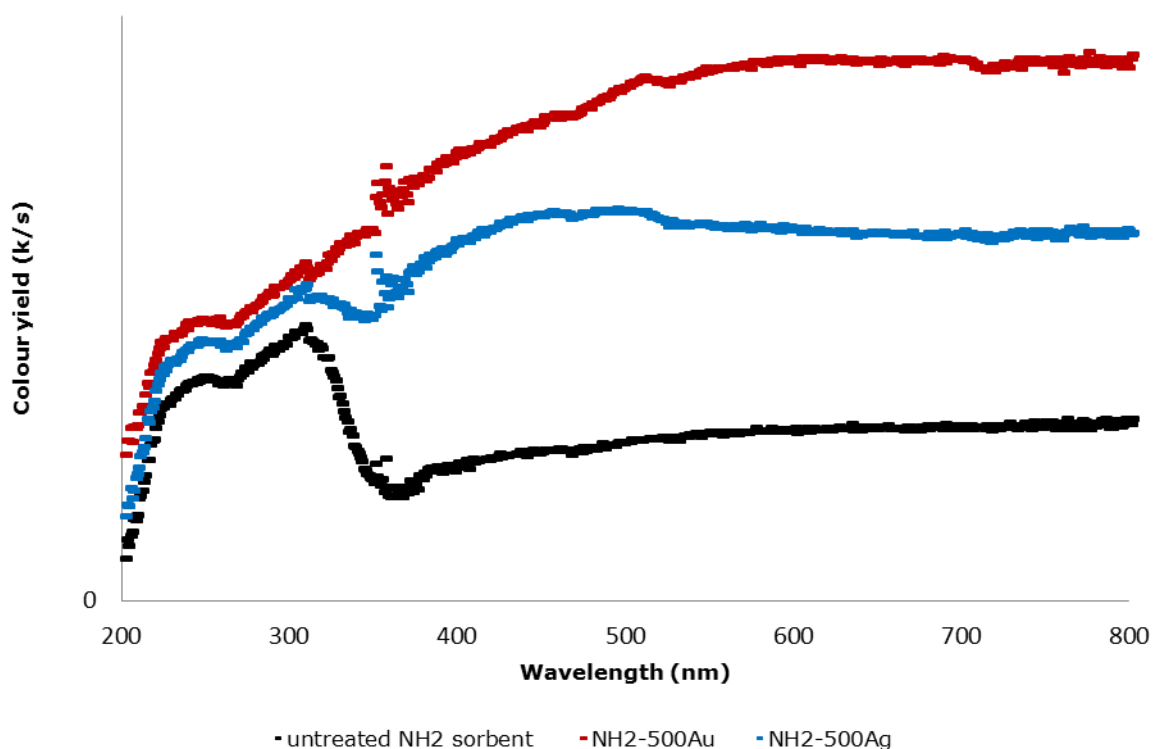


Figure 4.7: Kubelka Munk transformed UV-Vis reflectance spectra of the untreated NH2 sorbent particles, nanogold and nanosilver hybrid NH2 sorbent materials.

As such, the UV-Vis spectroscopy analyses confirmed that both substrates (PET and NH2 sorbent material) when exposed to gold or silver ion solutions are able to reduce Au^{3+} and Ag^+ to gold and silver nanoparticles respectively.

4.4 SEM and EDS analyses of hybrid PET sail cloth and silica based BULK ISOLUTE® NH₂ sorbent materials

SEM and EDS analyses were carried out on the PET-50Au, PET-50Ag, NH₂-500Au and NH₂-500Ag samples in order to view the morphology of the produced hybrid materials and to confirm the formation of gold or silver nanoparticles on their surface. To observe the interior of the hybrid PET polymer materials, cross sections of the sail cloth samples were made by cutting the samples with a clean razor blade into two halves.

Figure 4.8 offers SEM micrographs of the surface of the PET-50Au sample at increasing magnifications, confirming the presence of gold nanoparticles. The gold nanoparticles are observable in the backscatter mode as white dots. The contrast between the metal and the polymer is due to the higher atomic weight of gold and the lower atomic weight of the polymers. At a magnification of 25 times, the PET fibres of the PET-50Au sample, which are woven together to make the sail cloth (Figure 4.8a), do not differ from the fibres of the untreated PET sail cloth. However, with further magnification to 2500 times and 23000 times (Figure 4.8b-c) a surface with a rich coverage of gold nanoparticles can be observed. The gold nanoparticles are predominantly spherical accompanied by some bigger triangular gold platelets. The nanoparticles vary in size, most of the spherical nanoparticles were below 100 nm in diameter. Some particle agglomerates were also present. This is consistent with the results obtained from the UV-Vis analysis of these materials (Section 4.3). EDS elemental analysis confirmed that the nanoparticles present on the PET surface were gold (Figure 4.8d). The distribution of the gold nanoparticles is reasonably uniform across the PET fibres. Due to the intense surface plasmon band of these gold nanoparticles the hybrid PET sail cloth exhibits a purple hue (Figure 4.4).

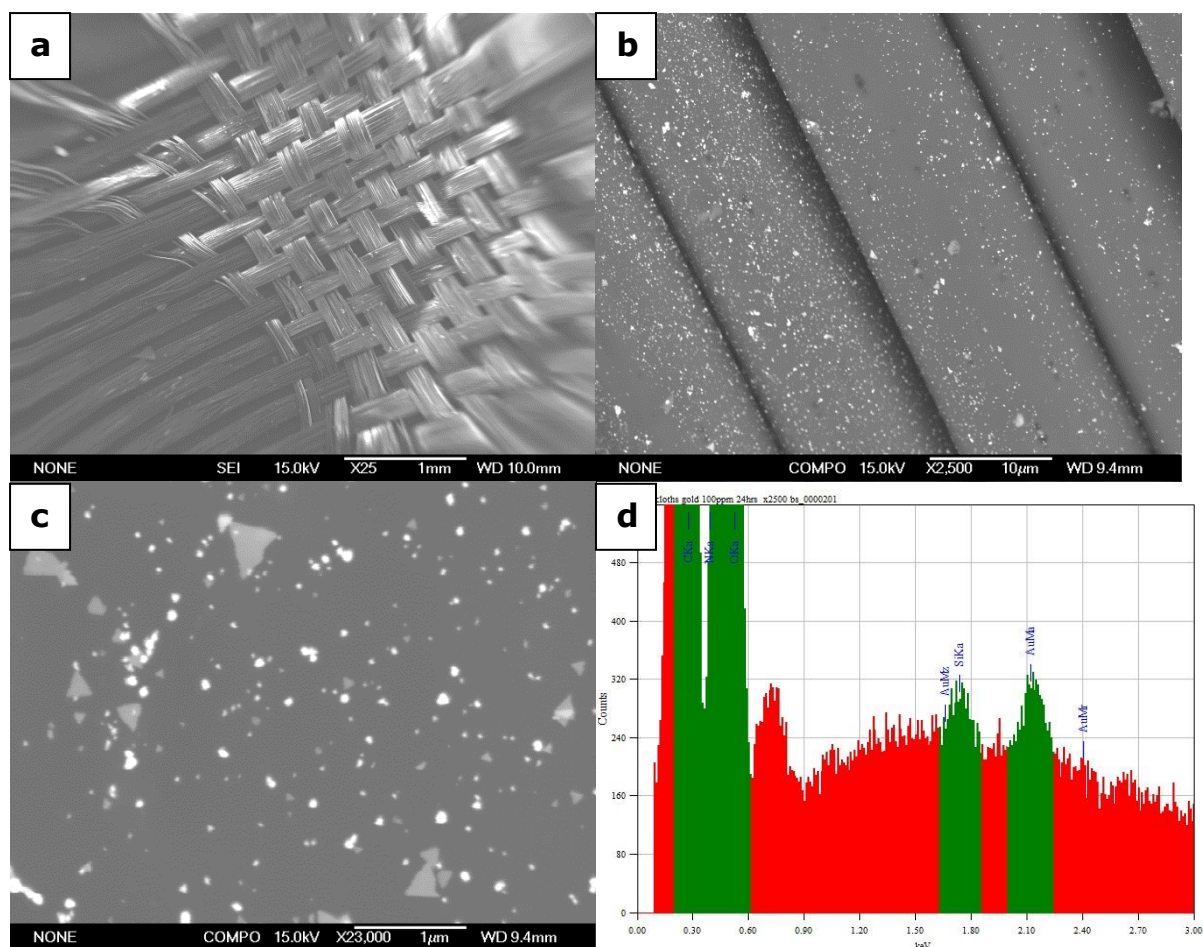


Figure 4.8: SEM micrographs of the surface of the PET-50Au sample a) at 25 times (SEI), b) 2500 times (COMPO), c) 23000 times magnification (COMPO) with d) the respective EDS elemental analysis spectrum.

The SEM analysis of the surface of the PET-50Ag sample confirmed the presence of silver nanoparticles (Figure 4.9). EDS analyses of the samples provided information about the elemental composition of the analysed surface of the hybrid sample. Similar to the PET-50Au sample, the surface analysis revealed high and uniform coverage over the entire surface of the sail cloth fibre, indicating that the absorbed Ag^+ ions were reduced to Ag^0 and simultaneously stabilised by the PET polymer matrix. The resulting nanoparticles were verified as silver by the EDS analysis (Figure 4.9b). The particles of the surface were spherical and generally smaller than the one found on the surface of the PET-50Au sample. However, particle aggregates were also present. These particles give rise to the surface of the PET fibres being yellow coloured (Figure 4.4).

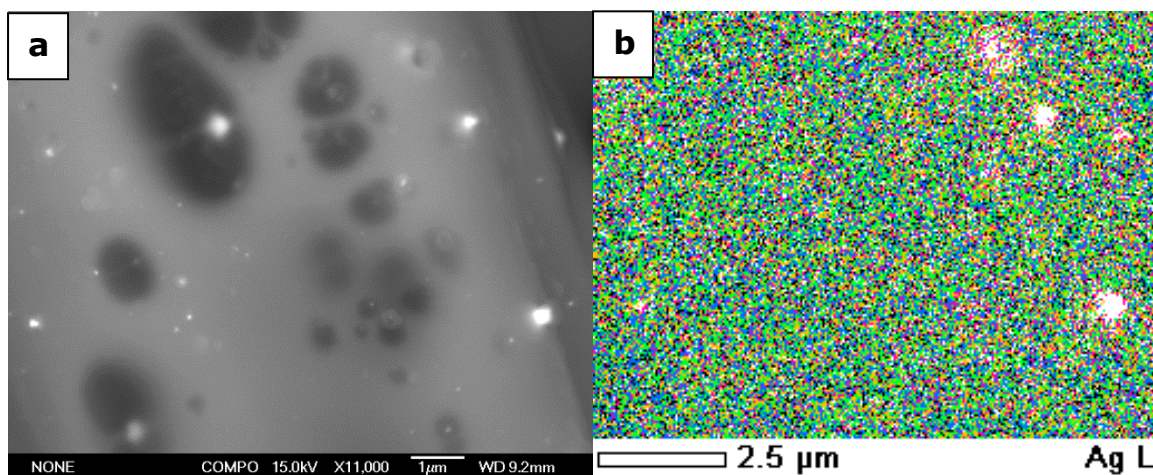


Figure 4.9: SEM micrographs of the PET-50Ag surface a) at 11000 times (COMPO) with b) the respective EDS elemental analysis map.

Figure 4.10 shows SEM image of a cross section of the PET-50Au sample recorded in backscatter mode. It is evident that the gold nanoparticles in these hybrid PET materials were confined to the surface of the fibres, rather than spread throughout the centre of the fibre. The SEM analysis of the cross section of the PET-50Ag sample led to the same result, the silver nanoparticles were formed on the surface of the PET fibres (not displayed). Hence, it can be assumed that the stabilisers containing the nitrogen groups which are essential for the Au^{3+} or Ag^+ reduction are located on the surface of the PET fibres.

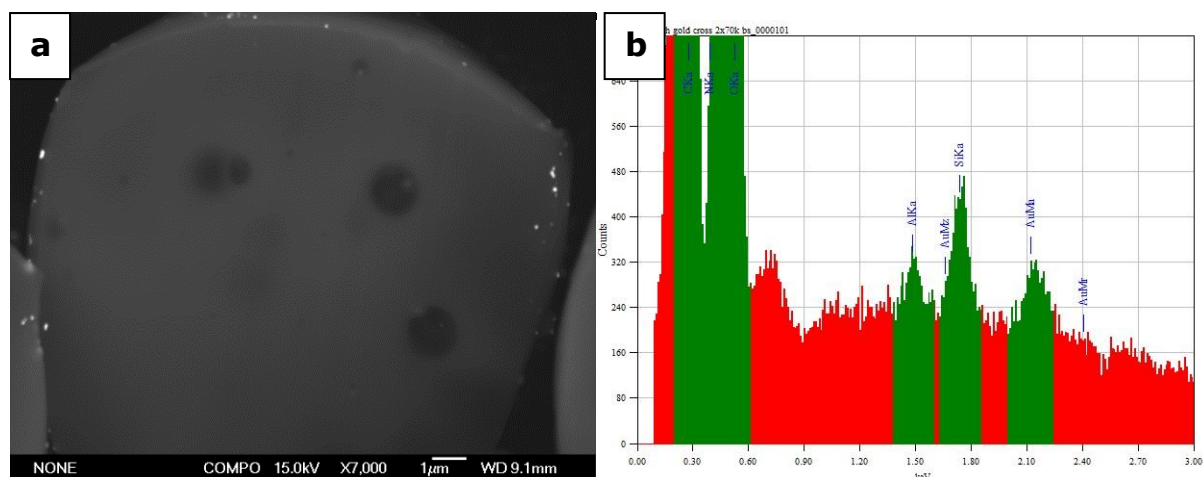


Figure 4.10: SEM micrograph (COMPO) of a cross section of the PET-50Au sample at a) 7000 times magnification (COMPO) with b) the respective EDS elemental analysis spectrum.

Figure 4.11 presents the SEM micrographs recorded in backscatter mode of the NH₂-500Au sample. At a low magnification of 170 times the irregular shapes of the silica based NH₂ sorbent particles can be seen (Figure 4.11a). Further magnifications of the sample to 1300 and 23000 times (Figure 4.11b-c) show a surface with a high coverage of bright white spots, which were confirmed by EDS elemental analysis to be gold (Figure 4.11d-e). In general the particles appeared to be spherical and smaller than 100 nm in size, however some larger triangles and particle agglomerates were observed. The distribution of these gold nanoparticles is uniform across the hybrid NH₂ sorbent particles. As mentioned in Section 4.3, the intense surface plasmon resonance absorption band in the visible region is responsible for the dark purple colouration of the sample (Figure 4.5).

Figure 4.12 shows a SEM micrograph and the corresponding EDS spectrum of the NH₂-500Ag sample. The bright white spots visible in the backscatter mode are silver nanoparticles which was confirmed by the EDS analysis. This implies that during the synthesis of the hybrid material silver ions were reduced to silver nanoparticles by the NH₂ sorbent material. These silver nanoparticles are predominantly spherical with a diameter of less than 100 nm. However, occasional large agglomerations were observed.

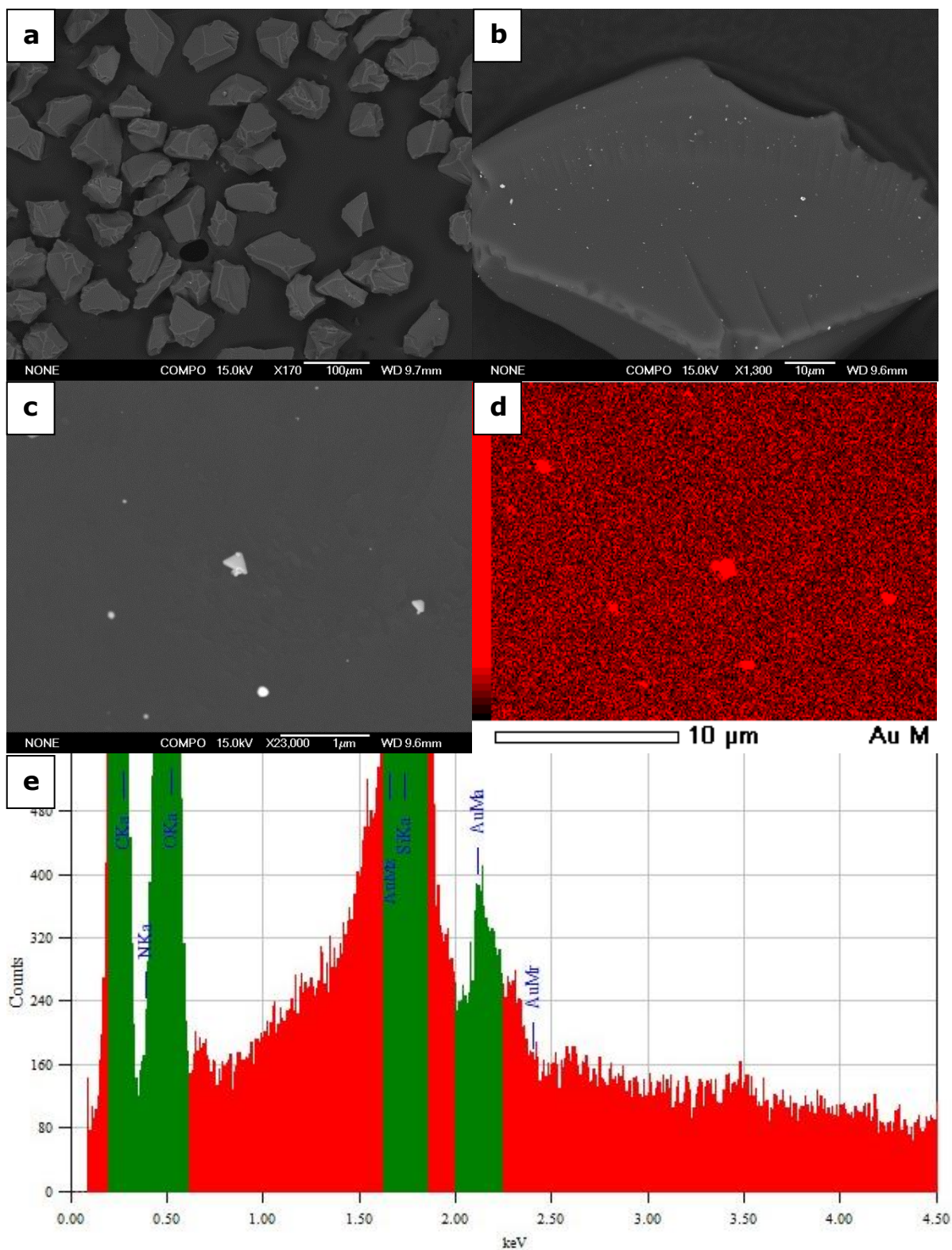


Figure 4.11: SEM micrographs in backscatter mode of the NH2-500Au surface a) at 170 times, b) 1300 times and c) 23000 times magnification with d) the respective EDS elemental analysis spectrum.

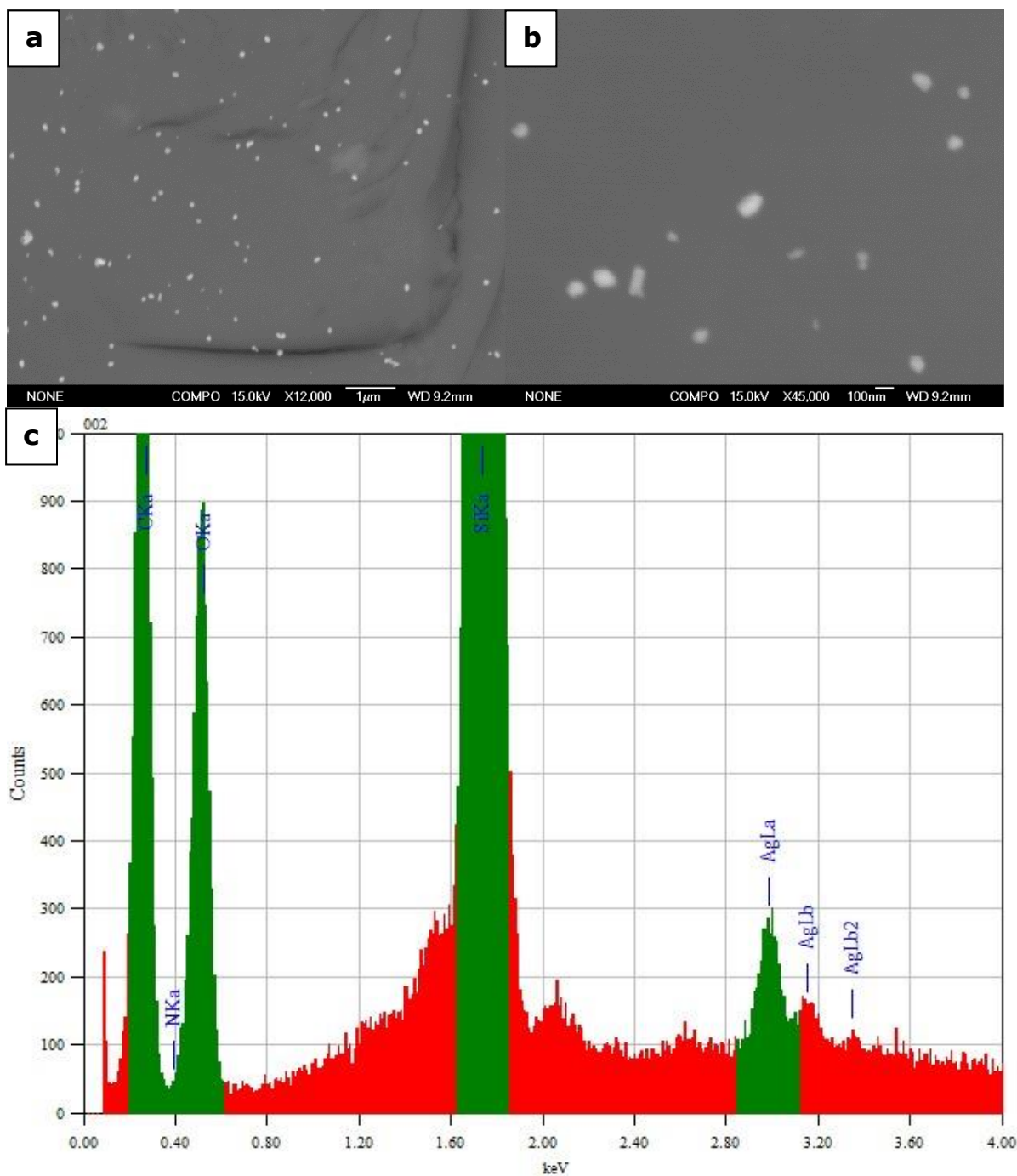


Figure 4.12: SEM micrographs in backscatter mode of the NH2-500Ag surface a) at 12000 times and b) 45000 times with c) the respective EDS elemental analysis spectrum.

4.5 X-ray diffraction on nanogold and nanosilver hybrid PET sail cloth and silica based BULK ISOLUTE® NH2 sorbent materials

XRD characterisation of nanogold and nanosilver hybrid PET and NH2 sorbent materials was carried out in order to confirm the formation of crystalline gold and silver nanoparticles. In the XRD patterns, the Bragg peak positions and their intensities were compared with the standard PDF 04-001-2616 for gold and PDF 04-001-2617 for silver pattern.²⁴² FWHM values were used in the Scherrer equation which was introduced in Section 2.3.4 in order to determine the mean particle size.

The XRD patterns of the untreated PET sail cloth together with the nanogold and nanosilver hybrid PET materials (PET-50Au and PET-50Ag samples) are presented in Figure 4.13. For the PET-50Au sample only one diffraction peak is observed. The discernible peak at $2\theta = 38.26^\circ$ can be indexed to the (1 1 1) lattice plane of a cubic unit cell, which corresponds to the cubic structure of gold (PDF 04-001-2616).²⁴² This XRD pattern confirms that Au^{3+} ions were reduced to Au^0 and simultaneously stabilised by the PET polymer matrix. The average crystallite size of the gold nanoparticles was estimated from the FWHM of the (1 1 1) diffraction peak. The particles were found to be ca. 19 nm for the PET-50Au sample. Although the UV-Vis and SEM analyses of the nanosilver hybrid PET material confirmed the presence of silver nanoparticles (Sections 4.3 and 4.4), the XRD pattern obtained for the PET-50Ag sample did not show any of the typical diffraction peaks for fcc silver. A possible reason for the absence of the diffraction peaks is that the silver nanoparticles on the surface of the PET sail cloth are very small, resulting in a low signal to noise ratio.

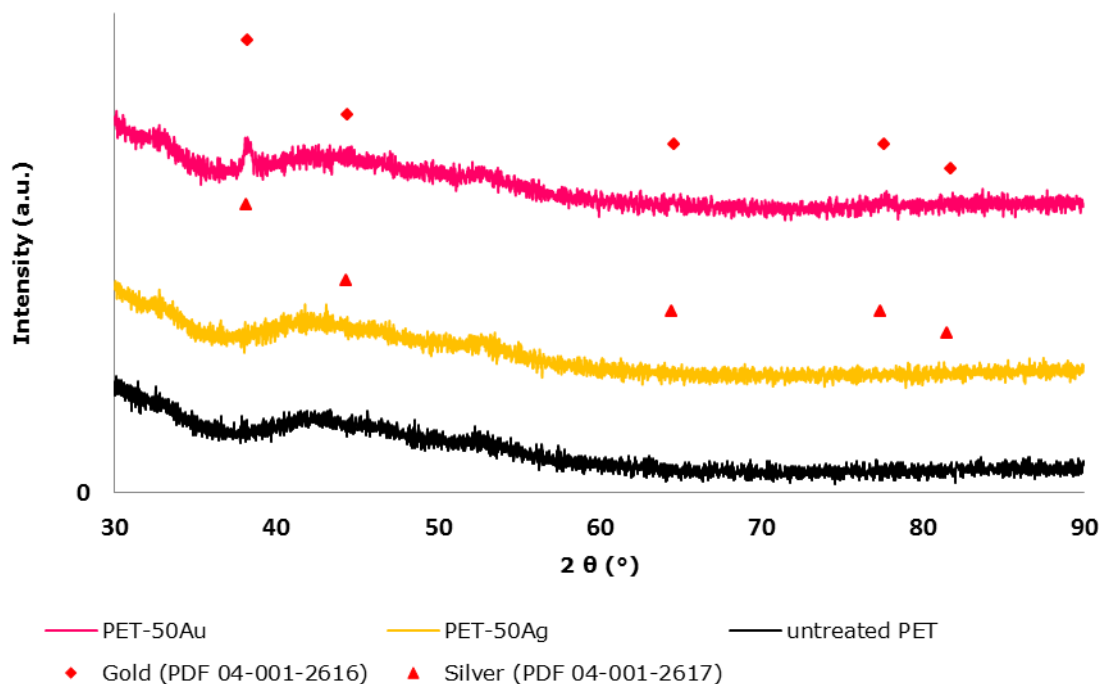


Figure 4.13: XRD patterns of the untreated PET sail cloth and the nanogold and nanosilver hybrid PET materials.

Figure 4.14 illustrates the XRD patterns obtained from the untreated NH₂ sorbent material as well as the nanogold and nanosilver hybrid NH₂ materials. The diffraction pattern of the NH₂-500Au sample provided further confirmation that during the synthesis of the hybrid material crystalline gold was formed within the NH₂ sorbent matrix. The diffraction peaks at $2\theta = 38.18^\circ$, 44.28° , 64.58° , 77.57° and 81.71° can be indexed as the (1 1 1), (2 0 0), (2 2 0), (3 1 1) and (2 2 2) diffraction peaks of face centred cubic structure of gold (PDF 04-001-2616).²⁴² Using the Scherrer equation the mean crystallite size of the gold nanoparticles was estimated to be 25 nm. Similar to the PET-50Ag sample described above, the XRD pattern obtained for the NH₂-500Ag sample did not show the presence of the typical diffraction peaks for crystalline silver. This might be due to the small size of the silver nanoparticles and low level of Ag in the materials.

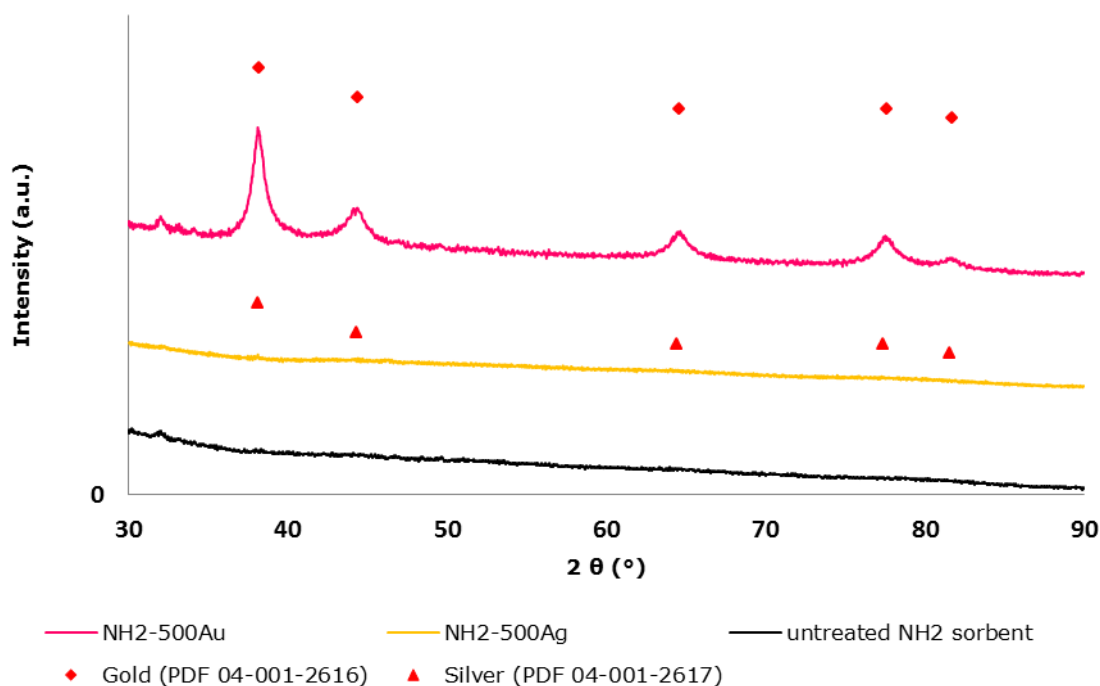


Figure 4.14: XRD patterns of the untreated PET sail cloth and the nanogold and nanosilver hybrid PET materials at higher concentration of Au and Ag.

4.6 X-ray photoelectron spectroscopy on nanogold and nanosilver hybrid PET sail cloth materials

As described in Section 1.3.1.4, PET is mainly composed of hydrocarbon backbones which contain ester linkages. However, it is important to note that polymers also contain stabilisers which are used to protect them from the effects of light, UV radiation, heat or aging. Incorporation of such compounds to the polymers such as PET sail cloth materials impart these polymers with new functional groups which are able to reduce absorbed Au^{3+} or Ag^+ to Au^0 or Ag^0 respectively. XPS analyses of the untreated and the nanogold and nanosilver hybrid PET sail cloth materials were carried out in order to investigate how the PET sail cloth was involved in the reduction of gold or silver ions to the respective metallic nanoparticles. Additionally, the nature of the bonding between the gold or silver nanoparticles and the PET sail cloth was studied.

An initial survey scan from a binding energy of 600 to 0 eV for the untreated PET sail cloth, the PET-50Au and the PET-200Ag samples showed the presence of carbon, oxygen groups as well as a weak peak for nitrogen on the PET sail cloth surface, together with gold and silver for the nanogold and nanosilver hybrid PET (Figure 4.15). This confirmed that the stabilisers present on the surface of the PET sail cloth contain nitrogen-containing functional groups. X-ray peaks for calcium and silicon should be ignored due to common laboratory contamination of the samples. Subsequently high resolution scans were carried out on carbon, nitrogen and oxygen for all samples, in addition to gold and silver for the hybrid PET sail cloth materials. Comparison of the C 1s XPS spectra for the PET sail cloth alone with its analogue nanogold and nanosilver hybrid samples did not show any significant changes.

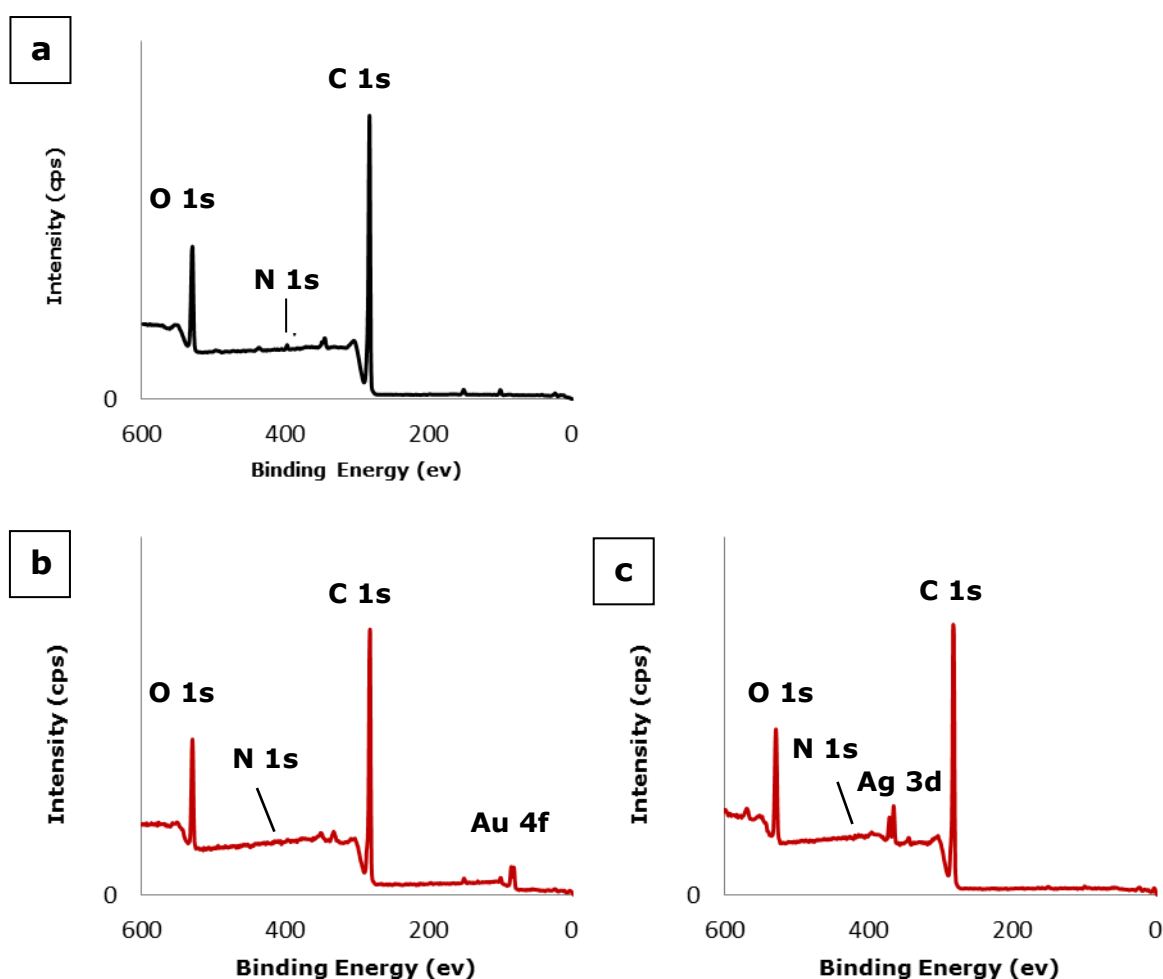


Figure 4.15: Survey XPS scans of the surface of a) the untreated PET sail cloth b) the PET-50Au and c) the PET-50Ag samples.

The N 1s spectra of the untreated PET sail cloth and the nanogold hybrid PET sample (PET-50Au) are presented in Figure 4.16a-b. When comparing both spectra, both N 1s peaks are located at ca. 399.7 eV and were attributed to amines^{275,299} related to the stabilising compounds on the surface of the sail cloth materials. Despite the unchanged position of the N 1s peak upon reaction of sail cloth with gold, a minimal broadening of the FWHM by around 0.3 eV was observed. The increase in the FWHM of the nitrogen in the amine groups suggests a greater range in the nature of the nitrogen species in addition to changes in the surrounding environment of these N entities. Because only 0.25 wt % of gold was employed to produce this nanogold hybrid PET material, very small changes are expected. Hence, it is not possible to exclude that the N 1s peak would mask further minor peaks at lower binding energies related to an Au-N interaction, but also a peak at higher binding energies representing oxidised nitrogen species, which provide the required electrons for the reduction of Au³⁺ to Au⁰.

Two distinct peaks were observed in the high resolution Au 4f spectrum obtained for the PET-50Au sample (Figure 4.16c). These peaks showed an intensity ratio of 4:3 and a spin orbital separation of 3.7 eV which matches the spacing of the bulk gold.^{275,299} The peaks centred at approximately 83.7 eV (4f_{7/2}) and 87.4 eV (4f_{5/2}) were assigned to Au⁰^{275,299} confirming that during the reaction Au³⁺ ions were reduced to metallic gold nanoparticles. Similar to the N 1s spectrum of the sample, due to the broadness of the FWHM of the doublet (1.2 eV) there is a possibility for an existence of an additional gold species attributable to Au⁺ in form of a Au-N interaction or partially reduced Au⁺ ions located on the surface of the formed Au⁰ nanoparticles. Similar results were obtained from the XPS analysis of the nanogold hybrid PU materials (Section 3.8.1).

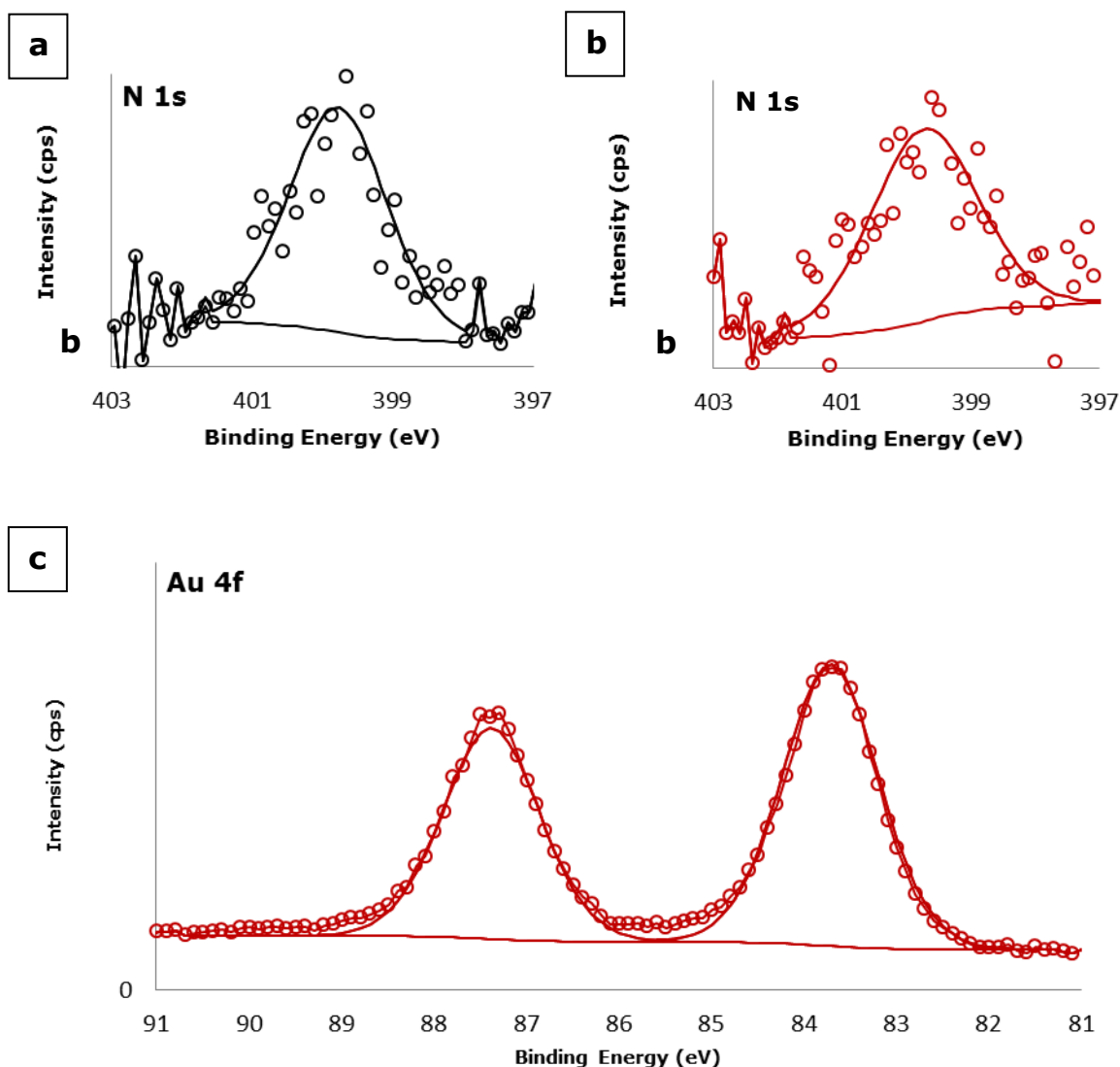


Figure 4.16: Deconvoluted high resolution XPS N 1s spectra for a) the untreated PET sail clot and b) the PET-50Au sample. Deconvoluted high resolution Au 4f XPS spectrum for the hybrid PET sail cloth prepared from a 50 mg kg⁻¹ gold solution at 80 °C for 24 hours is shown in c). Experimental data points are shown by circles.

The N 1s spectrum of the nanosilver hybrid PET sample, when compared to the N 1s spectrum obtained for the untreated PET sample (Figure 4.17a-b), did not show any change in the position of the N 1s peak (~ 399.7 eV). However, a minimal broadening of the FWHM by around 0.3 eV was detected. As for the N 1s spectrum obtained for the PET-50Au sample (described above), the increase in the FWHM of the nitrogen in the amine groups of the stabiliser on the surface

of the PET sail cloth indicates a variability of the environments surrounding these N entities. Thus, an interaction between the formed Ag nanoparticles and N is possible. Due to the low intensity and high amount of background noise in both N 1s spectra, it was not possible to assure the nature of the association existing between silver and the nitrogen atoms located on the surface of the PET polymer matrix.

The high resolution Ag 3d spectrum for the PET-50Ag sample is shown in Figure 4.17c. The spectrum was deconvoluted into one doublet with an intensity ratio of 3:2 and a spin orbit splitting of 6 eV which is typical for bulk silver.^{275,299} The two peaks positioned at around 368.0 ($3d_{5/2}$) eV and 374.0 ($3d_{3/2}$) eV are attributable to Ag^0 , which confirmed that silver ions were reduced to metallic silver when PET sail cloth was exposed to $AgNO_3$ solution at 80 °C for 24 hours of reaction time. Due to the broad FWHM of 1.6 eV it is possible that another silver species is masked by the Ag^0 peaks which associates with Ag^+ in form of an Ag-N interaction.

In light of these results, during the preparation of the nanogold and nanosilver hybrid PET materials, the reduction of Au^{3+} or Ag^+ to Au^0 or Ag^0 respectively by the PET sail cloth can be confirmed. There is an indication of an Au-N or Ag-N interaction between the formed metallic nanoparticles and the sail cloth. However, due to the low concentration of the metal ion solutions used and hence the metals in the polymers, high noise and low intensity of the spectra the exact nature of the bonding between the metal nanoparticles and the substrate cannot be ascertained.

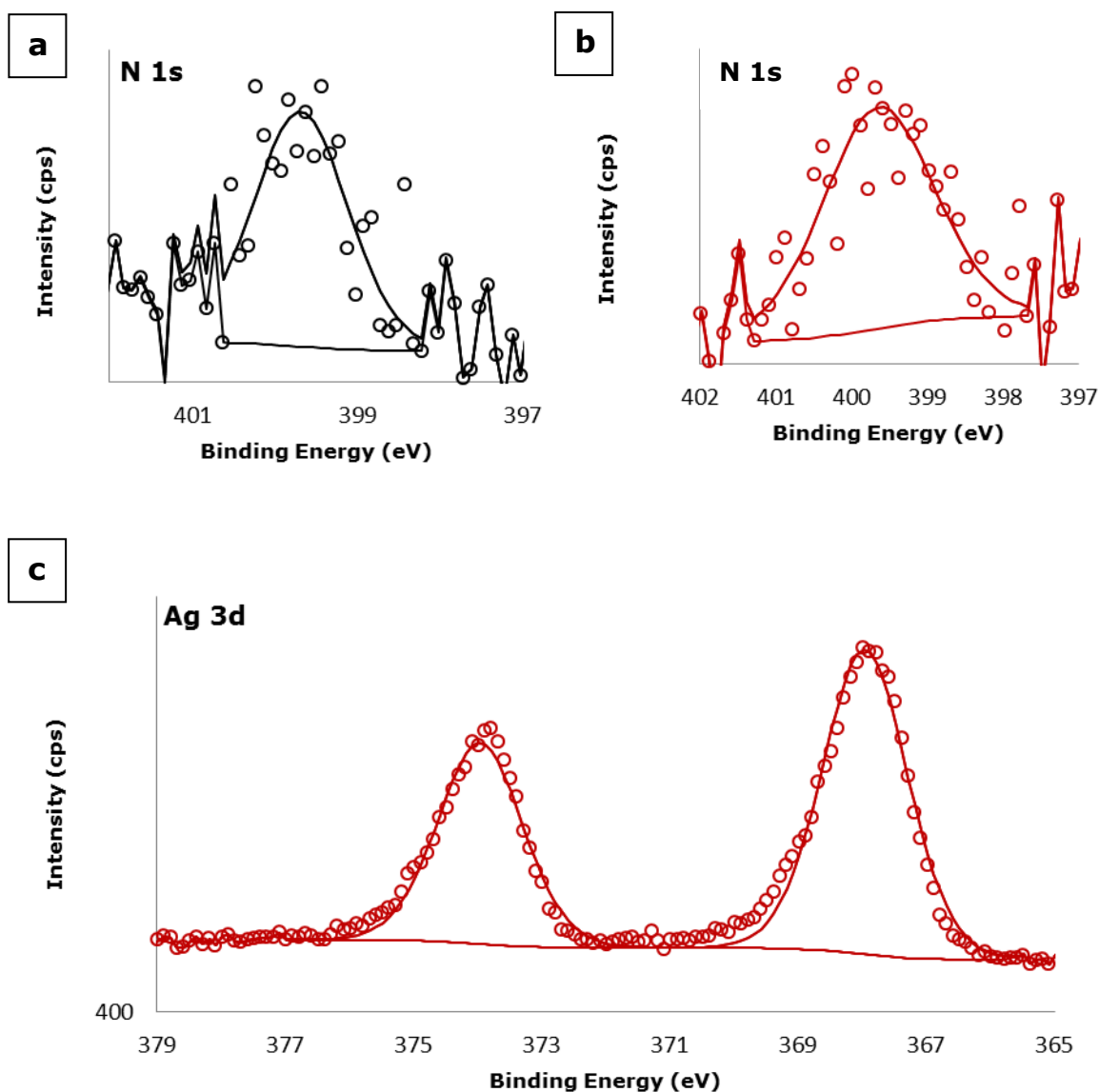


Figure 4.17: Deconvoluted high resolution XPS N 1s spectra for a) the untreated PET sail clot and b) the PET-50Ag sample. Deconvoluted high resolution Ag 3d XPS spectrum for the hybrid PET sail cloth prepared from a 50 mg kg⁻¹ silver solution at 80 °C for 24 hours is shown in c). Experimental data points are shown by circles.

4.7 Conclusions

In order to build up a simple model for the confirmation of the nitrogen's chemical affinity for gold and silver amine coated polyethylene terephthalate sail cloth and silica based Bulk isolate® sorbent (NH₂) were utilised as alternative substrates for the production of hybrid materials.

The temperature for the redox reaction was set to 70 °C for the production of nanogold and 80 °C for nanosilver hybrid polymer materials. After 24 hours of reaction time Atomic absorption studies showed that the majority of gold (in the form of AuCl₄⁻) and ca. 40 % of silver ions were absorbed by the PET polymer substrates.

Produced hybrid PET sail cloth and silica based Bulk isolate® sorbent (NH₂) materials were shown to exhibit absorption bands in the visible region of light. These absorption bands are consistent with the surface plasmon resonance bands of gold and silver nanoparticles respectively.

Electron microscopy studies of the nanogold and nanosilver hybrid PET sail cloth materials revealed that the nanoparticles varied in size, most of the spherical nanoparticles were below 100 nm in diameter. Some particle agglomerates were also present. It was evident that the nanoparticles in the hybrid PET materials were confined to the surface of the fibres, rather than spread throughout the centre of the fibre. SEM analyses of the nanogold and nanosilver hybrid isolate® sorbent (NH₂) materials showed that the metal nanoparticles appeared to be spherical and smaller than 100 nm in size, however some larger triangles and particle agglomerates were also observed. The distribution of the gold and silver nanoparticles was uniform across the hybrid NH₂ sorbent particles. In general, silver nanoparticles seem to be smaller than gold nanoparticles in both PET and isolate® sorbent (NH₂) substrates.

XRD analyses confirmed the presence of crystalline gold in the nanogold hybrid PET and isolate® sorbent samples. XRD patterns obtained for the nanosilver

hybrid PET and isolite® sorbent materials did not show the presence of the typical diffraction peaks for crystalline silver.

XPS studies confirmed that during the preparation of the nanogold and nanosilver hybrid PET materials, the reduction of Au^{3+} or Ag^+ to Au^0 or Ag^0 respectively by the amine coated PET sail took place. There was an indication of an Au-N or Ag-N interaction between the formed metallic nanoparticles and the sail cloth. Due to the low concentration of the metal nanoparticles in the polymers the exact nature of the bonding between the metal nanoparticles and the substrate could not be ascertained.

5 Nanogold and nanosilver hybrid materials: nanoparticles formed directly in polyurethane K5000 latex paint base material

Nanogold and nanosilver hybrid PU K5000 materials containing gold and silver nanoparticles were produced. The amine groups in the polyurethane were used to reduce Au^{3+} and Ag^+ to Au^0 and Ag^0 respectively and bind the resulting nanoparticles to the polymer matrix. Simultaneously the nanoparticles were stabilised by the polymer matrix. The preparation of the hybrid polyurethane K5000 latex paint polymer materials used the methodology described in Section 2.2.2. The approach comprised the slow addition of aqueous gold tetrachloride or silver nitrate solution to the liquid polyurethane K5000 paint base via a pipette under vigorous stirring. High concentrations of acidic metal ion solutions can destabilise the polyurethane suspension and cause flocculation of the paint. To prevent this, the metal ion solution was first diluted with distilled water, however too much water led to a undesirable watery paint product. For preparation of more concentrated nanogold and nanosilver hybrid PU K5000 paint samples (0.1 wt % metal content in paint) the two dilution volumes, 2.5 or 1.25 ml of metal ion solution to 5 g of PU K5000 paint base were chosen whilst keeping the polymer to metal ion ratio constant. The pH of all employed gold solutions was adjusted with NaOH to a value around 4.5 - 5 in order to avoid a possible flocculation of the paint substrate. Once the Au^{3+} / Ag^+ solutions were added to the PU K5000 paint respectively, the reaction tubes were heated in a water bath (50 °C for gold samples and 70 °C for silver samples) for 24 hours in order to affect the redox reaction. These temperatures however, proved to be too high resulting in polymerisation of the paint. Thus, the ideal temperature for the preparation of the nanogold and nanosilver hybrid PU K5000 materials was found to be room temperature. For this temperature, seven days of reaction time was required to reduce Au^{3+} or Ag^+ to Au^0 or Ag^0 respectively. During this time the sample vials were kept on a shaking table. The reduction of metal ions to Au^0 and Ag^0 was indicated by the development of stable purple colour for gold samples and brown colour for silver samples. The shade and intensity of the

colour could be altered by systematically altering the concentration of Au^{3+} or Ag^+ ions.

The sample names for the hybrid polyurethane K5000 latex paint base materials and their respective reaction parameters are summarised in Table 5.1.

Table 5.1: The names and their respective reaction parameters for the nanogold and nanosilver hybrid polyurethane K5000 latex paint base materials. All samples were prepared at room temperature, reaction time was seven days.

| Name of hybrid material | Mass of K5000 substrate [g] | Metal ion species | Metal ion conc. [mg kg^{-1}] | Vol. of metal ion solution [ml] | wt % of metal in K5000 paint |
|-------------------------|-----------------------------|-------------------|---|---------------------------------|------------------------------|
| K5000-100Au-1:2 | 5 | Au^{3+} | 20 | 2.5 | 0.01 |
| : | : | : | : | : | : |
| K5000-1000Au-1:2 | 5 | Au^{3+} | 2000 | 2.5 | 0.1 |
| K5000-100Au-1:4 | 5 | Au^{3+} | 40 | 1.25 | 0.01 |
| : | : | : | : | : | : |
| K5000-1000Au-1:4 | 5 | Au^{3+} | 4000 | 1.25 | 0.1 |
| K5000-100Ag-1:2 | 5 | Ag^+ | 20 | 2.5 | 0.01 |
| : | : | : | : | : | : |
| K5000-1000Ag-1:2 | 5 | Ag^+ | 2000 | 2.5 | 0.1 |
| K5000-100Ag-1:4 | 5 | Ag^+ | 40 | 1.25 | 0.01 |
| : | : | : | : | : | : |
| K5000-1000Ag-1:4 | 5 | Ag^+ | 4000 | 1.25 | 0.1 |

For the initial scale performance testing, the nanogold and nanosilver hybrid PU K5000 materials were produced in 80 times greater quantity (Figure 5.1). The preparation process was scaled up by a direct scaling of the procedure described above.

The nanogold and nanosilver hybrid PU K5000 paints were sent to The Polymer Group Ltd in Auckland, where the hybrid PU K5000 paint samples were further formulated into a marine paint which was used to coat surfaces of pieces of

wood. These pieces were subsequently immersed in seawater for six months in order to test the hybrid materials for their antifouling properties.



Figure 5.1: Picture nanogold (left) and nanosilver (right) hybrid polyurethane K5000 paint materials containing 0.1 wt % of Au^{3+} / Ag^{+} .

5.1 Formation of gold and silver nanoparticles within the polyurethane K5000 latex paint base polymer

During the reaction time for the reduction of gold or silver ions by the polyurethane K5000 substrate, a visible colour development was observed. The pink-violet-purple and yellow-brown colours of the resulting hybrid PU K5000 paint materials were evidence of the formation of gold and silver nanoparticles respectively. The excitation of surface plasmon resonances of nanoparticles by incident light gives rise to a very selective absorption of the light thus imparting distinct colours to the nanogold and nanosilver hybrid materials (Section 1.4.2).

K5000 is a polyurethane latex paint base polymer with a polyether/polyester/acrylic composite backbone. As previously shown (Chapter 3), polyurethane is able to reduce gold or silver ions to metallic nanoparticles and stabilise these nanoparticles within the polymer matrix. Here,

the PU K5000 paint simultaneously acts as the substrate, stabilising and reducing agent due to its carbamate functional groups.

Depending on the employed metal ion concentration, the colour change of the PU K5000 paint base from original white to pink or yellow can occur within the first day due to the formation of gold or silver nanoparticles respectively. Figure 5.2 presents the photographs of the nanogold hybrid polyurethane K5000 paint samples with different amounts of gold after different reaction times in days compared to the untreated PU K5000 paint sample. All samples were prepared at room temperature. When preparing the K5000-1000Au-1:2 and K5000-1000Au-1:4 samples, the sample turned pink within the first two hours of the reaction time, increasing in intensity and eventually turning dark purple in the following seven days. No visual difference was noted between these two samples. When preparing the K5000-200Au-1:2 or the K5000-200Au-1:4 materials, the samples did not change their colour after the first 24 hours of reaction time. In the subsequent seven days the samples became violet. Similarly, during the preparation of the K5000-1000Ag-1:2 and K5000-1000Ag-1:4 samples, a light brown colour was observed within the first two hours of the reaction. This colour increased in intensity and became dark brown during the following seven days. Figure 5.3 shows the photographs of the untreated PU K5000 paint sample and the colour development of the K5000-1000Ag-1:2 sample during the seven days of the reaction. No visual difference was observable to the human eye between the samples which were prepared from a 1.25 ml Ag^+ solution to their analogue samples prepared from a 2.5 ml Ag^+ solution.

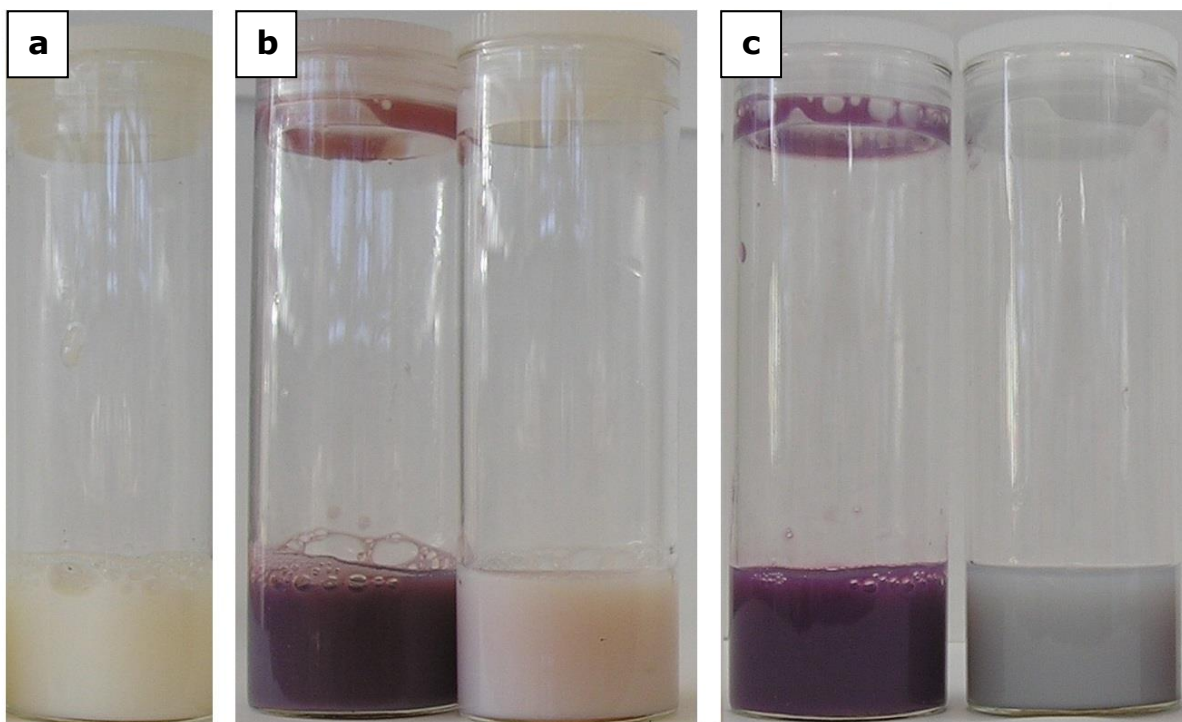


Figure 5.2: Photographs of the a) untreated PU K5000 paint base, b) K5000-1000Au-1:2 (left) and K5000-200Au-1:2 (right) after 24 hours of reaction time and c) K5000-1000Au-1:2 (left) and K5000-200Au-1:2 (right) after seven days of reaction time.

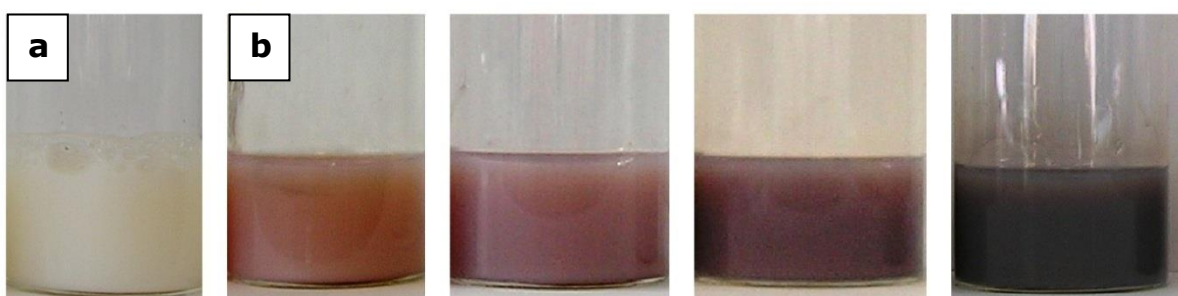


Figure 5.3: Photographs of the a) untreated PU K5000 paint base and b) the K5000-1000Ag-1:2 sample on day 1, day 2, day 3 and day 7 of reaction time (from left to right).

5.2 UV Visible spectroscopy - colour of nanogold and nanosilver hybrid polyurethane K5000 latex paint base materials

The colours of the nanogold and nanosilver hybrid PU K5000 paint base materials were studied with UV-Vis spectroscopy. Bulk gold exhibits an intense yellow colour, due to its absorption of light in the blue region of the UV-Vis spectrum as its interband transition takes place at around 470 nm. Bulk silver appears in shiny grey colour due to its interband transition occurring in the ultraviolet region at 320 nm.^{259,260} When the particle size is reduced to a size in the nanometer range the metals will no longer have their characteristic colour appearance. For example by tuning the particle size or shape of the gold nanoparticles, the colour can be varied from pink through violet to red.³⁰⁰ For gold nanoparticles the absorption is generally centred between 500–700 nm¹⁰⁶ and for silver nanoparticles between ca. 320-800 nm.^{260,301} These absorptions range over a broad wavelength as they are significantly influenced by not only the size and the shape of the nanoparticle but also on the dielectric constant of surrounding medium, presence of adsorbed species and the distance between neighbouring nanoparticles.²⁵²

For the UV-Vis absorption measurements, the prepared nanogold and nanosilver hybrid PU K5000 paint base materials were dried on glass slides after seven days of reaction time, during which gold or silver ions were reduced to gold or silver nanoparticles and simultaneously stabilised by the PU K5000 polymer matrix. Once the hybrid PU K5000 paint base dried, it was peeled off and rinsed with distilled water. Figure 5.4 shows a picture of the nanogold and nanosilver hybrid polyurethane K5000 paint samples. At low gold concentrations, when 2.5 ml or 1.25 ml of 400 or 800 mg kg⁻¹ Au³⁺ solution was added to the PU K5000 latex paint base (K5000-200Au-1:2 or K5000-200Au-1:4 sample), the nanogold hybrid PU K5000 paint was light violet in colour. When the gold concentration of the solution was increased to 1200 or 2400 mg kg⁻¹ Au³⁺ to produce the K5000-600Au-1:2 or the K5000-600Au-1:4 sample respectively, the colour of both samples turned to purple. Increasing the gold concentration of the reaction solution further to 2000 or 4000 mg kg⁻¹ Au³⁺ (K5000-600Au-1:2 or

K5000-600Au-1:4 sample) respectively resulted in a slight increased intensity of the purple colour. However, this change was hardly visible to the human eye.

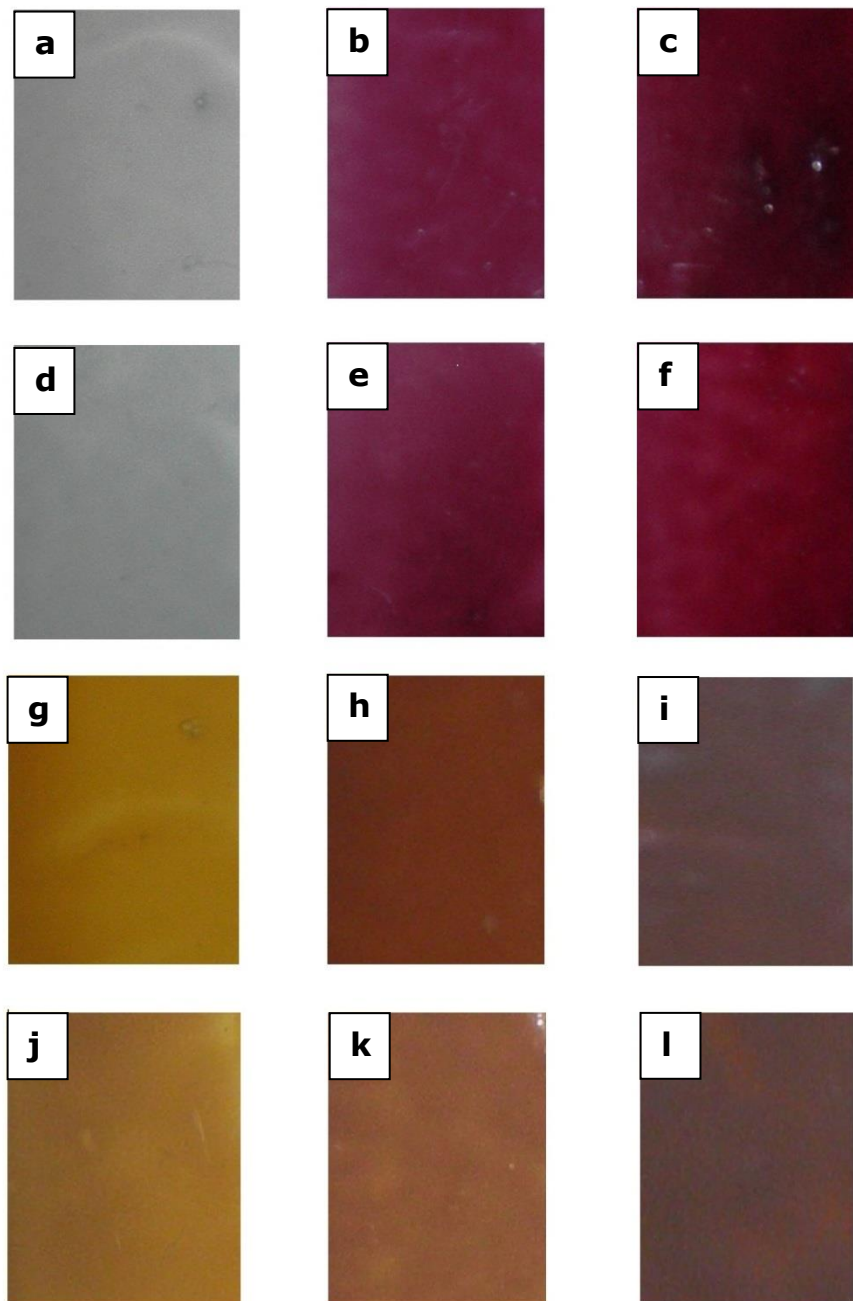


Figure 5.4: Photographs of dried nanogold and nanosilver hybrid PU K5000 paint films: a) K5000-200Au-1:4, b) K5000-600Au-1:4, c) K5000-1000Au-1:4, d) K5000-200Au-1:2, e) K5000-600Au-1:2, f) K5000-1000Au-1:2, g) K5000-200Ag-1:4, h) K5000-600Ag-1:4, i) K5000-1000Ag-1:4, j) K5000-200Ag-1:2, k) K5000-600Ag-1:2 and l) K5000-1000Ag-1:2.

Similarly, with increasing initial silver concentrations, the colour of the resultant hybrid paint materials turned from dark orange to dark brown. By contrast, the untreated PU K5000 paint base dried to give a colourless, transparent film (not displayed in Figure 5.4).

Figure 5.5 shows the UV-Vis absorption spectra for the nanogold hybrid PU K5000 paint materials prepared from 2.5 ml solutions containing different amounts of gold ranging from 800 to 4000 mg kg⁻¹. As previously mentioned, small gold nanoparticles with a diameter of 10 - 20 nm exhibit the surface plasmon resonance absorption band at around 520 nm,¹⁰⁸ these nanoparticles show the typical ruby red colour.³⁰² However, with increasing particle sizes there is a shift in the absorption band to longer wavelengths, for example as the diameter of the spherical gold nanoparticles increases from 20 to 100 nm, the SPR band shifts from about 520 to 580 nm and the bandwidth of the peak also increases.^{108,303} The absorption peak for the violet coloured K5000-200Au-1:4 sample (Figure 5.4a) is broadened and its maximum is centred at around 570 nm (Figure 5.5), an unusual result. As this sample was prepared from the most diluted gold solution, smaller nanoparticles would be expected providing a blue-shifted SPR absorption band in comparison to the K5000-600Au-1:4 sample with higher gold content. A possible reason for such SPR absorption of the sample is that during the reduction of gold ions to gold nanoparticles only a small number of nucleation centres were formed. These nucleation centres are sufficiently stabilised by the surrounding PU K5000 polymer matrix. As such, nanoparticle growth occurs through the reduction of gold ions adsorbed onto the nanocluster surface, resulting in the formation of larger particles, rather than forming a higher number of nucleation centres which grow into smaller gold particles. The low intensity of the absorption peak is consistent with the formation of only a small number of larger gold nanoparticles present in the sample. The sizes and shapes of the gold particles formed within the K5000-200Au-1:4 sample could not be ascertained by the TEM as the nanoparticle concentration was too low for them to be observed. Hence, the variation of particle sizes cannot be excluded. The UV-Vis analyses of the K5000-600Au-1:4 and K5000-1000Au-1:4 samples showed absorption peaks with their maxima located at ca. 540 nm. An increase in the intensities of the surface plasmon resonance bands was observed. Thus, it is assumed that the particle size of gold is not changing but more particles are

formed when increasing the Au^{3+} concentration of the solution added to the PU K5000 paint base. This results in no colour change but an increase in intensity of the purple colour shown in Figure 4.4b-c. Due to the similar shape and position of the peak observed for the analogue concentrated K5000-1000Au-1:2 sample (see below) the gold particles formed in the K5000-600Au-1:4 and K5000-1000Au-1:4 samples are likely to be spherical and 20 - 40 nm in diameter (Section 5.4).

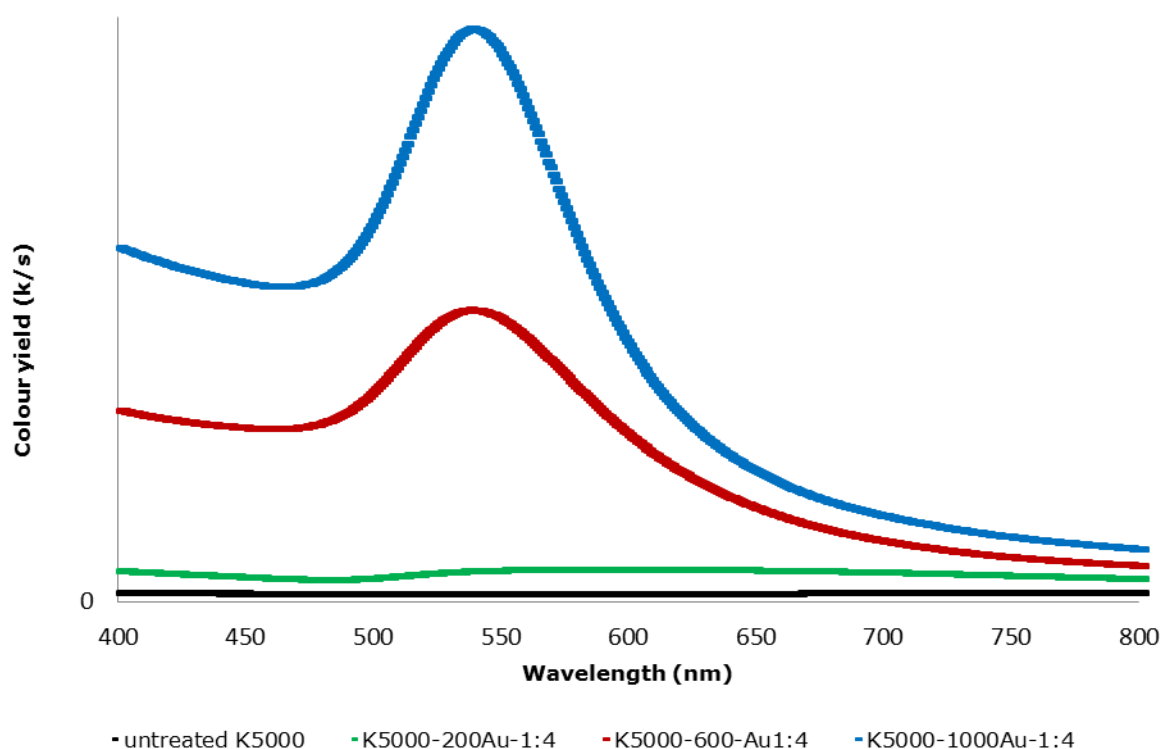


Figure 5.5: UV-Vis absorption spectra of the nanogold hybrid polyurethane K5000 latex paint base materials prepared from 1.25 ml solution with different amounts of Au^{3+} to 5 g of polyurethane K5000 paint base.

The UV-Vis spectra for the dried nanogold hybrid PU K5000 paint materials that were prepared from a 2.5 ml solution containing different levels of gold ranging from 400 to 2000 mg kg^{-1} Au^{3+} are shown in Figure 5.6. Their respective colour can be seen in Figure 5.4d-f. In general, the peak shapes and positions are similar to their analogue samples which were prepared from 1.25 ml gold

solutions (Figure 5.5). The sample with the lowest concentration of gold, the K5000-200Au-1:2 sample, showed the broad SPR band with the absorption maxima at around 570 nm. As reported above, the unusual absorption band is ascribed to the formation of the fewer nuclei, which subsequently grew to larger gold particles resulting in the violet colouration of the sample. The very low intensity of the peak suggests the formation of only a small number of gold nanoparticles. The purple K5000-600Au-1:2 sample exhibits its absorption peak at ca. 540 nm, the identical position of its analogue concentrated K5000-600Au-1:4 sample, confirming the formation of gold nanoparticles. No visual difference between the dried samples could be noted by the eye. When increasing the gold concentration from 1200 to 2000 mg kg⁻¹ Au³⁺ to produce the K5000-1000Au-1:2 sample, there is essentially no shift or broadening of the absorption peak, confirming the particle size does not change. Rather, more nanoparticles of the same size are formed which results in an increased intensity of the purple colour of the K5000-1000Au-1:2 sample (Figure 5.4e-f). TEM analysis of the K5000-1000Au-1:2 sample confirmed the presence of mostly spherical gold nanoparticles with a diameter ranging from ca. 20 – 40 nm (Section 5.4).

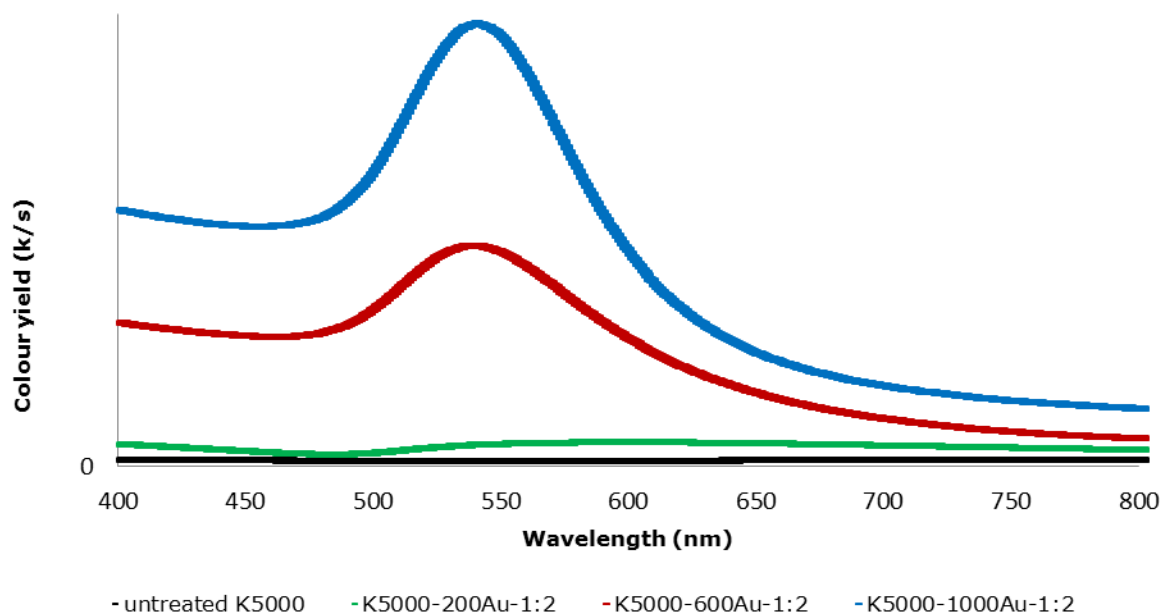


Figure 5.6: UV-Vis absorption spectra of the nanogold hybrid polyurethane K5000 latex paint base materials prepared from 2.5 ml solution with different amounts of Au^{3+} to 5 g of PU K5000 paint base.

Figure 5.7 shows the UV-Vis absorption spectra for the dried nanosilver hybrid PU K5000 paint materials prepared from a 1.25 ml solution containing different levels of silver ranging from 800 to 4000 mg kg^{-1} Au^{3+} . The respective colours of these samples are shown in Figure 5.4g-i. The absorption maxima of the K5000-200Ag-1:4, K5000-600Ag-1:4 and K5000-1000Ag-1:4 samples are centred at 424, 434 and 436 nm respectively. These surface plasmon absorption bands are characteristic for silver nanoparticles, confirming that silver ions were reduced to metallic nanoparticles. With their blue-shifted surface plasmon resonance band, silver nanoparticles in the K5000-1000Ag-1:4 sample are most likely to be slightly smaller than those in the analogue K5000-1000Ag-1:2 sample, on average smaller than 50 nm (see below). Similarly sized spherical silver nanoparticles in aqueous solution protected by PVP polymer (50 nm) have been reported to exhibit their absorption maximum at 424 nm.³⁰⁴ As such, this absorption is centred at a somewhat lower wavelength. Since the SPR properties of nanoparticles depend on their size, shape and surrounding dielectric medium, the position of SPRB of silver nanoparticles embedded in the K5000-1000Ag-1:4 or K5000-1000Ag-1:2 sample shifts towards higher wavelengths because the

refractive index of PU (ca. 1.5) is higher than that of water (1.33). The red shift upon increased added silver ion content in the PU K5000 paint samples implies nanoparticle growth either through the reduction of silver ions adsorbed onto the nanocluster surface or through coalescence/aggregation of the particles. As previously mentioned, larger nanoparticles scatter more light²⁵⁷ as a result of the larger optical cross sections and increasing ratio of scattering to total extinction with increasing size. Moreover, all three peaks are broadened, exhibiting a shoulder towards higher wavelengths. The broadening suggests inhomogeneity in particle size and shape. Furthermore, when nanoparticles are sufficiently close together, the conduction electrons near each particle surface become delocalized and are shared amongst adjacent nanoparticles. Thus, the models for isolated particles do not apply, and the optical absorption of the agglomerates is observed, resulting in a broadening and a shift to longer wavelengths of the peak.³⁰⁵

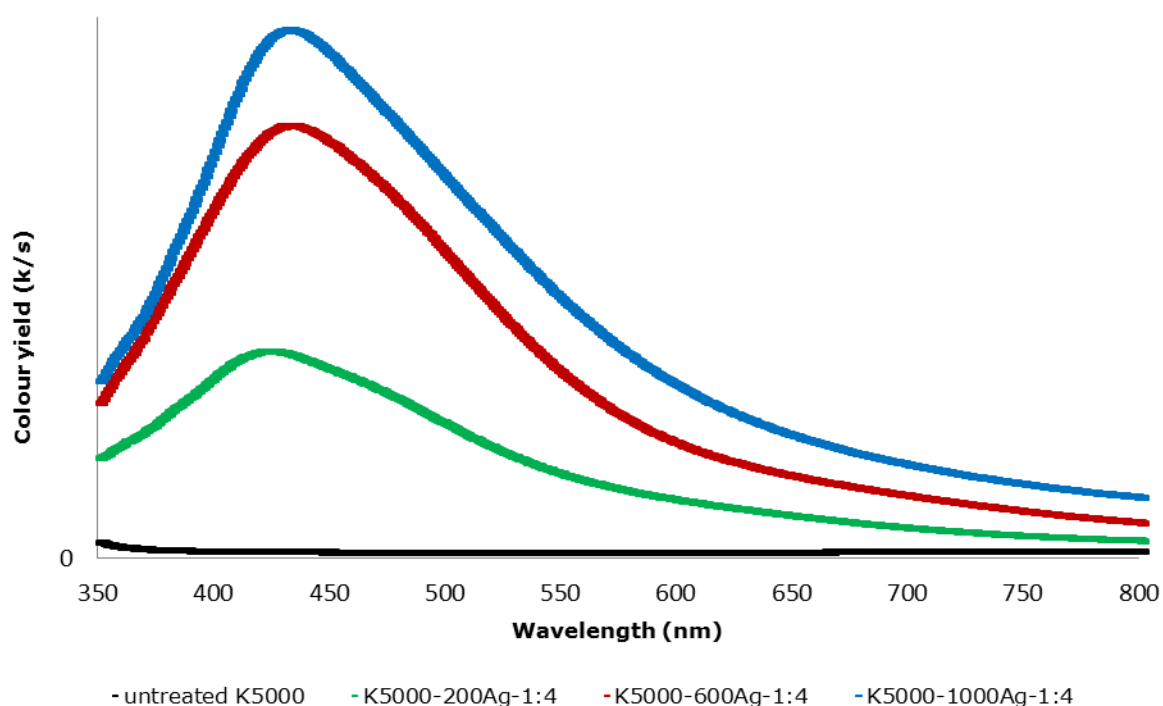


Figure 5.7: UV-Vis absorption spectra of nanosilver hybrid polyurethane K5000 latex paint base materials prepared from 1.25 ml solution with different amounts of Ag^+ to 5 g of PU K5000 paint base.

There were no visible differences noticeable in the colouring between the nanosilver hybrid PU K5000 paint samples prepared from a 1.25 ml silver solution to their analogue concentrated samples prepared from a 2.5 ml silver solution (Figure 5.4j-l). However, the UV-Vis spectra of the K5000-200Ag-1:2, K5000-600Ag-1:2 and K5000-1000Ag-1:2 samples showed a slight red shift in absorption maxima as well as an increase in full width at half maximum for all three samples (Figure 5.8). The peaks were centred at 428, 436 and 448 nm. Both, the red shift and the broadening of the peaks suggest a broader size distribution as well as particle agglomeration. The silver solutions used for the preparation of these samples contained a greater quantity of water (whilst the polymer to Ag⁺ ratio was kept constant) in comparison to the samples prepared from the 1.25 ml silver solution. Thus, the concentration of polyurethane K5000 paint base is decreased, resulting in a reduced ability of the polymer paint to stabilise the formation of silver nanoparticles in the polymer matrix. Generally, polymers sterically prevent direct contact between the nanoclusters by ligation of surface atoms of a nanocluster and also by physically occupying space around the nanoclusters. Some studies have shown that any H₂O present during nanocluster formation influences their formation and stability.³⁰⁶ More water content in the polymer ensures less of a strong protective surface coverage; small nanocrystals have a strong affinity to coalescence and form either large particles or large 'clumps' of smaller nanoparticles. As a result of coalescence, the particles decrease their exposed surface area, resulting in a lower surface energy and therefore increasing their stability in the polyurethane matrix in the PU K5000 paint formulation. TEM analysis of the K5000-1000Ag-1:2 sample showed the presence of predominantly spherical silver or spherical-like nanoparticles ranging in size from 10 to 60 nm. However, some scarce rod like and triangular particles as well as particle agglomerates were observed (Section 5.4).

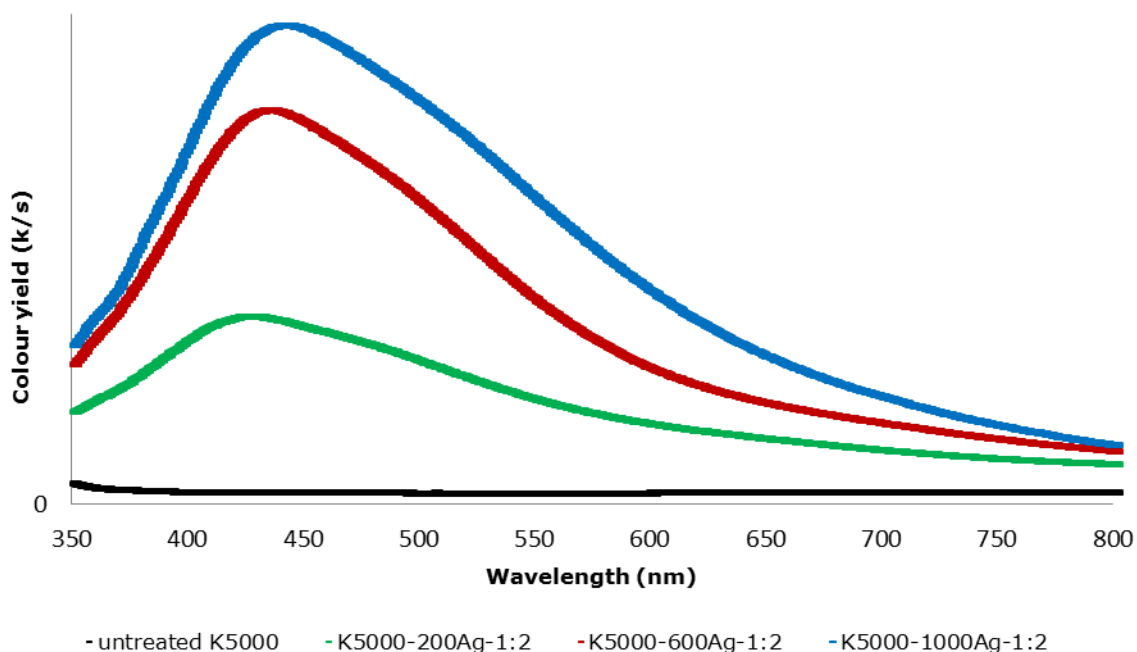


Figure 5.8: UV-Vis absorption spectra of nanosilver hybrid polyurethane K5000 latex paint base materials prepared from 2.5 ml solution with different amounts of Ag⁺ to 5 g of PU K5000 paint base.

5.3 Scanning electron microscopy and energy dispersive X-ray analysis of nanogold and nanosilver hybrid polyurethane K5000 latex paint base materials

The morphologies of the dried hybrid polyurethane K5000 paint samples were analysed by scanning electron microscopy. Dried films of the PU K5000 paint were broken into two halves providing a clean cross sectional area for the SEM analyses. Additionally, in order to investigate the internal structure of the produced nanogold and nanosilver hybrid polyurethane K5000 materials, Cryo-SEM analyses were undertaken allowing the pristine conditions of the samples to be preserved. The EDS analyses under cryogenic conditions proved to be difficult. The irradiation of a surface by the electron beam was only allowed to happen over a short period of time as the energy of the beam increased the temperature, causing the sample to melt. Analyses of the hybrid PU K5000 paint samples at higher magnifications were not possible. Only samples with higher

concentrations of gold and silver (K5000-1000Au-1:2 and K5000-1000Ag-1:2) were examined. EDS analyses of the samples provide information about the elemental composition of the analysed surface of a sample. X-ray peaks for elements such as calcium, magnesium, silicon and sodium are either due to impurities in the PU K5000 paint samples or from other contaminations in the laboratory. The X-ray peaks for aluminium and copper derive from sample holders and platinum peaks are due to the coating process of the samples. Hence, these peaks can be ignored.

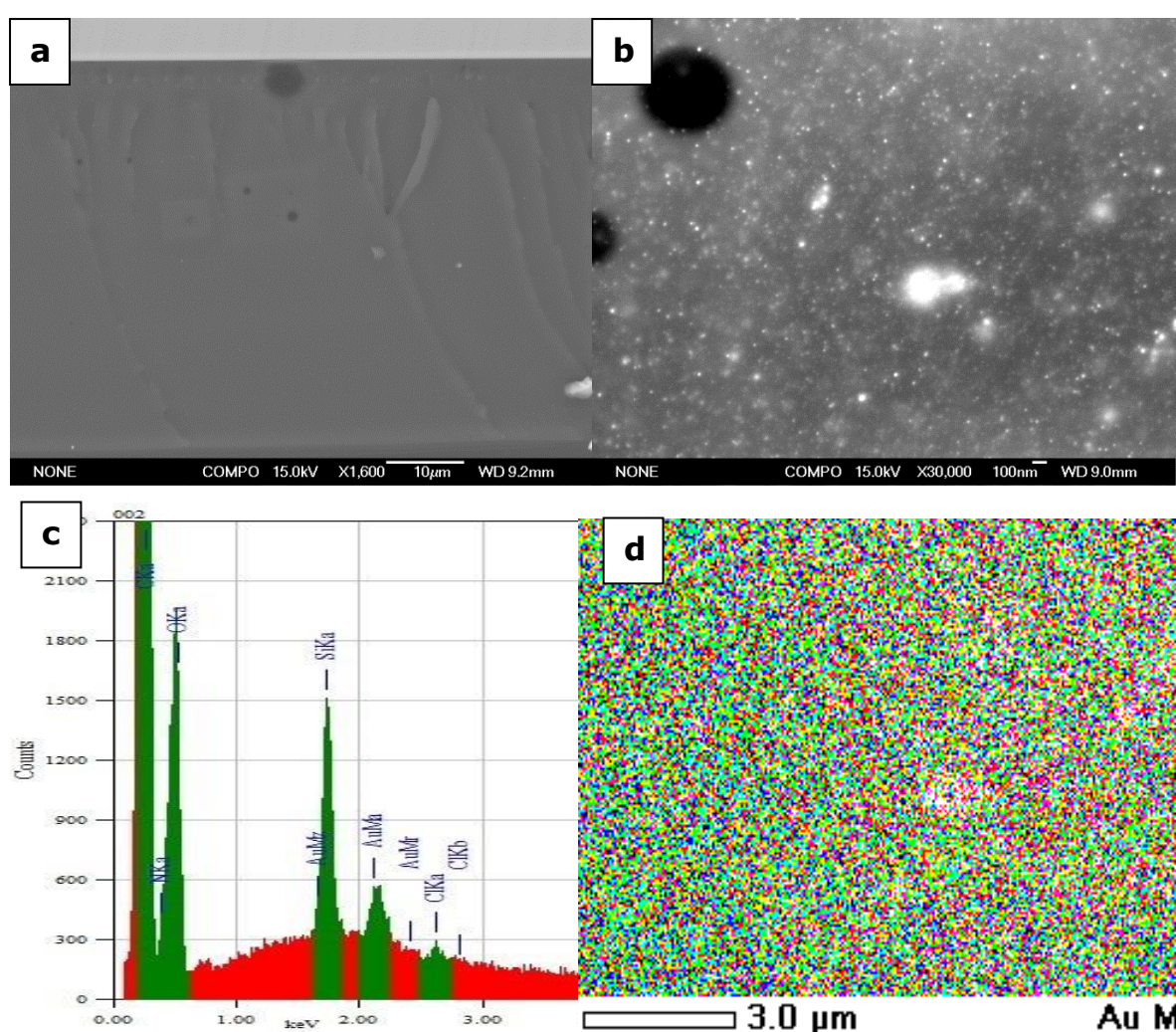


Figure 5.9: a-b) Cross sectional SEM micrographs in backscatter mode of the dry film nanogold hybrid polyurethane K5000 latex paint base sample (K5000-1000Au-1:2) at increasing magnification with c-d) the corresponding elemental analysis spectrum and gold EDS map.

Figure 5.9 presents cross sectional SEM micrographs of the K5000-1000Au-1:2 sample. Organic matrices, for example PU, seem to suffer under high energy electron beam resulting in dark areas. An example for such electron beam damage can be seen in the micrographs shown in Figure 5.9a-b. The surface of the sample at low magnification appears to be smooth and similar to the surface cross section of the untreated PU K5000 paint base sample (not displayed). A further magnification of the K5000-1000Au-1:2 sample to 30000 times (Figure 5.9b) shows a surface with a high coverage of gold nanoparticles. The intensity of the backscatter signal is directly related to the atomic number of an element, with heavier elements reflecting more signal than lighter elements and consequently appearing whiter, or brighter. When observed under backscatter conditions, the metal nanoparticles, which have higher atomic numbers in comparison to the main constituents of the PU K5000 polymer matrix, particularly C, O and N, should appear much brighter. The high concentrations of Au depicted in the EDS micrograph (Figure 5.9d) match with the white dots confirming that these are in fact nanoparticles of gold on the surface cross section of the nanogold hybrid PU K5000 paint sample. These gold nanoparticles are predominantly spherical with a diameter of less than 100 nm. However, occasional large agglomeration was observed. This is in agreement with the TEM micrographs (Section 5.4). The distribution of these gold nanoparticles is uniform across the hybrid polyurethane K5000 latex paint base, and the intense surface plasmon resonance band of these gold nanoparticles is responsible for the dark purple colouration of the hybrid polymer material (Figure 5.4f). There are also low concentrations of chlorine, as can be seen in the EDS spectrum (Figure 5.9c), likely a residue of $[\text{AuCl}_4^-]$ or free Cl^- ions.

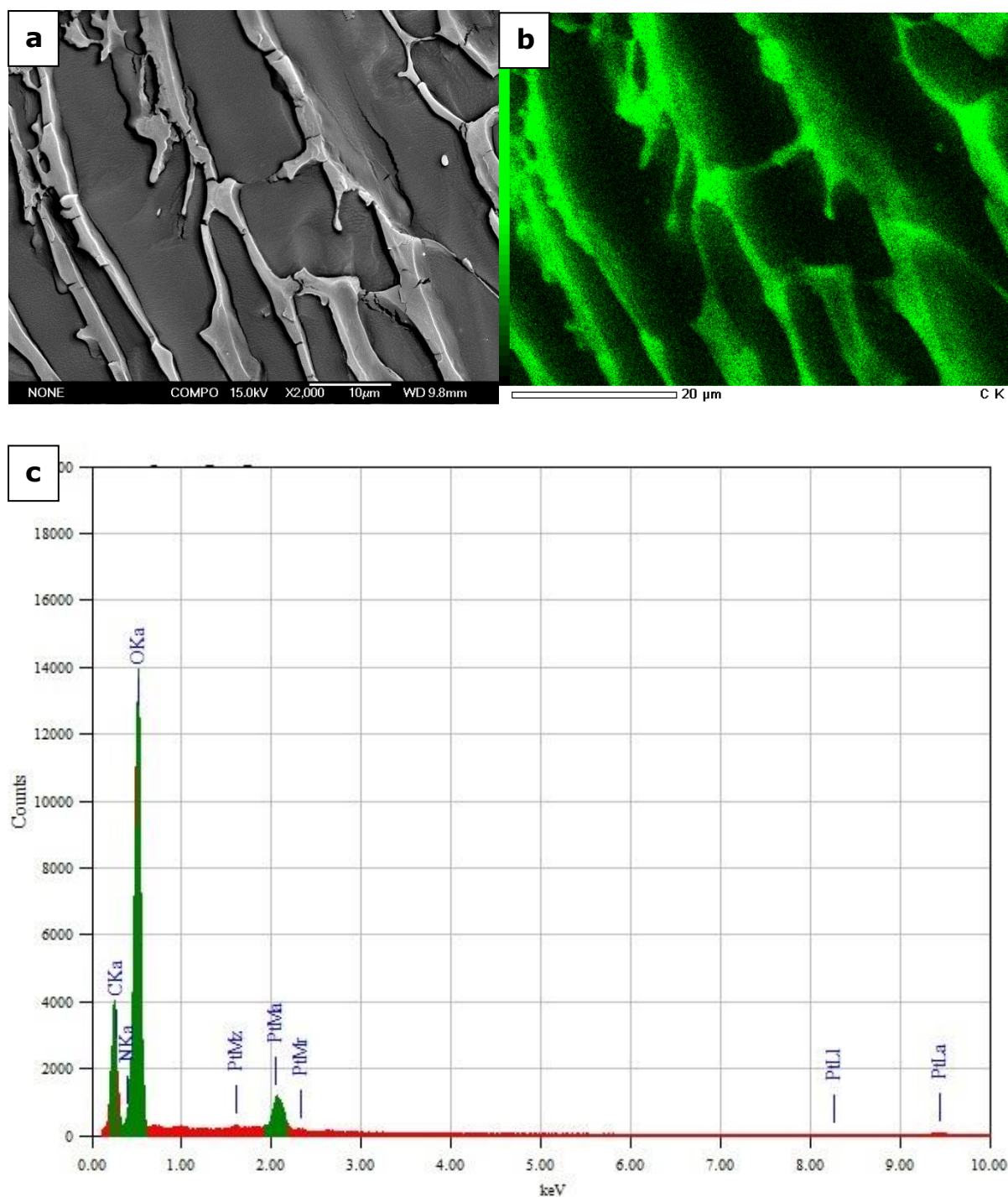


Figure 5.10: Cryo-SEM micrograph in backscatter mode of a) an untreated polyurethane K5000 latex paint base with b) the corresponding EDS micrograph and c) EDS spectrum.

Figure 5.10a-b illustrates the Cryo-SEM micrograph recorded in backscatter mode and the corresponding EDS micrograph of the untreated PU K5000 paint base sample comprised 5 g of the PU K5000 paint base and 2.5 ml H₂O, whilst

Figure 5.10c shows the EDS spectrum of the sample with C, N and O peaks. The sample exhibits two domains, the smooth and slightly darker areas (Figure 5.10a) represent water whereas the lighter areas are the carbon-based polyurethane polymer itself which can be seen as a green colour on the EDS map (Figure 5.10b).

Figure 5.11 offers a Cryo-SEM micrograph recorded in backscatter mode and the corresponding EDS micrographs of the K5000-1000Au-1:2 sample. The bright white spots which can be seen in the backscatter mode are gold nanoparticles. Of note is that where there are high concentrations of carbon, from the polymer, there are also bright white dots of gold nanoparticles. These are most apparent in the overlay micrograph (Figure 5.11d) as yellow-orange areas, implying that gold ions were reduced to metallic gold nanoparticles within the polymer domain and not within the adjacent aqueous solution of the PU K5000 paint base.

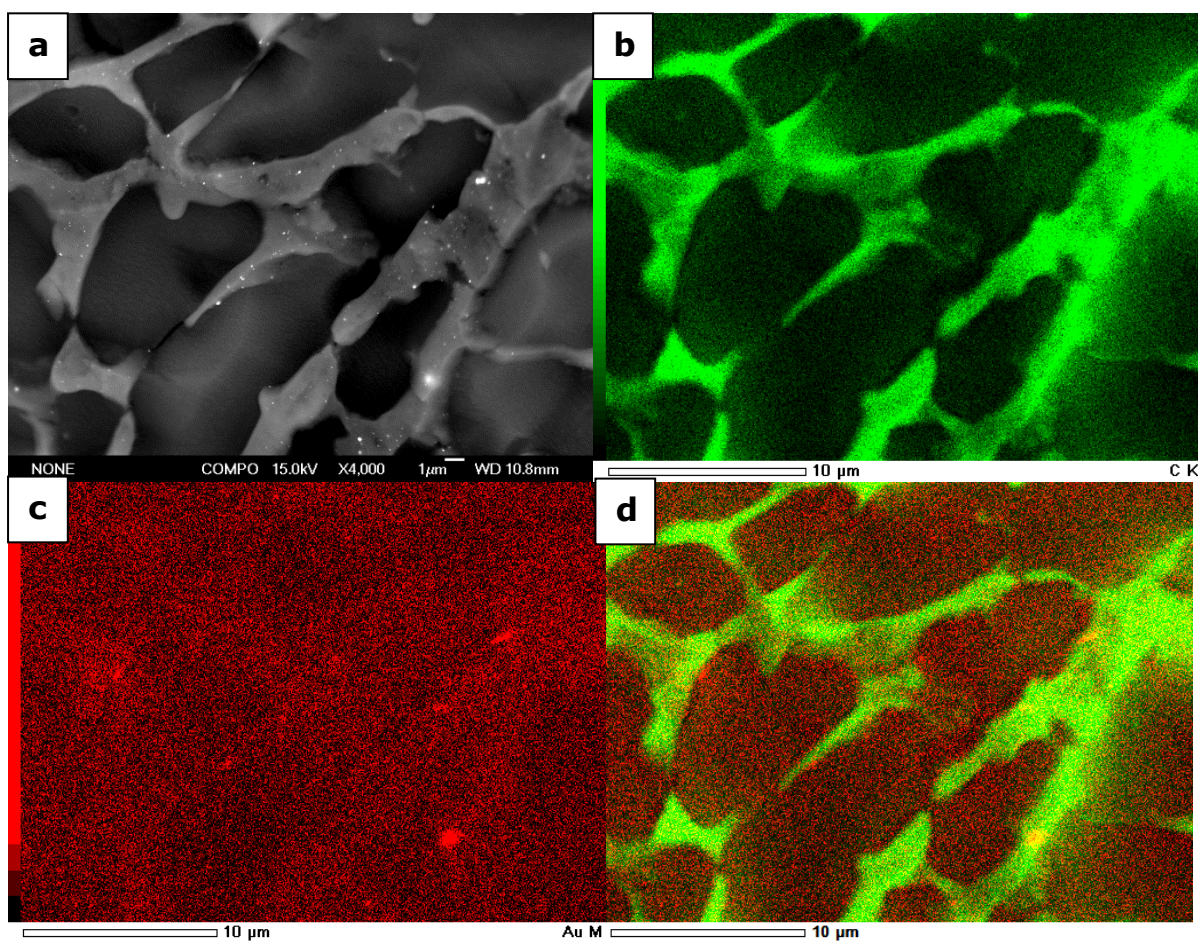


Figure 5.11: Cryo-SEM micrograph in backscatter mode of a) the K5000-1000Au-1:2 sample with b-c) the corresponding EDS micrographs and d) the EDS C and Au overlay map.

A Cryo-SEM micrograph of the K5000-1000Au-1:2 sample at a higher magnification of 30000 times is shown in Figure 5.12a. The concentrated energy of the electron beam caused melting of the sample leading to some vibrational movements. Due to these vibrations EDS mapping of the surface and collection of crisp images at this magnification proved to be difficult. The spherical bright dots, which are smaller than 100 nm in diameter, were found to be relatively well distributed on the surface of the polyurethane K5000 latex paint base. The EDS spectral analysis confirmed that the particles are gold (Figure 5.12b).

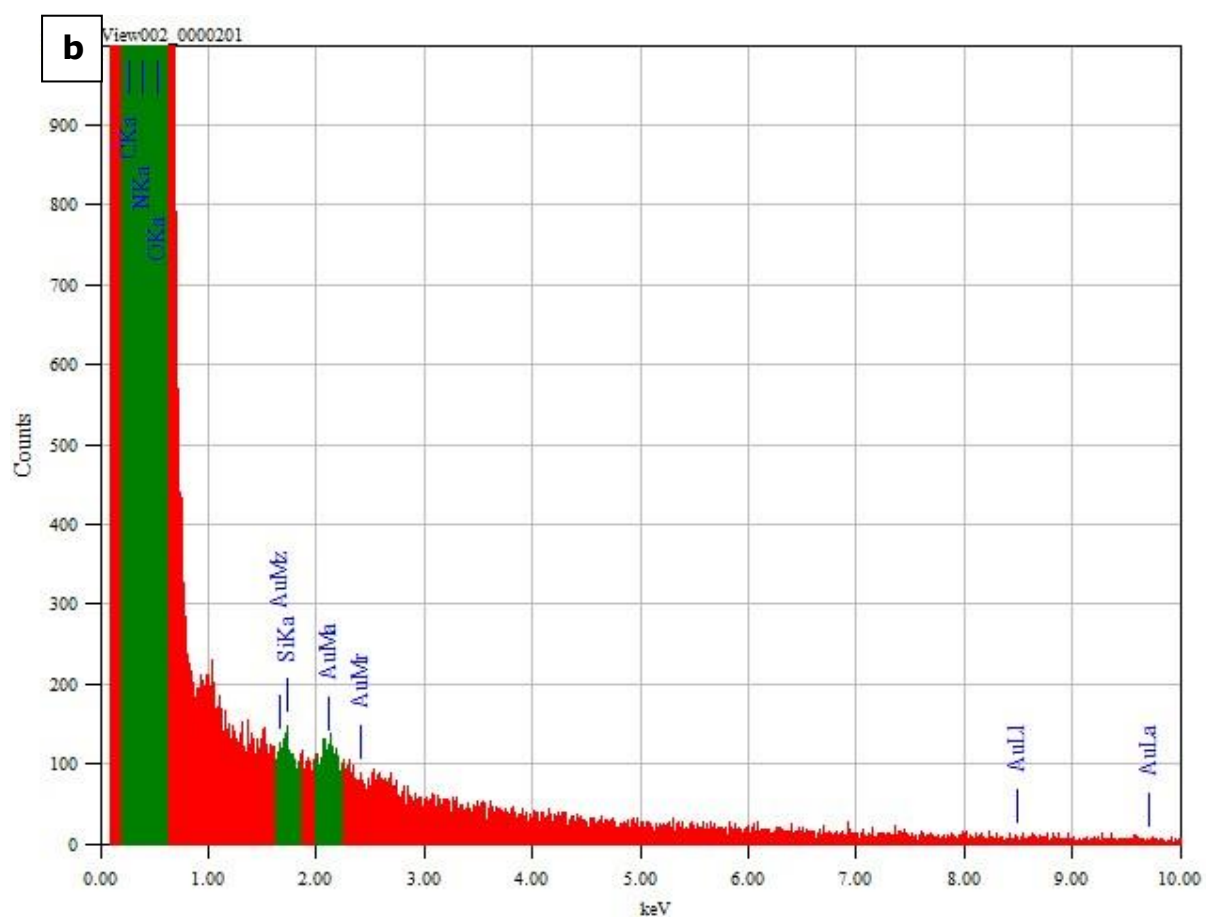
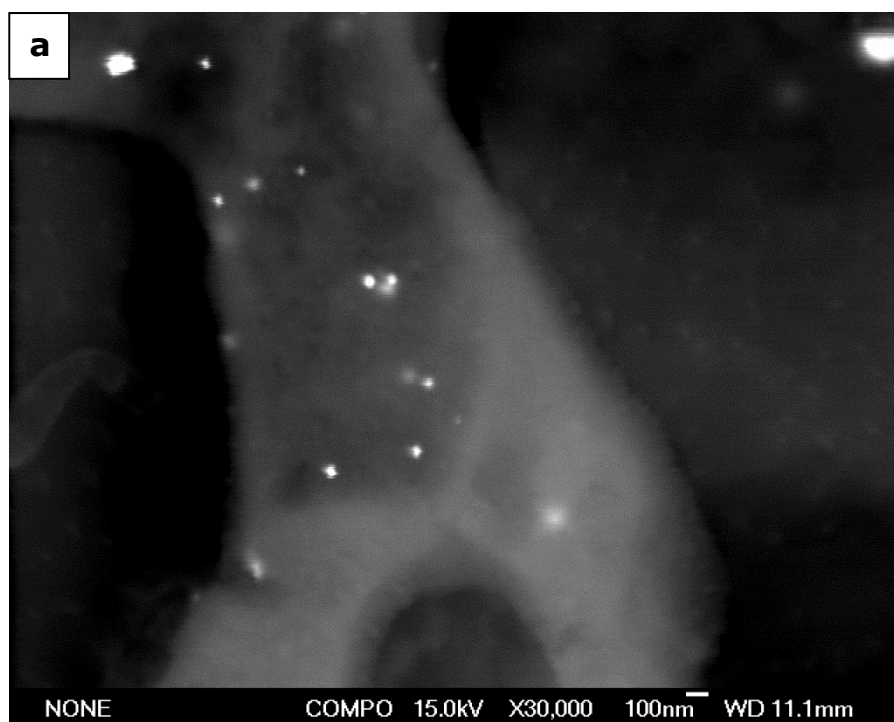


Figure 5.12: Cryo-SEM micrograph in backscatter mode a) of a K5000-1000Au-1:2 sample and b) respective EDS spectrum at higher magnification.

The Cryo SEM micrograph recorded in secondary electron mode and the respective EDS micrographs of the nanosilver hybrid PU K5000 paint sample (K5000-1000Ag-1:2) are shown in Figure 5.13. Unfortunately, due to the sample instability under the electron beam, EDS mapping could not be collected for a significant period of time in order to obtain better resolved EDS micrographs. Additionally, obtaining clearer images of the sample at higher magnifications proved to be difficult. Similar to the analogue gold sample, silver nanoparticles were found to be confined to the polymer rather than simply dispersed throughout the liquid phase. This can be seen as yellow spots on the overlay EDS micrograph (Figure 5.13d). The silver nanoparticles found in the polyurethane K5000 polymer matrix were spherical and smaller than 100 nm in diameter. However, it was not possible to ascertain the exact size of silver nanoparticles by SEM. TEM analyses of the K5000-1000Ag-1:2 revealed that the silver nanoparticles were mostly spherical and 10 nm - 60 nm in diameter.

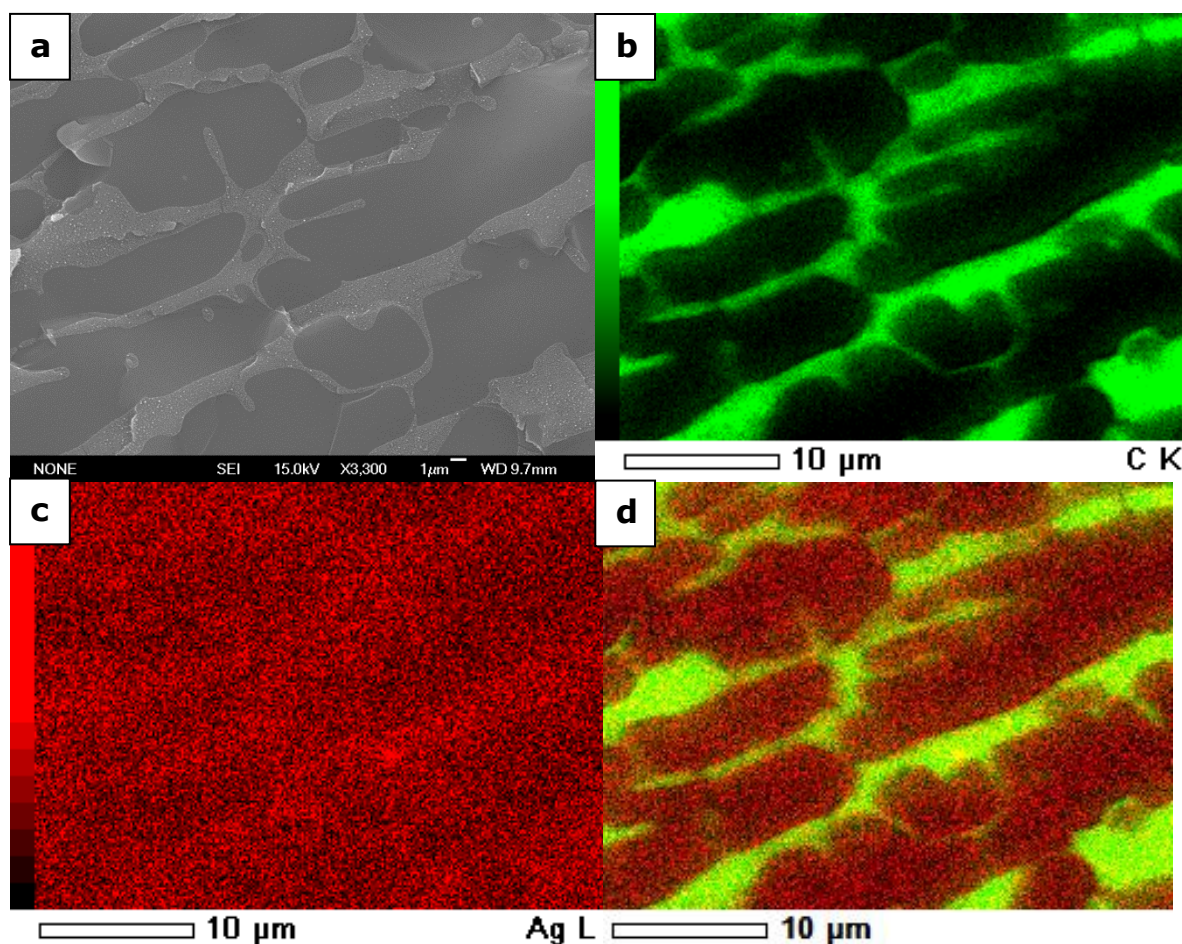


Figure 5.13: Cryo-SEM micrograph of a) a nanosilver hybrid PU K5000 paint sample with b-c) the corresponding EDS micrographs and d) the EDS Ag and C overlay map.

5.4 Transmission electron microscopy and energy dispersive X-ray analysis of nanogold and nanosilver hybrid polyurethane K5000 latex paint base materials

TEM offers increased spatial resolution thus allowing for a more precise identification of the size and shape of gold and silver nanoparticles formed within the polyurethane K5000 paint matrix. Relative to the amount of the polyurethane K5000 paint, the metal nanoparticles are present in very low concentrations. To increase the chance of detecting these particles under TEM, only higher concentration samples containing 0.1 wt % of metal

(K5000-1000Au-1:2 and K5000-1000Ag-1:2 samples) were analysed. In order to characterise the nanoparticles, the samples were dissolved in high purity methanol, and a drop of resulting solution was placed on a copper grid. Once the solvent was evaporated the residual grid was carbon coated. All imaged particles were verified by EDS elemental analyses. EDS showed the existence of carbon, nitrogen and oxygen which are the main constituents of the polyurethane K5000 paint polymer matrix, as well as a copper X-ray peak from the copper grid on which the sample was placed. The X-ray peaks for silicon should be ignored as this arises from laboratory contamination.

Figure 5.14 offers TEM micrographs of the nanogold hybrid PU K5000 paint material which was prepared from 2.5 ml of 1000 mg kg⁻¹ Au³⁺ solution in 5 g of PU K5000 paint base (K5000-1000Au-1:2). The presence of gold within the nanogold hybrid PU K5000 paint material was confirmed by a peak at 2.12 keV corresponding to the Au M_α line in EDS spectrum (Figure 5.14b). The analysis of the sample revealed the gold nanoparticles to be predominantly spherical in morphology and approximately 20-40 nm in diameter. Particle aggregates were also present, but in much lower concentrations (Figure 5.14d). This is in agreement with the UV-Vis analysis of the sample (Section 5.2), which suggested particle aggregation due to the broadening of the surface plasmon resonance absorption band. Due to equipment constraints, it was not possible to carry out TEM analysis of the analogue concentrated K5000-1000Au-1:4 sample. However, from comparisons of the colour of the sample and also the position of its surface plasmon resonance absorption peak (Section 5.2), it is likely that the gold nanoparticles present in the K5000-1000Au-1:4 sample are of the same morphology and size as the particles found in the K5000-1000Au-1:2 sample.

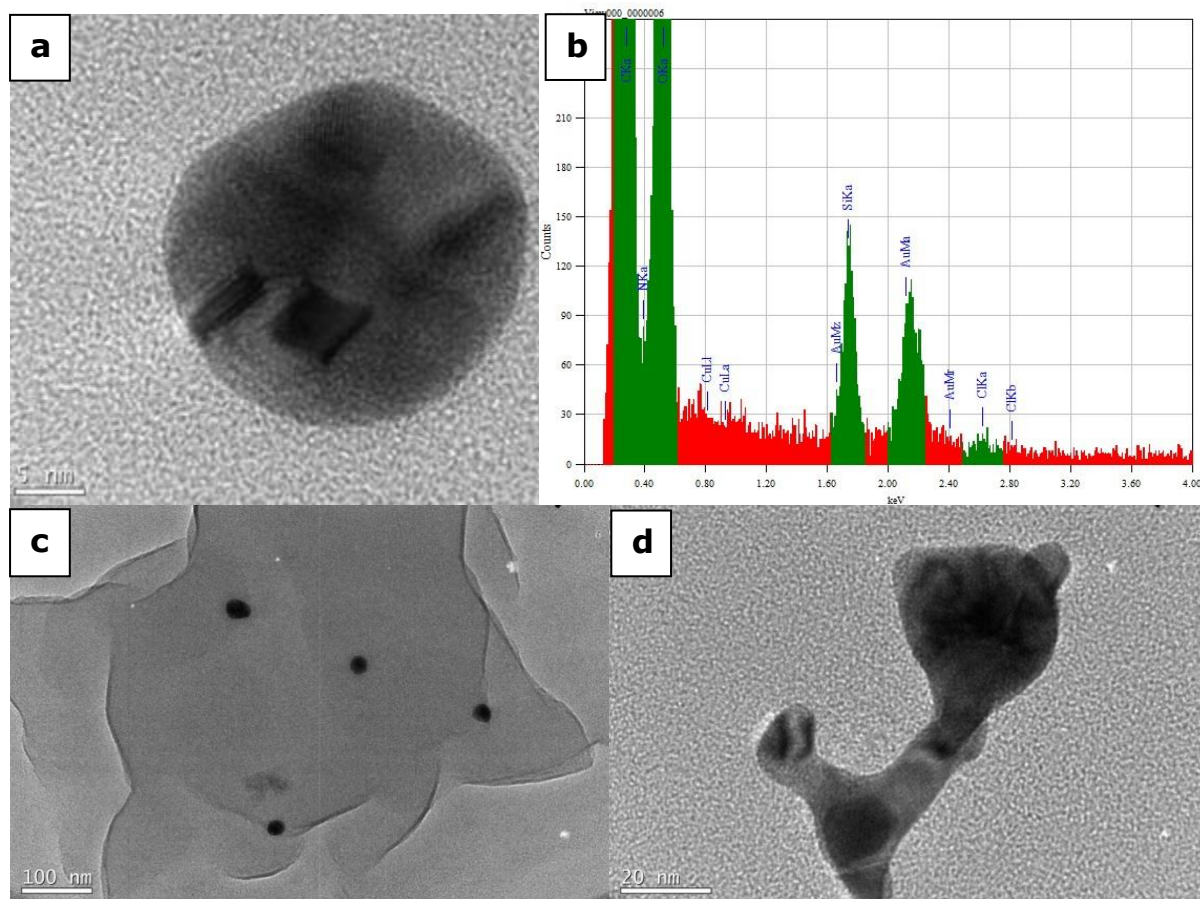


Figure 5.14: TEM micrographs of a,c,d) gold nanoparticles found in the K5000-1000Au-1:2 sample with b) the EDS spectrum of the particle shown in a).

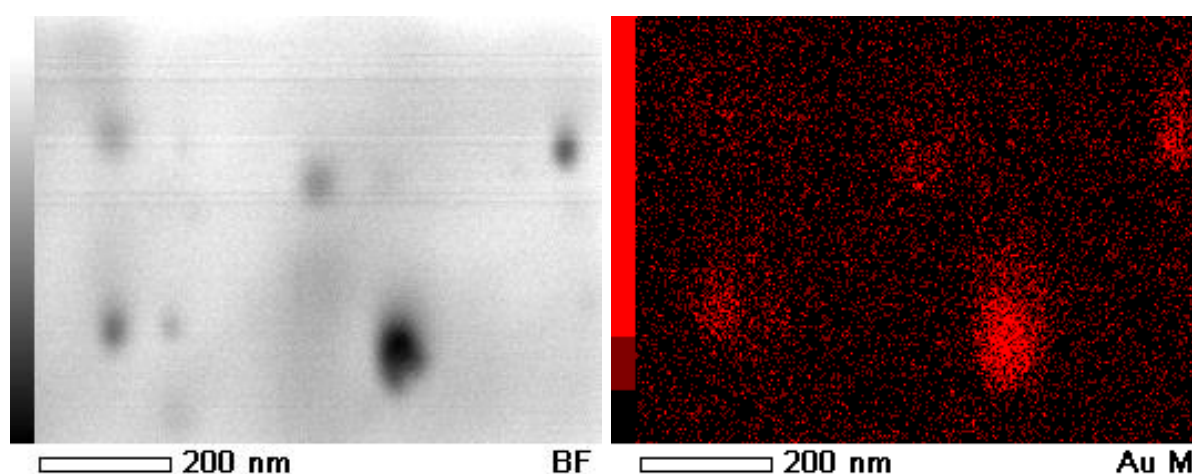


Figure 5.15: TEM and corresponding Au STEM micrographs of the K5000-1000Au-1:2 sample.

Scanning transmission electron microscopy (STEM) also confirmed the nanoparticles in the K5000-1000Au-1:2 sample to be gold. Figure 5.15a offers a TEM micrograph of the nanogold hybrid PU K5000 paint material, whereas the corresponding Au STEM map (Figure 5.15b) shows that where the nanoparticles are located, there are very high concentrations of gold (illustrated in red).

Figure 5.16 shows TEM micrographs of the nanosilver hybrid PU K5000 paint sample which was prepared from 2.5 ml of 1000 mg kg⁻¹ Ag⁺ solution in 5 g of PU K5000 paint base (K5000-1000Ag-1:2 sample). The silver in this hybrid material is present as a variety of nanoparticulate morphological forms. The most commonly found particles were spherical or spherical-like shapes including five-fold twinned particles in a broad size distribution from 10 to 60 nm in diameter. Additionally, alternate anisotropic geometric shapes were observed. The formation of anisotropic particles might be attributed to preferential addition of silver atoms at the twin sites, which are of high energy, leading to the formation of relatively short rods, truncated triangles, or to the geometric limitations imposed by the faceted character of the silver crystal.³⁰⁵ Particle aggregates were also found in the sample. This is consistent with the UV-Vis analysis result of the K5000-1000Ag-1:2 sample (Section 5.2). This UV-Vis spectrum shows a broad surface plasmon resonance absorption peak with a shoulder towards higher wavelengths, suggesting a non-uniform size and shape distribution of the particles as well as a presence of particle aggregation. The presence of silver within the nanosilver hybrid PU K5000 material was confirmed by a peak at 2.98 keV corresponding to the Ag L_α line in EDS elemental analysis (Figure 5.16b, d, f). Similar to the analogue K5000-1000Au-1:4 sample, TEM analysis of the K5000-1000Ag-1:4 sample could not be carried out due to limited equipment availability. However, it is likely that the silver nanoparticles present in this sample are slightly smaller in size. This assumption is inferred from the UV-Vis spectral analysis of the sample, which showed that the UV-Vis absorption peak was slightly blue-shifted (Section 5.2). Additional confirmation about the sizes of silver nanoparticles in both samples was achieved by analysing the XRD patterns and calculating the mean particle diameter by using the Scherrer equation (Section 2.3.4).

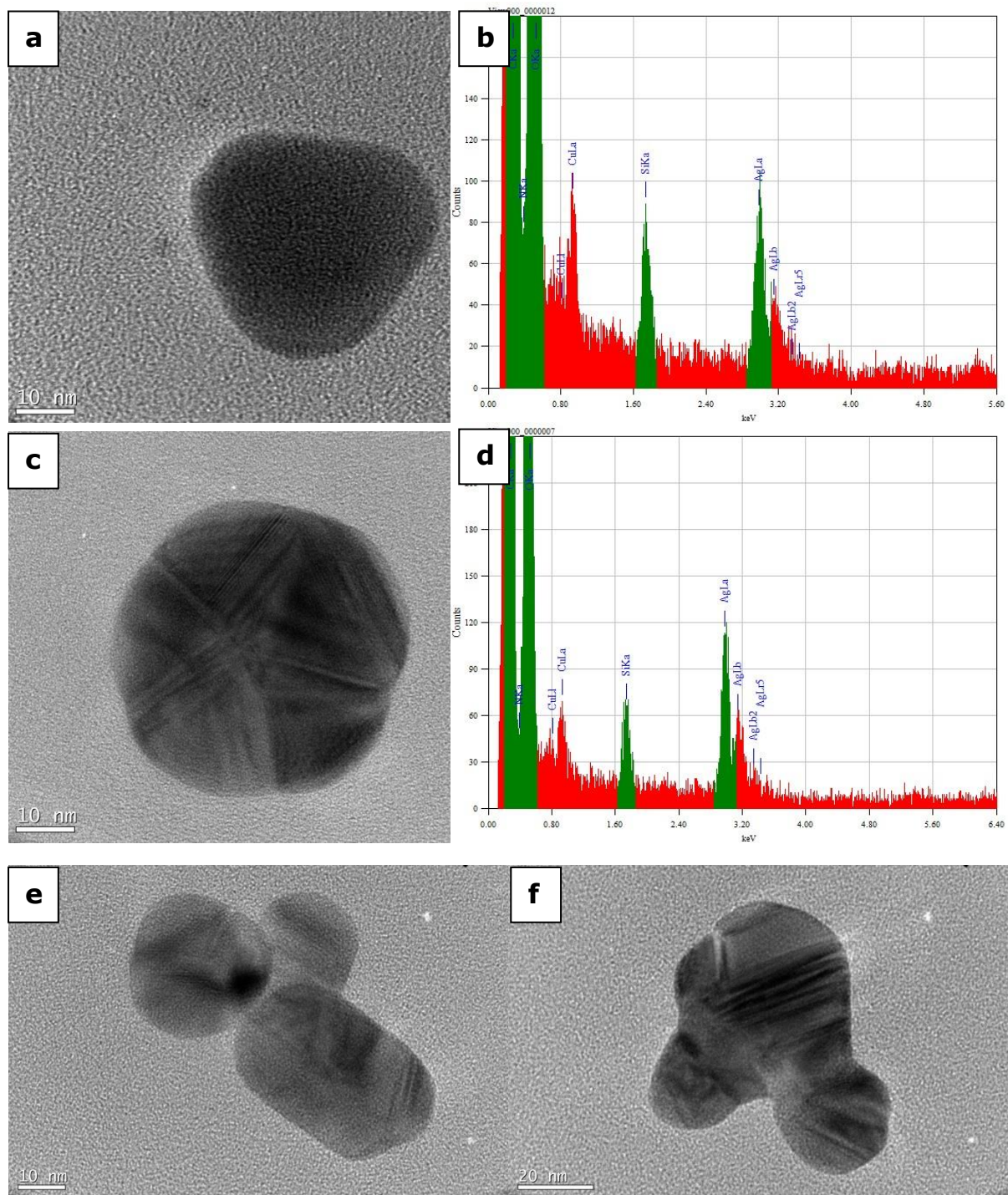


Figure 5.16: TEM micrographs of the K5000-1000Ag-1:2 sample: a, c) various shaped silver nanoparticles with b, d) their respective EDS spectra, e-f) nanosilver particle aggregates.

5.5 X-ray diffraction analysis of nanogold and nanosilver hybrid polyurethane K5000 latex paint base materials

XRD characterisation was carried out in order to confirm the formation of crystalline gold and silver nanoparticles in the nanogold and nanosilver hybrid polyurethane K5000 latex paint base materials. In the XRD patterns, the Bragg peak positions and their intensities were compared with the standard PDF 04-001-2616 for gold and PDF 04-001-2617 for silver pattern.²⁴² The mean particle size of the gold or silver nanoparticles was determined using Scherrer's equation, which was described in Section 2.3.4. The calculated mean crystallite particle sizes and the parameters for X-ray diffraction patterns for the nanogold and nanosilver hybrid polyurethane K5000 samples which are presented in Figure 5.17 - Figure 5.20 can be seen in Table 5.2 and Table 5.3 respectively.

Figure 5.17 and Figure 5.18 show XRD patterns of the nanogold hybrid PU K5000 paint materials prepared from 1.25 and 2.5 ml solution with different quantities of gold. For the samples containing 0.2 wt % of gold (K5000-200Au-1:4 and K5000-200Au-1:2), only diffraction peaks with low intensity are observed as the signal to noise ratio is very low. The discernible peak at $2\theta = 38.20^\circ$ and 38.90° respectively can be indexed to the (1 1 1) lattice plane of a cubic unit cell, which corresponds to the cubic structure of gold (PDF 04-001-2616).²⁴² These XRD results confirm that Au^{3+} ions were reduced to Au^0 and simultaneously stabilised by the PU K5000 polymer matrix. By increasing the concentration of the gold solutions employed to produce the K5000-600Au-1:4 sample and its more concentrated analogue K5000-600Au-1:2 sample, the (1 1 1) peak for both samples increased in intensity. Calculations for the mean crystallite size were done using Scherrer's equation and the results are given in Table 5.2. The mean crystallite size was found to be ca. 40 nm for both samples. The XRD patterns for samples containing the highest loading of gold (K5000-1000Au-1:4 and K5000-1000Au-1:2 samples) showed four peaks of Bragg reflections at $2\theta = 38.07^\circ$, 44.27° , 64.55° and 77.50° for the K5000-1000Au-1:4 sample and at 2θ angles = 38.12° , 44.29° , 64.64° and 77.61° for the K5000-600Au-1:2 sample. These peaks can be indexed to the (1 1 1), (2 0 0), (2 2 0) and (3 1 1) diffraction peaks based on the face centred

cubic structure of gold. Thus, XRD patterns confirm that the gold nanoparticles formed in both samples are crystalline in nature. The average sizes of the gold nanoparticles were estimated from the FWHM of the most intense respective (1 1 1) peaks. The mean crystallite size was estimated to be 43 nm for the K5000-1000Au-1:4 sample and 48 nm for the K5000-1000Au-1:2 sample. The results are consistent with those obtained in the UV-Vis analyses results (Section 5.2) for both samples exhibiting a similar purple colour. The UV-Vis spectra show that the surface plasmon resonance absorption bands for both samples are located at the same position suggesting that similar particle sizes are present in the K5000 1000Au-1:4 and K5000-1000Au-1:2 sample respectively.

Table 5.2: Parameters for X-ray diffraction patterns of the nanogold hybrid K5000 samples shown in Figure 5.17 -Figure 5.18.

| Hybrid material | Peak position [° 2 θ] | FWHM [° 2 θ] | Mean crystal diameter [nm] |
|------------------|----------------------------------|-------------------------|-------------------------------|
| K5000-1000Au-1:4 | 38.07 | 0.39 | 43 |
| K5000-1000Au-1:2 | 38.21 | 0.35 | 48 |
| K5000-600Au-1:4 | 38.07 | 0.39 | 40 |
| K5000-600Au-1:2 | 38.51 | 0.42 | 40 |

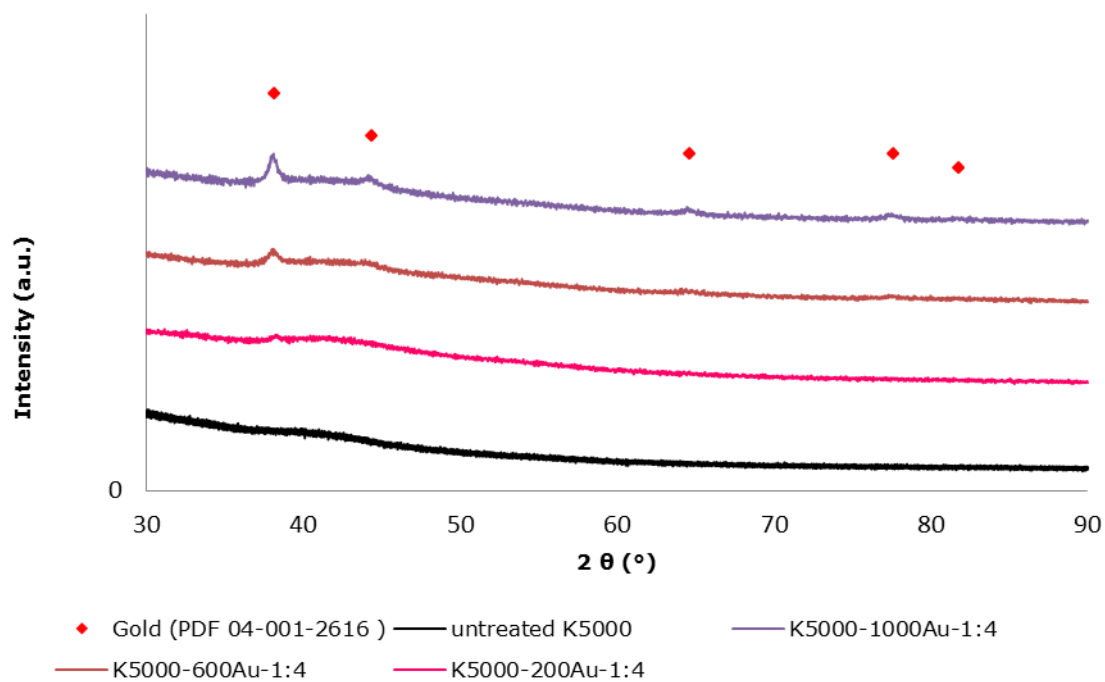


Figure 5.17: XRD patterns of the nanogold hybrid PU K5000 latex paint base materials prepared from 1.25 ml solution with different quantities of gold.

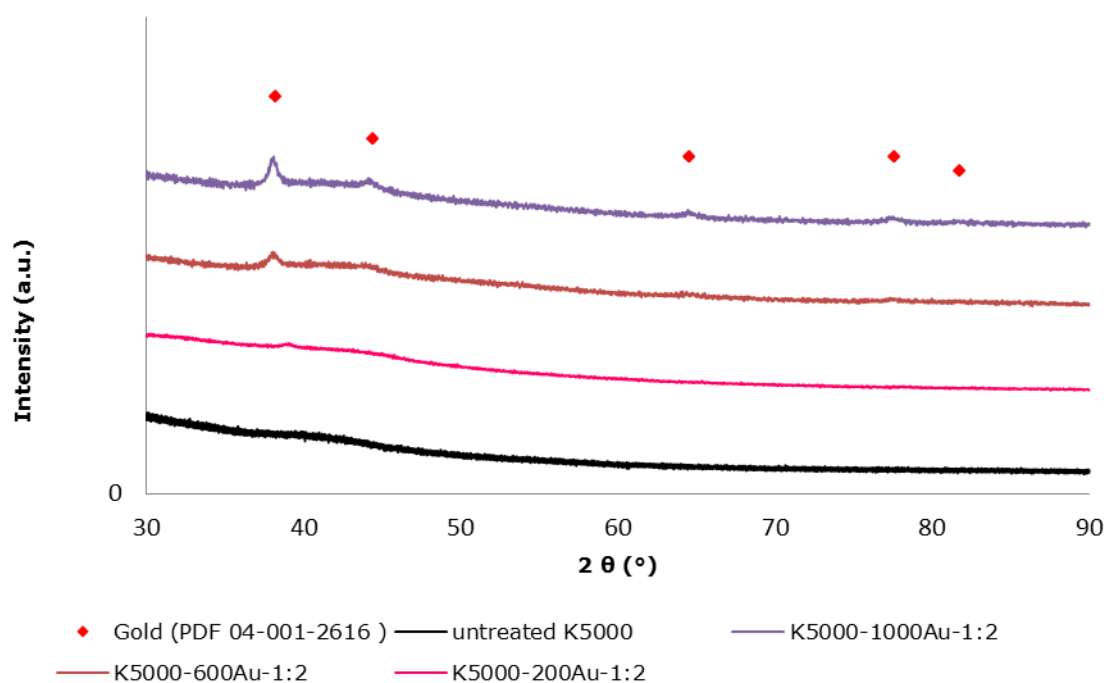


Figure 5.18: XRD patterns of the nanogold hybrid PU K5000 latex paint base materials prepared from 2.5 ml solution with different quantities of gold.

The XRD patterns of the nanosilver hybrid PU K5000 polymer samples prepared with different quantities of silver in 1.25 and 2.5 ml solution are shown in Figure 5.19 and Figure 5.20. All samples indicate the presence of silver. Similar to their analogue concentrated gold samples, the K5000-200Ag-1:4 and K5000-200Ag-1:2 samples exhibit only low X-ray intensity diffraction peaks at around $2\theta = 38^\circ$. The scarcely discernible Bragg diffraction peak present in both samples is identified as the (1 1 1) lattice plane of a cubic unit cell, corresponding to the cubic structure of silver (PDF 04-001-2617)²⁴². As the Ag^+ concentration was increased to produce the K5000-600Ag-1:4 or K5000-600Ag-1:2 samples, the (1 1 1) peak in both samples became more pronounced. The results are consistent with the colour change of these samples from yellow to brown (Figure 5.1). The peak positions ($2\theta = 38.30^\circ$ for the K5000-600Ag-1:4 sample and $2\theta = 38.17^\circ$ for the K5000-600Ag-1:2 sample) and their FWHM have been employed in Scherrer's equation to calculate the mean crystallite size of the silver particles. For the K5000-600Ag-1:4 sample the particle size was estimated to be 54 nm whereas for the K5000-600Ag-1:2 sample the particle size was found to be approximately 62 nm (Table 5.3). As the silver concentration was further increased to produce the K5000-1000Ag-1:4 or the K5000-1000Ag-1:2 sample, the XRD patterns of both samples showed the characteristic number of Bragg diffraction peaks for silver in the face centred cubic phase unequivocally indicating that the particles present in the K5000-1000Ag-1:4 and K5000-1000Ag-1:2 samples are composed of silver. In both samples three additional broad bands are observed at angle $2\theta = 44.44^\circ$, 64.58° and 77.53° (K5000-1000Ag-1:4 sample) or 44.33° , 64.52° and 77.46° (K5000-1000Ag-1:2 sample) which correspond to the (2 0 0), (2 2 0), and (3 1 1) planes of silver, matching the database pattern well²⁴². The peaks at $2\theta = 38.30^\circ$ or $2\theta = 38.17^\circ$ were used to calculate the crystallite size of the formed silver nanoparticles as these are primarily dominated by the (1 1 1) facets. The size of the silver nanoparticles was found to be ca. 58 nm for the K5000-1000Ag-1:4 sample and 67 nm for the K5000-1000Ag-1:2 sample (Table 5.3). This agrees well with TEM analysis results of the K5000-1000Ag-1:2 sample, where the spherical particle diameter was measured to be between 10 nm and 60 nm.

Table 5.3: Parameters for X-ray diffraction patterns of the nanosilver hybrid PU K5000 samples shown in Figure 5.19 -Figure 5.20.

| Hybrid material | Peak position [° 2 θ] | FWHM [° 2 θ] | Mean crystal diameter [nm] |
|------------------|----------------------------------|-------------------------|----------------------------------|
| K5000-1000Ag-1:4 | 38.30 | 0.29 | 58 |
| K5000-1000Ag-1:2 | 38.12 | 0.25 | 67 |
| K5000-600Ag-1:4 | 38.16 | 0.31 | 54 |
| K5000-600Ag-1:2 | 38.17 | 0.27 | 62 |

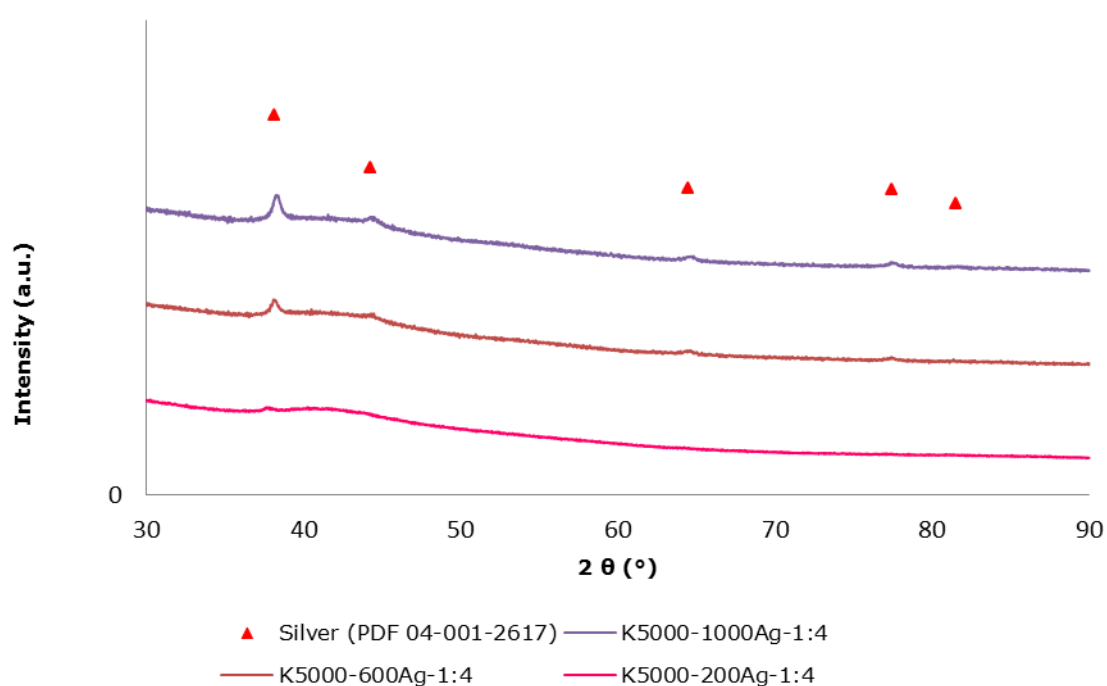


Figure 5.19: XRD patterns of the nanosilver hybrid polyurethane K5000 latex paint base materials prepared from 1.25 ml solution with different quantities of silver.

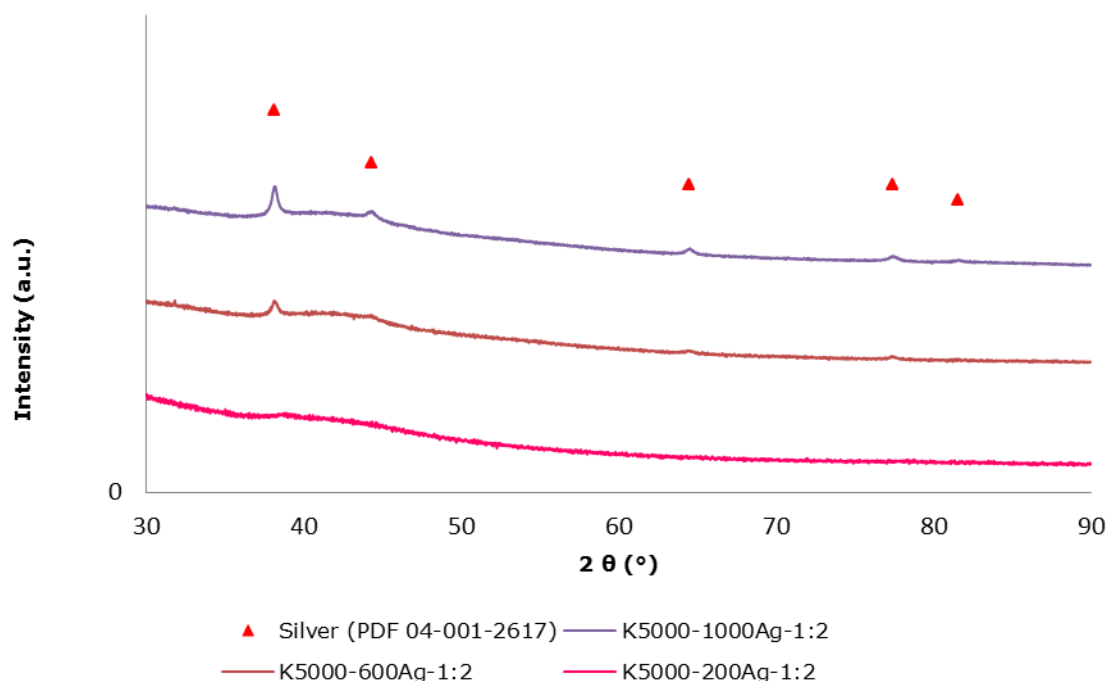


Figure 5.20: XRD patterns of the nanosilver hybrid polyurethane K5000 latex paint base materials prepared from 2.5 ml solution with different quantities of silver.

It is significant to note that the mean crystallite size of the silver nanoparticles is not only increasing with increased concentration of silver solutions, but also with the increased water content of those silver solutions. As previously mentioned, when preparing the hybrid PU K5000 materials from 2.5 ml of metal ion solution instead of 1.5 ml (whilst keeping the polymer to metal ion ratio constant), the concentration of the PU K5000 polymer is diluted and therefore decreased. The protective surface coverage of these silver particles, which is provided by the polymer, is reduced, leading to further growth and agglomeration of the particles. This also matches the results acquired from the UV-Vis analyses (Section 5.2) of the hybrid PU K5000 paint samples. Nanosilver hybrid samples with higher H_2O content underwent a red shift of their surface plasmon resonance absorption bands, suggesting particle growth.

5.6 X-ray photoelectron spectroscopy analysis of nanogold and nanosilver hybrid polyurethane K5000 latex paint base materials

As described in x, K5000 is a polyurethane latex paint base polymer with a polyether/polyester/acrylic composite backbone. Polyurethane possesses nitrogen-containing carbamate groups. An XPS study of the hybrid PU K5000 paint materials was carried out in order to understand how these carbamate groups were involved in the reduction of Au^{3+} or Ag^0 to their respective metallic nanoparticles and their subsequent binding to the PU K5000 polymer matrix. As representatives for nanogold and nanosilver hybrid PU K5000 paint materials, the K5000-1000Au-1:2 and K5000-1000Ag-1:2 samples were chosen for the XPS analyses due to the high concentration of formed metal nanoparticles at the analysed hybrid polymer surfaces. During the preparation of both samples, the reaction vials containing the samples were heated for 24 hours (50 °C for gold and 90 °C for silver). As reference samples, two samples each containing 5 g of PU K5000 paint base were heated at 50 and 90 °C respectively for 24 hours. By increasing the reaction temperature from room temperature to 50 °C and 90 °C respectively, it was hoped to increase the amount of gold or silver ions reduced to their respective metal nanoparticles. Thus, the probability of detecting any changes between the spectra of the reference PU K5000 paint samples and their respective hybrid polymers will be increased, as the formation of an increased amount of nanoparticles would require the oxidation of an increased percentage of functional groups of the PU K5000 polymer matrix. An initial survey scan from a binding energy of 600 to 0 eV for all PU K5000 latex paint polymer samples showed the presence of carbon, nitrogen and oxygen groups on the PU K5000 paint polymer surface, together with gold for the nanogold hybrid PU K5000 polymers and silver for the nanosilver hybrid PU K5000 polymers. High resolution scans were carried out across the peaks for each of the elements in the nanogold and nanosilver hybrid PU K5000 polymer materials, and also for carbon, nitrogen and oxygen in the reference PU K5000 paint samples. X-ray peaks for calcium and silicon should be ignored due to contamination of the samples.

5.6.1 X-ray photoelectron spectroscopy analysis of nanogold hybrid polyurethane K5000 latex paint base materials - proposed mechanism for gold nanoparticles formation and their binding to the PU K5000 matrix

Figure 5.21 presents wide XPS scans for the reference PU K5000 paint used as a sample and the nanogold hybrid PU K5000 paint sample (K5000-1000Au-1:2) with their characteristic elements (C, N, O and Au), confirming the presence of gold in the nanogold hybrid PU K5000 sample.

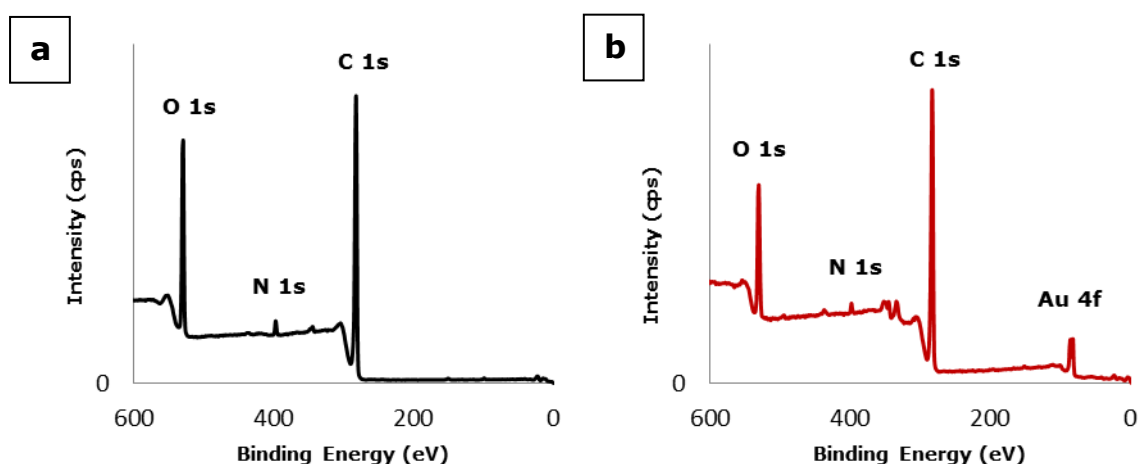


Figure 5.21: Survey XPS scans of a) the reference PU K5000 paint sample and b) the K5000-1000Au-1:2 sample which was heated to 50 °C during its preparation.

Figure 5.22 offers high resolution C 1s, N 1s and O 1s XPS spectra collected from both samples, the reference PU K5000 paint and the nanogold hybrid PU K5000 paint sample. A complete list of peak assignments is given in Table 5.4. The examination of the deconvoluted, high resolution C 1s spectrum of the reference PU K5000 paint sample revealed the presence of four components corresponding to aliphatic C–C or C–H (285 eV), C–N (285.6 eV), C–O (286.1 eV) and C=O (289.2 eV) bonds in the polymer chain.²⁶⁴ The high resolution N 1s spectrum was deconvoluted into one peak at 400.0 eV which is attributable to the nitrogen

of the carbamate group in the polymer matrix of the reference PU K5000 sample. The high resolution O 1s XPS spectrum can be deconvoluted into two peaks with their maxima at ca. 531.8 eV and 533.5 eV. These peaks were assigned to the carbonyl oxygen (C=O) and the oxygen singly bound to the carbon (C-O) in the PU K5000 matrix.

Table 5.4: XPS assignments for dry films of the reference PU K5000 paint sample and the K5000-1000Au-1:2 sample.

| | | Reference K5000 | Nanogold hybrid K5000 |
|--------------|--|-------------------------------------|-----------------------|
| | | Binding energy [eV] and (FWHM) [eV] | |
| C 1s | C-C, C-H | 285.00 (1.10) | 285.00 (1.10) |
| | C-N | 285.63 (0.81) | 285.56 (0.81) |
| | C-O | 286.14 (1.80) | 286.17 (1.96) |
| | O-C=O | 289.16 (1.21) | 289.11 (1.06) |
| N 1s | N-H | 400.00 (1.74) | 399.97 (1.67) |
| | N-Au | - | 398.36 (1.01) |
| | NO _x | | 407.69 (1.24) |
| O 1s | O=C | 531.84 (1.64) | 531.86 (1.64) |
| | O-C | 533.48 (1.92) | 533.53 (1.72) |
| Au 4f | Au ⁰ _{7/2} | - | 83.57 (1.24) |
| | Au ⁺ /Au ³⁺ _{7/2} | - | 84.75 (2.48) |
| | Au ⁰ _{5/2} | - | 87.33 (1.24) |
| | Au ⁺ /Au ³⁺ _{5/2} | - | 88.42 (2.48) |

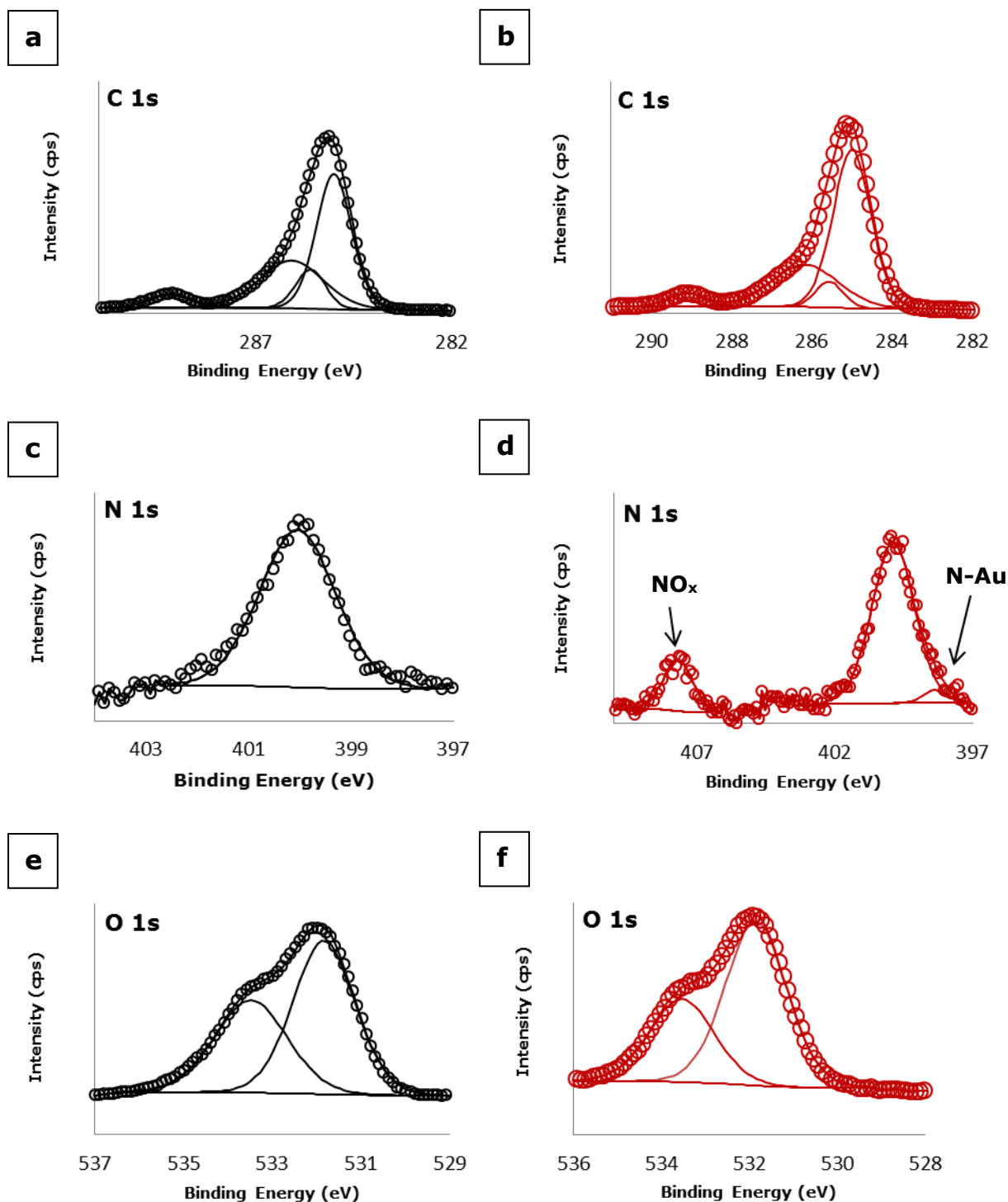


Figure 5.22: Deconvoluted high resolution XPS spectra for the reference PU K5000 paint sample: a) C 1s peaks, c) N 1s peak and e) O 1s peaks; for the K5000-1000Au-1:2 sample: b) C 1s peaks, d) N 1s peaks and f) O 1s peaks. Experimental data points are shown by circles.

The analysis of the high resolution C 1s XPS spectrum acquired for the nanogold hybrid PU K5000 sample did not show any significant changes in relation to the reference sample. The deconvolution of the C 1s spectrum using a four-peak fitting routine revealed four carbon species attributable to an aliphatic carbon bound to adjacent carbon or hydrogen (285 eV), a carbon singly bound to nitrogen environment (285.6 eV), carbon singly bound to oxygen (286.2 eV) and a carbonyl carbon derived from the PU K5000 matrix (289.1 eV). The values for their binding energies and the respective FWHM can be seen in Table 5.4.

As mentioned in Chapter 3, nitrogen in the carbamate group of PU shows an affinity for gold. As such, the PU K5000 latex paint base polymer offers an opportunity to attract and reduce gold ions to gold nanoparticles, stabilise the particles and subsequently bind them to the PU K5000 polymer matrix. The gold nitrogen interaction was first detected in the high resolution N 1s scan obtained for the nanogold hybrid PU K5000 paint sample. Although the binding energy of the peak for nitrogen in the carbamate group of the matrix did not change (~ 400.0 eV), Figure 5.22d shows that the treatment of 5 g of the PU K5000 paint base with 2.5 ml of a $1000 \text{ mg kg}^{-1} \text{ Au}^{3+}$ solution for 24 hours at 50°C resulted in the formation of two new nitrogen components. This confirms that N-containing moieties of the PU K5000 matrix were involved in the reduction of gold ions to gold nanoparticles. The peak at ca. 398.4 eV is consistent with the formation of a N-Au bond^{21,24,265,266} confirming the chemical affinity of gold for nitrogen. The interaction between the electrons on the nitrogen with gold to form an Au-N bond decreases the electron density on the nitrogen atom leading to the peak formation at lower binding energies. The K5000-1000Au-1:2 sample only contains 0.1 wt % of gold, hence, the changes of the nitrogen are expected to be minimal, as most of the nitrogen is associated with the remaining polymer and only 3.5 % area of nitrogen species form bonds to gold. Due to the extra columbic interaction between the photo-electron and the ion core, atoms of a higher positive oxidation state exhibit a higher binding energy.³⁰⁷ Therefore, the third N 1s spectral component which is located at 407.7 eV suggests the presence of a new nitrogen moiety of a higher oxidation state (NO_x). This oxidation of the nitrogen in the carbamate groups of the PU K5000 paint base is facilitated by the reduction of the Au^{3+} ions to Au^0 . Similar binding energies were reported for nitrate compounds.^{275,308,309}

Figure 5.22f shows that the envelope of the O 1s spectrum for the nanogold hybrid PU K5000 material has two maxima. The spectrum was deconvoluted into two components attributable to C-O and C=O bonds with the maxima centred at 531.9 eV and 533.5 eV respectively. When comparing the spectrum to that of the reference PU K5000 sample, it is evident that the chemical environment of oxygen does not change to any significant extent. This is to be expected, as it should be noted that because of the low concentration of employed gold solution in the production of these nanogold hybrid PU K5000 materials (approximately 0.1 wt %), following the reduction of Au^{3+} to Au^0 , a large proportion of the polymer will still remain unoxidised.

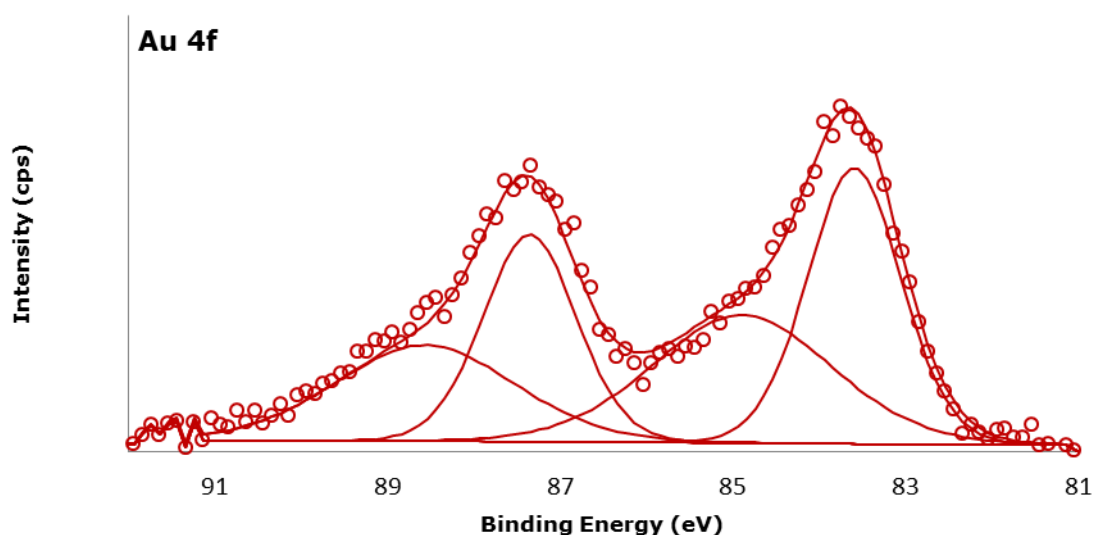


Figure 5.23: Deconvoluted high resolution Au 4f XPS spectrum for the nanogold hybrid PU K5000 paint sample (K5000-1000Au-1:2).

The high resolution Au 4f XPS spectra of the purple coloured nanogold hybrid PU K5000 sample (prepared from 2.5 ml of a 1000 mg kg^{-1} gold solution, at 50 °C for 24 hours) is shown in Figure 5.23. The deconvolution of the line shape resulted in two doublets, indicating two different species of gold present in the sample. Both doublets with an intensity ratio of 4:3 show a spin orbital separation of 3.67 eV matching the spacing of the bulk metal.²⁷⁵ The doublet

peaks centred at approximately 83.6 eV ($4f_{7/2}$) and 87.3 eV ($4f_{5/2}$), are attributable to Au^0 according to the literature^{275,310,311} and provide further confirmation that gold ions are reduced to metallic gold during the reaction of the PU K5000 matrix with gold solution at 50 °C for 24 hours. These values for the binding energies show a slight shift towards lower binding energies in comparison to those of bulk gold.²⁷⁵ The negative shift is assumed to be due to the nitrogen of the carbamate functional groups bound to the gold resulting in greater negative charge at the gold surface, which in turn leads to greater screening of the gold. Similar shifts have been reported in the literature.^{21,24} A second set of broader doublet peaks found at around 84.8 eV ($4f_{7/2}$) and 88.42 eV ($4f_{5/2}$), indicates the existence of a higher oxidation state of gold. It is considered that the gold nanoparticles possess Au^0 cores which are surrounded by Au^+ ions. Thus, these latter peaks were assigned to partially reduced Au^+ that are bound to the PU K5000 matrix via Au-N bonds through the nitrogen-containing carbamate group of the polyurethane K5000 matrix. However, they may also represent partially reduced Au^+ on the surface of the nanoparticles, which do not undergo any bond to the polymer matrix. Due to the broadness of the peaks, it is not possible to exclude the fact that they may mask an additional set of doublet peaks attributable to unreduced Au^{3+} in form of $[AuCl_4]^-$ ions. These ions may accumulate on the surface of the gold nanoparticles or exist freely in the PU K5000 polymer matrix. SEM analysis of the sample showed the presence of chlorine (Section 5.3).

From the XPS results discussed the following is proposed for the mechanisms of the formation of gold nanoparticles within the polyurethane K5000 polymer matrix. When adding the aqueous gold solution to the PU K5000 paint base substrate, the dissociated H^+ and $[AuCl_4]^-$ diffuse through the PU K5000 polymer. Hydrogen ions protonate the nitrogen-containing groups. The resulting positively charged nitrogen groups electrostatically attract Cl^- ions and destabilise the $[AuCl_4]^-$ complex, leading to the reduction of Au^{3+} to Au^+ by the carbamate functional groups of polyurethane. Subsequently the resultant Au^+ ions associate with the polymer matrix via Au-N bonds, through the carbamate group of polyurethane. Additional Au^{3+} ions will be reduced to Au^0 simultaneously coupled with a further oxidation reaction of carbamate groups which gives rise to a formation of a new NO_x species. Owing to the aurophilicity

effect²¹ it is likely that the Au^+ in the Au-N bonds would be attracted to each other resulting in the formation of nanoclusters on which the additional Au^{3+} may accumulate and be further reduced to Au^0 , forming gold nanoparticles within the PU K5000 polymer. It is not necessary for the nitrogen-containing carbamate groups to be in direct contact with the gold nanoclusters because the reaction is carried out in ionic solution. Thus, electrons released from the carbamate oxidation can be transported to the adjacent gold nanoclusters, providing the required electrons for the Au^{3+} to Au^0 reduction. Since these gold nanoparticles are bound to the polymer matrix via Au-N bonds, the surface energy of the nanoparticles will be decreased, making the nanoparticles stable against the aggregation.

Since only a low concentration of gold solution is employed (up to 0.1 wt % of gold loading in the PU K5000 polymer) in the production of these nanogold hybrid PU K5000 materials, most of the nitrogen is associated with the bulk polymer.

5.6.2 X-ray photoelectron spectroscopy analysis of nanosilver hybrid polyurethane K5000 latex paint base materials – proposed mechanism for silver nanoparticles formation and their binding to the PU K5000 matrix

The survey XPS scans for the reference PU K5000 paint sample and the nanosilver hybrid PU K5000 paint sample (K5000-1000Ag-1:2) with their respective characteristic elements (C, N, O and Ag) are presented in Figure 5.24.

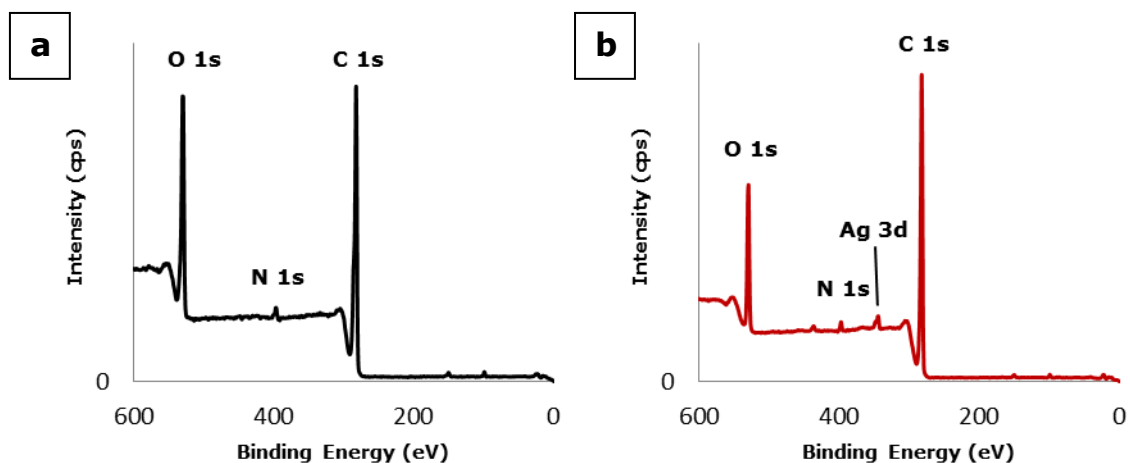


Figure 5.24: Survey XPS scans of the surfaces for a) the reference PU K5000 paint and b) the K5000-1000Ag-1:2 sample.

The high resolution C 1s, N 1s and O 1s XPS spectra acquired for the reference PU K5000 paint and the nanosilver hybrid PU K5000 paint sample are shown in Figure 5.25. Table 5.5 presents a complete list of peak assignments.

Table 5.5: XPS assignments for dry films of the reference PU K5000 paint sample and K5000-1000Ag-1:2 sample.

| | | Reference K5000 | Nanosilver hybrid K5000 |
|--------------|--------------------------------|-------------------------------------|-------------------------|
| | | Binding energy [eV] and (FWHM) [eV] | |
| C 1s | C-C, C-H | 285.00 (0.98) | 285.00 (1.00) |
| | C-N | 285.51 (0.79) | 285.53 (0.78) |
| | C-O | 286.52 (1.29) | 286.53 (1.28) |
| | O-C=O | 288.96 (0.87) | 288.97 (0.87) |
| | | | |
| N 1s | N-H | 399.82 (1.53) | 399.83 (1.64) |
| | N-Ag | - | 397.77 (1.00) |
| | NO _x | - | 407.11 (1.25) |
| O 1s | O=C | 532.03 (1.19) | 532.06 (1.22) |
| | O-C | 533.48 (1.31) | 533.49 (1.30) |
| Ag 3d | Ag ⁰ _{5/2} | - | 368.10 (0.98) |
| | Ag ⁰ _{3/2} | - | 374.10 (0.98) |

The comparison of the deconvoluted high resolution C 1s spectra for the reference PU K5000 sample and the K5000-1000Ag-1:2 sample revealed that the chemical environment of C does not change upon the reaction of the PU K5000 polymer matrix with silver. The XPS C 1s spectra for both samples were deconvoluted into three peaks (Figure 5.25a-b). As for the polyurethane K5000 samples described in Section 5.6.1, the peaks located at 285.0 eV are associated with aliphatic C-C or C-H carbons in the PU K5000 polymer matrix, whilst the peaks centred at ca. 285.5 eV and 286.5 eV were attributed to the carbon nitrogen (C-N) and the carbon oxygen bond (C-O) respectively. The peaks at higher binding energies found at around 289.0 eV for both samples correspond to the carbonyl carbon (O=C-N) of polyurethane chains in the PU K5000 matrix. All values for binding energies are a good match with the values found for PU in the literature.^{264,312}

Similar to gold, silver is known to have an affinity for nitrogen.^{241,313} As expected, the interaction between nitrogen and silver was observed by comparing the high resolution N 1s spectra obtained for the reference PU K5000 sample and the nanosilver hybrid PU K5000 paint sample (Figure 5.25c-d). After the reaction of the PU K5000 matrix with silver (2.5 ml of a 1000 mg kg⁻¹ Ag⁺ solution at 90°C for 24 hours) two new peaks emerged in addition to the unchanged peak located at 399.8 eV which was attributed to the nitrogen in the carbamate group of PU.²⁶⁴ The peak at lower binding energies, centred at ca. 397.8 eV, is consistent with the formation of a N-Ag bond³¹⁴. Again, since the nanosilver hybrid PU K5000 materials only contain 0.1 wt % silver, very minor changes to the N 1s spectrum are expected, thus only 3.3 % by area of nitrogen is in the form of bonds to silver. A further indication for the involvement of nitrogen-containing moieties of the PU K5000 matrix in the reduction of Ag⁺ to Ag⁰ was noted by the formation of a peak at around 407.1 eV. The peak was assigned to an oxidised species of nitrogen (NO_x). As previously reported, a peak with similar binding energy value was observed for the nanogold hybrid PU K5000 materials (Section 5.6.1), confirming that the reduction of gold ions to metallic gold was facilitated by the oxidation of carbamate groups in the polymer.

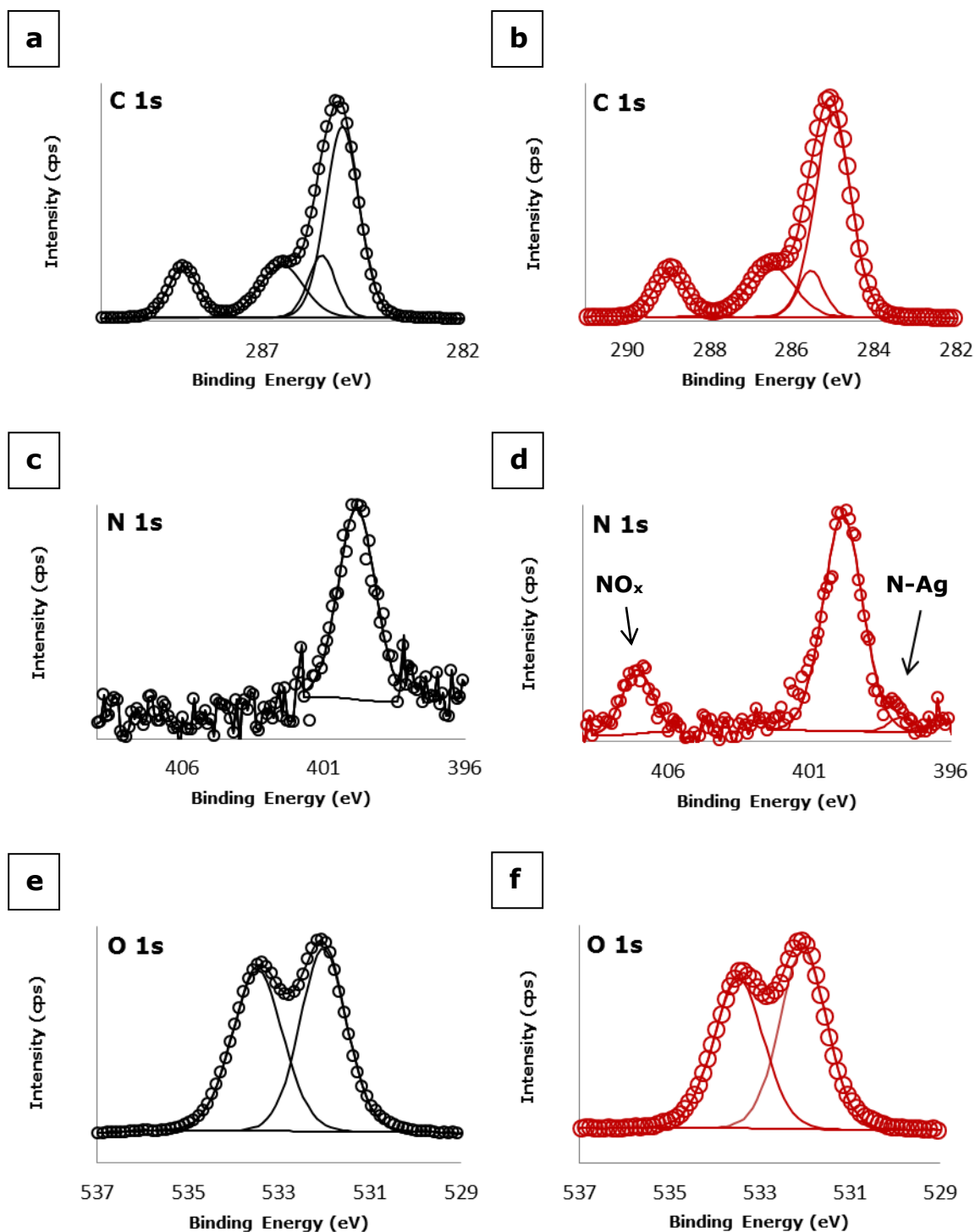


Figure 5.25: Deconvoluted high resolution XPS spectra for the reference PU K5000 paint sample: a) C 1s peaks, c) N 1s peak and e) O 1s peaks; for the K5000-1000Ag-1:2 sample: b) C 1s peaks, d) N 1s peaks and f) O 1s peaks. Experimental data points are shown by circles.

Similar to carbon, a comparison of the high resolution O 1s spectra for the reference PU K5000 sample and the K5000-1000Ag-1:2 sample showed that there was no significant change in the oxygen environment upon reaction of the PU K5000 matrix with silver (Figure 4.25e-f). Considering the small amount of silver used to prepare the sample (0.1 wt % Ag) and there is no chemical interaction between the silver and oxygen in the PU polymer, it is expected that the change of the oxygen environment is negligible and the oxygen environment is that of the polymer itself. The XPS O 1s spectra were deconvoluted into two oxygen components found at 532.0 eV and 533.5 eV for both samples. The latter peak is consistent with the oxygen singly bound to a carbon (C-O) and the peak at lower binding energies is attributable to a carboxyl oxygen in the carbamate group of the PU K5000 polymer matrix.²⁶⁴

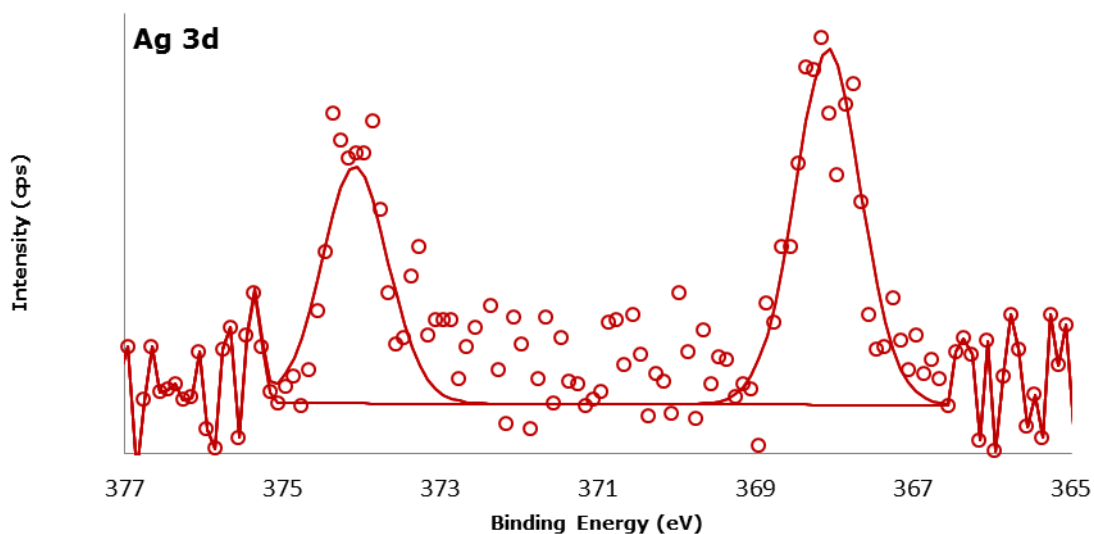


Figure 5.26: Deconvoluted high resolution Ag 3d XPS spectrum for the nanosilver hybrid PU K5000 paint sample (K5000-1000Ag-1:2).

The high resolution Ag 3d spectrum of the K5000-1000Ag-1:2 sample is shown in Figure 5.26. It was difficult to achieve a good signal to noise ratio in this spectrum because of the low level of silver. The spectrum was deconvoluted into one set of doublet peaks with an intensity ratio of 3:2 and the spin orbit splitting

of 6 eV. The peaks are positioned around 368.1 ($3d_{5/2}$) and 374.1 ($3d_{3/2}$) eV. These peaks are attributable to metallic silver²⁷⁵ which further confirm that silver ions were reduced to metallic silver when the PU K5000 paint was exposed to AgNO_3 solution at 90 °C for 24 hours. Owing to the affinity that silver has for nitrogen, it was hoped that another set of doublet peaks would be detected, showing an association of silver with the nitrogen atoms of the PU K5000 matrix. However, due to the low intensity and high amount of background noise in the Ag 3d spectrum, it was not possible to ascertain the nature of the bonding existing between silver and the PU K5000 polymer matrix using the Ag 3d XPS spectrum.

In light of the XPS results, the following is suggested for the mechanism of the formation of silver nanoparticles within the polyurethane K5000 polymer matrix. On addition of an aqueous AgNO_3 solution to the PU K5000 substrate, silver ions diffuse through the polymer matrix. Owing to its affinity for nitrogen, silver ions undergo an interaction with nitrogen-containing carbamate groups in PU resulting in an Ag-N bond. Adjacent carbamate functional groups act as a reducing agent, providing electrons for reduction of Ag^+ to Ag^0 . Coupled oxidation reaction of the nitrogen groups leads to the formation of oxidised NO_x species. The PU K5000 polymer matrix ensures the stabilisation of formed silver nanoparticles.

5.7 Infrared spectroscopy analysis of nanogold and nanosilver hybrid polyurethane K5000 latex paint base materials

Infrared spectroscopy analyses were carried out in an attempt to provide additional clarification on the bonding nature between the gold and silver nanoparticles and the polymer matrix of the polyurethane K5000 paint base. It was hoped that the comparisons of the IR spectra of the nanogold and nanosilver hybrid PU K5000 paint materials with the untreated PU K5000 paint would provide further information on the nature of the interaction between the nanoparticles and the substrate and confirm the role of carbamate groups in this bonding. The K5000-1000Au-1:2 and K5000-1000Ag-1:2 samples were chosen

as representatives of the nanogold and nanosilver hybrid K5000 materials. These samples have higher concentration of metal nanoparticles at the hybrid polymer surfaces, increasing the probability of detecting any changes between the IR spectra of the substrate and its respective hybrid polymers, as the formation of an increased amount of nanoparticles would require the oxidation of an increased percentage of functional groups of the polymer matrix. The IR spectra of the untreated PU K5000, K5000-1000Au-1:2 and K5000-1000Ag-1:2 samples are given in Figure 5.27. From the figure it can be observed that there are no distinguishable differences in the IR spectra of the untreated K5000 paint sample and the hybrid PU K5000 materials upon reaction with gold or silver; all three samples show identical peaks which are characteristic for PU (Section 3.9). Hence, the IR spectroscopy did not provide any further information on the bonding between the gold and silver nanoparticles and the polymer matrix of the PU K5000 paint base. This is probably attributable to the fact that IR spectroscopy is a bulk analysis method on such samples, thus it is not particularly sensitive to the small quantity of nanoparticles on the surface of the PU K5000 paint polymer relative to the bulk quantity of paint present

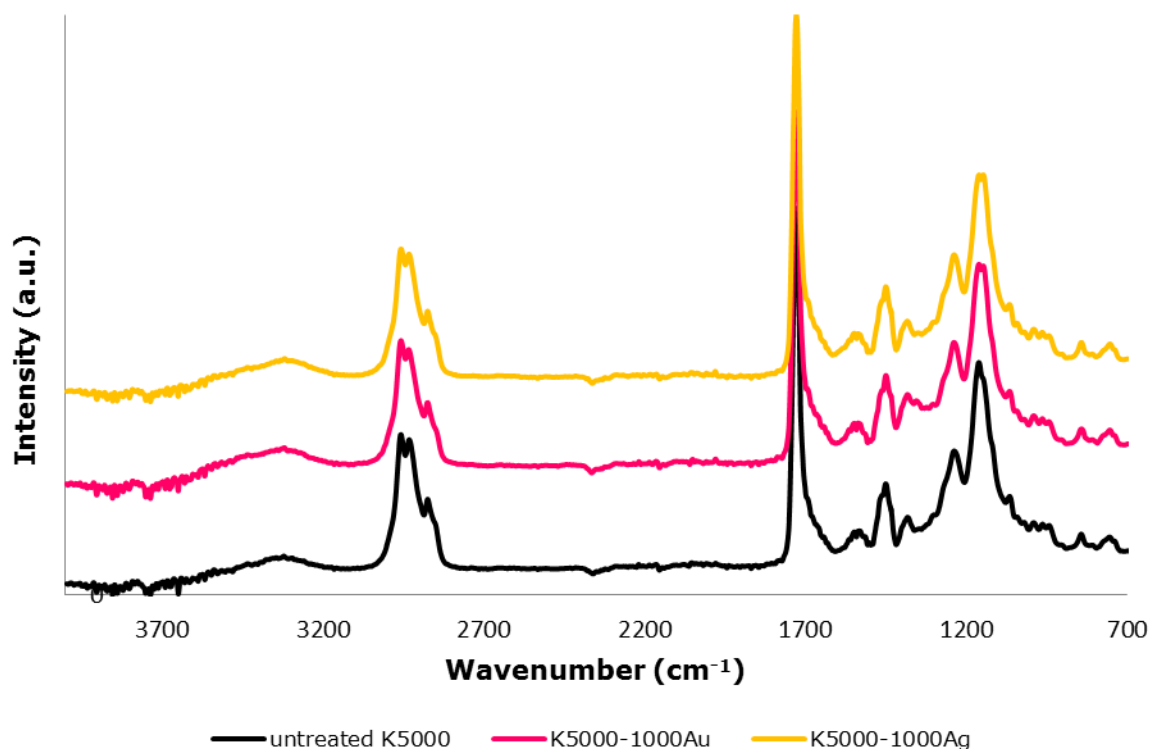


Figure 5.27: FT-IR spectra of the dry untreated PU K5000 paint and the nanogold and nanosilver hybrid PU K5000 paint materials.

5.8 Leaching tests on nanogold and nanosilver hybrid polyurethane K5000 latex paint base materials

The list of consumer products containing metal nanoparticles is growing despite the fact that little is known about the long term health or environmental impacts of these nanoparticles. Thus, it is essential to limit their leaching from consumer products. As such, quantitative AA analyses of the leaching solutions were carried out in order to determine the amount of gold and silver leached from the nanogold and nanosilver hybrid PU K5000 materials. The K5000-1000Au-1:2 and K5000-1000Ag-1:2 samples were chosen as representatives of the hybrid PU K5000 materials. The leaching solutions of these samples were prepared as described in Section 2.2.5. Briefly, this was achieved by drying the produced nanogold or nanosilver hybrid PU K5000 paint samples on microscope slides, rinsing the resultant dry films with distilled water and placing them in 30 ml of distilled water. Subsequently the samples were agitated for seven days at room temperature and the residual leaching solution was analysed by means of AA spectroscopy for any gold or silver content respectively. AA spectroscopy studies revealed that a small percentage value of gold (0.15 wt % of total gold loading in paint) and silver (0.07 wt % of total silver loading in paint) was leached from the hybrid PU K5000 materials (Table 5.6). These amounts complement the results obtained from XPS analyses of the materials which suggest that most of the gold and silver nanoparticles are chemically bound to the polymer matrix via Au-N and Ag-N bonds respectively (Section 5.6). The detected amounts of gold or silver arise from the free gold or silver ions, which are trapped in the PU K5000 matrix due to an uncompleted reduction reaction.

Table 5.6: Gold or silver leached from nanogold and nanosilver hybrid PU K5000 materials, leaching tests were carried out at room temperature for seven days.

| Sample | Metal species | Amount of metal in polymer [wt %] | Amount of leached metal [µg] | Amount of leached metal (% total metal loading) |
|------------------|---------------|-----------------------------------|------------------------------|---|
| K5000-1000Au-1:2 | gold | 0.1 | 7.5 | 0.15 |
| K5000-1000Ag-1:2 | silver | 0.1 | 3.6 | 0.07 |

5.9 Antimicrobial and antifouling properties of nanogold and nanosilver hybrid polyurethane K5000 latex paint base materials

Bacterial infection remains a leading cause of death in both the Western and developing world.³¹⁵ Most notable is that due to the growing occurrence of antibiotic resistance by common microbes, the treatment of microbial infections has become more challenging. Also traditional biocides, which are components of antifouling paints, have revealed limited efficacy against biofouling in aquatic and terrestrial environments. Hence, in order to ascertain the potential to create more effective antimicrobial and antifouling surfaces which inhibit the growth of biofilms and thus preventing the spread of microbial infections in healthcare, commercial and domestic facilities, or the attachment of undesired marine life to boat hulls, nanogold and nanosilver hybrid PU K5000 paint base materials were tested for their antimicrobial and antifouling activity.

For reasons of time constraints, it was only possible to test the K5000-1000Au-1:2 and the K5000-1000Ag-1:2 samples against the gram negative *Escherichia coli* bacteria (strain W3110). The test was performed via the method described in Section 2.3.8.1. In summary, the untreated PU K5000 reference sample, the K5000-1000Au-1:2 and the K5000-1000Ag-1:2 samples were spread out on a microscope slide and dried at room temperature. The dry films of the PU K5000 paint base samples were then peeled off and rinsed with distilled H₂O. Dry paint samples were cut into small pieces and dispersed in aqueous standard phosphate-buffered saline (PBS) suspension containing *E. coli*

bacteria to provide contact between the hybrid materials and bacteria. On the basis of the relative difference in total colony-forming units (CFU) between the nanogold and nanosilver hybrid PU K5000 samples and their reference samples, it was possible to determine the change in antimicrobial activity after two and four days of contact with the bacteria. CFU is a measure of viable bacterial numbers.

Figure 5.28 and Figure 5.29 show the percentages of remaining CFU after contact with the untreated PU K5000, the K5000-1000Au-1:2 and K5000-1000Ag-1:2 samples after two and four days of exposure. After two days of testing the CFU for the K5000-1000Au-1:2 and K5000-1000Ag-1:2 samples was ca. 82.1 % and 0.02 % respectively. It was expected for the sample containing silver nanoparticles to be more effective than its analogue sample containing gold nanoparticles because silver has a greater toxicity than gold towards microorganisms. The results obtained after four days of testing revealed a 30.7 % reduction in bacteria count after the contact with the K5000-1000Au-1:2 sample. The value of CFU for the tested K5000-1000Ag-1:2 sample showed the bacteria count decreased by 99.99% which demonstrates the excellent antimicrobial properties of this nanosilver hybrid PU K5000 paint.

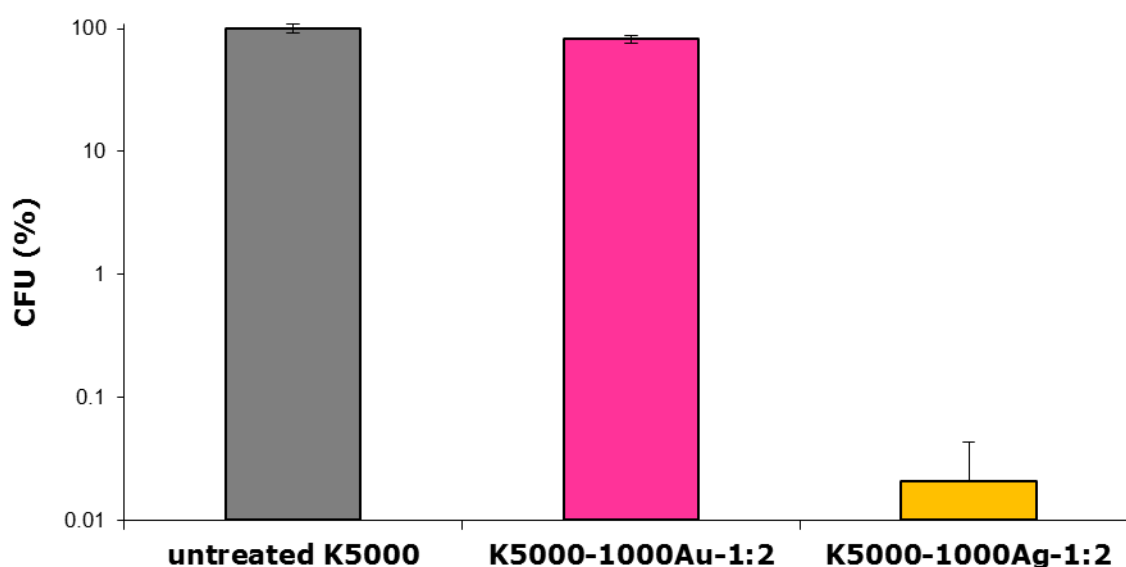


Figure 5.28: Percentage cell survival relative to untreated PU K5000 paint as control after two days of bacteria being in contact with the control, gold and silver hybrid PU K5000 materials. (Note the vertical axis is a log scale.)

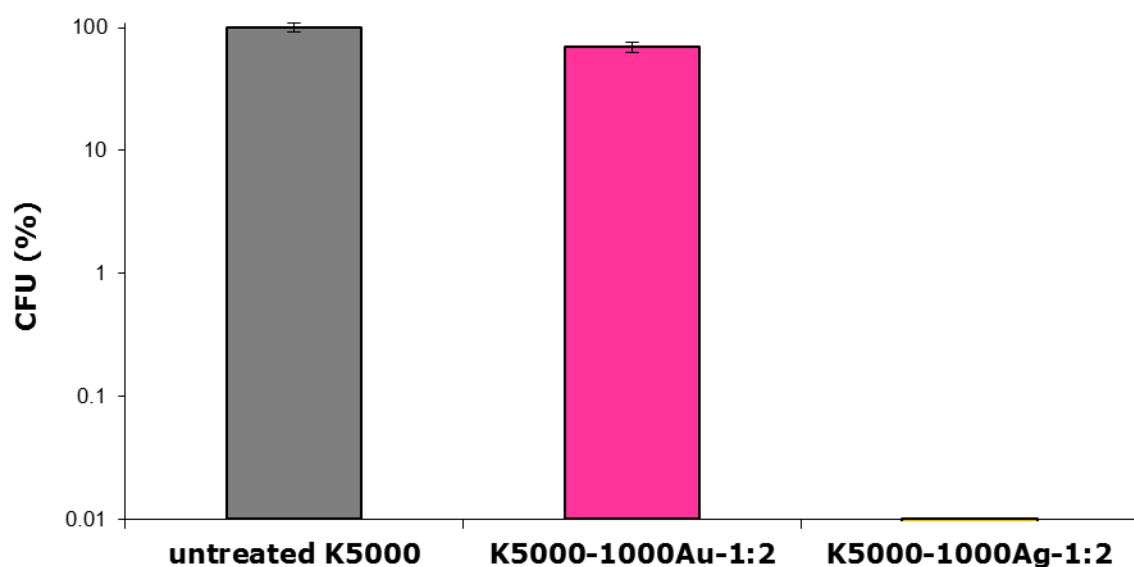


Figure 5.29: Percentage cell survival relative to untreated PU K5000 paint as control after four days of bacteria being in contact with the control, gold and silver hybrid PU K5000 materials. (Note the vertical axis is a log scale.)

As previously reported (Section 3.11), gold and silver nanoparticles possess a broad spectrum of antimicrobial effectiveness.^{192,203,204,290,291} Although, gold and silver nanoparticles exhibit a strong binding affinity to the electron-donating groups in the bacterial cells, resulting in their antimicrobial activity¹⁹², the mechanism of antimicrobial effects is still not entirely understood (Section 3.11).

The metallic nanoparticles present in the hybrid PU K5000 paint materials are considered to be chemically bound to the polymer matrix (Sections 5.6.1 and 5.6.2). Consequently, the gold or silver nanoparticles will not be released into the pathogenic environment where they are able to interact physically with the *E. coli* bacteria. It has been reported that gold nanoparticles which were chemically attached to wool were classified as bacteriostatic; these wool composites resisted *Staphylococcus aureus* growth²¹. As such, the nanogold hybrid PU K5000 paint materials provide surfaces that kill microbes on contact, i.e., they do not release gold nanoparticles or gold ions into the bacteria and they are not exhausted.

It is important to note that the antimicrobial properties of the nanogold hybrid PU K5000 paint materials could be due to the presence of partially reduced Au^+ ions on the surface of the gold nanoparticles (Section 5.6.1). Hence, an electrostatic attraction between the positively charged gold ions and negatively charged bacterial cell walls, which results in an association between the gold nanoparticles of the K5000-1000Au-1:2 sample and the bacteria, should not be excluded. This association can facilitate electron transfer between the bacteria and the gold resulting in an interference of bacteria's cell function. Additionally, it should be noted that the antibacterial activity of the nanogold hybrid PU K5000 materials could be related to the formation of free reactive oxygen species from the surface of gold nanoparticles. Previously this also was suggested as a possible mechanism for the antimicrobial properties of hybrid nanogold PU materials (Section 3.11). Metal ions are able to catalyse the production of reactive oxygen species²⁹² which subsequently oxidise the molecular structure of bacteria, attack membrane lipids and lead to a breakdown of membrane function, damage bacterial DNA or mitochondria.^{207,316} The direct contact between the gold nanoparticles within the PU K5000 matrix and the bacteria is not needed to induce harm to the microorganism since the reactive oxygen species diffuse through the polymer matrix to the surrounding medium.

Regarding the nanosilver hybrid PU K5000 materials, the comparison between the antimicrobial activities of the K5000-1000Au-1:2 and K5000-1000Ag-1:2 samples, (Figure 5.28 - Figure 5.29) revealed an almost complete reduction in the percentage of surviving *E. coli* cells for the sample containing silver nanoparticles. The nanogold hybrid PU K5000 materials were less effective. Despite many recent publications on the antimicrobial activity of silver particles and their polymer composites, which is believed to be attributable to morphological and structural changes found in the bacterial cells, so far the exact mechanism remains unclear.

Researchers attribute the toxicity of silver nanoparticles to dissolved silver.^{216,217} Unlike gold, silver nanoparticles are sensitive to oxidation.^{215,317} Partial oxidation of silver nanoparticles leads to dissolution Ag^0 and the slow release of silver ions to an aqueous or moist environment.^{216,217}

The required conditions for the dissolution of silver nanoparticles are provided when the K5000-1000Ag-1:2 sample is added to the suspension containing the *E. coli* bacteria. The contact between the silver nanoparticles and water molecules within the hybrid PU K5000 sample results in the slight release of mobile silver ions which subsequently migrate through the polymer matrix into the surrounding aqueous media. The possible consequences of the contacts between the bacteria and the released silver ions have been mentioned previously (Section 3.11). However, the brief explanation of the antimicrobial mechanism of silver ions provided is that: metal ions can damage or cross the cell membrane, where they bond to the –SH groups of cellular enzymes.³¹⁸ The resulting serious decrease of enzymatic activity of the microorganism causes a metabolism change and inhibits its growth leading to the cell's death.

An additional factor that may give rise to the antimicrobial activity of the tested K5000-1000Ag-1:2 sample is the electrostatic interaction between the negatively charged bacterial cell walls and the positively charged silver ions. The attachment of Ag⁺ to the bacteria results in cell death via the rupturing of the cell membrane.²⁹⁶

Antifouling effects of the nanogold and nanosilver hybrid PU K5000 materials were investigated. The K5000-1000Au-1:2, K5000-1000Au-1:4, K5000-1000Ag-1:2 and K5000-1000Ag-1:4 samples were sent to Polymer Group Ltd in Auckland. The hybrid PU K5000 materials together with the untreated K5000 paint were used to paint surfaces of panels (dimensions) which subsequently were set in the sea for approximately six months. After the testing period the surfaces containing the nanogold and nanosilver hybrid PU K5000 materials were compared to the surface which was painted with the untreated PU K5000 paint base. Figure 5.30 presents photographs of such surfaces after the panels were taken out of the sea water. In contrast to the panel containing the untreated PU K5000 paint (Figure 5.30a), the panels painted with the nanogold and nanosilver PU K5000 samples are free of shell and macro fouling (Figure 5.30b-e). The minimal growth on these panels is micro alga that is exhibiting some adhesion to the coating but they are free of the usual diatomaceous slime.

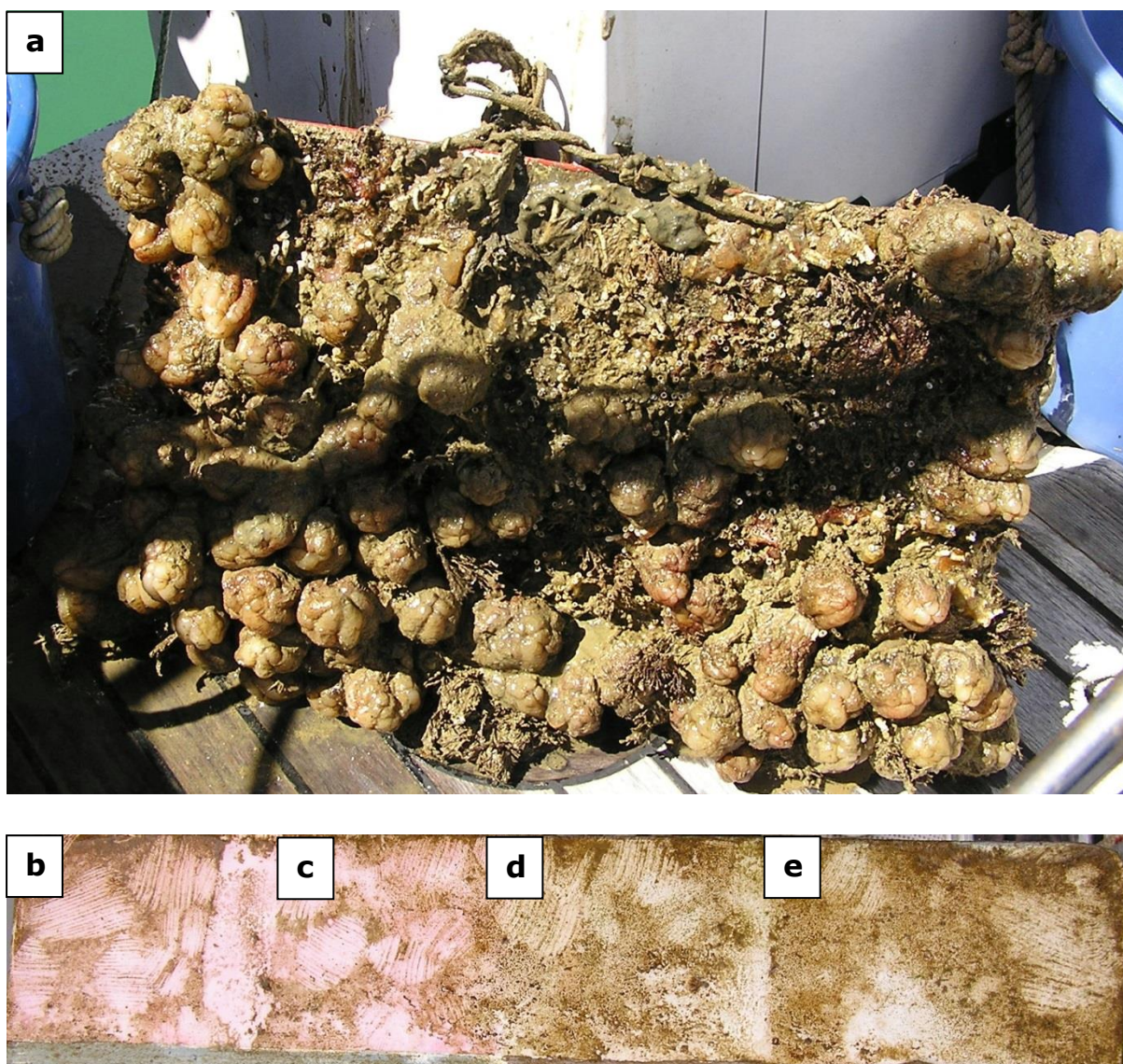


Figure 5.30: Photographs of panel surfaces painted with a) the untreated PU K5000 paint, b) the K5000-1000Au-1:2, c) the K5000-1000Au-1:4, d) the K5000-1000Ag-1:2 and e) the K5000-1000Ag-1:4 samples after being submerged in seawater for six months.

In light of the preliminary results obtained for the antimicrobial and antifouling tests of the nanogold and nanosilver hybrid PU K5000 materials, the following can be concluded. Nanogold and nanosilver hybrid PU K5000 materials were successfully tested against *Escherichia coli* bacteria, in particular the hybrid materials containing silver nanoparticles showed almost a complete reduction of the bacteria after four days of testing. Furthermore, these materials effectively prevented the growth of marine organisms on treated surfaces during the six

months of the antifouling tests. Hence, these materials have a great potential as antimicrobial and antifouling materials for applications in the health and biomedical device industry, food industry, personal hygiene industry and marine coating industry.

5.10 Conclusions

Nanogold and nanosilver hybrid PU K5000 polymer materials were successfully produced. For the redox reaction the carbamate functional groups of the K5000 material were used with the aim to reduce Au^{3+} or Ag^+ to Au^0 or Ag^0 respectively. Simultaneously formed gold or silver nanoparticles were chemically bound to the polymer matrix of the PU K5000 paint. The polymer matrix provided stabilisation for these gold and silver nanoparticles.

For the synthesis of the hybrid materials the ideal temperature was determined to be room temperature. The hybrid PU K5000 materials were produced at two dilutions, one set of samples used a 2.5 ml Au^{3+} / Ag^+ solution and the second was produced from a 1.25 ml metal ion solution whilst the polymer to metal ion ratio for these samples was kept constant. The reaction parameters, such as time and the concentration of the utilised metal ion solution influenced the colour of the resultant nanogold and nanosilver hybrid PU K5000 materials. However, there was no visual difference between the samples produced with the two dilution factors.

The nanogold and nanosilver hybrid polyurethane K5000 materials were shown to exhibit the characteristic UV-Vis absorption bands for gold and silver nanoparticles in the visible region of light. It was demonstrated that the SPR absorption bands of the nanogold hybrid PU K5000 samples prepared from a 2.5 ml Au^{3+} solution were comparable to those obtained for the samples prepared from a 1.25 ml Au^{3+} solution. The nanosilver hybrid polyurethane K5000 samples prepared from the more diluted solution showed a red shift of the respective

absorption peaks as well as an increase in FWHM suggesting a broader particle size distribution and particle agglomeration.

Electron microscopy analyses of the nanogold and nanosilver hybrid PU K5000 materials demonstrated that the metal nanoparticles were formed and uniformly distributed in the PU K5000 polymer phase and not the water phase. The gold nanoparticles in the samples containing 0.1 wt % of gold are predominantly spherical with a diameter of 20 - 40 nm. The silver nanoparticles of the analogue nanosilver hybrid PU K5000 samples were mostly spherical and 10 – 60 nm in diameter.

The XRD studies of these materials confirmed the presence of crystalline gold / silver within the PU K5000 materials. It was found that the mean crystallite size of the formed metal nanoparticles increased with increased concentration of employed ion solutions, and with the increased water content of those solutions.

XPS studies suggest the gold and silver nanoparticles bind to the PU K5000 matrix through the covalent Au-N and Ag-N bonds respectively in the nitrogen-containing carbamate functional groups.

The proposed mechanism of formation of the nanogold and nanosilver hybrid PU K5000 materials involves the reduction of Au^{3+} or Ag^+ to nanoparticulate Au^0 or Ag^0 by the carbamate functional groups of polyurethane in the PU K5000 matrix coupled with the oxidation reaction of these functional groups. It is proposed that the addition of a gold ion solution to the PU K5000 latex paint base leads to a reduction of Au^{3+} to Au^+ by the carbamate entities of polyurethane. The resultant Au^+ ions bind to the polymer matrix via Au-N bonds. Additional Au^{3+} ions are reduced to Au^0 , coupled by a further oxidation reaction of the carbamate groups resulting in a formation of the NO_x species. Au-N bonds are attracted to each other resulting in the formation of nanoclusters on which the additional Au^{3+} ions accumulate and are further reduced to Au^0 , resulting in gold nanoparticles within the polymer matrix. For the nanosilver hybrid PU K5000 materials it is proposed that due to the affinity for nitrogen, silver ions simultaneously undergo an interaction with nitrogen atoms in the carbamate groups of the PU K5000 matrix resulting in an Ag-N bond. Adjacent carbamate

functional groups act as a reducing agent, providing electrons for the reduction of Ag^+ to Ag^0 . Coupled oxidation reaction of the nitrogen groups leads to the formation of oxidised NO_x species. The polyurethane K5000 polymer matrix ensures the stabilisation of formed gold and silver nanoparticles in these materials. The leaching tests confirmed that the gold and silver nanoparticles were chemically bound to the polymer matrix. It was shown that only a very small amount of gold and silver leached out of the hybrid PU K5000 latex paint base materials after seven days of leaching. These amounts are believed to be due to residual unreduced gold or silver ions which are trapped in the polymer matrix.

The production of the nanogold and nanosilver hybrid PU K5000 materials has been scaled up to produce larger amounts of the paints which were successfully tested for their antifouling properties at The Polymer Group Ltd in Auckland. Additionally, it was found that the nanogold and nanosilver hybrid PU K5000 paint materials are antimicrobial against gram negative *E. coli* bacteria.

6 Nanosilver halide hybrid materials: silver halide formed in the presence of polyurethane, nylon 6,6 and polyurethane K5000 latex paint base materials

Nanosilver halide hybrid PU, nylon 6,6 and polyurethane K5000 latex paint base materials were produced using the experimental procedure outlined in Sections 2.2.3.1 and 2.2.3.2. The methodology for solid substrates comprised the immersing of PU (1.5 g) or nylon 6,6 (0.5 g) as sheets in 10 mL of 0.1 M NaX (X= Cl, I, Br) solution, then agitating the reaction vials on a shaking table for 12 hours. It was hoped that the polymer sheets would absorb the Cl⁻, I⁻ or Br⁻ ions. Following the soaking process, the doped samples were then rinsed with distilled water and allowed to air dry. The doped plastics were then added to a silver nitrate solution (10 mL, 200 mg kg⁻¹ Ag⁺) and agitated for 12 hours. For the synthesis of nanosilver halide hybrid polyurethane K5000 latex paint base materials, the procedure was slightly altered. 1 mL of 0.5 molar NaX solution was added to 5 g of liquid polyurethane Kamthane 5000 paint base. The mixture was agitated for two hours on a shaking table. Subsequently, the reaction was completed by the drop-wise addition of 1.5 mL of a 3333 mg kg⁻¹ Ag⁺ solution under vigorous stirring and agitating the samples for further two hours on a shaking table. All reaction steps were carried out at room temperature. As mentioned in Section 1.4.5 silver halide particles are not stable under light irradiation. Thus, before the addition of the silver nitrate solution the reaction vials were wrapped in aluminium foil. As a result of their photosensitive properties, upon exposure to light, the AgX particles in matrices of the resultant hybrid polymer materials were converted to Ag/AgX particles. Samples containing silver chloride and silver bromide particles changed their colour from white to purple. Hybrid materials containing silver iodide nanoparticles remained yellow under direct light exposure.

The sample names for the nanosilver halide hybrid polymer materials and their respective reaction parameters are summarised in Table 6.1.

Table 6.1: The sample names and their respective reaction parameters for the silver hybrid PU, nylon 6,6 and polyurethane K5000 latex paint base materials. All samples were prepared at room temperature.

| Names of hybrid materials | | | | | | | | | |
|---|------------|------------|-----------|------------|------------|-----------|----------------|----------------|---------------|
| | PU-200AgCl | PU-200AgBr | PU-200AgI | Ny-200AgCl | Ny-200AgBr | Ny-200AgI | K5000-1000AgCl | K5000-1000AgBr | K5000-1000AgI |
| Substrate species | PU | PU | PU | Nylon 6,6 | Nylon 6,6 | Nylon 6,6 | K5000 | K5000 | K5000 |
| Substrate mass [g] | 1.5 | 1.5 | 1.5 | 0.5 | 0.5 | 0.5 | 5 | 5 | 5 |
| NaX | NaCl | NaBr | NaI | NaCl | NaBr | NaI | NaCl | NaBr | NaI |
| Conc. of NaX sol. [M] | 0.1 | 0.1 | 0.1 | 0.1 | 0.1 | 0.1 | 0.5 | 0.5 | 0.5 |
| Vol. of NaX sol. [mL] | 10 | 10 | 10 | 10 | 10 | 10 | 1 | 1 | 1 |
| Soaking time [hr] | 12 | 12 | 12 | 12 | 12 | 12 | 2 | 2 | 2 |
| AgNO₃ sol. conc. [mg kg⁻¹] | 200 | 200 | 200 | 200 | 200 | 200 | 3333 | 3333 | 3333 |
| Vol. of AgNO₃ sol. [mL] | 10 | 10 | 10 | 10 | 10 | 10 | 1.5 | 1.5 | 1.5 |
| wt % of AgX in polymer | 0.1 | 0.1 | 0.1 | 0.4 | 0.4 | 0.4 | 0.1 | 0.1 | 0.1 |
| Soaking time [hr] | 12 | 12 | 12 | 12 | 12 | 12 | 2 | 2 | 2 |

6.1 UV Visible spectroscopy - colour of nanosilver halide hybrid polymer materials

Silver chloride and silver bromide have wide band gaps (Table 6.2). Therefore, absorption of light with a wavelength larger than 380 nm is not possible. By contrast, silver iodide's direct band of ca. 3 eV allows the material to absorb light in the visible region giving the material its yellow appearance. Figure 6.1, Figure 6.2 and Figure 6.3 show photographs of the produced nanosilver halide hybrid PU, nylon 6,6 and PU K5000 materials. Silver chloride and silver bromide hybrid materials are white in colour. Although not clearly visible on the photographs, the silver iodide hybrid polymer materials appeared to have a slight yellow colouration. These white and yellow colours were indicative of AgX particles being formed within the polymer substrates. Owing to their photosensitive properties, silver halides are not stable under UV visible light radiation (Section 1.4.5). With exposure to light, silver halide particles undergo a self-photosensitisation process resulting in partial reduction of Ag^+ to Ag^0 nanodomains or nanoparticles at the surface of the silver halide particles and releasing small amounts of halides as their respective halogen gas.^{168,319} As a result of the process the AgX nanoparticles within the polymer matrix will be converted *in situ* to Ag/AgX nanoparticles. The self-photosensitisation process has an effect on the colours of the hybrid polymer materials. Once exposed to light, the hybrid materials containing silver chloride (PU-200AgCl, Ny-200AgCl, K5000-1000AgCl samples) or silver bromide nanoparticles (PU-200AgBr, Ny-200AgBr, K5000-1000AgBr samples) changed from being white to purple (Figure 6.1 - Figure 6.3). The purple colour is due to the broad visible spectral absorption of these materials (which will be discussed further in following sections). The purple colour development of the nanosilver chloride hybrid PU, nylon 6,6 and polyurethane K5000 materials could be observed within the first 30 minutes of direct light exposure. In the following four days of natural light radiation the hybrid PU, nylon 6,6 and polyurethane K5000 latex paint base materials turned from purple to brown indicating an increased formation of silver nanoparticles. The brown colour is consistent with the formation of silver nanoparticles and was previously reported for nanosilver hybrid PU, nylon 6,6 and PU K5000 materials (Chapters 3 and 4). The hybrid polymer materials

containing silver bromide nanoparticles needed at least one day of direct light in order to change their colour from white to purple. However, the colour of the hybrid materials containing silver iodide nanoparticles (PU-200AgI, Ny-200AgI, K5000-1000AgI samples) remained unchanged upon exposure to light. Kelly and Tate have reported on similar colours of wool composites containing silver chloride, silver bromide and silver iodide nanoparticles.^{22,180}

Table 6.2: Band gap values for silver halides.³²⁰

| Silver halide | Indirect band gap [eV] | Direct band gap [eV] |
|---------------|------------------------|----------------------|
| AgCl | 3.3 | 5.2 |
| AgBr | 2.7 | 4.3 |
| AgI | 2.0 | 3.0 |

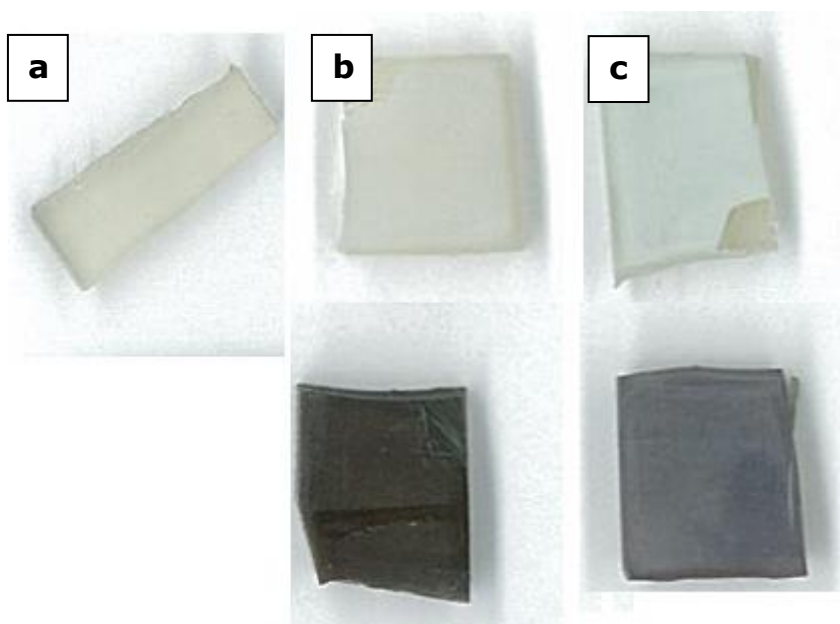


Figure 6.1: Photographs of a) the untreated polyurethane sheet and nanosilver hybrid polyurethane sheets; b) the PU-200AgCl sample before (top) and after exposure to light for four days (bottom); c) the PU-200AgBr sample before (top) and after exposure to light for four days (bottom).

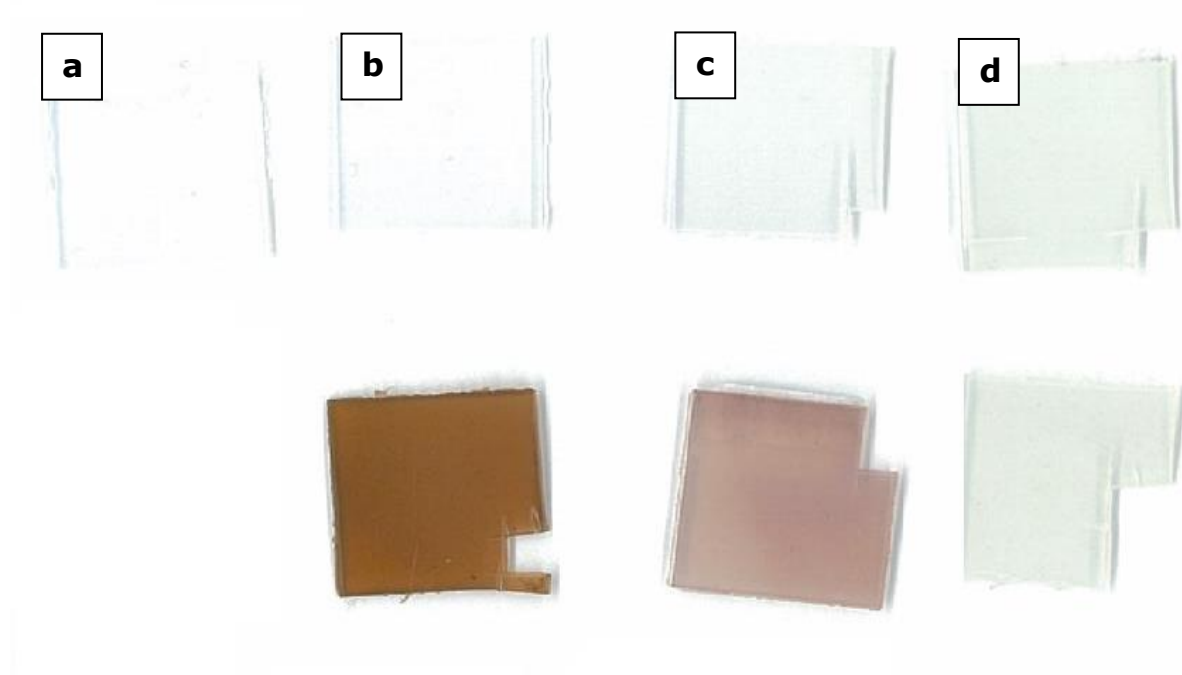


Figure 6.2: Photographs of a) the untreated nylon 6,6 sheet and nanosilver hybrid nylon 6,6 sheets; b) the Ny-200AgCl sample before (top) and after exposure to light for four days (bottom); c) the Ny-200AgBr sample before (top) and after exposure to light for four days (bottom); d) the Ny-200AgI sample before (top) and after exposure to light for four days (bottom).

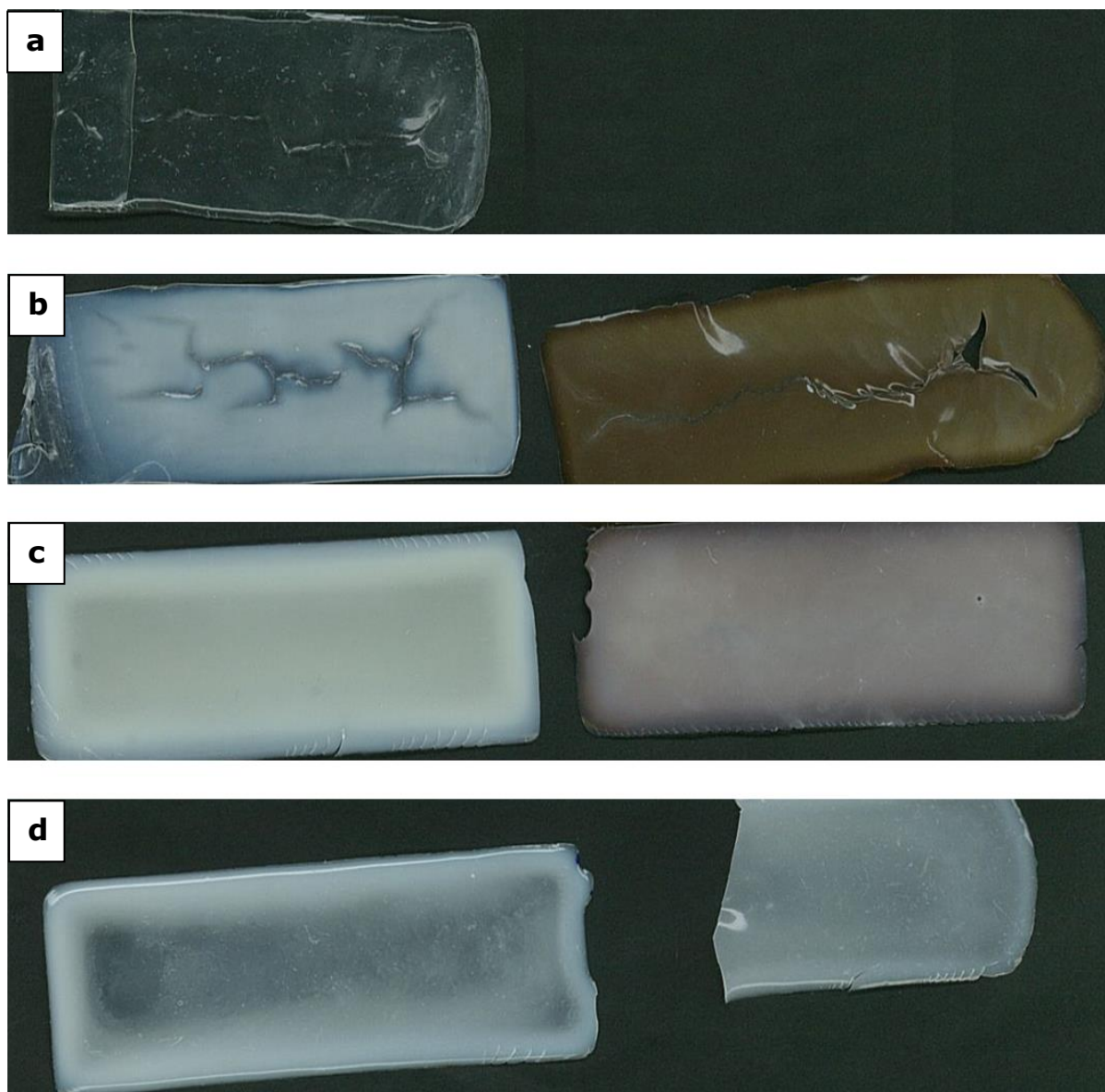
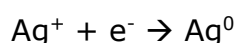


Figure 6.3: Photographs of dried films of a) the untreated PU K5000 sample; b) the K5000-1000AgCl sample before (left) and after exposure to light for four days (right); c) the K5000-1000AgBr sample before (left) and after exposure to light for four days (right); d) the K5000-1000AgI sample before (left) and after exposure to light for four days (right). The photographs were taken on a black background in order to improve the image contrast.

UV-Vis spectroscopy was utilised in order to demonstrate the presence of silver halide nanoparticles in the hybrid polymer materials as well as the formation of Ag/AgX nanoparticles as the result of the self-photosensitisation process. Due to their uniform thickness, nanosilver halide hybrid nylon 6,6 sheets appeared to be most suitable for the UV-Vis absorbance measurements. Thus, these materials

were chosen as representatives for the nanosilver halide hybrid polymer materials. The UV-Vis absorption spectra obtained for the nanosilver halide nylon 6,6 materials before and after light exposure are shown in Figure 6.4, Figure 6.5 and Figure 6.6. The spectra are typical for the semi-conductor silver halides. Figure 6.4 shows the absorption spectra for the Ny-200AgCl sample. The sample before being exposed to direct light shows the typical UV-Vis absorption between 230 – 300 nm corresponding to the direct band gap of AgCl.^{321–323} After being exposed to light the Ny-200AgCl sample shows absorption of light not only in the UV region with a discernible shoulder peak at ca. 380 nm but also in the visible region. AgCl exhibits direct and indirect band gap of 5.15 eV (~ 240 nm) and 3.25 eV (~ 380 nm), respectively (Table 6.2). As such, absorption of light with a wavelength greater than 380 nm is not possible by AgCl alone. This visible light absorption is due to the formation of Ag nanodomains on the surface of the AgCl particles. As described in the introduction, these Ag nanodomains develop through the photochemical reaction where the Ag⁺ in the AgCl lattice is partially reduced to Ag⁰ (Section 1.4.5). This photographic process is described through the mechanism first proposed by Gurney and Mott:¹⁵⁷



It is believed that on the nanoscale, once sufficient Ag⁰ particles are formed, the resultant Ag/AgX nanoparticles become photostable under further irradiation, preventing a total reduction of Ag⁺ to Ag⁰.^{173–175} As mentioned in the introduction, noble metal nanoparticles, such as silver, display unique optical properties in contrast to their bulk forms (Section 1.4). The colour reflected by the metal nanoparticles is due to strong visible absorptions known as Surface Plasmon Resonances (SPR).⁹² As such, the broad absorption peak in the visible region for the Ny-200AgCl sample with the maximum at around 470 nm is consistent with the SPR absorption band of Ag nanoparticles. Surface plasmon resonance absorption bands of spherical Ag nanoparticles in aqueous solutions

can vary in position ranging from 375 to 405 nm.⁹⁷ The red-shift of the absorption band to 470 nm and the reflected purple-brown colour of the Ny-200AgCl sample after exposure to light (Figure 6.2) is due to the dielectric constant of the AgCl surface ($n=2$) on which the Ag nanodomains are formed.

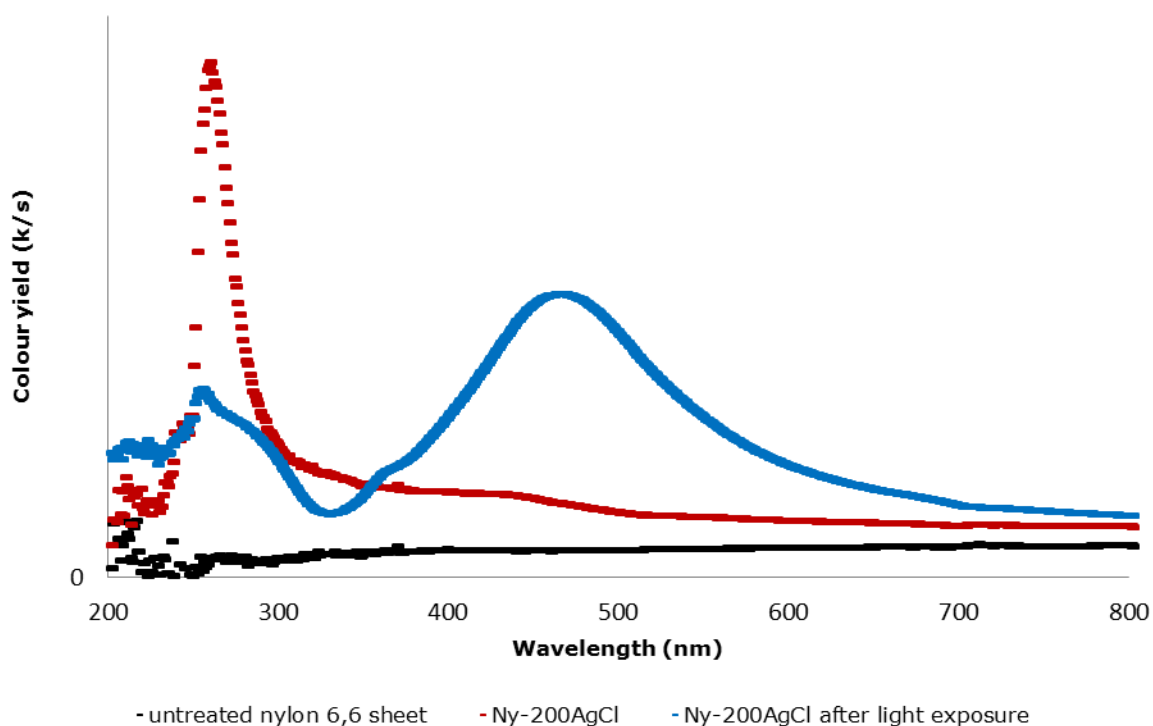


Figure 6.4: UV-Vis spectra of nanosilver chloride hybrid nylon 6,6 materials before and after light exposure.

The UV-Vis absorption spectra for the Ny-200AgBr sample before and after exposure to light are presented in Figure 6.5. The respective colours of the hybrid nylon 6,6 materials are shown in Figure 6.2. The spectrum for the sample before being exposed to light shows that the wavelengths in the range between 240 and 350 nm were absorbed, indicating the presence of the AgBr particles. These values are well in agreement with the absorption maxima for AgBr reported in the literature.^{324–326} Similar to the Ny-200AgCl sample, the spectrum recorded for the Ny-200AgBr sample after exposure to light shows an absorption in both the ultraviolet and visible region. Silver bromide undergoes a self-sensation process for the same reasons discussed previously. However, the

absorption in the visible spectral region seems to be broader and less intense than that of the Ny-200AgCl sample. This can be due to a lower number of silver nanodomains formed on the AgBr particles, reflecting a broader size and shape distribution.

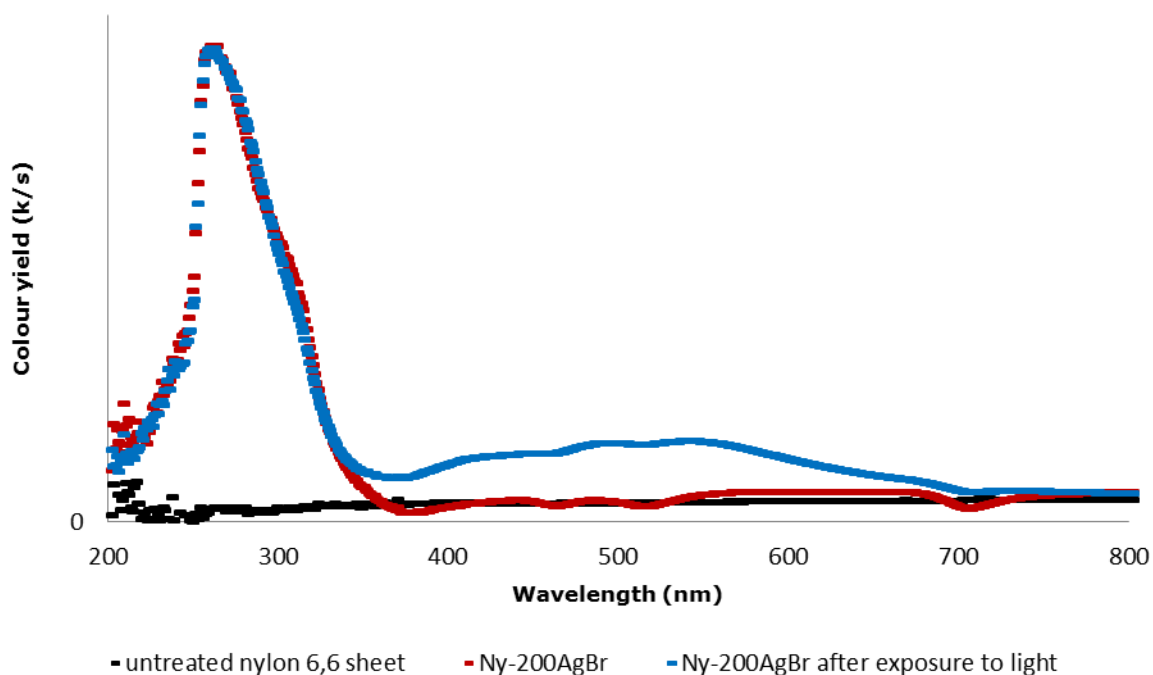


Figure 6.5: UV-Vis spectra of nanosilver bromide hybrid nylon 6,6 materials before and after light exposure.

As mentioned previously, the nanosilver iodide hybrid polymer materials are yellow in colour and this colour remains despite light exposure (Figure 6.2). This is noticeable when comparing the UV-Vis absorbance spectra of the Ny-200AgI sample before and after light exposure (Figure 6.6). Both spectra feature the typical absorbance for AgI confirming its presence.^{327,328} A peak with the absorption maximum at around 420 nm is responsible for the yellow colouration of the nanosilver iodide hybrid polymer materials. However, there was no obvious difference in the UV-Vis spectra of the Ny-200AgI sample after being the exposed to light. The reason for the observed phenomenon could be due to the low susceptibility of AgI to photolysis when compared to AgCl and AgBr, thus only a small amount of AgI is converted to Ag/AgI.³²⁹ Although the mechanism

of the photolysis is the same as for AgCl and AgBr, the rate is much slower.³³⁰ This is believed to be due to the direct smaller band gap of AgI (Table 5.2) which causes a shorter lifetime of the excited state.³³¹ In AgCl and AgBr the indirect band gaps result in a long lifetime of the excited state before the recombination of a photoelectron and an electron hole. This promotes the likelihood of a combination of a photoelectron with an interstitial Ag^+ ion resulting in the formation of Ag^0 . The shorter lifetime of the excited state of AgI is inconvenient for the combination of an interstitial Ag^+ ion with a photoelectron in order to form this Ag^0 . Moreover, the Ag–Ag binding energy between interstitial Ag^+ ions and lattice cations is smaller as compared to the Ag–I bonding energy.³³⁰

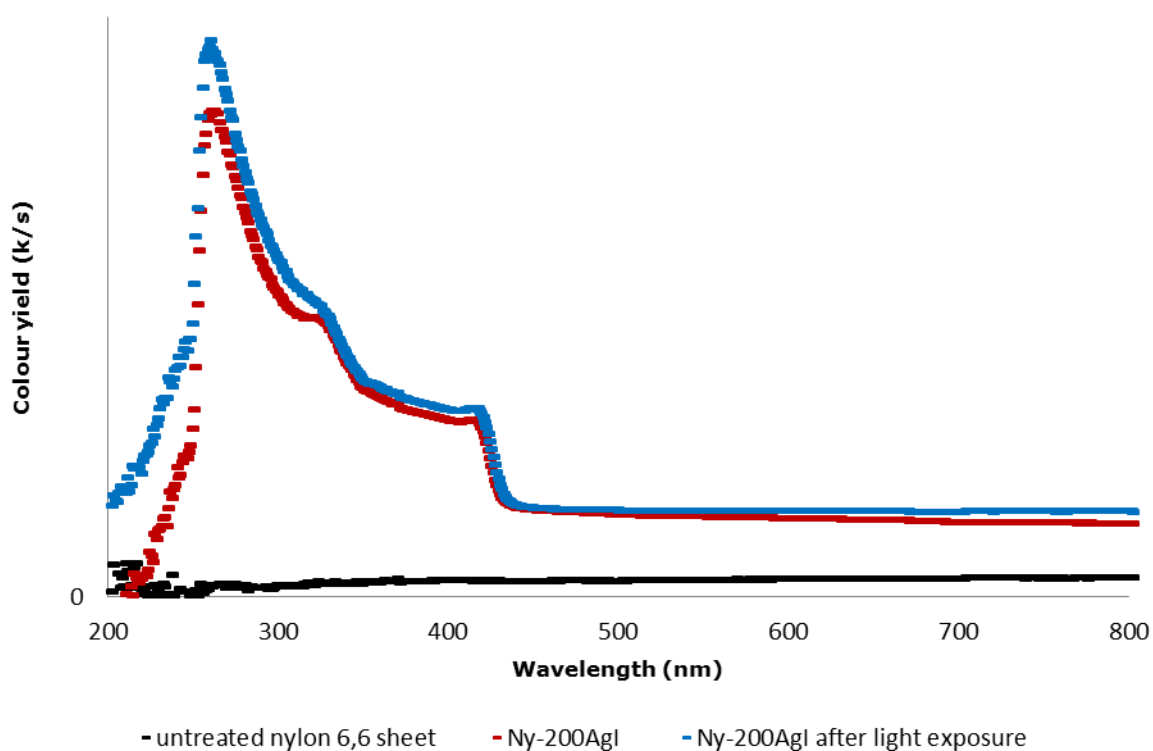


Figure 6.6: UV-Vis spectra of nanosilver iodide hybrid nylon 6,6 materials before and after light exposure.

6.2 Scanning electron microscopy and energy dispersive X-ray analysis of nanosilver halide polymer materials

SEM was used as a characterisation method to investigate the morphologies of the nanosilver halide hybrid polymer materials (PU, nylon 6,6 and polyurethane K5000 paint), to confirm the presence of the silver halide nanoparticles within the polymer substrates and to study the distribution of these nanoparticles. To observe the interior of the hybrid polymer materials, cross sections of the PU and nylon 6,6 samples were made by freezing the materials in liquid nitrogen and subsequently breaking them into two fractions. Furthermore, the internal structure of the nanosilver halide hybrid PU K5000 materials as frozen latexes was studied by Cryo-SEM analyses. The EDS analyses of the samples provided information about the elemental composition of the analysed surface of a sample. X-ray peaks for elements such as calcium, magnesium, nickel, phosphorus and silicon are either due to impurities in the paint samples or from other contaminations in the laboratory. Due to pre-treatment of the substrates with NaX (Cl, Br and I) X-ray peaks for sodium are common. Peaks for aluminium arise from sample holders and platinum peaks are due to the coating process of the samples. Hence, these X-ray peaks can be ignored. Some EDS mapping images show dark areas. These areas should be ignored. The sample preparation for the SEM analyses created an uneven polymer surface. The dark areas represent the hollows in the surface, thus, the EDS detector was not able to observe these areas.

6.2.1 Scanning electron microscopy and energy dispersive X-ray analysis of nanosilver halide hybrid polyurethane materials

Figure 6.7a presents the SEM micrograph of a surface cross section of the PU-200AgCl sample recorded in the backscatter mode. The sample was exposed to light prior to SEM analysis. At a magnification of 200 times, a bright line about 20 μm from the edge into the PU sheet interior was observed, which depicted

the presence of the AgCl particles (white dots). In backscatter mode, the contrast between the metal and the polymer is due to the higher atomic weight of silver chloride and the lower atomic weight of the polymer atoms (C, H, O, N). The presence of silver chloride was confirmed by the EDS analysis (Figure 6.7e). The corresponding images of the EDS mapping analysis show that where the particles, which form the bright line, are located, there are very high concentrations of silver and chlorine (Figure 6.7b-c). Their overlay image, shown in Figure 6.7d, further confirms that there has been silver halide nanoparticle formation within the PU matrix during the synthesis. The concentration of the formed silver chloride particles in the PU matrix decreases quickly with the increasing distance from the edge towards the centre of the substrate.

The mechanism for the formation of the silver halide particles within the polymer matrix is believed to be one of precipitation. The porous polymer matrix provides the stabilisation of the particles and the control of their size. The doped substrates contain halide ions distributed throughout the polymer matrix. The subsequent washing process removes the detached halide ions from the surface of the polymer leaving only halide ions beneath the surface and in the bulk of the substrate. Once introduced to a silver nitrate solution the Ag^+ ions will migrate through the porous polymer surface resulting in diffusion of the Ag^+ ions through the polymer matrix. Simultaneously, the mobile halide ions migrate towards the Ag^+ ions within the polymer matrix. Once the Ag^+ and X^- ($\text{X} = \text{Cl}, \text{Br}, \text{I}$) encounter each other, the silver halide nanoparticles precipitate in the polymer matrix, which are insoluble in aqueous environments. A higher number of silver halide particles are formed just below the surface of the polymer compared to the centre of the polymer sheet.

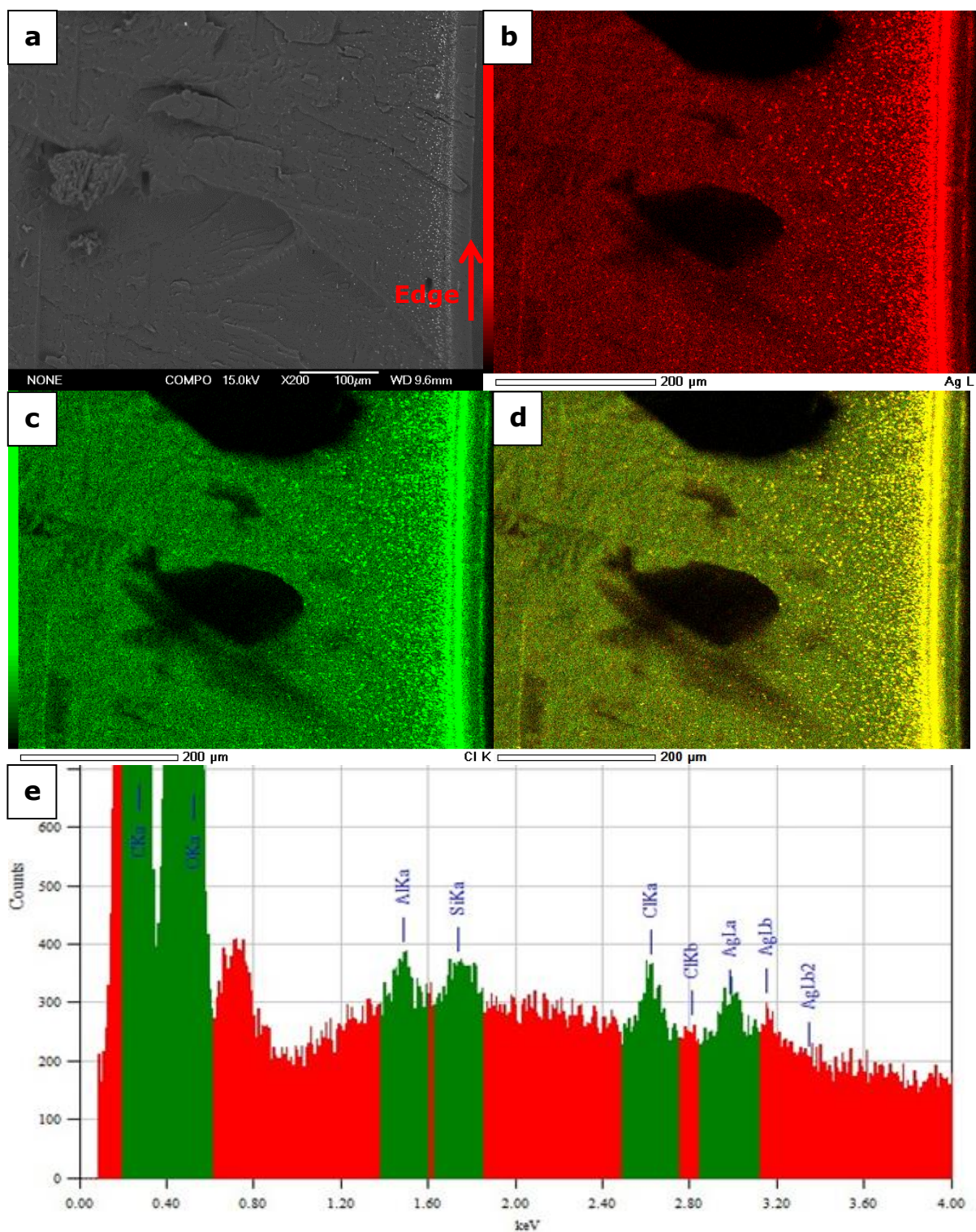


Figure 6.7: SEM micrograph in backscatter mode of the surface cross section of the PU-200AgCl sample at a magnification of 200 times with b-c) the corresponding EDS micrographs, d) the EDS Ag and Cl overlay map and e) the corresponding elemental analysis spectrum. The sample surface is located to the right side of the red arrow.

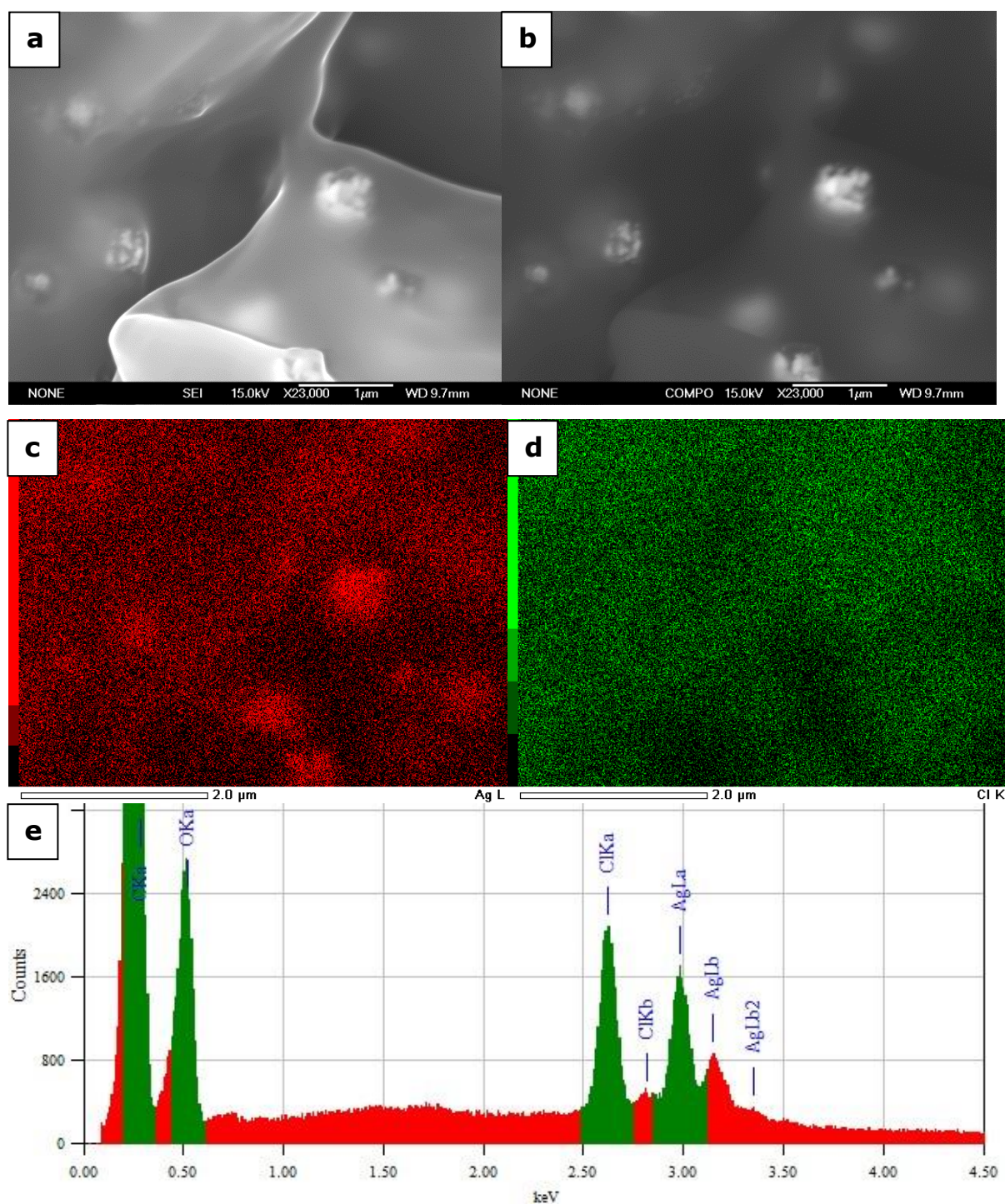


Figure 6.8: SEM micrographs a-b) of the surface cross section of the PU-200AgCl sample (secondary electron and backscatter mode) at a magnification of 23000 times with c-d) the corresponding EDS micrographs and e) the corresponding elemental analysis spectrum.

The magnification of 23000 times has revealed that the particles within the bright line observed in Figure 6.7a are cubic, a very common shape for silver

halide particles (Figure 6.8a-b).³³¹ EDS analysis confirmed that the particles were indeed silver chloride (Figure 6.8e). At this magnification, the particles observed were generally between 100 and 1000 nm in size, suggesting that the PU matrix is not able to provide a sufficient stabilisation of the silver halide particles. It is important to note, that the surfaces of these particles were covered by smaller sized nanoparticles of higher atomic weight. The micrographs presenting the EDS mapping analysis show that the nanoparticles on the surface are silver (Figure 6.8c). This confirms that the produced nanosilver halide hybrid PU materials are sensitive to photolysis under exposure to light, resulting in a formation of nanosized silver particles or domains on the surface of the AgCl particles through a photolytic reaction described above. It is also not possible to exclude the fact that the electron beam of the SEM promotes further photolysis of the AgCl to Ag⁰ nanoparticles. A closer look at one of those AgCl cubes, which is shown in Figure 6.9, reveals that the formed silver nanoparticles are not uniform in size and shape. Due to the surface plasmon resonance phenomenon (Section 1.4.2) a typical colour for spherical silver nanoparticles with an uniform size dispersed in water is yellow. The resonance wavelength not only depends on the size and the shape of the nanoparticle but also on the dielectric constant of the surrounding medium.²⁵² Because the Ag nanoparticles on the surface of the AgCl particles in the PU-200AgCl sample show a variety of particle sizes and shapes and the dielectric constant of AgCl is higher than water, the colour visible to the human eye of these materials is brown (Figure 6.1). At a further magnification of 55000 times, the AgCl particles smaller than 100 nm could be seen, however, it is difficult to determine the precise size by SEM (Figure 6.10a). EDS spectral analysis verified that the nanoparticles were silver chloride (Figure 6.10b).

Figure 6.11a-b presents the SEM micrographs of a surface cross section of the PU-200AgBr sample recorded in the secondary electron and backscatter mode. The edge which separates the interior area from the surface of the sheet is depicted by a red arrow. At a magnification of 2000 times, several bright lines which are formed just below the surface were observed.

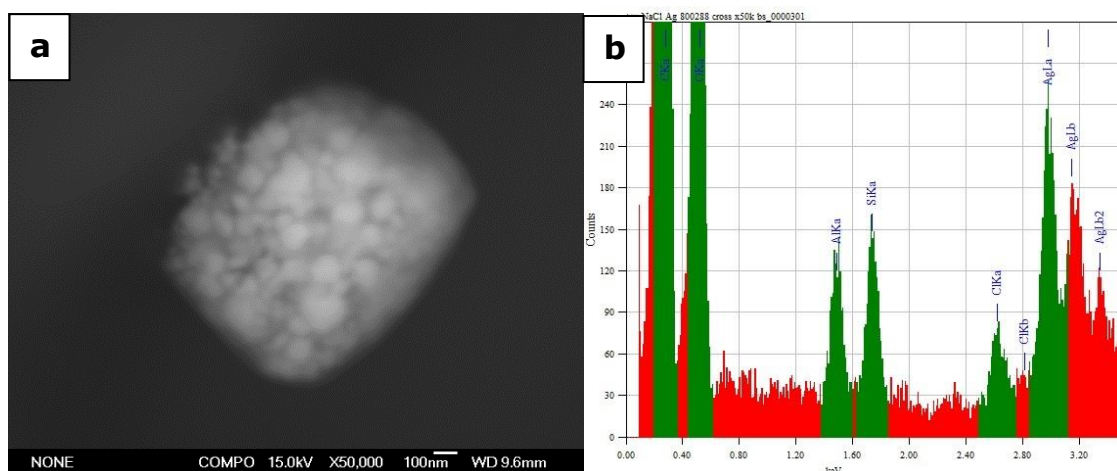


Figure 6.9: SEM micrograph in backscatter mode of the surface cross section of the PU-200AgCl sample at a magnification of 50000 times with b) the respective EDS elemental analysis spectrum.

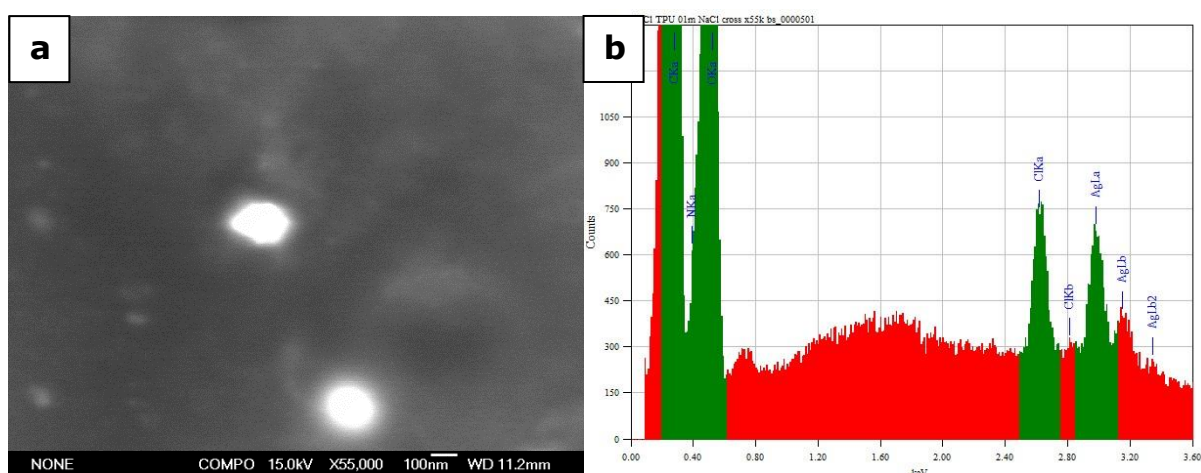


Figure 6.10: SEM micrograph in backscatter mode of the surface cross section of the PU-200AgCl sample at a magnification of 55000 times with b) the respective EDS elemental analysis spectrum.

The total thickness of the formed lines is ca. 20 μm , starting below the surface and becoming brighter, more concentrated towards the centre of the sheet. EDS spectral analysis verified that the particles which form these lines were AgBr (Figure 6.11d). The images taken at a magnification of 30000 times have revealed that the AgBr particles have irregular shapes and sizes, ranging from less than 100 nm to ca. two hundred nanometres (Figure 6.11c). Similar to for the PU-200AgCl sample, the PU matrix is not able to provide a sufficient

stabilisation for the silver bromide particles. It was not possible to determine the precise size of the AgBr nanoparticles by SEM. Analyses at higher magnifications caused damage to the samples due to the instability of the organic matrices such as PU and nylon 6,6 under higher energy SEM beam. As reported above, the mechanism of the particle formation within the PU substrate is believed to be one of precipitation.

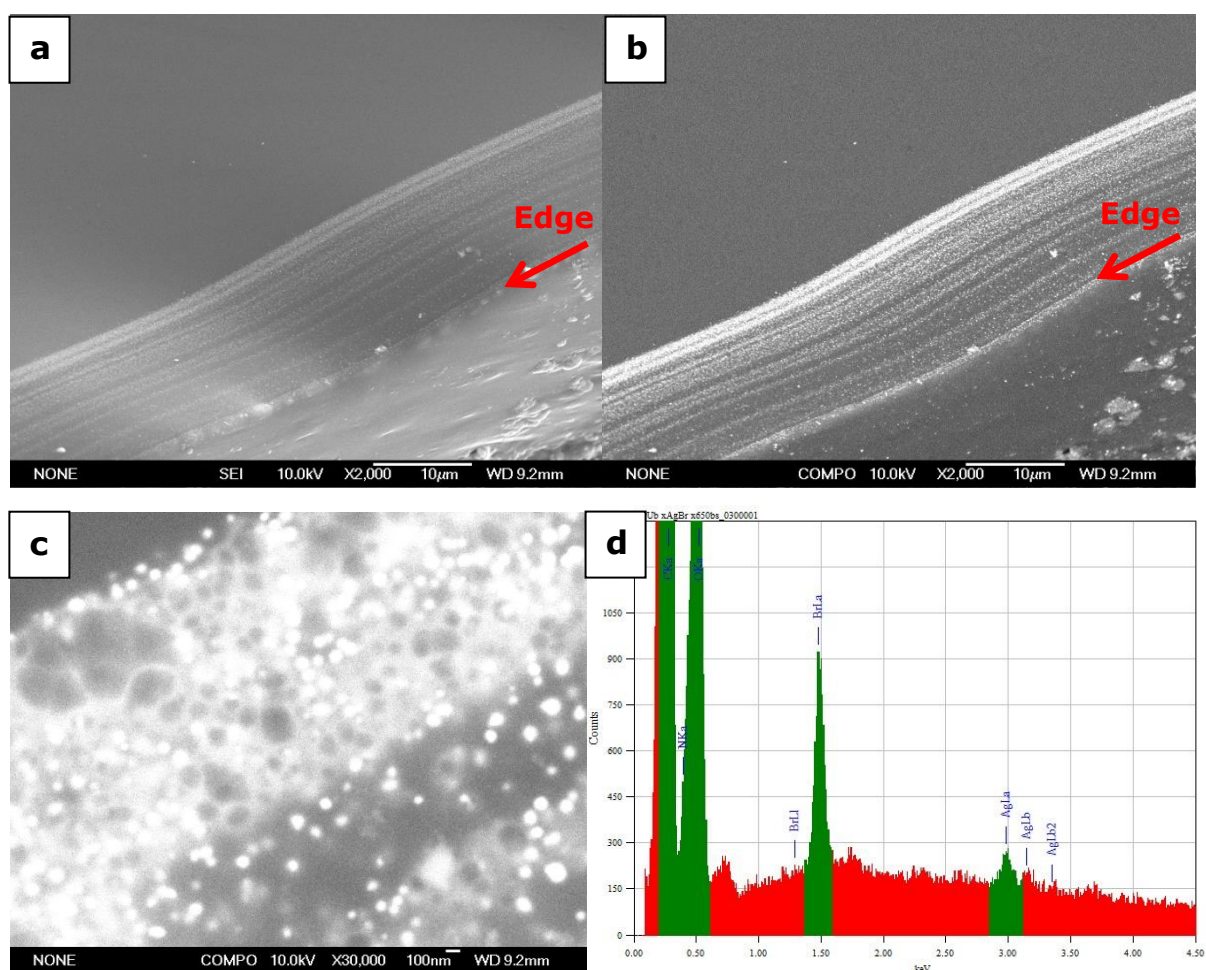


Figure 6.11: SEM micrographs a-b) of the surface cross section of the PU-200AgBr sample (secondary electron and backscatter mode). Above the red arrow is the interior, below the red arrow is the surface of the PU sheet and the red represents the edge of the sheet), c) at an increasing magnification of 30000 times with d) the respective EDS elemental analysis spectrum.

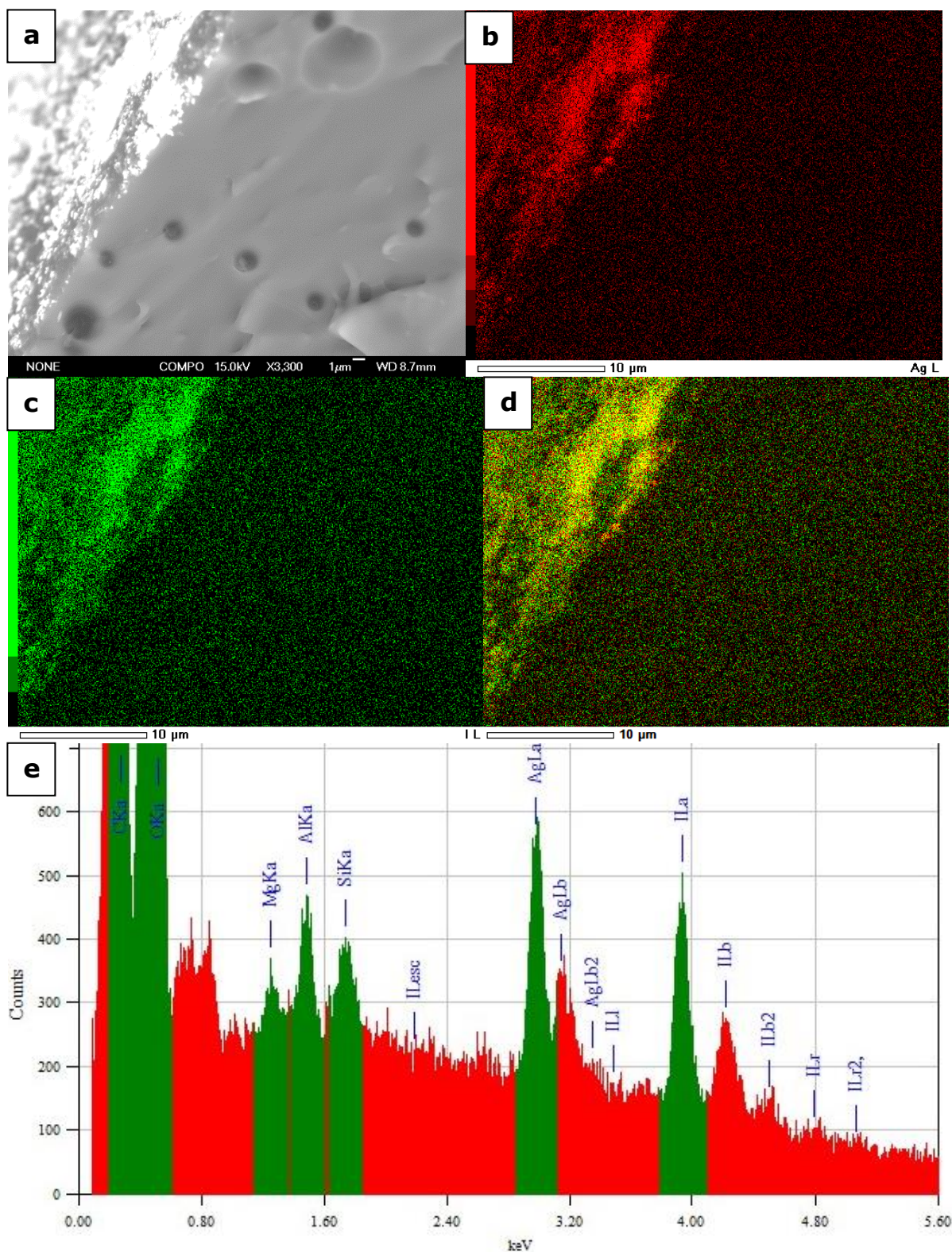


Figure 6.12: SEM micrograph in backscatter mode of the surface cross section of the PU-200AgI sample at a magnification of 3300 times with b-c) the corresponding EDS micrographs, d) the EDS Ag and Cl overlay map and e) the corresponding elemental analysis spectrum.

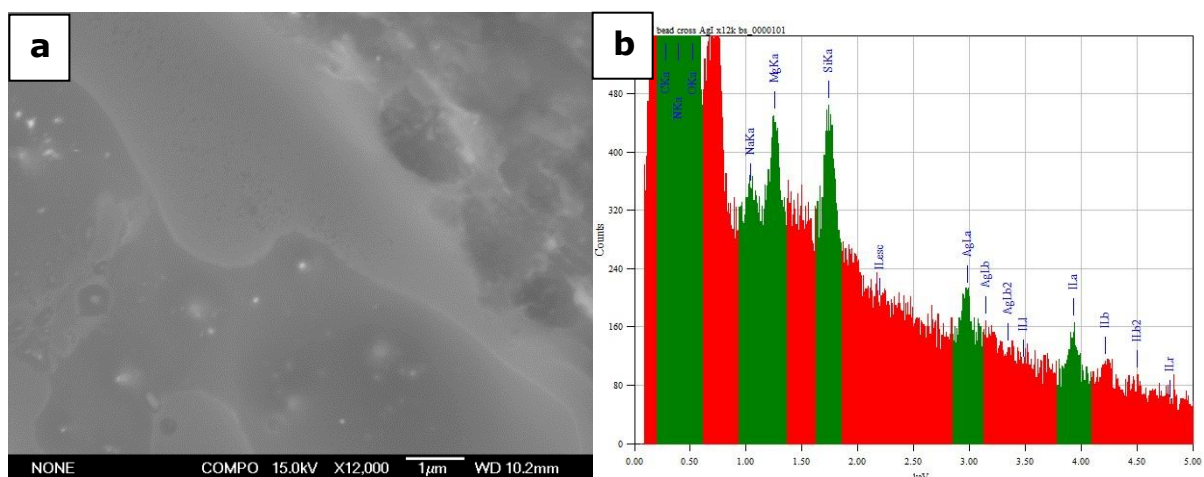


Figure 6.13: SEM micrograph in backscatter mode of the surface cross section of the PU-200AgI sample at a magnification of 12000 times with b) the respective EDS elemental analysis spectrum.

The nanosilver iodide hybrid PU materials differ slightly from the nanosilver chloride and bromide hybrid PU materials. The SEM micrograph of the cross sectioned PU-200AgI sample is shown in Figure 6.12a. The EDS elemental mapping analysis of the sample shows high concentration of silver and iodine on the surface of the PU sheet (Figure 6.12b-c). There was good overlap (Figure 6.12d) for silver with the respective iodine, confirming that there has been silver iodide nanoparticle formation, mostly on the surface of the PU sheet. However, at a higher magnification of 12000 times, the analysis of the interior PU-200AgI sample, has shown that some sparsely distributed silver iodide nanoparticles were formed just below the surface of the sample (Figure 6.13).

6.2.2 Scanning electron microscopy and energy dispersive X-ray analysis of nanosilver halide hybrid nylon 6,6 materials

Due to time limitations only the nanosilver chloride hybrid nylon 6,6 sheet was analysed by the SEM. Figure 6.15 offers the SEM micrograph of a surface cross section of the PU-200AgCl sample recorded in the backscatter mode. Similar to the PU-200AgCl sample (Section 6.2.1), bright spots were found just below the

surface of the nylon 6,6 sheet, ca. 2 μm from the edge towards the centre of the (Figure 6.14a). These bright spots were assigned to the AgCl nanoparticles, as the presence of AgCl was confirmed by the EDS analysis (Figure 6.14b).

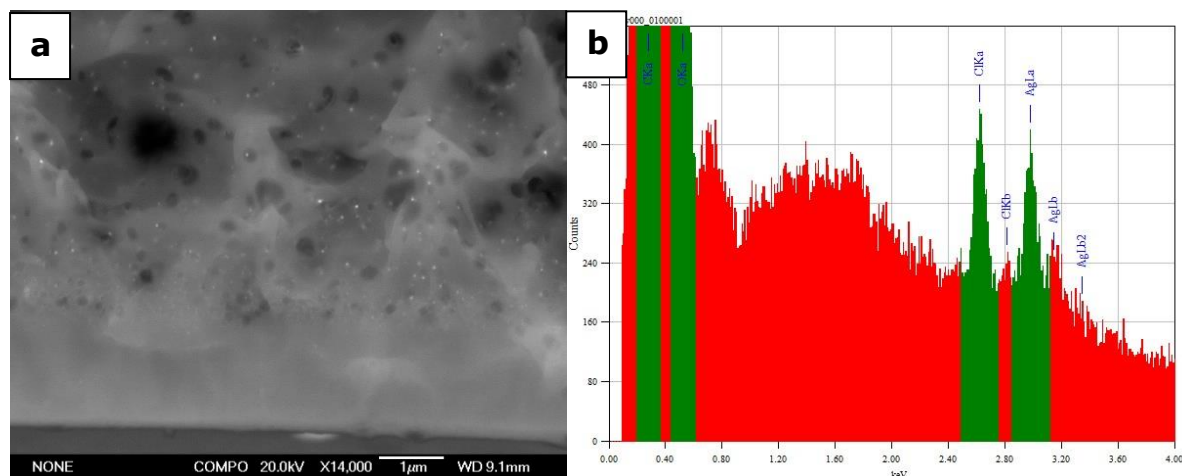


Figure 6.14: SEM micrograph in backscatter mode of the surface cross section of the Ny-200AgCl sample with b) the respective EDS elemental analysis spectrum.

Figure 6.15 presents a SEM micrograph of the Ny-200AgCl sample at a higher magnification. The corresponding images of the EDS mapping analysis show that where the particles are located, there are high concentrations of silver and chlorine (Figure 5.15b-c). Additionally, their overlay image further confirms the formation of silver chloride within the nylon 6,6 matrix during the synthesis of this material (Figure 5.15d).

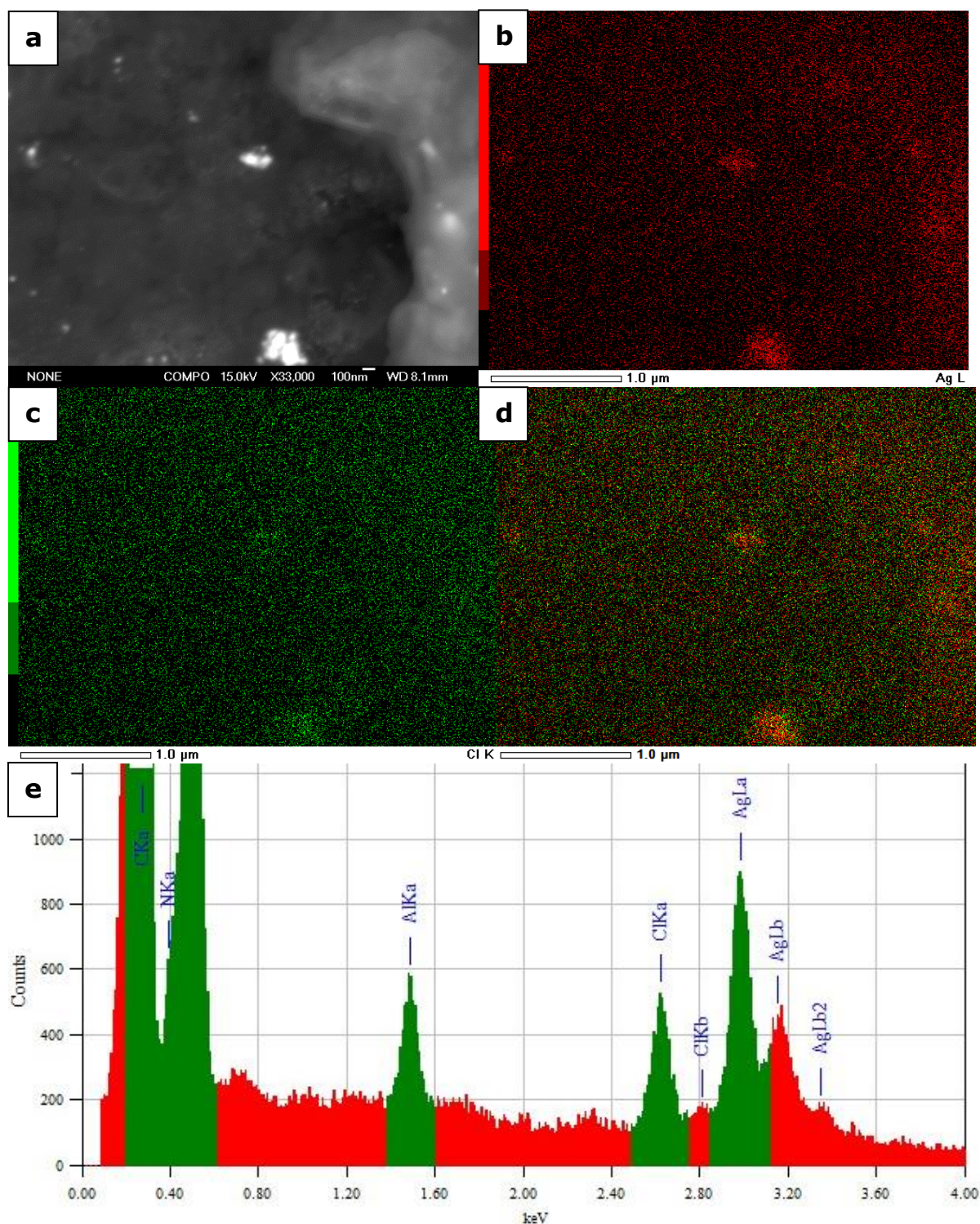


Figure 6.15: SEM micrograph in backscatter mode of the surface cross section of the Ny-200AgCl sample with b-c) the corresponding EDS micrographs, d) the EDS Ag and Cl overlay map and e) the corresponding elemental analysis spectrum.

The particles with non-uniform shapes were generally smaller than 100 nm. However, some larger AgCl particles as well as particle agglomerates were observed. The mechanism of the silver chloride formation within the nylon 6,6 would be the same as the nanosilver halide hybrid PU materials (Section 6.2.1). This is the mechanism via precipitation, where growth is controlled by the nylon 6,6 matrix.

6.2.3 Scanning electron microscopy and energy dispersive X-ray analysis of nanosilver halide hybrid polyurethane K5000 latex paint base materials

Due to the limited equipment availability only nanosilver chloride hybrid PU K5000 material was analysed by Cryo-SEM. Figure 6.16 illustrates a Cryo-SEM micrograph recorded in backscatter mode of the K5000-1000AgCl sample which comprised 5 g of the PU K5000 latex paint base, 1 ml NaCl (0.5 molar) and 1.5 ml of a 3333 mg kg⁻¹ Ag⁺ solution. The sample consists of two domains, namely the smooth and slightly lighter shaded areas which represent the carbon-based polyurethane polymer whereas the darker shaded areas are water. A magnification of 7000 times on one of these light shaded areas recorded in backscatter mode is shown in Figure 6.17a. The bright dots in the polymer have been assigned to AgCl, confirming the precipitation reaction during the synthesis of these products. EDS spectral analysis verified the nanoparticles as AgCl (Figure 6.17e). The high concentrations of Ag and Cl depicted in the EDS micrographs (Figure 6.17b-c) provide a good overlay and match with the white dots further confirming that these are nanoparticles of silver chloride in the nanosilver chloride hybrid PU K5000 paint sample. The particles were found to be relatively well distributed in the polyurethane K5000 latex paint base. It was not possible to ascertain the exact size of silver chloride nanoparticles by SEM. TEM analyses of the K5000-1000AgCl sample revealed that the silver chloride nanoparticles were approximately 15 – 100 nm in size (Section 6.3). It is important to note that the silver chloride nanoparticles were formed only within

the PU K5000 domains and not in the water phase. The polymer matrix of PU K5000 latex paint base provides stabilisation for the nanoparticles.

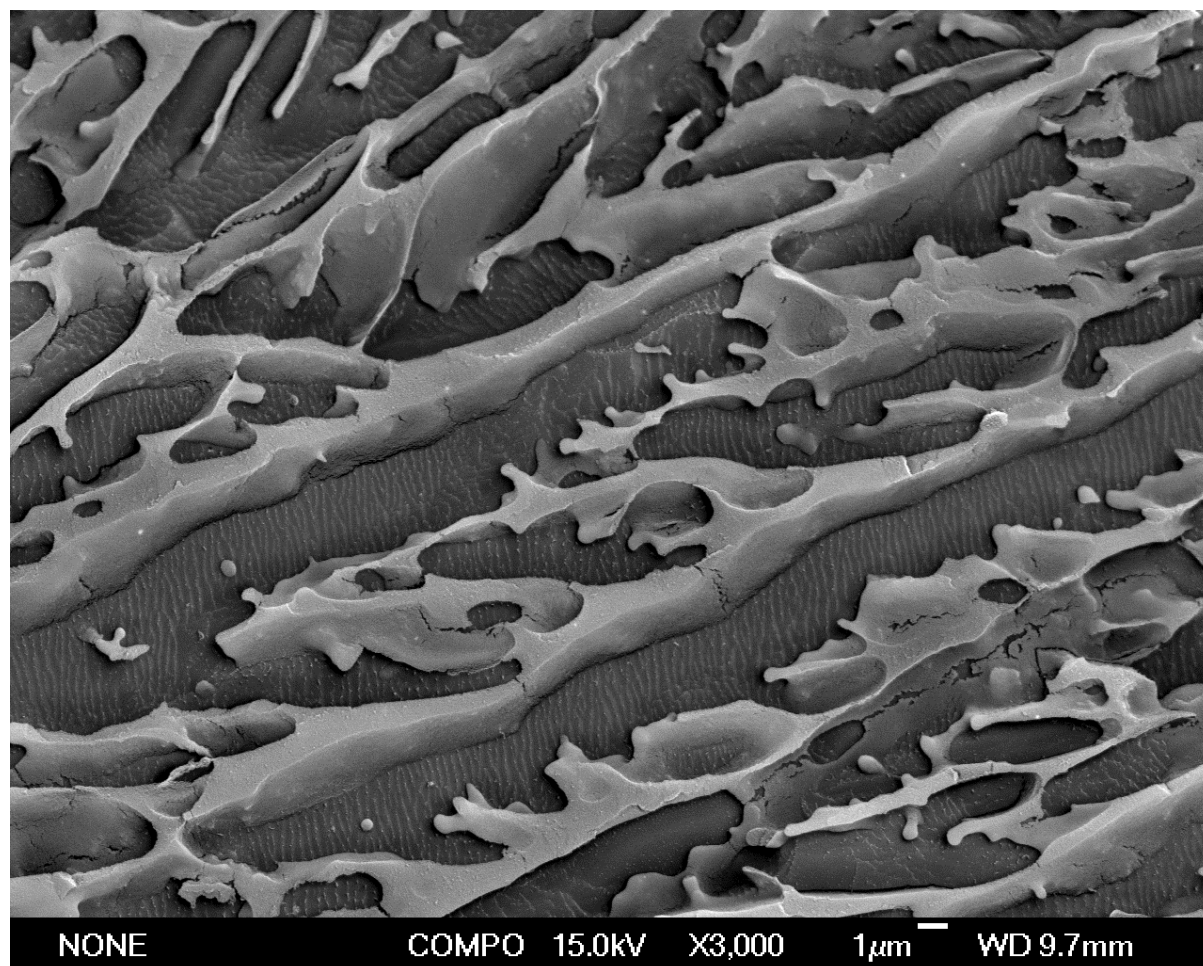


Figure 6.16: Cryo-SEM micrograph in backscatter mode of the K5000-1000AgCl sample.

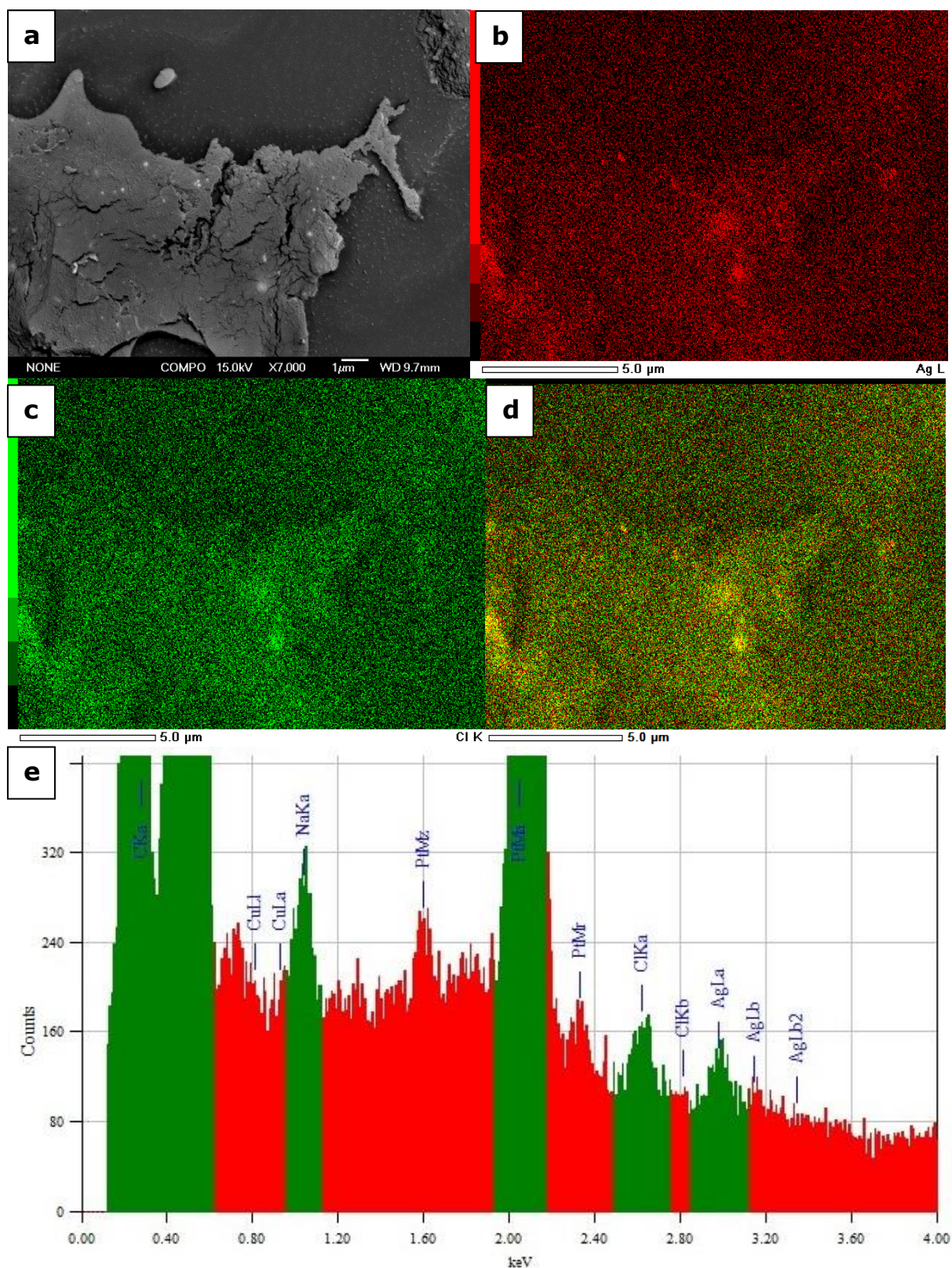


Figure 6.17: Cryo-SEM micrograph in backscatter mode of the K5000-1000AgCl sample with b-c) the corresponding EDS micrographs, d) the EDS Ag and Cl overlay map and e) the corresponding elemental analysis spectrum.

6.3 Transmission electron microscopy and energy dispersive X-ray analysis of nanosilver halide hybrid polymer materials

TEM was used to analyse the nanosilver halide hybrid polyurethane K5000 latex paint base materials in order to obtain information on the size and shape of silver halide particles formed within the polymer matrix. Due to instrument constraints, the ease of the sample preparation and the high concentration of silver halide particles present in the polymer matrix, the K5000-1000AgCl, K5000-1000AgBr and K5000-1000AgI samples were chosen as representatives of these hybrid materials. After exposure to light the samples were dissolved in high purity methanol, and a drop of resulting solution was placed on a copper grid. After the evaporation of the solvent the residual grid was carbon coated. All imaged particles were verified by EDS elemental analyses. The copper X-ray peak in the EDS spectra arises from the copper grid on which the sample was placed. Due to laboratory contamination, the peaks for silicon and zinc should be ignored. Due to the presence of dried polymer in the sample it was difficult to obtain crisp images of the lattice fringes of the analysed silver halide nanoparticles.

The TEM analyses of the K5000-1000AgCl, K5000-1000AgBr and K5000-1000AgI samples revealed a wide variety of shapes and sizes for the AgX nanoparticles. All particles were found to exhibit darker regions on the surface and edges of the central structure. The particles were difficult to image due to the electron beam causing increased decomposition of such silver halide particles. This was observed by continuous movements and growth of the dark regions under the irradiation with the electron beam. Figure 6.18 shows TEM micrographs of some examples of the nanoparticles found in the K5000-1000AgCl sample. The respective EDS spectral analyses, present on the right side of each photograph, confirmed the presence of silver chloride. These silver chloride nanoparticles in the hybrid PU K5000 polymer paint base had a predominantly cubic structure of AgCl. However, some spherical, irregular shaped particles and particle agglomerates could be observed. There was a range of particle sizes from approximately 15 – 100 nm.

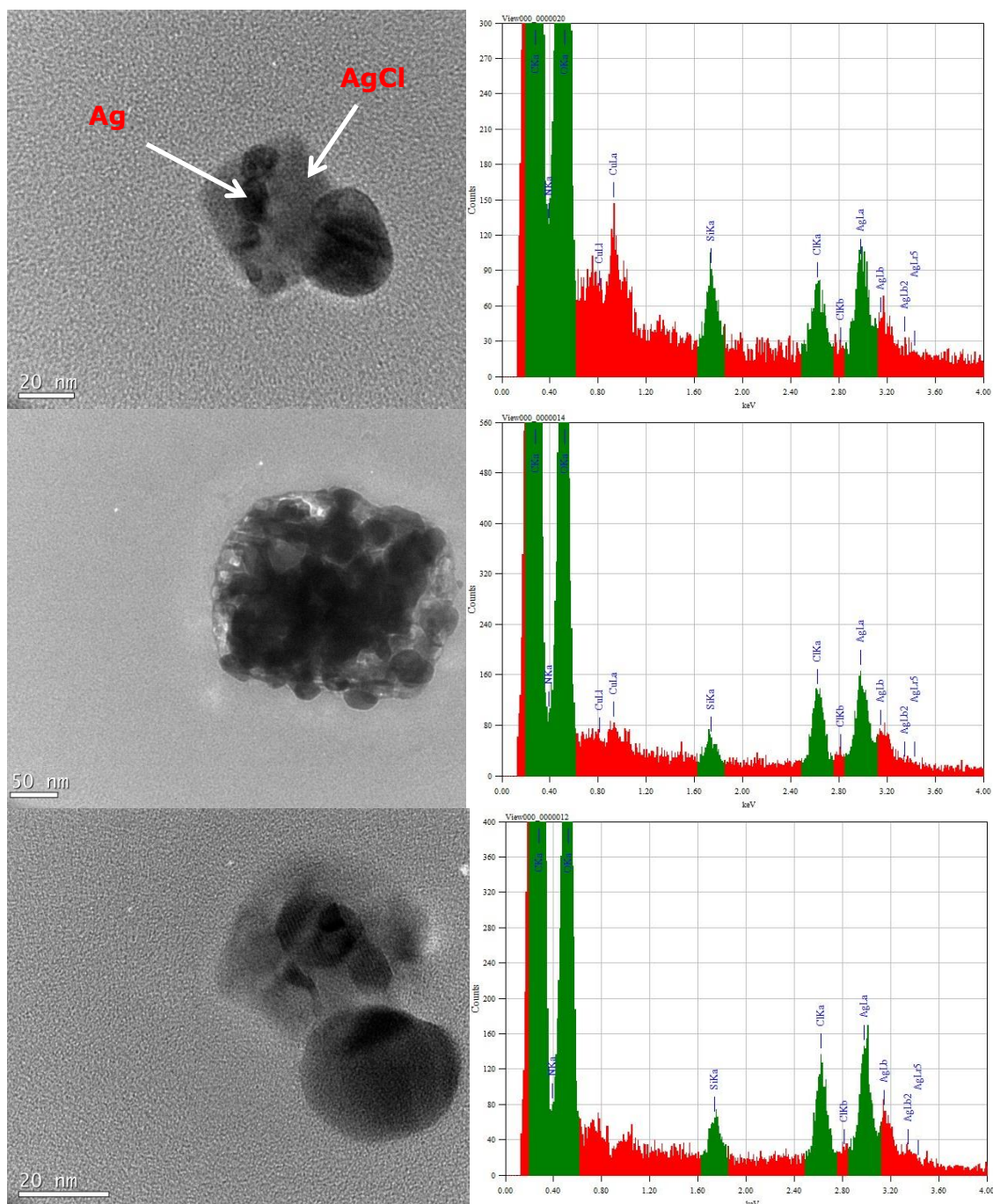


Figure 6.18: TEM micrographs of the Ag/AgCl nanoparticles found in the K5000-1000AgCl sample after the exposure to light (left) with their corresponding EDS spectra (right).

As mentioned above, mostly spherical-like particles and particle agglomerates, which are of darker contrast, could be found on the surface and edges of the AgCl nanoparticles. In the literature these dark regions have been previously identified as metallic silver.^{168,332} This further indicates that during light

irradiation, the silver halide particles in the nanosilver halide hybrid polymer materials are converted to Ag/AgX particles. The size of these non-uniformly shaped Ag⁰ nanodomains varies between very small discrete domains (ca. 5 nm), to large agglomerates (> 100 nm) (Figure 6.18).

Elemental mapping of the nanoparticles within the nanosilver halide hybrid polyurethane K5000 latex paint base materials was accomplished using Scanning Transmission Electron Microscopy. STEM confirmed the distinct relationship between silver and chlorine and additionally that the dark regions on the surface of the central AgCl nanoparticle were metallic silver. Figure 6.19 offers a TEM micrograph of a typical AgCl nanoparticle found in the K5000-1000AgCl sample. The corresponding Ag and Cl STEM maps suggest that the particle is composed of silver chloride. Furthermore, where the dark regions are located, there are very high concentrations of silver (depicted in red).

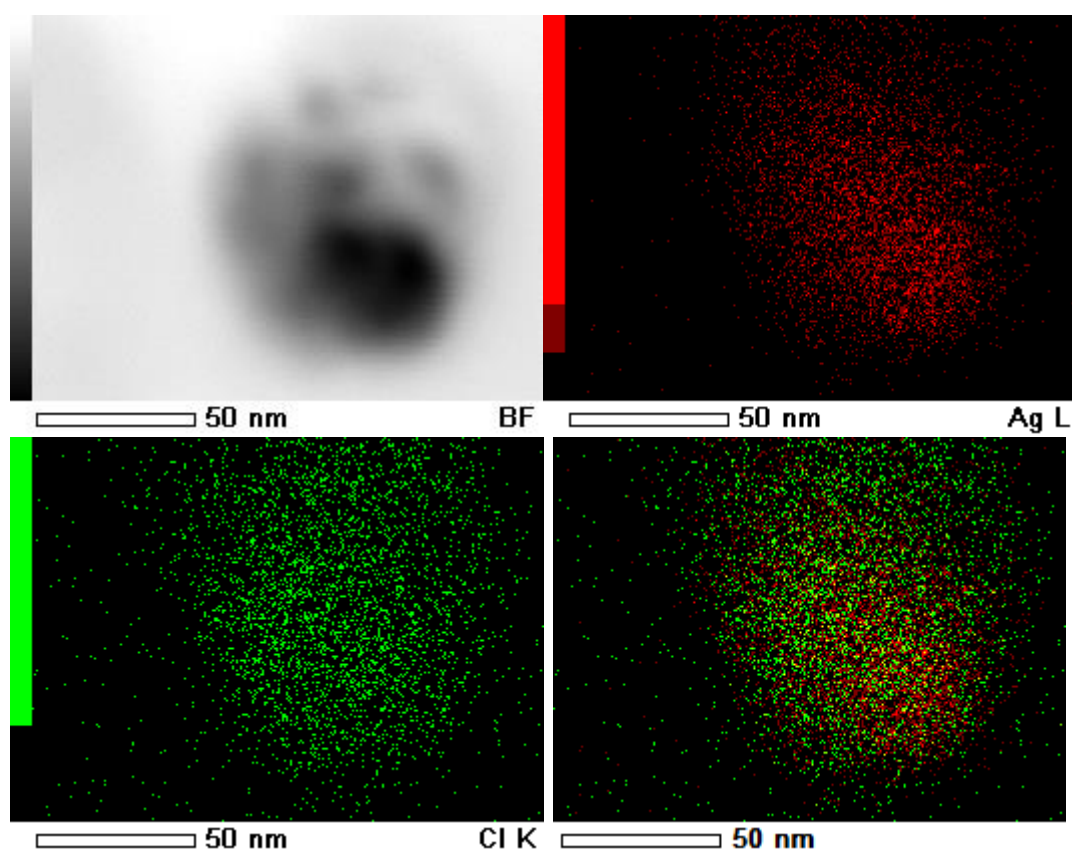


Figure 6.19: TEM micrograph of the silver chloride particle in the K5000-1000AgI sample, the corresponding Ag and Cl STEM micrographs and the Ag and Cl overlay.

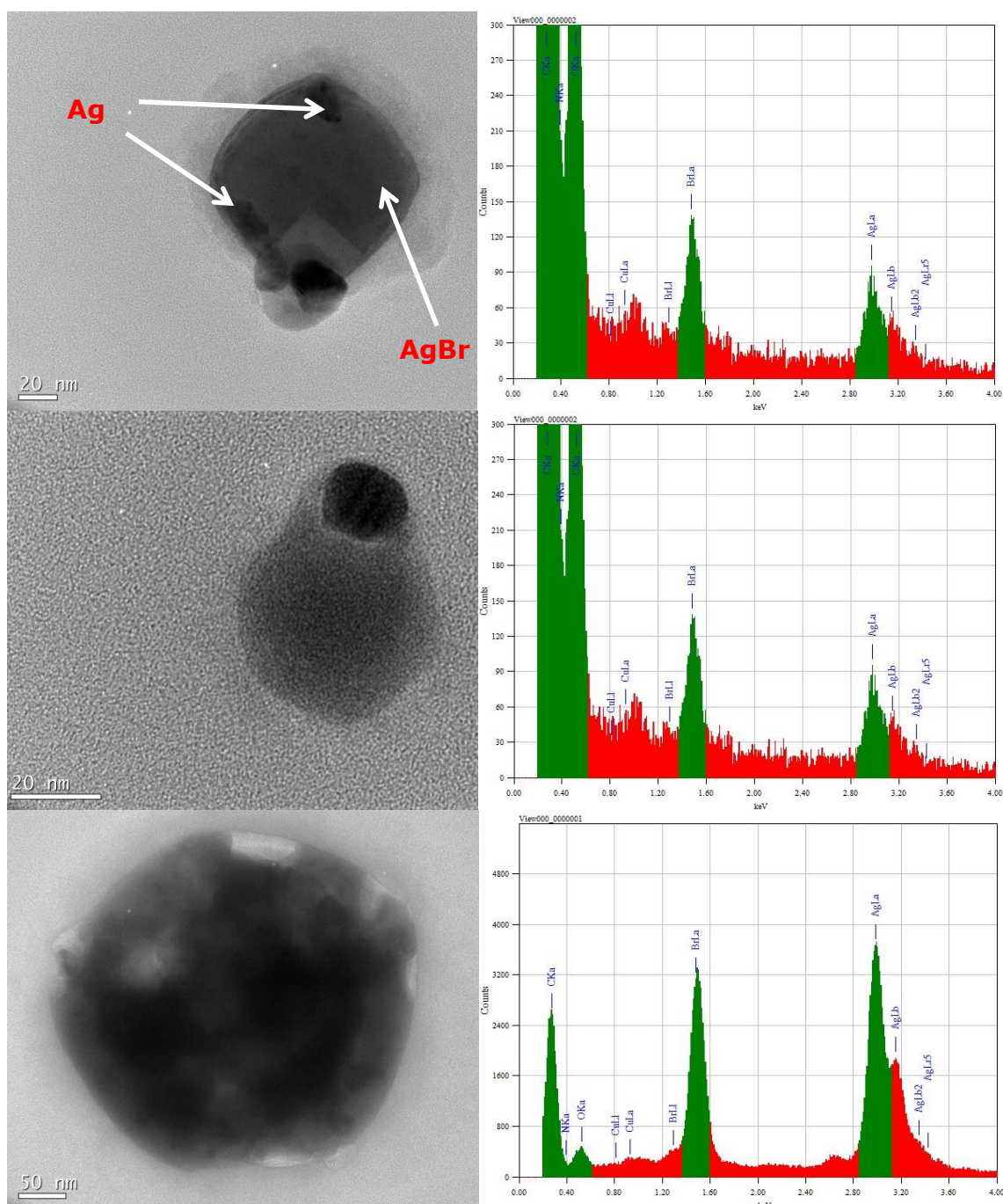


Figure 6.20: TEM micrographs of the Ag/AgCl nanoparticles found in the K5000-1000AgCl sample after the exposure to light (left) with their corresponding EDS spectra (right).

TEM examination of the K5000-1000AgBr sample, which was exposed to light prior to the analysis, showed that the AgBr particles appear to be cubic or spherical in morphology (although some irregular shapes were present) with a wide size distribution between 40 nm to 500 nm. Figure 6.20 offers some TEM

images with the corresponding EDS analyses spectra of the AgBr particles in the K5000-1000AgBr sample. The particles exhibit dark areas, similar to the AgCl particles mentioned above, which are assigned to Ag⁰ nanodomains (depicted with the arrows in the Figure 6.20).

During the exposure of the K5000-1000AgBr sample to the TEM beam, movements of the darker Ag⁰ nanodomains on the surface of the central AgBr crystal were observed. The series of images (Figure 6.21a-c), which was taken over a period of three minutes, show the dark silver nanodomains of the Ag/AgBr particle undergo agglomeration. Similar to an Ostwald ripening mechanism, the smaller dark regions are slowly growing into a larger region. The growth of these dark regions, which continued as long as the crystal was irradiated, could easily be followed. A likely explanation for such observation is that the beam causes a photolysis of the AgBr to Ag⁰ nanoparticles or nanodomains, resulting in two different phases within the one particle. The existence of these two different phases is in agreement with forming silver nanodomains on the AgBr nanoparticle upon exposure to light resulting in Ag/AgBr particles (Sections 6.1 and 6.4). Furthermore, although the self-photosensitisation is taking place under the electron beam, the particle does not fully convert to a single silver particle. During the electron beam irradiation period the spherical geometry and size of the AgBr crystal remains unchanged. A strong X-ray peak for bromine could still be detected by the EDS spectral analysis confirming the presence of AgBr (Figure 6.21d).

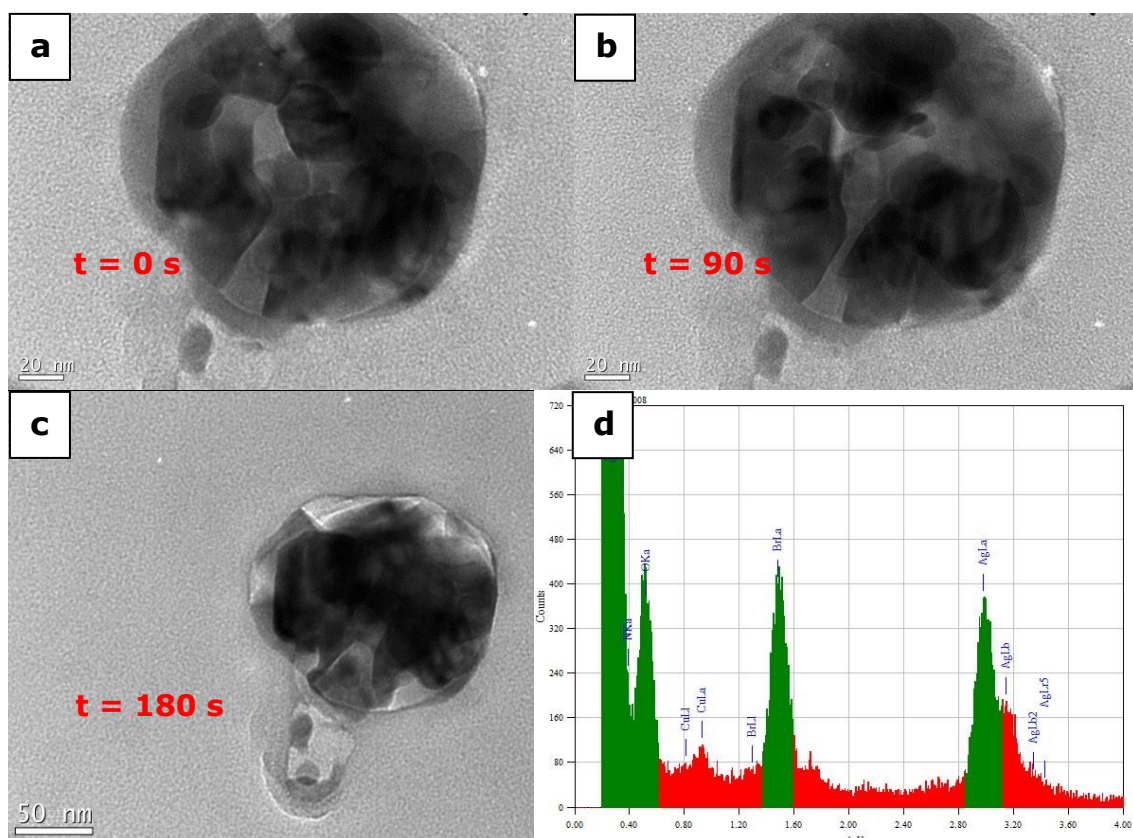


Figure 6.21: a-c) TEM micrographs of an Ag/AgBr particle found in the K5000-1000AgBr sample taken over a period of three minutes with d) the respective EDS analysis spectrum of the particle shown in a).

Figure 6.22 offers TEM micrographs of the nanosilver iodide hybrid PU K5000 paint base material (K5000-1000AgI) which was exposed to light. The presence of silver iodide within the hybrid PU K5000 paint base material was confirmed by the peaks at 2.98 keV and 3.94 keV corresponding to the Ag L_α and I L_α line respectively in the EDS spectra (Figure 6.22). Generally, the most common shapes of the AgI particles were spherical, hexagonal and triangular. Additionally, anisotropic geometric shapes and particle agglomerates were also present. The particles have a broad size distribution, ranging from 20 nm to 500 nm and exhibit dark regions on the surface of the central AgI crystal, comparable to the analogue K5000-1000AgCl and K5000-1000AgBr samples described above. The dark regions were attributed to Ag⁰ nanoparticles which are formed through a photolysis process with exposure to light (Section 1.4.5). Although the mechanism of the photolysis for the AgI is the same as for AgCl and AgBr, the rate is believed to be much slower.³³⁰

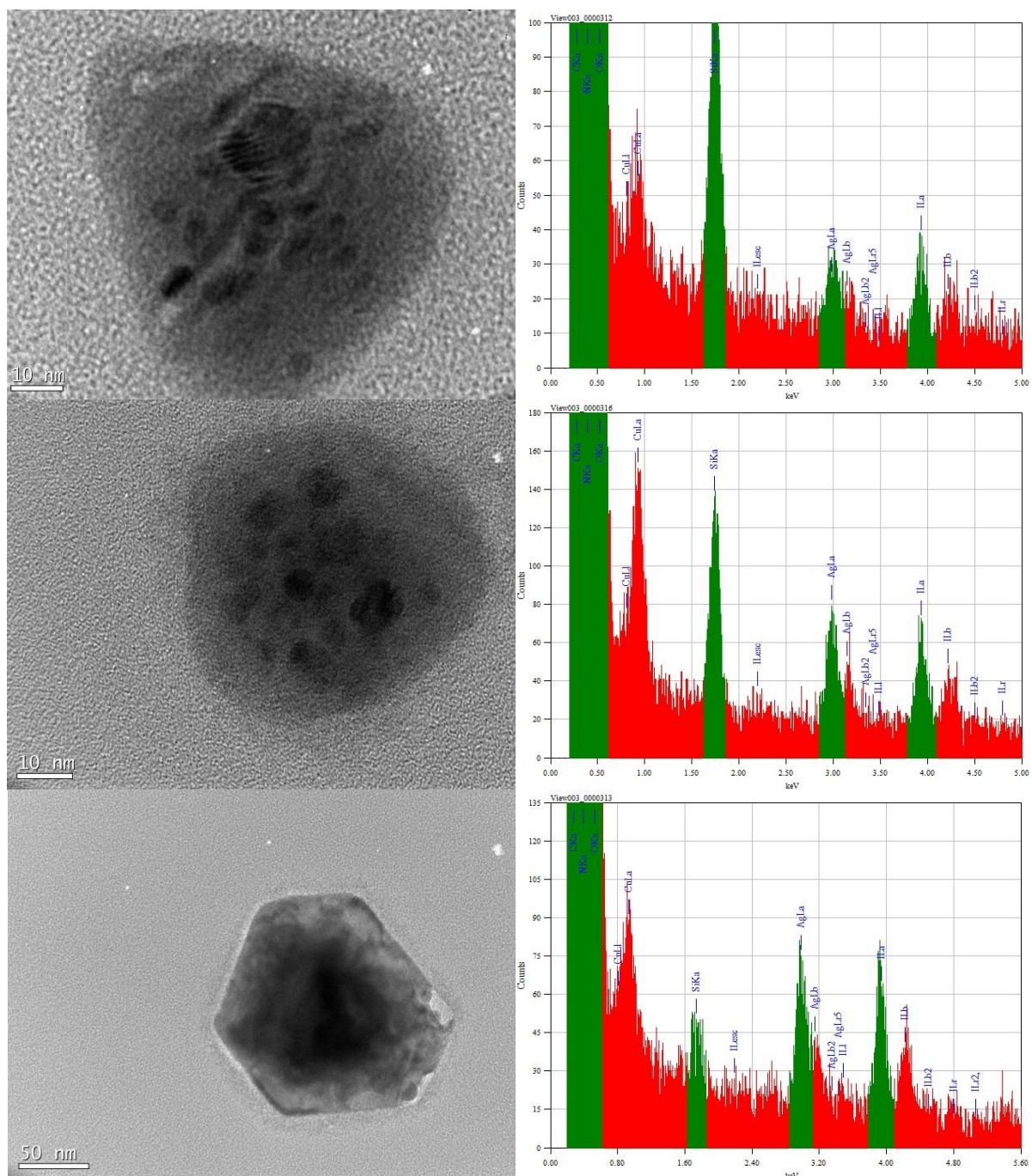


Figure 6.22: TEM micrographs of the Ag/AgI nanoparticles found in the K5000-1000AgCl sample after the exposure to light (left) with their corresponding EDS spectra (right).

A typical AgI particle was further analysed by STEM. Figure 6.23 presents a TEM micrograph of the nanosilver iodide hybrid polyurethane K5000 paint base material with the corresponding Ag and I STEM maps. The overlay map of Ag and I substantiates that the particle consists of silver iodide. This is confirmed by

the distinct relationship between silver and iodine; whereby again high levels of silver correspond to high levels of iodine. Additionally, it can be seen where the most dark regions of the particle are located there is a higher concentration of silver (illustrated in red in the Ag and I overlay map). As such, silver iodide nanoparticles were successfully formed within the polyurethane K5000 matrix and converted to Ag/AgI particles during the exposure of the sample to natural light.

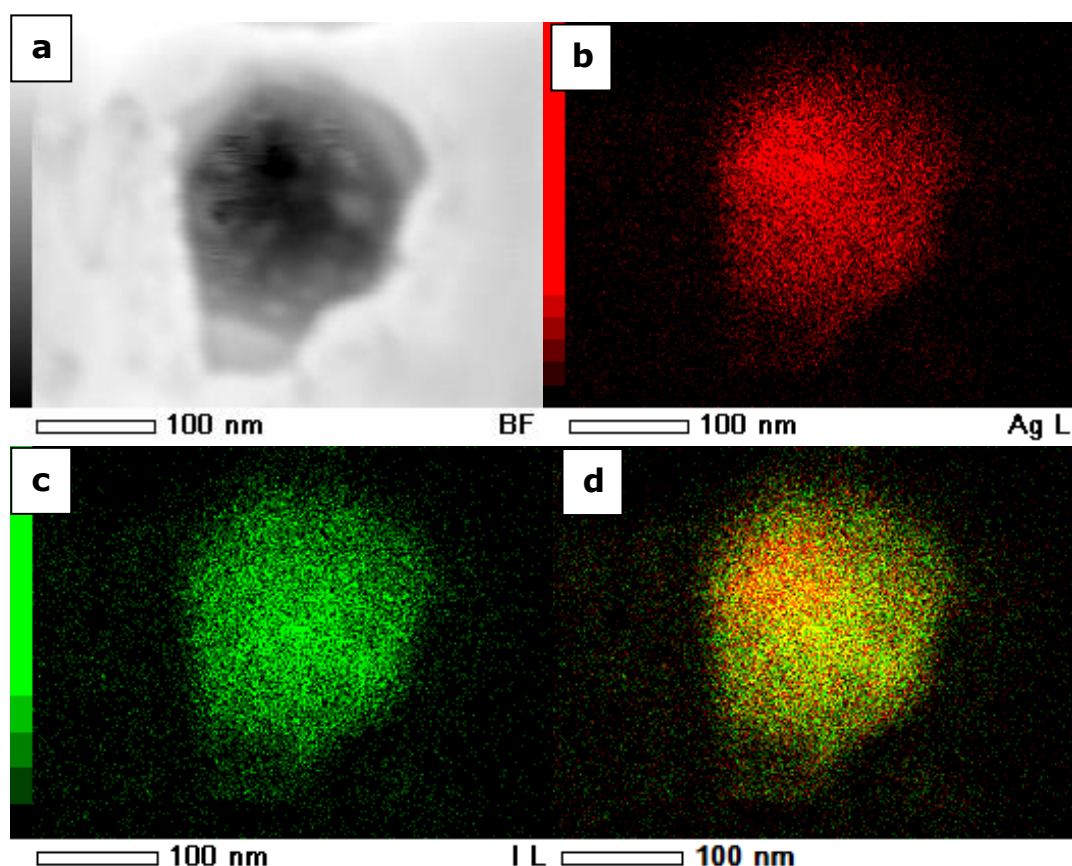


Figure 6.23: a) TEM micrograph of the silver iodide particles in the K5000-1000AgI sample, the corresponding b) Ag and c) I STEM micrographs. The Ag and I overlay is shown in d).

6.4 X-ray diffraction analysis of nanosilver halide hybrid polymer materials

XRD analyses were carried out in order to confirm the presence of silver halide nanoparticles in the hybrid polymer materials. The XRD patterns were used to compare the Bragg peak positions and their intensities with the standard PDF 04-001-2617 for silver, PDF 01-071-5209 for silver chloride, PDF 04-005-4490 for silver bromide and PDF 00-009-0374 for silver iodide diffraction patterns.²⁴² The mean particle size of the silver halides was calculated using Scherrer's equation, which was introduced in Section 2.3.4. For the samples containing AgCl and AgBr, the most intense (2 0 0) peak was used for the calculation, whereas for the sample containing AgI particles the most intense (1 1 0) peak seemed to be suitable for the calculation. The calculated mean crystallite particle sizes and the parameters for X-ray diffraction patterns for the nanosilver halide hybrid PU and polyurethane K5000 samples are listed in Table 6.3.

Figure 6.24 illustrates the XRD patterns obtained from the nanosilver halide hybrid PU sheets prior to their exposure to light. For all three samples, the PU-200AgCl, PU-200AgBr and PU-200AgI, the patterns confirm that during the syntheses of the hybrid materials crystalline silver halides were formed within the PU matrix. The diffraction peaks at $2\theta = 27.84^\circ, 32.26^\circ, 46.26^\circ, 54.84^\circ, 57.50^\circ$ and 76.75° in the XRD pattern for the PU-200AgCl sample can be indexed as the (1 1 1), (2 0 0), (2 2 0), (3 1 1), (2 2 2) and (4 2 0) reflection peaks of face centred cubic AgCl (PDF 01-071-5209).²⁴² The XRD pattern for the PU-200AgBr sample showed six reflection peaks at $2\theta = 26.72^\circ, 30.94^\circ, 44.29^\circ, 54.98^\circ, 64.44^\circ, 73.18^\circ$ and 81.55° which can be attributed to the (1 1 1), (2 0 0), (2 2 0), (2 2 2), (4 0 0), (4 2 0) and (4 2 2) reflection peaks of the fcc AgBr (PDF 04-005-4490).²⁴² The XRD pattern obtained for the PU-200AgI sample showed the presence of seven broader Bragg reflection peaks in comparison to peaks found in the PU-200AgCl and PU-200AgBr samples respectively, indicating smaller crystallite size.³³³ The peaks found at $2\theta = 22.29^\circ, 23.60^\circ, 25.17^\circ, 32.77^\circ, 39.04^\circ, 42.43^\circ$ and 46.12° correspond respectively to the (1 0 0), (0 0 2), (1 0 1), (1 0 2), (1 1 0), (1 0 3) and (1 1 2)

crystal planes of the hexagonal wurtzite β -AgI (PDF 00-009-0374).²⁴² As expected, it is noted that for all three samples no peaks corresponding to elemental Ag were discerned. The mean crystallite size of the silver halide particles was estimated to be 86 nm for the PU-200AgCl sample, 69 nm for the PU-200AgBr sample and 40 nm for the PU-200AgI sample (Table 6.3).

Table 6.3: Parameters for X-ray diffraction patterns of the nanosilver halide hybrid PU and polyurethane K5000 latex paint base samples.

| Hybrid material | Peak position [° 2 θ] | FWHM [° 2 θ] | Mean crystal diameter [nm] |
|-----------------|----------------------------------|-------------------------|-------------------------------|
| PU-200AgCl | 32.30 | 0.19 | 86 |
| PU-200AgBr | 30.94 | 0.24 | 69 |
| PU-200AgI | 39.04 | 0.42 | 40 |
| K5000-1000AgCl | 32.28 | 0.29 | 56 |
| K5000-1000AgBr | 30.90 | 0.27 | 62 |

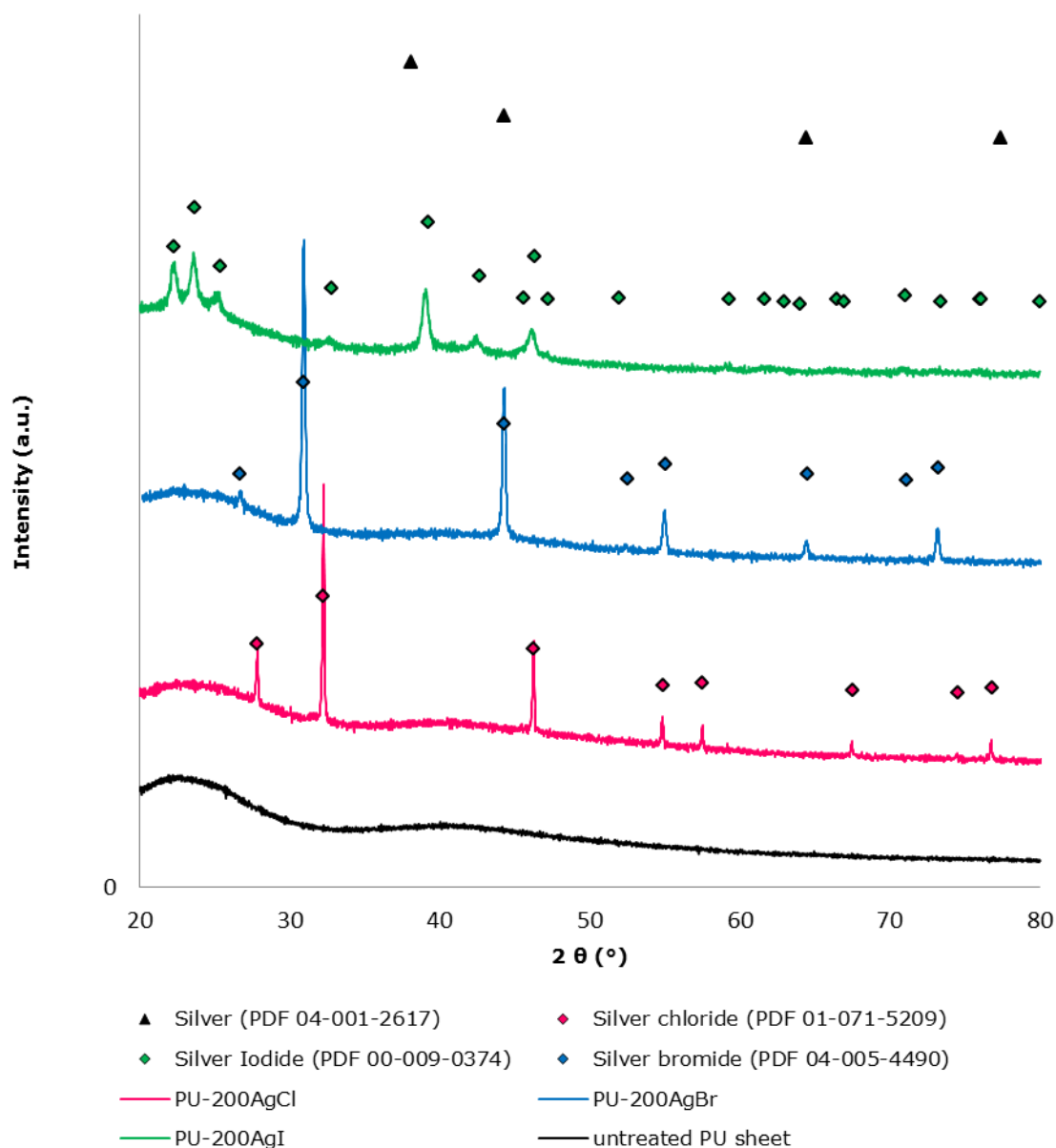


Figure 6.24: XRD patterns of the nanosilver halide hybrid PU materials before exposure to light.

The XRD patterns obtained from the nanosilver halide hybrid nylon 6,6 sheets are presented in Figure 6.25. Although UV-Vis and SEM analyses of these materials showed the presence of silver halide particles within the nylon 6,6 matrix (Sections 6.1 and 6.2.2), the XRD patterns of the nanosilver halide hybrid nylon 6,6 samples did not show any of the typical Bragg diffraction peaks for AgCl, AgBr or AgI. A possible reason for the absence of the diffraction peaks for all three samples is that the formation of the halide particles in the nylon 6,6

matrix took place below the penetration depth of the X-rays into the samples. Furthermore, pore structure in nylon 6,6 substrates is likely to be smaller than in PU substrates hence the silver halide particles may be very small. The small size of the particles results in a low signal to noise ratio. Due to the semicrystalline nature of nylon 6,6 matrix the weak diffraction peaks can be masked. To verify this proposed statement, further XRD studies accompanied by TEM analyses of these materials are required.

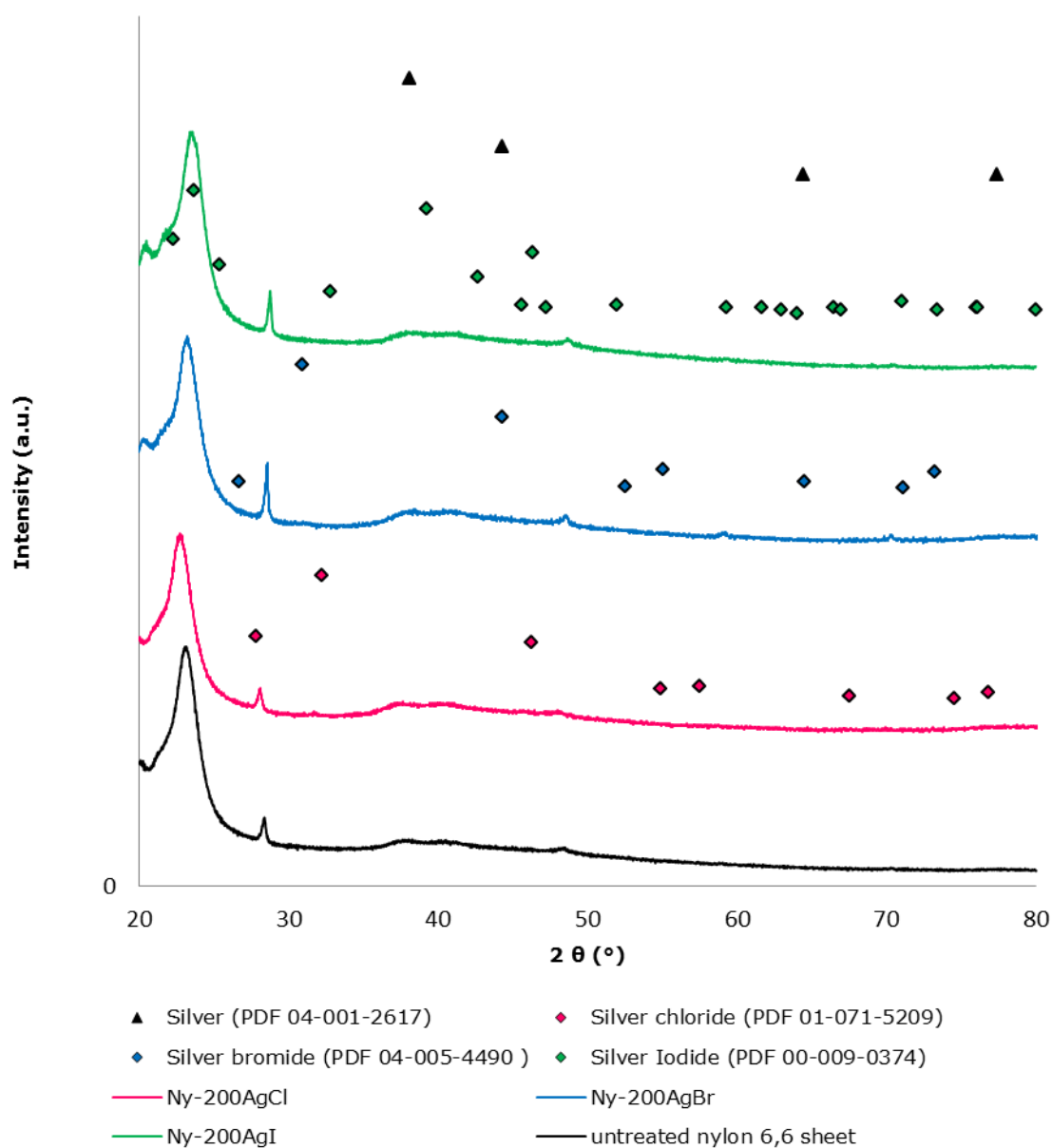


Figure 6.25 XRD patterns of the nanosilver halide hybrid nylon 6,6 materials before exposure to light.

Figure 6.26 presents the XRD patterns obtained from the nanosilver halide hybrid polyurethane K5000 latex paint base materials. Silver chloride- and silver bromide-containing hybrid polyurethane K5000 materials (K5000-1000AgCl and K5000-1000AgBr sample) were found to have formed their respective silver halides in the polyurethane K5000 matrix. Silver iodide could not be detected in the K5000-1000AgI sample. Four Bragg diffraction peaks were found in the K5000-1000AgCl sample at $2\theta = 27.88^\circ$, 32.28° , 46.25° and 54.842° and indexed as the (1 1 1), (2 0 0), (2 2 0) and (3 1 1) peaks based on the face centred cubic structure of AgCl (PDF-01-071-5209).²⁴² The mean particle size of the silver chloride nanoparticles was estimated to be 56 nm. The K5000-1000AgBr sample revealed five diffraction peaks at $2\theta = 30.90^\circ$, 44.30° , 55.02° , 64.46° and 73.24° identifiable as the (2 0 0), (2 2 0), (2 2 2), (4 0 0) and (4 2 0) reflection peaks, corresponding to the fcc structure of AgBr (PDF 04-005-4490).²⁴² Using the position and the FWHM of the most intensive (2 0 0) peak the mean particle size was found to be ca. 62 nm (Table 6.3). Although the presence of the AgI nanoparticles in the K5000-1000AgI sample was confirmed by TEM analysis (Section 6.3), for unknown reasons, the XRD pattern of the sample did not detect any AgI within the PU K5000 paint base matrix. It is likely the concentration was too diluted. Therefore further XRD studies of more concentrated samples containing AgI particles are required.

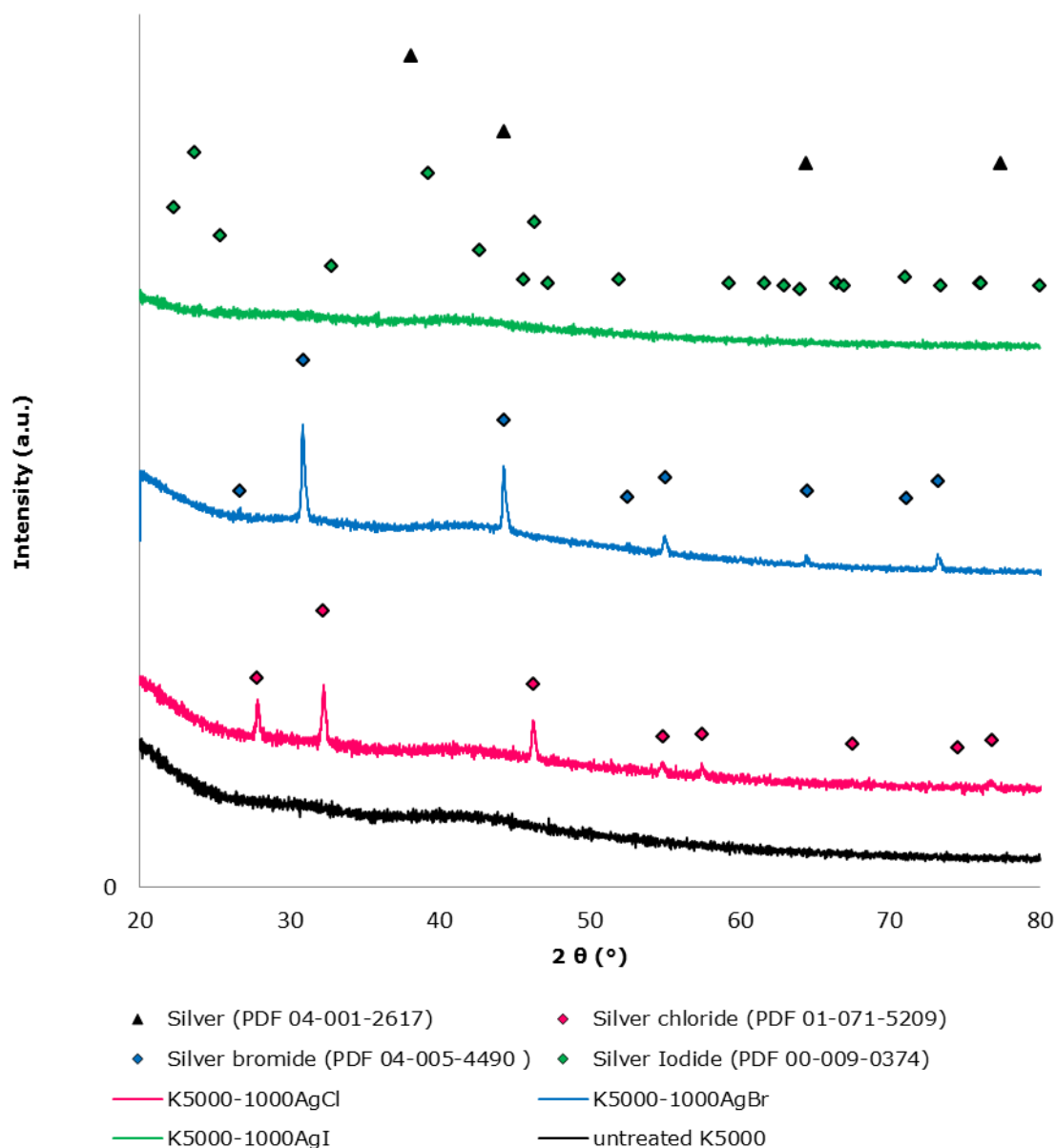


Figure 6.26: XRD patterns of the nanosilver halide hybrid polyurethane K5000 latex paint base materials before exposure to light.

XRD analyses were also carried out on the nanosilver halide hybrid PU and polyurethane K5000 materials in order to confirm if light exposure did in fact cause photolysis of silver halides particles leading to the formation of metallic silver nanoparticles on the surface of the silver halides within the polymer matrices.

The XRD analyses of the PU-200AgCl and PU-200AgBr samples were carried out over a period of time, on the day of the synthesis before the samples were exposed to light, and after the samples were exposed to natural light for 4, 26 and 61 days respectively. Figure 6.27 and Figure 6.29a illustrate the XRD patterns and the respective photographs of the PU-200AgCl sample upon exposure to light. As expected, before exposure to light, the sample only exhibited the typical diffraction peaks of the fcc AgCl as discussed earlier. Immediately after the sample was prepared, its colour was white, also characteristic for AgCl due to the wide band gaps (Sections 1.4.5 and 6.1). After four days of natural light, the sample showed dark purple colouration and the XRD pattern indicated the presence of two new discernible peaks which were indexed to the (1 1 1) and (2 0 0) diffraction peaks of fcc silver (PDF 04-001-2617).²⁴² The longer the PU-200AgCl sample was exposed to light the more pronounced these diffraction peaks for Ag became and the colour of the PU-200AgCl sample grew browner. A similar effect was noted for the PU-200AgBr sample. Figure 6.28 and Figure 6.29b present the XRD patterns and the respective photographs of the sample upon exposure to light. Before exposure to light, the sample was white in colour and showed the characteristic Bragg diffraction peaks of the fcc AgBr structure. Although the purple colouration of the sample was well noticeable on day four of natural light exposure, the XRD pattern from the sample obtained after 61 days of light first showed the presence of a very weak peak which was identifiable as the (1 1 1) Bragg diffraction peak of fcc silver (PDF 04-001-2617).²⁴² As such, it is assumed that more metallic silver was formed in the PU-200AgCl sample compared to the PU-200AgBr sample after being exposed to natural light for 61 days.

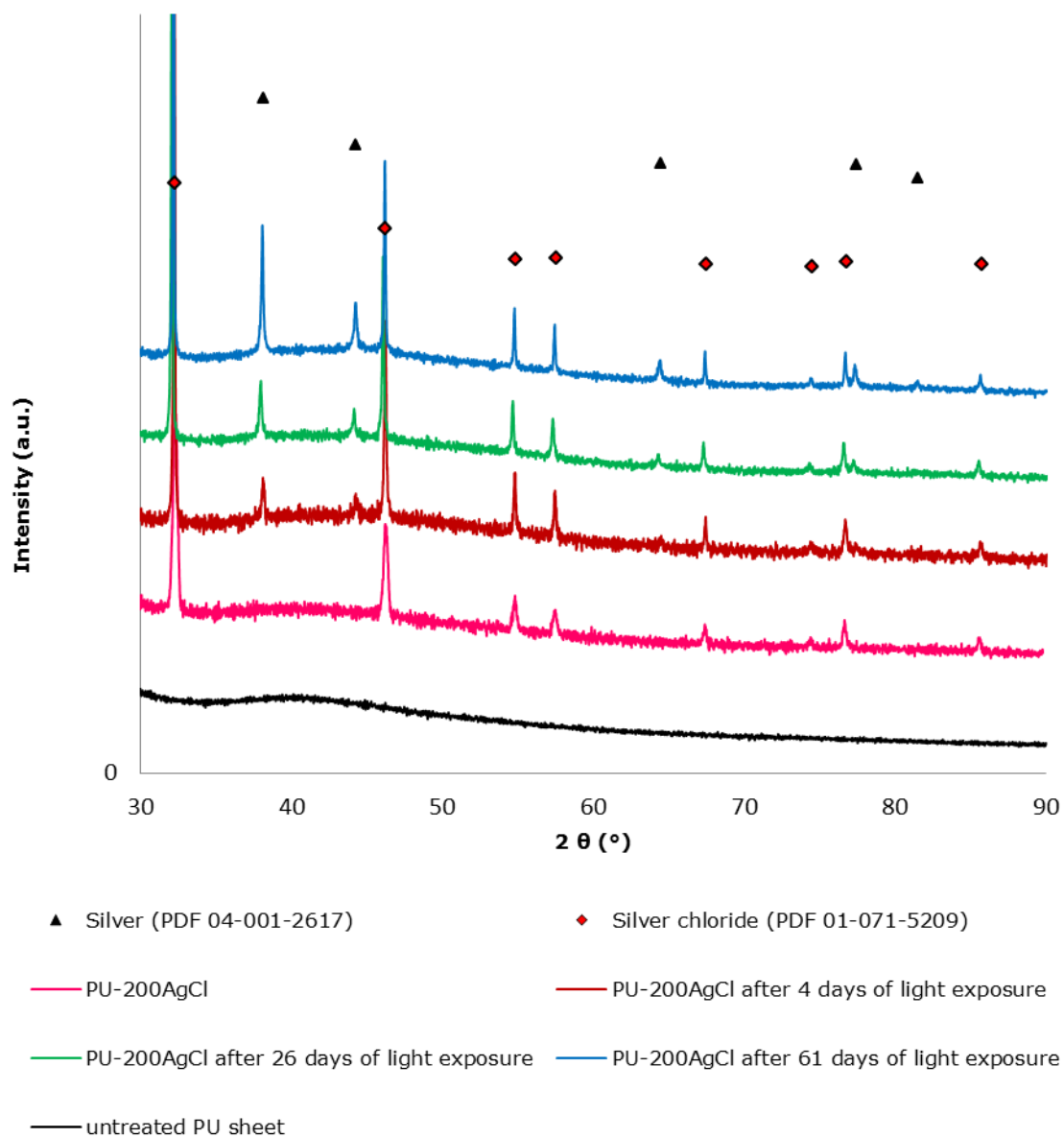


Figure 6.27: XRD patterns of the nanosilver chloride hybrid PU materials before and after exposure to light.

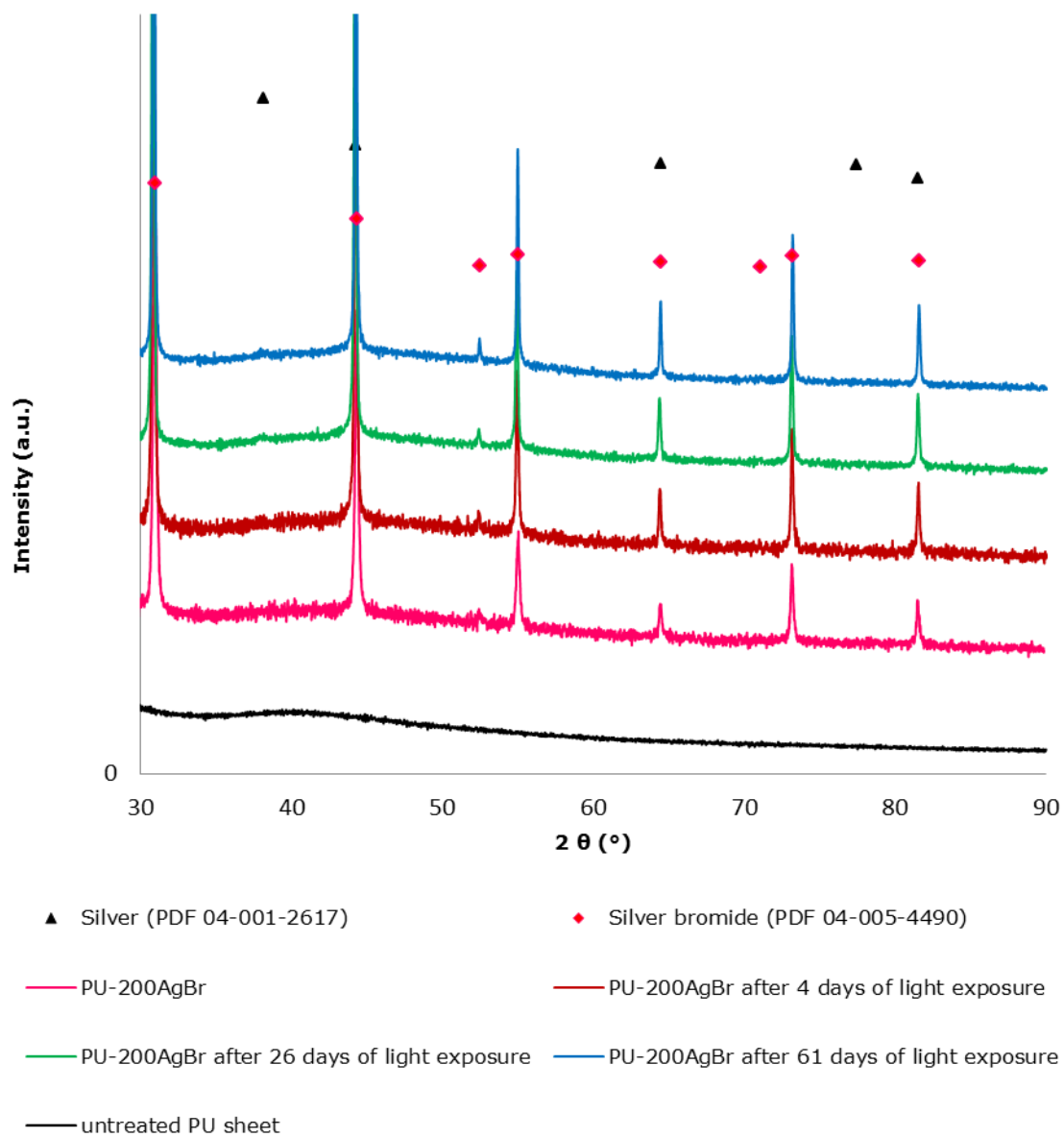


Figure 6.28: XRD patterns of the nanosilver bromide hybrid PU materials before and after exposure to light.

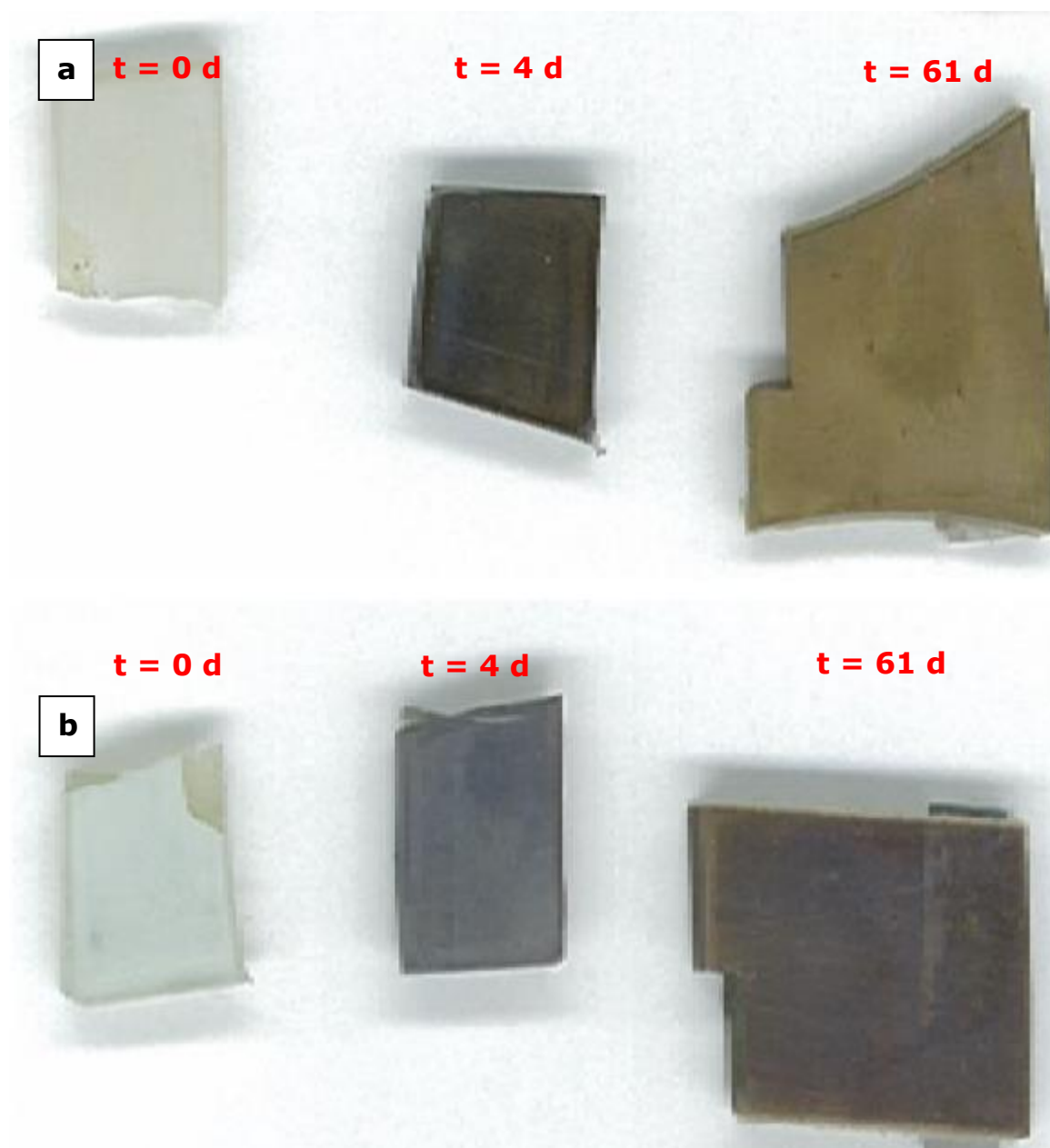


Figure 6.29: Photographs of a) the PU-200AgCl sample before the exposure to light, 4 and 61 days of exposure to natural light (from left to right) and b) the PU-200AgBr sample before the exposure to light, 4 and 61 days of exposure to natural light (from left to right).

The XRD patterns obtained for the K5000-1000AgCl and K5000-1000AgBr samples before and after exposure to natural light (4 days) are shown in Figure 6.30 and Figure 6.31. The respective photographs of the samples are shown in Figure 6.3. Upon exposure to natural light for four days, the K5000-1000AgCl sample changed the colour from white to brown, whereas the K5000-1000AgBr

sample turned purple. The XRD patterns for the K5000-1000AgCl sample showed in addition to the expected characteristic diffraction peaks of the fcc AgCl the (1 1 1) peak of the fcc Ag (PDF-04-001-2617).²⁴² However, the intensity of the silver peak was very weak suggesting that very small amount of Ag was formed. In the XRD analysis of the K5000-1000AgBr sample after being exposed to light, no peaks corresponding to elemental Ag were discernable.

As reported in Sections 1.4.5 and 6.1, due to their photosensitive characteristics, silver halides are not stable under UV visible light. Once exposed to light, these silver halide particles go through a self-photosensitisation process leading to a partial reduction of Ag^+ to Ag^0 nanodomains or nanoparticles at the surface of the silver halide particles.^{168,319} Thus, it can be assumed that the AgX nanoparticles within the PU and PU K5000 polymer matrix were converted *in situ* to Ag/AgX nanoparticles. Due to their wide band gaps (Table 6.2), silver chloride and bromide are not able to absorb light above 380 nm as was shown by the UV-Vis analyses of the nanosilver halide hybrid nylon 6,6 materials (Section 6.1). Therefore, the purple/brown colour is due to the SPR effect of the formed Ag^0 domains resulting in a broad visible spectral absorption of these materials (Sections 1.4.5). XRD analyses revealed that the hybrid PU and polyurethane K5000 polymer materials containing AgCl are more photosensitive than the ones containing AgBr.

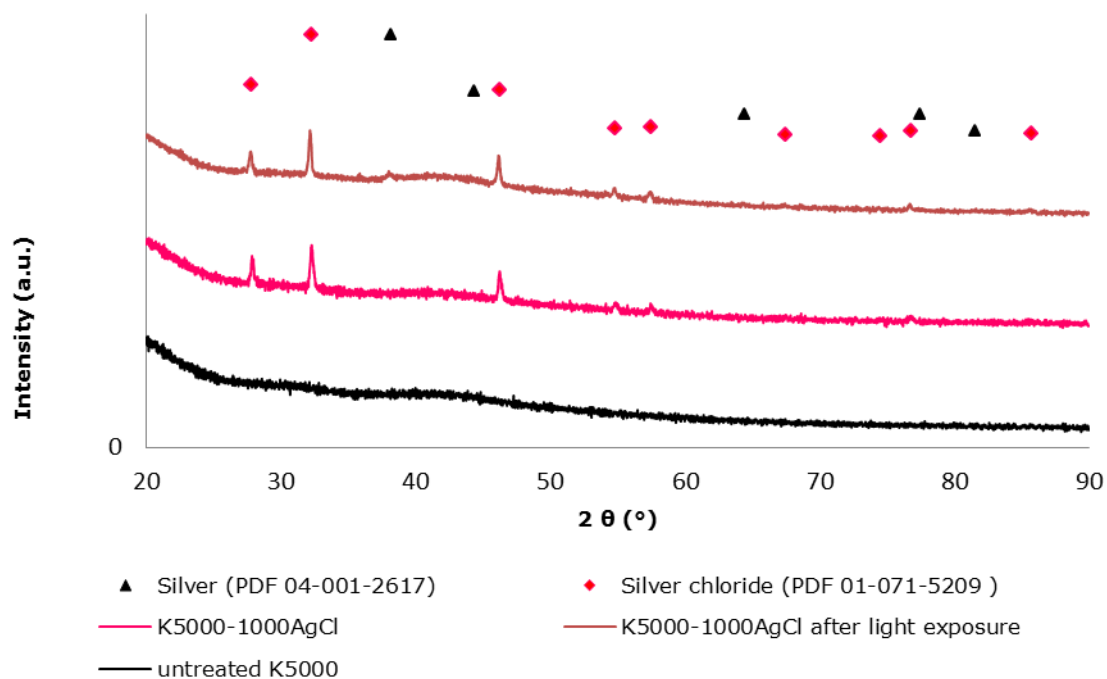


Figure 6.30: XRD patterns of the nanosilver chloride hybrid polyurethane K5000 latex paint base materials before and after exposure to light.

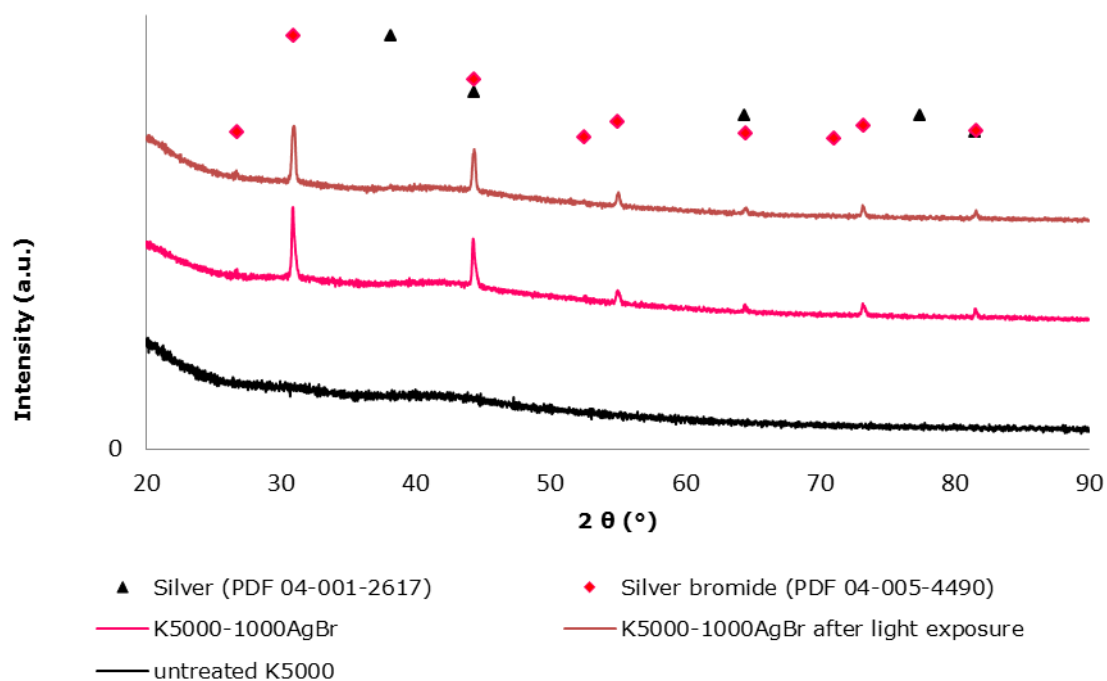


Figure 6.31: XRD patterns of the nanosilver bromide hybrid polyurethane K5000 latex paint base materials before and after exposure to light.

6.5 X-ray photoelectron spectroscopy analysis of nanosilver halide hybrid polymer materials

An XPS study of the hybrid PU materials was carried out in order to further confirm the formation of silver halide nanoparticles within the polymer matrix and to investigate their chemical interaction with the polymer matrix. As representatives for the nanosilver halide hybrid polymer materials the PU-200AgCl, PU-200AgBr and PU-200AgI samples were chosen for the XPS studies. For every nanosilver halide PU sample, a reference sample was prepared. The preparation of the reference samples was attempted via the same method as the preparation of the nanosilver halide hybrid PU samples (Section 2.2.3.1), however, instead of immersing the NaX-doped PU sheets in the AgNO₃ solution, distilled H₂O was used. During the preparation and the loading process of the samples into the X-ray photoelectron spectrometer, the samples were kept out of light in order to avoid the photolysis of the silver halide nanoparticles. However, the complete prevention of the light radiation could not be guaranteed. An initial survey scan from a binding energy of 700 to 0 eV for all polyurethane samples showed the presence of carbon, nitrogen and oxygen groups on the polymer surface, together with silver, chlorine, bromine and iodine for the nanosilver halide hybrid PU polymers respectively. High resolution scans were carried out across the peaks for each of the elements. X-ray peaks for calcium and silicon should be ignored due to contamination of the samples.

The wide XPS scans for the nanosilver halide hybrid PU materials (PU-200AgCl, PU-200AgBr and PU-200AgI samples) and their respective PU sheet reference samples are shown in Figure 6.32. Each sample shows the presence of the characteristic elements (C, N and O) of PU. Additionally, for the nanosilver halide hybrid PU samples the peaks for Ag and the respective halides were observed.

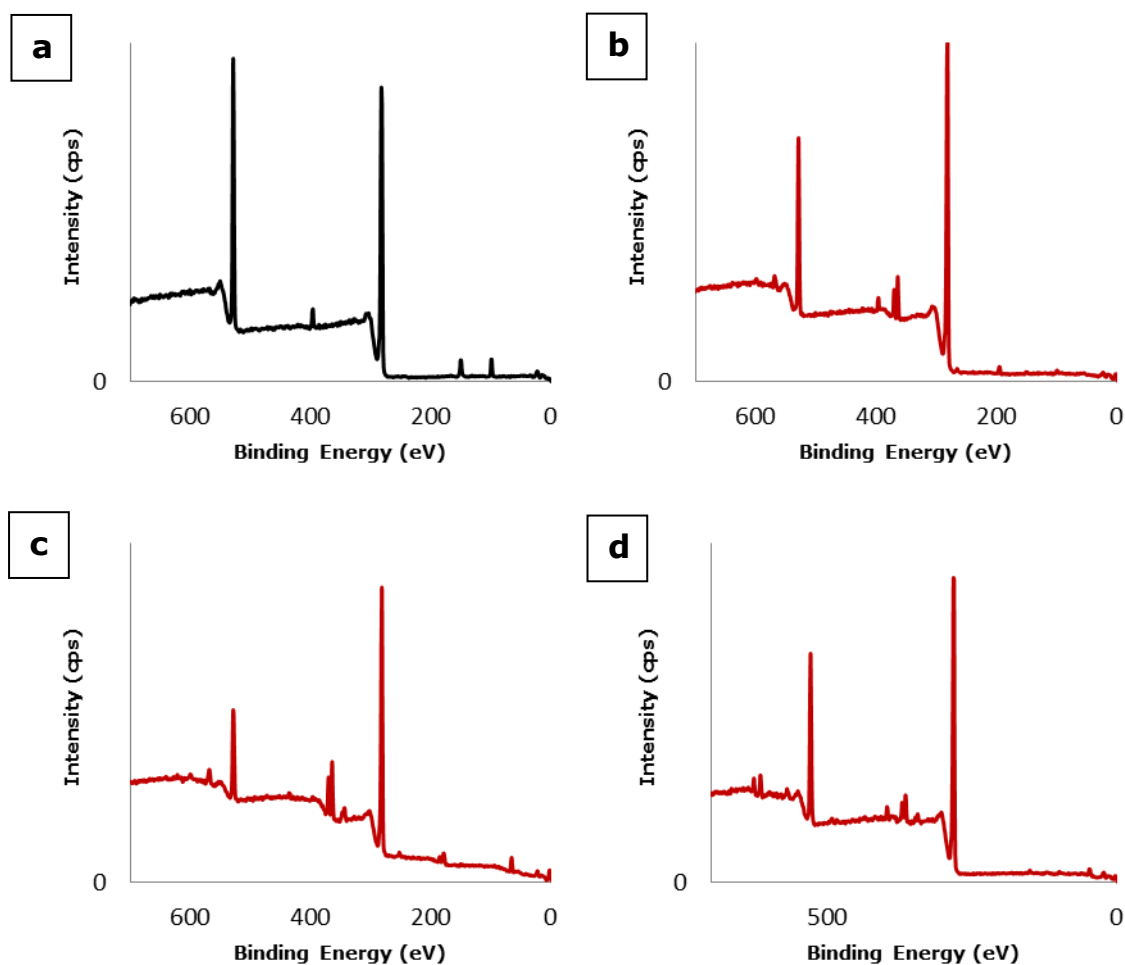


Figure 6.32: Survey XPS scans of a) the PU sheet used as reference sample, b) the PU-200AgCl sample, c) the PU-200AgBr sample and d) the PU-200AgI sample.

The high resolution C 1s, N 1s and O 1s XPS spectra obtained for both samples, the PU reference and nanosilver chloride hybrid PU samples, are presented in Figure 6.33. A complete list of peak assignments is shown in Table 6.4. The analyses of the high resolution C 1s, N 1s and O 1s XPS spectra collected for the PU-200AgCl sample do not show any significant changes in comparison to the spectra obtain for the PU reference sample. In agreement with the literature²⁶⁴, the deconvolution of the C 1s spectrum revealed the presence of four carbon species attributable to an aliphatic carbon bound to an adjacent carbon or a hydrogen (285 eV), a carbon singly bound to a nitrogen (285.7 eV), a carbon singly bound to an oxygen (286.7 eV) and a carbonyl carbon (289.5 eV) in the PU polymer matrix. The deconvoluted, high resolution N 1s spectrum of the

reference (Figure 6.33c) and the PU-200AgCl sample (Figure 6.33d) show the presence of one nitrogen species which is attributable to the nitrogen of the carbamate group in the PU polymer matrix. Just as with the PU reference sample, the XPS O 1s spectrum of the PU-200AgCl sample was deconvoluted into one peak with the maximum at around 532.9 eV and was assigned to the average oxygen environment of PU. The values for the binding energies and the respective FWHM are presented in Table 6.4.

Table 6.4: XPS assignments for the PU sheet as the reference sample and the nanosilver chloride hybrid PU material.

| | | | Reference PU | PU-200AgCl |
|--------------|---------------------|---|-------------------------------------|---------------|
| | | | Binding energy [eV] and (FWHM) [eV] | |
| C 1s | C-C, C-H | | 285.00 (1.02) | 285.00 (1.03) |
| | C-N | | 285.65 (0.65) | 285.74 (0.67) |
| | C-O | | 286.70 (1.16) | 286.64 (1.15) |
| | O-C=O | | 289.43 (1.18) | 289.51 (0.75) |
| N 1s | N-H | | 400.32 (1.34) | 400.31 (1.21) |
| O 1s | Average environment | O | 532.86 (1.75) | 532.91 (1.67) |
| Ag 3d | Ag ⁰ 5/2 | - | - | - |
| | Ag ⁺ 5/2 | - | - | 367.80 (0.88) |
| | Ag ⁰ 3/2 | - | - | - |
| | Ag ⁺ 3/2 | - | - | 373.80 (0.88) |
| Cl 2p | Cl ⁻ 3/2 | - | - | 198.14 (0.86) |
| | Cl ⁻ 1/2 | - | - | 199.74 (0.86) |

Two distinct peaks were observed in the high resolution Ag 3d spectrum relating to the PU-200AgCl sample (Figure 6.34a). The doublet with an intensity ratio of 3:2 shows a spin orbital separation of 6.0 eV which matches the spacing of the bulk silver.^{275,299} According to the literature the peaks centred at ca. 367.8 eV (3d_{5/2}) and 373.8 eV (3d_{3/2}) were assigned to Ag⁺ in form of AgCl^{179,181,334} thereby confirming the formation of silver chloride in the PU matrix.

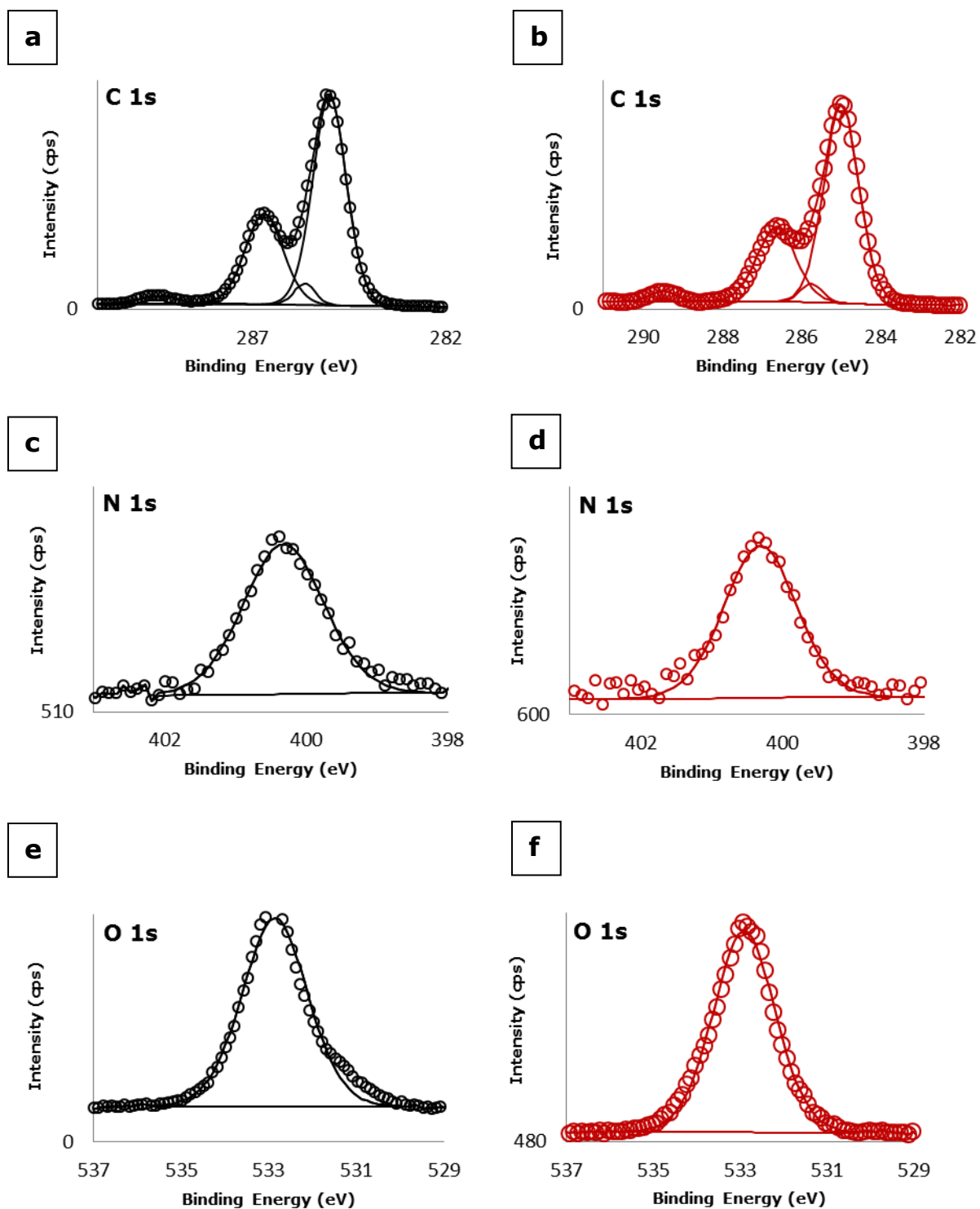


Figure 6.33: Deconvoluted high resolution XPS spectra for the PU sheet used as reference sample: a) C 1s peaks, c) N 1s peak and e) O 1s peaks; for the PU-200AgCl sample: b) C 1s peaks, d) N 1s peaks and f) O 1s peaks. Experimental data points are shown by circles.

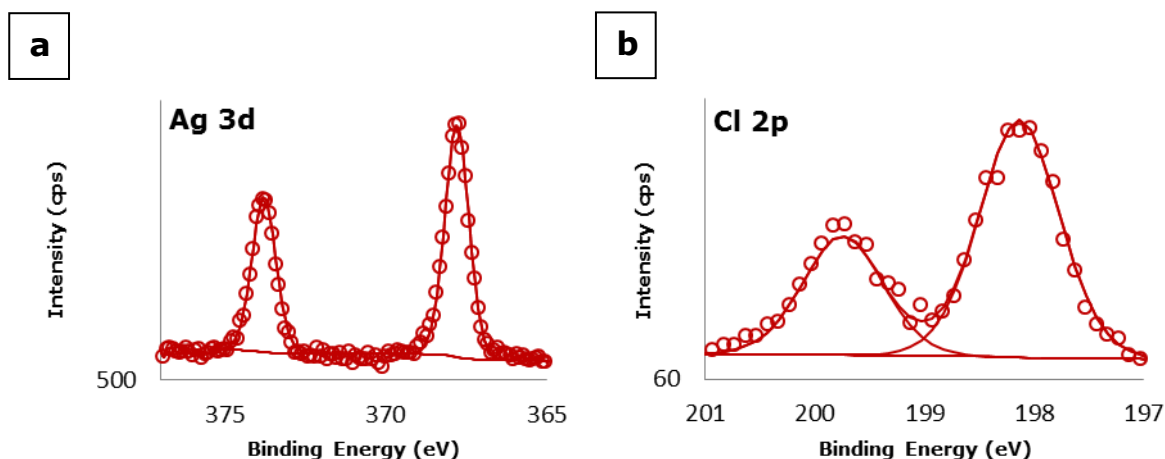


Figure 6.34: Deconvoluted high resolution XPS spectra for the PU-200AgCl sample: a) Ag 3d peaks and b) Cl 2p peaks. Experimental data points are shown by circles.

The high resolution Cl 2p spectrum of the PU-200AgCl sample is presented in Figure 6.34b. The binding energies of Cl 2p_{1/2} and Cl 2p_{3/2} deriving from Cl⁻ are 198.1 eV and 199.8 eV, respectively. The doublet has the required intensity ratio of 2:1 and the spin orbital separation of 1.6 eV. These values are in good agreement with the reported values for AgCl nanoparticles.^{177,179,275,299,335} Hence, the XPS results are in agreement with the results obtained from the SEM and XRD analyses of the PU-200AgCl sample (Sections 6.2.1 and 6.4) further confirming that the AgCl nanoparticles were successfully formed within the PU polymer matrix.

The high resolution C 1s, N 1s and O 1s spectra collected for the nanosilver bromide hybrid PU material (PU-200AgBr sample) and the respective PU reference sample are shown in Figure 6.35. The values for the binding energies and their respective FWHM are given in Table 6.5.

Table 6.5: XPS assignments for the PU sheet as the reference sample and the nanosilver bromide hybrid PU material.

| | | | Reference PU | PU-200AgBr |
|--------------|--------------------------------|---|-------------------------------------|---------------|
| | | | Binding energy [eV] and (FWHM) [eV] | |
| C 1s | C-C, C-H | | 285.00 (0.98) | 285.00 (0.95) |
| | C-N | | 285.59 (0.79) | 285.67 (0.73) |
| | C-O | | 286.74 (1.14) | 286.66 (1.17) |
| | COO-Ag | | - | 288.79 (1.16) |
| | O-C=O | | 289.68 (0.86) | 289.58 (0.80) |
| N 1s | N-H | | 400.43 (1.07) | 400.39 (1.35) |
| O 1s | Average | O | 532.84 (1.56) | 532.84 (1.62) |
| | environment | | | |
| | O-Ag | | - | 531.51 (1.29) |
| Ag 3d | Ag ⁰ _{5/2} | | - | 368.09 (1.18) |
| | Ag ⁺ _{5/2} | | - | 367.86 (0.77) |
| | Ag ⁰ _{3/2} | | - | 374.09 (1.18) |
| | Ag ⁺ _{3/2} | | - | 373.86 (0.77) |
| Br 3d | Br ⁻ _{5/2} | | - | 68.51 (0.83) |
| | Br ⁻ _{3/2} | | - | 69.56 (0.83) |

When comparing the C 1s spectra of the PU-200AgBr sample to the respective PU sheet reference sample (Figure 6.35a-b), it can be clearly seen that the exposure of PU sheet to the sodium bromide solution followed by a treatment of silver nitrate solution leads to changes in relative intensities of the C 1s peaks. The decrease in intensity of the C 1s peak located at approximately 286.7 eV attributable to C-O, and a formation of a new C 1s peak centred at ca. 288.8 eV, indicate that the chemical environment of carbon is perturbed by the presence of the formed AgBr nanoparticles. A reason for the decrease in the intensity of the C 1s peaks for C-O after the formation of AgBr particles, as well as the new peak at higher binding energies is possibly due to a formation of a new interaction between silver and oxygen (Ag-O-C) in the PU matrix. The formation of this Ag-O-C species would induce a charge transfer to the carbon atoms through the oxygen atoms. Hence, this decrease in the intensity results in a change in the chemical environment of carbon. Additionally, it can be assumed that the presence of AgBr nanoparticles on the surface of the PU can also influence the

intensity of the C-O due to a screening effect. Such an effect causes the photoelectrons which are ejected from carbon atoms to be partially trapped by the silver bromide present on the surface of PU. Similar behaviour regarding the decrease in the intensity of components in an XPS spectrum has been reported previously in the literature.^{314,336}

The N 1s spectrum of the nanosilver bromide hybrid PU sample, when compared to the PU reference sample (Figure 6.35c-d), sees a minimal broadening of the FWHM by around 0.3 eV. The increase in the FWHM of the nitrogen in the carbamate group of the PU indicates a variability of the environments surrounding these N entities. Thus, an interaction between the formed AgBr and N is possible.

Figure 6.35f shows the envelope of the O 1s spectrum for the PU-200AgBr sample with one maximum and an apparent shoulder towards lower binding energies. The spectrum was deconvoluted into two oxygen components. The peak at higher binding energies, at ca. 532.8 eV, is attributable to the average oxygen environment of the PU matrix. When comparing this O 1s peak to that of the PU sheet reference sample (Figure 6.35e), the position of the peak remains comparable. However, a slight increase in the FWHM value of this peak means that more varied surrounding environment for the oxygen is provided upon formation of the AgBr in the PU matrix. The second peak located at approximately 531.5 eV is indicative of a formation of a new oxygen species which was ascribed to a Ag-O-C bond. Compounds containing Ag-O-C bonds have been shown to possess binding energies of around 531.5 eV.^{314,337,338} This supports the statement for the C 1s spectrum made above, further confirming the formation of the new interaction between silver and oxygen upon formation of the AgBr nanoparticles in the polymer matrix.

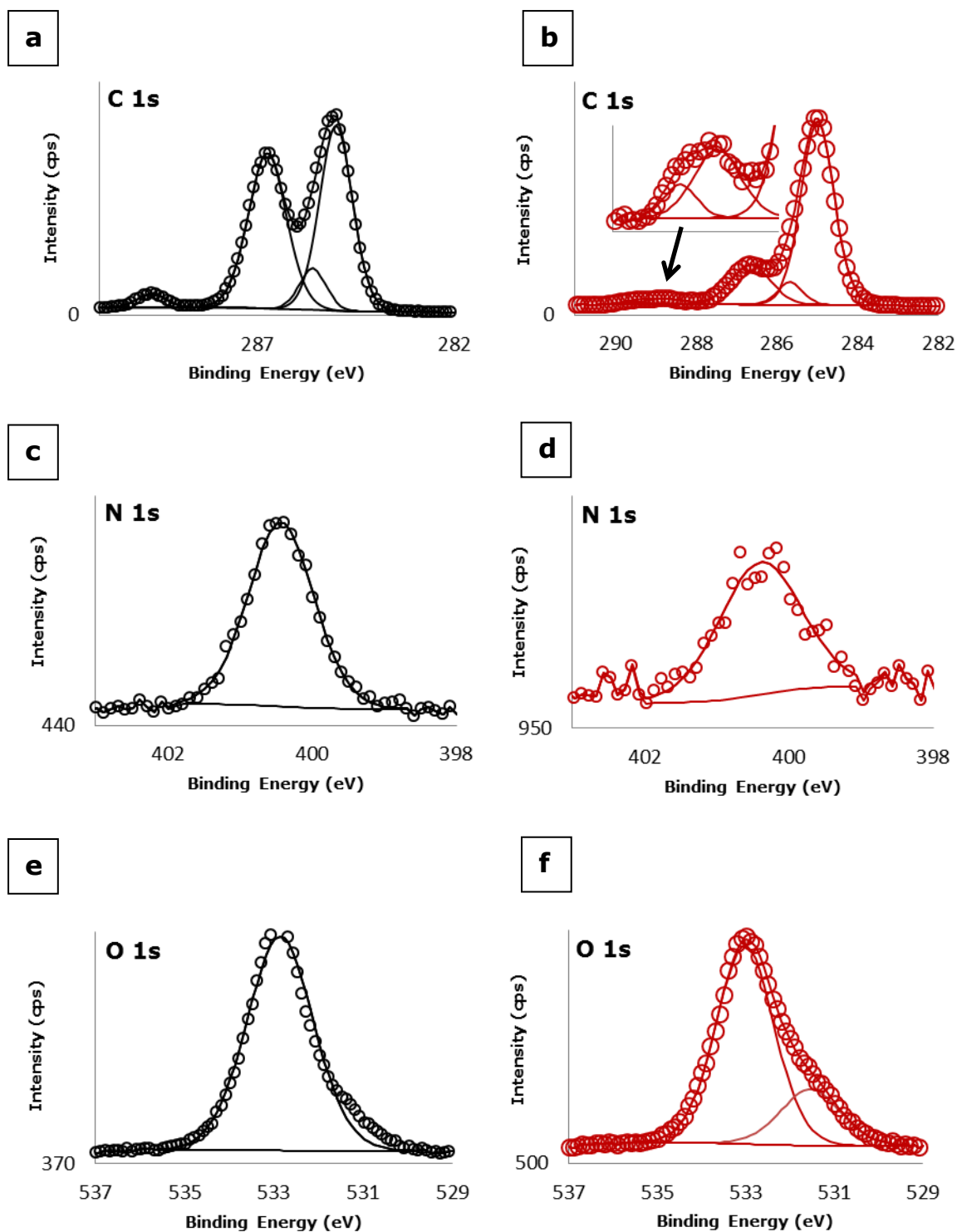


Figure 6.35: Deconvoluted high resolution XPS spectra for the PU sheet used as reference sample: a) C 1s peaks, c) N 1s peak and e) O 1s peaks; for the PU-200AgBr sample: b) C 1s peaks, d) N 1s peaks and f) O 1s peaks. Experimental data points are shown by circles.

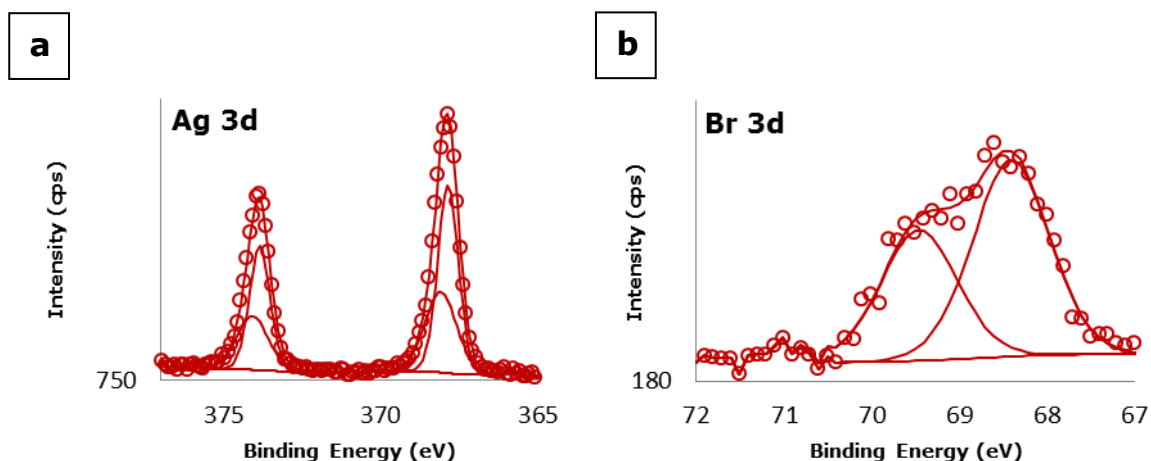


Figure 6.36: Deconvoluted high resolution XPS spectra for the PU-200AgBr sample: a) Ag 3d peaks and b) Br 3d peaks. Experimental data points are shown by circles.

The high resolution Ag 3d XPS spectrum for the nanosilver bromide hybrid PU sample (PU-200AgBr) is shown in Figure 6.36a. The deconvolution of the line shape resulted in two doublets, implying that two different species of silver are present in the sample. Both doublets with an intensity ratio of 3:2 show a spin orbital separation of 6 eV matching the spacing of the bulk silver.^{275,299} The doublet peaks at lower binding energies, namely at ca. 367.9 eV ($3d_{5/2}$) and 373.9 eV ($3d_{3/2}$), have been ascribed to Ag^+ in AgBr.^{182,275,299,339} A second set of broader doublet peaks centred at around 368.1 eV ($3d_{5/2}$) and 374.1 eV ($3d_{3/2}$) respectively, is indicative of the existence of metallic silver.^{182,275,299,339} The sample was protected from light during the preparation process; however the chamber storing the samples during the XPS analyses has a glass window. Thus, a photolysis of the sample which results in a formation of Ag^0 nanodomains on the surface of the AgBr particles cannot be ruled out. Such nanodomains were observed in the TEM analyses of hybrid polymer materials containing Ag/AgBr nanoparticles (Section 6.3). The spectrum of the Br 3d electrons in Figure 6.36b shows that the binding energies of Br $3d_{5/2}$ and Br $3d_{3/2}$ are approximately 68.5 eV and 69.5 eV respectively. These values match well the values for Br^- in AgBr found in the literature.^{175,179}

Figure 6.37 presents the high resolution C 1s, N 1s and O 1s spectra obtained for the nanosilver iodide hybrid PU material (PU-200AgI sample) and for the

respective PU reference sample. The values for the binding energies and their respective FWHM are given in Table 6.6.

Again comparing the high resolution XPS C 1s spectra for the PU-200AgI and the PU reference sample revealed similar changes observed for the PU-200AgBr sample (Figure 6.37a-b). The Ag-O-C bond was evident in the high resolution C 1s spectrum of the hybrid PU material incorporating AgI nanoparticles. The spectrum showed a new peak centred at 288.7 eV, which was absent in the PU reference sample. This peak has been reported to be representative of a Ag-O-C bond.^{340,341} Additional changes to the spectrum upon formation of the AgI nanoparticles included the decrease in intensities of the C-O and C-N peak respectively. As mentioned previously, the decrease may have been caused by the formation of a new interaction of oxygen and nitrogen groups in the PU matrix with the silver iodide nanoparticles. The new bonds (Ag-O-C or Ag-N-C) induce a charge transfer to the carbon atoms through the oxygen and nitrogen atoms respectively resulting in a change in the chemical environment of carbon and thus causing the decrease of the intensities.

The N 1s spectrum of the PU-200AgI sample, when compared to the PU reference sample, shows a new peak which was not present in the reference sample (Figure 6.37c-d). This peak exhibits a shift of ca. 0.8 eV towards lower binding energies from the N 1s peak of the reference sample consistent with the nitrogen of the carbamate groups in PU found in both samples. The peak may suggest a further interaction of silver from the AgBr particles to the nitrogen groups of PU. As previously reported in Chapters 3 and 4, nitrogen has an affinity for silver.^{241,313} Thus, an Ag-N-C bond is likely.

Table 6.6: XPS assignments for the PU sheet as the reference sample and the nanosilver iodide hybrid PU material.

| | | | Reference PU | PU-200AgI |
|--------------|--------------------------------|--|-------------------------------------|---------------|
| | | | Binding energy [eV] and (FWHM) [eV] | |
| C 1s | C-C, C-H | | 285.00 (0.99) | 285.00 (1.12) |
| | C-N | | 285.65 (0.60) | 285.87 (0.79) |
| | C-O | | 286.71 (1.13) | 286.78 (1.15) |
| | COO-Ag | | - | 288.72 (1.37) |
| | O-C=O | | 289.62 (0.88) | 289.51 (0.75) |
| N 1s | N-H | | 400.40 (1.17) | 400.41 (1.16) |
| | N-Ag | | - | 399.59 (1.53) |
| O 1s | Average O environment | | 532.80 (1.63) | 532.90 (1.70) |
| | COO-Ag | | - | 531.22 (1.19) |
| | | | | |
| Ag 3d | Ag ⁰ _{5/2} | | - | 368.01 (1.09) |
| | Ag ⁺ _{5/2} | | - | 366.68 (0.77) |
| | Ag ⁰ _{3/2} | | - | 374.01 (1.09) |
| | Ag ⁺ _{3/2} | | - | 372.68 (0.77) |
| I 3d | I ⁻ _{5/2} | | - | 619.06 (1.38) |
| | I ⁻ _{3/2} | | - | 630.56 (1.38) |

The high resolution O 1s spectra for the nanosilver iodide and the respective PU reference sample are shown in Figure 6.37e-f. For the PU-200AgI sample the XPS O 1s spectrum was deconvoluted into two oxygen components. The position of the peak owing to the average oxygen environment of the PU remains at 532.9 eV, the same position as the PU reference sample. The new peak at a lower binding energy, 531.2 eV, again indicates significant changes in the surrounding environment. It suggests an interaction of oxygen to silver of the AgI nanoparticles, a potential Ag-O-C bond which was also detected for the PU-200AgBr sample. This complements the observation made for the C 1s spectrum above.

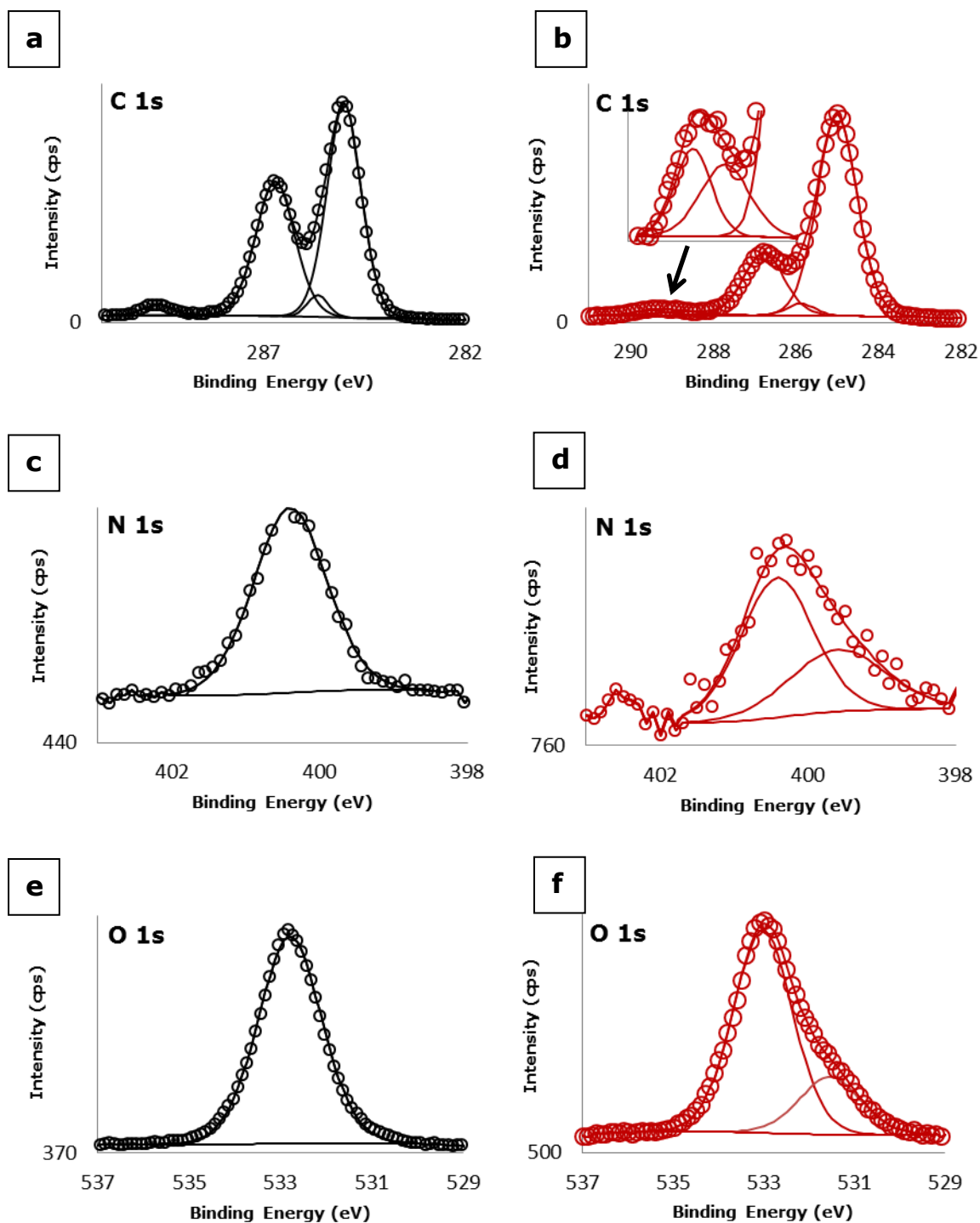


Figure 6.37: Deconvoluted high resolution XPS spectra for the PU sheet used as used as reference sample: a) C 1s peaks, c) N 1s peak and e) O 1s peaks; for the PU-200AgI sample: b) C 1s peaks, d) N 1s peaks and f) O 1s peaks. Experimental data points are shown by circles.

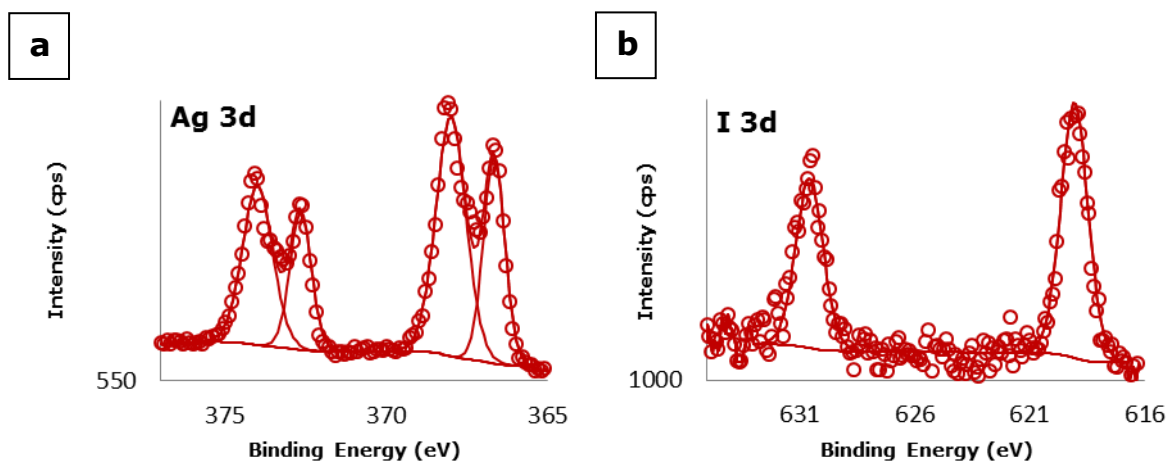


Figure 6.38: Deconvoluted high resolution XPS spectra for the PU-200AgI sample: a) Ag 3d peaks and b) I 3d peaks. Experimental data points are shown by circles.

The high resolution Ag 3d spectrum of the PU-200AgI sample is presented in Figure 6.38a. The deconvolution of the spectrum revealed two sets of doublet peaks. The peaks centred at 366.68 eV ($3d_{5/2}$) and 372.68 eV ($3d_{3/2}$) relate to Ag^+ of the AgI nanoparticles.^{182,275,299,339} According to the literature, the doublet positioned at higher binding energies, around 368.0 ($3d_{5/2}$) and 374.0 ($3d_{3/2}$) eV, is attributable to Ag^0 .^{182,275,299,339,342} This suggests that silver ions of the AgI nanoparticles were converted to Ag^0 nanodomains via the photolysis process, similar to the PU-200AgBr sample described above. Both doublets have the required intensity ratio of 3:2 and the spin orbital separation of 6.0 eV.^{275,299} Figure 6.38b shows the high resolution I 3d spectrum. It can be seen that the doublet possesses binding energies of ca. 619.1 eV ($3d_{5/2}$) and 630.6 eV ($3d_{3/2}$), matching the values found in the literature for the I^- as AgI well.^{343–346} As such, this further confirms that silver iodide nanoparticles have been successfully formed within the PU matrix.

From the XPS results discussed above, it can be concluded that silver halide nanoparticles have been successfully produced *in situ* within the PU polymer matrix. The PU polymer matrix provides stabilisation of the halide nanoparticles. XPS results show that the hybrid PU materials containing AgBr and AgI nanoparticles respectively underwent a photolysis process resulting in a

formation of Ag^0 nanodomains on the surface of these silver halide nanoparticles. The C 1s and O 1s spectra for these materials imply an interaction between the silver on the surface of the silver bromide and iodide respectively and the oxygen groups present within the PU matrix. In addition to silver - oxygen interaction, nitrogen is also implied to interact with the silver on the silver iodide nanoparticles. This interaction is suggested by the position of the new N 1s peak of the nanosilver iodide hybrid PU material.

6.6 Infrared spectroscopy analysis of nanosilver halide hybrid polymer materials

Infrared spectroscopy analyses were carried out in an attempt to complement the XPS results obtained from the nanosilver halide hybrid polymers (Section 6.5). It was hoped get a clarification on the nature of the interaction between the silver halide nanoparticles and the polymer matrix. The K5000-1000AgCl, K5000-1000AgBr and K5000-1000AgI samples were chosen as representatives of the nanosilver halide hybrid PU K5000 materials. Because these materials have higher concentration of silver halide particles at the hybrid polymer surfaces, the probability of detecting any changes between the IR spectra of an untreated PU K5000 sample and its respective hybrid polymers is increased.

The IR spectra of the untreated PU K5000, K5000-1000AgCl, K5000-1000AgBr and K5000-1000AgI samples are presented in Figure 6.39. When comparing the IR spectra of the untreated PU K5000 sample to the nanosilver halide hybrid U K5000 samples no distinguishable differences can be observed. All four samples show identical peaks characteristic for PU (Section 3.9). As such, the IR spectroscopy analysis of these materials did not provide any further indication on the nature of the interaction between the silver halide nanoparticles and the polyurethane K5000 polymer matrix. This is probably due to the fact that IR spectroscopy is a bulk analysis method on such samples, and is not particularly sensitive to the small quantity of nanoparticles present on the surface of the polymer relative to the bulk quantity of the paint.

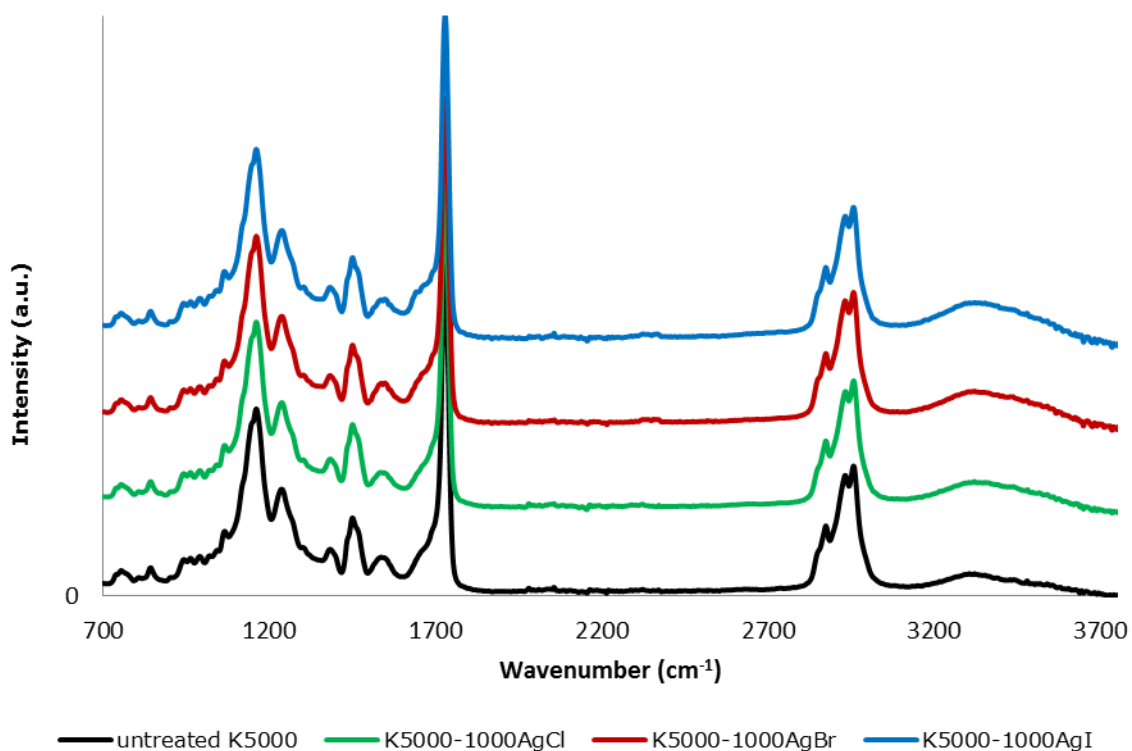


Figure 6.39: FT-IR spectra of the dry untreated PU K5000 paint base and the nanosilver halide hybrid polyurethane K5000 latex paint base materials.

6.7 Antimicrobial properties of nanogold and nanosilver hybrid polymer materials

In recent years the availability of medicines to treat infections effectively with resistant organisms has become a major concern. As mentioned in Chapters 3 and 4, the creation of new antimicrobial materials has attracted increasing interest in order to combat the challenge of antimicrobial resistance. Silver and silver compounds have a great potential as antimicrobial agents and have been used as such for many centuries. They have low toxicity toward mammalian cells and do not easily provoke microbial resistance.³⁴⁷ Hence, the nanosilver halide hybrid polymer materials were tested for their antimicrobial activity. In order to see whether the photolysis of the samples would influence their antimicrobial activity, two sets of samples were prepared and tested. For the duration of the preparation and testing process respectively, one set of the samples was

prepared under natural light exposure while the other set was prepared in dark conditions. Due to the time limitations, only nanosilver halide hybrid PU K5000 materials were tested against the gram negative *E. coli* bacteria (strain W3110). The tests were carried out following the technique described in Section 2.3.8. However briefly, this included cutting the dried films of the K5000-1000AgCl, K5000-1000AgBr and K5000-1000AgI samples into small pieces and immersing them in aqueous standard phosphate-buffered saline (PBS) suspension containing *E. coli* bacteria in order to create a contact between the hybrid polymer materials and the microbes. The determination of the antimicrobial activity was achieved on the basis of the relative difference in total colony-forming units (CFU) between the nanosilver halide hybrid PU K5000 samples and the control sample after five days of contact with the bacteria. As the control sample the dry untreated polyurethane K5000 polymer was used.

The graphical result of the antimicrobial test is provided in Figure 6.40 illustrating the percentage of CFU remaining after the reference sample and the nanosilver halide hybrid PU K5000 samples were exposed to bacteria for five days. Table 6.7 represents the obtained CFU values for the nanosilver halide hybrid PU K5000 materials. As expected, the untreated PU K5000 sample used as the reference did not show any effect on the bacteria. When analysing the results obtained for both sets of samples, which were tested in natural light and in dark conditions, the samples containing silver chloride nanoparticles seem to show higher efficacy against the bacteria compared to the samples containing silver bromide nanoparticles. AgBr-containing samples, in turn, are more antimicrobial than their analogue AgI-containing samples. Despite many recent publications on the antimicrobial activity of silver, silver compounds and their polymer composites, the exact mechanism still remains unclear. The proposed modes of action for silver towards the microbes that have been reported in the literature are discussed in detail in Sections 1.4.6 and 3.1.11. It has been accepted that the antimicrobial effects of silver depend on the dissolution rate of silver nanoparticles and silver compounds, releasing the effective silver ions into the pathogenic environment.^{217,348} Hence, the reason for the greater antimicrobial activity of the hybrid materials containing AgCl nanoparticles over those containing the AgBr and AgI particles respectively could be due to their

corresponding solubility constants. The solubility constants of some silver compounds are given in Table 1.5.

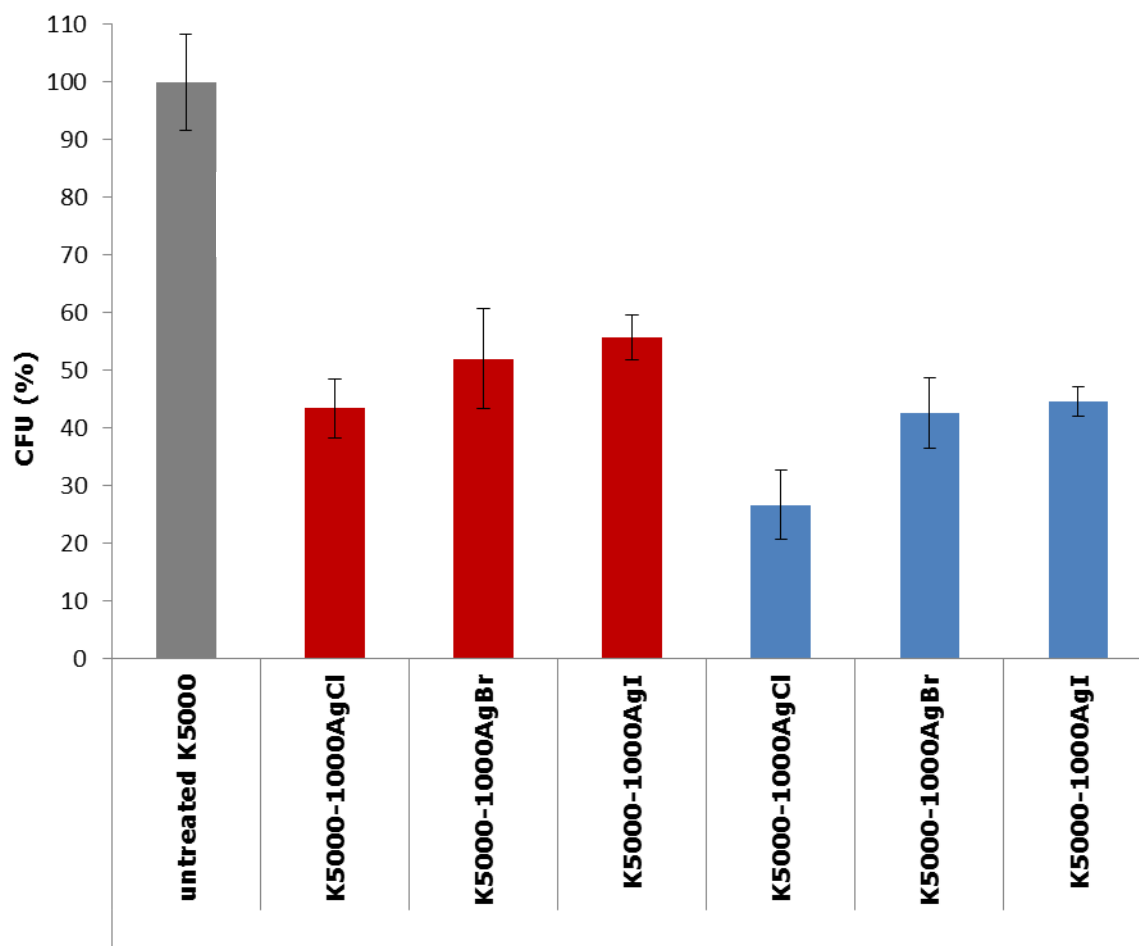


Figure 6.40: Percentage cell survival relative to untreated PU K5000 paint as control after five days of bacteria being in contact with the control and the nanosilver halide hybrid PU K5000 samples. The bars depicted in red represent the samples tested in dark conditions, whereas the bars depicted in blue relate to the samples tested in natural light. (Note the vertical axis is in log scale.)

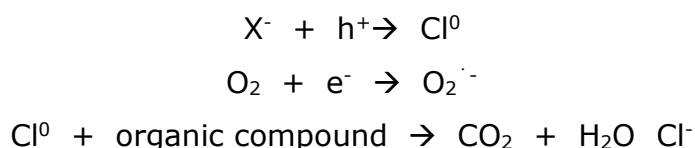
Table 6.7: Remaining percentage of *E. coli* CFU after being in contact with the nanosilver halide hybrid PU K5000 materials for five days.

| | K5000-1000AgCl | K5000-1000AgBr | K5000-1000AgI | K5000-1000AgCl | K5000-1000AgBr | K5000-1000AgI |
|--|-------------------------|----------------|---------------|---------------------------|----------------|---------------|
| | Tested in natural light | | | Tested in dark conditions | | |
| CFU after 5 days of testing against <i>E. coli</i> [%] | 43 | 52 | 56 | 27 | 43 | 45 |

When comparing the samples which were tested in dark conditions to their analogue samples tested in natural light, it is clearly observable the nanosilver halide hybrid PU K5000 samples tested in the natural light are more effective against *E. coli* than the analogue samples tested in dark conditions. As previously mentioned, as a result of their photosensitive characteristic silver halide nanoparticles are not stable under light irradiation. The absorption of a photon by the semiconductor AgX results in the corresponding generation of an electron and a positive hole. The formed electron will combine with an interstitial silver ion to form a separate silver atom. With repeating cycles of light absorption partial reduction of Ag^+ will lead to formation of Ag^0 nanodomains on the surface of the AgX particles. As such, the enhanced antibacterial activity of the hybrid materials may be correlated with the release of the silver ions deriving both from silver halide nanoparticles and from metallic silver nanoparticles present on the AgX surface.

Silver/silver halide nanoparticles have been found to be active in visible light photocatalysis and progressively used as plasmonic photocatalysts. These materials have been reported to show excellent photocatalytic performance in the degradation of dyes, decomposition of harmful organic compounds and killing microorganisms.^{175,177,342,348,349} The literature suggests the mechanism for the degradation of these organic compounds is through radical formation. When

excited by light the electron-hole pair is created in the Ag/AgX system which then separates and migrates to the Ag and AgX regions of the particle respectively. Then both the electron and hole induce the radical formation. In an aqueous environment, the Ag^0 region forms super oxide and other radical oxygen species that are able to oxidise and therefore degrade the organic compounds by the reduction of dissolved oxygen in solution.^{225,335,348,349} Additionally, in a similar manner the hole in the AgX region forms X^0 radical species. These X^0 radical species are also able to degrade organic compounds by becoming reduced to halide ions again.^{168,174,178} Some examples for free radical formations are shown in the chemical equations below:



Hence, the enhanced antimicrobial activity of the nanosilver halide hybrid polyurethane K5000 latex paint base materials under exposure to light may be due to the photocatalytic destruction of microbial cells by formed radical species. Nevertheless, detailed investigations are required on the releasing mechanism of silver from the nanosilver halide hybrid polyurethane K5000 latex paint base materials as well as on formation of radical species.

The nanosilver halide hybrid materials may find use as antimicrobial coatings for a wide variety of applications in the health and biomedical device industry, food industry, and personal hygiene industry.

6.8 Conclusions

Nanosilver halide hybrid polymer materials were successfully produced using the synthesis procedures outlined in Section 2.2.3. The polymer matrices included polyurethane, nylon 6,6 and PU K5000 latex paint base. The silver halide nanoparticles were formed within the polymer matrices which provided simultaneously stabilisation for these nanoparticles.

Owing to their wide band gaps silver chloride and silver bromide are not able to absorb light in the visible region. However, silver iodide absorbs light in the visible region. As such, nanosilver chloride and bromide hybrid polymers were white in colour; silver iodide containing hybrid polymer materials had slight yellow colouration. Because silver halide nanoparticles are photo-sensitive materials, upon exposure to light silver halide hybrid polymers changed in colour. In a self-photosensitisation process the Ag^+ in the AgX are partially reduced to Ag^0 nanodomains or nanoparticles at the surface of the AgX nanoparticles and small amounts of halides as their respective halogen gas are released.^{168,319} UV-Vis spectroscopy analyses of the nanosilver halide hybrid nylon 6,6 materials have shown that the samples containing AgCl and AgBr nanoparticles exhibit the characteristic absorbance in the UV region. Once exposed to light, the samples exhibit the absorbance in the UV and also in the visible region of light. The visible light absorbance is due to the SPR effect of the silver nanodomains formed at the AgX nanoparticle surface. It was demonstrated that the absorption peaks in the visible region of light are broad indicating the existence of a variety of silver nanoparticle sizes and shapes. These samples were purple-brown in colour. For the nanosilver iodide hybrid nylon 6,6 sample there was no obvious difference in the UV-Vis spectra after exposure to light which was ascribed to the low susceptibility of AgI to photolysis when compared to AgCl and AgBr.

Electron microscopy analyses of the nanosilver halide hybrid polymer materials showed that silver halide particles were formed on the surface and within the polymer substrates. It was shown that a higher number of silver halide particles are formed just below the surface compared to the centre of the polymer

substrates. In the case of polyurethane as the substrate, the AgCl particles were varying in size between less than about 100 nm and up to about 1000 nm. Mostly the AgCl particles were found as cubes covered by non-uniform shaped and sized silver nanoparticles as a result of self-photosensitisation process. The AgBr particles were found to have irregular shapes and sizes, ranging from less than 100 nm to two hundred nanometres. For the nanosilver iodide hybrid PU materials the particles were mostly found on the surface of the polymer. For the nylon 6,6 samples the AgCl particles with non-uniform shapes were generally smaller than 100 nm. Occasionally some larger AgCl particles as well as particle agglomerates were observed. The AgX particles with a wide variety of shapes and sizes found in the nanosilver halide hybrid PU K5000 materials were well distributed within the PU K5000 matrix. The K5000-1000AgCl sample showed the presence of the AgCl nanoparticles between 15 and 100 nm in size. For the K5000-1000AgBr sample the formed AgBr nanoparticles were between 40 and 500 nm in size, whereas the AgI particles in the K5000-1000AgI sample ranged from 20 nm to 500 nm in size. Upon exposure to light, it was shown that all AgX particles possessed non-uniform shaped silver nanoparticles formed on their surfaces.

The XRD studies of these materials before exposure to direct light confirmed the presence of crystalline silver halides within the PU and polyurethane K5000 materials. No diffraction peaks were detected for the nanosilver halide nylon 6,6 materials presumably due to the low concentration of AgX particles in the polymer matrix. After being exposed to light the nanosilver halide hybrid PU and PU K5000 materials showed the presence of metallic silver which is due to the photosensitive characteristics of silver halide nanoparticles. The samples containing AgCl nanoparticles were more susceptible to light than those containing AgBr nanoparticles. The longer the samples were exposed to light the more silver halide was converted to metallic silver.

XPS studies suggest an interaction between the silver on the surface of the AgX nanoparticles and the nitrogen and oxygen groups present in the PU matrix.

Nanosilver halide hybrid polymer materials were shown to exhibit antimicrobial performance against the gram negative *E. coli* bacteria. The K5000-1000AgCl

sample was more effective against the bacteria than the K5000-1000AgBr which in turn killed more bacteria than the K5000-AgI sample. This fact was attributed to the relative solubilities of the silver halides which are responsible for the dissolution of different amounts of active Ag^+ ions. The samples which were tested in direct light in comparison with the samples tested in dark conditions showed greater antimicrobial activity. The enhanced antibacterial activity of these hybrid materials is correlated with the release of the silver ions originating from silver halide nanoparticles and from metallic silver nanoparticles present on the AgX surface which are formed in the direct light.

7 Summary of Thesis

This thesis has been focused on the synthesis of the new generation hybrid polymer materials and the characterisation of their novel optical, antimicrobial and antifouling properties.

7.1 Nanogold and nanosilver hybrid polyurethane and nylon 6,6, materials

Nanogold and nanosilver hybrid polyurethane and nylon 6,6 polymer materials have been successfully synthesised. For the redox reaction the carbamate and amide functional groups in PU and nylon 6,6 matrices respectively have been used to reduce Au^{3+} or Ag^+ to Au^0 or Ag^0 . Simultaneously, the polymer matrices stabilise the metal nanoparticles. The formed gold or silver nanoparticles are chemically bound to the surface and within the polymer matrix of PU or nylon 6,6. The resultant hybrid materials exhibit the characteristic pink/purple and yellow/brown colours for gold and silver nanoparticles respectively due to their surface plasmon resonance effects. The reaction took place at 50 °C and 90 °C for the reduction of gold and silver ions respectively to metal nanoparticles. After 24 hours the atomic absorption analyses demonstrated that the majority of gold and more than 60 % of silver ions were absorbed by the polymer substrates. The reaction parameters, such as time, temperature and the concentration of the metal ion solution influenced the uptake rate of Au^{3+} / Ag^+ by the substrates and therefore the resultant colours of the hybrid materials. The hybrid polymer materials exhibit the characteristic SPR bands in the visible region of light for gold and silver. Increased metal ion contents in the solution for the synthesis of the hybrid polymer materials resulted in the peak broadening and peak shifts towards higher wavelengths reflecting the increase of the particle size and indicating the presence of particle agglomerations.

Electron microscopy studies of the nanogold and nanosilver hybrid PU and nylon 6,6 materials have shown that the metal nanoparticles are formed on the surfaces and within the polymer matrices. The polymer interior provided better stabilisation of the nanoparticles resulting in smaller particle size compared to the particles found on the surface of the polymers. Silver nanoparticles are smaller than gold nanoparticles in both PU and nylon 6,6 substrates. The particles found in the PU polymer are larger than the analogue hybrid nylon 6,6 materials which is believed to be due to the higher amount of metal ion uptake by PU compared to nylon 6,6 substrates. The gold nanoparticles in the hybrid polymer materials are spherical or spherical like in shape, few hexagonal, truncated triangular and rod shaped particles are also present. Silver nanoparticles are predominantly spherical.

XPS studies suggest the gold and silver nanoparticles bind to the PU or nylon 6,6 matrix through the covalent Au-N and Ag-N bonds respectively in the nitrogen-containing carbamate or amine groups. There is also an ionic interaction between the unreduced negatively charged $[\text{AuCl}_4]^-$ complex and the protonated nitrogen groups of nylon 6,6.

The proposed mechanism of formation of the nanogold hybrid polyurethane and nylon 6,6 materials involves the reduction of Au^{3+} in the $[\text{AuCl}_4]^-$ complex to nanoparticulate Au^0 by the coupled oxidation of the carbamate groups of PU or amide groups of nylon 6,6. During the reaction some of the Au^{3+} ions will be reduced to Au^+ by the nitrogen groups, forming the Au-N bonds and acting as nucleation sites. Further Au^{3+} are attracted to these Au-N nucleation sites where they are reduced to Au^0 , facilitated by the oxidation of adjacent nitrogen groups of the polymers. As a result of their affinity for nitrogen, silver ions interact with nitrogen groups in carbamates or amides. Additionally, the interaction between the silver ions and oxygen atoms of the polymer matrices is likely. Nitrogen entities are oxidised and provide the electrons for Ag^+ ions to be reduced to Ag^0 , resulting in the formation of silver nanoparticles in the polymer matrix. The matrix restricts the size of the nanoparticles. The leaching tests have confirmed that the gold and silver nanoparticles are chemically bound to the polymer matrix. Only a very small amount of gold and silver leached out of the hybrid PU

materials within seven days of testing. These amounts are likely due to loosely bound gold or silver nanoparticles on the surface of the polymers.

The nanogold and nanosilver hybrid polyurethane materials exhibit antimicrobial properties against gram negative *E. coli* bacteria. The production of the nanogold and nanosilver hybrid PU materials has been scaled up to produce larger amounts of the materials which were moulded into *dog bone* test strips via a conventional thermoplastic moulding process by the Centre for Advanced Composite Materials and the Plastics Centre of Excellence at the University of Auckland. The test strips show that the metal nanoparticles are distributed evenly through the moulded plastic, confirming that these nanoparticles do not affect the thermoplastic forming properties of the polymer substrates.

7.2 Nanogold and nanosilver hybrid polyethylene terephthalate and silica based BULK ISOLUTE® SORBENTS (NH₂)

In order to build up a simple model for the confirmation of the nitrogen's chemical affinity for gold and silver amine coated polyethylene terephthalate sail cloth and silica based Bulk isolate® sorbent (NH₂) were utilised as alternative substrates for the production of hybrid materials. UV-Vis, SEM, XRD and XPS analyses demonstrated that the nitrogen-containing functional groups in these substrates are able to reduce Au³⁺ and Ag⁺ to Au⁰ and Ag⁰ respectively and subsequently bind the resultant metal nanoparticles to the substrate matrix.

7.3 Nanogold and nanosilver hybrid polyurethane K5000 latex paint base materials

Nanogold and nanosilver hybrid PU K5000 polymer materials have been successfully produced. In the redox reaction the carbamate functional groups of the PU K5000 material have been utilised to reduce *in situ*, the Au³⁺ or Ag⁺ to

Au^0 or Ag^0 respectively. The formed metal nanoparticles are chemically bound to the polymer matrix of the PU K5000 paint. The polymer matrix provides stabilisation for these gold and silver nanoparticles. The reaction took place at room temperature for 24 hours. The hybrid PU K5000 materials were produced at two dilutions, one set of samples (5g of liquid K5000 paint) has been produced from a 2.5 ml Au^{3+} / Ag^+ solution and the second set from a 1.25 ml metal ion solution whilst the polymer to metal ion ratio for these samples was kept constant. The reaction parameters, such as time and the concentration of the utilised metal ion solution influenced the extent of nanoparticle formation and hence the colour of the resultant hybrid PU K5000 materials. The nanogold and nanosilver hybrid polyurethane K5000 materials have the characteristic SPR bands for gold and silver nanoparticles in the visible region of light. The SPR absorption bands of the nanogold hybrid PU K5000 samples prepared from a 2.5 ml Au^{3+} solution are comparable to the SPR bands of the samples prepared from a 1.25 ml Au^{3+} solution. The nanosilver hybrid polyurethane K5000 samples prepared from the 2.5 ml Ag^+ solution show a red shift and an increase in FWHM of the respective absorption peaks suggesting a broader particle size distribution and particle agglomeration.

The electron microscopic analyses of the nanogold and nanosilver hybrid PU K5000 materials demonstrate that the metal nanoparticles are uniformly distributed in the PU K5000 polymer phase and not the water phase of the paint formulation. The gold ($\sim 20 - 40$ nm) and silver ($\sim 10 - 60$ nm) nanoparticles are mostly spherical.

The XRD studies of these materials confirm the presence of crystalline gold / silver within the hybrid PU K5000 materials. The mean crystallite size of the formed metal nanoparticles increases with increased concentration of employed ion solutions, and with the increased water content of those solutions. The XPS studies suggest the gold and silver nanoparticles bind to the PU K5000 matrix through the covalent Au-N and Ag-N bonds respectively to the nitrogen-containing carbamate functional groups. The proposed mechanism of formation of the nanogold and nanosilver hybrid PU K5000 materials when metal ion solution is added to the PU K5000 latex paint base is believed to be the same one as for the formation of gold and silver nanoparticles in the hybrid

polyurethane materials as described in Section 7.1. Briefly, the metal ions are reduced by a coupled oxidation reaction of the carbamate groups in PU resulting in the formation of a new NO_x species in the polymer matrix. The polymer matrix ensures the stabilisation of formed gold and silver nanoparticles in these materials. The leaching tests confirm the integrity of the chemical bond between the gold and silver nanoparticles and the polymer matrix. Only a very small amount of gold and silver leached out of the hybrid PU K5000 latex paint base materials after seven days of leaching. These amounts are believed to be due to residual unreduced gold or silver ions which are trapped in the polymer matrix. The production of the nanogold and nanosilver hybrid PU K5000 materials has been scaled up to produce larger amounts of the paints which were successfully tested by The Polymer Group Ltd in Auckland for their antifouling properties. Furthermore these materials show antimicrobial effects against gram negative *E. coli* bacteria.

7.4 Nanosilver halide hybrid polyurethane, nylon 6,6 and PU K5000 latex paint base materials

Nanosilver halide hybrid polymer materials have successfully produced. Polyurethane, nylon 6,6 and PU K5000 latex paint base have been used as substrates. The substrate matrices were first doped with Cl^- , Br^- or I^- (X^-) ions and the reaction is completed by addition of silver nitrate solution. The mechanism of particle formation within the polymer matrix is believed to be one of precipitation of nanosize particles of AgX , with size control and stabilisation of the particles being mediated by the polymer itself. Due to their wide band gaps silver chloride and silver bromide do not absorb light in the visible region. Silver iodide, however, absorbs light in the visible region. As such, nanosilver chloride and bromide hybrid polymers are white in colour; nanosilver iodide hybrid polymer materials have yellow colouration. Silver halide nanoparticles are photo-sensitive, as such, upon exposure to light, silver halide hybrid polymers change in colour. In a self-photosensitisation process the Ag^+ in the AgX are partially reduced to Ag^0 nanodomains or nanoparticles at the surface of the AgX

nanoparticles and small amounts of halides as their respective halogen gas are released. The UV-Vis spectroscopic analyses of the nanosilver chloride and bromide hybrid polymer materials have shown that the samples exhibit the characteristic absorbance peaks for AgCl and AgBr respectively in the UV region. After exposure to light, the samples exhibit an absorbance in the UV and the visible region of light. The visible light absorbance is due to the SPR effect of the silver nanodomains formed at the AgX nanoparticle surface. It has been demonstrated that the absorption peaks in the visible region are broad indicating the existence of a variety of silver nanoparticle sizes and shapes resulting in a purple-brown colouration of the samples. For the nanosilver iodide hybrid polymer materials no obvious difference in the UV-Vis spectra after exposure to light could be observed which is justified by the low susceptibility of AgI to photolysis when compared to AgCl and AgBr.

Electron microscopy analyses of the nanosilver halide hybrid polymer materials confirm the silver halide particles form on the surface and within the matrix of the polymer substrates. It has been shown that a higher number of silver halide particles are formed just below the surface compared to the centre of the polymer substrates. For the polyurethane samples, the AgCl particles are cube shaped and vary in size between less than about 100 nm and up to about 1000 nm. These AgCl particles are covered by non-uniform shaped and sized silver nanoparticles as a result of self-photosensitisation process. The AgBr particles have irregular shapes and sizes, ranging from less than about 200 nm. For the nanosilver iodide hybrid PU materials the particles were mostly found on the surface of the polymer. For the hybrid nylon 6,6 samples the AgCl particles with non-uniform shapes are smaller than 100 nm. However, some larger AgCl particles as well as particle agglomerates have been found. The AgX particles with a wide variety of shapes and sizes found in the nanosilver halide hybrid PU K5000 materials are well distributed within the PU K5000 matrix. The AgCl nanoparticles are between 15 and 100 nm in size, the AgBr nanoparticles are between 40 and 500 nm in size, whereas the AgI particles range from 20 nm to 500 nm in size. Upon exposure to light, it has been demonstrated that all AgX particles possess non-uniform shaped silver nanoparticles formed on their surfaces.

The XRD studies of these materials before exposure to direct light confirmed the presence of crystalline silver halides within the PU and polyurethane K5000 materials. No diffraction peaks were detected for the nanosilver halide nylon 6,6 materials presumably due to the low concentration of AgX particles in the polymer matrix. After the exposure to light the nanosilver halide hybrid PU and PU K5000 materials show diffraction peaks for metallic silver which due to the photosensitive characteristics of these silver halide nanoparticles. The samples containing AgCl nanoparticles are more susceptible to light than those containing AgBr nanoparticles. The longer the samples are exposed to light the more silver halide is converted to metallic silver. The XPS analyses suggest an interaction between the silver on the surface of the AgX nanoparticles and the nitrogen and oxygen groups present in the PU matrix.

The nanosilver halide hybrid polymer materials show antimicrobial performance against the gram negative *E. coli* bacteria. The sample containing AgCl nanoparticles is more effective against the bacteria than the one containing AgBr which in turn kills more bacteria than the sample with AgI nanoparticles. This effect is believed to be due to the solubilities of the silver halides which are responsible for the dissolution of different amounts of active Ag⁺ ions. The samples tested in direct light in comparison with the samples tested in dark conditions show greater antimicrobial activity which is correlated with the release of the silver ions originating from silver halide nanoparticles and also from metallic silver nanoparticles present on the AgX surface.

8 References

- (1) Kickelbick, G. *Hybrid materials: synthesis, characterization, and applications*; WILEY-VCH Verlag, 2006; Vol. Weinheim, p. 498.
- (2) Ashby, M. F.; Shercliff, H.; Cebon, D. *Materials: engineering, science, processing and design*; Butterworth-Heinemann: Burlington, 2007; p. 528.
- (3) Konsta-Gdoutos, M. S. *Measuring, Monitoring and Modeling Concrete Properties*; MARIA S. KONSTA-GDOUTOS, Ed.; Springer: Netherlands, 2006; p. 805.
- (4) Shrive, N. G. *Constr. Build. Mater.* **2006**, 20, 269–277.
- (5) Katti, D. R.; Katti, K. S.; Raviprasad, M.; Gu, C. J. *Nanomater.* **2012**, 2012, 1–15.
- (6) Becker, O.; Simon, G. P. *Adv. Polym. Sci.* **2005**, 179, 29–82.
- (7) Usuki, A.; Hasegawa, N.; Kato, M. *Adv. Polym. Sci.* **2005**, 179, 135–195.
- (8) Nicolais, L.; Carotenuto, G. *Metal-Polymer Nanocomposites*; Wiley: New Jersey, 2004; p. 324.
- (9) Ravindra, S.; Murali Mohan, Y.; Narayana Reddy, N.; Mohana Raju, K. *Colloids Surfaces, A Physicochem. Eng. Asp.* **2010**, 367, 31–40.
- (10) Nguyen, T.-H.; Lee, K.-H.; Lee, B.-T. *Mater. Sci. Eng. C Mater. Biol. Appl.* **2010**, 30, 944–950.
- (11) Ciobanu, L.-C.; Ciobanu, C.; Dorohoi, D. *High Perform. Polym.* **2010**, 22, 56–68.
- (12) Mayer, A. B. R. *Polym. Adv. Technol.* **2001**, 12, 96–106.
- (13) Jain, P.; Pradeep, T. *Biotechnol. Bioeng.* **2005**, 90, 59–63.

- (14) Sawant, S. N.; Selvaraj, V.; Prabhawathi, V.; Doble, M. *PLoS One* **2013**, *8*, e63311.
- (15) Perelshtein, I.; Applerot, G.; Perkas, N.; Guibert, G.; Mikhailov, S.; Gedanken, A. *Nanotechnology* **2008**, *19*, 245705/1–245705/6.
- (16) Abbasi, A. R.; Kalantary, H.; Yousefi, M.; Ramazani, A.; Morsali, A. *Ultrason. Sonochem.* **2012**, *19*, 853–857.
- (17) Moosavi, R.; Abbasi, A. R.; Yousefi, M.; Ramazani, A.; Morsali, A. *Ultrason. Sonochem.* **2012**, *19*, 1221–1226.
- (18) Min, S.-H.; Yang, J.-H.; Kim, J. Y.; Kwon, Y.-U. *Microporous Mesoporous Mater.* **2010**, *128*, 19–25.
- (19) Shi, Q.; Vitichuli, N.; Nowak, J.; Noar, J.; Caldwell, J. M.; Breidt, F.; Bourham, M.; McCord, M.; Zhang, X. *J. Mater. Chem.* **2011**, *21*, 10330.
- (20) Hsu, S.; Tseng, H.-J.; Lin, Y.-C. *Biomaterials* **2010**, *31*, 6796–6808.
- (21) BurrIDGE, K. A. Gold and silver nanoparticles as high-value colourants and multi-functional entities for natural fibres and minerals, Victoria University of Wellington, New Zealand, 2009.
- (22) Kelly, F. M. Multifunctional Textiles from Natural Fibres and Synthetic Fabrics Coloured with Silver and Silver Halide Nanoparticles, Victoria University of Wellington, New Zealand, 2009.
- (23) Richardson, M. J.; Johnston, J. H.; Borrmann, T. *Eur. J. Inorg. Chem.* **2006**, 2618–2623.
- (24) Richardson, M. J.; Johnston, J. H. *J. Colloid Interface Sci.* **2007**, *310*, 425–430.
- (25) Legge, N. R.; Holden, G.; Schroeder, H. E. *Thermoplastic elastomers: a comprehensive review*; Hanser Publishers: Munich, 1987; p. 574 pp.
- (26) Coleman, D. J. *Polym. Sci.* **1954**, *14*, 15–28.

- (27) Latimer, W. M.; Rodebush, W. H. *J. Am. Chem. Soc.* **1920**, *42*, 1419–1433.
- (28) Söntjens, S. H. M.; Renken, R. a. E.; van Gemert, G. M. L.; Engels, T. a. P.; Bosman, A. W.; Janssen, H. M.; Govaert, L. E.; Baaijens, F. P. T. *Macromolecules* **2008**, *41*, 5703–5708.
- (29) Bonart, R. *J. Macromol. Sci. Part B Phys.* **1968**, *2*, 115–138.
- (30) Bonart, R.; Morbitzer, L.; Hentze, G. *J. Macromol. Sci. Phys.* **1969**, *3*, 339–358.
- (31) Bayer, O.; Muller, E.; Petersen, S.; Piepenbrink, H. F.; Windemuth, E. *Angew. Chemie* **1950**, *62*, 57–66.
- (32) Versteegen, R. M.; Sijbesma, R. P.; Meijer, E. W. *Macromolecules* **2005**, *38*, 3176–3184.
- (33) Bonart, R.; Morbitzer, L.; Mueller, E. H. *J. Macromol. Sci. Phys.* **1974**, *9*, 447–461.
- (34) Jeon, H. J.; Kim, J. S.; Kim, T. G.; Kim, J. H.; Yu, W.-R.; Youk, J. H. *Appl. Surf. Sci.* **2008**, *254*, 5886–5890.
- (35) <http://www.chemicals-technology.com/projects/BASF-HPPO/BASF-HPPO2.html>.
- (36) <http://www.polyone.com/en-us/products/engresincompound/Pages/EdgetekCopolyester.aspx>.
- (37) <http://www.kinsang.com/index.php/whatsnews/en/14>.
- (38) Bhowmick, A. K. *Current topics in elastomers research*; First Edit.; CRC Press, 2008; p. 1104.
- (39) Bayer, O.; Rinke, H.; Siefken, W.; Ortner, L.; Schild, H. A process for the production of polyurethanes and polyureas. DRP 728981, 1937.
- (40) Carothers, W. H. Synthetic fibers. US 2130948, 1938.

- (41) Carothers, W. H. Linear condensation polymers. US 2071253, 1937.
- (42) Christ, A. E.; Hanford, W. E. Treatment of polyesters and product therefrom. US 2333639, 1940.
- (43) Hanford, W. E.; Holmes, D. F. Process for making polymeric products and for modifying polymeric products. US 2284896, 1942.
- (44) Habgood, B. J.; Harper, D. A.; Reynolds, R. J. W. Modified polyesters and polyester-amides. GB 580524, 1941.
- (45) Schollenberger, C. S.; Scott, H.; Moore, G. R. *Rubber World* **1958**, 137, 549-555.
- (46) Olabisi, O. *Handbook of Thermoplastics*; Volume 41 .; Marcel Dekker: New York, 1997; p. 1053.
- (47) Bhat, G.; Chand, S.; Yakopson, S. *Thermochim. Acta* **2001**, 367-368, 161-164.
- (48) Li, W.; Liu, J.; Hao, C.; Jiang, K.; Xu, D.; Wang, D. *Polym. Eng. Sci.* **2008**, 48, 249-256.
- (49) Woo, L.; Anderson, B. *Annu. Tech. Conf. - Soc. Plast. Eng.* **2008**, 66th, 1564-1566.
- (50) Rogulska, M.; Kultys, A.; Pikus, S. *J. Appl. Polym. Sci.* **2008**, 110, 1677-1689.
- (51) Siddhamalli, S. K.; Hewitt, L. E. *Proc. Int. Wire Cable Symp.* **2008**, 57th, 342-346.
- (52) Hepburn, C. *Polyurethane Elastomers*; Applied Science: London, 1982; p. 412.
- (53) Feijen, D. H. W.; Mueller, J. L.; Julia, J.; Salvatella, D.; Riba, M. J. *TPE Conf. 2001, Two-Day Conf. Brussels, Belgium, June 18-19, 2001* **2001**, Paper14/1-Paper14/5.

- (54) Abouzahr, S.; Wilkes, G. L. *J. Appl. Polym. Sci.* **1984**, 29, 2695–2711.
- (55) Ojha, U.; Kulkarni, P.; Faust, R. *Polymer (Guildf)*. **2009**, 50, 3448–3457.
- (56) Drobny, J. G. *Handbook of thermoplastic elastomers*; First Edit.; William Andrew Inc.: Norwich, 2007; p. 520.
- (57) Ma, H.; Yang, Y. *Polym. Test.* **2008**, 27, 441–446.
- (58) Wang, X.; Luo, X.; Wang, X. *Polym. Test.* **2005**, 24, 18–24.
- (59) Tartarini, C.; Schrinner, K.; Hornbach, K. H. *Rubber World* **2009**, 241, 26–28,30,32.
- (60) Dan, C. H.; Lee, M. H.; Kim, Y. D.; Min, B. H.; Kim, J. H. *Polymer (Guildf)*. **2006**, 47, 6718–6730.
- (61) De, S. K.; White, J. R. *Rubber Technologists Handbook*; Rapra Technology Limited: UK, 2001; p. 576.
- (62) Romaskevicius, T.; Budriene, S.; Pielichowski, K.; Pielichowski, J. *Chemija* **2006**, 17, 74–89.
- (63) Walder, A. *Proc. Int. Wire Cable Symp.* **2005**, 54th, 78–79.
- (64) Schollenberger, C. S. Simulated vulcanizates of polyurethane elastomers. US 2871218, 1959.
- (65) Singer, S. M.; Allott, M. T. Thermoplastic polyurethane elastomer based on a hydroxyl terminated polyol, an aromatic chain extender and 1,5 naphthalene diisocyanate. US 5599874, 1997.
- (66) Ishimar, F.; Nakamura, S.; Sugitawa, C.; Imagawa, O. Thermoplastic polyurethane. US 5695884, 1997.
- (67) Handlin, D. L. Method for producing mixed polyol thermoplastic polyurethane compositions. US 6323299 B1, 2001.

- (68) Martin, D. J.; Warren, L. A. P.; Gunatillake, P. A.; McCarthy, S. J.; Meijs, G. F.; Schindhelm, K. *Biomaterials* **2000**, *21*, 1021–1029.
- (69) Kim, H.-D.; Lee, T.-J.; Huh, J.-H.; Lee, D.-J. *J. Appl. Polym. Sci.* **1999**, *73*, 345–352.
- (70) Holden, G.; Kricheldorf, H. R.; Quirk, R. P. *Thermoplastic Elastomers*; Third Edit.; Hanser Gardner Publications: Munich, 2004; p. 540.
- (71) Bhowmick, A. K.; Stephens, H. L. *Handbook of Elastomers*; 2. Edition.; CRC Press: USA, 2000; p. 944.
- (72) Feijen, D. H. W.; Muller, J. L.; Julia, J.; Salvatella, D.; Riba, M. J. *PU Lat. Am. 2001, Int. Polyurethanes Conf. Exhib. Lat. Am. Conf. Pap. Sao Paulo, Brazil, Aug. 28-30, 2001* **2001**, P28/1–P28/5.
- (73) Kannan, M.; Bhagawan, S. S.; Joseph, K.; Thomas, S. J. *Compos. Mater.* **2009**, *43*, 1915–1925.
- (74) Frisch, K. C. *Fundamental chemistry and catalysis of polyurethanes, Polyurethane Technology*; Interscience: New York, 1969; pp. 1–38.
- (75) Sandler, S. R.; Karo, W. *Polymer syntheses*; 2. Edition.; Academic Press: New York, 1991; p. 512.
- (76) Bertsch McGrayne, S. *Prometheans in the Lab: Chemistry and the Making of the Modern World*; First Edit.; McGraw-Hill Trade, 2001; p. 243.
- (77) Giles, H. F. J.; Mount, E. M. I.; Wagner, J. R. J. *Extrusion: The definitive processing guide and handbook*; 1. Edition.; William Andrew, 2007; p. 560.
- (78) Avery, J. *Injection molding alternatives: a guide for designers and product engineers*; Hanser Gardner Publications, Inc., 331AD; p. 1998.
- (79) Kim, K. J.; Dhevi, D. M.; Lee, J. S.; Cho, Y. D.; Choe, E. K. *Polym. Degrad. Stab.* **2006**, *91*, 1545–1555.

- (80) Kohan, M. I. *Nylon plastics handbook*; Hanser Gardner Publications, Inc.: New York, 1995; p. 631.
- (81) Braun, D.; Cherdrón, H.; Rehahn, M.; Ritter, H.; Voit, B. *Polymer synthesis: theory and practice: fundamentals, methods, experiments*; 4. Edition.; Springer, 2004; p. 403.
- (82) Bernstein, R.; Derzon, D. K.; Gillen, K. T. *Polym. Degrad. Stab.* **2005**, *88*, 480–488.
- (83) Page, I. B. *Polyamides As Engineering Thermoplastic Materials*; Volume 11.; Rapra Publishing, 2000; p. 143.
- (84) Barnetson, A. *Advances in Polymers: Market and Technical Trends*; Rapra Technology Limited, 1997; p. 122.
- (85) DIANE Publishing Company. *New Materials Society, Challenges and Opportunities: New Materials Science and Technology*; DIANE Publishing, 1993; p. 300.
- (86) Koo, J. H. *Polymer nanocomposites: processing, characterization, and applications*; McGraw-Hill Trade: The University of Michigan, 2006; p. 272.
- (87) Edwards, S. A. *The Nanotech Pioneers*; First Edit.; WILEY-VCH Verlag: Weinheim, Germany, 2006; p. 257.
- (88) Rao, C. N. R.; Müller, A.; Cheetham, A. K. *Nanomaterials chemistry: recent developments and new direction*; Wiley-VCH Verlag GmbH & Co. KGaA, 2007; p. 403.
- (89) Freestone, I.; Meeks, N.; Sax, M.; Higgitt, C. *Gold Bull.* **2007**, *40*, 270–277.
- (90) Schmid, G.; Corain, B. *Eur. J. Inorg. Chem.* **2003**, *2003*, 3081–3098.
- (91) Faraday, M. *Philos. Trans. R. Soc. London* **1857**, *147*, 145–181.
- (92) Mie, G. *Ann. Phys.* **1908**, *25*, 377–445.

- (93) Burda, C.; Chen, X.; Narayanan, R.; El-Sayed, M. *Chem. Rev.* **2005**, *105*, 1025–1102.
- (94) Hutter, E.; Fendler, J. H. *Adv. Mater.* **2004**, *16*, 1685–1706.
- (95) Liz-Marzán, L. M. *Langmuir* **2006**, *22*, 32–41.
- (96) Liz-Marzán, L. M. *Mater. Today* **2004**, *7*, 26–31.
- (97) Mulvaney, P. *Langmuir* **1996**, *12*, 788–800.
- (98) Sun, Y.; Xia, Y. *Analyst* **2003**, *128*, 686–691.
- (99) Endo, T.; Ikeda, R.; Yanagida, Y.; Hatsuzawa, T. *Anal. Chim. Acta* **2008**, *611*, 205–211.
- (100) Arvizo, R.; Bhattacharya, R.; Mukherjee, P. *Expert Opin. Drug Deliv.* **2010**, *7*, 753–763.
- (101) Sau, T. K.; Rogach, A. L.; Jäckel, F.; Klar, T. a; Feldmann, J. *Adv. Mater.* **2010**, *22*, 1805–1825.
- (102) Schulte, J. *Nanotechnology: Global Strategies, Industry Trends and Applications*; Wiley, 2005; p. 194.
- (103) Bigall, N. C.; Reitzig, M.; Naumann, W.; Simon, P.; van Pée, K.-H.; Eychemüller, A. *Angew. Chemie* **2008**, *47*, 7876–7879.
- (104) Ko, K. D.; Toussaint, K. C. *J. Quant. Spectrosc. Radiat. Transf.* **2009**, *110*, 1037–1043.
- (105) Ghosh, K.; Maiti, S. N. *J. Appl. Polym. Sci.* **1996**, *60*, 323–331.
- (106) Eustis, S.; El-Sayed, M. a. *Chem. Soc. Rev.* **2006**, *35*, 209–217.
- (107) Link, S.; El-Sayed, M. a. *Int. Rev. Phys. Chem.* **2000**, *19*, 409–453.
- (108) Toderas, F.; Baia, M.; Maniu, D.; Astilean, S. *J. Optoelectron. Adv. Mater.* **2008**, *10*, 2282–2284.

- (109) Mustafa, D. E.; Yang, T.; Xuan, Z.; Chen, S.; Tu, H.; Zhang, A. *Plasmonics* **2010**, *5*, 221–231.
- (110) Daniel, M.-C.; Astruc, D. *Chem. Rev.* **2004**, *104*, 293–346.
- (111) Hu, J.; Wang, Z.; Li, J. *Sensors* **2007**, *7*, 3299–3311.
- (112) Maillard, M.; Giorgio, S.; Pileni, M.-P. *Adv. Mater.* **2002**, *14*, 1084.
- (113) Callegari, A.; Tonti, D.; Chergui, M. *Nano Lett.* **2003**, *3*, 1565–1568.
- (114) Sambhy, V.; MacBride, M. M.; Peterson, B. R.; Sen, A. *J. Am. Chem. Soc.* **2006**, *128*, 9798–9808.
- (115) Vu, L. Van; Long, N. N.; Doanh, S. C.; Trung, B. Q. *J. Phys. Conf. Ser.* **2009**, *187*, 012077.
- (116) Yu, C.-C.; Yang, K.-H.; Liu, Y.-C.; Chen, B.-C. *Mater. Res. Bull.* **2010**, *45*, 838–843.
- (117) Kutsenko, A. S.; Granchak, V. M.; Nauky, P. *Theor. Exp. Chem.* **2009**, *45*, 300–305.
- (118) Zhou, J.; Ralston, J.; Sedev, R.; Beattie, D. *J. Colloid Interface Sci.* **2009**, *331*, 251–262.
- (119) Pastoriza-Santos, I.; Liz-Marzán, L. M. *Adv. Funct. Mater.* **2009**, *19*, 679–688.
- (120) Liu, Y.; Male, K. B.; Bouvrette, P.; Luong, J. H. T. *Chem. Mater.* **2003**, *15*, 4172–4180.
- (121) Mayer, A. B. R.; Mark, J. E. *Eur. Polym. J.* **1998**, *34*, 103–108.
- (122) Mitsudome, T.; Noujima, A.; Mizugaki, T.; Jitsukawa, K.; Kaneda, K. *Adv. Synth. Catal.* **2009**, *351*, 1890–1896.
- (123) Sun, K.; Qiu, J.; Liu, J.; Miao, Y. *J. Mater. Sci.* **2008**, *44*, 754–758.

- (124) Pastoriza-santos, I.; Liz-Marzán, L. M. *Pure Appl. Chem.* **2000**, 72, 83–90.
- (125) Malikova, N.; Pastoriza-santos, I.; Schierhorn, M.; Kotov, N. A.; Liz-Marzán, L. M. *Langmuir* **2002**, 18, 3694–3697.
- (126) Turkevich, J.; Stevenson, P. C.; Hillier, J. *Discuss. Faraday Soc.* **1951**, 11, 55–75.
- (127) Brust, M.; Walker, M.; Bethell, D.; Schiffrin, D. J.; Whyman, R. *J. Chem. Soc. Chem. Commun.* **1994**, 7, 801–802.
- (128) Brust, M.; Fink, J.; Bethella, D.; Schiffrina, D. J.; Kielyb, C. *J. Chem. Soc. Chem. Commun.* **1995**, 16, 1655–1656.
- (129) Sardar, R.; Funston, A. M.; Mulvaney, P.; Murray, R. W. *Langmuir* **2009**, 25, 13840–13851.
- (130) Philip, D. *Phys. E Low-dimensional Syst. Nanostructures* **2010**, 42, 1417–1424.
- (131) Huang, X.; Wu, H.; Liao, X.; Shi, B. *Green Chem.* **2010**, 12, 395.
- (132) MubarakAli, D.; Thajuddin, N.; Jeganathan, K.; Gunasekaran, M. *Colloids Surfaces B Biointerfaces* **2011**, 85, 360–365.
- (133) Das, S. K.; Das, A. R.; Guha, A. K. *Langmuir* **2009**, 25, 8192–8199.
- (134) Thakkar, K. N.; Mhatre, S. S.; Parikh, R. Y. *Nanomedicine Nanotechnology, Biol. Med.* **2010**, 6, 257–262.
- (135) Anandan, S.; Oh, S.-D.; Yoon, M.; Ashokkumar, M. *Spectrochim. Acta Part A Mol. Biomol. Spectrosc.* **2010**, 76, 191–196.
- (136) Anandan, S.; Grieser, F.; Ashokkumar, M. *J. Phys. Chem. C* **2008**, 112, 15102–15105.
- (137) Brito-Silva, A. M.; Gómez, L. a.; de Araújo, C. B.; Galembeck, A. *J. Nanomater.* **2010**, 2010, 1–7.

- (138) Sakai, T.; Enomoto, H.; Torigoe, K.; Sakai, H.; Abe, M. *Colloids Surfaces A Physicochem. Eng. Asp.* **2009**, *347*, 18–26.
- (139) Liu, Y.-C.; Lin, L.-H.; Chiu, W.-H. *J. Phys. Chem. B* **2004**, *108*, 19237–19240.
- (140) Irzh, A.; Perkas, N.; Gedanken, A. *Langmuir* **2007**, *23*, 9891–9897.
- (141) Navaladian, S.; Viswanathan, B.; Varadarajan, T. K.; Viswanath, R. P. *Nanotechnology* **2008**, *19*, 045603.
- (142) Peng, Z.; Spliethoff, B.; Tesche, B.; Walther, T.; Kleinermanns, K. *J. Phys. Chem. B* **2006**, *110*, 2549–2554.
- (143) Yin, Y.; Xu, X. *Chem. Commun.* **1998**, *8*, 941–942.
- (144) Navaladian, S.; Viswanathan, B.; Viswanath, R.; Varadarajan, T. *Nanoscale Res. Lett.* **2006**, *2*, 44–48.
- (145) Nunes, G. S.; Allen, P. B.; Martins, J. L. *Solid State Commun.* **1998**, *105*, 377–380.
- (146) Sugimoto, T.; Shiba, F.; Sekiguchi, T.; Itoh, H. *Colloids Surfaces A Physicochem. Eng. Asp.* **2000**, *164*, 183–203.
- (147) Zhou, Z.; Long, M.; Cai, W.; Cai, J. *J. Mol. Catal. A Chem.* **2012**, *353–354*, 22–28.
- (148) Ashokkumar, M.; Marignier, J.-L. *Int. J. Hydrogen Energy* **1999**, *24*, 17–20.
- (149) Kakuta, N.; Goto, N.; Ohkita, H.; Mizushima, T. *J. Phys. Chem. B* **1999**, *103*, 5917–5919.
- (150) Wyckoff, R. W. G. *Crystal structures*; 2. Edition.; Interscience Publishers: New York, 1963.
- (151) Maskasky, J. E. *Phys. Rev. B* **1991**, *43*, 5769.

- (152) Yoshiasa, A.; Inaba, A.; Ishii, T.; Koto, K. *Solid State Ionics* **1995**, 79, 67–70.
- (153) Vogelsang, H.; Husberg, O.; Osten, W. Von Der. **2000**, 86, 87–94.
- (154) Funke, K.; Wilmer, D.; Lauxtermanna, T.; Holzgreve, R.; Bennington, S. M. *Solid State Ionics* **1996**, 86-88, 141–146.
- (155) Hayes, W.; Stoneham, A. M. *Defects and Defect Processes in Nonmetallic Solids*; Dover Publications, 2004; p. 480.
- (156) Rogez, J.; Garnier, A.; Knauth, P. J. *Phys. Chem. Solids* **2002**, 63, 9–14.
- (157) Gurney, R. W.; Mott, N. F. *Proc. R. Soc. A Math. Phys. Eng. Sci.* **1938**, 164, 151–167.
- (158) Pileni, M. P. *Langmuir* **1997**, 13, 3266–3276.
- (159) Husein, M.; Rodil, E.; Vera, J. H. *J. Colloid Interface Sci.* **2004**, 273, 426–434.
- (160) Xu, S.; Li, Y. *J. Mater. Chem.* **2003**, 13, 163–165.
- (161) Husein, M. M.; Rodil, E.; Vera, J. H. *Langmuir* **2006**, 22, 2264–2272.
- (162) Pillai, V.; Kumar, P.; Hou, M. J.; Ayyub, P.; Shah, D. O. *Adv. Colloid Interface Sci.* **1995**, 55, 241–269.
- (163) Nagarajan, R.; Ruckenstein, E. *Langmuir* **2000**, 16, 6400–6415.
- (164) Jeunieu, L.; Verbouwe, W.; Rousseau, E.; Auweraer, M. Van Der; Nagy, J. B. *Langmuir* **2000**, 16, 1602–1611.
- (165) Monnoyer, P.; Fonseca, A.; Nagy, J. B. *Colloids Surfaces A Physicochem. Eng. Asp.* **1995**, 100, 233–243.
- (166) Ohde, H.; Ye, X.-R.; Wai, C. M.; Rodriguez, J. M. *Chem. Commun.* **2000**, 23, 2353–2354.

- (167) Feng, X.; Liu, Y.; Lu, C.; Hou, W.; Zhu, J.-J. *Nanotechnology* **2006**, *17*, 3578–3583.
- (168) Choi, M.; Shin, K.-H.; Jang, J. *J. Colloid Interface Sci.* **2010**, *341*, 83–87.
- (169) Glaus, S.; Calzaferri, G. *Photochem. Photobiol. Sci.* **2003**, *2*, 398–401.
- (170) Ves, S.; Glotzel, D.; Cardona, M.; Overhof, H. *Phys. Rev. B Condens. Matter Mater. Phys.* **1981**, *24*, 3073–3085.
- (171) Tamura, S.; Takeuchi, K.; Mao, G.; Csencsits, R.; Fan, L.; Otomo, T.; Sabounji, M.-L. *J. Electroanal. Chem.* **2003**, *559*, 103–109.
- (172) Mellor, J. W. *A Comprehensive Treatise on Inorganic and Theoretical Chemistry*; Wiley: New York, 1961.
- (173) Lanz, M.; Schuerch, D.; Calzaferri, G. *J. Photochem. Photobiol. A Chem.* **1999**, *120*, 105–117.
- (174) Wang, P.; Huang, B.; Qin, X.; Zhang, X.; Dai, Y.; Wei, J.; Whangbo, M.-H. *Angew. Chemie* **2008**, *47*, 7931–7933.
- (175) Wang, P.; Huang, B.; Zhang, Q.; Zhang, X.; Qin, X.; Dai, Y.; Zhan, J.; Yu, J.; Liu, H.; Lou, Z. *Chemistry (Easton)*. **2010**, *16*, 10042–10047.
- (176) Kuai, L.; Geng, B.; Chen, X.; Zhao, Y.; Luo, Y. *Langmuir* **2010**, *26*, 18723–18727.
- (177) Wang, P.; Huang, B.; Lou, Z.; Zhang, X.; Qin, X.; Dai, Y.; Zheng, Z.; Wang, X. *Chemistry (Easton)*. **2010**, *16*, 538–544.
- (178) An, C.; Peng, S.; Sun, Y. *Adv. Mater.* **2010**, *22*, 2570–2574.
- (179) Wang, P.; Huang, B.; Zhang, X.; Qin, X.; Dai, Y.; Wang, Z.; Lou, Z. *ChemCatChem* **2011**, *3*, 360–364.
- (180) Tate, E. W. Synthesis and Characterisation of Photocatalyst Silver/Silver Halide Nanocomposites, Victoria University of Wellington, New Zealand.

- (181) Chen, D.; Li, T.; Chen, Q.; Gao, J.; Fan, B.; Li, J.; Li, X.; Zhang, R.; Sun, J.; Gao, L. *Nanoscale* **2012**, 4, 5431–5439.
- (182) Xu, X.; Shen, X.; Zhou, H.; Qiu, D.; Zhu, G.; Chen, K. *Appl. Catal. A Gen.* **2013**, 455, 183–192.
- (183) Tang, Y.; Jiang, Z.; Deng, J.; Gong, D.; Lai, Y.; Tay, H. T.; Joo, I. T. K.; Lau, T. H.; Dong, Z.; Chen, Z. *Appl. Mater. Interfaces* **2012**, 4, 438–446.
- (184) Ware, M. *Mechanisms of Image Deterioration in Early Photographs: The Sensitivity to Light of W. H. F. Talbot's Halide-Fixed Images 1834-1844*; NMSI Trading Ltd, 1994; p. 89.
- (185) Binh, N. T.; Ly, D. T.; Hue, N. T.; Quyen, L. T. *VNU J. Sci. Math. - Phys.* **2008**, 24, 1–5.
- (186) M., E. A.; M., H.-M. J.; Brumfitt, W.; Noble, W. C. *J. Antimicrob. Chemother.* **1996**, 37, 911–918.
- (187) Sadler, P. J. *Struct. Bond.* **1976**, 29, 171–214.
- (188) Aaseth, J.; Haugen, M.; Førre, O. *Analyst* **1998**, 123, 3–6.
- (189) Smith, W. E.; Brown, D. H.; Cappell, H. a. *Inorganica Chim. Acta* **1985**, 106, L23–L24.
- (190) Naik, A. J. T.; Ismail, S.; Kay, C.; Wilson, M.; Parkin, I. P. *Mater. Chem. Phys.* **2011**, 129, 446–450.
- (191) Narband, N.; Mubarak, M.; Ready, D.; Parkin, I. P.; Nair, S. P.; Green, M. A.; Beeby, A.; Wilson, M. *Nanotechnology* **2008**, 19, 445102.
- (192) Zhang, Y.; Peng, H.; Huang, W.; Zhou, Y.; Yan, D. *J. Colloid Interface Sci.* **2008**, 325, 371–376.
- (193) Chen, X.; Schluesener, H. J. *Toxicol. Lett.* **2008**, 176, 1–12.
- (194) Cioffi, N.; Rai, M. *Nano-Antimicrobials: Progress and Prospects*; Springer Berlin / Heidelberg: New York, 2012; p. 556.

- (195) Lagaron, J. M.; Ocio, M. J.; Lopez-Rubio, A. *Antimicrobial Polymers*; First Edit.; Wiley, 2012; p. 608.
- (196) Fabrega, J.; Luoma, S. N.; Tyler, C. R.; Galloway, T. S.; Lead, J. R. *Environ. Int.* **2011**, *37*, 517–531.
- (197) Amendola, V.; Polizzi, S.; Meneghetti, M. *Langmuir* **2007**, *23*, 6766–6770.
- (198) Kaegi, R.; Sinnet, B.; Zuleeg, S.; Hagendorfer, H.; Mueller, E.; Vonbank, R.; Boller, M.; Burkhardt, M. *Environ. Pollut.* **2010**, *158*, 2900–2905.
- (199) Dastjerdi, R.; Mojtahedi, M. R. M.; Shoshtari, a. M. *Macromol. Res.* **2009**, *17*, 378–387.
- (200) Abou El-Nour, K. M. M.; Eftaiha, A.; Al-Warthan, A.; Ammar, R. A. A. *Arab. J. Chem.* **2010**, *3*, 135–140.
- (201) Morones, J. R.; Elechiguerra, J. L.; Camacho, A.; Holt, K.; Kouri, J. B.; Ramírez, J. T.; Yacaman, M. J. *Nanotechnology* **2005**, *16*, 2346–2353.
- (202) Pal, S.; Tak, Y. K.; Song, J. M. *Appl. Environ. Microbiol.* **2007**, *73*, 1712–1720.
- (203) Lok, C.; Ho, C.; Chen, R.; He, Q.; Yu, W.; Sun, H.; Tam, P. K.; Chiu, J.; Che, C. J. *Proteome Res.* **2006**, 916–924.
- (204) Jeong, S. H.; Hwang, Y. H.; Yi, S. C. *J. Mater. Sci.* **2005**, *40*, 5413–5418.
- (205) Bugla-Ploskonska, G.; Leszkiewicz, A. *Kosmos* **2007**, *56*, 115–122.
- (206) Jeong, S. H.; Yeo, S. Y.; Yi, S. C. *J. Mater. Sci.* **2005**, *40*, 5407–5411.
- (207) Kim, J. S.; Kuk, E.; Yu, K. N.; Kim, J.-H.; Park, S. J.; Lee, H. J.; Kim, S. H.; Park, Y. K.; Park, Y. H.; Hwang, C.-Y.; Kim, Y.-K.; Lee, Y.-S.; Jeong, D. H.; Cho, M.-H. *Nanomedicine Nanotechnology, Biol. Med.* **2007**, *3*, 95–101.

- (208) Chaloupka, K.; Malam, Y.; Seifalian, A. M. *Trends Biotechnol.* **2010**, *28*, 580–588.
- (209) Rai, M.; Yadav, A.; Gade, A. *Biotechnol. Adv.* **2009**, *27*, 76–83.
- (210) Matsumura, Y.; Yoshikata, K.; Kunisaki, S.; Tsuchido, T. *Appl. Environ. Microbiol.* **2003**, *69*, 4278–4281.
- (211) Guzman, M.; Dille, J.; Godet, S. *Nanomedicine Nanotechnology, Biol. Med.* **2012**, *8*, 37–45.
- (212) Son-di, I.; Salopek-Son-di, B. *J. Colloid Interface Sci.* **2004**, *275*, 177–182.
- (213) Choi, O.; Hu, Z. *Environ. Sci. Technol.* **2008**, *42*, 4583–4588.
- (214) Nel, A.; Xia, T.; Mädler, L.; Li, N. *Science (80-.)*. **2006**, *311*, 622–627.
- (215) Henglein, A. *Chem. Mater.* **1998**, *10*, 444–450.
- (216) Xiu, Z.-M.; Zhang, Q.-B.; Puppala, H. L.; Colvin, V. L.; Alvarez, P. J. J. *Nano Lett.* **2012**, *12*, 4271–4275.
- (217) Lok, C.-N.; Ho, C.-M.; Chen, R.; He, Q.-Y.; Yu, W.-Y.; Sun, H.; Tam, P. K.-H.; Chiu, J.-F.; Che, C.-M. *J. Biol. Inorg. Chem.* **2007**, *12*, 527–534.
- (218) Song, H. Y.; Ko, K. K.; Oh, I. H.; Lee, B. T. *Eur. Cells Mater.* **2006**, *11*, 58.
- (219) Muñoz-Bonilla, A.; Fernández-García, M. *Prog. Polym. Sci.* **2012**, *37*, 281–339.
- (220) Perkash, N.; Amirian, G.; Dubinsky, S.; Gazit, S.; Gedanken, A. *J. Appl. Polym. Sci.* **2007**, *104*, 1423–1430.
- (221) Dong, G.; Xiao, X.; Liu, X.; Qian, B.; Liao, Y.; Wang, C.; Chen, D.; Qiu, J. *Appl. Surf. Sci.* **2009**, *255*, 7623–7626.
- (222) Lee, S. H.; Sung, K.; Chung, T.-M.; Lee, S.-G.; Min, K. D.; Koo, S.; Kim, C. G. *J. Nanosci. Nanotechnol.* **2008**, *8*, 4734–4737.

- (223) Onsuratoom, S.; Rujiravanit, R.; Sreethawong, T.; Tokura, S.; Chavadej, S. *Plasma Chem. Plasma Process.* **2009**, *30*, 191–206.
- (224) Deka, H.; Karak, N.; Kalita, R. D.; Buragohain, A. K. *Polym. Degrad. Stab.* **2010**, *95*, 1509–1517.
- (225) Hu, C.; Lan, Y.; Qu, J.; Hu, X.; Wang, A. *J. Phys. Chem. B* **2006**, *110*, 4066–4072.
- (226) Faÿ, F.; Carteau, D.; Linossier, I.; Vallée-Réhel, K. *Prog. Org. Coatings* **2011**, *72*, 579–585.
- (227) Turner, A. *Mar. Pollut. Bull.* **2010**, *60*, 159–171.
- (228) Yebra, D. M.; Kiil, S.; Dam-Johansen, K. *Prog. Org. Coatings* **2004**, *50*, 75–104.
- (229) Almeida, E.; Diamantino, T. C.; de Sousa, O. *Prog. Org. Coatings* **2007**, *59*, 2–20.
- (230) Woods Hole Oceanographic Institution, U. S. N. D. B. of S. *Marine fouling and its prevention*; United States Naval Institute: the University of Michigan, 1952; p. 388.
- (231) Watermann, B. T.; Daehne, B.; Sievers, S.; Dannenberg, R.; Overbeke, J. C.; Klijnstra, J. W.; Heemken, O. *Chemosphere* **2005**, *60*, 1530–1541.
- (232) Parks, R.; Donnier-Marechal, M.; Frickers, P. E.; Turner, A.; Readman, J. W. *Mar. Pollut. Bull.* **2010**, *60*, 1226–1230.
- (233) Voulvoulis, N.; Scrimshaw, M. D.; Lester, J. N. *Appl. Organomet. Chem.* **1999**, *13*, 135–143.
- (234) Dafforn, K. a; Lewis, J. a; Johnston, E. L. *Mar. Pollut. Bull.* **2011**, *62*, 453–465.
- (235) Lewis, J. A. *Mater. Forum* **1998**, *22*, 41–61.
- (236) Gadd, J.; Depree, C.; Hickey, C. *NIWA Taihoro Nukurangi* **2011**.

- (237) Thomas, K. V; Brooks, S. *Biofouling* **2010**, 26, 73–88.
- (238) Hellio, C.; Yebra, D. *Advances in Marine Antifouling Coatings and Technologies*; Woodhead Publishing Limited: Cambridge, 2009; p. 764.
- (239) Maréchal, J.-P.; Hellio, C. *Int. J. Mol. Sci.* **2009**, 10, 4623–4637.
- (240) Chief Executive ERMA, N. Z. **2012**.
- (241) Nath, S.; Ghosh, S. K.; Kundu, S.; Praharaj, S.; Panigrahi, S.; Pal, T. *J. Nanoparticle Res.* **2006**, 8, 111–116.
- (242) *Powder Diffraction File*; International Centre for Diffraction Data: Pennsylvania, U.S.A., 2007; p. Version 4+.
- (243) Guinier, A. *X-ray diffraction in crystals, imperfect crystals, and amorphous bodies*; Courier Dover Publications: Toronto, 1994; p. 378.
- (244) Monshi, A.; Foroughi, M. R.; Monshi, M. R. *World J. Nano Sci. Eng.* **2012**, 02, 154–160.
- (245) Kubelka, P. *J. Opt. Soc. Am.* **1948**, 38, 448–457.
- (246) Hayhurst, C. *E. Coli*; First Edit.; The Rosen Publishing Group, Inc.: New York, 2004; p. 64.
- (247) Cussler, E. L. *Diffusion: Mass Transfer in Fluid Systems*; 2. Edition.; Cambridge University Press: Cambridge, 1997.
- (248) Johnston, J. H.; Nilsson, T. *J. Mater. Sci.* **2011**, 47, 1103–1112.
- (249) Marsden, J. O.; House, C. I. *The Chemistry of Gold Extraction*; 2. Edition.; The Society for Mining, Metallurgy, and Exploration, Inc., 2006; p. 680.
- (250) Le Ru, E. C.; Etchegoin, P. G. *Principles of Surface-Enhanced Raman Spectroscopy: And Related Plasmonic Effects*; Elsevier: Amsterdam, 2008.
- (251) Sun, Y.; Xia, Y. *Analyst* **2003**, 128, 686.

- (252) Chhatre, A.; Solasa, P.; Sakle, S.; Thaokar, R.; Mehra, A. *Colloids Surfaces A Physicochem. Eng. Asp.* **2012**, *404*, 83–92.
- (253) Grunwaldt, J.-D.; Kiener, C.; Wögerbauer, C.; Baiker, A. *J. Catal.* **1999**, *181*, 223–232.
- (254) Chen, L.; Hu, J.; Richards, R. *J. Am. Chem. Soc.* **2009**, *131*, 914–915.
- (255) Yang, S.; Zhang, T.; Zhang, L.; Wang, S.; Yang, Z.; Ding, B. *Colloids Surfaces A Physicochem. Eng. Asp.* **2007**, *296*, 37–44.
- (256) Geddes, C. D.; Lakowicz, J. R. *Radiative Decay Engineering*; Springer Science+Business Media, Inc.: New York, 2005.
- (257) Evanoff, D. D.; Chumanov, G. *J. Phys. Chem. B* **2004**, *108*, 13957–13962.
- (258) Hu, M.; Chen, J.; Li, Z.-Y.; Au, L.; Hartland, G. V.; Li, X.; Marquez, M.; Xia, Y. *Chem. Soc. Rev.* **2006**, *35*, 1084–1094.
- (259) Kreibig, U. *J. Phys. F Met. Phys.* **1974**, *4*, 999–1014.
- (260) Henglein, A. *J. Phys. Chem.* **1993**, *97*, 5457–5471.
- (261) Berry, C. R. *J. Appl. Phys.* **1971**, *42*, 2818.
- (262) Sau, T. K.; Rogach, A. L. *Complex-shaped Metal Nanoparticles: Bottom-Up Syntheses and Applications*; Wiley-VCH Verlag GmbH & Co. KGaA: Weinheim, Germany, 2012.
- (263) Montazer, M.; Shamei, A.; Alimohammadi, F. *Prog. Org. Coatings* **2012**, *74*, 270–276.
- (264) Beamson, G.; Briggs, D. *High resolution XPS of organic polymers, the scienta ESCA300 database*; John Wiley & Sons: Chichester, 1992; p. 280.
- (265) Ashwell, G. J.; Williams, A. T.; Barnes, S. a; Chappell, S. L.; Phillips, L. J.; Robinson, B. J.; Urasinska-wojcik, B.; Wierzchowicz, P.; Gentle, I. R.; Wood, B. J. *J. Phys. Chem. C* **2011**, *115*, 4200–4208.

- (266) Devia, a.; Castillo, H. a.; Benavides, V. J.; Arango, Y. C.; Quintero, J. H. *Mater. Charact.* **2008**, 59, 105–107.
- (267) Wagner, C. D.; Zatko, D. a.; Raymond, R. H. *Anal. Chem.* **1980**, 52, 1445–1451.
- (268) Torres, J.; Perry, C. C.; Bransfield, S. J.; Fairbrother, D. H. *J. Phys. Chem. B* **2002**, 106, 6265–6272.
- (269) Boyen, H.-G.; Kästle, G.; Weigl, F.; Koslowski, B.; Dietrich, C.; Ziemann, P.; Spatz, J. P.; Riethmüller, S.; Hartmann, C.; Möller, M.; Schmid, G.; Garnier, M. G.; Oelhafen, P. *Science (80-.)*. **2002**, 297.
- (270) Eley, D. D.; Moore, P. B. *Surf. Sci.* **1978**, 76, 599–602.
- (271) Pireaux, J.-J.; Liehr, M.; Thiry, P. A.; Delrue, J. P.; Caudano, R. *Surf. Sci.* **1984**, 141, 221–232.
- (272) Haruta, M.; Tsubota, S.; Kobayashi, T.; Kageyama, H.; Genet, M. J.; Delmon, B. *J. Catal.* **1993**, 144, 175–192.
- (273) Juodkazis, K.; Juodkazyte, J.; Jasulaitiene, V.; Lukinskas, A.; Sebek, B. *Electrochem. commun.* **2000**, 2, 503–507.
- (274) Wang, D.; Hao, Z.; Cheng, D.; Shi, X.; Hu, C. *J. Mol. Catal. A Chem.* **2003**, 200, 229–238.
- (275) Wagner, C. D.; Riggs, W. M.; Davis, L. E.; Moulder, J. F.; Muilenberg, G. E. *Handbook of X-ray Photoelectron Spectroscopy*; Perkin-Elmer Corporation: Eden Prairie, Minnesota, USA, 1979; p. 190.
- (276) Wagner, C. D.; Naumkin, A. V.; Kraut-Vass, A.; Alisson, J. W.; Powell, C. J.; Rumble, J. R. *J. Natl. Inst. Stand. Technol.* **2003**.
- (277) Larson, R. A.; Weber, E. J. *Reaction mechanisms in environmental organic chemistry*; Lewis Publishers: United States, 1994; p. 448.

- (278) Dodero, G.; Michieli, L. De; Cavalleri, O.; Rolandi, R.; Oliveri, L.; Daccà, A.; Parodi, R. *Colloids Surfaces A Physicochem. Eng. Asp.* **2000**, *175*, 121–128.
- (279) Tseng, R. J.; Tsai, C.; Ma, L.; Ouyang, J.; Ozkan, C. S.; Yang, Y. *Nat. Nanotechnol.* **2006**, *1*, 72–77.
- (280) Chapman, T. M. *J. Polym. Sci. Part A Polym. Chem.* **1989**, *27*, 1993–2005.
- (281) Dicenzo, S. B.; Wertheim, G. K. *Comments Solid State Phys.* **1985**, *11*, 203–219.
- (282) Kitagawa, H.; Kojima, N.; Sakai, H. *J. Chem. Soc. Dalt. Trans. Inorg. Chem.* **1991**, *11*, 3121–3125.
- (283) Mcneillie, A.; Brown, D. H.; Smith, W. E.; Chemistry, A.; Gibson, M. J. *Chem. Soc. Dalt. Trans. Inorg. Chem.* **1980**, 767–770.
- (284) Gerenser, L. J.; Goppert-Berarducci, K. E.; Baetzold, R. C.; Pochan, J. M. *J. Chem. Phys.* **1991**, *95*, 4641.
- (285) Wagner, C. D. *Faraday Discuss. Chem. Soc.* **1975**, *60*, 291–300.
- (286) Xie, Y.-B.; Zhang, C.; Li, J.-R.; Bu, X.-H. *Dalt. Trans.* **2004**, *21*, 562–569.
- (287) Park, H. B.; Lee, Y. M. *J. Memb. Sci.* **2002**, *197*, 283–296.
- (288) Lobo, H.; Bonilla, J. V. *Handbook of Plastics Analysis*; CRC Press, 2003; p. 650.
- (289) Roohpour, N.; Moshaverinia, A.; Wasikiewicz, J. M.; Paul, D.; Wilks, M.; Millar, M.; Vadgama, P. *Biomed. Mater.* **2012**, *7*, 015007.
- (290) Hernández-Sierra, J. F.; Ruiz, F.; Pena, D. C. C.; Martínez-Gutiérrez, F.; Martínez, A. E.; Guillén, A. D. J. P.; Tapia-Pérez, H.; Castañón, G. M. *Nanomedicine Nanotechnology, Biol. Med.* **2008**, *4*, 237–240.

- (291) Shanmugam, S.; Viswanathan, B.; Varadarajan, T. K. *Mater. Chem. Phys.* **2006**, *95*, 51–55.
- (292) Dastjerdi, R.; Montazer, M. *Colloids Surfaces B Biointerfaces* **2010**, *79*, 5–18.
- (293) Lansdown, A. B. G. *J. Wound Care* **2002**, *11*, 173–177.
- (294) Castellano, J. J.; Shafii, S. M.; Ko, F.; Donate, G.; Wright, T. E.; Mannari, R. J.; Payne, W. G.; Smith, D. J.; Robson, M. C. *Int. Wound J.* **2007**, *4*, 114–122.
- (295) Kaur, P.; Saxena, M.; Vadehra, D. V. *Indian J. Med. Res.* **1985**, *82*, 122–126.
- (296) Sathishkumar, M.; Sneha, K.; Won, S. W.; Cho, C.-W.; Kim, S.; Yun, Y.-S. *Colloids Surfaces B Biointerfaces* **2009**, *73*, 332–338.
- (297) Dastjerdi, R.; Montazer, M.; Shahsavan, S. *Colloids Surfaces A Physicochem. Eng. Asp.* **2009**, *345*, 202–210.
- (298) Percival, S. L.; Bowler, P. G.; Russell, D. J. *Hosp. Infect.* **2005**, *60*, 1–7.
- (299) Moulder, J. F.; Stickle, W. F.; Sobol, P. E. *Handbook of X-ray Photoelectron Spectroscopy*; Physical Electronics, 1993; p. 275.
- (300) Ghosh, S. K.; Pal, T. *Chem. Rev.* **2007**, *107*, 4797–4862.
- (301) Sarkar, P.; Bhui, D. K.; Bar, H.; Sahoo, G. P.; Samanta, S.; Pyne, S.; Misra, A. *Nanoscale Res. Lett.* **2010**, *5*, 1611–1618.
- (302) Qian, H.; Zhu, M.; Wu, Z.; Jin, R. *Acc. Chem. Res.* **2012**, *45*, 1470–1479.
- (303) Haiss, W.; Thanh, N. T. K.; Aveyard, J.; Fernig, D. G. *Anal. Chem.* **2007**, *79*, 4215–4221.
- (304) MacCuspie, R. I.; Rogers, K.; Patra, M.; Suo, Z.; Allen, A. J.; Martin, M. N.; Hackley, V. a. *J. Environ. Monit. JEM* **2011**, *13*, 1212–1226.

- (305) Wiley, B.; Sun, Y.; Mayers, B.; Xia, Y. *Chemistry (Easton)*. **2005**, *11*, 454–463.
- (306) Ott, L. S.; Finke, R. G. *Coord. Chem. Rev.* **2007**, *251*, 1075–1100.
- (307) Verma, H. R. *Atomic and nuclear analytical methods. XRF, Moessbauer, XPS, NAA and ion-beam spectroscopic techniques*; Springer Berlin / Heidelberg: New York, 2007.
- (308) Suárez, S.; Martín, J. A.; Yates, M.; Avila, P.; Blanco, J. J. *Catal.* **2005**, *229*, 227–236.
- (309) Jirsak, T.; Dvorak, J.; Rodriguez, J. a. *Surf. Sci.* **1999**, *436*, 683–690.
- (310) McLean, W.; Colmenares, C. A.; Smith, R. L.; Somorjal, G. A. *J. Phys. Chem.* **1983**, *87*, 788–793.
- (311) Lindau, I.; Pianetta, P.; Yu, K.; Spicer, W. *Phys. Rev. B* **1976**, *13*, 492–495.
- (312) Gray, J. E.; Norton, P. R.; Griffiths, K. *Appl. Surf. Sci.* **2003**, *217*, 210–222.
- (313) Sebastian, J.; Jasra, R. V. *Ind. Eng. Chem. Res.* **2005**, *44*, 8014–8024.
- (314) Serghini-Monim, S.; Norton, P. R.; Puddephatt, R. J.; Pollard, K. D.; Rasmussen, J. R. *J. Phys. Chem. B* **1998**, *102*, 1450–1458.
- (315) Toone, E. J. *Advances in Enzymology and Related Areas of Molecular Biology*; Wiley Hoboken, 2011; p. Volume 77.
- (316) Kim, S.-H.; Lee, H.; Ryu, D.; Choi, S.; Lee, D. *Korean J. Microbiol. Biotechnol.* **2011**, *39*, 77–85.
- (317) Li, X.; Lenhart, J. J. *Environ. Sci. Technol.* **2012**, *46*, 5378–5386.
- (318) Wright, T. *Chem. Fibers Int.* **2002**, *25*, 125.

- (319) An, C.; Wang, J.; Jiang, W.; Zhang, M.; Ming, X.; Wang, S.; Zhang, Q. *Nanoscale* **2012**, *4*, 5646–5650.
- (320) Träger, F. *Handbook of Lasers and Optics*; 2. Edition.; Springer Berlin / Heidelberg, 2012; p. 1726.
- (321) Kim, S.-W.; Chung, H.-E.; Kwon, J.-H.; Yoon, H.-G.; Kim, W. *Bull. Korean Chem. Soc.* **2010**, *31*, 2918–2922.
- (322) Liu, C.-Y.; Zhang, Z.-Y.; Wang, C.-Y. *J. Imaging Sci. Technol.* **1999**, *43*, 492–497.
- (323) Husein, M. M.; Rodil, E.; Vera, J. H. *J. Colloid Interface Sci.* **2005**, *288*, 457–467.
- (324) Husein, M.; Rodil, E.; Vera, J. H. *J. Colloid Interface Sci.* **2004**, *273*, 426–434.
- (325) Correa, N. M.; Zhang, H.; Schelly, Z. A. *JACS* **2000**, 6432–6434.
- (326) Zhang, H.; Schelly, Z. A.; Marynick, D. S. *J. Phys. Chem. A* **2000**, *104*, 6287–6294.
- (327) Kumar, P. S.; Dayal, P. B.; Sunandana, C. S. *Thin Solid Films* **1999**, *357*, 111–118.
- (328) Wang, Y.; Mo, J.; Cai, W.; Yao, L.; Zhang, L. *Mater. Lett.* **2002**, *56*, 502–506.
- (329) Gavriluk, A. I. *Tech. Phys. Lett.* **2007**, *33*, 779–781.
- (330) Matsunaga, K.; Tanaka, I.; Adachi, H. *J. Phys. Soc. Japan* **1998**, *67*, 2027–2036.
- (331) Maskasky, J. E.; Jones, R. W. Silver halide photographic emulsions with novel grain faces. EP 213964 A2 19870311, 1987.
- (332) Goessens, C.; Schryvers, D.; Van Landuyt, J.; De Keyzer, R. *Ultramicroscopy* **1992**, *40*, 151–162.

- (333) Sanchezbajo, F.; Ortiz, a; Cumbreira, F. *Acta Mater.* **2006**, *54*, 1–10.
- (334) Wang, W.; Li, W.; Ye, J.; Zhang, R.; Wang, J. *Synth. Met.* **2010**, *160*, 2203–2207.
- (335) Tang, Y.; Subramaniam, V. P.; Lau, T. H.; Lai, Y.; Gong, D.; Kanhere, P. D.; Cheng, Y. H.; Chen, Z.; Dong, Z. *Appl. Catal. B Environ.* **2011**, *106*, 577–585.
- (336) Clabes, J. G. *J. Vac. Sci. Technol. A* **1988**, *6*, 2887–2892.
- (337) Morales, J.; Sánchez, L.; Martín, F.; Ramos-Barrado, J. R.; Sánchez, M. J. *Electrochem. Soc.* **2004**, *151*, A151.
- (338) Salaita, G. N.; Hazos, Z. F.; Hoflund, G. B. *J. Electron Spectros. Relat. Phenomena* **2000**, *107*, 73–81.
- (339) Wang, P.; Huang, B.; Qin, X.; Zhang, X.; Dai, Y.; Whangbo, M.-H. *Inorg. Chem.* **2009**, *48*, 10697–10702.
- (340) Peng, P.; Hu, A.; Zheng, W.; Su, P.; He, D.; Oakes, K. D.; Fu, A.; Han, R.; Lee, S. L.; Tang, J.; Zhou, Y. N. *RSC Adv.* **2012**, *2*, 11359–11365.
- (341) Hammond, J. S.; Gaarenstroom, S. W.; Winograd, N. *Anal. Chem.* **1975**, *47*, 2193–2199.
- (342) Cheng, H.; Huang, B.; Dai, Y.; Qin, X.; Zhang, X. *Langmuir* **2010**, *26*, 6618–6624.
- (343) Li, Y.; Zhang, H.; Guo, Z.; Han, J.; Zhao, X.; Zhao, Q.; Kim, S.-J. *Langmuir* **2008**, *24*, 8351–8357.
- (344) Xu, H.; Yan, J.; Xu, Y.; Song, Y.; Li, H.; Xia, J.; Huang, C.; Wan, H. *Appl. Catal. B Environ.* **2013**, *129*, 182–193.
- (345) Gaarenstroom, S. W.; Winograd, N. *J. Chem. Phys.* **1977**, *67*, 3500.
- (346) Guo, J.-Z.; Cui, H. *J. Phys. Chem. C* **2007**, *111*, 12254–12259.

- (347) Ghosh, S.; Saraswathi, A.; Indi, S. S.; Hoti, S. L.; Vasan, H. N. *Langmuir* **2012**, 28, 8550–8561.
- (348) Rehan, M.; Hartwig, A.; Ott, M.; Gätjen, L.; Wilken, R. *Surf. Coatings Technol.* **2013**, 219, 50–58.
- (349) Jiang, J.; Zhang, L. *Chemistry (Easton)*. **2011**, 17, 3710–3717.